VASCULAR SMOOTH MUSCLE CELL FATE AND VASCULAR REMODELING: MECHANISMS, THERAPEUTIC TARGETS, AND DRUGS, VOLUME I

EDITED BY: Ping Song, Xiaoyan Dai, Qilong Wang and Vicky E. MacRae
PUBLISHED IN: Frontiers in Pharmacology

frontiers Research Topics

frontiers

ISSN 1664-8714
ISBN 978-2-83250-070-5
DOI 10.3389/978-2-83250-070-5

About Frontiers

Frontiers is more than just an open-access publisher of scholarly articles: it is a pioneering approach to the world of academia, radically improving the way scholarly research is managed. The grand vision of Frontiers is a world where all people have an equal opportunity to seek, share and generate knowledge. Frontiers provides immediate and permanent online open access to all its publications, but this alone is not enough to realize our grand goals.

Frontiers Journal Series

The Frontiers Journal Series is a multi-tier and interdisciplinary set of open-access, online journals, promising a paradigm shift from the current review, selection and dissemination processes in academic publishing. All Frontiers journals are driven by researchers for researchers; therefore, they constitute a service to the scholarly community. At the same time, the Frontiers Journal Series operates on a revolutionary invention, the tiered publishing system, initially addressing specific communities of scholars, and gradually climbing up to broader public understanding, thus serving the interests of the lay society, too.

Dedication to Quality

Each Frontiers article is a landmark of the highest quality, thanks to genuinely collaborative interactions between authors and review editors, who include some of the world's best academicians. Research must be certified by peers before entering a stream of knowledge that may eventually reach the public - and shape society; therefore, Frontiers only applies the most rigorous and unbiased reviews.
Frontiers revolutionizes research publishing by freely delivering the most outstanding research, evaluated with no bias from both the academic and social point of view. By applying the most advanced information technologies, Frontiers is catapulting scholarly publishing into a new generation.

What are Frontiers Research Topics?

Frontiers Research Topics are very popular trademarks of the Frontiers Journals Series: they are collections of at least ten articles, all centered on a particular subject. With their unique mix of varied contributions from Original Research to Review Articles, Frontiers Research Topics unify the most influential researchers, the latest key findings and historical advances in a hot research area! Find out more on how to host your own Frontiers Research Topic or contribute to one as an author by contacting the Frontiers Editorial Office: frontiersin.org/about/contact

VASCULAR SMOOTH MUSCLE CELL FATE AND VASCULAR REMODELING: MECHANISMS, THERAPEUTIC TARGETS, AND DRUGS, VOLUME I

Topic Editors:
Ping Song, Georgia State University, United States
Xiaoyan Dai, Guangzhou Medical University, China
Qilong Wang, Tianjin University of Traditional Chinese Medicine, China
Vicky E. MacRae, University of Edinburgh, United Kingdom

Citation: Song, P., Dai, X., Wang, Q., MacRae, V. E., eds. (2022). Vascular Smooth Muscle Cell Fate and Vascular Remodeling: Mechanisms, Therapeutic Targets, and Drugs, Volume I. Lausanne: Frontiers Media SA. doi: 10.3389/978-2-83250-070-5

Table of Contents

frontiers | Frontiers in Pharmacology

TYPE Editorial
PUBLISHED 16 August 2022
DOI 10.3389/fphar.2022.989689

OPEN ACCESS

EDITED AND REVIEWED BY
Francesco Rossi,
University of Campania Luigi Vanvitelli, Italy

*CORRESPONDENCE
Qilong Wang,
wangqilong_00@tjutcm.edu.cn
Ping Song,
psong@gsu.edu

SPECIALTY SECTION
This article was submitted to Cardiovascular and Smooth Muscle Pharmacology, a section of the journal Frontiers in Pharmacology

RECEIVED 08 July 2022
ACCEPTED 15 July 2022
PUBLISHED 16 August 2022

CITATION
Wang Q, Dai X, MacRae VE and Song P (2022), Editorial: Vascular smooth muscle cell fate and vascular remodeling: Mechanisms, therapeutic targets, and drugs, volume I. *Front. Pharmacol.* 13:989689. doi: 10.3389/fphar.2022.989689

Editorial: Vascular smooth muscle cell fate and vascular remodeling: Mechanisms, therapeutic targets, and drugs, volume I

Qilong Wang[1]*, Xiaoyan Dai[2], Vicky E. MacRae[3] and Ping Song[4]*

[1]Institute of Traditional Chinese Medicine, Tianjin University of Traditional Chinese Medicine, Tianjin, China, [2]Guangzhou Municipal and Guangdong Provincial Key Laboratory of Molecular Target & Clinical Pharmacology, the NMPA and State Key Laboratory of Respiratory Disease, School of Pharmaceutical Sciences, Guangzhou Medical University, Guangzhou, China, [3]The Roslin Institute and R(D)VS, University of Edinburgh, Easter Bush, United Kingdom, [4]Center for Molecular and Translational Medicine, Georgia State University, Atlanta, GA, United States

KEYWORDS

VSMC, neointimal hyperplasia, vascular dilation, arterial stiffness, calcification, atherosclerosis

Editorial on the Research Topic
Vascular smooth muscle cell fate and vascular remodeling: Mechanisms, therapeutic targets, and drugs, volume I

Introduction

Vascular smooth muscle cells (VSMCs), an essential cell type of the blood vessel, are required for maintaining vascular structure and function with unique phenotypes. However, under a pathological state VSMC fate changes such as proliferation, migration, apoptosis, quiescence, senescence and trans-differentiation, can lead to altered structure and arrangement of blood vessels. This can subsequently result in the development of critical cardiovascular diseases including atherosclerosis, aneurysm, hypertension, vascular calcification and arterial stiffness. Currently, there is limited therapy to prevent VSMC phenotype switching and vascular remodeling. Therefore, investigating the cellular and molecular basis of VSMC cell fate change will enable the discovery of novel therapeutic targets and develop effective medicines to treat cardiovascular diseases.

To understand the underlying mechanisms of VSMC fate regulation and issue future perspectives, we actively bring together this Research Topic "*Vascular Smooth Muscle Cell Fate and Vascular Remodeling: Mechanisms, Therapeutic Targets, and Drugs*" for the readers of Frontiers in Pharmacology. This Research Topic has twelve papers, including

ten original research articles and two literature reviews, highlighting novel mechanisms and medicines underpinning VSMC fate and vascular remodeling.

VSMCs and neointimal hyperplasia

Neointimal hyperplasia is a pathological process associated with dysregulated VSMC proliferation and migration within the vessel during atherosclerosis and in-stent restenosis. Zhang et al. showed that VSMC-specific deletion of lethal giant larvae 1 (LGL1), which functions as cell polarity regulator and tumor suppressor, caused promotion of neointimal hyperplasia *in vivo*. Moreover, LGL1 knockdown enhanced the proliferation and migration of VSMCs *in vitro*. The authors proposed that this effect may be mediated by the loss of LGL1-STAT3 binding and enhanced STAT3-mediated proliferation/migration-related gene transcription.

In-stent restenosis is a common complication following stent placement. Identifying the biomarker for the onset of in-stent restenosis in the patients is critical after stent implantation. Guo et al. (2022) recruited patients from 6 months and 2 years post percutaneous coronary intervention (PCI) and measured serum homocysteine. The authors observed a positive correlation between homocysteine and severity of restenosis after PCI, suggesting that serum homocysteine level might be a predictive biomarker for stent restenosis severity.

Additionally, new therapeutic medicines useful for suppressing neointima formation are illustrated here. Wu et al. (2022) found that theaflavin-3,3′-digallate, a natural product isolated from black tea, attenuated neointimal hyperplasia *in vivo*. Meanwhile, theaflavin-3,3′-digallate (TF3) decreased the proliferation and migration of primary rat aortic smooth cells *in vitro*. The authors further showed that TF3 reduced phosphorylation of PDGFRβ, leading to the blockage of PDGF-induced phenotypic switching of VSMCs, suggesting that TF3 might be a potential therapeutic candidate for the treatment of neointima formation.

VSMCs and vascular dilation

VSMC contraction and relaxation contributes to the function of the vessel. However, abnormal vasoconstriction and vasospasm leads to vascular disease pathogenesis, particularly hypertension, angina and stroke. Zhang et al. found that benzoylaconitine, a monoester alkaloid from *Aconitum carmichaelii*, reduced blood pressure in spontaneously hypertensive rats. Studies demonstrated that benzoylaconitine directly binds with angiotensin-converting enzymes (ACE)/ACE2 and activates ACE/ACE2 activity, through virtual docking, surface plasmon resonance, enzyme activity assays and HUVEC cell culture experiments. Benzoylaconitine enhanced endothelium-dependent vasorelaxation and reduced vascular inflammation, and therefore maybe a potential modulator of the renin-angiotensin system for the treatment of hypertension.

Cui et al. (2022) found that allicin, an active molecular derived from garlic, exaggerated coronary artery relaxation induced by 5-hydroxytryptamine (5-HT), 9,11-dideoxy-9α,11α-methanoepoxy-prosta-5Z,13E-dien-1-oic acid (U46619), or endothelin-1 (ET-1). Allicin relaxed VSMCs via activation of the ATP-sensitive potassium (K_{ATP}) channels. Moreover, Allicin enhanced hydrogen sulfide (H_2S) production and cystathionine-γ-lyase levels in serum and myocardial tissue. These moleculesmay be involved in the mechanism of allicin action in acute myocardial infarction.

Traditional Chinese medicine has been used to treat cardiovascular disease for thousands of years. Guo et al. (2022) demonstrated that Danggui Buxue Decoction, consisting of *Angelicae Sinensis* Radix and *Astragali Radix*, induces a relaxation effect on rat middle cerebral artery. Danggui Buxue decoction, *Angelicae Sinensis* Radix, and *Astragali Radix* extracts relax KCl and U46619-contracted middle cerebral artery, with activation of K_{ATP} and K_{ir} channels underpinning this mechanism. Moreover, extracellular Ca^{2+} influx and internal Ca^{2+} from organelles also contribute to the action of Danggui Buxue Decoction. Fan et al. (2021) have further found that SaiLuoTong capsule attenuated cerebral infarction and neurological deficit in the middle cerebral artery occlusion rat model. SaiLuoTong capsule increased tight junction proteins via upregulation of a Nrf2-mediated anti-oxidative pathway in vascular endothelium and bone marrow microvascular endothelial cells, suggesting that SaiLuoTong capsule's therapeutic effect on brain ischemia might be related to Nrf2-dependent endothelial cell protection.

VSMCs and arterial stiffness

Arterial stiffness refers to the loss of elastic characteristics within the arterial wall, leading to systolic blood pressure and cardiac dysfunction. VSMC collagen deposition and hypercontraction contribute to arterial stiffness. Previous studies have measured the intrinsic mechanical properties of VSMCs to evaluate cell stiffness using atomic force microscopy. Ahmed et al. (2022) have provided a novel technique to record the tensegrity model of cellular mechanics using polyacrylamide hydrogels to mimic the physiological stiffness of the aortic wall. Angiotensin II inhibited the VSMC morphology and enhanced traction stress, whereas colchicine increased VSMC morphology, suggesting that VSMC morphology and actomyosin activity are the major reason for the contractile response. Moreover, microtubule destabilization by paclitaxel blocked the angiotensin II-induced morphology change, revealing that microtubules are essential in regulating the morphology and contractility of the isolated VSMCs.

Zhang et al. found that ginsenoside Rb1, a natural compound from ginseng, improved aortic stiffness in diabetic mice. Rb1 regulated pulse pressure and aortic compliance and

restored acetylcholine-induced endothelium-dependent vasorelaxation. Rb1 induced phosphorylation of AMPK and inhibited TGFβ1/smad2/3, ROS production, and MMP2/9 expression. Moreover, AMPK silencing blocked Rb1-mediated reduction of collagen deposition, fibronectin expression, and elastic fiber alignment, suggesting that Rb1 ameliorates diabetic arterial stiffness via AMPK activation.

VSMCs and arterial calcification

Arterial calcification is characterized by the deposition of calcium phosphate crystals in the artery wall. VSMC transdifferentiation and mineralization can induce arterial calcification. Daprodustat is a medicine employed to increase erythropoiesis via stabilization of HIF1α. Toth et al. (2022) demonstrated that Daprodustat increased aortic calcification in a high phosphate-induced chronic kidney disease mice model. Daprodustat could stabilize HIF1α and HIF2α to accelerate medial calcification, suggesting that there is a possible risk that Daprodustat treatment could accelerate medial calcification in CKD patients with hyperphosphatemia.

VSMCs and atherosclerosis

VSMCs are the primary source of plaque cells and extracellular matrix in both early- and late-stage atherosclerosis. Li et al. (2022) have reviewed the effect of extracellular vesicles on VSMC in atherosclerosis. The extracellular vesicles could be secreted by multiple cell types, including endothelial cells, macrophages, and mesenchymal stem cells. Extracellular vesicles are essential for intercellular communication via their contents, such as miRNA and lncRNA. The author suggested that extracellular vesicles might function as diagnostic indicators of atherosclerosis and drug vectors. Wang et al. (2022) have summarized the role of IL-17 in the pathogenesis of rheumatoid arthritis and atherosclerosis. Serum IL-17 level is significantly upregulated in patients with rheumatoid arthritis and atherosclerosis. Then, IL-17 regulates proliferation, migration, and apoptosis of vascular endothelial cells and VSMC, leading to cytokine production and the development of atherosclerosis. IL-17 also regulates bone destruction and synovial hyperplasia. Therefore, IL-17 might be used as a potential therapeutic target for the occurrence and development of cardiovascular disease in patients with rheumatoid arthritis.

In conclusion, this Research Topic provides valuable articles describing novel molecular mechanisms and innovative therapeutic medicines to treat cardiovascular diseases.

Author contributions

QW, XD, and PS wrote the manuscript. VM revised the manuscript. All the authors listed have made a substantial, direct, and intellectual contribution to the work and approved it for publication.

Funding

This work was supported by grants from Innovation Team and Talents Cultivation Program of National Administration of Traditional Chinese Medicine, China (ZYYCXTD-C-202203) and Science and Technology Program of Tianjin, China (21ZYJDJC00080) to QW; the Natural Science Foundation of Guangdong (2022A1515012502) to XD; Biotechnology and Biological Sciences Research Council (BBSRC) in the form of an Institute Strategic Programme Grant (BB/J004316/1) to VM; and National Heart, Lung, and Blood Institute (HL140954) to PS.

Conflict of interest

The authors declare that the research was conducted in the absence of any commercial or financial relationships that could be construed as a potential conflict of interest.

Publisher's note

References

Ahmed, S., Johnson, R. T., Solanki, R., Afewerki, T., Wostear, F., and Warren, D. T. (2022). Using polyacrylamide hydrogels to model physiological aortic stiffness reveals that microtubules are critical regulators of isolated smooth muscle cell morphology and contractility. *Front. Pharmacol.* 13, 836710. doi:10.3389/fphar.2022.836710

Cui, T., Liu, W., Yu, C., Ren, J., Li, Y., Shi, W., et al. (2022). Protective effects of allicin on acute myocardial infarction in rats via hydrogen sulfide-mediated regulation of coronary arterial vasomotor function and myocardial calcium transport. *Front. Pharmacol.* 12, 752244. doi:10.3389/fphar.2021.752244

Fan, X.-D., Yao, M.-J., Yang, B., Han, X., Zhang, Y.-H., Wang, G.-R., et al. (2021). Chinese herbal preparation SaiLuoTong alleviates brain ischemia via Nrf2 antioxidation pathway–dependent cerebral microvascular protection. *Front. Pharmacol.* 12, 748568. doi:10.3389/fphar.2021.748568

Guo, J., Gao, Y., Ahmed, M., Dong, P., Gao, Y., Gong, Z., et al. (2022). Serum homocysteine level predictive capability for severity of restenosis post percutaneous coronary intervention. *Front. Pharmacol.* 13, 816059. doi:10.3389/fphar.2022.816059

Li, T., Wang, B., Din, H., Chen, S., Cheng, W., Li, Y., et al. (2022). Effect of extracellular vesicles from multiple cells on vascular smooth muscle cells in atherosclerosis. *Front. Pharmacol.* 13, 857331. doi:10.3389/fphar.2022.857331

Toth, A., Csiki, D. M., Nagy, B., Jr, Balogh, E., Lente, G., Ababneh, H., et al. (2022). Daprodustat accelerates high phosphate-induced calcification through the activation of HIF-1 signaling. *Front. Pharmacol.* 13, 798053. doi:10.3389/fphar.2022.798053

Wang, J., He, L., Li, W., and Lv, S. (2022). A role of IL-17 in rheumatoid arthritis patients complicated with atherosclerosis. *Front. Pharmacol.* 13, 828933. doi:10.3389/fphar.2022.828933

Wu, Y., Chen, M., Chen, Z., Shu, J., Zhang, L., Hu, J., et al. (2022). Theaflavin-3,3'-digallate from black tea inhibits neointima formation through suppression of the PDGFRβ pathway in vascular smooth muscle cells. *Front. Pharmacol.* 13, 861319. doi:10.3389/fphar.2022.861319

frontiers in Pharmacology

ORIGINAL RESEARCH
published: 12 October 2021
doi: 10.3389/fphar.2021.753881

Ginsenoside Rb1 Ameliorates Diabetic Arterial Stiffening *via* AMPK Pathway

Xinyu Zhang[1], *Lei Wang*[1], *Rong Guo*[2], *Jie Xiao*[1], *Xiaoling Liu*[1], *Mei Dong*[1], *Xiaorong Luan*[1], *Xiaoping Ji*[1]* *and Huixia Lu*[1,3]*

[1]*The Key Laboratory of Cardiovascular Remodeling and Function Research, Chinese Ministry of Education, Chinese National Health Commission and Chinese Academy of Medical Sciences, The State and Shandong Province Joint Key Laboratory of Translational Cardiovascular Medicine, Department of Cardiology, Qilu Hospital, Cheeloo College of Medicine, Shandong University, Jinan, China,* [2]*Department of Cardiology, Ji'an Municipal Center People's Hospital, Ji'an, China,* [3]*Dr. Gilbert Hung Ginseng Laboratory, Department of Biology, Faculty of Science, Hong Kong Baptist University, Hong Kong, Hong Kong, SAR China*

Background and Purpose: Macrovascular complication of diabetes mellitus, characterized by increased aortic stiffness, is a major cause leading to many adverse clinical outcomes. It has been reported that ginsenoside Rb1 (Rb1) can improve glucose tolerance, enhance insulin activity, and restore the impaired endothelial functions in animal models. The aim of this study was to explore whether Rb1 could alleviate the pathophysiological process of arterial stiffening in diabetes and its potential mechanisms.

Experimental Approach: Diabetes was induced in male C57BL/6 mice by administration of streptozotocin. These mice were randomly selected for treatment with Rb1 (10–60 mg/kg, i. p.) once daily for 8 weeks. Aortic stiffness was assessed using ultrasound and measurement of blood pressure and relaxant responses in the aortic rings. Mechanisms of Rb1 treatment were studied in MOVAS-1 VSMCs cultured in a high-glucose medium.

Key Results: Rb1 improved DM-induced arterial stiffening and the impaired aortic compliance and endothelium-dependent vasodilation. Rb1 ameliorated DM-induced aortic remodeling characterized by collagen deposition and elastic fibers disorder. MMP2, MMP9, and TGFβ1/Smad2/3 pathways were involved in this process. In addition, Rb1-mediated improvement of arterial stiffness was partly achieved via inhibiting oxidative stress in DM mice, involving regulating NADPH oxidase. Finally, Rb1 could blunt the inhibition effects of DM on AMPK phosphorylation.

Conclusion and Implications: Rb1 may represent a novel prevention strategy to alleviate collagen deposition and degradation to prevent diabetic macroangiopathy and diabetes-related complications.

Keywords: Rb1, arterial stiffening, AMPK, diabetes, ginsenoside

OPEN ACCESS

Edited by:
Qilong Wang,
Tianjin University of Traditional Chinese Medicine, China

Reviewed by:
Jinlong He,
Tianjin Medical University, China
Ding Zhao,
Hebei Medical University, China

***Correspondence:**
Xiaoping Ji
jixiaoping@sdu.edu.cn
Huixia Lu
luhuixia@sdu.edu.cn

Specialty section:
This article was submitted to Cardiovascular and Smooth Muscle Pharmacology, a section of the journal Frontiers in Pharmacology

Received: *05 August 2021*
Accepted: *14 September 2021*
Published: *12 October 2021*

Citation:
Zhang X, Wang L, Guo R, Xiao J, Liu X, Dong M, Luan X, Ji X and Lu H (2021) Ginsenoside Rb1 Ameliorates Diabetic Arterial Stiffening via AMPK Pathway. Front. Pharmacol. 12:753881. doi: 10.3389/fphar.2021.753881

INTRODUCTION

Diabetes mellitus (DM) is one of the costliest and most burdensome chronic diseases worldwide. It has become a pandemic health disaster, especially among the elderly. In addition to the disease, consequent chronic vascular complications are a major cause of the increased morbidity and mortality of diabetic patients (Delbin and Trask, 2014). Several clinical trials have confirmed that

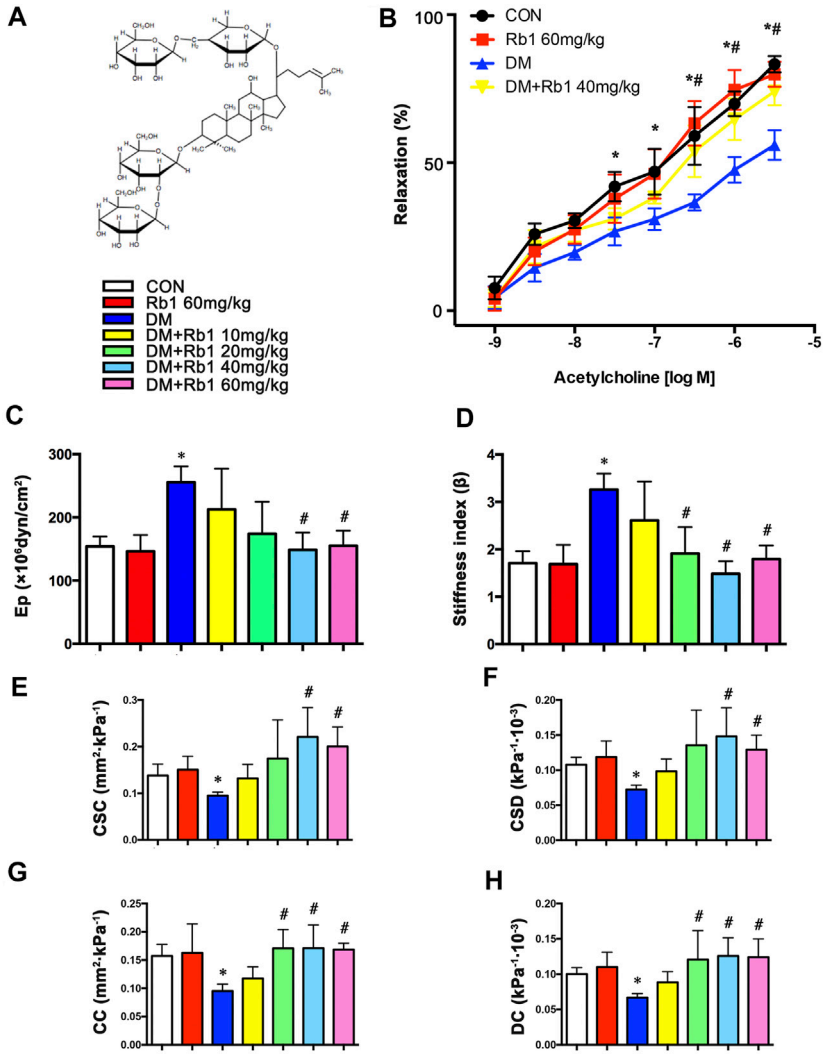

FIGURE 1 | Rb1 improves aortic compliance and restores acetylcholine-induced endothelium-dependent vasorelaxation. **(A)** Chemical structure of ginsenoside Rb1. **(B)** After the addition of phenylephrine, cumulative doses of acetylcholine (1×10^{-9}–$1 \times 10^{-5.5}$ M) were added to check the endothelial functions. **(C)** Peterson's elastic modulus (Ep). **(D)** Arterial stiffness index (β). **(E)** Cross-sectional compliance (CSC), **(F)** cross-sectional distensibility (CSD), **(G)** compliance coefficient (CC), and **(H)** distensibility coefficient (DC). Data are mean ± SEM. n = 5–6, *$p < 0.05$ vs. Control; #$p < 0.05$ DM + Rb1 vs. DM.

intensive glycemic control in people with diabetes contributes to reducing the risk of microvascular (Holman et al., 2008). However, there was no evidence that it has advantages in terms of mortality or diabetic macroangiopathy (Zoungas et al., 2014). Macrovascular complications of DM, characterized by increased aortic stiffness, are also associated with hypertension, aging, insulin resistance, atherosclerosis, and hypertriglyceridemia (Mitchell et al., 2007; Dietrich et al., 2010; Payne et al., 2010; Stacey et al., 2010). Increased aortic stiffness independently predicts future cardiovascular disease, especially in women (Laurent et al., 2012; Ben-Shlomo et al., 2014). It leads to many adverse clinical outcomes, including impaired coronary perfusion and subsequent cardiovascular mortality.

As a major active component of ginseng, ginsenoside Rb1 (Rb1) (**Figure 1A**) (Cho et al., 2004) is the most frequently used and studied Chinese medicine and object. Gabriel Hoi-huen Chan et al. have demonstrated that ginseng extract exerted a protective effect in restoring normal endothelial functions in models with diabetes (Chan et al., 2013). Min Liu et al. have demonstrated that Rb1 reduced body weight, improved glucose tolerance, enhanced insulin action, and decreased the accumulation of cellular lipid in the livers of obese animals induced by high-fat diet (HFD) by activating the adenosine monophosphate (AMP)-activated protein kinase (AMPK) signaling pathway (Xiong et al., 2010; Shen et al., 2013). Interestingly, the effects of metformin, thiazolidinediones, and some other antidiabetic drugs are mediated through AMPK activation. Previous studies have supported the notion that AMPK working as a metabolic sensor of cellular adenosine triphosphate (ATP) levels is an important therapeutic target of aortic stiffness in cardiovascular diseases (CVDs) (Nagata et al., 2004; Gu et al., 2014; Lin et al., 2016).

These studies prompted us to hypothesize that Rb1 might alleviate the pathophysiological process of arterial stiffening in diabetes via the AMPK pathway. We used an animal model of type 1 diabetes to verify this hypothesis.

MATERIALS AND METHODS

Cell Culture and Treatments

Dulbecco's modified Eagle's medium (DMEM) supplemented with 10% fetal bovine serum (FBS) and penicillin (100 U/ml) or streptomycin (100 μg/ml) maintained MOVAS-1 murine primary aortic vascular smooth muscle cells (VSMCs) (ATCC; Cat. no CRL-2797TM) at the temperature of 37°C with 5% CO_2 atmosphere in a humid incubator. Upon reaching 60–70% confluence, cells were incubated with control medium (NC, 5.5 mmol/L) and serum-free DMEM overnight before treatment with high-glucose medium (HG, 30 mmol/L) and Rb1. VSMCs were stimulated with Rb1 (40 μM) 2 h before HG (30 mM) stimulation and cultured for an additional 48 h. For the HG + Rb1 + compound C (p-AMPK inhibitor) group, VSMCs were pretreated with compound C (10 μM) for 2 h before Rb1 treatment. Compound C was purchased from Selleck (Houston, Texas, the United States) and dissolved in dimethylsulfoxide (DMSO). Cells and supernatant were harvested simultaneously.

Mice and Drug Treatment

This study followed the animal protocols approved by the Animal Care Committee of Shandong University and the Guide for the Care and Use of Laboratory Animals published by the National Institutes of Health. All mouse husbandry and experiments followed the Animal Management Rule of the Ministry of Health of the People's Republic of China (Document No. 55, 2001). Male C57BL/6 mice (6–8 weeks, 25–28 g, Vital River Laboratories, Beijing, China) were classified into control and diabetes mellitus groups (CON and DM (n = 15 and 90)). As mentioned earlier, streptozocin (STZ) induced diabetes (Wang et al., 2014; Zhang et al., 2016). In brief, mice (n = 75 and 15) from DM and CON groups were randomly selected for treatment with Rb1 dissolved in normal saline and intraperitoneally (ip) once every day for 8 weeks in DM + Rb1 and CON + Rb1 groups. The dose range of Rb1 (10–60 mg/kg) was based on other experimental studies (Jiang et al., 2007; Zhao et al., 2010).

Blood Pressure Measurement

As described previously, systolic and diastolic blood pressures (SBP and DBP) were measured using a noninvasive tail-cuff system (Softron BP-98A; Softron, Tokyo, Japan) (Kanda et al., 2005) and used for calculating pulse pressure (PP).

Arterial Stiffness Assessment

As previously mentioned, the Vevo2100 imaging system (Visual Sonics, Toronto, Canada) was utilized to perform aortic ultrasonography (Zhang et al., 2016). Isoflurane (1% in O_2) was inhaled by and anesthetized mice. Two-dimensional (2D), M-mode, and pulsed wave (PW) Doppler was used to obtain images. Three continuous cardiac cycles were averaged to get all measurements conducted by an operator. Minimum and maximum (end-diastolic, Dd; peak systolic, Ds) diameters were obtained from M-mode. 2D ultrasonography was applied to determine Peterson's elastic modulus (Ep), arterial stiffness index (β), cross-sectional distensibility and compliance (CSD and CSC), and distensibility and compliance coefficients (DC and CC), which were estimated automatically by the following formulae (Pannier et al., 2002):

$$EP = \left(\frac{\Delta P}{\Delta D}\right) \times Dd = \left[\frac{Ps - Pd}{Ds - Dd}\right] \times Dd\left(\frac{10^6 dym}{cm^2}\right)$$

$$\beta = ln\frac{Ps/Pd}{([Ds - Dd]/Dd)},$$

$$CSC = \frac{\Delta V/L}{\Delta P} = \frac{\Delta A}{\Delta P} = \frac{\pi \times \left(2Dd \times \Delta D \times \Delta D^2\right)}{4\Delta P}\left(mm^2 \cdot kPa^{-1}\right),$$

$$CSD = \Delta A{:}\ [A \times (Ps - Pd)] = \pi \times \left[\left(\frac{Ds}{2}\right)^2 - \left(\frac{Dd}{2}\right)^2\right]{:}\left[\pi \times \left(\frac{Dd}{2}\right)^2 \times (Ps - Pd) \times 0.13332\right] = \frac{2Dd \times \Delta D + Dd^2}{Dd^2 \times \Delta P}\left(kPa^{-1} \cdot 10^{-3}\right),$$

$$CC = \frac{2Dd \times \Delta D + Dd^2}{4\Delta P}\left(mm^2 \cdot kPa^{-1}\right),$$

$$DC = \frac{2\Delta d}{Dd \times \Delta P}\left(kPa^{-1} \cdot 10^{-3}\right)$$

where Ps and Pd are SBP and DBP, respectively; ΔP, ΔD, and ΔA represent the changes in BP, vascular diameter, and aortic cross-sectional lumen area, respectively; Ds and Dd stand for systolic and diastolic diameters, respectively; A refers to aortic cross-sectional lumen area.

Measurement of Relaxant Responses in the Aortic Rings

Measurement was implemented as described previously (Chan et al., 2013). Briefly, mice were anesthetized, whose thoracic aortas were cut from the aortic arch to the diaphragm and immediately put into dishes containing Krebs buffer maintained at 4°C. Adipose tissues were cut off from the aortas before being cut into 3 mm segment rings. Then, the segments were mounted cautiously between two platinum hooks in 10 ml of organ baths, maintaining Krebs buffer at 37°C and continuously bubbled with 95% O_2 to 5% CO_2. After the 60 min equilibration of resting tension determined by normalization, each aortic ring was added with the cumulative doses of KCL (20–80 mM) to detect their activation. After the wash-out of KCL, the addition of one-dose phenylephrine at 1×10^{-7} M was performed until aortic rings maintained 50% of maximum tension. Endothelial functions were checked by adding the cumulative doses of acetylcholine (1×10^{-9}–$1 \times 10^{-5.5}$ M). The plateau of responses was followed by the addition of all doses.

Experimental Procedure

At last, mice were dissected and perfused with saline before being anesthetized with 1% pentobarbital sodium, which was then sacrificed, with thoracic aortas removed from the chest and rinsed with saline. A portion of the aorta (approximately

5 mm) underwent 72 h fixing in 4% paraformaldehyde, followed by the dehydration of tissues by ethanol and their embedment in paraffin, and the use of cross-sections (a thickness of 5 μm) for histological and morphometric analyses. Liquid nitrogen was used to freeze the rest of the aortas at once and store them at −80°C for subsequent molecular experiments.

Histological and Morphometric Analyses

Sirius red and Verhoeff-Van Gieson (VVG) staining were used to stain the sections so as to shape and arrange collagen and elastin content, respectively. Sirius red slides are imaged using circularly polarized light showing newer, thinner collagen fibers as green and older, thicker fibers as red/orange. The VVG slides show both collagen (pink) and elastic fibers (black). The ratio of perivascular collagen area (PVCA) to the luminal area (LA) was utilized to represent perivascular collagen content for normalizing PVCA around vessels in a variety of sizes. Pictures were obtained under a microscope (BX52, Olympus, Tokyo, Japan) and analyzed using Image-Pro Plus 5.0 software (Media Cybernetics, US). The positive area and total tissue area of each image were obtained by analyzing the images. Collagen and elastic fibers content were quantified as a percentage of total tissue area. Histological and morphometric analyses were conducted by analyzing no less than three fields per section.

Immunohistochemical and Immunofluorescence Staining

Regarding immunohistochemistry, 0.05 M sodium citrate buffer (a pH value of 6.0) was applied to perform heat-mediated antigen retrieval after the rehydration of tissue sections (5 μm). Three percent of hydrogen peroxide and bovine serum albumin were used to prevent endogenous peroxidase activity and non-specific staining, respectively. Primary antibodies against collagens I and III, 3-ni0trotyrosine (Abcam, Cambridge, the United Kingdom), and fibronectin (Proteintech Group, Chicago, Illinois (IL), the United States) were added and incubated at 4°C in a humidified box for one night. A secondary antibody (Beijing Zhong Shan-Golden Bridge Biological Technology Co., Ltd. China) was applied to incubate the sections washed with phosphate-buffered saline at 37°C for half an hour for immunohistochemical staining. Diaminobenzidine (DAB) solution (Beijing Zhong Shan-Golden Bridge Biological Technology Co., Ltd. China) was used to incubate the sections washed with phosphate-buffered saline. Hematoxylin was used to counterstain nuclei. For immunofluorescence staining, the incubation of the sections was performed by fluorescein isothiocyanate (FITC)-conjugated antibodies (a ratio of 1:50, ZSGB-BIO, Beijing, China). 4′6-Diamidine-2-phenylindole dihydrochloride (DAPI) (a ratio of 1:200, Roche, Germany) was used to stain nuclei. The observation of tissue sections was conducted using a FV 1000 SPD laser-scanning confocal microscope (Olympus, Japan). The software Image-Pro Plus 5.0 was used to analyze the obtained images. The area and IOD of each image were obtained by analyzing the images, and the mean intensity can be calculated by IOD/area. The analysis of no less than three fields per section was carried out.

Assessment of Intracellular ROS Levels

The measurement of reactive oxygen species (ROS) production in VSMC was conducted by 2′,7′-dichlorodihydro-fluorescein diacetate (DCFH-DA; Biotime), Amplex Red (Molecular Probes, Invitrogen), and dihydroethidium (DHE; Biotime) according to the instructions of manufacturers.

Western Blot Analysis

After separation by 8–10% sodium dodecyl sulfate (SDS)-polyacrylamide gel electrophoresis, proteins were moved to polyvinylidene difluoride membranes (0.22 and 0.45 μm, Millipore, Billerica, Massachusetts (MA), the United States). Overnight incubation was performed using antibodies against phospho-AMPK (Thr172), AMPK, collagens I and III (Proteintech Group, Chicago, IL, the United States), phospho-Smad2 and Smad3, NOX1, NOX4 (Abcam, Cambridge, the United Kingdom), Smad2/3 (Millipore, Billerica, MA, the United States), glyceraldehyde-3-phosphate dehydrogenase (GAPDH) and β-actin (Beijing Zhong Shan-Golden Bridge Biological Technology Co., Ltd. China), matrix metalloprotein (MMP-9), and transforming growth factor-β1 (TGFβ1). The secondary antibody conjugated to horseradish peroxidase (Beijing Zhong Shan-Golden Bridge Biological Technology Co., Ltd. China) was used for the 1.5 h incubation of the membranes washed with Western washing buffer (TBS-T) at ambient temperature. The ECL kit (Millipore, Billerica, MA, the United States) was used to visualize immunoreactive bands, and the ChemiDoc™ Touch Imaging System (Bio-Rad Laboratories, Hercules, California, the United States) was utilized to obtain pictures.

Real-Time Quantitative Reverse-Transcriptase PCR (RT-qPCR)

A ribonucleic acid (RNA) extraction kit (Qiagen) was employed to prepare total cellular RNA. The following primers were used to perform real-time reverse-transcriptase quantitative polymerase chain reaction (RT-qPCR). For the analysis of vascular NOX1 messenger RNA (mRNA), the primer sequences are as follows: forward and reverse: 5′GCTCCA GACCTCCATTTGACA3′ and 5′AAGGCCAAGGCAGTT CCGAG3′, respectively. For the analysis of vascular NOX2 mRNA, the primer sequences are as follows: forward and reverse: 5′CACTTCACACGGCCATTCAC3′ and 5′ACC GAGTCACAGCCACATAC3′, respectively. For the analysis of vascular NOX4 mRNA, the primer sequences are as follows: forward and reverse: 5′ATGTGGGCCTAGGATTGT GT3′ and 5′CCTGCTAGGGACCTTCTGTG3′, respectively. For the analysis of GAPDH mRNA the primer sequences are as follows: forward and reverse: 5′GCTGTGATCCTGAGC TCCGAGAC3′ and 5′CATGTGGGCCAGGTCCACCAC3′, respectively. For the analysis of VSMC NOX1 mRNA, the primer sequences are as follows: forward and reverse: 5′GGT TGGGGCTGAACATTTTTC3′ and 5′TCGACACACAGG AATCAGGAT3′, respectively. For the analysis of VSMC NOX4 mRNA, the primer sequences are as follows: forward

TABLE 1 | Characteristics of the mice at the end of experiment.

	Control	Rb1	DM	DM + Rb1 (10 mg/kg)	DM + Rb1 (20 mg/kg)	DM + Rb1 (40 mg/kg)	DM + Rb1 (60 mg/kg)
HR (bpm)	626.143 ± 17.856	618.6 ± 11.717	610.6 ± 29.828	647.421 ± 16.831	591.529 ± 20.268	613.5 ± 18.853	612.632 ± 7.626
BW (g)	30.2 ± 0.961	29.575 ± 0.630	23.75 ± 1.386*	25.675 ± 0.669*	25.462 ± 0.662*	24.628 ± 0.434*	25.65 ± 0.715*
SBP (mmHg)	106.6 ± 5.653	102.3333 ± 6.386	102.25 ± 3.240	100.8 ± 7.276	106.25 ± 3.966	113.857 ± 4.295#	105.889 ± 1.867
DBP (mmHg)	78 ± 4.868	79.333 ± 9.333	60.438 ± 2.871*	66.4 ± 3.027	77 ± 4.916#	85.5 ± 2.754#	80.778 ± 3.833#
PP (mmHg)	20.75 ± 2.955	23 ± 4.359	41.813 ± 4.078*	34.4 ± 5.609	29.25 ± 7.825	25.429 ± 3.741#	25.111 ± 2.816#
PP/MBP	0.3325 ± 0.1021	0.2751 ± 0.0668	0.4826 ± 0.0249*	0.4367 ± 0.0563	0.3439 ± 0.0992	0.2752 ± 0.0432#	0.3148 ± 0.0389#
GLU (mmol/L)	8.488 ± 0.910	8.486 ± 1.063	25.263 ± 2.045*	24.362 ± 2.018*	22.233 ± 1.810*	23.222 ± 2.960*	21.500 ± 1.877*

Data are mean ± SEM, n = 5–8 per group. HR, heart rate; BW, body weight; SBP, systolic blood pressure; DBP, diastolic blood pressure; PP, pulse pressure; MBP, mean blood pressure; GLU glucose. p < 0.05 vs. Control; # p < 0.05 DM + +Rb1 vs. DM*

and reverse: 5′GAAGGGGTTAAACACCTCTGC3′ and 5′ATGCTCTGCTTAAACACAATCCT3′, respectively. Synergy brands (SYBR) green was used as fluorescence dye to carry out reactions on a real-time PCR system (LightCycler 96, Roche). Experiments were conducted twice. The $2^{-\triangle\triangle CT}$ method was adopted in relative expression analysis.

Statistical Analysis

Data were reported to be the mean ± standard error mean (SEM). First, the homogeneity of variance and Kolmogorov–Smirnov tests were performed. Then, the one-way analysis of variance (ANOVA) was conducted to analyze multiple groups, and *post hoc* individual comparisons were made. Finally, the least significant difference (LSD) test was performed to compare the means of every group and other columns in the case of homogeneous variance, and *p*-value was obtained by performing Dunnett's T3 test in the case of inhomogeneous variance. Differences were considered statistically significant at $p < 0.05$. Statistical Product and Service Solutions (SPSS) v20.0 (SPSS Inc., Chicago, IL, the United States) was used in all statistical analyses.

RESULTS

Characteristics of the Mice at the End of Experiments

At baseline, these groups showed no difference in BP, blood glucose, and body weight. In order to evaluate the relationship between Rb1 and body weight, parameters of mice, including blood glucose and BP, were measured after an 8-week Rb1 treatment. As shown in **Table 1**, the DM group had lower DBP and higher PP and PP/MBP compared with the CON one but saw a drop after Rb1 treatment (40 and 60 mg/kg). Body weight showed no significant differences after Rb1 treatment (**Table 1**). Glucose levels presented a decreasing trend in the high-dose group compared with those in the DM one, whereas both groups were not statistically different ($p = 0.537$).

Recovery of Endothelial Function and Aortic Compliance Following Rb1 Treatment

In the present study, we examined endothelial functions and aortic compliance. In the DM group, endothelium-dependent vasodilatory responses to acetylcholine were decreased compared with those in the CON group (E_{max} = 56.0 ± 8.8% vs. E_{max} = 83.3 ± 4.7%), indicating that DM has induced endothelial dysfunction. These defects were improved by Rb1 treatment (E_{max} = 74.1 ± 8.1%) (**Figure 1B**).

Reflecting worse aortic compliance, the increase of Ep and arterial stiffness index in DM mice (**Figures 1C,D**) was reverted after treatment with Rb1 as well. In contrast, Rb1-treated mice showed an increase in CSD, CSC, DC, and CC compared with DM ones (**Figures 1E–H**). It was observed that Rb1 had a maximum effect at 40 mg/kg, which was thus chosen for further research.

Rb1 Alleviated DM-Induced Aortic Remodeling

Collagen fibers were stained bright red, shown by Sirius red staining. Evaluated by collagen fiber area and PVCA/LA ratio, adventitial collagen accumulation showed an enhancement in DM mice relative to CON ones and was prevented by Rb1 treatment (**Figures 2A,B**). Additionally, diabetic mice exhibited higher values of PVCA/LA compared with CON ones, whereas enhanced values were reversed after treatment with Rb1 (**Figure 2A**). Elastic fibers were black shown by VVG staining, which suggested that focal irregularities and insufficient normal wavy contraction in the arrangement of elastic fibers in DM mice were not found in CON ones. Rb1 treatment contributed to improvement in the elastic lamina, with fewer inordinate patterns in the CON group than in the DM one (**Figure 2B**). Fibronectin in the adventitia was observed in all groups, whose accumulation was higher in the adventitia of the DM group than that of the CON one but regressed by Rb1 (**Figure 2C**). Moreover, the immunohistochemical detection of collagens I and III demonstrated that the aorta of the DM group had stronger immunostaining than that of the CON one (**Figures 2D,E**). Similarly, the protein expressions of collagens I and III

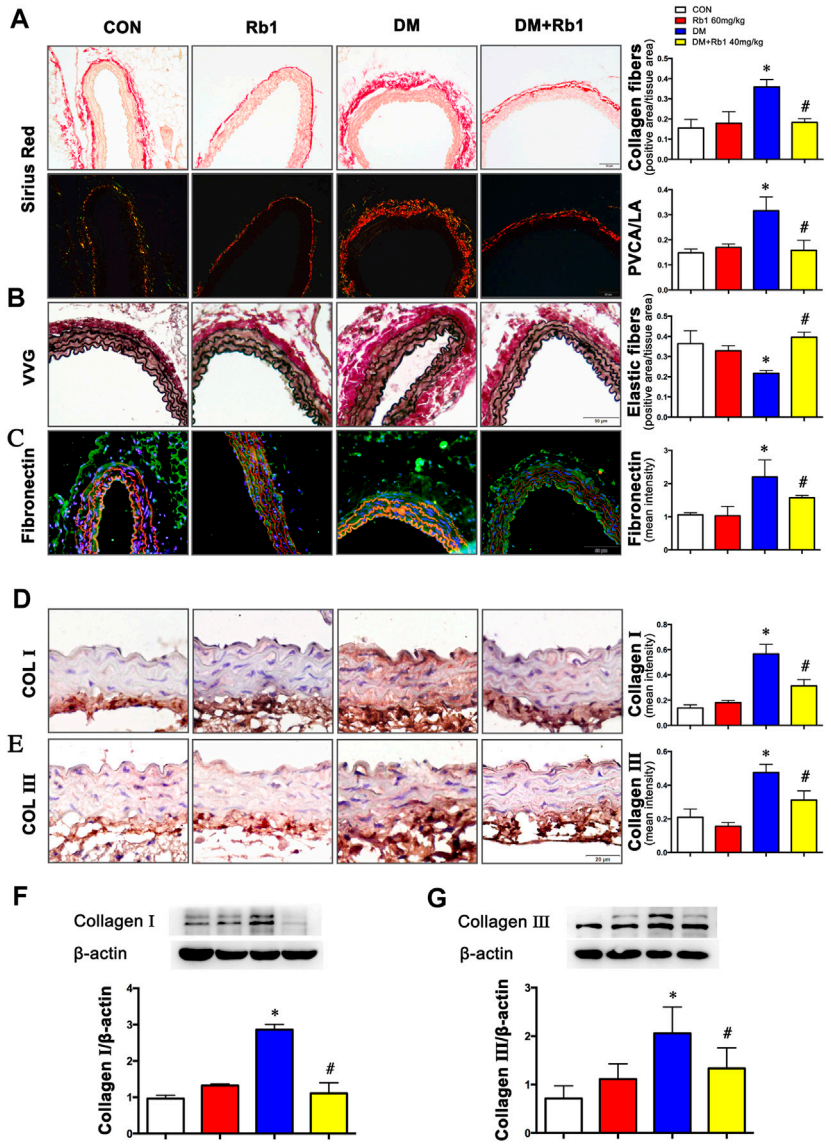

FIGURE 2 | Rb1 reduces DM-induced aortic remodeling **(A)** Sirius red staining (bright field and dark field) (scale bar 50 μm). Collagen fibers were stained bright red. Semiquantitative analysis of collagen fibers. Perivascular collagen content, shown as the perivascular collagen area/luminal area (PVCA/LA) ratio. **(B)** Elastic fibers shown by Verhoeff-Van Gieson staining (scale bar 50 μm). Elastic fibers are black, VSMCs are light red, and collagen fibers are pink. Semiquantitative analysis of elastic fibers. **(C)** Fibronectin accumulation (green: fibronectin, red: elastic lamina, blue: nuclei, scale bar 50 μm). Semiquantitative analysis of fibronectin expression. Representative immunohistochemical staining **(D)**, Western blot bands **(F)**, and semiquantitative analysis of collagen I expression (scale bar 20 μm). Representative immunohistochemical staining **(E)**, Western blot bands **(G)**, and semiquantitative analysis of collagen III expression (scale bar 20 μm). Data are mean ± SEM. n = 5–6, $^{*}p < 0.05$ vs. Control; $\#p < 0.05$ DM + Rb1 vs. DM.

exhibited higher levels in DM mice than in CON ones (**Figures 2F,G**). The accumulation of collagens I and III in diabetes was regressed after treatment with Rb1 (**Figures 2D–G**).

AMPK Involved in the Effects of Rb1 on Collagen Accumulation and TGFβ1-Smad2/3 Signaling Pathway

Aorta extracts from DM mice saw a decrease in AMPK phosphorylation and an increase in TGF β1 and phospho-Smad2/3 expressions compared with those from control ones (**Figures 3A–D**). After an 8-week Rb1 treatment, the inhibition of AMPK phosphorylation was reduced in Rb1-treated DM mice compared with the DM ones (**Figure 3A**). Meanwhile, TGFβ1 and phospho-Smad2/3 were suppressed in expression level (**Figures 3B–D**).

To clarify the potential role of Rb1 treatment in this signaling pathway *in vitro*, VSMCs were pretreated with the concentration gradient of Rb1 (from 10 to 60 μM) 2 h before high-glucose (30 mM) (HG) stimulation and were

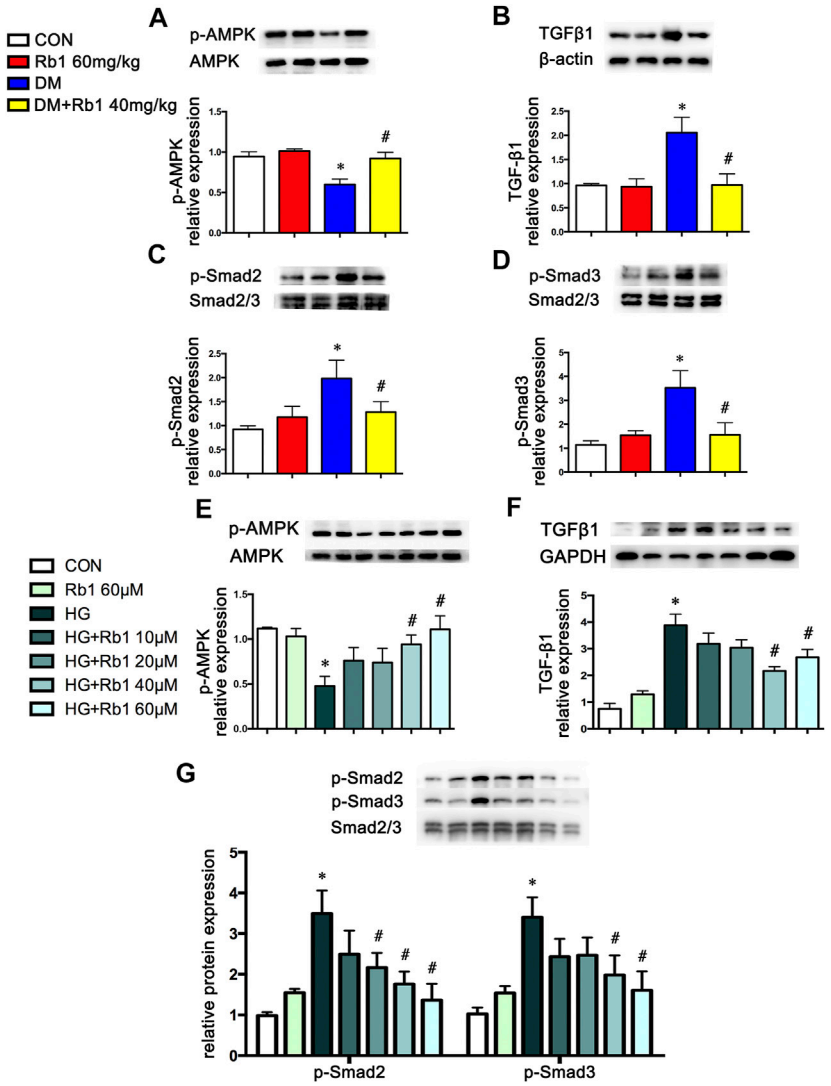

FIGURE 3 | AMPK pathway is involved in the effect of Rb1 on DM- and HG-mediated TGFβ1, Smad2/3, and collagen expression. Representative Western blot bands and semiquantitative analysis of **(A)** phosphorylated AMPK (p-AMPK), **(B)** TGFβ1, **(C)** phosphorylated Smad2 (p-Smad2), and **(D)** phosphorylated Smad3 (p-Smad3) in aorta extracts. **(E–G)** VSMCs were treated with Rb1 at doses of 10, 20, 40, and 60 μM in a high-glucose medium. Representative Western blot bands and semiquantitative analysis of phosphorylated AMPK (p-AMPK), TGFβ1, phosphorylated Smad2 (p-Smad2), and phosphorylated Smad3 (p-Smad3). Semiquantitative analysis of above proteins expressions. Data are mean ± SEM. n = 5–6, *$p < 0.05$ vs. Control; #$p < 0.05$ DM + Rb1 vs. DM and HG + Rb1 vs. HG.

cultured for an additional 48 h. We detected the levels of phospho-AMPK, TGFβ1, and phospho-Smad2/3 and selected 40 μM as the Rb1 treatment concentration (**Figures 3E–G**). Then, VSMCs were stimulated with Rb1 (40 μM) 2 h before high-glucose (30 mM) (HG) stimulation and were cultured for an additional 48 h. For the HG + Rb1+compound C group, VSMCs were pretreated with compound C for 2 h before the Rb1 treatment. The results exhibited that Rb1-mediated increase of phospho-AMPK, reduction of TGFβ1 and phospho-Smad2/3 in DM mice, and inhibition of collagenIand collagenIII accumulation were partly abolished by treatment with compound C, an inhibitor of AMPK (**Figures 4A–F**).

Rb1 Reduced the Collagen Deposition, MMP-2, and MMP-9 Expression in VSMC

In addition to the TGFβ1-phospho-Smad2/3 pathway involved in vascular remodeling, we also detected MMPs expression and activity in diabetes and HG-treated VSMC. The results showed that the levels of MMP-2 and MMP-9 were increased (**Figures 5A,B**). However, the above alterations were partly reversed by Rb1. Meanwhile, Rb1 treatment (40 μM) inhibited the protein expression of MMP-2 and MMP-9 compared with high glucose (HG) without Rb1 treatment (**Figures 5C,D**). These effects were eliminated by treatment with compound C, an inhibitor of AMPK. Thus, Rb1 suppressed HG-induced collagen deposition and MMPs expression *via* the AMPK pathway.

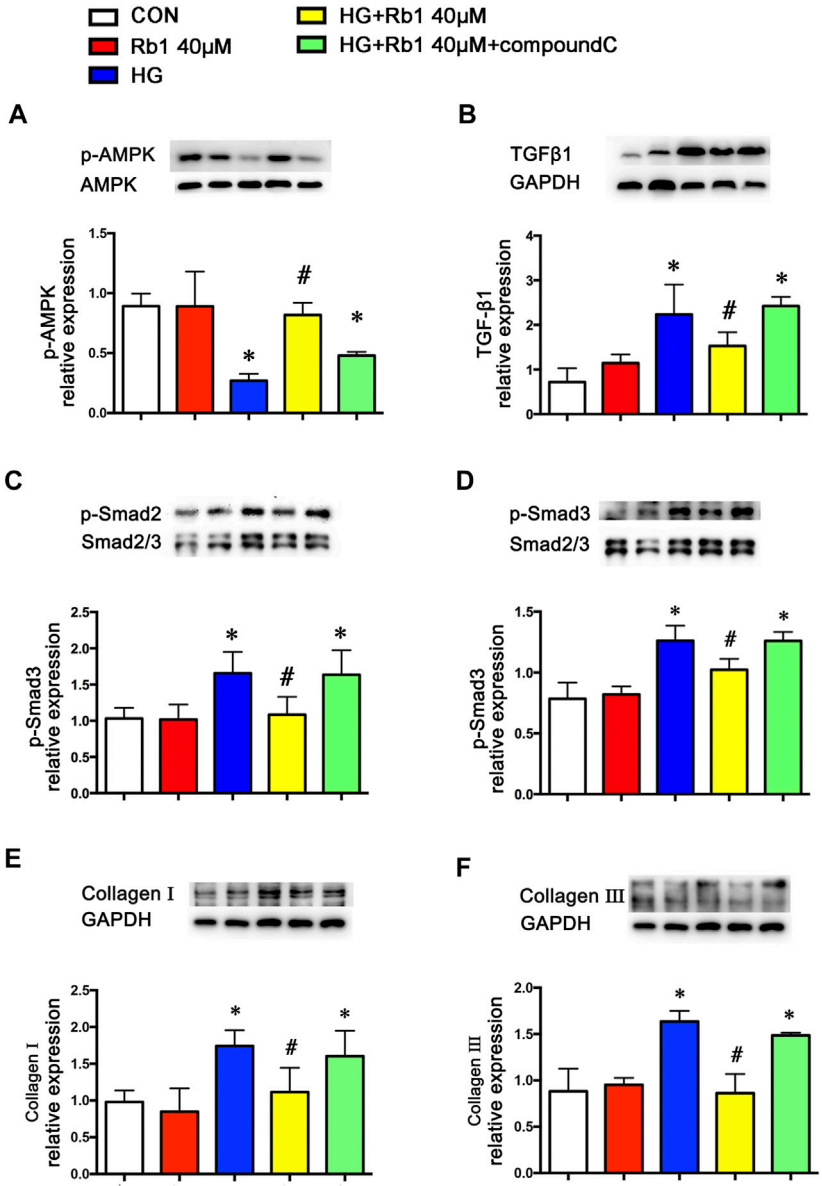

FIGURE 4 | Rb1-mediated reduction of TGFβ1 and phospho-Smad2/3 and collagen accumulation are partly abolished by treatment with compound C, an inhibitor of AMPK. VSMCs were treated with Rb1 at doses of 40 μM in a high-glucose medium and pretreated with compound C. Representative Western blot bands and semiquantitative analysis of **(A)** phosphorylated AMPK (p-AMPK), **(B)** TGFβ1, and **(C)** phosphorylated Smad2 (p-Smad2). **(D)** Phosphorylated Smad3 (p-Smad3). **(E)** Collagen I and **(F)** collagen III. Data are mean ± SEM. n = 5–6, $^{*}p < 0.05$ vs. Control; $\#p < 0.05$ HG + Rb1 vs. HG.

Rb1 Improved DM-Induced Oxidative Stress

To gain further insights into the potential protective mechanism of Rb1 in aortic remodeling, we assessed oxidative stress using 3-NT staining, an oxidative stress-induced lipid peroxidation marker. It was demonstrated that 3-NT staining was more evident in diabetic mice than in controls (**Figure 6A**). Staining was most intense in the endothelium, which is less in the adventitia and relatively minimal in the medial layer. Rb1 treatment prevented 3-NT accumulation in the endothelium and adventitia markedly. To further confirm whether Rb1 could decrease the production of ROS *in vitro*. ROS was assessed by three different methods, DCFH-DA, Amplex Red, and DHE in VSMCs (**Figures 6B–F**). Cells pretreated with Rb1 or compound C were exposed to high glucose (HG) for 48 h. Rb1 attenuated the HG-induced ROS level in cells. The protective effect of Rb1 was eliminated by treatment with compound C (**Figures 6B–F**), indicating that the inhibitory effect of Rb1 on ROS was AMPK-dependent.

NOX Isoforms Involved in Effects of Rb1 on DM-Induced Oxidative Stress

To clarify the potential effect of Rb1 treatment on the inhibition of oxidative stress, the mRNA levels of NOX1,

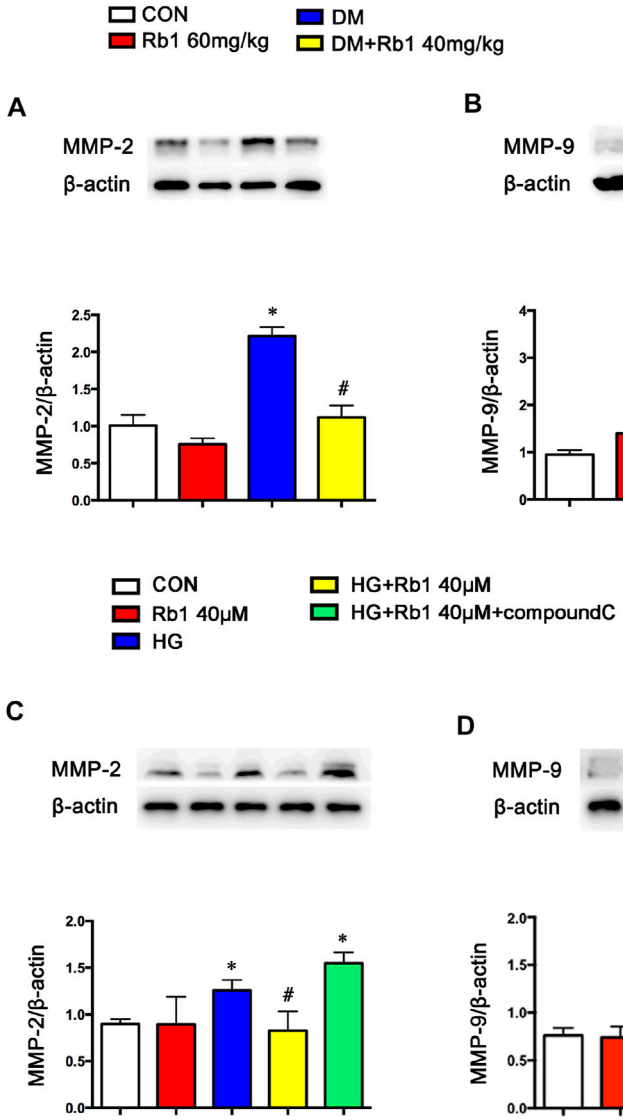

FIGURE 5 | Rb1 suppresses MMP-2 and MMP-9 expression. Representative Western blot bands and semiquantitative analysis of **(A)** MMP-2 and **(B)** MMP-9 protein expression in aorta. Representative Western blot bands and semiquantitative analysis of **(C)** MMP-2 and **(D)** MMP-9 protein expression in VSMCs. Data are mean ± SEM. n = 5–6, *$p < 0.05$ vs. Control; #$p < 0.05$ DM + Rb1 vs. DM and HG + Rb1 vs. HG.

NOX2, NOX4, and other NOX isoforms in aorta extracts were detected, indicating the inhibiting effect of Rb1 treatment on the mRNA expression levels of NOX1 and NOX4, which exhibited a rise in DM mice (**Figures 7A–C**). However, the DM group was not significantly different from the DM + Rb1 one in NOX2 (**Figure 7B**). Furthermore, the mRNA levels of NOX1, NOX2, and NOX4 in VSMCs were detected. The results showed that Rb1 had the same effect as aorta extracts (**Figures 7D–F**), and the changes of NOX1, NOX2, and NOX4 were confirmed in protein expression level (**Figures 7G–I**). In addition, these effects on the inhibition of NOX1 and NOX4 were partly eliminated by treatment with compound C, an inhibitor of AMPK.

DISCUSSION

In the present study, we found that Rb1 could alleviate arterial stiffness by reducing aortic remodeling. The beneficial effects of Rb1 on vascular stiffness were achieved by suppressing oxidative stress and inhibiting the expression of collagenI, collagen III, MMPs, and TGFβ1/Smad2/3, which were, at least partially, AMPK-dependent.

Rb1 is a major active component of *Panax ginseng*, whose protective action against a few CVDs (Bai et al., 2018; Zhou et al., 2019), including abdominal aortic aneurysm (Zhang et al., 2015), hypertension-induced carotid arterial remodeling (Lin et al., 2015), myocardial ischemia/reperfusion injury (Wu et al.,

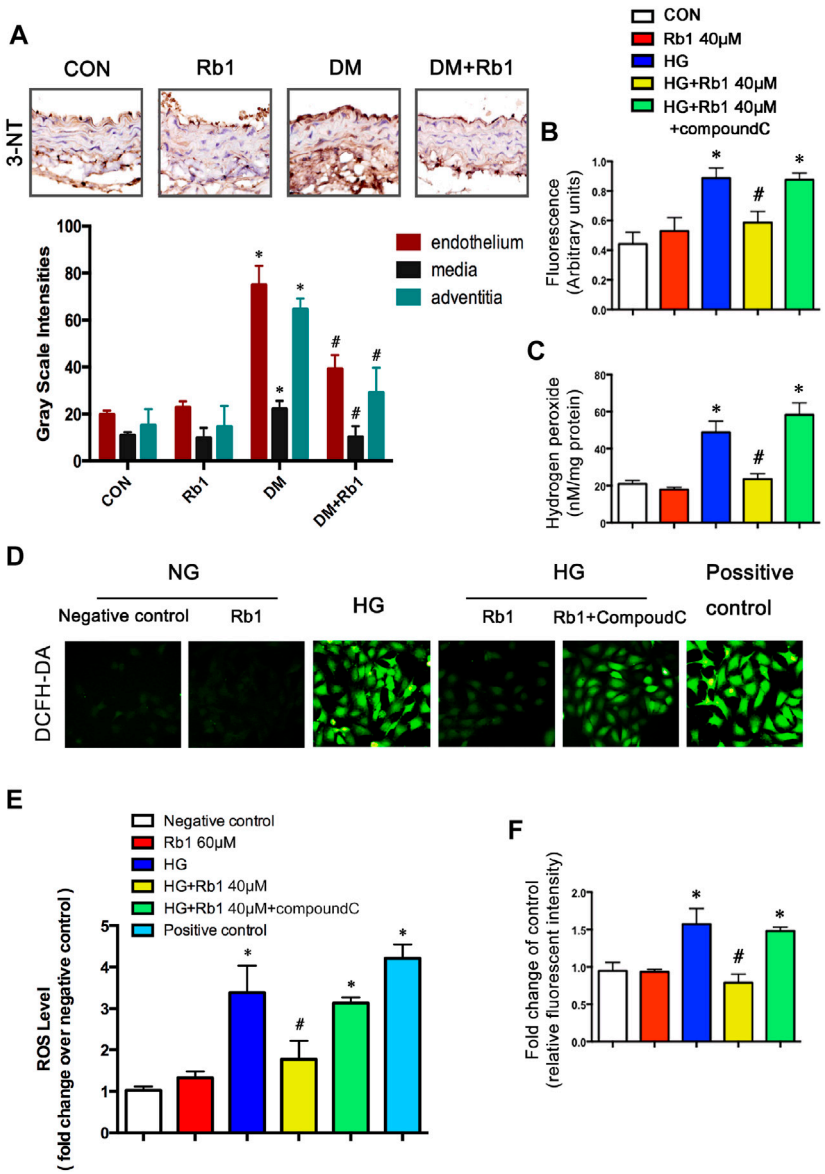

FIGURE 6 | Rb1 improves DM and HG-induced oxidative stress. **(A)** Immunohistochemical staining and semiquantitative analysis of 3-nitrotyrosine (3-NT). ROS was assessed by three different methods: **(B)** DCFH-DA, **(C)** Amplex Red, and **(F)** DHE in VSMCs **(D)** ROS levels. in each group. Original magnification × 200. **(E)** Semiquantitative analysis of ROS levels in each group. The positive control is the active oxygen donor from the DCFH-DA kit, which contains H_2O_2. Data are mean ± SEM. n = 5–6, *p < 0.05 vs. Control; #p < 0.05 DM + Rb1 vs. DM and HG + Rb1 vs. HG.

2011; Xia et al., 2011), and hypertrophy (Kanda et al., 2005; Jiang et al., 2007), has been recently proved by *in vivo* and *in vitro* studies. Previous research discovered that Rb1 led to a decline in the accumulation of lipid and the area of atherosclerotic plaques through the skew of macrophages to the M2 phenotype and the improvement of lipid metabolism and autophagy in macrophage foam cells (Qiao et al., 2017; Zhang et al., 2018). Nevertheless, the effect of Rb1 on vascular diseases under hyperglycemia is unclear, whose contributing molecular mechanisms remain to be elucidated. This study found that treatment with Rb1 could alleviate DM-induced arterial stiffness.

As a key pathway linking diabetes to CVDs, arterial stiffness can decrease diastolic pressure and increase PP. Philips, J C et al. have demonstrated that PP increased and concomitantly decreased in DBP according to T1DM duration, in agreement with accelerated arterial stiffening due to chronic hyperglycemia. They have confirmed the validity of using the index PP/MBP previously proposed as a surrogate marker of arterial stiffness (Philips et al., 2009). It is a complex phenomenon that arises from the qualitative and quantitative variations in arterial wall components, giving rise to the redistribution of mechanical loads towards elastic materials, endothelial dysfunction,

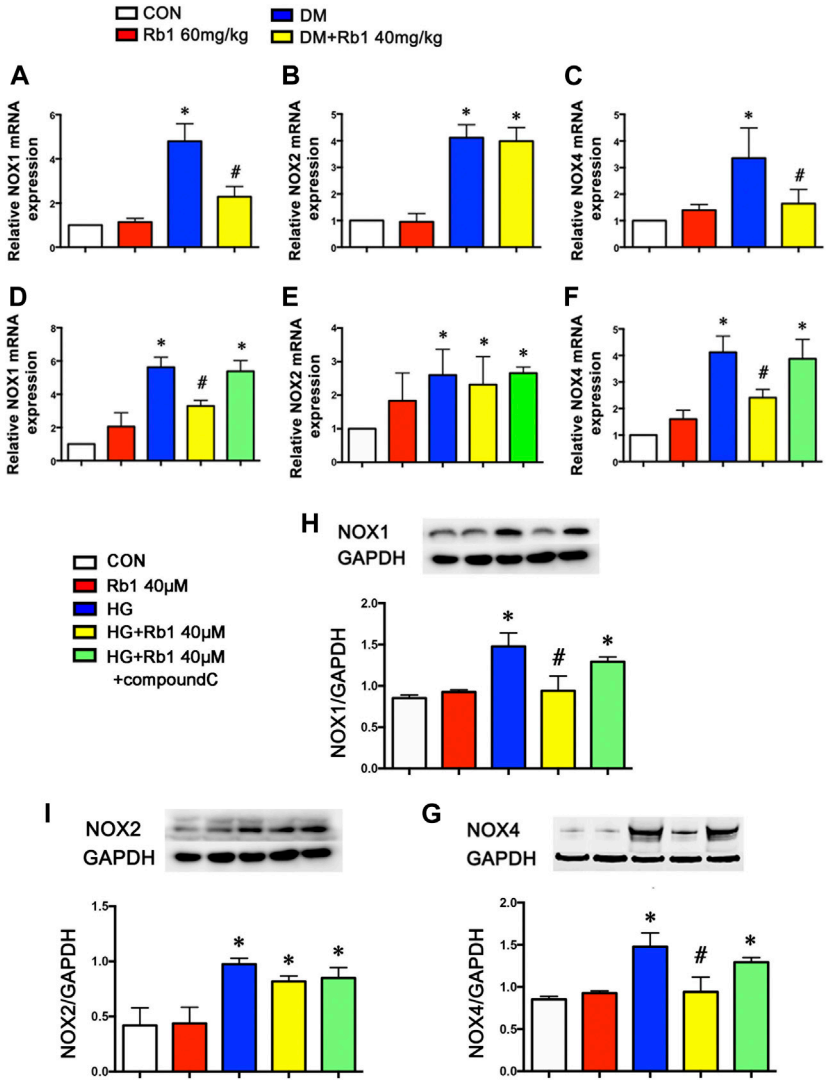

FIGURE 7 | NOX isoforms involved in the effects of Rb1 on DM-induced oxidative stress. Quantitative analysis of **(A)** NOX1 **(B)** NOX2 and **(C)** NOX4 mRNA expression in the aorta. Quantitative analysis of **(D)** NOX1 **(E)** NOX2 and **(F)** NOX4 mRNA expression in VSMCs. Representative Western blot bands and semiquantitative analysis of **(H)** NOX1 **(I)** NOX2 and **(G)** NOX4 protein expression in VSMCs. Data are mean ± SEM. n = 5–6, **p* < 0.05 vs. Control; #*p* < 0.05 DM + Rb1 vs. DM and HG + Rb1 vs. HG.

increased smooth muscle tone, the phenotypic modulation of adventitial fibroblasts to myofibroblasts, and chronic inflammation (Zhou et al., 2012). Research has shown that Rb1 treatment could decrease PP and PP/MBP, restore DBP, endothelial function, and aortic compliance, and suppress aortic remodeling. Endothelial-independent relaxation (e.g., SNP-induced relaxation) should be analyzed to confirm the possible effects of Rb1 on smooth muscle cells in further study. Rb1 treatment failed to decrease glucose levels. Based on previous studies, no consensus reports evaluated the effect of Rb1 on serum glucose. In this study, glucose levels showed a decreasing trend in the high-dose group compared with those in the DM one, whereas both groups were not statistically different (p = 0.537). Rb1 protected arteries from stiffening, which was independent of decreased glucose levels.

Previous studies have supported the notion that AMPK was an important therapeutic target of diabetes (Lin et al., 2016; Luo et al., 2016), including DM-induced macrovascular complications (Gu et al., 2014; Nagata et al., 2004). AMPK played a key role in protecting vascular dysfunction from hyperglycemia involving reversing oxidant damage (Sambuceti et al., 2009), reducing inflammation (Ha et al., 2014), and attenuating endothelial dysfunction (Tang et al., 2016). Of interest, multiple molecular mechanisms of Rb1 treatment have been proposed, including reduction of oxidative stress, apoptosis, and protein synthesis, *via* AMPK-dependent pathway and some other pathways (Cho et al., 2004; Zhao et al., 2010; Xia et al., 2011; Shen et al., 2013; Zhang et al., 2015). In our study, we found that Rb1 could reduce the suppression of AMPK caused by hyperglycemia. Diabetes is accompanied by oxidative stress characterized by elevated ROS

levels in the cardiovascular system (Jay et al., 2006). We found oxidative stress in aortic sections from diabetic mice and abundant ROS production in VSMCs, consistent with other reports (San Martín et al., 2007).

The anti-oxidative stress mechanisms of Rb1 may involve both direct ROS scavenging (Lü et al., 2012) and indirect signaling effects. Recent studies have demonstrated that activating AMPK contributed to reversing oxidant damage (Sambuceti et al., 2009) partly by reducing ROS generation and increasing nitric oxide (NO) production (An et al., 2016). The NADPH oxidases protein family was a major source of ROS in vascular cells (Brown and Griendling, 2009; Lassègue and Griendling, 2010; Amanso and Griendling, 2012). Our findings have supported that Rb1 treatment inhibited DM-induced overexpression of NOX1 and NOX4, but not NOX2. These benefits in suppressing NADPH oxidase and ROS production were partly eliminated by treatment with compound C, an inhibitor of AMPK. It seemed that Rb1 treatment took part in inhibiting ROS production, at least partially, via the AMPK pathway. As for why Rb1 did not suppress NOX2, the relative study needs to be performed in the future.

Previous studies have demonstrated that the activation of matrix metalloproteinase (MMP)-2/9 was strongly correlated with the disorganization, stiffness, and calcification of elastic fibers and the dysfunction of vasomotion in the arterial vasculature (Longo et al., 2002; Yasmin et al., 2005; Chung et al., 2009). The lack of elastin fibers or collagen deposition in the arterial wall resulted in aortic remodeling and increased stiffness (Sangartit et al., 2014; Herrmann et al., 2015; Li et al., 2015). It was found that DM mice exhibited increased 3-nitrotyrosine (NT) staining, MMP2/9 expressions and perivascular fibrosis/lumen area, disorganized elastic, and collagen fibers. Besides, the increased expressions of collagens I and III indicated an increase in the deposition of collagen in the DM group. Concomitant Rb1 treatment prevented the above-mentioned changes and retained the normal morphology of aortic specimens, which confirmed the anti-arterial stiffness effect of Rb1.

Another important factor regulating collagen production in aortic remodeling is the TGFβ1/Smad2/3 pathway, which is closely related to oxidative stress. The data of this study supported that TGF signaling got involved in the production of HG-induced collagens and the accumulation of extracellular matrices, which are in line with previous reports (Kubota et al., 2003; Ha et al., 2016). Cytoplasmic signals are transmitted into the intracellular domain by TGF-β via its type I and II receptors. After direct phosphorylation by the TGF-β receptor I kinase, Smad2 and Smad3 regulate target gene expression by shuttling from the cytoplasm into the nucleus (Shi and Massagué, 2003). It was interesting to notice that Rb1 was shown to eliminate the HG-induced overexpressions of TGFβ1 and phospho-Smad2/3 *in vitro*, which suggested that the inhibitory effect of Rb1 on the production of HG-mediated collagens may also be involved in TGFβ1. Furthermore, this effect of Rb1 on collagen production could be reversed by compound C, indicating that the effect of Rb1 on the TGFβ1/Smad2/3 pathway was AMPK-dependent.

The findings supported that Rb1 had therapeutic potential in preventing cardiovascular complications in patients with diabetes mellitus, which was independent of decreased glucose levels. Rb1 can reverse the inhibition of AMPK, which, however, may not explain all of its therapeutic effects. Notably, Rb1 was reported to have pleiotropic cardiovascular protection effects on multiple molecular targets independently, mainly including AMPK, PI3K/Akt, NF-κB, and mitogen-activated protein kinase (MAPK) pathways and endoplasmic reticulum stress. AMPK participates in the cardiovascular protection effect of Rb1 against reperfusion injury/myocardial ischemia, coronary atherosclerotic, heart failure, cardiac hypertrophy, and fibrosis by mediating apoptosis (Kong et al., 2010), autophagy (Qiao et al., 2017; Dai et al., 2019), mitochondrial fission (Li et al., 2016), fatty acid β-oxidation (Kong et al., 2018), and aging (Zheng et al., 2020). In the meantime, the changes in Akt signaling are of importance in atherosclerosis, cardiac hypertrophy, vascular remodeling, and many other cardiovascular pathological processes. Rb1 has a cardioprotective effect partly by mediating PI3K pathway activation and Akt phosphorylation and regulating inflammatory response (Yang et al., 2019), oxidative stress (Chen et al., 2019), apoptosis (Nanao-Hamai et al., 2019), autophagy (Yang et al., 2018), and mitochondrial function (Zheng et al., 2017). It was demonstrated that Akt and AMPK pathways in the cardiovascular protection effect of Rb1 were cross and independent of each other. Further studies are necessary to elucidate its integration with other signaling pathways that are predicted to account for this effect.

CONCLUSION

Ginsenoside Rb1 ameliorates DM-related vascular remodeling, at least partially, *via* reducing the inhibition of AMPK caused by hyperglycemia. This effect is obtained by alleviating oxidative stress and suppressing TGFβ1/Smad2/3 pathway, leading to regulating collagen production and degradation. Our findings have shown the effect and possible mechanism of Rb1 in treatment for diabetic macroangiopathy and diabetes-related complications prevention.

DATA AVAILABILITY STATEMENT

The raw data supporting the conclusions of this article will be made available by the authors, without undue reservation.

ETHICS STATEMENT

The animal study was reviewed and approved by the Animal Care Committee of Shandong University.

AUTHOR CONTRIBUTIONS

XJ, HL, and XZ contributed to the study concept and design. XZ and HL wrote the paper. XZ, RG, MD, and XL performed *in vitro* work. XZ, LW, JX, and XL performed *in vivo* mice model studies. All authors revised the article and approved the final version to be published.

FUNDING

This work was supported by the National Natural Science Foundation of China (81900444, 81873516, 81873522, 81270403, 81173427), the National Key Research and Development Program of China (2017YFC1308303), the Clinical Research Center of Shandong University (2020SDUCRCA009) the Author of National Excellent Doctoral Dissertation of PR China (201181), the Program for Hong Kong Scholars (201104629), China Postdoctoral Science Foundation (2012M521353, 2014M551914), and the Natural Science Foundation of Shandong Province (ZR2019PH030, 2014ZRE27067, ZR2014CM010). The funders had no role in the study design, data collection and analysis, decision to publish, or preparation of the manuscript.

ACKNOWLEDGMENTS

The authors thank Ricky Ngok-Shun Wong (Chair Professor, Department of Biology, Faculty of Science, Hong Kong Baptist University, Hong Kong SAR, Hong Kong, China) for his guidance in shaping this research.

REFERENCES

Amanso, A. M., and Griendling, K. K. (2012). Differential Roles of NADPH Oxidases in Vascular Physiology and Pathophysiology. *Front. Biosci. (Schol Ed.* 4, 1044–1064. doi:10.2741/s317

An, H., Wei, R., Ke, J., Yang, J., Liu, Y., Wang, X., et al. (2016). Metformin Attenuates Fluctuating Glucose-Induced Endothelial Dysfunction through Enhancing GTPCH1-Mediated eNOS Recoupling and Inhibiting NADPH Oxidase. *J. Diabetes Complications* 30, 1017–1024. doi:10.1016/j.jdiacomp.2016.04.018

Bai, L., Gao, J., Wei, F., Zhao, J., Wang, D., and Wei, J. (2018). Therapeutic Potential of Ginsenosides as an Adjuvant Treatment for Diabetes. *Front. Pharmacol.* 9, 423. doi:10.3389/fphar.2018.00423

Ben-Shlomo, Y., Spears, M., Boustred, C., May, M., Anderson, S. G., Benjamin, E. J., et al. (2014). Aortic Pulse Wave Velocity Improves Cardiovascular Event Prediction: an Individual Participant Meta-Analysis of Prospective Observational Data from 17,635 Subjects. *J. Am. Coll. Cardiol.* 63, 636–646. doi:10.1016/j.jacc.2013.09.063

Brown, D. I., and Griendling, K. K. (2009). Nox Proteins in Signal Transduction. *Free Radic. Biol. Med.* 47, 1239–1253. doi:10.1016/j.freeradbiomed.2009.07.023

Chan, G. H., Law, B. Y., Chu, J. M., Yue, K. K., Jiang, Z. H., Lau, C. W., et al. (2013). Ginseng Extracts Restore High-Glucose Induced Vascular Dysfunctions by Altering Triglyceride Metabolism and Downregulation of Atherosclerosis-Related Genes. *Evid. Based Complement. Alternat Med.* 2013, 797310. doi:10.1155/2013/797310

Chen, S., Li, X., Wang, Y., Mu, P., Chen, C., Huang, P., et al. (2019). Ginsenoside Rb1 Attenuates Intestinal Ischemia/reperfusion-induced I-nflammation and O-xidative S-tress via A-ctivation of the PI3K/Akt/Nrf2 S-ignaling P-athway. *Mol. Med. Rep.* 19, 3633–3641. doi:10.3892/mmr.2019.10018

Cho, J., Park, W., Lee, S., Ahn, W., and Lee, Y. (2004). Ginsenoside-Rb1 from Panax Ginseng C.A. Meyer Activates Estrogen Receptor-Alpha and -beta, Independent of Ligand Binding. *J. Clin. Endocrinol. Metab.* 89, 3510–3515. doi:10.1210/jc.2003-031823

Chung, A. W., Yang, H. H., Kim, J. M., Sigrist, M. K., Chum, E., Gourlay, W. A., et al. (2009). Upregulation of Matrix Metalloproteinase-2 in the Arterial Vasculature Contributes to Stiffening and Vasomotor Dysfunction in Patients with Chronic Kidney Disease. *Circulation* 120, 792–801. doi:10.1161/CIRCULATIONAHA.109.862565

Dai, S. N., Hou, A. J., Zhao, S. M., Chen, X. M., Huang, H. T., Chen, B. H., et al. (2019). Ginsenoside Rb1 Ameliorates Autophagy of Hypoxia Cardiomyocytes from Neonatal Rats via AMP-Activated Protein Kinase Pathway. *Chin. J. Integr. Med.* 25, 521–528. doi:10.1007/s11655-018-3018-y

Delbin, M. A., and Trask, A. J. (2014). The Diabetic Vasculature: Physiological Mechanisms of Dysfunction and Influence of Aerobic Exercise Training in Animal Models. *Life Sci.* 102, 1–9. doi:10.1016/j.lfs.2014.02.021

Dietrich, T., Schaefer-Graf, U., Fleck, E., and Graf, K. (2010). Aortic Stiffness, Impaired Fasting Glucose, and Aging. *Hypertension* 55, 18–20. doi:10.1161/HYPERTENSIONAHA.109.135897

Gu, Q., Wang, B., Zhang, X. F., Ma, Y. P., Liu, J. D., and Wang, X. Z. (2014). Chronic Aerobic Exercise Training Attenuates Aortic Stiffening and Endothelial Dysfunction through Preserving Aortic Mitochondrial Function in Aged Rats. *Exp. Gerontol.* 56, 37–44. doi:10.1016/j.exger.2014.02.014

Ha, D. M., Carpenter, L. C., Koutakis, P., Swanson, S. A., Zhu, Z., Hanna, M., et al. (2016). Transforming Growth Factor-Beta 1 Produced by Vascular Smooth Muscle Cells Predicts Fibrosis in the Gastrocnemius of Patients with Peripheral Artery Disease. *J. Transl Med.* 14, 39. doi:10.1186/s12967-016-0790-3

Ha, Y. M., Park, E. J., Kang, Y. J., Park, S. W., Kim, H. J., and Chang, K. C. (2014). Valsartan Independent of AT_1 Receptor Inhibits Tissue Factor, TLR-2 and -4 Expression by Regulation of Egr-1 through Activation of AMPK in Diabetic Conditions. *J. Cel Mol Med* 18, 2031–2043. doi:10.1111/jcmm.12354

Herrmann, M., Sullivan, D. R., Veillard, A. S., McCorquodale, T., Straub, I. R., Scott, R., et al. (2015). Serum 25-hydroxyvitamin D: a Predictor of Macrovascular and Microvascular Complications in Patients with Type 2 Diabetes. *Diabetes Care* 38, 521–528. doi:10.2337/dc14-0180

Holman, R. R., Paul, S. K., Bethel, M. A., Matthews, D. R., and Neil, H. A. (2008). 10-year Follow-Up of Intensive Glucose Control in Type 2 Diabetes. *N. Engl. J. Med.* 359, 1577–1589. doi:10.1056/NEJMoa0806470

Jay, D., Hitomi, H., and Griendling, K. K. (2006). Oxidative Stress and Diabetic Cardiovascular Complications. *Free Radic. Biol. Med.* 40, 183–192. doi:10.1016/j.freeradbiomed.2005.06.018

Jiang, Q. S., Huang, X. N., Dai, Z. K., Yang, G. Z., Zhou, Q. X., Shi, J. S., et al. (2007). Inhibitory Effect of Ginsenoside Rb1 on Cardiac Hypertrophy Induced by Monocrotaline in Rat. *J. Ethnopharmacol* 111, 567–572. doi:10.1016/j.jep.2007.01.006

Kanda, T., Hayashi, K., Wakino, S., Homma, K., Yoshioka, K., Hasegawa, K., et al. (2005). Role of Rho-Kinase and P27 in Angiotensin II-Induced Vascular Injury. *Hypertension* 45, 724–729. doi:10.1161/01.HYP.0000153316.59262.79

Kong, H. L., Hou, A. J., Liu, N. N., Chen, B. H., Dai, S. N., and Huang, H. T. (2018). The Effects of Ginsenoside Rb1 on Fatty Acid β-oxidation, Mediated by AMPK, in the Failing Heart. *Iran J. Basic Med. Sci.* 21, 731–737. doi:10.22038/IJBMS.2018.24002.6016

Kong, H. L., Li, Z. Q., Zhao, Y. J., Zhao, S. M., Zhu, L., Li, T., et al. (2010). Ginsenoside Rb1 Protects Cardiomyocytes against CoCl2-Induced Apoptosis in Neonatal Rats by Inhibiting Mitochondria Permeability Transition Pore Opening. *Acta Pharmacol. Sin* 31, 687–695. doi:10.1038/aps.2010.52

Kubota, K., Okazaki, J., Louie, O., Kent, K. C., and Liu, B. (2003). TGF-beta Stimulates Collagen (I) in Vascular Smooth Muscle Cells via a Short Element in the Proximal Collagen Promoter. *J. Surg. Res.* 109, 43–50. doi:10.1016/s0022-4804(02)00037-9

Lassègue, B., and Griendling, K. K. (2010). NADPH Oxidases: Functions and Pathologies in the Vasculature. *Arterioscler Thromb. Vasc. Biol.* 30, 653–661. doi:10.1161/ATVBAHA.108.181610

Laurent, S., Alivon, M., Beaussier, H., and Boutouyrie, P. (2012). Aortic Stiffness as a Tissue Biomarker for Predicting Future Cardiovascular Events in Asymptomatic Hypertensive Subjects. *Ann. Med.* 44 Suppl 1 (Suppl. 1), S93–S97. doi:10.3109/07853890.2011.653398

Li, F., Fan, X., Zhang, Y., Pang, L., Ma, X., Song, M., et al. (2016). Cardioprotection by Combination of Three Compounds from ShengMai Preparations in Mice with Myocardial Ischemia/reperfusion Injury through AMPK Activation-Mediated Mitochondrial Fission. *Sci. Rep.* 6, 37114. doi:10.1038/srep37114

Li, Y., Han, L., Ding, W. Y., Ti, Y., Li, Y. H., Tang, M. X., et al. (2015). Prostaglandin F2α Receptor Silencing Attenuates Vascular Remodeling in Rats with Type 2 Diabetes. *Exp. Mol. Pathol.* 99, 517–523. doi:10.1016/j.yexmp.2015.09.011

Lin, X. H., Hong, H. S., Zou, G. R., and Chen, L. L. (2015). Upregulation of TRPC1/6 May Be Involved in Arterial Remodeling in Rat. *J. Surg. Res.* 195, 334–343. doi:10.1016/j.jss.2014.12.047

Lin, Y., Chen, J., and Sun, Z. (2016). Antiaging Gene Klotho Deficiency Promoted High-Fat Diet-Induced Arterial Stiffening via Inactivation of AMP-Activated Protein Kinase. *Hypertension* 67, 564–573. doi:10.1161/HYPERTENSIONAHA.115.06825

Longo, G. M., Xiong, W., Greiner, T. C., Zhao, Y., Fiotti, N., and Baxter, B. T. (2002). Matrix Metalloproteinases 2 and 9 Work in Concert to Produce Aortic Aneurysms. *J. Clin. Invest.* 110, 625–632. doi:10.1172/JCI15334

Lü, J. M., Weakley, S. M., Yang, Z., Hu, M., Yao, Q., and Chen, C. (2012). Ginsenoside Rb1 Directly Scavenges Hydroxyl Radical and Hypochlorous Acid. *Curr. Pharm. Des.* 18, 6339–6347. doi:10.2174/138161212803832254

Luo, T., Nocon, A., Fry, J., Sherban, A., Rui, X., Jiang, B., et al. (2016). AMPK Activation by Metformin Suppresses Abnormal Extracellular Matrix Remodeling in Adipose Tissue and Ameliorates Insulin Resistance in Obesity. *Diabetes* 65, 2295–2310. doi:10.2337/db15-1122

Mitchell, G. F., Guo, C. Y., Benjamin, E. J., Larson, M. G., Keyes, M. J., Vita, J. A., et al. (2007). Cross-sectional Correlates of Increased Aortic Stiffness in the Community: the Framingham Heart Study. *Circulation* 115, 2628–2636. doi:10.1161/CIRCULATIONAHA.106.667733

Nagata, D., Takeda, R., Sata, M., Satonaka, H., Suzuki, E., Nagano, T., et al. (2004). AMP-activated Protein Kinase Inhibits Angiotensin II-Stimulated Vascular Smooth Muscle Cell Proliferation. *Circulation* 110, 444–451. doi:10.1161/01.CIR.0000136025.96811.76

Nanao-Hamai, M., Son, B. K., Komuro, A., Asari, Y., Hashizume, T., Takayama, K. I., et al. (2019). Ginsenoside Rb1 Inhibits Vascular Calcification as a Selective Androgen Receptor Modulator. *Eur. J. Pharmacol.* 859, 172546. doi:10.1016/j.ejphar.2019.172546

Pannier, B. M., Avolio, A. P., Hoeks, A., Mancia, G., and Takazawa, K. (2002). Methods and Devices for Measuring Arterial Compliance in Humans. *Am. J. Hypertens.* 15, 743–753. doi:10.1016/s0895-7061(02)02962-x

Payne, R. A., Wilkinson, I. B., and Webb, D. J. (2010). Arterial Stiffness and Hypertension: Emerging Concepts. *Hypertension* 55, 9–14. doi:10.1161/HYPERTENSIONAHA.107.090464

Philips, J. C., Marchand, M., and Scheen, A. J. (2009). Pulse Pressure and Cardiovascular Autonomic Neuropathy According to Duration of Type 1 Diabetes. *Diabetes Metab. Res. Rev.* 25, 442–451. doi:10.1002/dmrr.969

Qiao, L., Zhang, X., Liu, M., Liu, X., Dong, M., Cheng, J., et al. (2017). Corrigendum: Ginsenoside Rb1 Enhances Atherosclerotic Plaque Stability by Improving Autophagy and Lipid Metabolism in Macrophage Foam Cells. *Front. Pharmacol.* 8, 964. doi:10.3389/fphar.2017.00964

Sambuceti, G., Morbelli, S., Vanella, L., Kusmic, C., Marini, C., Massollo, M., et al. (2009). Diabetes Impairs the Vascular Recruitment of normal Stem Cells by Oxidant Damage, Reversed by Increases in pAMPK, Heme Oxygenase-1, and Adiponectin. *Stem Cells* 27, 399–407. doi:10.1634/stemcells.2008-0800

San Martín, A., Du, P., Dikalova, A., Lassègue, B., Aleman, M., Góngora, M. C., et al. (2007). Reactive Oxygen Species-Selective Regulation of Aortic Inflammatory Gene Expression in Type 2 Diabetes. *Am. J. Physiol. Heart Circ. Physiol.* 292, H2073–H2082. doi:10.1152/ajpheart.00943.2006

Sangartit, W., Kukongviriyapan, U., Donpunha, W., Pakdeechote, P., Kukongviriyapan, V., Surawattanawan, P., et al. (2014). Tetrahydrocurcumin Protects against Cadmium-Induced Hypertension, Raised Arterial Stiffness and Vascular Remodeling in Mice. *PLoS One* 9, e114908. doi:10.1371/journal.pone.0114908

Shen, L., Xiong, Y., Wang, D. Q., Howles, P., Basford, J. E., Wang, J., et al. (2013). Ginsenoside Rb1 Reduces Fatty Liver by Activating AMP-Activated Protein Kinase in Obese Rats. *J. Lipid Res.* 54, 1430–1438. doi:10.1194/jlr.M035907

Shi, Y., and Massagué, J. (2003). Mechanisms of TGF-Beta Signaling from Cell Membrane to the Nucleus. *Cell* 113, 685–700. doi:10.1016/s0092-8674(03)00432-x

Stacey, R. B., Bertoni, A. G., Eng, J., Bluemke, D. A., Hundley, W. G., and Herrington, D. (2010). Modification of the Effect of Glycemic Status on Aortic Distensibility by Age in the Multi-Ethnic Study of Atherosclerosis. *Hypertension* 55, 26–32. doi:10.1161/HYPERTENSIONAHA.109.134031

Tang, S.-T., Su, H., Zhang, Q., Tang, H.-Q., Wang, C.-J., Zhou, Q., et al. (2016). Sitagliptin Inhibits Endothelin-1 Expression in the Aortic Endothelium of Rats with Streptozotocin-Induced Diabetes by Suppressing the Nuclear Factor-Kb/iκbα System through the Activation of AMP-Activated Protein Kinase. *Int. J. Mol. Med.* 37, 1558–1566. doi:10.3892/ijmm.2016.2578

Wang, L., Zheng, M., Wang, Y., Zhang, Y., Qian, H., Zhang, H., et al. (2014). Anti-diabetic Activity of Cassava Cross-Linked Octenyl Succinic Maltodextrin in STZ-Induced Diabetic Mice. *Int. J. Biol. Macromol* 64, 247–251. doi:10.1016/j.ijbiomac.2013.11.017

Wu, Y., Xia, Z. Y., Dou, J., Zhang, L., Xu, J. J., Zhao, B., et al. (2011). Protective Effect of Ginsenoside Rb1 against Myocardial Ischemia/reperfusion Injury in Streptozotocin-Induced Diabetic Rats. *Mol. Biol. Rep.* 38, 4327–4335. doi:10.1007/s11033-010-0558-4

Xia, R., Zhao, B., Wu, Y., Hou, J. B., Zhang, L., Xu, J. J., et al. (2011). Ginsenoside Rb1 Preconditioning Enhances eNOS Expression and Attenuates Myocardial Ischemia/reperfusion Injury in Diabetic Rats. *J. Biomed. Biotechnol.* 2011, 767930. doi:10.1155/2011/767930

Xiong, Y., Shen, L., Liu, K. J., Tso, P., Xiong, Y., Wang, G., et al. (2010). Antiobesity and Antihyperglycemic Effects of Ginsenoside Rb1 in Rats. *Diabetes* 59, 2505–2512. doi:10.2337/db10-0315

Yang, G., Zhuo, J., Lin, Y., Zhang, M., Liu, L., Chen, X., et al. (2019). Ginsenoside Rb1 Prevents Dysfunction of Endothelial Cells by Suppressing Inflammatory Response and Apoptosis in the High-Fat Diet Plus Balloon Catheter-Injured Rabbit Model via the G Protein-Coupled Estrogen Receptor-Mediated Phosphatidylinositol 3-Kinases (PI3K)/Akt Pathway. *Med. Sci. Monit.* 25, 7407–7417. doi:10.12659/MSM.912986

Yang, T., Miao, Y., Zhang, T., Mu, N., Ruan, L., Duan, J., et al. (2018). Ginsenoside Rb1 Inhibits Autophagy through Regulation of Rho/ROCK and PI3K/mTOR Pathways in a Pressure-Overload Heart Failure Rat Model. *J. Pharm. Pharmacol.* 70, 830–838. doi:10.1111/jphp.12900

YasminMcEniery, C. M., Wallace, S., Dakham, Z., Pulsalkar, P., Pusalkar, P., et al. (2005). Matrix Metalloproteinase-9 (MMP-9), MMP-2, and Serum Elastase Activity Are Associated with Systolic Hypertension and Arterial Stiffness. *Arterioscler Thromb. Vasc. Biol.* 25, 372. doi:10.1161/01.ATV.0000151373.33830.41

Zhang, X., Liu, M. H., Qiao, L., Zhang, X. Y., Liu, X. L., Dong, M., et al. (2018). Ginsenoside Rb1 Enhances Atherosclerotic Plaque Stability by Skewing Macrophages to the M2 Phenotype. *J. Cel Mol Med* 22, 409–416. doi:10.1111/jcmm.13329

Zhang, X., Xiao, J., Li, R., Qin, X., Wang, F., Mao, Y., et al. (2016). Metformin Alleviates Vascular Calcification Induced by Vitamin D3 Plus Nicotine in Rats via the AMPK Pathway. *Vascul Pharmacol.* 81, 83–90. doi:10.1016/j.vph.2016.01.002

Zhang, X. J., He, C., Tian, K., Li, P., Su, H., and Wan, J. B. (2015). Ginsenoside Rb1 Attenuates Angiotensin II-Induced Abdominal Aortic Aneurysm through Inactivation of the JNK and P38 Signaling Pathways. *Vascul Pharmacol.* 73, 86–95. doi:10.1016/j.vph.2015.04.003

Zhao, H., Lv, D., Zhang, W., Dong, W., Feng, J., Xiang, Z., et al. (2010). Ginsenoside-Rb1 Attenuates Dilated Cardiomyopathy in cTnT(R141W) Transgenic Mouse. *J. Pharmacol. Sci.* 112, 214–222. doi:10.1254/jphs.09314fp

Zheng, X., Wang, S., Zou, X., Jing, Y., Yang, R., Li, S., et al. (2017). Ginsenoside Rb1 Improves Cardiac Function and Remodeling in Heart Failure. *Exp. Anim.* 66, 217–228. doi:10.1538/expanim.16-0121

Zheng, Z., Wang, M., Cheng, C., Liu, D., Wu, L., Zhu, J., et al. (2020). Ginsenoside Rb1 Reduces H2O2-induced HUVEC D-ysfunction by S-timulating the sirtuin-1/AMP-activated P-rotein K-inase P-athway. *Mol. Med. Rep.* 22, 247–256. doi:10.3892/mmr.2020.11096

Zhou, P., Xie, W., He, S., Sun, Y., Meng, X., Sun, G., et al. (2019). Ginsenoside Rb1 as an Anti-diabetic Agent and its Underlying Mechanism Analysis. *Cells* 8. doi:10.3390/cells8030204

Zhou, R. H., Vendrov, A. E., Tchivilev, I., Niu, X. L., Molnar, K. C., Rojas, M., et al. (2012). Mitochondrial Oxidative Stress in Aortic Stiffening with Age: the Role of Smooth Muscle Cell Function. *Arterioscler Thromb. Vasc. Biol.* 32, 745–755. doi:10.1161/ATVBAHA.111.243121

Zoungas, S., Chalmers, J., Neal, B., Billot, L., Li, Q., Hirakawa, Y., et al. (2014). Follow-up of Blood-Pressure Lowering and Glucose Control in Type 2 Diabetes. *N. Engl. J. Med.* 371, 1392–1406. doi:10.1056/NEJMoa1407963

Conflict of Interest: The authors declare that the research was conducted in the absence of any commercial or financial relationships that could be construed as a potential conflict of interest.

Publisher's Note: All claims expressed in this article are solely those of the authors and do not necessarily represent those of their affiliated organizations, or those of the publisher, the editors and the reviewers. Any product that may be evaluated in this article, or claim that may be made by its manufacturer, is not guaranteed or endorsed by the publisher.

frontiers in Pharmacology

ORIGINAL RESEARCH
published: 02 November 2021
doi: 10.3389/fphar.2021.748568

Chinese Herbal Preparation SaiLuoTong Alleviates Brain Ischemia *via* Nrf2 Antioxidation Pathway–Dependent Cerebral Microvascular Protection

Xiao-Di Fan[1,2], *Ming-Jiang Yao*[1,2], *Bin Yang*[3], *Xiao Han*[1,2], *Ye-Hao Zhang*[1,2], *Guang-Rui Wang*[1,2], *Peng Li*[1,2]*, *Li Xu*[1,2]* and *Jian-Xun Liu*[1,2]*

[1]*Institute of Basic Medical Sciences, Xiyuan Hospital of China Academy of Chinese Medical Sciences, Beijing, China,* [2]*Key Laboratory of Pharmacology of Chinese Materia Medica, Beijing, China,* [3]*The Department of Pathology, Xiyuan Hospital of China Academy of Chinese Medical Sciences, Beijing, China*

Stroke is one of the most devastating diseases worldwide. The Chinese herbal preparation SaiLuoTong (SLT) capsule showed outstanding therapeutic effects on stroke and its sequelae. The aim of this study was to further elucidate its therapeutic mechanism. We duplicated a permanent cerebral ischemia model in rats by MCAO and used SLT (33 and 16.5 mg/kg) to intervene. The results showed SLT dose dependently decreased infarction volumes, relieved neuron degeneration and loss, and ameliorated neurological functions, and the dose of 33 mg/kg had statistical significance (compared with the model group, $p < 0.05$); SLT of 33 mg/kg also significantly inhibited the elevation in brain water content and the loss in claudin-1 and occludin expressions; additionally, it significantly increased nucleus translocation of Nrf2, elevated the expression of HO-1, and raised the activity of SOD and content of GSH (compared with the model group, $p < 0.05$ or 0.01). These results testified SLT's anti-brain ischemia effect and hint this effect may be related to the protection of brain microvascular endothelial cells (BMECs) that is dependent on the Nrf2 pathway. To further testify, we cultured hCMEC/D3 cells, duplicated OGD/R model to simulate ischemia, and used SLT (3.125, 6.25, and 12.5 mg/L) to treat. SLT dose dependently and significantly inhibited the drop in cell viabilities, and activated the Nrf2 pathway by facilitating Nrf2 nucleus translocation, and increasing HO-1 expression, SOD activity, and GSH content (compared with the model group, $p < 0.05$ or 0.01); last, the anti-OGD/R effects of SLT, including raising cell viabilities, inhibiting the elevation in dextran permeability, and preserving expressions of claudin-1 and occludin, were all abolished by Nrf2 siRNA interference. The *in vitro* experiment undoubtedly confirmed the direct protective effect of SLT on BMECs and the obligatory role of the Nrf2 pathway in it. Collectively, data of this study suggest that SLT's therapeutic effect on brain ischemia is related to its Nrf2-dependent BMECs protection.

Keywords: cerebral ischemia, SaiLuoTong capsule, brain microvascular endothelial cells, anti-oxidation, nuclear factor–E2–related factor 2

OPEN ACCESS

Edited by:
Qilong Wang,
Tianjin University of Traditional Chinese Medicine, China

Reviewed by:
Abraham Jacob Al-Ahmad,
Texas Tech University Health Sciences Center, United States
Malgorzata Burek,
Julius Maximilian University of Würzburg, Germany

***Correspondence:**
Peng Li
pengli1972cn@126.com
Li Xu
xuli1230@126.com
Jian-Xun Liu
liujx0324@sina.com

Specialty section:
This article was submitted to Cardiovascular and Smooth Muscle Pharmacology, a section of the journal Frontiers in Pharmacology

Received: *28 July 2021*
Accepted: *27 September 2021*
Published: *02 November 2021*

Citation:
Fan X-D Yao M-J Yang B, Han X, Zhang Y-H Wang G-R Li P, Xu L and Liu J-X (2021) Chinese Herbal Preparation SaiLuoTong Alleviates Brain Ischemia via Nrf2 Antioxidation Pathway–Dependent Cerebral Microvascular Protection. Front. Pharmacol. 12:748568. doi: 10.3389/fphar.2021.748568

INTRODUCTION

Stroke is one of the leading causes of disability and death worldwide, which produces immense health and economic burdens. Taking the case of China, tens of millions of people suffer from stroke each year, in which nearly ten percent of them die, and most of the remaining people are afflicted to different extents by the sequelae such as sensory and motor impediments, cognition impairments, and affective and speech disorders, which badly influences their lives as well as their families.

Most of strokes are the ischemic type, which occupies 80% of the total cases. It is usually triggered by obstructions of one or more cerebral arteries, which then lead to a critical reduction of regional cerebral blood flow, causing a waterfall-like cascade, and finally resulting in massive neuron deaths (Donnan et al., 2008). In this damage cascade, the ruin of the brain–blood barrier (BBB) plays a pivotal role.

The endothelium of cerebral microvascular is unique compared to that in other tissues, as they have continuous intercellular tight junctions (TJs) and efflux transporters, and thus the endothelium and their TJs form a barrier-like structure, which can greatly limit both the paracellular and transcellular diffusion of vascular inclusions, and constitute the BBB (Bazzoni et al., 2004; Abbott et al., 2006).

Growing evidences demonstrate that brain ischemia causes loss of endothelial cells and TJs, leading to enhanced BBB permeability including not only extravasations of blood plasma constituents and some neurotoxins but also the infiltrations of neutrophils and monocytes, which further cause neuron damage, significantly amplifying the effects of ischemia and making the injury irreversible (Jiao et al., 2011; Obermeier et al., 2013; Sladojevic et al., 2019).

Oxidative stress is the major cause of BBB damage in ischemia that refers to a state in which the generation of reactive oxygen species (ROS) exceeds far behind the body's dispose ability, leading to serious impairments (Kuźma et al., 2018; Chen et al., 2020). Redressing this imbalance between ROS and ROS scavenging in the brain vascular endothelial cells is necessary and urgent for stroke treatment. In comparison to directly eliminating ROS, inspiring the innate antioxidation system is a better choice as it has a higher efficiency, longer effecting duration, and more safety (Kuźma et al., 2018; Chen et al., 2020).

The nuclear factor erythroid 2–related factor 2 (Nrf2) belongs to the cap "n" collar (Cnc)-bZIP (basic leucine zipper) family and is a transcription factor regulating the expressions of a series of antioxidant, anti-inflammatory, and detoxifying proteins (Loboda et al., 2016). The Nrf2 pathway is the most important antioxidation machinery of the body and is also closely related to cerebral vascular endothelium preservation and the outcome of brain ischemia.

A large number of studies showed that the activation of the Nrf2 pathway can lead to strong antioxidative and antiapoptotic effects and BBB protection in the brain infarction (Zhao et al., 2007; Nguyen et al., 2009; Zhang et al., 2017; Hu et al., 2018; Li et al., 2018; Wang et al., 2018; Liu et al., 2019). In contrast, mass reports exhibited that the deletion or downregulation of Nrf2 exacerbated brain injuries in ischemia, in which the acceleratedly destroyed TJs in cerebral blood vessels, increased BBB breakdown, and brain edema played a pivotal role (Zhao et al., 2007; Li et al., 2014). These results indicate that the Nrf2 pathway is a pivotal target for vascular endothelial cell protection and stroke therapy.

SaiLuoTong capsule (SLT) is an outstanding representative of new type Chinese herbal preparation, which is composed of refined herbal extracts, instead of crude drugs, thus having a definite and controllable composition, in which the high efficient ingredients are enriched, and the lower and even inefficient ones are removed. This characteristic renders SLT to overcome the shortcomings of traditional Chinese herbal preparations, significantly enhances the controllability in production and safety, and increases the therapeutic effects.

SLT is composed of extracts of three Chinese herbal medicines, that is, the roots of *Panax ginseng* (ginseng), the leaves of *Ginkgo biloba* (ginkgo), and the flowers of *Crocus sativus* (saffron), with the proportion of 5:5:1 that is derived from pharmacodynamic optimization experiments in animals (Jia et al., 2018; Steiner et al., 2018). The main active components of SLT are ten compounds, including three ginsenosides, three flavones, three ginkgolides, and one crocin (Jia et al., 2018).

Numerous studies have testified the remarkable protective effect of SLT against brain ischemia. And the therapeutic mechanism was revealed as anti-inflammation, antioxidative stress, and antiapoptotic and platelet aggregation, as well as improving blood flow and brain tissue acetylcholine (ACh) content (Xu et al., 2008; Seto et al., 2017; Steiner et al., 2018; Zhang et al., 2019; Fan et al., 2020). More encouragingly, in a strictly designed clinical trial with multiple centers, large sample, and double-blinded placebo control, SLT showed a significant ameliorative effect in patients with mild to moderate vascular dementia; meanwhile, no significant toxicities were exhibited (Jia et al., 2018; Steiner et al., 2018). At present, an internationally cooperated phase III clinical trial about the effects of SLT on brain ischemia–related cognition impairments is well ongoing in both China and Australia. Thus, SLT has a good chance to be accepted as an official drug for the remedy of stroke and its sequelae by the international mainstream, which will possibly be the first worldwide applied Chinese herbal drug in the major diseases, not only being a milestone of Chinese medicine but also bringing a light to the unsatisfying situation of stroke remedy.

Therefore, further exploring SLT's therapeutic mechanisms has a particular significance and should be a long-lasting issue. The relationship between SLT's anti-stroke effect and Nrf2 pathway–mediated cerebral vascular endothelial cell protection has not been clarified. In the present study, we investigated this issue with experiments on both rats and cultured cells. This study may be significant for clarifying the therapeutic mechanism of SLT on stroke and for searching effective drugs for stroke remedy.

MATERIALS AND METHODS

Animal Preparation

Male Sprague–Dawley rats (200–230 g) were purchased from SPF Biotechnology Co., Ltd. (Beijing, China, No. 1103241911033018).

Rats were maintained in an air-conditioned room (temperature: 21 ± 2°C) under a 12 h day–night cycle with free access to food and water, and they were acclimated for 3 days prior to the experiment. Animal handling procedures were performed in accordance with the guide of the Ethics Committee of Xi Yuan Hospital of China Academy of Chinese Medical Sciences (Protocol No. 2019XLC015-2). And all animal housing, care, feeding, and experimental procedures were in compliance with the National Guidelines for Animal Protection.

Establishment of Cerebral Infarction Model in Rats With Permanent Middle Cerebral Artery Occlusion

Rats were anesthetized by an intraperitoneal injection with 1% pentobarbital sodium (80 mg/kg). Under anesthesia, the right common carotid, the right external carotid, and the right internal carotid were carefully separated and exposed. The right external carotid and the right common carotid were ligated with a suture silk. Thereafter, a 3–0 monofilament nylon suture with a rounded tip of 0.32 mm diameter (Item#2432A1, Beijing Sunbio Biotech Co Ltd.) was introduced into the bifurcation of the right common carotid and then was intracranially inserted for approximately 18 mm to block the blood flow of the right middle cerebral artery. During this procedure, the body temperature was maintained at 37°C using a warm pad. For the sham-operated group, only skin incisions were performed under anesthesia.

Drug Treatments in Rats

SLT was provided by the ShenWei Pharmaceutical Corporation (Heibei, China). SLT was soluted in saline and was injected into the duodenum immediately after the right middle cerebral artery was blocked. The doses of SLT were set as 16.5 mg/kg (SLT-L) and 33 mg/kg (SLT-H). Rats in the sham group and model group were injected with saline in the same way and at the same time point.

Measurement of Neurological Deficits

The neurological function deficit scores of rats were blindly evaluated 24 h after MCAO. A five-point scale was used as follows: 0, no neurological deficits; 1, failure to fully extend the left forelimb; 2, decreased resistance to a lateral push toward the right side and failure to fully extend the left forepaw; 3, circling to the left side; and 4, inability to walk spontaneously and lack of response to stimulation (Bederson et al., 1986).

Assessment of Infarct Volumes

After neurological function tests, the rats were killed by decapitation, and their brains were taken out and were sectioned into slices of 2 mm thickness; the slices were incubated in a 2% 2,3,5-triphenyltetrazolium chloride (TTC) solution at 37°C for 15 min. TTC stained the non-infarcted region with a deep red pigment, while the infarcted brain areas were stained with white (Bederson et al., 1986). Stained sections were photographed, and the images were analyzed to calculate the infarct volumes by using an Image Pro-Plus 6.0 analysis system (Media Cybernetics, Rockville, MD, United States).

Brain Tissue Fixation, Embedding, and Sectioning, and HE Staining

24 h after MCAO, the rats were killed by decapitation, and the brains were then rapidly taken out and were placed in 4% paraformaldehyde for 7 days. The brains were then embedded in paraffin and were sectioned into slices of 7 μm thickness. The sections were stained with HE and were observed using an Olympus BX51 microscope.

Evaluation of Water Content of the Brain

24 h after MCAO, rats were sacrificed by decapitation, and their brains were taken out. The wet brains were weighed and were dried at 60°C for 3 days, and then the weights of the dry brains were measured. The brain water content = (1-dry weight/wet weight)×100%.

Immunohistochemistry Examination

The brain sections were deparaffinized, rehydrated, and blocked. Next, the sections were incubated overnight at 4°C with anti–claudin-1 antibody (1:500, ab15098, abcam), anti-occludin antibody (1:500, 27260-1-AP, ProteinTech), and anti–heme oxygenase-1 (HO-1) antibody (1:500, 66743-1-Ig, ProteinTech). The sections were rinsed with PBS three times, then were incubated with horseradish peroxidase (HRP)-conjugated goat anti-rabbit IgG at 37 °C for 20 min, and were colorized with DAB. Last, hematoxylin restaining was performed. The sections were observed using an Olympus BX51 microscope.

Western Blot Assay

The nuclear and cytosol protein extractions and total protein extractions from the samples (in *in vivo* experiments, were cerebral cortex; in *in vitro* experiment, were hCMEC/D3 cells) were performed using the nuclear-cytosol extraction kit (Applygen Technologies Inc., Beijing) and the total protein extraction kit (Solarbio Science and Technology Co. Ltd., Beijing), respectively. Equal amounts of protein (50 μg) were loaded into 10% or 12.5% SDS-PAGE gels, and then were subjected to electrophoresis; last, they were transferred to nitrocellulose membranes (Millipore, Billerica, MA, United States). The membranes were blocked with 5% bovine serum albumin (BSA) for 1 h at room temperature, and then were incubated overnight at 4°C with anti–claudin-1 antibody (1:1000), anti-occludin antibody (1:1000), anti-Nrf2 antibody (1:1000), anti–HO-1 antibody (1:1000), anti-GAPDH antibody (1:1000,60004-1-Ig, ProteinTech), anti–β-actin antibody (1:1000, 60008-1-Ig, ProteinTech), or anti–histone H3 antibody (17168-1-AP, ProteinTech). The membranes were incubated with HRP-conjugated secondary antibodies for 1.5 h at room temperature. The protein bands were enlightened with an enhanced chemiluminescence kit,

and their brightness was quantified by using Image LabTM software.

Determinations of the Activities of Superoxide Dismutase and the Contents of Glutathione

All samples (brains and cells) were made into homogenates by using an ultrasonic cell disrupter at 0°C. SOD activities and GSH contents in the homogenates were analyzed with the merchant kits (Institute of Biological Engineering of Nanjing Jiancheng, Nanjing, China).

Cell Culture

Human brain microvascular endothelial cell lines (hCMEC/D3, iCellBioscience, Inc. Shanghai, China) were cultured at 37 °C with 5% CO_2 in the endothelial cell medium (ECM, PriMed-iCell-0016, China) supplemented with 5% fetal bovine serum, 1% ECGS, 100 U/mL penicillin, and 100 μg/ml streptomycin, and were passaged with 0.25% trypsin.

Oxygen-Glucose Deprivation and Reoxygenation Model and SLT Treatments

For oxygen-glucose deprivation (OGD), hCMEC/D3 cells were incubated with a glucose-free Dulbecco's modified Eagle's medium (DMEM, Gibco, United States) and were placed in a customer-made chamber, which was then filled with 95% N_2/5% CO_2 and kept at 37°C for 4 h. After OGD, for reoxygenation, the incubation media were replaced with the normal ECM, and the cells were cultured under normal atmosphere with 5% CO_2. The mock group was incubated in normal DMEM under normal atmosphere with 5% CO_2 at 37°C for 4 h and was then incubated with ECM. SLT was soluted with DMSO, and the solutions were added into the incubation medium with the volume ratio of 1: 1000 at the beginning of OGD and reoxygenation. The mock group and the OGD/R model group were treated with DMSO in the same way at the same time points.

Cell Viability Measurement

The cells were incubated with CCK8 (Dojindo Corporation, Japan)-ECM solution (1:10) at 37°C for 2 h. The absorbance at 450 nm was measured using a microplate reader. Then the cell viabilities were obtained through normalization to the average absorbance of the mock (normal control) group.

Immunofluorescence Assay

Paraformaldehyde-fixed hCMEC/D3 cells were incubated with anti-Nrf2 antibody or anti–HO-1 antibody (both 1:200), followed by the incubation with secondary antibodies, that is, fluorescein-conjugated AffiniPure goat anti-rabbit IgG (1: 100, Yuabio, China), and were stained with DAPI finally. Cells were observed and imaged using an Olympus IX81 live cell station.

RNA Interference of Nrf2

Transfections in HCMEC/D3 cells were conducted with Lipofectamine 3000 reagent (Thermo Fisher Scientific, United States). High purity control siRNAs (negative control siRNA and GAPDH siRNA) and Nrf2 siRNAs were obtained from JTSBIO (Wuhan, China). The Nrf2 siRNA sequences were as follows: Nrf2 siRNA-1, forward, CCCUGAAAGCACAGCAGAATT, and reverse, UUCUGCUGUGCUUUCAGGGTT; Nrf2 siRNA-2, forward, CCAGAACACUCAGUGGAAUTT, and reverse, AUUCCACUGAGUGUUCUGGTT; and Nrf2 siRNA-3, forward, GCCUGUAAGUCCUGGUCAUTT, and reverse, AUGACCAGGACUUACAGGCTT. Negative control (NC) siRNA sequences were as follows: forward, UUCUCCGAA CGUGUCACGUTT, and reverse, ACGUGACACGUUCGG AGAATT. GAPDH sequences were as follows: forward, UGA CCUCAACUACAUGGUUTT, and reverse, AACCAUGUA GUUGAGGUCATT.

Paracellular Permeability Measurement

Cell monolayer integrity was assessed by diffusion of fluorescein isothiocyanate (FITC)-dextran (4kDa, Lot: 64,878, MCE, United States) as previously described (Hu et al., 2018). After OGD/R, 400 μL FITC-dextran (0.5 mg/ml) solutions were added to the upper chamber of the 12-well transwell culture plate inserts (A190059, Millicell, Germany) on the bottom of which the hCMEC/D3 cell confluents grew. Inserts were placed in the 12-well culture plates containing 1000 μL of DMEM/F12 media (without serum and phenol red) per well. Then the cells were incubated at 37°C for 60 min in the dark. Inserts were removed, and the solutions in the wells were collected and transferred into a black 96-well plate. The fluorescence intensities were measured by using the excitation and emission wavelengths at 490 and 520 nm, respectively, and were converted to the concentrations of FITC-dextran with the calibration curve.

Statistical Analysis

The data are expressed as mean ± SD and were statistically analyzed by using the Statistical Product and Service Solutions (SPSS) 16.0 software; data comparisons between two groups were conducted with the t-test, and those among multiple groups were conducted with one-way or two-way analysis of variance (ANOVA) followed by the LSD test. The statistical significance level was set to 0.05.

RESULTS

SLT Attenuated Cerebral Infarctions and Improved the Neurological Functions in MCAO Rats

No infarction was detected in the sham group, while infarctions of large volumes were developed in the model group. SLT treatments alleviated the brain infarctions, and the infarct volumes in the SLT-H group were significantly lower than

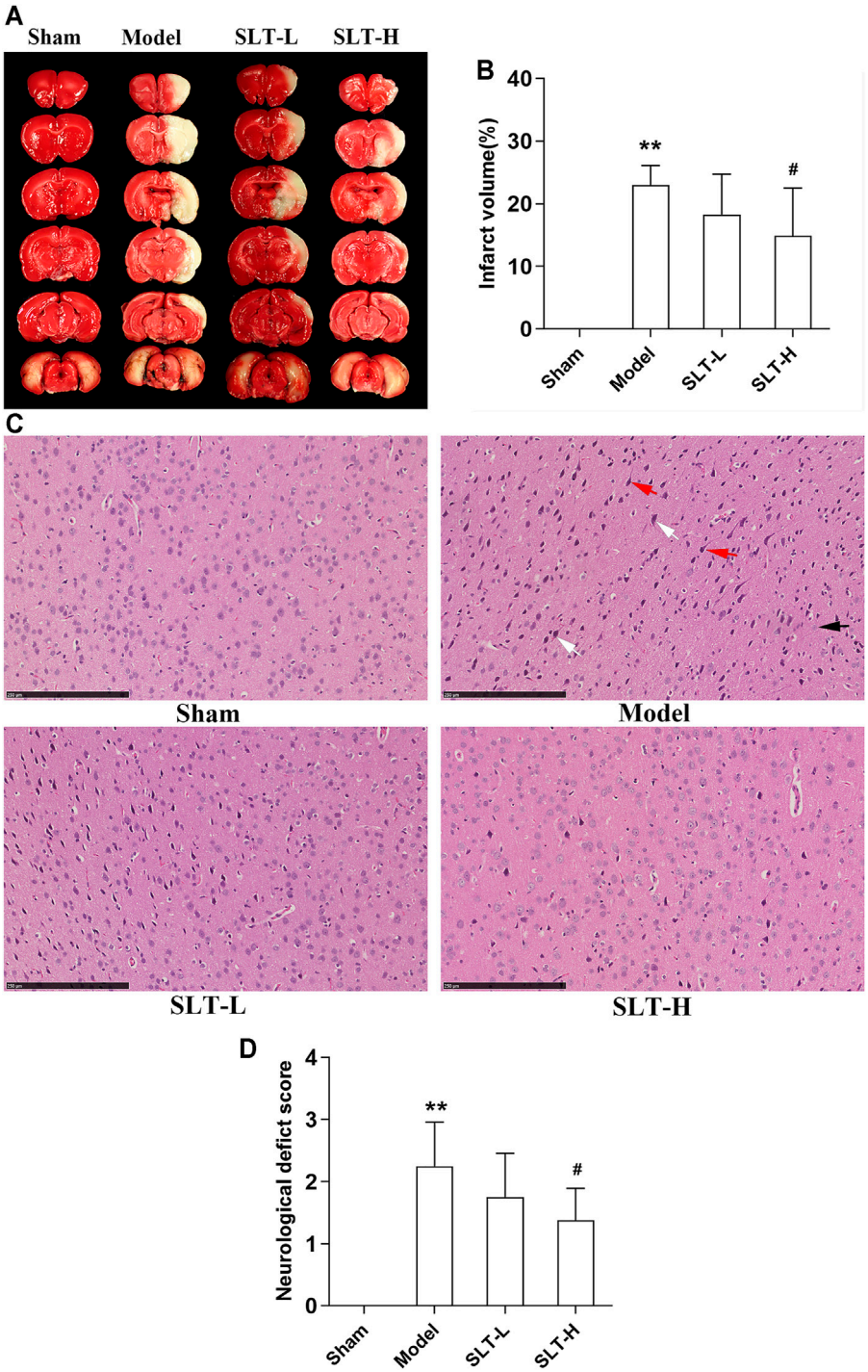

FIGURE 1 | SLT attenuated cerebral infarction and neurological deficit in rats undergoing MCAO. 24 h after MCAO, the rats were neurologically tested, then were killed, and their brains were harvested for TTC and HE stainings. **(A)** Representative images of TTC staining. The white regions are the infarct tissues, while the red regions are the viable tissues. **(B)** Infarct volumes of the brains ($n = 8$). **(C)** Representative images of HE staining of the brain cortex in all the groups. The ischemic brain region in the model group presented severe neuronal loss and neuron degeneration, including cytoplasm acidophilic degeneration (indicated with white arrows), nuclear pyknosis (indicated with red arrows), and hydropic degeneration (indicated with black arrow). The neuronal damages were alleviated in SLT-L and SLT-H groups (scale bar in all panels = 250 μm). **(D)** Neurological deficit scores of all the groups ($n = 8$). Data are expressed as mean ± SD. $^{*}p < 0.05$, $^{**}p < 0.01$, in comparison to the sham group; $\#p < 0.05$, in comparison to the model group.

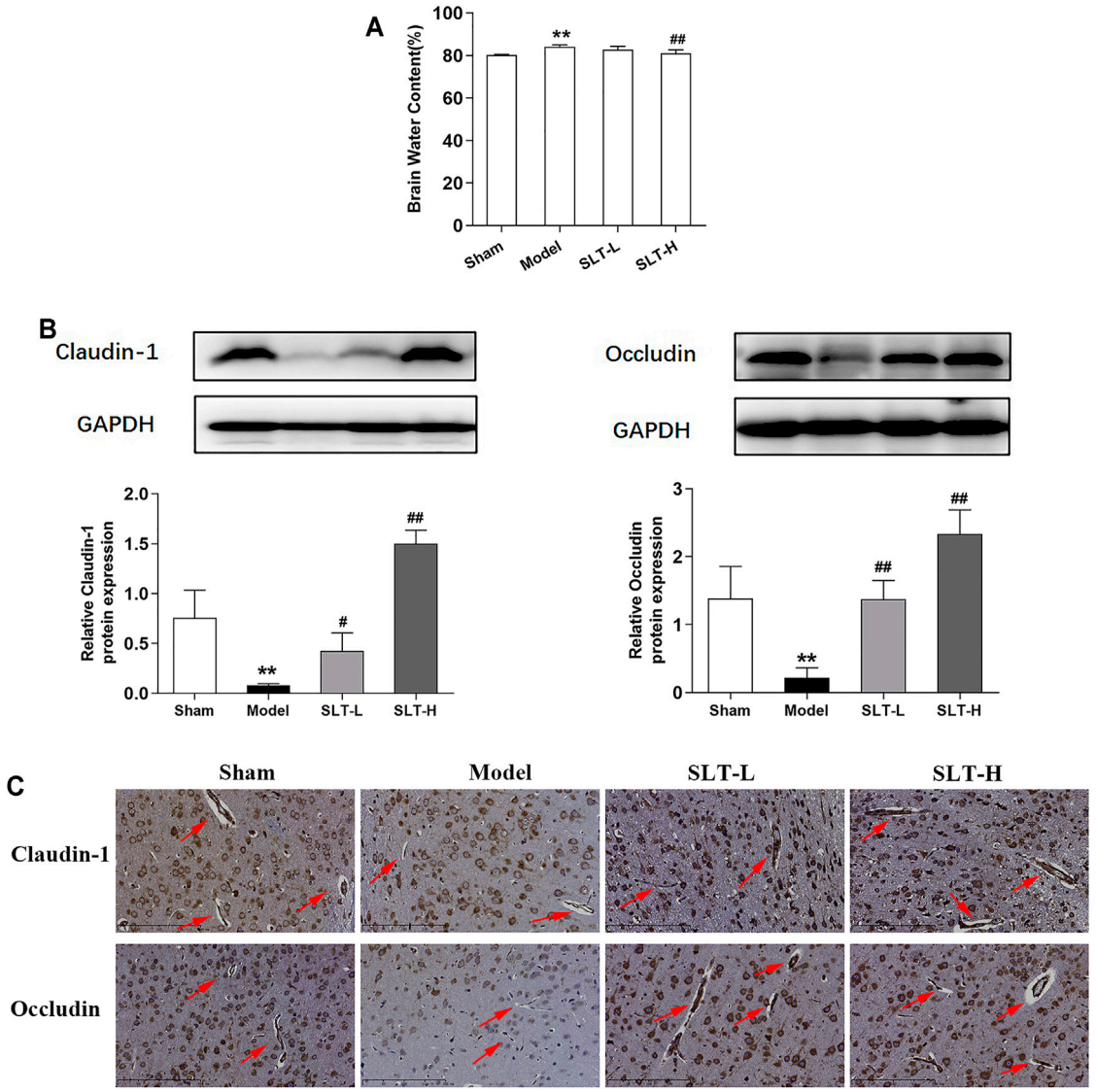

FIGURE 2 | SLT decreased brain edema and prevented the loss of tight junction proteins in the cerebral vascular endothelium in MCAO rats. **(A)** Brain water contents of the ischemic hemispheres measured by the wet and dry weight method (n = 7). **(B)** Western blot assays for claudin-1 and occludin expressions in the ischemic hemispheres (n = 3). **(C)** Representative images of immunohistochemistry examination for claudin-1 and occludin in the ischemia areas. The arrows point to the blood vessels (scale bar = 200 μm). Data are represented as mean ± SD. *p < 0.05, **p < 0.01, compared with the sham group; #p < 0.05, ##p < 0.01, compared with the model group.

those in the model group (p < 0.05, **Figures 1A,B**). Accordingly, in the sham group, no neuron damage, neuron loss, or other notable morphological abnormalities were shown in the brain microscopy; however, necrosis of large areas was observed in the model group, in which severe neuron loss, neuron cell degeneration including cytoplasm acidophilic degeneration, and nuclear pyknosis were shown; tissue edema and neuron hydropic degeneration were shown in the regions peripheral to necrosis, and these lesions were notably attenuated in SLT-treated groups, especially in the SLT-H group (**Figure 1C**).

Neurological deficit scores were significantly elevated in the model group in comparison to the sham group (p < 0.01), indicating a severe injury in neurological function was induced by brain ischemia. However, treatment with SLT alleviated the elevation in neurological deficit scores, especially with the high dose, of which the effect was significant (p < 0.05, compared with the model group; **Figure 1D**).

SLT Decreased Water Content of the Brain and Inhibited the Drop in Expression Levels of Claudin-1 and Occludin in MCAO Rats

The water contents of the infarcted hemispheres in the model group were significantly increased in comparison to the ipsilateral

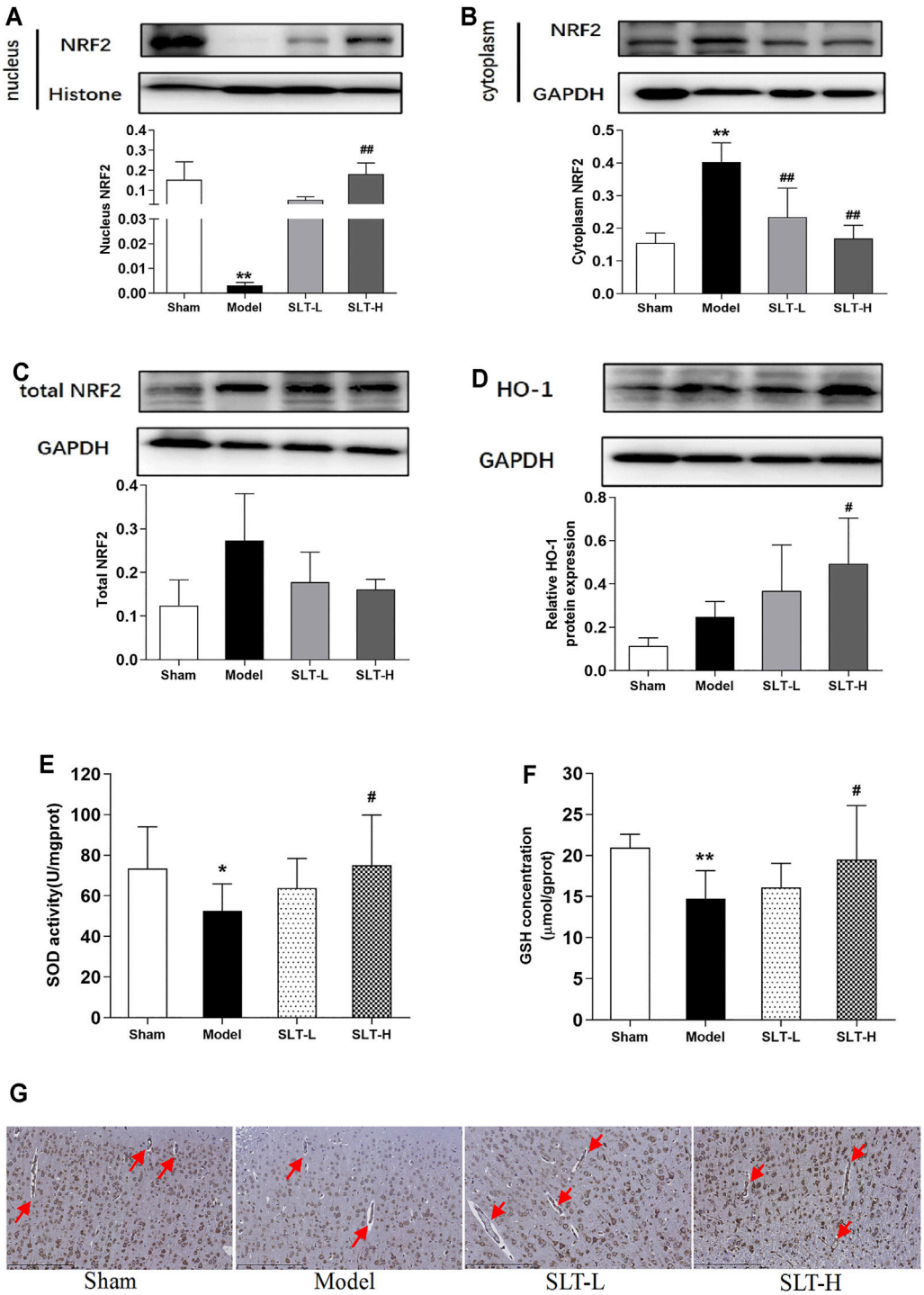

FIGURE 3 | SLT activated the Nrf2 pathway in the brain after ischemia. **(A–C)** Western blot assays for the protein levels in the ischemic hemispheres of nucleus Nrf2, cytoplasm Nrf2, and the total Nrf2 ($n = 3$). **(D)** HO-1 expressions in the ischemic hemispheres. **(E)** and **(F)** SOD activities and GSH contents in the ischemic hemispheres ($n = 8$). **(G)** Immunochemistry examination of HO-1 expressions in the ischemic regions. Red arrows indicate the blood vessels (scale bar = 250 μm). Data are expressed as mean ± SD. *$p < 0.05$, **$p < 0.01$, vs. the sham group; #$p < 0.05$, ##$p < 0.01$, vs. the model group.

hemispheres in the sham group ($p < 0.01$); however, water contents of the infarcted hemispheres in SLT groups were decreased, especially in the SLT-H group, which were significantly lower than those in the model group ($p < 0.01$, **Figure 2A**). These results hint that SLT may have the effect of protecting cerebral microvascular, thus alleviating its leakage.

Additionally, the examinations on claudin-1 and occludin, two key TJ-related proteins that play pivotal roles in maintaining BBB integrity, showed similar results. The results of the Western blot assay showed that the expression levels of claudin-1 and occludin in the infarcted hemispheres significantly decreased in the model group, compared with the ipsilateral hemispheres in the sham group ($p < 0.01$); however, the expression levels of claudin-1 and occludin were significantly increased in SLT-administrated groups in comparison to the model group ($p < 0.05$ or $p < 0.01$, **Figure 2B**). Immunohistochemistry examination results showed that the expression levels of claudin-1 and occludin in cerebral microvascular endothelial cells in the infarcted area were attenuated in the model group, in comparison to the same positions in the sham group; however, these downregulations in claudin-1 and occludin expressions were prevented by SLT treatments (**Figure 2C**).

Collectively, these results hint that the cerebral microvascular may be a key target of SLT, and the protection on them may constitute the foundation for SLT's therapeutic effects on brain ischemia.

SLT Activated the Nrf2 Pathway in the Brain of MCAO Rats

The nuclear contents of Nrf2 in the infarcted hemispheres in the model group were significantly lower than those in the ipsilateral hemispheres in the sham group ($p < 0.01$); correspondingly, Nrf2 contents in the cytoplasm of the model group were significantly higher ($p < 0.01$). This result indicates that after MCAO, the Nrf2 pathway was drastically compromised in rat brains. However, SLT treatments rescued this fall down; in SLT-H groups, Nrf2 levels in the nucleus were significantly increased ($p < 0.01$, compared with the model group), and the contents of Nrf2 in the cytoplasm of SLT-L and SLT-H groups were significantly lower than those in the model group (both $p < 0.01$, **Figures 3A,B**). Besides, the total protein levels of Nrf2 between all the groups showed no significant difference, suggesting the changes in the Nrf2 pathway were mainly derived from posttranslational modifications, which are also the major regulation fashion of the Nrf2 pathway (**Figure 3C**).

The downstream of Nrf2 exhibited similar changes. Treatments with SLT increased the protein expressions of HO-1 in the ischemia hemisphere, especially with SLT-H, which showed a significance in statistics (compared with the model group, $p < 0.05$, **Figure 3D**). Immunohistochemistry examination revealed that the upregulation of HO-1 by SLT treatments also happened in cerebral vascular endothelial cells (**Figure 3G**). The activities of SOD and the contents of GSH in the infarcted hemispheres in the model group were also significantly decreased in comparison to the ipsilateral hemispheres in the sham group ($p < 0.05$ in SOD activities and $p < 0.01$ in GSH contents), and these decreases were inhibited in SLT treatment groups as well, with better effects in the SLT-H group, which has statistical significances in comparison to the model group ($p < 0.05$ in SOD activities and $p < 0.05$ in GSH contents, **Figures 3E,F**).

Taken together, these results showed SLT treatments activated the Nrf2 pathway in the brain and imply that it may play a key role in SLT's therapeutic effects on brain ischemia including the protection of cerebral microvascular endothelium.

SLT Protected hCMEC/D3 Cells and Activated the Nrf2 Pathway in hCMEC/D3 Cells in OGD/R Injury

The above results of *in vivo* experiments suggest that SLT may exert its anti-brain ischemia effect through cerebral microvascular protection, which may be related to the activation of the Nrf2 pathway. To confirm this assumption, we selected a human brain microvascular endothelial cell line, hCMEC/D3, and observed the direct effect of SLT on it.

First, we observed the safety range of SLT on normal hCMEC/D3 cells with the CCK8 test. In the concentration range of 3.125–100 mg/L, SLT did not significantly decrease the cell viabilities; on the contrary, at concentrations of 25, 50, and 100 mg/L, SLT significantly increased the cell viabilities ($p < 0.01$, compared with the mock group; **Figure 4A**). This result indicates that up to 100 mg/L, SLT has no toxicities on hCMEC/D3 cells because there was no significant decline shown in cell viabilities.

Second, we duplicated the OGD/R model in hCMEC/D3 cells, which simulates ischemia injury *in vivo*, and treated the cells with SLT. The results showed that OGD/R injury significantly decreased the cell viabilities ($p < 0.01$, compared with the mock group); however, SLT treatments at concentrations of 3.125, 6.25, and 12.5 mg/L significantly increased the cell viabilities (all $p < 0.01$, compared with the model group, **Figure 4B**), confirming that SLT has a direct protective effect on microvascular endothelial cells against ischemia assault.

Third, we investigated the activities of the Nrf2 pathway in SLT's intervening. We selected the medium effective concentration, that is, 6.25 mg/L, of SLT to treat hCMEC/D3 cells. The results of immunocytofluorescent examinations showed that cells in the mock group exhibited weak expressions of Nrf2 and HO-1; in contrast, cells in the model group displayed slightly enhanced expressions. However, the expressions of these two proteins in cells of SLT-treated groups were strongly enhanced in comparison to the model group; furthermore, the enhancedly expressed Nrf2 was mainly nuclear distributed (**Figures 5A,B**). SOD activities and GSH levels in hCMEC/D3 cells showed an accordant situation. They were significantly decreased in the OGD/R group ($p < 0.01$, compared with the mock group); however, compared with the model group, the SOD activities and GSH levels in the SLT-treated group were significantly increased ($p < 0.01$, **Figures 5C,D**). This result directly testified that SLT treatment activates the Nrf2 pathway in microvascular endothelial cells and further links the Nrf2 pathway to SLT's vascular endothelium protection.

Nrf2 siRNA Interference Inhibited SLT's Protective Effect Against OGD/R Injury in hCMEC/D3 Cells

To finally confirm the role of the Nrf2 pathway in SLT's therapeutic effect, we performed a counterevidence experiment.

First, we constituted siRNAs to knock down Nrf2. The optimal transfection concentration of plasmid that leads to minimum cytotoxicity and can efficiently downregulate target gene

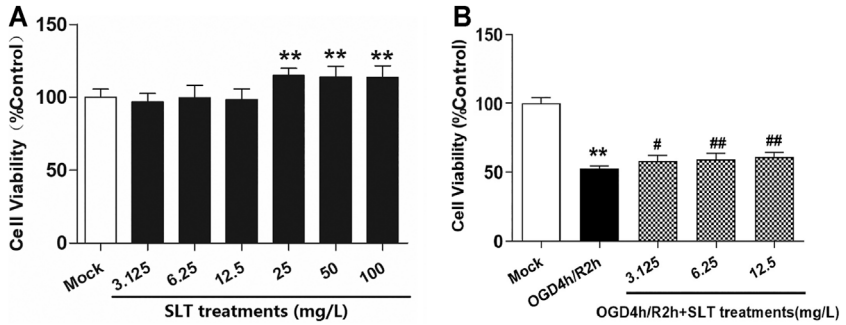

FIGURE 4 | SLT alleviated OGD/R injury in hCMEC/D3 cells. **(A)** Toxicity test of SLT on hCMEC/D3 cells ($n = 6$). The cells were cultured with different concentrations of SLT (3.125, 6.25, 12.5, 25, 50, and 100 mg/L) for 24 h, and the cell viabilities were examined by the CCK-8 method. **(B)** The therapeutic effects of SLT on OGD/R injury in hCMEC/D3 cells ($n = 6$). Data are expressed as mean ± SD. $^{*}p < 0.05$, $^{**}p < 0.01$, vs. the mock group; $\#p < 0.05$, $\#\#p < 0.01$, vs. the OGD/R group.

expressions was determined as 50 nmol/L (**Figure 6A**). Then, three Nrf2 siRNA (siRNA-1, siRNA-2, and siRNA-3) and negative control siRNA (NC siRNA) sequences were designed, synthesized, and transfected into hCMEC/D3 cells. The results showed that Nrf2 siRNA-3 had the strongest ability to inhibit Nrf2 protein expression, and interestingly, this siRNA also significantly decreased the cell viability in OGD/R injury, which is agreed with the well-recognized safeguard role of the Nrf2 pathway in ischemia injury ($p < 0.01$, compared with NC siRNA + OGD/R group, **Figures 6B–D**). Therefore, Nrf2 siRNA-3 was selected to study the role of Nrf2 in SLT's therapeutic effect on OGD/R injury of hCMEC/D3 cells.

Next, we duplicated OGD/R injury in hCMEC/D3 cells, treated it with SLT, and observed the blocking effect of Nrf2 siRNA on SLT's therapy. As expected, the elevations of protein expressions of Nrf2 and HO-1 by SLT treatment ($p < 0.05$ or 0.01, NC siRNA + OGD/R + SLT group vs. NC siRNA + OGD/R group) were significantly prevented by Nrf2 siRNA interference, indicating the Nrf2 pathway was specifically blocked (all $p < 0.01$, OGD/R + SLT + Nrf2 siRNA group vs. NC siRNA + OGD/R + SLT group, **Figure 7**). The alleviating effects of SLT on OGD/R injury in hCMEC/D3 cells include significantly increasing the cell viabilities, reducing endothelium permeability, and elevating expressions of claudin-1 and occludin ($p < 0.05$ or 0.01, NC siRNA + OGD/R + SLT group vs. NC siRNA + OGD/R group); however, these protective effects were all significantly inhibited by Nrf2 siRNA interference ($p < 0.05$ or $p < 0.01$, OGD/R + SLT + Nrf2 siRNA group vs. NC siRNA + OGD/R + SLT group; and $p > 0.05$, OGD/R + Nrf2 siRNA group vs. OGD/R + SLT + Nrf2 siRNA group; **Figures 8A–C**). This result undoubtedly indicates the protective effect of SLT on OGD/R injury of hCMEC/D3 cells is Nrf2 pathway dependent.

DISCUSSION

The mass and devastating neuron damages are the ultimate consequence of cerebral infarction; however, with the deepening of the research on the mechanism of brain ischemia, factors out of the neural cells deserve more and more attentions (Andjelkovic et al., 2019). Ischemia leads to a drastic drop in the supplies of oxygen and nutrients mainly including glucose, which injures neurons and also injures brain vascular endothelial cells at the same time (Brouns et al., 2009). The vascular endothelial cells exhibit severe cellular edema, that is, hydropic degeneration, even death, which results in disruption in the endothelium TJs, and attenuates its barrier function, leading to serious exudations from the blood vessels, which finally cause grievous edema and inflammation in the brain tissue, generating additive injuries to the neurons (Andjelkovic et al., 2019). These injuries secondary to ischemia are far more detrimental, both more violent and more extensive, which could expand to semi-ischemic and even non-ischemic regions, thus significantly amplifying the damages, even by fold (Brouns et al., 2009). Actually, most of the fatally devastating events elicited by cerebral infarction, such as cerebral edema, intracranial hypertension, cerebral hernia, coma, and even death, are largely related to vascular damages (Rahimi et al., 2017). Thus, the vascular factor plays a pivotal role in the pathogenesis of cerebral ischemia, even more important than ischemia itself.

The formation of endothelial TJs is dependent on a sort of specific proteins, of which claudin and occludin are two major members. These two proteins have a similar action mode; that is, the same kind of molecules in membranes of the two neighboring cells combine each other and form homological complexes, thus sealing off the intercellular gap, blocking the passing of blood contents (Rahimi et al., 2017). Besides, these two proteins also have a protective effect on endothelial cells against hazardous stimuli. For example, knockdown of occludin potentiated cytokine secretion, inflammasome activation, and pyroptosis occurrence in TNF-α–treated bEnd.3 cells (Zhang et al., 2020).

It should be noted that claudin has some subtypes; however, it is acknowledged that claudin-1 is the main type of that expressed in the brain blood vessels. Berndt et al. reported that claudin-1 was expressed in human brain capillaries as the strongest claudin, even significantly more than claudin-5 (Berndt et al., 2019). A recent study showed that claudin-1 replaced claudin-5 at the TJs of brain capillary endothelial cells during the regeneration phase after stroke (Sladojevic et al., 2019). Furthermore, knockout of claudin-1 in null mice is lethal, suggesting its irreplaceable role for TJ preservation (Furuse et al., 2002).

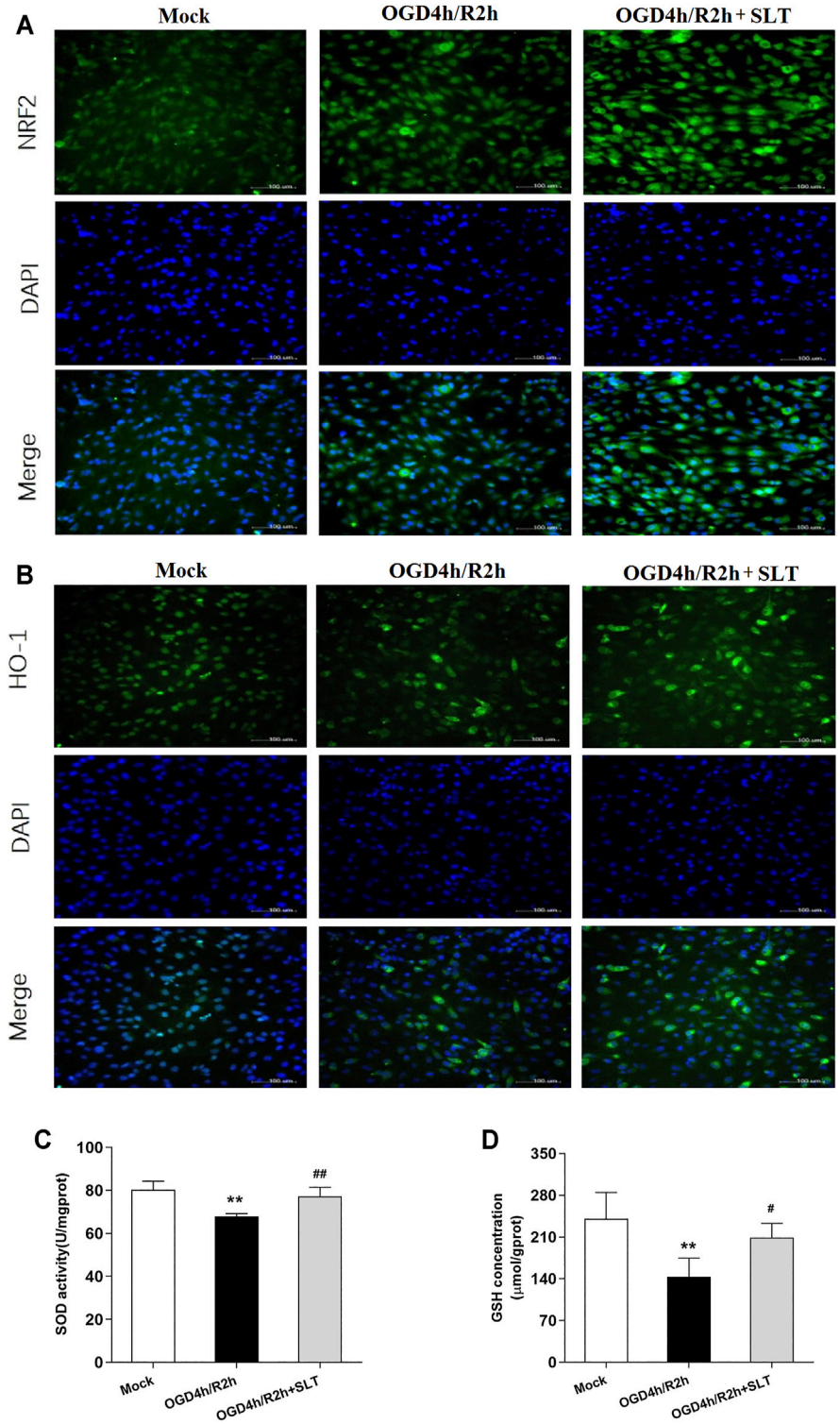

FIGURE 5 | SLT activated Nrf2 pathway in OGD/R-injured hCMEC/D3 cells. **(A,B)** Images of cytoimmunofluorescent examination of Nrf2 and HO-1 expressions in cells undergoing OGD/R injury (scale bar = 100 μm). **(C,D)** SOD activities and GSH contents in hCMEC/D3 cells undergoing OGD/R injury (n = 5 each). Data are expressed as mean ± SD. *p < 0.05, **p < 0.01, vs. the mock group; #p < 0.05, ##p < 0.01 vs. the OGD/R group.

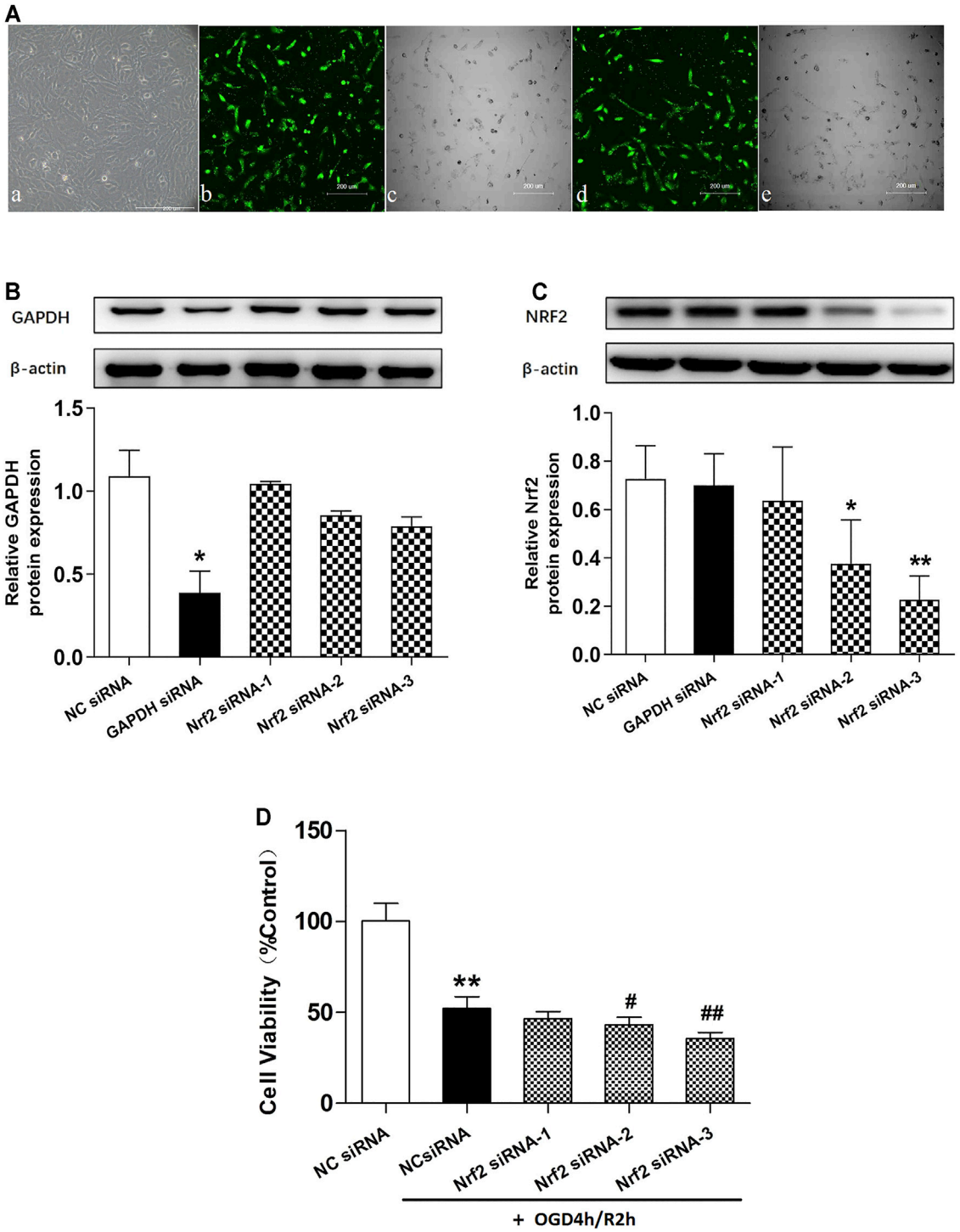

FIGURE 6 | Effects of different Nrf2 siRNA interferences on Nrf2 expressions and hCMEC/D3 cell viabilities in OGD/R. **(A)** (a) hCMEC/D3 cells under normal culture condition. (b,c,d,e) Different concentrations of the negative control siRNA labeled with green fluorescence were applied to hCMEC/D3 cells to help optimize the transfection conditions. (b,c) Fluorescence and bright field images of hCMEC/D3 cells treated with 50 nmol/L plasmid. (d,e) Fluorescence and bright field images of hCMEC/D3 cells treated with 100 nmol/L plasmid. Plasmids of the two concentrations showed similar transfection efficiency, while the lower one showed less cell loss; thus, 50 nmol/L was selected as the optimal concentration for transfection and was used in the subsequent experiments. **(B,C)** Western blot assays for expressions of GAPDH and Nrf2 in hCMEC/D3 cells. The cells were transfected with GAPDH siRNA plasmid or Nrf2 siRNA plasmid (Nrf2 siRNA-1, Nrf2 siRNA-2, and Nrf2 siRNA-3); the results showed the expressions of target genes were specifically knocked down by aiming siRNAs, testifying specificities and efficiencies of the siRNAs. Besides, Nrf2 siRNA-3 showed the strongest ability to interfere with the expression of Nrf2. **(D)** Effects of different Nrf2 siRNAs on OGD/R injury of hCMEC/D3 cells. Data are expressed as mean ± SD (n = 3). $^{*}p < 0.05$, $^{**}p < 0.01$ vs. negative control siRNA (NC siRNA); $\#p < 0.05$, $\#\#p < 0.01$ vs. NC siRNA + OGD/R.

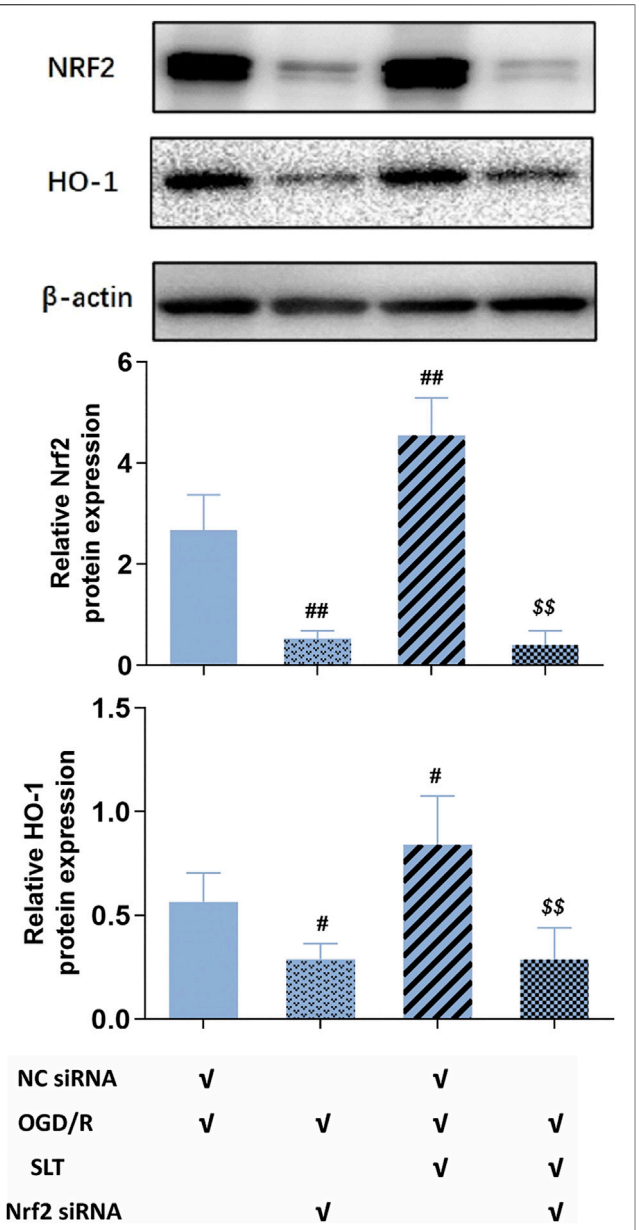

FIGURE 7 | Nrf2 siRNA abrogated activation of SLT on the Nrf2 pathway in cerebral microvascular endothelial cells in OGD/R injury. Data are expressed as mean ± SD ($n = 3$). #$p < 0.05$, ##$p < 0.01$ vs. NC siRNA + OGD/R group; $ $p < 0.05$, $$ $p < 0.01$, vs. NC siRNA + OGD/R + SLT group.

Cerebral ischemia induces a rapid degradation of claudin and occludin, which disrupts the TJ structure and renders the endothelial cells more vulnerable, accelerating their damage (Zhang et al., 2017). These finally result in the collapse of the blood vessel barrier and severe edema in the brain (Sandoval et al., 2008). In contrast, preventing the loss of claudin and occludin can alleviate brain edema and lesions (Takenaga et al., 2009; Stamatovic et al., 2016).

In the present study, the administrations of SLT significantly and dose dependently reduced the infarct size, alleviated neural morphological injuries, and improved neurological functions in rats 24 h after MCAO, indicating that SLT has an explicit protective effect against bran ischemia. Additionally, SLT treatments also significantly decreased the brain water content and elevated the expressions of endothelial TJ proteins including claudin-1 and occludin. This result is in accordance with our previous reports, and further hints that SLT may exert its therapeutic effects on brain ischemia through protection of cerebral vascular endothelial cells (Seto et al., 2017; Fan et al., 2020).

Cerebral microvascular endothelium is highly vulnerable to oxidative stress. It has been suggested that the disruptions of blood vascular endothelial TJs and endothelial cell damage in brain infarction are all closely related to peroxidation (Musch et al., 2006; Freeman et al., 2012).

Oxidative stress refers to a relative surplus of ROS, which is a sort of oxygen molecule derivatives having an extremely vivacious oxidative activity and mainly includes super oxygen anions, hydroxyl radicals, and hydrogen peroxides. The origin of ROS in endothelial cells includes the mitochondrial electronic transition chain, the cytoplasm hypoxanthine–xanthine oxidase system, and NAPDH oxidase system (Fraser et al., 2011). Usually, super oxygen anions are first generated, and are then soon metabolized into hydroxyl radicals and hydrogen peroxides, which even have more strong oxidative abilities.

The targets of ROS are mainly biological macromolecules including DNA in the nucleus and in the mitochondria, cytomembrane lipids, and proteins. ROS break their unsaturated links, leading to severe abnormalities in their structures and functions, which further cause disorders in cellular signal transductions and organelle functions; even generate cessation in pivotal physiological procedures such as energy metabolism, cellular structure repairs, and eliminations of damaged organelles; and finally result in cell degenerations, even cell death (Olmez et al., 2012).

The Nrf2 pathway is the major antioxidation system in most cell types, including vascular endothelial cells. Nrf2 is a nuclear transcription factor; however, in the quiescent state, most of which are detained in the cytoplasm and faced to ubiquitin-mediated degradation (Itoh et al., 1999). Upon oxidative assaults, Nrf2 is released, then translocates into the nucleus, and combines with DNA, promoting the transcriptions of a series of antioxidative genes including HO-1, SOD, and GST-1 (Otterbein et al., 2000; Harvey et al., 2009). HO-1 catalyzes the generation of carbon monoxide, which has strong reduction ability; SOD degrades super oxygen anions; and GST-1 promotes the generation of GSH, which is a powerful and broad-spectrum ROS scavenger. Thus, with these potent downstream effectors, the Nrf2 pathway exerts an efficient elimination on free radicals, making a mighty counterattack to the oxidation assault.

However, interestingly, this passive defense system can play active roles in some conditions. In the ischemia preconditioning, small amount ROS generated from a transient ischemia-reperfusion can activate the Nrf2 pathway, endowing the cells strong antioxidation ability to confront the following severe ischemia challenge (Nguyen et al., 2009; Zhang et al., 2017). Another example is the preconditioning-like effects elicited by some chemicals, which have strong redox activities and can liberate

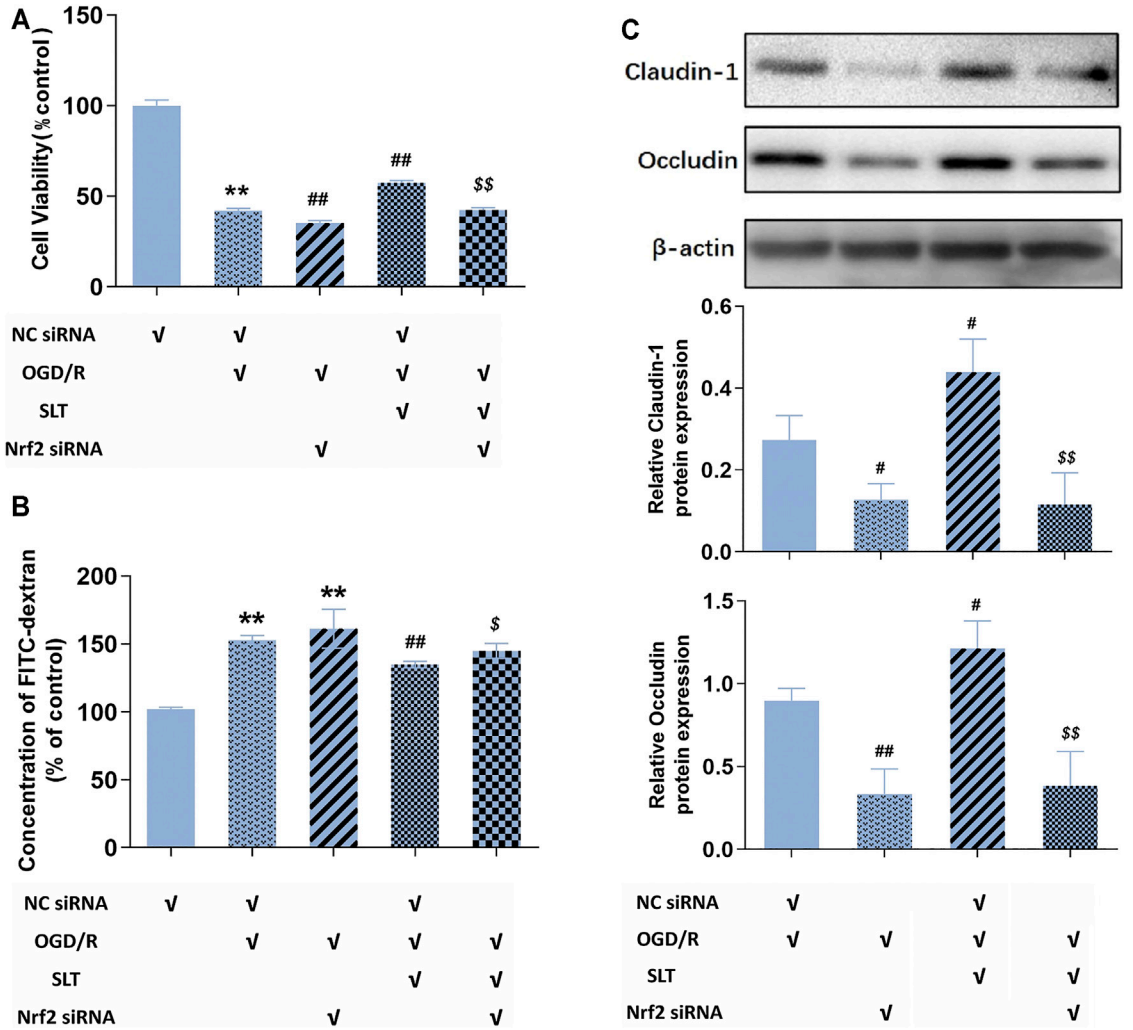

FIGURE 8 | Blocking of the Nrf2 pathway ablated SLT's protection against OGD/R injury in cerebral microvascular endothelial cells. **(A,B)** Effects Nrf2 siRNA interference on SLT's ameliorations on cell viabilities and FITC-dextran permeabilities in OGD/R-injured hCMEC/D3 cells ($n = 6$). **(C)** Effects of Nrf2 siRNA interference with SLT's ameliorations on claudin-1 and occludin expressions in OGD/R-injured hCMEC/D3 cells ($n = 3$). Data are expressed as mean ± SD. *$p < 0.05$, **$p < 0.01$, vs. negative control siRNA (NC siRNA) group; #$p < 0.05$, ##$p < 0.01$, vs. NC siRNA + OGD/R group; $ $p < 0.05$, $$ $p < 0.01$, vs. NC siRNA + OGD/R + SLT group.

Nrf2 in the similar way with ROS (Ashabi et al., 2015; Ding et al., 2015). Many natural substances have this effect, such as some dietary phytochemicals including epicatechin, catechin, quercetin, and kaempferol; more importantly, numerous Chinese herbal ingredients are also included, among which the famous ones comprise salviolic acids, ligustrazine, and luteolin. Thus, the Nrf2 pathway forms a bridge for natural compounds to exert the physical modulatory effects (Alfieri et al., 2013; Hu et al., 2018; Li et al., 2018; Farkhondeh et al., 2019; Yamagata et al., 2020).

In consideration of the key role of peroxidation in vascular endothelium damage in ischemia and the key role of Nrf2 in antioxidation, we next investigated the role of the Nrf2 pathway in SLT's endothelial protective effects. In *in vivo* experiments, SLT treatments significantly elevated the function of Nrf2 in the brain infarction; accordingly, the expression of HO-1, activity of SOD, and content of GSH in the brain were all increased by SLT, indicating the downstreams of Nrf2 were activated. Notably, the immunochemistry examination positioned this Nrf2 pathway activation to cerebral vascular endothelial cells. These data preliminarily demonstrate the central role of the Nrf2 pathway in SLT's vascular endothelium protection.

To obtain the direct evidence, we performed an *in vitro* experiment. We selected hCMEC/D3, a human brain microvascular endothelial cell line as the experimental material. Interestingly, this cell line was found to express claudin-1 as one of the most dominant claudin subtypes, which is similar to the situation of *in vivo* brain vascular endothelial cells (Bederson et al., 1986; Brouns et al., 2009; Andjelkovic et al., 2019). And we selected the OGD/R model in which the cells are incubated with glucose-free medium in an anoxia circumstance to simulate ischemia *in vivo* and are then returned to normal medium and circumstance to simulate reperfusion.

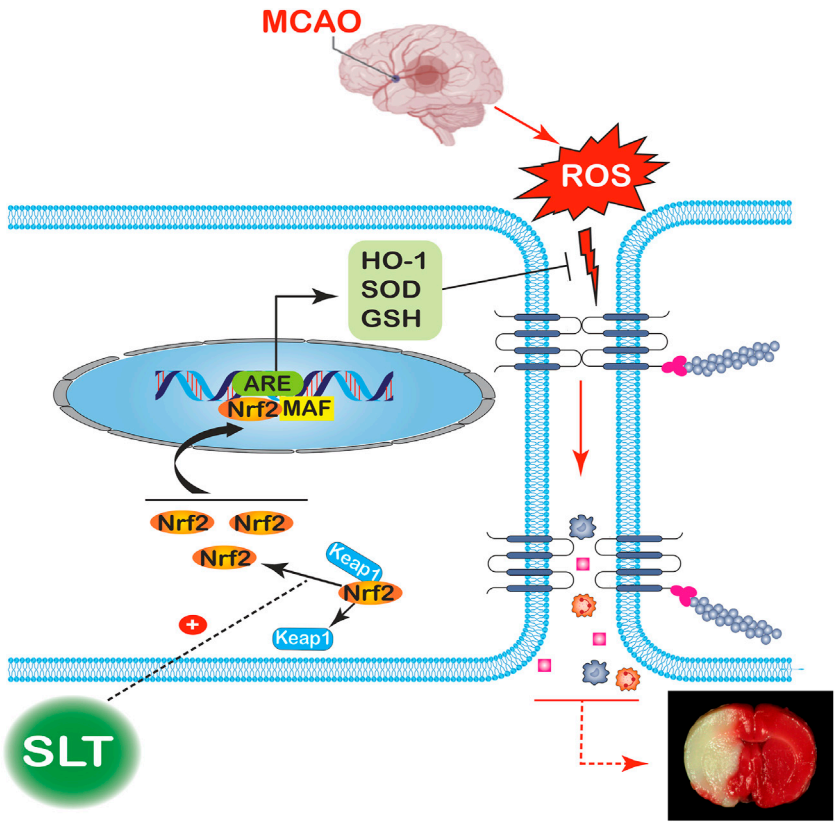

FIGURE 9 | Putative mechanism for the therapeutic effect of SLT on brain ischemia. Occlusions in the cerebral arteries induce a drastic elevation in ROS contents; the excess ROS severely disrupts the brain blood barriers, leading to serious leakages from the blood vessels and brain edema, finally resulting in an infarction of large volume. SLT dramatically releases Nrf2 detained in the cytoplasm and promotes its nucleus translocation, thus priming the downstream transcriptions and increasing the contents of HO-1, SOD, and GSH, which then lead to massive elimination of ROS, cutting off the injury cascade and finally rescuing the brain from ischemia.

At first, SLT significantly inhibited OGD/R-induced drop in viabilities of hCMEC/D3 cells, confirming its direct protective effects on brain vascular endothelial cells against ischemia. Moreover, the Nrf2 pathway was also activated in hCMEC/D3 cells by SLT treatments, further revealing the relationship between Nrf2 pathway and SLT's therapeutic effects. Last, we used siRNA to block the function of Nrf2, and expectedly, the protective effects of SLT on hCMEC/D3 cells against OGD/R injury were all diminished, conclusively confirming the obligatory role of the Nrf2 pathway in SLT's protection on the brain vascular endothelium. Furthermore, combining the results of *in vivo* and *in vitro* experiments, it can be inferred that the Nrf2 pathway–dependent protection on cerebral microvascular endothelial cells underlies the therapeutic effect of SLT on brain ischemia (the putative mechanism of SLT's anti-brain ischemia effect is shown in **Figure 9**).

However, as a redox active drug, SLT also has the ability to directly scavenge ROS, then does this activity play a role in SLT's effects? As shown in our experiment results, the knockdown of Nrf2 expression resulted in a nearly total ablation in SLT's protective effects on hCMEC/D3 cells; thus, it indicates that the direct antioxidation effect of SLT does not make a significant contribution to its vascular endothelium protection in brain ischemia.

At last, an interesting issue should be discussed. SLT has multiple ingredients, then which exert this Nrf2-dependent therapeutic effect? The main ingredients of SLT include ginsenosides, flavones, ginkgolides, and crocin. Although, according to the published studies, all of them have active redox characteristics and the potential to activate Nrf2, there exist differences in their activities. Flavones and crocin possessed the strongest redox activities, which are far more than that of the others (Ma et al., 2012; Barbagallo et al., 2013). Additionally, their amounts occupy nearly a half of that of SLT's main active ingredients. Thus, the flavones and crocin in SLT seem to be associated most with the Nrf2-dependent endothelium protection. However, what are the exact roles of SLT's ingredients in its therapy, and what are the relationships between them, simple additive relation, or synergic relation, or even antagonistic relation, need to be further studied in the future.

This study also has some limitations. In *in vitro* experiments, we used a monoculture of brain microvascular endothelial cells (BMECs). Although BMECs are a major and key component of the BBB, they are not the only one as astrocytes and pericytes also participate in the constitution of the BBB (Rahman NA et al., 2016). Thus, to further understand the effects of SLT on the BBB, an *in vitro* coculture model of BMECs with astrocytes or pericytes may

be necessary. We consider performing related experiments in the future studies.

In conclusion, data of this study suggest that SLT's prevention against brain ischemia is related to its protection on the cerebral vascular endothelial cells, which is dependent on the activation of the Nrf2 antioxidation pathway.

DATA AVAILABILITY STATEMENT

The original contributions presented in the study are included in the article; further inquiries can be directed to the corresponding authors.

ETHICS STATEMENT

The animal study was reviewed and approved by Xi Yuan Hospital of China Academy of Chinese Medical Sciences (Protocol No. 2019XLC015-2).

AUTHOR CONTRIBUTIONS

X-DF, LX, and J-XL conceived and coordinated the study. X-DF and PL designed the experiments and wrote the paper. All authors performed the experiments *in vitro* and *in vivo*. X-DF, BY, and G-RW analyzed the data. X-DF and PL reviewed and edited the manuscript. All authors read and approved the final manuscript.

FUNDING

This work was supported by the Beijing Natural Science Foundation (7194314), MiaoPu Funding of Xiyuan Hospital (2019XYMP-11), National Science and Technology Major Projects (2018ZX09737-009), and the National Natural Science Foundation of China (81973594,82104444).

ACKNOWLEDGMENTS

The authors acknowledge the Department of Pathology of Xiyuan Hospital, China Academy of Chinese Medical Science for providing helpful advice.

SUPPLEMENTARY MATERIAL

The Supplementary Material for this article can be found online at: https://www.frontiersin.org/articles/10.3389/fphar.2021.748568/full#supplementary-material

REFERENCES

Abbott, N. J., Rönnbäck, L., and Hansson, E. (2006). Astrocyte-endothelial Interactions at the Blood-Brain Barrier. *Nat. Rev. Neurosci.* 7 (1), 41–53. doi:10.1038/nrn1824

Alfieri, A., Srivastava, S., Siow, R. C. M., Cash, D., Modo, M., Duchen, M. R., et al. (2013). Sulforaphane Preconditioning of the Nrf2/HO-1 Defense Pathway Protects the Cerebral Vasculature against Blood-Brain Barrier Disruption and Neurological Deficits in Stroke. *Free Radic. Biol. Med.* 65, 1012–1022. doi:10.1016/j.freeradbiomed.2013.08.190

Andjelkovic, A. V., Xiang, J., Stamatovic, S. M., Hua, Y., Xi, G., Wang, M. M., et al. (2019). Endothelial Targets in Stroke: Translating Animal Models to Human. *Arterioscler Thromb. Vasc. Biol.* 39 (11), 2240–2247. doi:10.1161/ATVBAHA.119.312816

Ashabi, G., Khalaj, L., Khodagholi, F., Goudarzvand, M., and Sarkaki, A. (2015). Pre-treatment with Metformin Activates Nrf2 Antioxidant Pathways and Inhibits Inflammatory Responses through Induction of AMPK after Transient Global Cerebral Ischemia. *Metab. Brain Dis.* 30 (3), 747–754. doi:10.1007/s11011-014-9632-2

Barbagallo, I., Galvano, F., Frigiola, A., Cappello, F., Riccioni, G., Murabito, P., et al. (2013). Potential Therapeutic Effects of Natural Heme Oxygenase-1 Inducers in Cardiovascular Diseases. *Antioxid. Redox Signal.* 18 (5), 507–521. doi:10.1089/ars.2011.4360

Bazzoni, G., and Dejana, E. (2004). Endothelial Cell-To-Cell Junctions: Molecular Organization and Role in Vascular Homeostasis. *Physiol. Rev.* 84 (3), 869–901. doi:10.1152/physrev.00035.2003

Bederson, J. B., Pitts, L. H., Tsuji, M., Nishimura, M. C., Davis, R. L., and Bartkowski, H. (1986). Rat Middle Cerebral Artery Occlusion: Evaluation of the Model and Development of a Neurologic Examination. *Stroke* 17 (3), 472–476. doi:10.1161/01.str.17.3.472

Berndt, P., Winkler, L., Cording, J., Breitkreuz-Korff, O., Rex, A., Dithmer, S., et al. (2019). Tight junction Proteins at the Blood-Brain Barrier: Far More Than Claudin-5. *Cell Mol Life Sci.* 76 (10), 1987–2002. doi:10.1007/s00018-019-03030-7

Brouns, R., and De Deyn, P. P. (2009). The Complexity of Neurobiological Processes in Acute Ischemic Stroke. *Clin. Neurol. Neurosurg.* 111 (6), 483–495. doi:10.1016/j.clineuro.2009.04.001

Chen, H., He, Y., Chen, S., Qi, S., and Shen, J. (2020). Therapeutic Targets of Oxidative/nitrosative Stress and Neuroinflammation in Ischemic Stroke: Applications for Natural Product Efficacy with Omics and Systemic Biology. *Pharmacol. Res.* 158, 104877. doi:10.1016/j.phrs.2020.104877

Ding, Y., Chen, M., Wang, M., Li, Y., and Wen, A. (2015). Posttreatment with 11-Keto-β-Boswellic Acid Ameliorates Cerebral Ischemia-Reperfusion Injury: Nrf2/HO-1 Pathway as a Potential Mechanism. *Mol. Neurobiol.* 52 (3), 1430–1439. doi:10.1007/s12035-014-8929-9

Donnan, G. A., Fisher, M., Macleod, M., and Davis, S. M. (2008). Stroke. *The Lancet* 371, 1612–1623. doi:10.1016/s0140-6736(08)60694-7

Fan, X., Yao, M., Li, P., and Xu, L. (2020). Sailuotong Improves OGD/R Induced Injury of Brain Microvascular Endothelial Cells by Up-Regulating Nrf2/HO-1 Signaling Pathway. *Chin. Pharmacol. Bull.* 36 (07), 1018–1023. doi:10.3969/j.issn.1001-1978.2020.07.023

Farkhondeh, T., Yazdi, H. S., and Samarghandian, S. (2019). The Protective Effects of Green Tea Catechins in the Management of Neurodegenerative Diseases: A Review. *Curr. Drug Discov. Technol.* 16 (1), 57–65. doi:10.2174/1570163815666180219115453

Fraser, P. A. (2011). The Role of Free Radical Generation in Increasing Cerebrovascular Permeability. *Free Radic. Biol. Med.* 51 (5), 967–977. doi:10.1016/j.freeradbiomed.2011.06.003

Freeman, L. R., and Keller, J. N. (2012). Oxidative Stress and Cerebral Endothelial Cells: Regulation of the Blood-Brain-Barrier and Antioxidant Based Interventions. *Biochim. Biophys. Acta* 1822, 822–829. doi:10.1016/j.bbadis.2011.12.009

Furuse, M., Hata, M., Furuse, K., Yoshida, Y., Haratake, A., Sugitani, Y., et al. (2002). Claudin-based Tight Junctions Are Crucial for the Mammalian Epidermal Barrier: a Lesson from Claudin-1-Deficient Mice. *J. Cel Biol.* 156 (6), 1099–1111. doi:10.1083/jcb.200110122

Harvey, C. J., Thimmulappa, R. K., Singh, A., Blake, D. J., Ling, G., Wakabayashi, N., et al. (2009). Nrf2-regulated Glutathione Recycling Independent of Biosynthesis Is Critical for Cell Survival during Oxidative Stress. *Free Radic. Biol. Med.* 46 (4), 443–453. doi:10.1016/j.freeradbiomed.2008.10.040

Hu, S., Wu, Y., Zhao, B., Hu, H., Zhu, B., Sun, Z., et al. (2018). Panax Notoginseng Saponins Protect Cerebral Microvascular Endothelial Cells against Oxygen-Glucose Deprivation/Reperfusion-Induced Barrier Dysfunction via Activation of PI3K/Akt/Nrf2 Antioxidant Signaling Pathway. *Molecules* 23 (11), 2781. doi:10.3390/molecules23112781

Itoh, K., Wakabayashi, N., Katoh, Y., Ishii, T., Igarashi, K., Engel, J. D., et al. (1999). Keap1 Represses Nuclear Activation of Antioxidant Responsive Elements by Nrf2 through Binding to the Amino-Terminal Neh2 Domain. *Genes Dev.* 13 (1), 76–86. doi:10.1101/gad.13.1.76

Jia, J., Wei, C., Chen, S., Li, F., Tang, Y., Qin, W., et al. (2018). Efficacy and Safety of the Compound Chinese Medicine SaiLuoTong in Vascular Dementia: A Randomized Clinical Trial. *Alzheimers Dement (N Y)* 4, 108–117. doi:10.1016/j.trci.2018.02.004

Jiao, H., Wang, Z., Liu, P., Wang, P., and Xue, Y. (2011). Specific Role of Tight junction Proteins Claudin-5, Occludin, and ZO-1 of the Blood-Brain Barrier in a Focal Cerebral Ischemic Insult. *J. Mol. Neurosci.* 44 (2), 130–139. doi:10.1007/s12031-011-9496-4

Kuźma, E., Lourida, I., Moore, S. F., Levine, D. A., Ukoumunne, O. C., and Llewellyn, D. J. (2018). Stroke and Dementia Risk: A Systematic Review and Meta-Analysis. *Alzheimers Dement* 14 (11), 1416–1426. doi:10.1016/j.jalz.2018.06.3061

Li, C., Wang, R., Hu, C., Wang, H., Ma, Q., Chen, S., et al. (2018). Pyridoxine Exerts Antioxidant Effects in Cell Model of Alzheimer's Disease via the Nrf-2/HO-1 Pathway. *Cel Mol Biol (Noisy-le-grand)* 64, 119–124. doi:10.14715/cmb/2018.64.10.19

Li, H., Wang, P., Huang, F., Jin, J., Wu, H., Zhang, B., et al. (2018). Astragaloside IV Protects Blood-Brain Barrier Integrity from LPS-Induced Disruption via Activating Nrf2 Antioxidant Signaling Pathway in Mice. *Toxicol. Appl. Pharmacol.* 340, 58–66. doi:10.1016/j.taap.2017.12.019

Li, T., Wang, H., Ding, Y., Zhou, M., Zhou, X., Zhang, X., et al. (2014). Genetic Elimination of Nrf2 Aggravates Secondary Complications except for Vasospasm after Experimental Subarachnoid Hemorrhage in Mice. *Brain Res.* 1558, 90–99. doi:10.1016/j.brainres.2014.02.036

Liu, J., Jiang, Y., Zhang, G., Lin, Z., and Du, S. (2019). Protective Effect of Edaravone on Blood-Brain Barrier by Affecting NRF-2/HO-1 Signaling Pathway. *Exp. Ther. Med.* 18 (4), 2437–2442. doi:10.3892/etm.2019.7859

Loboda, A., Damulewicz, M., Pyza, E., Jozkowicz, A., and Dulak, J. (2016). Role of Nrf2/HO-1 System in Development, Oxidative Stress Response and Diseases: an Evolutionarily Conserved Mechanism. *Cel Mol Life Sci.* 73 (17), 3221–3247. doi:10.1007/s00018-016-2223-0

Ma, Q., and He, X. (2012). Molecular Basis of Electrophilic and Oxidative Defense: Promises and Perils of Nrf2. *Pharmacol. Rev.* 64 (4), 1055–1081. doi:10.1124/pr.110.004333

Musch, M. W., Walsh-Reitz, M. M., and Chang, E. B. (2006). Roles of ZO-1, Occludin, and Actin in Oxidant-Induced Barrier Disruption. *Am. J. Physiol. Gastrointest. Liver Physiol.* 290 (2), G222–G231. doi:10.1152/ajpgi.00301.2005

Nguyen, T., Nioi, P., and Pickett, C. B. (2009). The Nrf2-Antioxidant Response Element Signaling Pathway and its Activation by Oxidative Stress. *J. Biol. Chem.* 284 (20), 13291–13295. doi:10.1074/jbc.R900010200

Obermeier, B., Daneman, R., and Ransohoff, R. M. (2013). Development, Maintenance and Disruption of the Blood-Brain Barrier. *Nat. Med.* 19 (12), 1584–1596. doi:10.1038/nm.3407

Olmez, I., and Ozyurt, H. (2012). Reactive Oxygen Species and Ischemic Cerebrovascular Disease. *Neurochem. Int.* 60 (2), 208–212. doi:10.1016/j.neuint.2011.11.009

Otterbein, L. E., and Choi, A. M. (2000). Heme Oxygenase: Colors of Defense against Cellular Stress. *Am. J. Physiol. Lung Cel Mol Physiol.* 279 (6), L1029–L1037. doi:10.1152/ajplung.2000.279.6.L1029

Rahimi, N. (2017). Defenders and Challengers of Endothelial Barrier Function. *Front. Immunol.* 8, 1847. doi:10.3389/fimmu.2017.01847

Rahman, N. A., Rasil, A. N. H. M., Meyding-Lamade, U., Craemer, E. M., Diah, S., Tuah, A. A., et al. (2016). Immortalized Endothelial Cell Lines for *In Vitro* Blood-Brain Barrier Models: A Systematic Review. *Brain Res.* 1642, 532–545. doi:10.1016/j.brainres.2016.04.024

Sandoval, K. E., and Witt, K. A. (2008). Blood-brain Barrier Tight junction Permeability and Ischemic Stroke. *Neurobiol. Dis.* 32 (2), 200–219. doi:10.1016/j.nbd.2008.08.005

Seto, S. W., Chang, D., Ko, W. M., Zhou, X., Kiat, H., Bensoussan, A., et al. (2017). Sailuotong Prevents Hydrogen Peroxide (H_2O_2)-Induced Injury in EA.Hy926 Cells. *Int. J. Mol. Sci.* 18 (1), 95. doi:10.3390/ijms18010095

Sladojevic, N., Stamatovic, S. M., Johnson, A. M., Choi, J., Hu, A., Dithmer, S., et al. (2019). Claudin-1-Dependent Destabilization of the Blood-Brain Barrier in Chronic Stroke. *J. Neurosci.* 39 (4), 743–757. doi:10.1523/JNEUROSCI.1432-18.2018

Stamatovic, S. M., Johnson, A. M., Keep, R. F., and Andjelkovic, A. V. (2016). Junctional Proteins of the Blood-Brain Barrier: New Insights into Function and Dysfunction. *Tissue Barriers* 4 (1), e1154641. doi:10.1080/21688370.2016.1154641

Steiner, G. Z., Bensoussan, A., Liu, J., Hohenberg, M. I., and Chang, D. H. (2018). Study Protocol for a Randomised, Double-Blind, Placebo-Controlled 12-week Pilot Phase II Trial of Sailuotong (SLT) for Cognitive Function in Older Adults with Mild Cognitive Impairment. *Trials* 19 (1), 522. doi:10.1186/s13063-018-2912-0

Takenaga, Y., Takagi, N., Murotomi, K., Tanonaka, K., and Takeo, S. (2009). Inhibition of Src Activity Decreases Tyrosine Phosphorylation of Occludin in Brain Capillaries and Attenuates Increase in Permeability of the Blood-Brain Barrier after Transient Focal Cerebral Ischemia. *J. Cereb. Blood Flow Metab.* 29, 1099–1108. doi:10.1038/jcbfm.2009.30

Wang, W., Wang, X., Zhang, X. S., and Liang, C. Z. (2018). Cryptotanshinone Attenuates Oxidative Stress and Inflammation through the Regulation of Nrf-2 and NF-Kb in Mice with Unilateral Ureteral Obstruction. *Basic Clin. Pharmacol. Toxicol.* 123, 714–720. doi:10.1111/bcpt.13091

Xu, L., Liu, J. X., Cong, W. H., and Wei, C. E. (2008). Effects of Weinaokang Capsule on Intracephalic Cholinergic System and Capability of Scavenging Free Radicas in Chronic Cerebral Hypoperfusion Rats. *Zhongguo Zhong Yao Za Zhi* 33 (5), 531–534.

Yamagata, K. (2020). Protective Effect of Epigallocatechin Gallate on Endothelial Disorders in Atherosclerosis. *J. Cardiovasc. Pharmacol.* 75 (4), 292–298. doi:10.1097/FJC.0000000000000792

Zhang, R., Xu, M., Wang, Y., Xie, F., Zhang, G., and Qin, X. (2017). Nrf2-a Promising Therapeutic Target for Defensing against Oxidative Stress in Stroke. *Mol. Neurobiol.* 54, 6006–6017. doi:10.1007/s12035-016-0111-0

Zhang, X., Fan, Z., and Jin, T. (2017). Crocin Protects against Cerebral- Ischemia-Induced Damage in Aged Rats through Maintaining the Integrity of Blood-Brain Barrier. *Restor Neurol. Neurosci.* 35 (1), 65–75. doi:10.3233/RNN-160696

Zhang, Y., Liu, J., Yao, M., Song, W., Zheng, Y., Xu, L., et al. (2019). Sailuotong Capsule Prevents the Cerebral Ischaemia-Induced Neuroinflammation and Impairment of Recognition Memory through Inhibition of LCN2 Expression. *Oxid Med. Cel Longev.* 2019, 8416105. doi:10.1155/2019/8416105

Zhang, Y., Li, X., Qiao, S., Yang, D., Li, Z., Xu, J., et al. (2020). Occludin Degradation Makes Brain Microvascular Endothelial Cells More Vulnerable to Reperfusion Injury *In Vitro*. *J. Neurochem.* 156, 352–366. doi:10.1111/jnc.15102

Zhao, J., Moore, A. N., Redell, J. B., and Dash, P. K. (2007). Enhancing Expression of Nrf2-Driven Genes Protects the Blood Brain Barrier after Brain Injury. *J. Neurosci.* 27 (38), 10240–10248. doi:10.1523/JNEUROSCI.1683-07.2007

Conflict of Interest: The authors declare that the research was conducted in the absence of any commercial or financial relationships that could be construed as a potential conflict of interest.

Publisher's Note: All claims expressed in this article are solely those of the authors and do not necessarily represent those of their affiliated organizations, or those of the publisher, the editors, and the reviewers. Any product that may be evaluated in this article, or claim that may be made by its manufacturer, is not guaranteed or endorsed by the publisher.

frontiers in Pharmacology

ORIGINAL RESEARCH
published: 08 November 2021
doi: 10.3389/fphar.2021.749915

Anticonstriction Effect of MCA in Rats by Danggui Buxue Decoction

Ying Guo[1,2], Yating Zhang[3], Ya Hou[3], Pengmei Guo[4], Xiaobo Wang[4], Sanyin Zhang[4,5]* and Peng Yang[2]**

[1]School of Basic Medical College, Chengdu University of Traditional Chinese Medicine, Chengdu, China, [2]Chengdu Fifth People's Hospital, Chengdu, China, [3]School of Pharmacy, Chengdu University of Traditional Chinese Medicine, Chengdu, China, [4]State Key Laboratory of Southwestern Chinese Medicine Resources, Innovative Institute of Chinese Medicine and Pharmacy, Chengdu University of Traditional Chinese Medicine, Chengdu, China, [5]Chengdu Integrated TCM and Western Medicine Hospital, Chengdu, China

Objective: Danggui Buxue decoction (DBD), consisting of Angelicae Sinensis Radix (ASR) and Astragali Radix (AR), is a famous prescription with the function of antivasoconstriction. This study intends to probe its mechanisms on the relaxation of the middle cerebral artery (MCA).

Methods: Vascular tension of rat MCA was measured using a DMT620 M system. First, the identical series of concentrations of DBD, ASR, and AR were added into resting KCl and U46619 preconstricted MCA. According to the compatibility ratio, their dilatation effects were further investigated on KCl and U46619 preconstricted vessels. Third, four K^+ channel blockers were employed to probe the vasodilator mechanism on KCl-contracted MCA. We finally examined the effects of DBD, ASR, and AR on the vascular tone of U46619-contracted MCA in the presence or absence of Ca^{2+}.

Results: Data suggested that DBD, ASR, and AR can relax on KCl and U46619 precontracted MCA with no effects on resting vessels. The vasodilator effect of ASR was greater than those of DBD and AR on KCl-contracted MCA. For U46619-contracted MCA, ASR showed a stronger vasodilator effect than DBD and AR at low concentrations, but DBD was stronger than ASR at high concentrations. Amazingly, the vasodilator effect of DBD was stronger than that of AR at all concentrations on two vasoconstrictors which evoked MCA. The vasodilator effect of ASR was superior to that of DBD at a compatibility ratio on KCl-contracted MCA at low concentrations, while being inferior to DBD at high concentrations. However, DBD exceeded AR in vasodilating MCA at all concentrations. For U46619-constricted MCA, DBD, ASR, and AR had almost identical vasodilation. The dilation of DBD and AR on KCl-contracted MCA was independent of K^+ channel blockers. However, ASR may inhibit the K^+ channel opening partially through synergistic interactions with Gli and $BaCl_2$. DBD, ASR, and AR may be responsible for inhibiting $[Ca^{2+}]_{out}$, while ASR and AR can also inhibit $[Ca^{2+}]_{in}$.

OPEN ACCESS

Edited by:
Qilong Wang,
Tianjin University of Traditional Chinese Medicine, China

Reviewed by:
Bin Wu,
Chongqing Hospital of Traditional Chinese Medicine, China
Mun Fei Yam,
Universiti Sains Malaysia (USM), Malaysia

****Correspondence:***
Peng Yang
tcmzsy@126.com
Sanyin Zhang
tcmzsy@cdutcm.edu.cn
Xiaobo Wang
VitaDrwang@cdutcm.edu.cn

Specialty section:
This article was submitted to Cardiovascular and Smooth Muscle Pharmacology, a section of the journal Frontiers in Pharmacology

Received: *30 July 2021*
Accepted: *29 September 2021*
Published: *08 November 2021*

Citation:
Guo Y, Zhang Y, Hou Y, Guo P, Wang X, Zhang S and Yang P (2021) Anticonstriction Effect of MCA in Rats by Danggui Buxue Decoction. Front. Pharmacol. 12:749915. doi: 10.3389/fphar.2021.749915

Abbreviations: 4-AP, 4-aminopyridine; AR, Astragali Radix; ASR, Angelicae Sinensis Radix; DBD, Danggui Buxue decoction; EGTA, ethylene glycol-bis (2-aminoethylether)-N, N, N′, N′-tetraacetic acid; Gli, glyburide; MCA, middle cerebral artery; TCM, traditional Chinese medicine; TEA, tetraethtylamine; U46619, 9, 11-dideoxy-9α, 11α-methanoepoxy prostaglandin F2α; $[Ca^{2+}]_{in}$, internal Ca^{2+} from organelles; $[Ca^{2+}]_{out}$, influx of extracellular Ca^{2+}.

Conclusion: DBD can relax MCA with no effects on resting vessels. The mechanism may be related to ASR's inhibition of K_{ATP} and K_{ir} channels. Meanwhile, the inhibition of $[Ca^{2+}]_{out}$ by DBD, ASR, and AR as well as the inhibition of $[Ca^{2+}]_{in}$ by ASR and AR may contribute to dilate MCA.

Keywords: Danggui Buxue decoction, middle cerebral artery, vascular tone, K^+ channel, Ca^{2+} channel

INTRODUCTION

Vascular diseases with a high fatality rate include cerebrovascular disease, cardiovascular disease, hypertension, and atherosclerosis, causing millions of deaths worldwide every year (George et al., 2015; Cainzos-Achirica et al., 2020). According to the "China Health Statistics Yearbook 2020 (National Health Commission, 2019)," the number of deaths of cerebrovascular diseases in China ranked the third following malignant tumors and heart diseases. As an extension of the internal carotid artery, the middle cerebral artery (MCA) tended to being affected by thromboembolism. Among these, evidence had indicated that MCA damage-evoked cerebral infarction events accounted for more than 80% of all cerebral infarctions (Virani et al., 2021). It was reported that brain disease-involved MCA damages constantly caused abnormal changes in vascular tension, especially abnormal contraction of brain vessels (Garg et al., 2021). It thus directly fluctuated the perfusion pressure and the body's blood supply circulation (Greenstein et al., 2020; Bai et al., 2021). Changes in these factors can lead to the symptoms such as vasospasm, sensory disturbances, and dyskinesia, which in turn result in abnormal changes in vascular tone (Pantoni, 2010; Lee and Lee, 2011; Mehanna and Jankovic, 2013; Krdžić et al., 2015). Also, this vicious circle will eventually be life-threatening.

At present, the main treatment methods for cerebrovascular diseases (such as cerebral hemorrhage, cerebral infarction, and subarachnoid hemorrhage) were surgical treatment and drug treatment (DeBaun et al., 2020; Hernandez Fustes et al., 2020; Sturiale et al., 2020). Of these, there are three main types of conventional drug therapy: 1) antihypertensive and antidiabetic drugs, such as nifedipine, valsartan, and metformin; 2) anticoagulant therapy, such as aspirin and warfarin; 3) symptomatic treatment of cognitive, emotional, and mental disorders, such as memantine hydrochloride, oxiracetam, and clozapine (Jiang et al., 2020; Li T. et al., 2021). However, taking these drugs for a long term was often accompanied by certain liver and kidney damage, gut reaction, perception abnormalities, and perception barriers (Kalantar-Zadeh et al., 2015; Yang et al., 2020).

For thousands of years, Chinese people had used traditional Chinese medicine (TCM) to prevent and treat diseases. TCM scholars had found that different herbs may produce better therapeutic effects according to specific combinations. Danggui Buxue decoction (DBD) was originally derived from *Differentiation on Endogenous* (Neiwaishang Bianhuo Lun,《内外伤辨惑论》), which was written by Gao Li in the Song dynasty (Li et al., 2007; Liu et al., 2021). Also, it was composed of the root of Angelica sinensis (Oliv.) Diels (Danggui or Angelicae Sinensis Radix, ASR), and the root of *Astragalus propinquus* and Schischkin (Huangqi or Astragali Radix, AR) are in the ratio of 1:5. In the view of Chinese medicine, it could achieve the purpose of "generating blood" through the way of "replenishing Qi" to treat medical miscellaneous diseases related to Qi deficiency and blood stasis (Lin et al., 2017). Modern pharmacological research found that the classic DBD had the function of hematopoietic characteristics (Yang et al., 2009; Dou et al., 2020; Shi et al., 2020), heart protection (Hu et al., 2018), immunity regulation (Gao et al., 2006a; Gao et al., 2006b), anti-inflammation (Gong et al., 2017; Li C. Y. et al., 2021), and antifibrosis (Chen et al., 2008; Wang and Liang, 2010; Lv et al., 2012). The origin and function of DBD in TCM are shown in **Figure 1**.

Our research group had found that DBD can promote angiogenesis in rats with myocardial infarction (Hu et al., 2018). In addition, astragaloside IV, a vital component of DBD, could relax the thoracic aorta of rats, and the mechanism involved is related to blocking the Ca^{2+} channel (Hu et al., 2016), which was an important ion channel for the surface of vascular smooth muscles to regulate vascular tension. Experiments have proved that ferulic acid in DBD has the effect of relaxing blood vessels via regulation of the Ca^{2+} channel (Zhou et al., 2017). However, the vasodilator mechanism of DBD remained unclear. Therefore, the purpose of this experiment was to clarify the regulating effect of DBD on vascular tension and to further illustrate whether its vasodilator effect was related to the regulation of K^+ and Ca^{2+} channels.

MATERIALS AND METHODS

Animals

Healthy male Sprague–Dawley (SD) rats weighing 180–220 g were purchased from Da Shuo Biotechnology Co., Ltd. (Chengdu, Sichuan, China). All rats were housed under identical conditions [the temperature at 25 ± 1°C, the air humidity at 50 ± 5%, and artificial illumination for 12 h (light period 7:00–19:00)]. Commercial solid food and tap water were available *ad libitum* to all animals. All the experimental procedures were performed under the guidelines of the Management Committee from Chengdu University of TCM (Chengdu, Sichuan, China) (Record No. 2015–03).

Herbs and Reagents

AR and ASR were purchased from the Affiliated Hospital of Chengdu University of TCM and were identified as authentic medicinal materials by Professor Sanyin Zhang of Chengdu University of TCM, and the medicinal materials meet the inclusion requirements of the 2020 Chinese Pharmacopoeia (Chinese Pharmacopoeia Commission et al., 2020). Tetraethtylamine (TEA, no. 134473), 4-aminopyridine (4-AP, no. 275875), $BaCl_2$ (no. 342920), glyburide (Gli, no. Y0001511), ethylene glycol-bis (2-aminoethylether)-N, N, N′, N′-tetraacetic acid (EGTA,

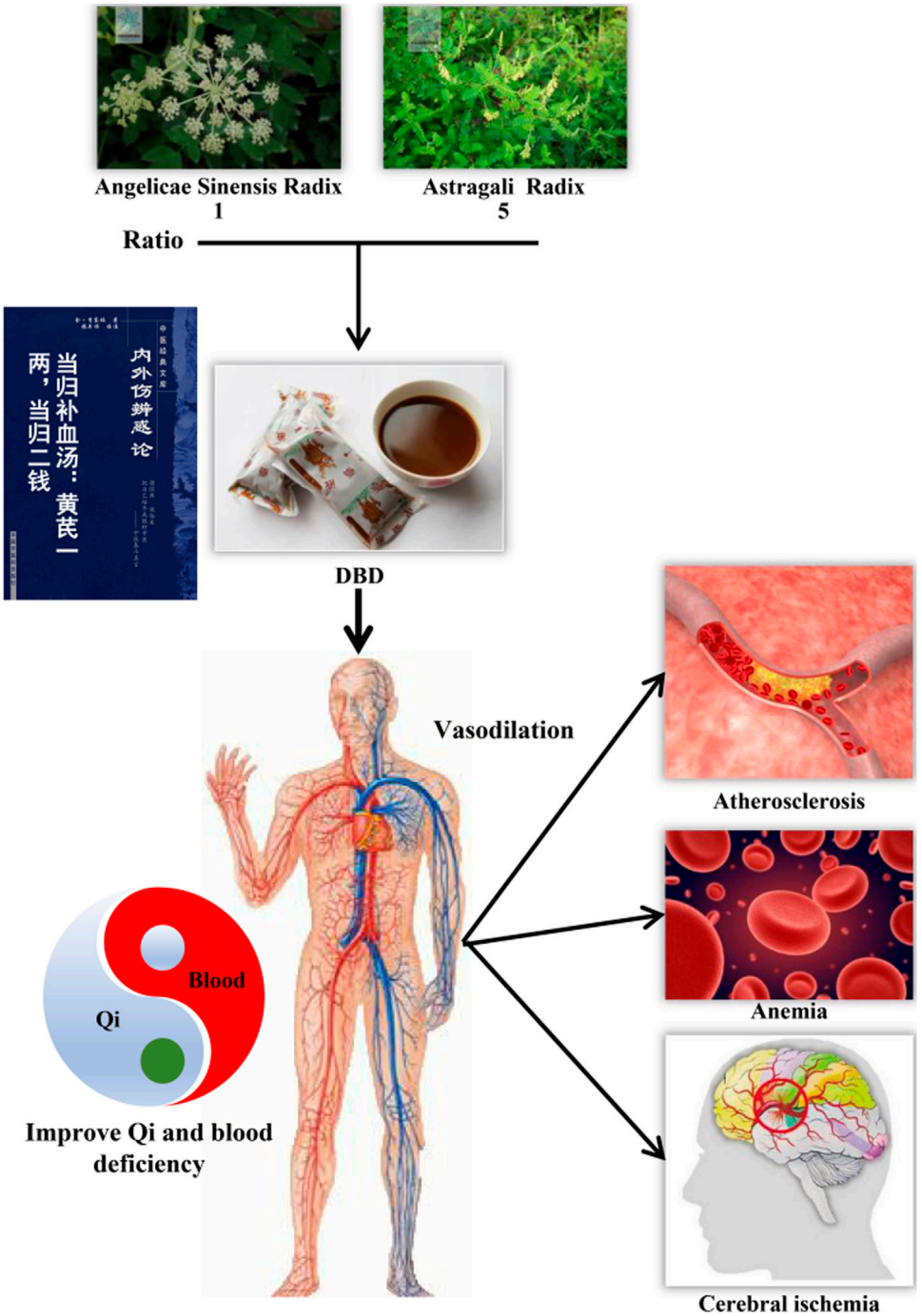

FIGURE 1 | Origin and function of DBD in traditional Chinese medicine. DBD was originally recorded in *Differentiation on Endogenous* (Neiwaishang Bianhuo Lun, 《内外伤辨惑论》), which was composed of AR and ASR in a ratio of 1:5. DBD ameliorated the deficiency of Qi and blood by tonifying Qi and generating blood, thus treating atherosclerosis, anemia, and diseases related to cerebrovascular injuries. AR, Astragali Radix. ASR, Angelicae Sinensis Radix. DBD, Danggui Buxue decoction.

no. E3889), and 9, 11-dideoxy-9α, 11α-methanoepoxy prostaglandin F2α (U46619, no. D8174) were purchased from Sigma. Astragaloside IV (no. wkq16042601) and ferulic acid (no. wkq17022303) were provided by Weikeqi Biological Technology Co., Ltd. Formononetin (no. DST201025-011) and ligustalide (no. DST200610-007) were procured from Lemeitian medicine.

Preparation of Lyophilized Powder

The strict quality control in the preparation of lyophilized powder must be carried out to ensure the consistency of drug quality during the research process. First, AR and ASR were pulverized using a pulverizer (RS-FS1401 grinder, Royalstar, China). Therefore, we accurately weighed ASR and AR according to the ratio of 1: 5. The mixture

with 10 times the volume of distilled water was boiled at 100°C for 1 h, and then, the supernatant was acquired by centrifugation at 5,000 rpm for 10 min. Afterward, the medicinal material precipitation was added with 5 times the volume of distilled water to repeat the above process. The supernatant was placed in a −80°C refrigerator to freeze overnight. Lyophilized powder of DBD was acquired using a freeze dryer (Eyel4 model freeze dryer, physicochemical Tokyo, Japan). Conformably, ASR and AR freeze-dried powders were prepared by the same method described above. These lyophilized powders were stored in the refrigerator at −20°C. Before the experiment, the concentration of lyophilized powder was prepared in 1 g/ml with distilled water. After centrifugation at 5,000 rpm for 10 min, the supernatant was filtered using a 0.22 μm microporous membrane. According to the minimum and maximum concentrations of DBD in dilating the MCA of rats in our pre-experiment (data were not provided), its series concentrations (8, 16, 32, 64, 128, and 256 mg/ml) were set to the following measures of vascular tension.

HPLC Analysis

High-performance liquid mass spectrometry (HPLC, Shimadzu L2030) was employed to determine the contents of astragaloside IV, ferulic acid, formononetin, and ligustalide in lyophilized powder of DBD (Jin et al., 2019). First, 0.1% formic acid–water (aqueous phase) and methanol (organic phase) were used as mobile phases, wherein the total flow rate was set at 1 ml/min with a column temperature of 303 K using a C18 column (Agilent 5 HC-C18). The UV detection wavelengths of the above four standards were set at 201 nm (astragaloside IV), 280 nm (ferulic acid and formononetin), and 338 nm (ligustilide). Afterward, all standards (10–20 mg) were diluted to 1 ml, which was defined as mother liquor. Take a certain amount of mother liquor and dilute it by 3.3, 10, 25, 50, and 100 times and filter and perform HPLC tests. All samples were analyzed three times to obtain the standard curves according to the relationship between peak area and concentration. The yield of the component concentration in DBD was determined by comparison with standard calibration curves.

MCA Vascular Preparation

The PSS liquid (mmol/L: 118 NaCl, 4.7 KCl, 2.5 $CaCl_2$, 1.2 KH_2PO_4, 1.2 $MgCl_2$, 2.5 $NaHCO_3$, 11 glucose, and 5 HEPES) was inflated to the saturation state with 95% O_2 + 5% CO_2 gas before the experiment. After sacrificing by neck removal, the skull of SD rats was stripped and the brain tissue was removed after bloodletting. The brain tissue was then placed in a Petri dish containing the 4°C cold PSS liquid. After washing the excess blood on the brain tissue with the PSS fluid, the MCAs of rats were then dissected and isolated under a light microscope (XTL-2400 optical microscope, Oka, China). The vessels were cut to 2–3 mm and fixed in the DMT 620 M slot with two 20 μm tungsten filaments, and the temperature was maintained at 37°C. After stabilizing for 20 min, the initial tension of MCA with 1.2 mN was acquired via adjusting the tension button gently four times in a row and being stable for 40 min. Then, the vascular activity was examined by constricting twice with the KPSS liquid (mmol/L: 58 NaCl, 60 KCl, 2.5 $CaCl_2$, 1.2 KH_2PO_4, 1.2 $MgCl_2$, 2.5 $NaHCO_3$, 11 glucose, and 5 HEPES), 10 min each time. After each contraction, the vessels were cleaned with the PSS fluid at least three times for 10 min each time to restore the tension as basal tension. The MCA with a vasoconstriction amplitude less than 15% and a vasotension greater than 1 mN between two independent KPSS stimuli was employed for further experiments. The values of vascular tension were recorded by using Labchart Pro professional software v8.3 (ADInstruments, Australia). The effects of all tested drugs at different concentrations on vascular tone were recorded for at least 10 min and repeated five times with different blood vessels.

Measurement for the Tension of DBD, ASR, and AR on Resting Vessels

The well-activated and eligible MCA vessels were used to investigate the effects of DBD, ASR, and AR at the concentrations of 8, 16, 32, 64, 128, and 256 mg/ml.

Measurement for the Tension of DBD, ASR, and AR on KCl Preconstricted Vessels

Referring to the previous method (Hu et al., 2016), the vessels of MCA were constricted with 60 mM KCl. Also, the vascular tension of DBD, ASR, and AR (8, 16, 32, 64, 128, and 256 mg/ml) on the KCl preconstricted MCA was recorded. Parallelly, KCl-constricted MCA vascular tension was also measured by the addition of ASR (1.5, 3, 6, 12, 24, 48 mg/ml) and AR (6.5, 13, 26, 52, 104, and 208 mg/ml), consistent with the DBD compatibility ratio.

Measurement for the Tension of DBD, ASR, and AR on U46619 Preconstricted Vessels

Similarly, another vasoconstrictor U46619 (thromboxane A2 analogue, TXA2; 1 μM) was used to stimulate the MCA contraction (Lv et al., 2014). We further detected the variations in vascular tone by incubation with DBD, ASR, and AR (8, 16, 32, 64, 128, and 256 mg/ml) as well as ASR (1.5, 3, 6, 12, 24, and 48 mg/ml) and AR (6.5, 13, 26, 52, 104, and 208 mg/ml).

The Effect of K^+ Channel Blockers on the Relaxation of DBD, ASR, and AR

Four K^+ channel blockers 4-AP (1×10^{-3} mol/L), $BaCl_2$ (1×10^{-4} mol/L), TEA, and Gli were administered after 60 mM KCl-evoked MCA vasoconstriction. Then, changes in vascular tone were recorded by adding DBD, ASR, and AR (64 mg/ml).

Measurement for the Tension of DBD, ASR, and AR on Surged Ca^{2+} in Cytoplasm-Evoked Vasoconstriction

According to the previous experimental method (Ma et al., 2020), we evaluated the effects of DBD, ASR, and AR on MCA contraction induced by the release of internal Ca^{2+} from organelles such as the endoplasmic reticulum and mitochondria into the cytoplasmic matrix ($[Ca^{2+}]_{in}$). After incubating the MCA vessels with EGTA containing the Ca^{2+}-free PSS fluid for 10 min to remove intracellular Ca^{2+}, the vessels were then administered with the EGTA- and Ca^{2+}-free PSS fluids containing DBD, ASR, and AR (64 mg/ml) for 10 min. Subsequently, 1 μM U46619 was employed to stimulate vasoconstriction and

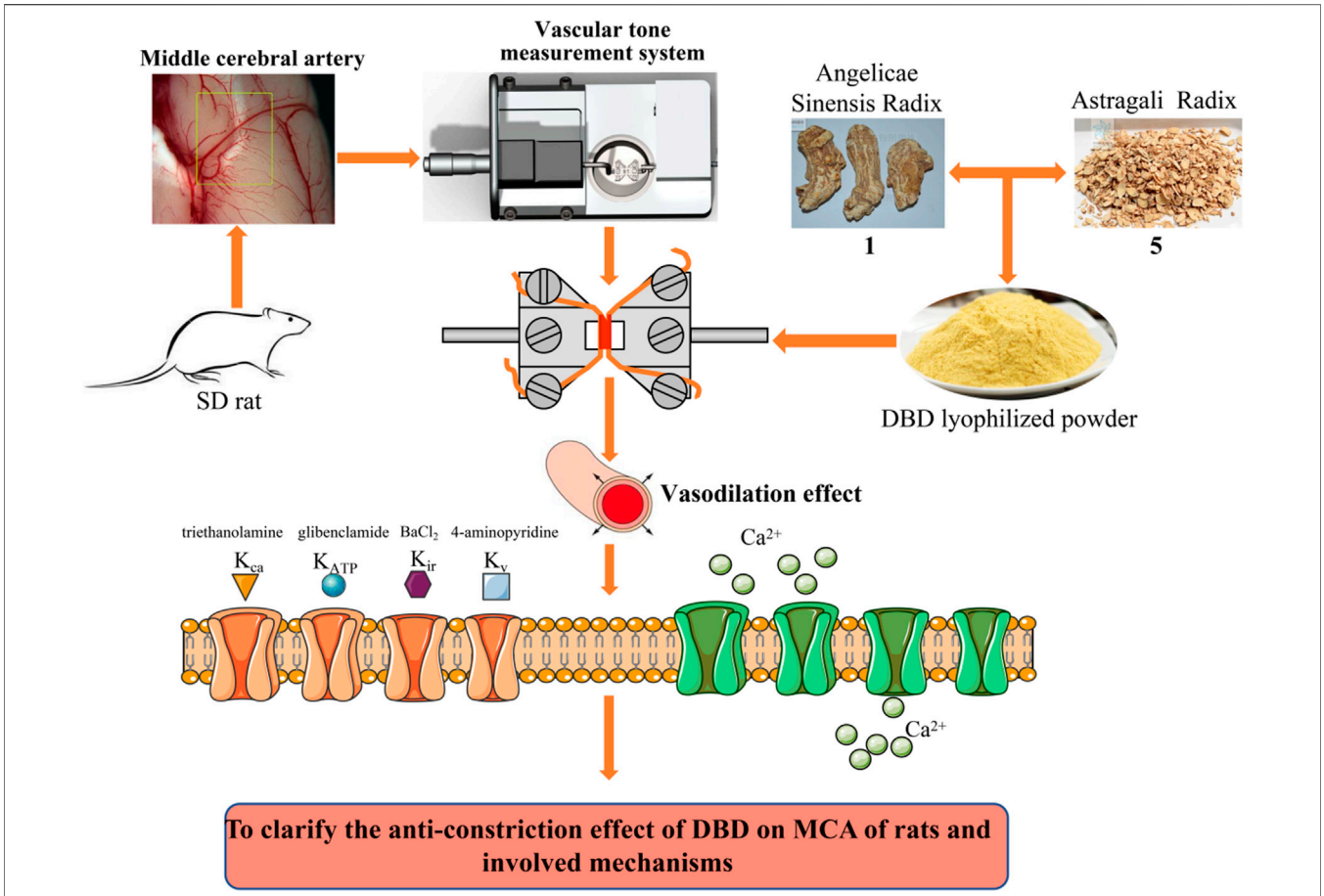

FIGURE 2 | Laboratory technology roadmap. After dissection and isolation of the MCA of rats, the changes of DBD, ASR, and AR on the vascular tension were monitored and recorded using the DMT620 M vascular tension detection system. The potential regulatory activities of K^+ and Ca^{2+} channels were further demonstrated to clarify the anticonstriction effect by DBD, ASR, and AR. AR, Astragali Radix. ASR, Angelicae Sinensis Radix. DBD, Danggui Buxue decoction. MCA, middle cerebral artery.

maintained for 10 min. Second, 2.5 mM Ca^{2+} was added to observe whether the above three tested drugs would resist the MCA vasoconstriction induced by the influx of extracellular Ca^{2+} ($[Ca^{2+}]_{out}$). The laboratory technology roadmap is shown in **Figure 2**.

Statistical Analysis

The experimental data were expressed as the mean ± standard error of the mean (S.E.M). Statistical differences among groups were evaluated by one-way ANOVA with the Tukey–Kramer multiple comparison test using Graph Pad Prism 6.0. $p < 0.05$ was considered statistically significant.

RESULTS

HPLC Analysis Results of Four Compounds in DBD

Compared with the retention time of the corresponding standards (**Figure 3**), four compounds in lyophilized powder of DBD were determined by HPLC. As shown in **Table 1**, the contents of astragaloside IV, ferulic acid, formononetin, and ligustalide were 0.1999, 0.0276, 0.0469, and 1.1296 mg/g, respectively.

DBD, ASR, and AR had No Effects on MCA Under Resting Tension

As shown in **Figure 4**, PSS solution, as a control, had no effect on MCA vessels under resting tension (**Figure 4A**). Unanimously, the cumulative addition of DBD (**Figure 4B**), ASR (**Figure 4C**), and AR (**Figure 4D**) (8, 16, 32, 64, 128, and 256 mg/ml) also had no effects on the resting tension of MCA vessels.

DBD, ASR, and AR Dilated KCl-Evoked MCA Vasoconstriction

The results in **Figure 5** showed the effects of DBD, ASR, and AR on the constricted MCA of KCl. Compared with the control group (**Figures 5A and E**), DBD (**Figures 5B and E**), ASR (**Figures 5C and E**), and AR (**Figures 5D and E**) (8, 16, 32, 64, and 128 mg/ml) enabled the KCl precontracted MCA to dilate in a concentration-dependent manner ($p < 0.05$). Amazingly, 256 mg/ml of them hardly continued to relax the MCA as compared to the concentration of 128 mg/ml. However, the concentrations of 128 and 256 mg/ml of ASR did not continue to dilate the MCA compared with the concentration of 256 mg/ml (**Figures 5C and E**).

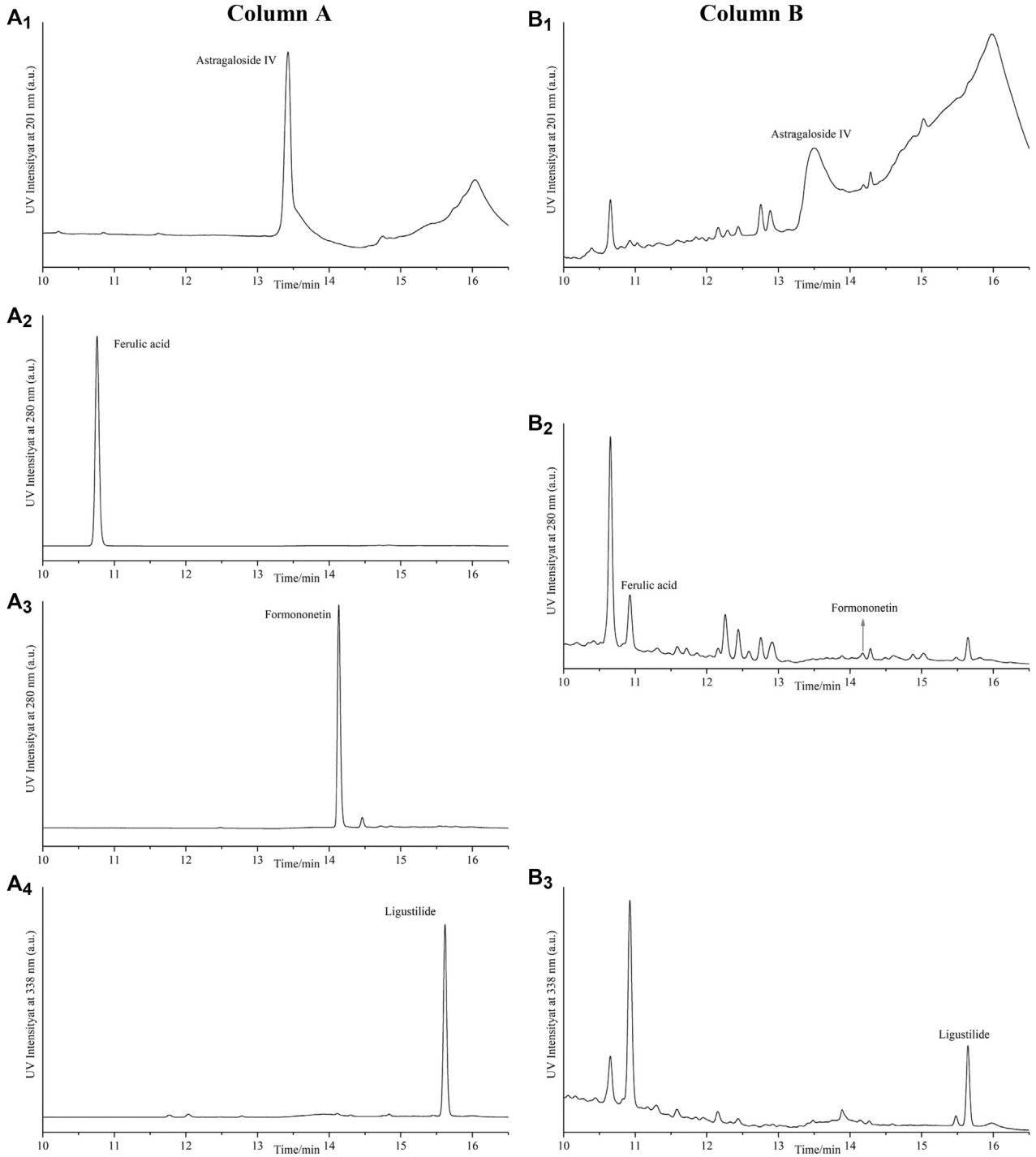

FIGURE 3 | HPLC analysis of four compounds in lyophilized powder of DBD. Column A represents HPLC chromatograms of standard substances astragaloside IV **(A_1)**, ferulic acid **(A_2)**, formononetin **(A_3)**, and ligustalide **(A_4)**. Column B represents HPLC chromatograms of astragaloside IV **(B_1)**, ferulic acid, and formononetin **(B_2)** and ligustalide **(B_3)** in lyophilized powder of the DBD sample.

To further compare the vasodilator effect of ASR, AR, and DBD on MCA of rats, ASR (1.5, 3, 6, 12, 24, and 48 mg/ml) and AR (6.5, 13, 26, 52, 104, and 208 mg/ml) were added to the MCA vessels constricted by KCl in the prescribed compatibility ratio. Consistently, both ASR and AR can dilate MCA in a concentration-dependent manner, in which the maximum vasodilation rate of ASR at the concentration of 48 mg/ml was 71.28 ± 16.18% (**Figures 6B, D**), while that of AR at the concentration of 208 mg/ml was 75.52 ± 17.5% (**Figures 6B, D**). Interestingly, the vasodilator of DBD was not the superimposition of the vasodilator of ASR and AR under the

TABLE 1 | Contents of astragaloside IV, ferulic acid, formononetin, and ligustalide in lyophilized powder of DBD identified by HPLC analysis.

NO.	Components	Wavelength (nm)	Retention time (min)	Content (mg/g)
1	Astragaloside IV	201	13.43	0.1999
2	Ferulic acid	280	10.75	0.0276
3	Formononetin	280	14.14	0.0469
4	Ligustalide	338	15.62	1.1296

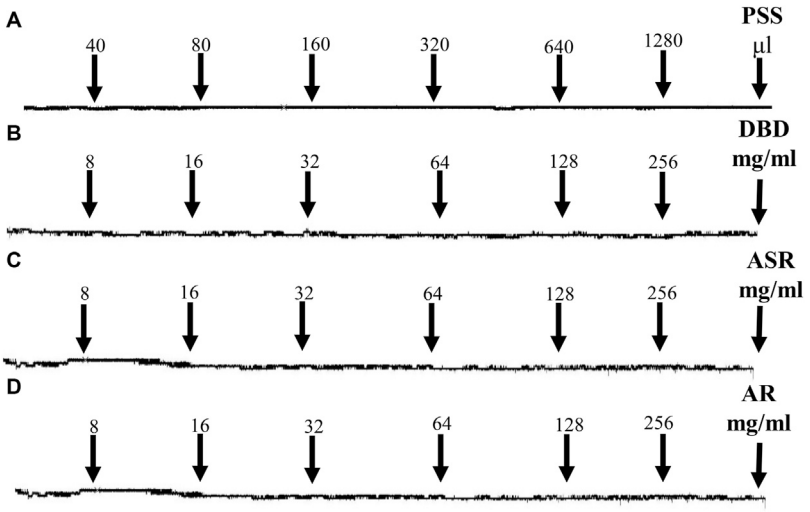

FIGURE 4 | Effects of serial concentrations of DBD, ASR, and AR (8, 16, 32, 64, 128, and 256 mg/ml) on MCA vessels under resting tension. PSS (control, **A**), DBD **(B)**, ASR **(C)**, and AR **(D)** had no effects on resting tension of MCA vessels. DBD, Danggui Buxue decoction. ASR, Angelicae Sinensis Radix. AR, Astragali Radix. MCA, middle cerebral artery.

compatibility ratio. At low concentrations (8–16 mg/ml), ASR was superior to DBD in vasodilating MCA, while DBD exceeded AR at concentrations of 128–256 mg/ml.

DBD, ASR, and AR Dilated U46619-Evoked MCA Vasoconstriction

Similarly, we further investigated the dilatation of DBD, ASR, and AR on U46619-induced MCA contraction in rats. Compared with the control group (**Figure 7A**), DBD, ASR, and AR all dilated MCA in a concentration-dependent manner with the vasodilator efficiency of ASR > DBD > AR in the concentration range of 8–32 mg/ml and DBD > ASR > AR at the concentrations of 128 and 256 mg/ml (**Figures 7B, D**). Similarly, ASR and AR disaggregated in prescribed proportions also exhibited concentration-dependent dilation of the constricted MCA vessels of U46619 (**Figures 8B, D**). However, the vasodilator efficiency of DBD was better than that of ASR and AR within the concentration range we set (**Figure 8D**) ($p > 0.05$).

DBD, ASR, and AR Dilated KCl-Constricted MCA Potentially via Inhibiting K^+ Channel Openness

To probe whether the vasodilator effect of DBD, ASR, and AR is related to the decrease of intracellular K^+ concentration via the inhibition of K^+ channel opening, we incubated the KCl-constricted MCA with four K^+ channel blockers: TEA (1×10^{-2} mM, a blocker of Ca^{2+}-sensitive K^+ channels), Gli (1×10^{-5} mM, a blocker of ATP-sensitive potassium channels), $BaCl_2$ (1×10^{-4} mM, a blocker of inwardly rectifer K^+ channels), and 4-AP (1×10^{-3} mM, a blocker of voltage-dependent K^+ channels). Subsequently, 64 mg/ml of DBD, ASR, and AR were added to investigate their effects on various K^+ channels. The results showed that the above four kinds of K^+ channel blockers had no significant effect on the vascular tone of KCl-constricted MCA in rats (**Figure 9**). In the presence of 4 K^+ channel blockers, further addition of DBD and AR showed no difference in vascular tone compared with the absence of K^+ channel blockers (**Figures 9A–D, I–M, O**) ($p > 0.05$). However, addition of ASR may dilate MCA in a way similar to those of GLI and $BaCl_2$ (Figures 9E–H, **N**) ($p < 0.05$) but not TEA and 4-AP.

DBD, ASR, and AR Dilated U46619-Constricted MCA Potentially via Inhibiting the $[Ca^{2+}]_{out}$ and $[Ca^{2+}]_{in}$

We further depleted the Ca^{2+} in the incubation solution to reveal whether the dilation of MCA by DBD, ASR, and AR was related to the inhibition of $[Ca^{2+}]_{out}$ or $[Ca^{2+}]_{in}$. The results showed that compared with the control group, 1 μM U46619 can induce MCA dilation in the absence of Ca^{2+} in the incubation solution, suggesting that $[Ca^{2+}]_{in}$ is involved in this event (**Figure 10**).

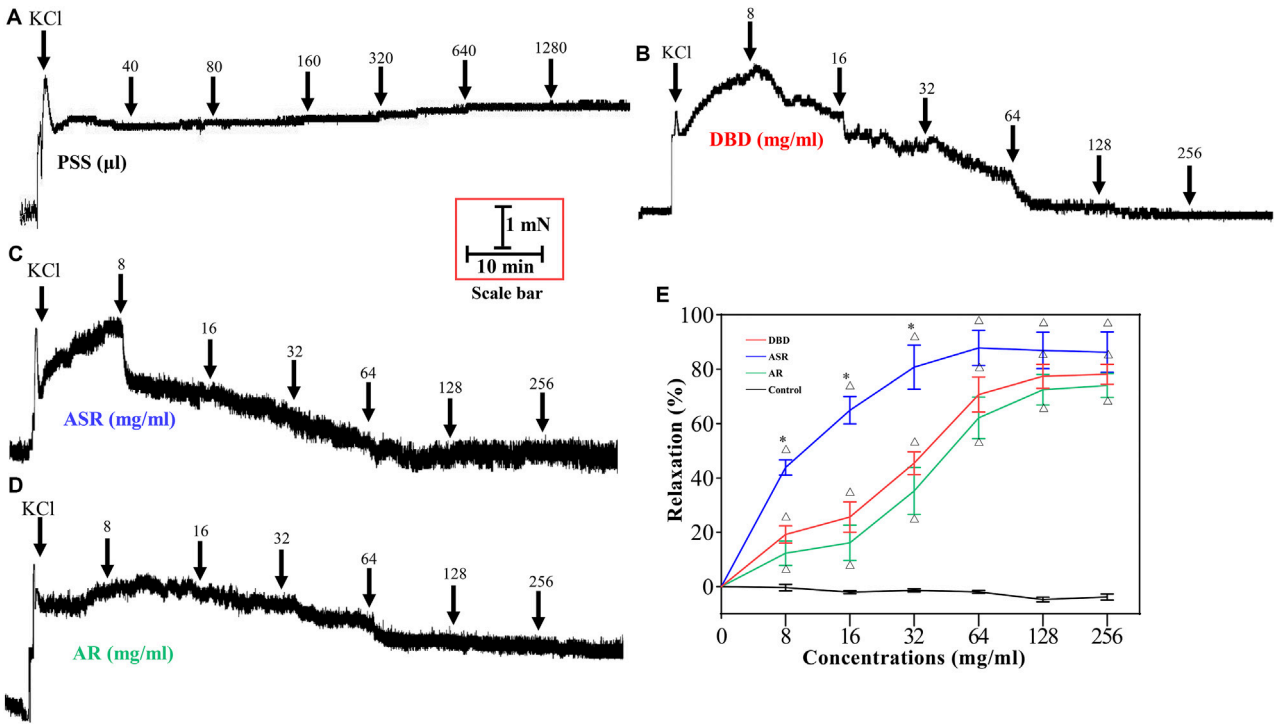

FIGURE 5 | Effect of DBD, ASR, and AR on vascular tension of 60 mM KCl precontracted MCA of rats. Diagrams of the effect of cumulative addition of PSS **(A)**, DBD **(B)**, AR **(C)**, and ASR **(D)** on KCl preconstricted MCA of rats. (E) Comparison of vasodilators by DBD, ARS, and AR on MCA of rats. Data were expressed as the mean ± S.E.M. (n = 5). $^{\triangle}p < 0.05$ vs the control group; $^{*}p < 0.05$ vs the DBD group. DBD, Danggui Buxue decoction. ASR, Angelicae Sinensis Radix. AR, Astragali Radix. MCA, middle cerebral artery.

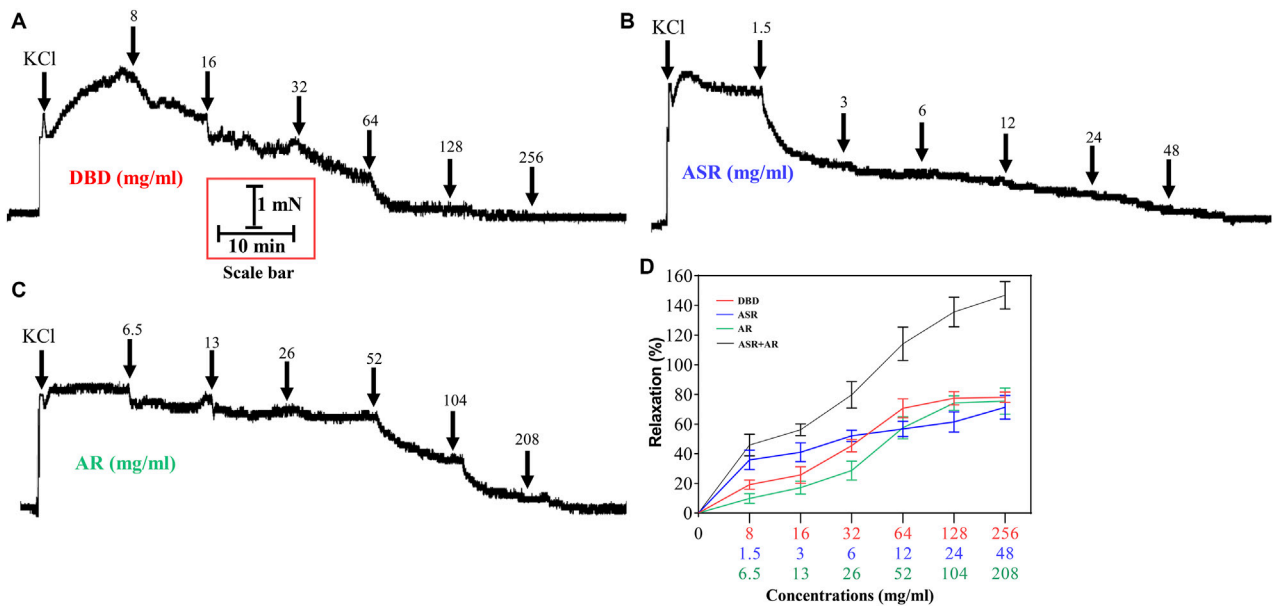

FIGURE 6 | Effect of DBD and its compatibility ratio of ASR and AR monotherapy on the regulation of 60 mM KCl precontracted vascular tension. Diagrams of the effect of cumulative addition of DBD **(A)**, ASR **(B)**, and AR **(C)** on KCl preconstricted MCA of rats. Data were expressed as the mean ± S.E.M. (n = 5). DBD, Danggui Buxue decoction. ASR, Angelicae Sinensis Radix. AR, Astragali Radix. MCA, middle cerebral artery.

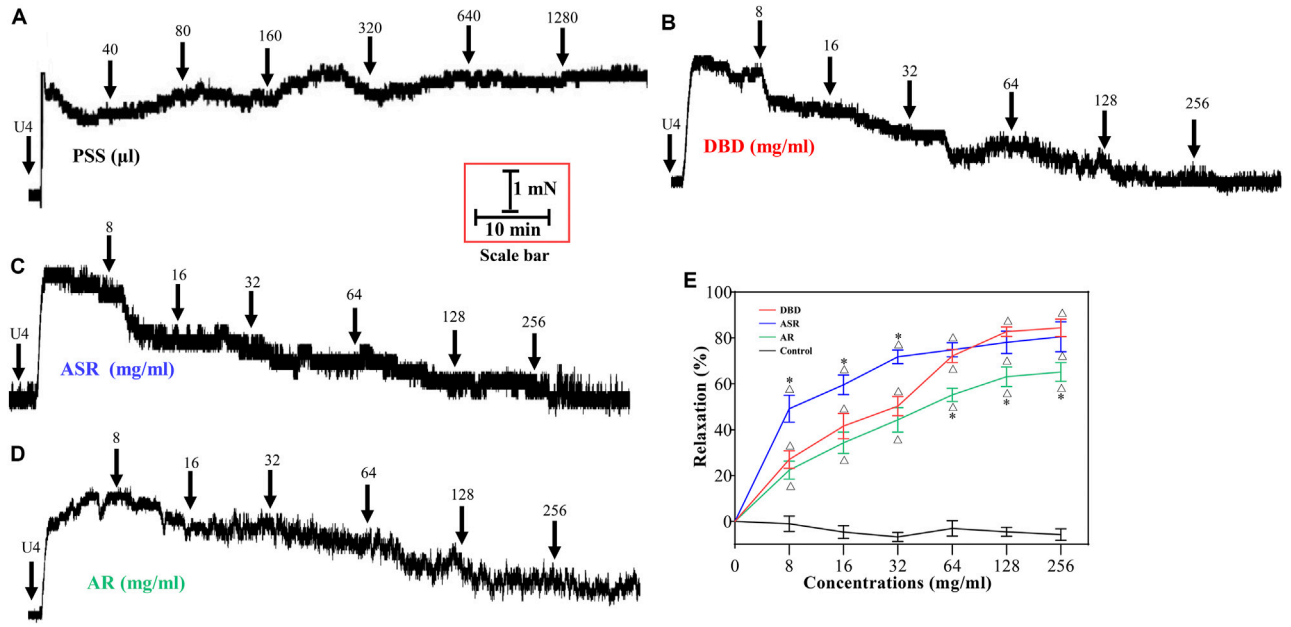

FIGURE 7 | Effect of DBD, ASR, and AR on vascular tension of MCA under 1 μM U46619 precontraction conditions. Diagrams of the effect of cumulative addition of PSS **(A)**, DBD **(B)**, ASR **(C)**, and AR **(D)** on U46619 preconstricted MCA of rats. **(E)** Comparison of vasodilators by DBD, ARS, and AR on MCA of rats. Data were expressed as the mean ± S.E.M. (n = 5). $^{\triangle}p < 0.05$ vs the control group; $^{*}p < 0.05$ vs the DBD group. DBD, Danggui Buxue decoction. ASR, Angelicae Sinensis Radix. AR, Astragali Radix. MCA, middle cerebral artery.

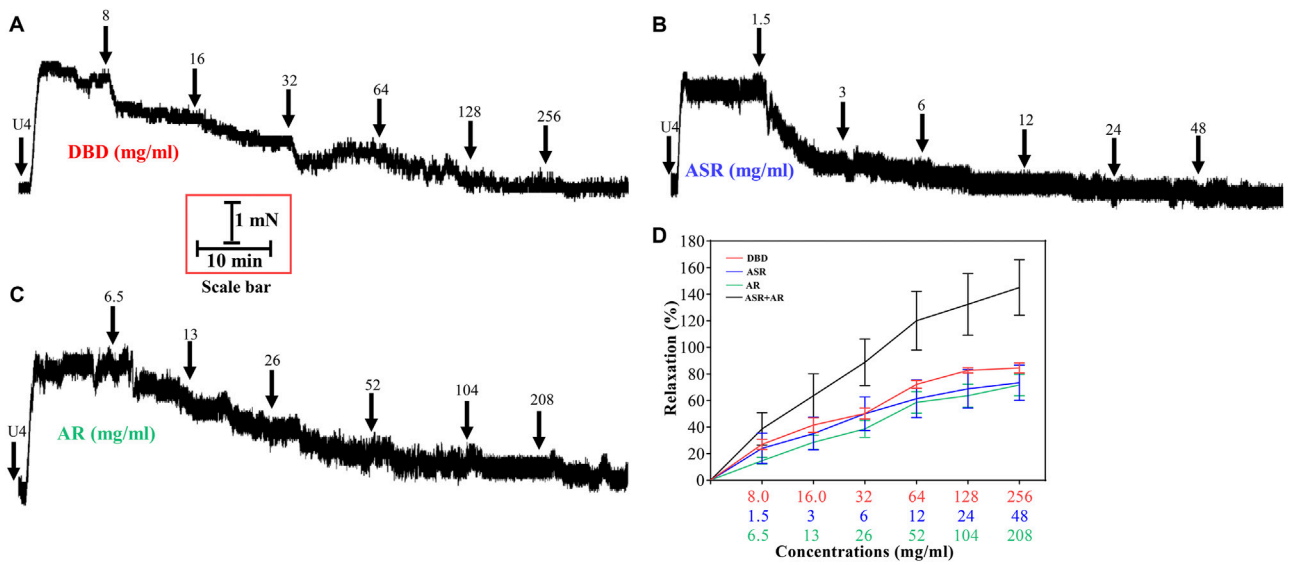

FIGURE 8 | Effect of DBD and its compatibility ratio of ASR and AR monotherapy on vascular tension of MCA under 1 μM U46619 precontraction condition. Diagrams of the effect of cumulative addition of DBD **(A)**, ASR **(B)**, and AR **(C)** on U46619 preconstricted MCA of rats **(D)** Comparison of vasodilators by DBD, ARS, and AR on MCA of rats. Data were expressed as the mean ± S.E.M. (n = 5). DBD, Danggui Buxue decoction. ASR, Angelicae Sinensis Radix. AR, Astragali Radix. MCA, middle cerebral artery.

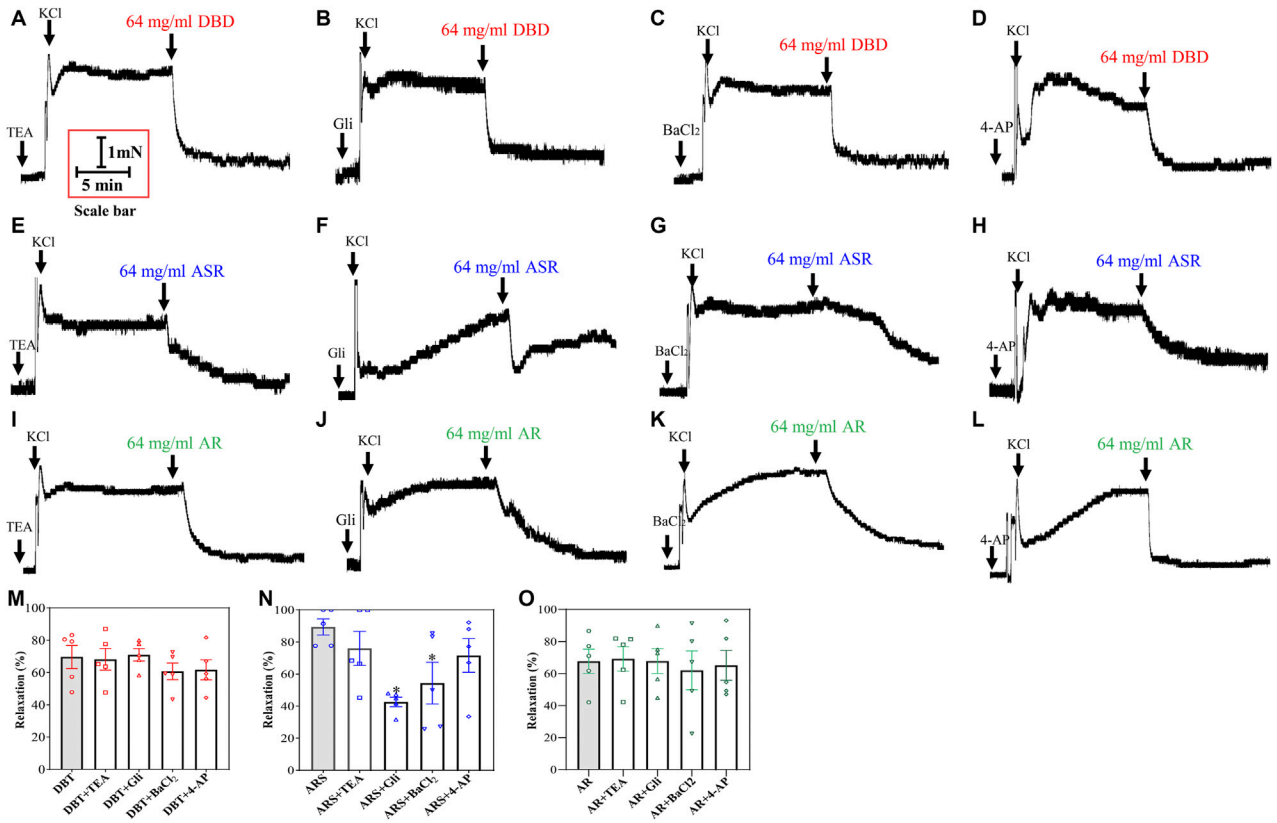

FIGURE 9 | Regulation of DBD, ASR, and AR on K^+ channels. Potentially inhibiting K^+ channels opening (TEA, K_{Ca} blocker; Gli, K_{ATP} blocker; $BaCl_2$, K_{IR} blocker; 4-AP, K_V blocker) by DBD **(A–D)**, ASR **(E–H)**, and AR **(I–L)** on 60 mM KCl precontracted MCA of rats. Statistical results and detailed values of DBD **(M)**, ASR DBD **(N)**, and AR DBD **(O)** dilating MCA of rats by regulating four kinds of K^+ channels. K_{Ca}, Ca^{2+}-activated K^+ channel. K_{ATP}, ATP-sensitive K^+ channel. K_{IR}, inwardly rectifer K^+ channel. K_V, voltage-dependent K^+ channel. Data were expressed as the mean ± S.E.M. (n = 5). *$p < 0.05$ vs the control group. DBD, Danggui Buxue decoction. ASR, Angelicae Sinensis Radix. AR, Astragali Radix. MCA, middle cerebral artery.

Amazingly, preincubation of ASR and AR counteracted U46619-evoked MCA contraction ($p < 0.05$), with the maximum contraction from 1.22 ± 0.07 mN to 0.45 ± 0.39 mN and 0.47 ± 0.38 mN, respectively, indicating the potential inhibition of organelle Ca^{2+} release partly by ASR and AR (Figures 10A, **C**, D). However, there was no statistically significant difference in DBD in decreasing MCA vascular tone compared with the control group ($p > 0.05$). To demonstrate whether the dilating MCA effect of DBD, ASR, and AR was related to the inhibition of $[Ca^{2+}]_{out}$, **Figure 10A** shows that 2.5 mM $CaCl_2$ stimulated the further contraction of MCA. However, the three drugs inhibited the $CaCl_2$-mediated secondary contraction of MCA ($p < 0.05$) with the maximum contraction from 1.92 ± 0.13 mN to 1.15 ± 0.22 mN (DBD), 0.52 ± 0.39 mN (ASR), and 0.46 ± 0.4 mN (AR) (**Figures 10B–E**). The above results collectively suggested that DBD, ASR, and AR may be responsible for inhibiting $[Ca^{2+}]_{out}$ against U46619-induced contraction of MCA, while ASR and AR can also inhibit the release of internal Ca^{2+}, resulting in the decrease of cytoplasmic Ca^{2+}-evoked MCA dilation.

DISCUSSION

DBD is a TCM prescription used in the treatment of cerebrovascular diseases with a long history. However, there is no evidence to reveal its regulation on the tension of MCA. The results of this experiment revealed the following: 1) vasodilator active ingredients of DBD may be astragaloside IV, ferulic acid, formononetin, and ligustalide. 2) DBD, ASR, and AR have no relaxing effect on the MCA of rats under resting tension. 3) DBD, ASR, and AR can relax the MCA vessels precontracted by KCl and U46619 in a concentration-dependent manner. The vasodilator effect of ASR is characterized by stronger relaxation at low concentrations and rapidly reaches the maximum relaxation rate with the increase of concentration. However, AR has a lower relaxation effect with the relaxation rate slowly increasing. The relaxation effect of DBD is the same as that of AR, but it is stronger than AR at all concentrations. 4) The relaxing effect of DBD on MCA is not the superimposition of ASR and AR. DBD can exert much stronger relaxing effect analogous to ASR at low concentrations as well as the stable relaxing effect analogous to AR on KCl and U46619 precontracted MCA of rats.

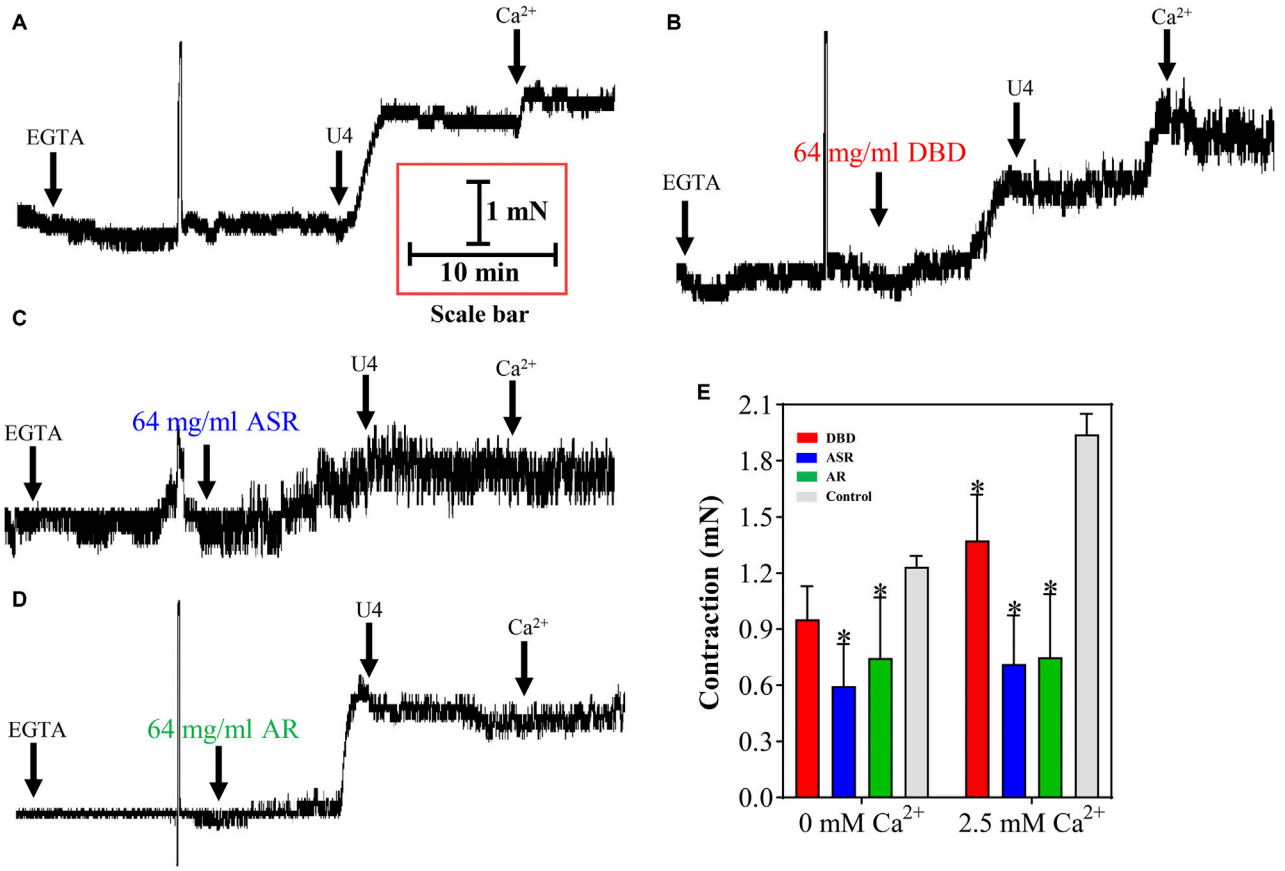

FIGURE 10 | Effect of DBD, ASR, and AR on 1 μM U46619 precontracted MCA of rats by regulation of $[Ca^{2+}]_{out}$ and $[Ca^{2+}]_{in}$. **(A)** U46619 contraction of vessels without Ca^{2+} and secondary contraction of vessels after recalcification. The effect of DBD **(B)**, ASR **(C)**, and AR **(D)** on vasodilation of MCA in the presence and absence of Ca^{2+}. **(E)** Statistical results and detailed values of DBD, ASR, and AR on $[Ca^{2+}]_{out}$ and $[Ca^{2+}]_{in}$. $[Ca^{2+}]_{out}$, the influx of extracellular Ca^{2+}. $[Ca^{2+}]_{in}$, the release of internal Ca^{2+} from organelles. Data were expressed as the mean ± S.E.M. (n = 5). *$p < 0.05$ vs the control group. DBD, Danggui Buxue decoction. ASR, Angelicae Sinensis Radix. AR, Astragali Radix. MCA, middle cerebral artery.

5) The vasodilator effect of both DBD and AR may be not related to the K^+ channel. However, ASR can dilate MCA by the inhibition of K_{ir} and K_{ATP}. In addition, ASR and AR can inhibit both the $[Ca^{2+}]_{in}$ and $[Ca^{2+}]_{out}$, but DBD can only inhibit the $[Ca^{2+}]_{out}$.

Cerebrovascular disease was a global disease that caused millions of deaths worldwide every year (Hammond–Haley et al., 2021). In recent years, it has been found that hypertension and vasculitis can both cause cerebrovascular diseases ((Mustanoja et al., 2018; Lersy et al., 2020; and Hou et al., 2021). These diseases are often related to the abnormal contraction of blood vessels, which can cause changes in the body's homeostasis and further aggravate its abnormal contractions. If this vicious circle is not broken, it will endanger life (Boguslavskyi et al., 2021). Being a very important vessel in the brain, MCA diseases account for a large proportion of all cerebrovascular diseases. Long-term use of traditional drugs for the treatment of cerebrovascular diseases is often accompanied by some adverse reactions. Therefore, the search for drugs that can treat or reduce abnormal vasoconstriction has become a research focus. DBD was used in clinics to treat various medical miscellaneous diseases caused by "deficiency of Qi and blood" (Wu et al., 2016; Chen et al., 2017). Our experiment can thus provide the experimental basis for the better use of DBD.

Concentrations of drugs do result in different pharmacological activities. First, the clinical dosage of DBD was 1 g/kg, and the equivalent dose for rat was 6.3 g/kg. Evidence has shown that astragaloside IV, ferulic acid, formononetin, and ligustilide can be detected in rat plasma after oral administration of DBD (Ji., 2013). Our pre-experimental data confirmed that DBD, lower than 8 mg/ml and higher than 256 mg/ml, had almost no effect on MCA vasodilation in rats with KCl contraction (data were not provided). According to the results of HPLC, the concentrations of astragaloside IV, ferulic acid, formononetin, and ligustilide in 256 mg/ml DBD were 0.0512, 0.0071, 0.012, and 0.2892 mg/ml, respectively. We have previously demonstrated that DBD can promote the proliferation of hypoxic vascular endothelial cells *in vitro* in the range of 3.75–15 mg/ml (Yang et al., 2013). Second, for *in vitro* organs, astragaloside IV (0.01–0.1 mg/ml), ferulic acid (0.1942–0.5825 mg/ml), formononetin (0.0027–0.0268 mg/ml), and ligustilide (0.001–0.4 mg/ml) have been reported to exhibit

excellent relaxation on isolated vessels or smooth muscles (Wang et al., 2006; Jia et al., 2014; Li, 2014; Fang et al., 2016; Song, 2018). Our previous investigation indicated that astragaloside IV (0.001–235.491 mg/ml) can dilate MCA of rats (Wang, 2017). At the cellular level, astragaloside IV (0.0075 mg/ml), ferulic acid (0.018 mg/ml), and formononetin (0.0125 mg/ml) showed superior antioxidative stress injury on vascular endothelial cells (Cai et al., 2021). The above evidence in whole-organ cells suggests that the concentrations of DBD (8, 16, 32, 64, 128, and 256 mg/ml) are, to some degree, all reasonable.

Vasoconstrictors are drugs that act on ion channels or specific receptors to cause vascular smooth muscle contraction. KCl-stimulated vasoconstriction is achieved by membrane depolarization (extracellular $K^+ > 20$ mM), which activates the opening of voltage-dependent Ca^{2+}channels (Hu et al., 2016). TXA2 is mainly produced by prostaglandin H2 in platelets under the action of TXA2 synthase with the effect of promoting platelet aggregation and contraction of vascular smooth muscles (Nguyen et al., 2016). As a representative analogue of TXA2, U46619 can contract vessels via activating cyclic nucleotide-gated channels, causing an increase in intracellular Ca^{2+} and activation of TXA2 receptors (Fang et al., 2016). Therefore, from the molecular level, the mechanisms of the above two vasoconstrictors are completely different. In this experiment, DBD, ASR, and AR did not affect vascular tension without adding vasoconstrictors. This shows that under normal circumstances, the three drugs will not relax uncontracted vessels. The relaxation effects of the three drugs reached the maximum at a certain concentration, indicating that DBD, ASR, and AR all had effects on MCA under the precontraction of the two stimulants. Studies have shown that the important components of DBD, ferulic acid, astragaloside IV, and formononetin can relax coronary arteries (Jia et al., 2014; Fang et al., 2016; and Lin et al., 2018). This is consistent with our experimental results. Dividing the DBD at a certain concentration according to the ratio of ASR: AR = 1:5, it can be found that the relaxing effect of DBD is not the superimposition of the vasodilator effect of ASR and AR. At a lower concentration (8 mg/ml), the relaxation effect of DBD is not stronger than that of the low concentration (1.5 mg/ml) of ASR sinensis at this ratio, but after reaching a certain concentration (64 mg/ml), the relaxing effect of DBD is gradually stronger than that of ASR at this ratio (20.8 mg/ml), which may be caused by the special compatibility mechanism of DBD. Studies have shown that there are differences in the composition of the decoction of different ratios of ASR and AR. The ratio of the classic DBD has been proven to release the effective ingredients better than other ratios (ASR:AR, 1:1, 1:2, 1:3, 1:4, 1:7, 1:10) (Don et al., 2006). This may be the reason why DBD is composed of a large amount of ASR and AR. The role of DBD in protecting blood vessels is closely related to concentration, which is consistent with previous studies (Yang et al., 2013).

K^+ is a very important ion in the human body. Most of it is stored in cells and a small amount in the extracellular fluid. K^+ channels are widely present in body tissues and organs and play a role in maintaining cell resting membrane potential, regulating muscle tension and action potential, and participating in cell membrane repolarization (Ykocki et al., 2017). There are four important K^+ channels distributed on vascular smooth muscles: K_V, K_{ir}, K_{Ca}, and K_{ATP}. This study showed that preincubation of the four K^+ channel blockers did not affect the relaxation effects of DBD and AR, while preincubation of the K_{ir} and K_{ATP} channel blockers Gli and $BaCl_2$ reduced the relaxation effects of ASR. It is worth noting that in this experiment, we chose a single concentration (64 mg/ml) for the experiment. At this concentration, the three drugs all show good vasodilation effects. It may be that the vasodilator effect of AR at this concentration can compensate for the effect of blockers on ASR, which may be the reason why DBD is not affected by K^+ channel blockers.

The contraction and relaxation of vascular smooth muscles are affected by not only K^+ ions but also the increase of $[Ca^{2+}]_{in}$, which can stimulate vasoconstriction (Mamo et al., 2014). This experiment shows that in the absence of Ca^{2+}, preincubation of DBD, ASR, and AR will not affect vascular tension, but both ASR and AR can inhibit U46619-induced vasoconstriction, while DBD has no obvious effect. On the other hand, the addition of exogenous Ca^{2+} can cause further contraction of vascular smooth muscles. Preincubation of the three drugs can inhibit the secondary contraction induced by exogenous Ca^{2+}. DBD, as a prescription for the compatibility of ASR and AR, did not show a more comprehensive inhibitory effect. The reason for this result may be related to the release of ingredients during prescription preparation and freeze-dried powder preparation. Experiments have shown that DBD decoction can promote the release of astragalus components, and the process of making freeze-dried powder may cause certain changes in the components of DBD (Yan et al., 2010; Tan et al., 2021). Simultaneously, we will further apply vascular organoids coupled with microfluidic mass spectrometry chips to define the potential pharmacological components and deep-level molecular mechanisms of DBD on dilating blood vessels (Wang et al., 2019 and, 2020; Trillhaase et al., 2021).

Collectively, our data demonstrated that DBD, ASR, and AR can dilate the rat MCA. In MCA with KCl contraction, the vasodilatation was ASR > DBD > AR. For U46619-contracted MCA, the vasodilatation was ASR > DBD > AR at concentrations less than 128 mg/ml, while DBD > ASR > AR at concentrations greater than 128 mg/ml. Nevertheless, the deep reason why TCM prescription and decomposed prescription show inconsistent pharmacological activities is worth further exploration. In the ischemic stroke model established by middle cerebral artery occlusion, a 14-day administration of Buyang Huanwu decoction can significantly ameliorate the neurological function score of rats. Compared to the model group, groups AR, and the combination of ASR, *Paeonia lactiflora*, *Ligusticum chuanxiong*, *Pheretima aspergillum*, *Carthamus tinctorius*, and *Prunus persica* had a tendency to decrease the neurological function score, separately, with no significant difference (Shu and Pan 2017). Guiqi Congzhi decoction was proved to be superior to groups *Ligusticum chuanxiong* and *Pheretima aspergillum*, *Radix Sophorae Flavescentis*, and *Acorus calamus Linn*, as well as AR and ASR in improving the memory capacity of vascular dementia rats (Ma et al., 2018). For *in vitro* investigation of prescription disassembly, both Xiaobanxia decoction and

Zingiber officinale Roscoe can counteract the isolated ileum contraction induced by acetylcholine, 5-hydroxytryptamine, and histamine in guinea pigs in a concentration dependent manner, and there was almost no difference in their relaxing effects (Lin, 2018). Evidence also indicated that Siwu decoction was better than any single herbs on oxytocin-induced *in vitro* uterine contractions of mice (Zhu et al., 2011). Meaningfully, the results confirmed that DBD, but not ASR, can significantly resist leukopenia induced by $^{60}Co\gamma$ -ray radiation in mice (Gu, 2009). In terms of regulating blood vessels, it was revealed that DBD, ASR, and AR can inhibit hepatic angiogenesis in rats with nonalcoholic fatty liver disease by decreasing the activity of nitric oxide synthase, while only DBD and AR can reduce the content of nitric oxide (Guo et al., 2014). The above relevant clues suggested that the pharmacological effects of any TCM prescription, including DBD, should not be identified with the numerical superposition of single herbs. Similarly, we cannot figure out, prescription or single herbs from disassembled prescription, what the strength of the action is. It was thus reasonable for us to believe that the synergistic effect of ASR and AR as well the regulation of other physiological functions may be responsible for the distinct vasodilation of DBD on rat MCA. The elucidation of pharmacological effects of TCM prescriptions involves pharmacokinetics as well as the regulation of multi-components on multi-organ functions (Li C. et al., 2021). Maybe the integrative pharmacology-based investigation is something we should learn from (Xu et al., 2021).

DATA AVAILABILITY STATEMENT

The raw data supporting the conclusions of this article will be made available by the authors, without undue reservation.

ETHICS STATEMENT

The animal study was reviewed and approved by the Management Committee from Chengdu University of Traditional Chinese Medicine.

AUTHOR CONTRIBUTIONS

PY, SZ and XW conceived the study. YG and YZ wrote the manuscript and drew the figures. YG, YZ, YH, and PG conducted the experiments. PY, SZ, and XW supervised the experiments and manuscript preparation and directed the final version of the manuscript. The final version of the manuscript was read and approved by all authors. The authors would like to thank JS and XF at the Innovative Institute of Chinese Medicine and Pharmacy, Chengdu University of Traditional Chinese Medicine, Chengdu, China, for providing technical guidance on manipulation and operation of the DMT microvascular tension detection system and HPLC analysis, respectively.

FUNDING

This work was supported by the Department of Science and Technology, Chengdu University of Traditional Chinese Medicine (030041042), the Key R&D project of the Provincial Department of Education (18ZA0180), the Science and Technology Department of Sichuan Province (319238 and 319807), and the National Natural Science Foundation of China (82004058 and 82104533).

REFERENCES

Bai, J., Zhang, Y., Tang, C., Hou, Y., Ai, X., Chen, X., et al. (2021). Gallic Acid: Pharmacological Activities and Molecular Mechanisms Involved in Inflammation-Related Diseases. *Biomed. Pharmacother.* 133, 110985. doi:10.1016/j.biopha.2020.110985

Boguslavskyi, A., Tokar, S., Prysyazhna, O., Rudyk, O., Sanchez-Tatay, D., Lemmey, H. A. L., et al. (2021). Phospholemman Phosphorylation Regulates Vascular Tone, Blood Pressure, and Hypertension in Mice and Humans. *Circulation* 143, 1123–1138. doi:10.1161/CIRCULATIONAHA.119.040557

Cainzos-Achirica, M., Miedema, M. D., McEvoy, J. W., Al Rifai, M., Greenland, P., Dardari, Z., et al. (2020). Coronary Artery Calcium for Personalized Allocation of Aspirin in Primary Prevention of Cardiovascular Disease in 2019: The MESA Study (Multi-Ethnic Study of Atherosclerosis). *Circulation* 141, 1541–1553. doi:10.1161/CIRCULATIONAHA.119.045010

Chen, X. Y., Wang, Z. C., Guo, C. X., and Wang, L. N. (2017). Preventive and Treatment Effect of Danggui Buxuetang and Liuwei Dihuang Tang on Early Hypertensive Renal Damage. *Chin. J. Exp. Traditional Med. Formulae* 23, 190–195. doi:10.13422/j.cnki.syfjx.2017090190

Chen, Y., Tao, Y. Y., and Li, F. H. (2008). Effects of Danggui Buxue Decoction on Liver Fibrosis and Hepatic Lipid Peroxidation in Rats. *Zhongguo Zhong Xi Yi Jie He Za Zhi* 28, 39–42.

Chinese Pharmacopoeia Commission (2020). *Chinese Pharmacopoeia 1*. Beijing: China Medical Science and Technology Press.

DeBaun, M. R., Jordan, L. C., King, A. A., Schatz, J., Vichinsky, E., Fox, C. K., et al. (2020). American Society of Hematology 2020 Guidelines for Sickle Cell Disease: Prevention, Diagnosis, and Treatment of Cerebrovascular Disease in Children and Adults. *Blood Adv.* 4, 1554–1588. doi:10.1182/bloodadvances.2019001142

Dong, T. T., Zhao, K. J., Gao, Q. T., Ji, Z. N., Zhu, T. T., Li, J., et al. (2006). Chemical and Biological Assessment of a Chinese Herbal Decoction Containing Radix Astragali and Radix Angelicae Sinensis: Determination of Drug Ratio in Having Optimized Properties. *J. Agric. Food Chem.* 54, 2767–2774. doi:10.1021/jf053163l

Dou, H. Y., Du, Y. G., Han, Y. H., Wang, Y. Y., Wang, X. L., and Wang, T. (2020). Mechanism of Hematopoietic Reconstruction in Mice Treated with Danggui Buxue Decoction Combined with Muscle-Derived Stem Cell Transplantation. *Zhongguo Shi Yan Xue Ye Xue Za Zhi* 28, 1177–1182. doi:10.19746/j.cnki.issn.1009-2137.2020.04.016

Fang, L. M., Hou, X. M., Yang, R., Fan, F. W., He, Z. F., Shi, M., et al. (2016). Vasodilatory Effect of Ferulic Acid on *In-Vitro* Rat Coronary Artery. *Chin. Pharmacol. Bull.* 32, 554–558. doi:10.3969/j.issn.1001-1978.2016.04.022

Gao, Q. T., Cheung, J. K., Li, J., Chu, G. K., Duan, R., Cheung, A. W., et al. (2006a). A Chinese Herbal Decoction, Danggui Buxue Tang, Prepared from Radix Astragali and Radix Angelicae Sinensis Stimulates the Immune Responses. *Planta Med.* 72, 1227–1231. doi:10.1055/s-2006-947186

Gao, Q. T., Cheung, J. K., Li, J., Jiang, Z. Y., Chu, G. K., Duan, R., et al. (2006b). A Chinese Herbal Decoction, Danggui Buxue Tang, Activates Extracellular Signal-Regulated Kinase in Cultured T-Lymphocytes. *FEBS Lett.* 581, 5087–5093. doi:10.1016/j.febslet.2007.09.053

Garg, A., Rocha, M., StarrOrtega-Gutierrez, M. S., and Ortega-Gutierrez, S. (2021). Predictors and Outcomes of Hemorrhagic Stroke in Reversible Cerebral Vasoconstriction Syndrome. *J. Neurol. Sci.* 421, 117312. doi:10.1016/j.jns.2021.117312

George, J., Rapsomaniki, E., Pujades-Rodriguez, M., Shah, A. D., Denaxas, S., Herrett, E., et al. (2015). How Does Cardiovascular Disease First Present in Women and Men? Incidence of 12 Cardiovascular Diseases in a Contemporary Cohort of 1,937,360 People. *Circulation* 132, 1320–1328. doi:10.1161/CIRCULATIONAHA.114.013797

Gong, A. G., Zhang, L. M., Lam, C. T., Xu, M. L., Wang, H. Y., Lin, H. Q., et al. (2017). Polysaccharide of Danggui Buxue Tang, an Ancient Chinese Herbal Decoction, Induces Expression of Pro-inflammatory Cytokines Possibly via Activation of NFκB Signaling in Cultured RAW 264.7 Cells. *Phytother. Res.* 31, 274–283. doi:10.1002/ptr.5745

Greenstein, A. S., Kadir, S. Z. A. S., Csato, V., Sugden, S. A., Baylie, R. A., Eisner, D. A., et al. (2020). Disruption of Pressure-Induced Ca2+ Spark Vasoregulation of Resistance Arteries, rather Than Endothelial Dysfunction, Underlies Obesity-Related Hypertension. *Hypertension* 75, 539–548. doi:10.1161/HYPERTENSIONAHA.119.13540

Gu, J. (2009). Effects of Huangqi in Danggui Buxue Decoction on Hematopoietic Functions in Mice. *Chin. J. Basic Med. Traditional Chin. Med.* 15, 215–217.

Guo, T., Zhao, Z. M., Yang, S. H., Tang, L. R., Tan, Y., Tao, Y. Y., et al. (2014). Therapeutic Effect of Danggui Buxue Decoction and its Separated Recipes on Liver Fibrosis and Angiogenesis and its Mechanism. *J. Clin. Hepatol.* 30, 324–329.

Hammond-Haley, M., Hartley, A., Essa, M., DeLago, A. J., Marshall, D. C., Salciccioli, J. D., et al. (2021). Trends in Ischemic Heart Disease and Cerebrovascular Disease Mortality in Europe: An Observational Study 1990-2017. *J. Am. Coll. Cardiol.* 77, 1697–1698. doi:10.1016/j.jacc.2021.02.013

Hernandez Fustes, O. J., Arteaga Rodriguez, C., and Hernandez Fustes, O. J. (2020). In-Hospital Mortality from Cerebrovascular Disease. *Cureus* 12, e8652. doi:10.7759/cureus.8652

Hou, Y., Wang, X., Zhang, Y., Wang, S., and Meng, X. (2021). Highland Mate: Edible and Functional Foods in Traditional Medicine for the Prevention and Treatment of Hypoxia-Related Symptoms. *Curr. Opin. Pharmacol.* 60, 306–314. doi:10.1016/j.coph.2021.07.018

Hu, G., Li, X., Zhang, S., and Wang, X. (2016). Association of Rat Thoracic Aorta Dilatation by Astragaloside IV with the Generation of Endothelium-Derived Hyperpolarizing Factors and Nitric Oxide, and the Blockade of Ca2+ Channels. *Biomed. Rep.* 5, 27–34. doi:10.3892/br.2016.680

Hu, G., Yang, P., Zeng, Y., Zhang, S., and Song, J. (2018). Danggui Buxue Decoction Promotes Angiogenesis by Up-Regulation of VEGFR1/2 Expressions and Down-Regulation of sVEGFR1/2 Expression in Myocardial Infarction Rat. *J. Chin. Med. Assoc.* 81, 37–46. doi:10.1016/j.jcma.2017.06.015

Ji, H. (2013). *Effects of Absorbed Components of Danggui-Buxue-Tang on Isolated Thoracic Aorta and its Mechanism [D]*. Xiangya Hospital Central South University.

Jia, X. N., Li, J. D., Shao, Z. W., and Wang, Q. Y. (2014). Influences of Formononetin on Contraction of Small Intestine Smooth Muscle of Rabbits *In Vitro*. *Chin. J. Gerontol.* 34, 2174–2176. doi:10.3969/j.issn.1005-9202.2014.08.073

Jiang, X., Liu, X., Liu, X., Wu, X., Jose, P. A., Liu, M., et al. (2020). Low-Dose Aspirin Treatment Attenuates Male Rat Salt-Sensitive Hypertension via Platelet Cyclooxygenase 1 and Complement Cascade Pathway. *J. Am. Heart Assoc.* 9, e013470. doi:10.1161/JAHA.119.013470

Jin, R. N., Qi, X. T., Sun, R., Dai, Y. T., Ma, L. Z., Tong, J. Y., et al. (2019). Research Progress on Pharmacodynamic Material Basis and Quality Control of Danggui Buxue Tan. *Chin. J. Exp. Traditional Med. Formulae* 25, 220–228. doi:10.13422/j.cnki.syfjx.20190648

Kalantar-Zadeh, K., and Rhee, C. M. (2015). Metformin in Chronic Kidney Disease: More Harm Than Help? *Lancet Diabetes Endocrinol.* 3, 579–581. doi:10.1016/S2213-8587(15)00133-3

Krdžić, I., Čovičković-Šternić, N., Katsiki, N., Isenović, E. R., and Radak, Đ. (2015). Correlation of Carotid Artery Disease Severity and Vasomotor Response of Cerebral Blood Vessels. *Angiology* 66, 481–487. doi:10.1177/0003319714538312

Lee, J. Y., and Lee, Y. S. (2011). Vasomotor Reactivity in Middle Cerebral Artery Stenosis. *J. Neurol. Sci.* 301, 35–37. doi:10.1016/j.jns.2010.11.008

Lersy, F., Anheim, M., Willaume, T., Chammas, A., Brisset, J. C., Cotton, F., et al. (2021). Cerebral Vasculitis of Medium-Sized Vessels as a Possible Mechanism of Brain Damage in COVID-19 Patients. *J. Neuroradiol.* 48, 141–146. doi:10.1016/j.neurad.2020.11.004

Li, C., Cheng, C., Jia, W. W., Yang, J. L., Yu, X., and Olajide, O. E. (2021a). Pharmacokinetic Research on Chinese Herbal Medicines: Identifying Potentially Therapeutic Compounds and Characterizing Their Disposition and Pharmacokinetics. *Acta Pharmaceutica Sinica* 56, 2426–2446. doi:10.16438/j.0513-4870.2021-0839

Li, C. Y., Zhu, F. L., Wang, S. S., Wang, J., and Wu, B. (2021b). Danggui Buxue Decoction Ameliorates Inflammatory Bowel Disease by Improving Inflammation and Rebuilding Intestinal Mucosal Barrier. *Evid-based Compl. Alt.* 2021, 8853141. doi:10.1155/2021/8853141

Li, G. (2007). *Neiwaishang Bianhuo Lun*. Beijing: People's Medical Publishing House, 22.

Li, L. (2014). *Study on Porcine Coronary Vasodilataion Mechanism and Pharmacology of Ligustilide [D]*. Lanzhou city: Lanzhou University.

Li, T., Providencia, R., Mu, N., Yin, Y., Chen, M., Wang, Y., et al. (2021c). Association of Metformin Monotherapy or Combined Therapy with Cardiovascular Risks in Patients with Type 2 Diabetes Mellitus. *Cardiovasc. Diabetol.* 20, 30. doi:10.1186/s12933-020-01202-5

Lin, H. Q., Gong, A. G., Wang, H. Y., Duan, R., Dong, T. T., Zhao, K. J., et al. (2017). Danggui Buxue Tang (Astragali Radix and Angelicae Sinensis Radix) for Menopausal Symptoms: A Review. *J. Ethnopharmacol.* 199, 205–210. doi:10.1016/j.jep.2017.01.044

Lin, X. P., Cui, H. J., Yang, A. L., Luo, J. K., and Tang, T. (2018). Astragaloside IV Improves Vasodilatation Function by Regulating the PI3K/Akt/eNOS Signaling Pathway in Rat Aorta Endothelial Cells. *J. Vasc. Res.* 55, 169–176. doi:10.1159/000489958

Lin, Y. Y. (2018). *Effects of XiaoBanXiaTang on Guined Pig Ileum Contractile Activity* in Vitro. *[D]*. Jinan city: Shandong University Of TCM.

Liu, C.-X., Tan, Y.-Z., and Deng, C.-Q. (2021). Main Active Components and Cell Cycle Regulation Mechanism of Astragali Radix and Angelicae Sinensis Radix in the Treatment of Ox-LDL-Induced HUVECs Injury and Inhibition of Their Cell Cycle. *Evidence-Based Complement. Altern. Med.* 2021, 1–12. doi:10.1155/2021/8087183

Liu, Y., Chang, M., Hu, Z., Xu, X., Wu, W., Ning, M., et al. (2021). Danggui Buxue Decoction Enhances the Anticancer Activity of Gemcitabine and Alleviates Gemcitabine-Induced Myelosuppression. *J. Ethnopharmacol.* 273, 113965. doi:10.1016/j.jep.2021.113965

Liu, Y., Niu, L., Cui, L., Hou, X., Li, J., Zhang, X., et al. (2014). Hesperetin Inhibits Rat Coronary Constriction by Inhibiting Ca(2+) Influx and Enhancing Voltage-Gated K(+) Channel Currents of the Myocytes. *Eur. J. Pharmacol.* 735, 193–201. doi:10.1016/j.ejphar.2014.03.057

Lv, J., Zhao, Z., Chen, Y., Wang, Q., Tao, Y., Yang, L., et al. (2012). The Chinese Herbal Decoction Danggui Buxue Tang Inhibits Angiogenesis in a Rat Model of Liver Fibrosis. *Evid. Based Complement. Alternat Med.* 2012, 284963. doi:10.1155/2012/284963

Ma, C. L., Chen, J., Cui, S. M., Zhu, K. M., Li, H. L., and Wu, H. Y. (2018). Effect of Guiqi Congzhi Decoction and its Disassembled Prescriptions onExpressions of HIF-1α, VEGF and HO-1 in Hippocampus Area ofVascular Dementia Rats. *Chin. J. Exp. Traditional Med. Formulae* 24, 143–148. doi:10.13422/j.cnki.syfjx.20181532

Ma, G., Zhang, J., Yang, X., Guo, P., Hou, X., Fan, Y., et al. (2020). TMEM16A-encoded Anoctamin 1 Inhibition Contributes to Chrysin-Induced Coronary Relaxation. *Biomed. Pharmacother.* 131, 110766. doi:10.1016/j.biopha.2020.110766

Mamo, Y. A., Angus, J. A., Ziogas, J., SoedingWright, P. F. C. E., and Wright, C. E. (2014). The Role of Voltage-Operated and Non-voltage-operated Calcium Channels in Endothelin-Induced Vasoconstriction of Rat Cerebral Arteries. *Eur. J. Pharmacol.* 742, 65–73. doi:10.1016/j.ejphar.2014.09.002

Mehanna, R., and Jankovic, J. (2013). Movement Disorders in Cerebrovascular Disease. *Lancet Neurol.* 12, 597–608. doi:10.1016/S1474-4422(13)70057-7

Mustanoja, S., Putaala, J., Koivunen, R. J., Surakka, I., and Tatlisumak, T. (2018). Blood Pressure Levels in the Acute Phase after Intracerebral Hemorrhage Are Associated with Mortality in Young Adults. *Eur. J. Neurol.* 25, 1034–1040. doi:10.1111/ene.13662

National Health Commission (2019). *China Health Statistics Yearbook*. Beijing: China Peking Union Medical University Press, 281–282.

Nguyen, H. T., Nguyen, H. T., Islam, M. Z., Obi, T., Pothinuch, P., Nguyen, T. V., et al. (2016). Antagonistic Effects of Gingko Biloba and Sophora Japonica on Cerebral Vasoconstriction in Response to Histamine, 5-Hydroxytryptamine,

U46619 and Bradykinin. *Am. J. Chin. Med.* 44, 1607–1625. doi:10.1142/S0192415X16500907

Pantoni, L. (2010). Cerebral Small Vessel Disease: from Pathogenesis and Clinical Characteristics to Therapeutic Challenges. *Lancet Neurol.* 9, 689–701. doi:10.1016/S1474-4422(10)70104-6

Shi, X. Q., Zhu, Z. H., Yue, S. J., Tang, Y. P., Chen, Y. Y., Pu, Z. J., et al. (2020). Integration of Organ Metabolomics and Proteomics in Exploring the Blood Enriching Mechanism of Danggui Buxue Decoction in Hemorrhagic Anemia Rats. *J. Ethnopharmacol.* 261, 113000. doi:10.1016/j.jep.2020.113000

Shu, T. H., and Pan, H. Y. (2017). Effects of Buyang Huanwu Decoction and its Decomposed Recipes on Neural Function and Angiogenesisafter Focal Cerebral Ischemia in Rats. *Chin. J. Cerebrovasc. Dis.* 14, 87–93.

Song, J. G. (2018). *Study on the Effects of Ferulic Acid and Astragaloside IV in Different Proportion on Regulating the Tension of Thoracic Aorta in Rats and its Mechanism [D]*. Chengdu city: Chengdu University of TCM.

Sturiale, C. L., Ricciardi, L., Marchese, E., Puca, A., Olivi, A., and Albanese, A. (2020). Surgical Treatment of Anterior Communicating Artery Aneurysms: Hints and Precautions for Young Cerebrovascular Surgeons. *J. Neurol. Surg. A. Cent. Eur. Neurosurg.* 81, 463–471. doi:10.1055/s-0039-3401985

Tan, X. X., Zhu, H. M., Tang, C., and Wang, X. (2021). HPLC-MS Identification on Flavonoids in Astragali Radix Decoction. *Drugs & Clinic* 36, 231–235. doi:10.7501/j.issn.1674-5515.2021.02.004

Trillhaase, A., Maertens, M., and Aherrahrou, Z. (2021). Induced Pluripotent Stem Cells (iPSCs) in Vascular Research: from Two- to Three-Dimensional Organoids. *Stem Stem Cel Rev. Rep.* 18, 1–13. doi:10.1007/s12015-021-10149-3

Tykocki, N. R., Boerman, E. M., and Jackson, W. F. (2017). Smooth Muscle Ion Channels and Regulation of Vascular Tone in Resistance Arteries and Arterioles. *Compr. Physiol.* 7, 485–581. doi:10.1002/cphy.c160011

Virani, S. S., Alonso, A., Aparicio, H. J., Benjamin, E. J., Bittencourt, M. S., Callaway, C. W., et al. (2021). Heart Disease and Stroke Statistics-2021 Update: A Report from the American Heart Association. *Circulation* 143, e254–e743. doi:10.1161/CIR.0000000000000950

Wang, P., and Liang, Y. Z. (2010). Chemical Composition and Inhibitory Effect on Hepatic Fibrosis of Danggui Buxue Decoction. *Fitoterapia* 81, 793–798. doi:10.1016/j.fitote.2010.04.007

Wang, X., Hou, Y., Ai, X., Sun, J., Xu, B., Meng, X., et al. (2020). Potential Applications of Microfluidics Based Blood Brain Barrier (BBB)-on-chips for *In Vitro* Drug Development. *Biomed. Pharmacother.* 132, 110822. doi:10.1016/j.biopha.2020.110822

Wang, X. H., Zhu, L., and Cheng, H. (2006). Effect of Astragaloside Ⅳ on Contraction and Relaxation in Isolated Rat Aortic Rings. *Chin. Pharmacol. Bull.* 11, 1319–1324. doi:10.3321/j.issn:1001-1978.2006.11.009

Wang, X., Liu, Z., Fan, F., Hou, Y., Yang, H., Meng, X., et al. (2019). Microfluidic Chip and its Application in Autophagy Detection. *Trac Trends Anal. Chem.* 117, 300–315. doi:10.1016/j.trac.2019.05.043

Wang, X. (2017). *Research on the Different Diastolic Effects of Astragaloside IV on Small Vessels in Different Organs and its Mechanism [D]*. Chengdu city: Chengdu University of TCM.

Wu, B. (2016). Clinical Effect of Shenqi Sichong Decoction Combined with Danggui Buxue Decoction in the Treatment of Vertebrobasilar Insufficiency Vertigo. *China Med. Herald* 13, 92–95.

Xu, H., Zhang, Y., Wang, P., Zhang, J., Chen, H., Zhang, L., et al. (2021). A Comprehensive Review of Integrative Pharmacology-Based Investigation: A Paradigm Shift in Traditional Chinese Medicine. *Acta Pharm. Sin. B* 11, 1379–1399. doi:10.1016/j.apsb.2021.03.024

Yan, X. K., Li, T. L., and Huang, Y. X. (2010). Studies on Chemical Components of Lyophilized Powder of Sinisan. *Chin. Traditional Herbal Drugs* 41, 854–859.

Yang, M., Chan, G. C., Deng, R., Ng, M. H., Cheng, S. W., Lau, C. P., et al. (2009). An Herbal Decoction of Radix Astragali and Radix Angelicae Sinensis Promotes Hematopoiesis and Thrombopoiesis. *J. Ethnopharmacol.* 124, 87–97. doi:10.1016/j.jep.2009.04.007

Yang, P., Feng, P., Yang, M., Zeng, Y., and Zhang, S. Y. (2013). Effect of Danggui Buxue Decoction on Proliferation and its Molecular Mechanism in Hypoxic Vascular Endothelial Cells. *Chin. J. Exp. Traditional Med. Formulae* 19, 178–181. doi:10.11653/syfj2013220178

Yang, X. W., Chen, Y., Xue, Q., Feng, Y. Y., Ding, Q., and Qiu, W. M. (2020). Analysis of Risk and Benefit of Alteplase Intravenous Thrombolysis in Patients with Acute Ischemic Stroke of Different Ages. *Chin. J. Hosp. Pharm.* 40, 2247–2250. doi:10.13286/j.1001-5213.2020.21.08

Zhou, Z. Y., Xu, J. Q., Zhao, W. R., Chen, X. L., Jin, Y., Tang, N., et al. (2017). Ferulic Acid Relaxed Rat Aortic, Small Mesenteric and Coronary Arteries by Blocking Voltage-Gated Calcium Channel and Calcium Desensitization via Dephosphorylation of ERK1/2 and MYPT1. *Eur. J. Pharmacol.* 815, 26–32. doi:10.1016/j.ejphar.2017.10.008

Zhu, M., Duan, J. A., Tang, Y. P., Hua, Y. Q., Chen, F., Su, S. L., et al. (2011). Inhibition of Contraction of Isolated Mouse Uterine by Siwu Decoction and It's Composite Drugs. *Chin. J. Exp. Traditional Med. Formulae* 17, 149–152. doi:10.13422/j.cnki.syfjx.2011.05.068

Conflict of Interest: The authors declare that the research was conducted in the absence of any commercial or financial relationships that could be construed as a potential conflict of interest.

Publisher's Note: All claims expressed in this article are solely those of the authors and do not necessarily represent those of their affiliated organizations or those of the publisher, the editors, and the reviewers. Any product that may be evaluated in this article or claim that may be made by its manufacturer is not guaranteed or endorsed by the publisher.

frontiers in Pharmacology

ORIGINAL RESEARCH
published: 03 January 2022
doi: 10.3389/fphar.2021.752244

Protective Effects of Allicin on Acute Myocardial Infarction in Rats *via* Hydrogen Sulfide-mediated Regulation of Coronary Arterial Vasomotor Function and Myocardial Calcium Transport

Tianwei Cui[1,2†], Weiyu Liu[1†], Chenghao Yu[1†], Jianxun Ren[1], Yikui Li[3], Xiaolu Shi[4], Qiuyan Li[5]* and Jinyan Zhang[1]**

[1]Institute of Basic Medical Sciences, Xiyuan Hospital, China Academy of Chinese Medical Sciences, Beijing, China, [2]Department of Reproductive Medicine, The First Affiliated Hospital of Henan University of Chinese Medicine, Zhengzhou, China, [3]Health Prevention Department, Xiyuan Hospital, China Academy of Chinese Medical Sciences, Beijing, China, [4]Beijing Key Laboratory of TCM Basic Research on Prevention and Treatment of Major Disease, Experimental Research Center, China Academy of Chinese Medical Sciences, Beijing, China, [5]Department of General Medicine, Xiyuan Hospital, China Academy of Chinese Medical Sciences, Beijing, China

Acute myocardial infarction (AMI) is a condition with high morbidity and mortality, for which effective treatments are lacking. Allicin has been reported to exert therapeutic effects on AMI, but the underlying mechanisms of its action have not been fully elucidated. To investigate this, a rat model of AMI was generated by ligating the left anterior descending branch of the coronary artery. DL-propargylglycine (PAG), a specific hydrogen sulfide (H_2S) synthetase inhibitor, was used to examine the effects of allicin on H_2S production. Isolated coronary arteries and cardiomyocytes were assessed for vascular reactivity and cellular Ca^{2+} transport using a multiwire myography system and a cell-contraction-ion detection system, respectively. Allicin administration improved cardiac function and myocardial pathology, reduced myocardial enzyme levels, and increased H_2S and H_2S synthetase levels. Allicin administration resulted in concentration-dependent effects on coronary artery dilation, which were mediated by receptor-dependent Ca^{2+} channels, ATP-sensitive K^+ channels, and sarcoplasmic reticulum (SR) Ca^{2+} release induced by the ryanodine receptor. Allicin administration improved Ca^{2+} homeostasis in cardiomyocytes by increasing cardiomyocyte contraction, Ca^{2+} transient amplitude, myofilament sensitivity, and SR Ca^{2+} content. Allicin also enhanced Ca^{2+} uptake via SR Ca^{2+}-ATPase and Ca^{2+} removal via the Na^+/Ca^{2+} exchanger, and it reduced SR Ca^{2+} leakage. Notably, the protective effects of allicin were partially attenuated by blockade of H_2S production with PAG. Our findings provide novel evidence that allicin-induced production of H_2S mediates coronary artery dilation and regulation of Ca^{2+} homeostasis in AMI. Our study presents a novel mechanistic insight into the anti-AMI effects of allicin and highlights the therapeutic potential of this compound.

Keywords: allicin, myocardial infarction, hydrogen sulfide, calcium homeostasis, coronary artery

OPEN ACCESS

Edited by:
Qilong Wang,
Tianjin University of Traditional Chinese Medicine, China

Reviewed by:
Eugenia Piragine,
University of Pisa, Italy
Zhen Li,
Louisiana State University, United States

***Correspondence:**
Jinyan Zhang
jinyanz@163.com
Qiuyan Li
liqiuyan1968@sohu.com
Xiaolu Shi
shixiaolu365@163.com

†These authors have contributed equally to this work

Specialty section:
This article was submitted to Cardiovascular and Smooth Muscle Pharmacology, a section of the journal Frontiers in Pharmacology

Received: *02 August 2021*
Accepted: *30 November 2021*
Published: *03 January 2022*

Citation:
Cui T, Liu W, Yu C, Ren J, Li Y, Shi X, Li Q and Zhang J (2022) Protective Effects of Allicin on Acute Myocardial Infarction in Rats via Hydrogen Sulfide-mediated Regulation of Coronary Arterial Vasomotor Function and Myocardial Calcium Transport. Front. Pharmacol. 12:752244. doi: 10.3389/fphar.2021.752244

1 INTRODUCTION

Acute myocardial infarction (AMI) is a condition with high morbidity and mortality (McAloon et al., 2016). Despite the substantial technological and pharmacological developments of the recent years, the steady increase in the incidence of AMI and its poor prognosis remain significant clinical problems. Therefore, there is an urgent need to develop novel therapeutic strategies for preventing AMI. In this regard, traditional Chinese medicine (TCM) offers various advantages including the ability to target multiple biological pathways, low toxicity and costs, and fewer side effects (Liu et al., 2011).

Allicin, the main pharmacologically active ingredient in crushed raw garlic cloves (Lawson and Hunsaker, 2018), has various cardioprotective properties (Mocayar Marón et al., 2020), including blood pressure reduction, blood lipid regulation, atherosclerosis prevention, and myocardium protection against AMI. Nevertheless, the biological mechanisms underlying the protective action of allicin against AMI have not been fully elucidated. Studies have reported that in a rat model of AMI, allicin reduced oxidative stress injury and apoptosis by modulating the JNK signaling pathway in cardiomyocytes (Xu et al., 2020), and inhibited inflammation by relieving myocardial ischemia-reperfusion injury (Liu et al., 2019). We previously demonstrated that allicin exerted anti-fibrotic and anti-apoptotic effects in the myocardium, thereby ameliorating cardiac dysfunction in a rat model of AMI (Ma et al., 2017). Extensive evidence supports the importance of coronary artery tension, which maintains sufficient blood supply to the myocardium, in AMI injury (Uren et al., 1994). In addition, Ca^{2+} homeostasis, which is regulated by Ca^{2+}-induced excitation-contraction coupling, is a critical determinant of cardiac contractile function. In fact, Ca^{2+} dyshomeostasis may lead to impaired systolic-diastolic function of cardiomyocytes after AMI (Zhang et al., 2021). Therefore, we speculated that the anti-AMI effects of allicin might be related to the coronary vasomotor function and Ca^{2+} transport in cardiomyocytes.

Hydrogen sulfide (H_2S) plays a crucial role in cardiovascular homeostasis. In the human body, H_2S production is predominantly catalyzed by cystathionine-γ-lyase (CSE), cystathionine-β-synthase (CBS), and 3-mercaptopyruvate sulfurtransferase (3-MST). To date, most scholars have proposed that CSE is the primary H_2S-producing enzyme in the cardiovascular system (Singh and Banerjee, 2011; Leigh et al., 2016). H_2S induces vasodilation, promotes angiogenesis, and regulates endothelial cell migration and inflammatory pathways (Li S. et al., 2017; Wang et al., 2021). Studies have showed that H_2S can mediate the vasoactivity of garlic (Benavides et al., 2007), and that diallyl disulfide, a compound found in garlic, is a H_2S-donor in both a cell-free system and vascular cells (Martelli et al., 2013; Martelli et al., 2020). As a sulfur compound, allicin has also been suggested to exert cardiovascular effects via the production of H_2S *in vivo* (Wang et al., 2010). We previously demonstrated that allicin reduced blood pressure by promoting vasodilation in spontaneously hypertensive rats by inducing H_2S production (Cui et al., 2020), a finding that was consistent with the literature. The present study aimed to evaluate the beneficial effects of allicin in a rat model of AMI and to elucidate the mechanisms related to H_2S production. We hypothesized that allicin might protect against AMI injury in rats by inducing coronary artery vasodilation and regulating Ca^{2+} homeostasis by favoring H_2S production.

2 MATERIALS AND METHODS

2.1 Chemicals and Reagents

Allicin was provided by Xinjiang Ailexin Pharmaceutical Co., Ltd. (Batch No. 20190428, Xinjiang, China). DL-propargylglycine (PAG, inhibitor of the hydrogen sulfide synthetase, cystathionine-gamma-lyase [CSE]) was purchased from Shanghai Yuanye Bio-Technology (S18M7L11462, Shanghai, China). Diltiazem (a Ca^{2+}-channel blocker) was purchased from Tianjin Tanabe Pharmaceutical Co., Ltd. (Batch No. 1905029, Tianjin, China). Potassium chloride (KCl), 5-hydroxytryptamine (5-HT), endothelin-1 (ET-1), tetraethylamine (TEA, inhibitor of Ca^{2+}-sensitive potassium channels), 4-aminopyridine (4-AP, inhibitor of voltage-dependent potassium channels), barium chloride ($BaCl_2$, inhibitor of inwardly rectifying potassium channels) and glibenclamide (Glib, inhibitor of ATP-sensitive potassium channels) were purchased from Sigma-Aldrich (St. Louis, MO, United States). All other reagents were of analytical purity.

2.2 Measurement of the Effects of Allicin on Acute Myocardial Infarction and Involvement of Hydrogen Sulfide

2.2.1 Animals

Male 8-week-old Sprague Dawley (SD) rats (weighing 200–220 g) were utilized in the present study.

2.2.2 Induction of Myocardial Infarction, Animal Grouping, and Treatment

The AMI model was generated via left anterior descending coronary artery (LAD) ligation in SD rats. Briefly, rats were anesthetized with 1% pentobarbital sodium. After left thoracotomy, the heart was exteriorized, and the LAD was ligated approximately 2 mm below the left atrium with a 6–0 silk suture. AMI was confirmed by elevation of the ST segment on an electrocardiogram and bulging of the relevant segment of the left ventricle (LV). In the sham group, the suture was removed without tying, and no infarction was generated. After establishment of the AMI model, rats were divided into six groups (n = 14–16 per group) by a random number table: sham, model, diltiazem (8.1 mg/kg), allicin (14 mg/kg), allicin (7 mg/kg), and allicin (14 mg/kg) + PAG (32 mg/kg) groups (Cui et al., 2020). All groups received intraperitoneal injection once a day for 7 days.

2.2.3 Echocardiography and Myocardial Staining

Cardiac function was assessed using a Vevo 3100 echocardiography system (Visual sonics Inc, Toronto, Canada). Rats were anesthetized with 1.5–2% isoflurane via

continuous inhalation and warmed on a heated pad (37°C). Ultrasound transmission gel was applied to the chest, and echocardiography (M-mode and B-mode imaging) was performed. The LV internal diameter and thickness of the anterior wall at end-diastole (LVID d, LVAW d) and end-systole (LVID s, LVAW s), as well as LV fractional shortening (FS), ejection fraction (EF), and stroke volume (SV) were measured in each rat in a blinded manner. All values were averaged using three to five cardiac cycles per rat. Rat hearts were harvested after 1% pentobarbital sodium overdose via intraperitoneal injection and sliced into five sections of 1-mm thickness across the left ventricular long axis under the ligature. To identify the infarction area, heart slices were incubated with nitro-blue tetrazolium chloride (Sigma-Aldrich) for 3 min at 22 ± 2°C. Infarction areas were measured using Image-Pro Plus software (Version 6.0; Media Cybernetics, Silver Springs, MD, United States) and presented as a percentage of infarct area to ventricular area or total area.

2.2.4 Serum cTnI, LDH, and CSE Levels

Before the rats were sacrificed, blood samples were collected from the abdominal aorta. Serum was incubated at 22 ± 2°C for 30 min and centrifuged at 975.87 ×g for 10 min. The supernatant was collected for determination of serum cardiac troponin I (cTnI), lactate dehydrogenase (LDH), and CSE levels. Levels of serum cTnI, LDH, and CSE were separately quantified with commercially available cTnI (Medical Discovery Leader, Beijing, China, 159632), LDH (Medical Discovery Leader, Beijing, China, 164752), and CSE ELISA kits (Bluegene, Shanghai, China, E02C0834); antibody and chromogenic agent were added according to the manufacturer's instructions. Absorbance was measured at 450 nm, detected by a microplate tester. Levels of LDH, cTnI, and CSE were calculated according to the standard curve (Chen et al., 2019; Li J. et al., 2020; Wu et al., 2020).

2.2.5 Immunofluorescence Assay of Myocardial CSE

The border zone of myocardial infarction tissues were fixed with 4% (v/v) paraformaldehyde and incubated with dimethylbenzene for 30 min before serum blocking for 60 min. Specimens were incubated with CSE antibody (Proteintech, Wuhan, China, 12217-1-AP) for 24 h at 4°C prior to incubation with goat anti-rabbit IgG (H + L) fluorescein isothiocyanate-conjugated polyclonal antibody (20200321, Bai Aotong Experimental Materials Center, Luoyang, China) in the dark at 37°C for 60 min. After washing specimens in phosphate buffer solution, nuclei were stained with 4′, 6-diamidino-2-phenylindole (Sigma-Aldrich). Images were obtained using an upright fluorescence microscope (DM-LFS, Leica, MH, Germany) under ×400 magnification.

2.2.6 Hydrogen Sulfide Levels

Levels of H_2S in serum and the border zone of myocardial infarction tissue were measured using methylene blue spectrophotometry at 665 nm according to manufacturer's instructions (Nanjing Jiancheng Bioengineering Institute, Nanjing, China).

2.2.7 Histologic Examination

Hearts were harvested, weighed, washed in phosphate buffer solution, fixed in 4% paraformaldehyde overnight, and embedded in paraffin. Each paraffin-embedded heart was cut into 4-μm thick sections through the infarction area and stained with hematoxylin and eosin (H&E) for morphological observation. Specimens were stained with Masson's trichrome stain to evaluate collagen volume. Sections were imaged using a stereomicroscope (Olympus SZ61, Tokyo, Japan).

2.3 Allicin Treatment of Isolated Coronary Arteries

2.3.1 Preparation of Rat Coronary Arterial Rings

The coronary arterial rings (diameter: 100–300 μm) of SD rats were then isolated and placed in a cold Krebs buffer [composition (mM): NaCl, 119; KCl, 4.6; $CaCl_2$, 1.5; NaH_2PO_4, 1.2; $MgCl_2$, 1.2; $NaHCO_3$, 15; Glucose, 5.6; pH 7.4]. RCARs were prepared and performed as previously described (Cui et al., 2020).

2.3.2 Allicin-Induced Vasodilation of Rat Coronary Arterial Rings

RCARs were contracted with KCl (6×10^{-2} M) until a plateau of contraction was reached. The rings were then divided equally into two groups (8 rings each): PAG or control. RCARs were incubated with PAG (10^{-2} M) or the same volume of saline, respectively, for 5 min. Both groups were treated with allicin (10^{-5}–$10^{-4.2}$ M) and cumulative concentration-response curves were obtained.

2.3.3 Effect of Allicin on Ca^{2+} Channel-Induced Contraction

KCl mediates the opening of voltage-dependent Ca^{2+} channels (VDCCs), whereas U46619, 5-HT, and ET-1 mediate the opening of receptor-dependent Ca^{2+} channels (RDCCs). In this study, RCARs were divided into three groups (8 rings each): allicin, allicin + PAG, and control groups. Rings were incubated with allicin ($10^{-4.8}$ M), allicin ($10^{-4.8}$ M) + PAG (10^{-2} M), or the equivalent volume of saline, respectively, for 5 min. Cumulative concentration-response curves for KCl ($10^{-1.54}$–$10^{-1.42}$ M), U46619 (10^{-8}–10^{-5} M), 5-HT (10^{-8}–10^{-4} M), and ET-1 (10^{-9}–10^{-6} M) were obtained.

2.3.4 Effects of Potassium Pathway Inhibitors on Allicin-Induced Vasodilation

To investigate the contribution of Ca^{2+}-sensitive potassium channels (K_{Ca}), voltage-dependent potassium channels (Kv), inwardly rectifying potassium channels (K_{ir}), and ATP-sensitive potassium channels (K_{ATP}) to allicin-induced vasodilation, the corresponding inhibitors, TEA (10^{-3} M), 4-AP (10^{-3} M), $BaCl_2$ (10^{-5} M) and Glib (10^{-5} M) were applied. RCARs were divided into two groups (8 rings each): control and inhibitor groups. The rings were incubated with the four respective inhibitors for each channel or the same volume of saline for 5 min. Cumulative concentration-response curves for allicin (10^{-5}–$10^{-4.2}$ M) were obtained.

If the maximum vasodilatory effect in the inhibitor group was lower than that in the control group, subsequent experiments were conducted, as follows. The rings were divided into three groups (8 rings each): inhibitor, PAG, and PAG + inhibitor groups. Cumulative concentration-response curves for allicin (10^{-5}–$10^{-4.2}$ M) were obtained as described above.

2.3.5 Effect of Allicin on Caffeine-Induced Contraction

The grouping and intervention for RCARs were performed as described above (See "Effect of Allicin on Ca^{2+} Channel-induced Contraction" section). Contraction-response curves for caffeine (3×10^{-2} M) were obtained.

2.4 Effects of Allicin on Ca^{2+} Transport in Cardiomyocytes

2.4.1 Measurement of Sarcomere Shortening and Cytosolic Ca^{2+} Transients

Isolated cardiomyocytes were loaded with 2 μM Fura-2 AM (Sigma-Aldrich) in the dark for 30 min at 22 ± 2°C. Cells were washed, resuspended twice in Tyrode's solution (concentration in mM: 137.0 NaCl, 1.2 NaH_2PO_4, 5.0 KCl, 1.2 $MgCl_2$, 10.0 HEPES, 10.0 glucose, and 1.2 $CaCl_2$ [pH 7.4]), and placed in a cell chamber. Myocytes were stimulated to contract at a pacing frequency of 1 Hz with 4 ms of electrical stimulation. Myocytes were exposed to 340 or 380 nm excitation wavelengths, and the emitted fluorescent signal was detected at 510 nm. Sarcomere length and fluorescence intensity (a proxy of Ca^{2+} concentration) were synchronously recorded with a cell contraction-ion detection system (IonOptix, Westwood, MA, United States). Contractility parameters including amplitude, peak time, systolic half-time of decay (T_{50}), diastolic T_{50}, and myofilament sensitivity were measured. Ca^{2+} transient parameters including amplitude, maximum ascending and descending velocity, and Ca^{2+} decline time constant were also recorded.

2.4.2 Measurement of Sarcoplasmic Reticulum Ca^{2+} Content

SR Ca^{2+} content is associated with caffeine-sensitive Ca^{2+} release (Santulli et al., 2017). Short puffs of 10 mM caffeine were applied to completely empty the SR, following a train of 1-Hz field stimulation to achieve steady-state SR Ca^{2+} loading in ventricular myocytes. SR Ca^{2+} content was assessed by measuring the amplitude of caffeine-elicited Ca^{2+} transients ($\triangle F/F_0$).

2.4.3 Assessment of Ca^{2+} Removal

Rapid and continuous application of 10 mM caffeine was employed to induce SR Ca^{2+} release and assess the contribution of the Na^+/Ca^{2+} exchanger (NCX) and slow transport systems (mitochondrial Ca^{2+} uniporter and sarcolemmal Ca^{2+}-ATPase). The contribution of the slow transport system to Ca^{2+} removal is only 1% and is often overlooked (Puglisi et al., 2014). With continuous caffeine superfusion, a decrease in fluorescence (F340/380) indicates Ca^{2+} removal, which is predominantly attributable to the NCX. Ca^{2+} removal was predominantly achieved by sarco/endoplasmic reticulum Ca^{2+}-ATPase (SERCA) uptake and NCX Ca^{2+} efflux with superfusion of Tyrode's solution. Based on these factors, the time of SERCA-mediated Ca^{2+} removal was calculated (Tau).

2.4.4 Ca^{2+} Leakage Assessment

Ca^{2+} leakage levels were assessed by perfusing myocytes with 1 mM tetracaine and reperfusing in 10 mM Na-, Ca-free Tyrode's solution (containing Li^+ and EGTA instead of Na^+ and Ca^{2+}). Levels of SR Ca^{2+} leakage were calculated based on the difference in cytosolic Ca^{2+} concentration before and after tetracaine perfusion.

2.5 Statistical Analysis

The SPSS statistical software (SPSS 20.0, IBM, Chicago, IL, United States) was used for statistical analysis. Vasodilation and vasocontraction are expressed as the percentage of precontraction amplitude. The negative logarithms of the concentration that produced the half-maximal effect (pEC_{50}) and maximum relaxation (R_{max}) or contraction (E_{max}) were determined using concentration negative logarithm-effect curves. The differences in vasomotor responses to allicin, as well as in the levels of KCl, 5-HT, U46619, and ET-1 were compared by a two-way analysis of variance (ANOVA), with a *post hoc* Bonferroni test for group comparison. Statistical significance was determined through a one-way ANOVA with Dunnett's test for multiple-group comparisons in other experiments. $^*p < 0.05$, $^{**}p < 0.01$ vs. sham group, $^{\triangle}p < 0.05$, $^{\triangle\triangle}p < 0.01$ vs. AMI model group, $^{\#}p < 0.05$, $^{\#\#}p < 0.01$ vs. allicin 14 mg/kg group in all figures. All data are presented as the mean ± S.E.M.

3 RESULTS

3.1 Effects of Allicin on Acute Myocardial Infarction and the Involvement of Hydrogen Sulfide

3.1.1 Cardiac Function

Ventricular size and function were measured to assess the effect of allicin treatment. There was no statistical difference in LVID d among the groups. LVID s was significantly greater in the model group than in the sham group (**Figure 1A**), whereas the values of LVAW s, LVAW d, EF, FS, and SV were significantly lower in the model group than in the sham group. On the contrary, LVID s was significantly lower, and LVAW s, LVAW d, EF, FS, and SV were significantly higher, in the diltiazem 8.1 mg/kg and allicin 14 mg/kg groups than in the model group. LVID s was significantly higher, and LVAW s, LVAW d, EF, FS, and SV were significantly lower in the allicin 14 mg/kg + PAG group than in the allicin 14 mg/kg group (**Figures 1B–F**). Hence, as shown in **Figure 1G**, we found that allicin significantly improved the cardiac function of AMI rats, and PAG partially weakened this effect.

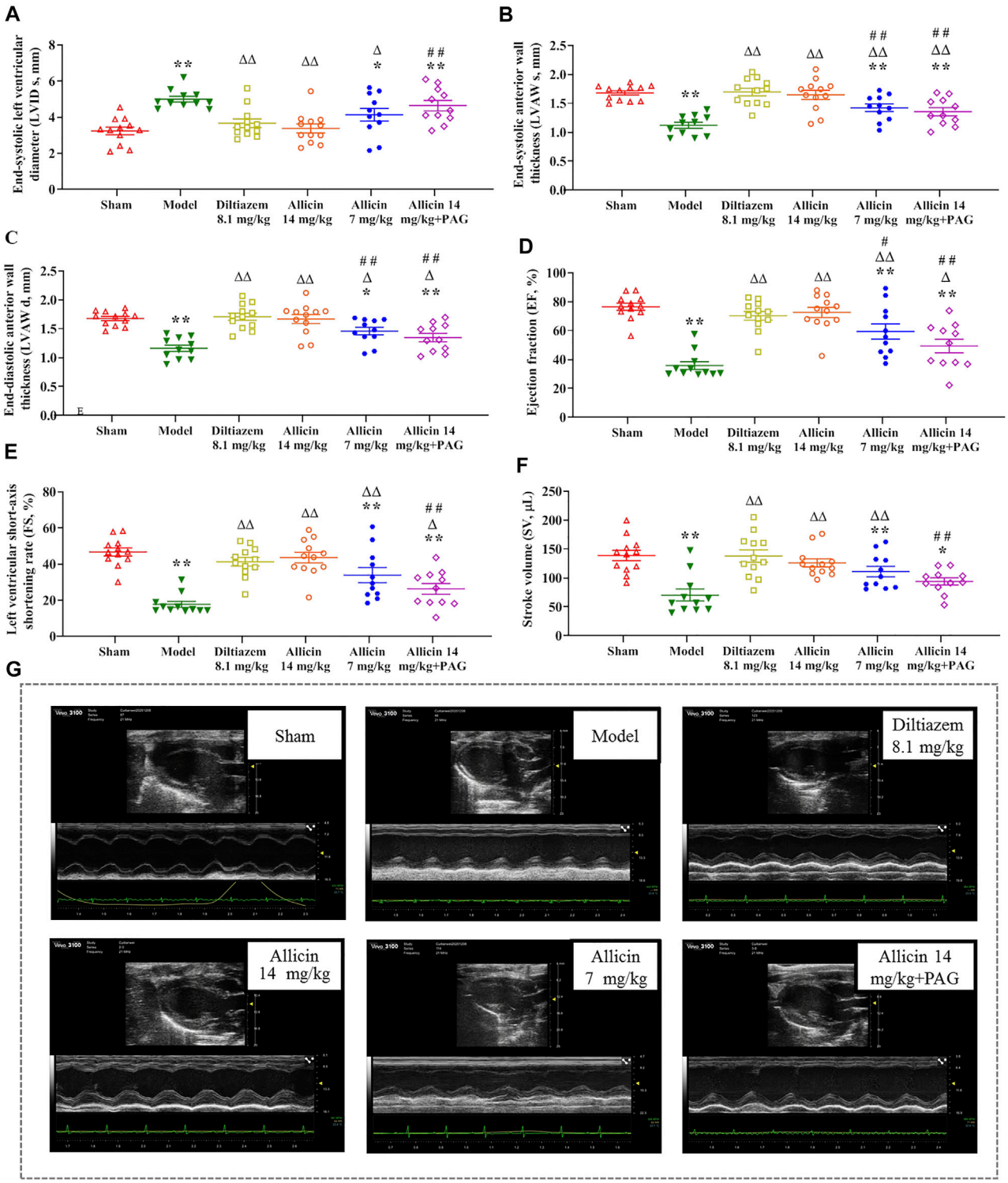

FIGURE 1 | Allicin improved cardiac function in AMI model rats. **(A–F)** The statistical scatter plots of **(A)** LVID s, **(B)** LVAW s, **(C)** LVAW d, **(D)** EF, **(E)** FS, and **(F)** SV in the experimental and control groups. **(G)** Representative images of ultrasonic function in experimental and control groups. Data are expressed as mean ± S.E.M ($n = 11–12$). $^{*}p < 0.05$, $^{**}p < 0.01$ vs. control; $^{\triangle}p < 0.05$, $^{\triangle\triangle}p < 0.01$ vs. the Model group; $^{\#}p < 0.05$, $^{\#\#}p < 0.01$ vs. the Allicin 14 mg/kg group. Abbreviations: LVID s, left ventricular internal diameter end systole; LVAW s, left ventricular end-systolic anterior wall thickness; LVAW d, left ventricular end-diastolic anterior wall thickness; EF, ejection fraction; FS, functional shortening; SV, stroke volume; PAG, DL-propargylglycine.

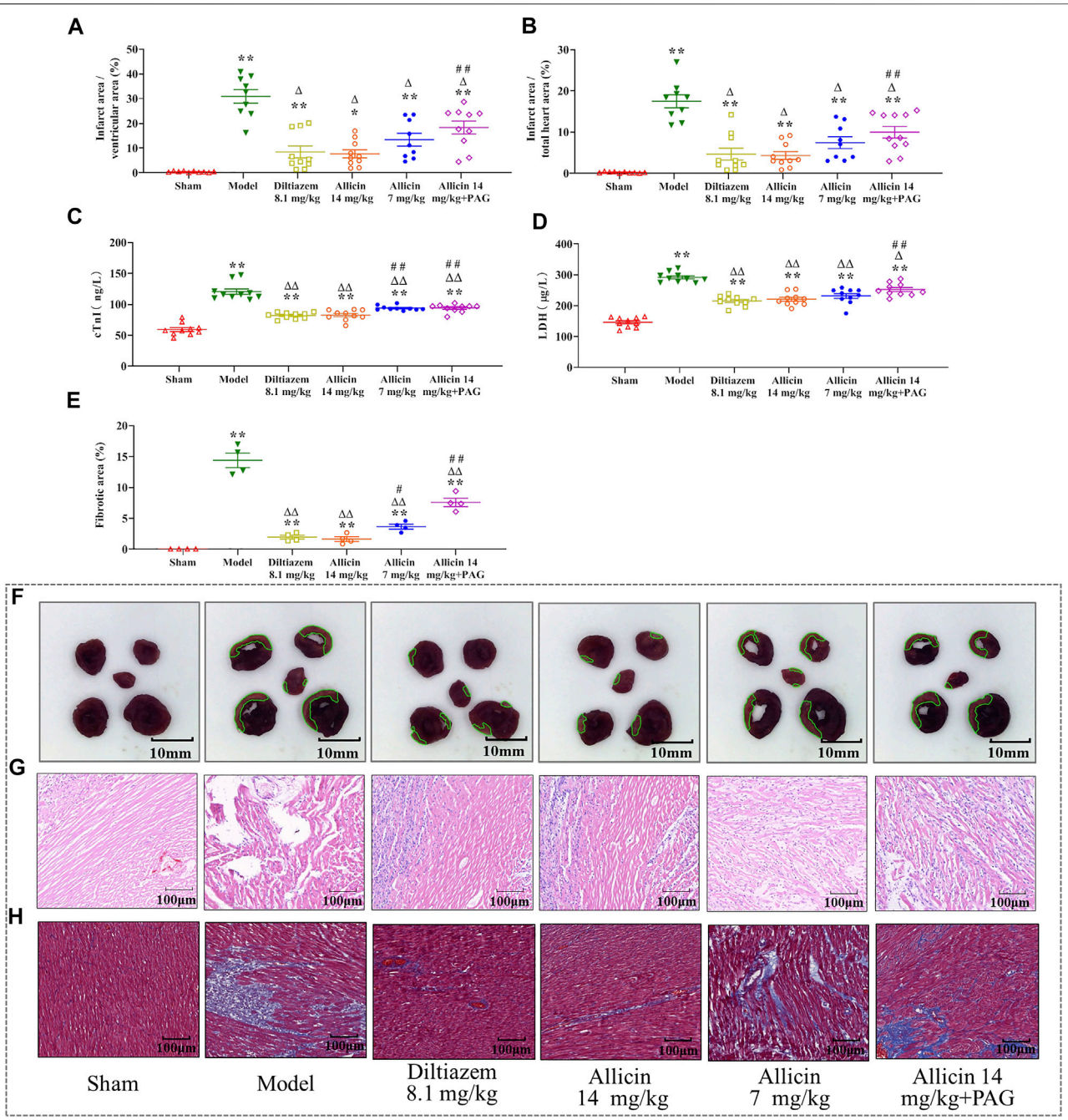

FIGURE 2 | Allicin reduced myocardial infarction area and improved morphological changes in myocardial tissue. **(A,B)** Percentage of myocardial infarction area over the ventricular and total heart area, respectively (n = 9–11). **(C,D)** Effects of allicin on serum cTnI and LDH levels (n = 9–11). **(E)** Percentage of myocardial fibrosis area stained with Masson's trichrome staining (n = 4). **(F)** Representative myocardial infarction areas in each group (n = 9–11). **(G,H)** Effects of allicin on the pathological morphology of the myocardium in rats with acute myocardial infarction by H&E staining and Masson staining (n = 9–11), magnification ×200. Data are expressed as mean ± S.E.M. $^{*}p < 0.05$, $^{**}p < 0.01$ vs. control; $^{\triangle}p < 0.05$, $^{\triangle\triangle}p < 0.01$ vs. the Model group; $^{\#}p < 0.05$, $^{\#\#}p < 0.01$ vs. the Allicin 14 mg/kg group. Abbreviations: LDH, lactate dehydrogenase; cTnI, cardiac troponin; PAG, DL-propargylglycine.

3.1.2 Myocardial Infarction Size

The percentages of myocardial infarction area to ventricular area (ITV) and total heart area (ITT) were significantly lower in the sham group (0.42 ± 0.26% and 0.23 ± 0.16%, respectively) than in the model group (30.89 ± 8.26% and 17.49 ± 4.75%, respectively). ITV and ITT were significantly reduced by treatment with 14 mg/kg of allicin (7.67 ± 5.15% and 4.33 ± 2.84%, respectively) and 8.1 mg/kg of diltiazem (8.27 ± 7.65% and

4.67 ± 4.57%, respectively). However, in the allicin 14 mg/kg + PAG group, ITV and ITT were significantly higher (17.57 ± 8.17% and 9.97 ± 4.63%, respectively) than in the allicin 14 mg/kg group, but significantly lower than in the model group (**Figures 2A,B**). Hence, allicin significantly decreased the myocardial infarction area of AMI rats, and PAG partially weakened the effect of allicin (**Figure 2E**).

3.1.3 Serum cTnI and LDH Levels

cTnI and LDH levels were significantly higher in the model group than in the sham group (cTnI: 120.53 ± 13.93 ng/L vs. 59.39 ± 9.81 ng/L; LDH: 291.81 ± 15.91 μg/L vs. 146.62 ± 16.20 μg/L), indicating that the model successfully mimicked AMI conditions. Levels of cTnI and LDH were significantly lower in the diltiazem 8.1 mg/kg group (82.12 ± 5.09 ng/L and 215.06 ± 16.16 μg/L, respectively), allicin 14 mg/kg group (82.82 ± 8.30 ng/L and 220.77 ± 19.85 μg/L, respectively), allicin 7 mg/kg group (94.04 ± 3.84 ng/L and 231.55 ± 24.56 μg/L, respectively), and allicin 14 mg/kg + PAG group (94.14 ± 6.28 ng/L and 252.20 ± 20.53 μg/L, respectively) than in the model group. cTnI and LDH levels were significantly higher in the allicin 14 mg/kg + PAG group than in the allicin 14 mg/kg group. These data suggest that treatment with diltiazem or allicin significantly alleviated the changes in cardiac function induced by AMI, and PAG partially reversed this effect (**Figures 2C,D**).

3.1.4 Pathological Morphology

H&E and Masson staining revealed that in the sham group, the structure of cardiomyocytes remained intact, the transverse and fiber striations of the myocardium were clear, and cells were arranged regularly. No degeneration, necrosis, hemorrhage, inflammatory cell infiltration, or collagen deposition was observed in the sham group. In the model group, the arrangement of myocardial fibers was disordered, swollen, and disjointed; the septum of the fiber bundles was widened; transverse lines of cells were absent, striations were disordered, normal cell structure was disrupted; and extensive cardiomyocyte necrosis, interstitial vascular hyperplasia, hyperemia, edema, inflammatory cell infiltration, and collagen deposition were observed. These features are typical of myocardial infarction. In the allicin 14 mg/kg and diltiazem 8.1 mg/kg groups, the arrangement of cardiomyocytes was slightly disordered, myocardial fibers were neatly arranged, the interstitium was broadened, the septum of the fiber bundles was not significantly widened, no cell necrosis was observed, and minimal cardiomyocyte edema and collagen deposition were noted. Hence, the degree of pathological damage observed in the allicin 7 mg/kg and allicin 14 mg/kg + PAG treatment groups was intermediate compared with that noted in the model and allicin 14 mg/kg groups (**Figures 2F,G**).

3.1.5 Hydrogen Sulfide Levels in Serum and Myocardial Tissue

The levels of the H_2S in serum and the border zone of the myocardial infarction tissues were significantly lower in the model group (36.23 ± 8.96 nM/ml and 342.18 ± 48.77 nM/g, respectively) than in the sham group (109.39 ± 11.44 nM/ml and 682.93 ± 56.83 nM/g, respectively) (**Figures 3A,B**). On the other hand, the levels of H_2S in the serum and myocardial tissue were significantly higher in the diltiazem 8.1 mg/kg (86.21 ± 7.03 nM/ml and 543.91 ± 49.15 nM/g, respectively), allicin 14 mg/kg (85.73 ± 9.06 nM/ml and 563.91 ± 34.28 nM/g, respectively), allicin 7 mg/kg (68.35 ± 7.18 nM/ml and 469.82 ± 48.25 nM/g, respectively), and allicin 14 mg/kg + PAG groups (62.00 ± 8.48 nM/ml and 490.53 ± 47.75 nM/g, respectively) than in the model group, suggesting that these treatments alleviated myocardial infarction symptoms. High levels of allicin were more effective than lower levels, as H_2S serum and tissue levels were significantly lower in the allicin 7 mg/kg and allicin 14 mg/kg + PAG groups than in the allicin 14 mg/kg group. Finally, the levels of H_2S in the serum and myocardial tissue were significantly higher in the allicin 14 mg/kg group than in the model group.

3.1.6 CSE Levels

Immunofluorescence analysis revealed that the average optical density (AOD) of CSE in myocardial tissue was significantly lower in the model group (0.039 ± 0.014) than in the sham group (0.141 ± 0.028). CSE showed a significantly higher level in the diltiazem 8.1 mg/kg (0.091 ± 0.009), allicin 14 mg/kg (0.101 ± 0.008), allicin 7 mg/kg (0.077 ± 0.010), and allicin 14 mg/kg + PAG groups (0.073 ± 0.003) than in the model group. On the other hand, CSE levels tended to be lower in the allicin 7 mg/kg and allicin 14 mg/kg + PAG groups than in the allicin 14 mg/kg group, but this trend did not reach statistical significance (**Figure 3C**). Similarly, serum CSE levels were significantly lower in the model group than in the sham group (CSE: 1.95 ± 0.52 μg/L vs. 4.07 ± 0.88 μg/L). Serum CSE levels were significantly higher in all treatment groups than in the model group. CSE levels were significantly lower in the allicin 14 mg/kg + PAG group than in the allicin 14 mg/kg group (**Figure 3D**). **Figure 3E** suggests that in rats with AMI, allicin treatment improved CSE levels partly via inducing H_2S production.

3.2 Allicin-Regulated Coronary Artery Vasomotor Function

3.2.1 Vasodilatory Effects of Allicin on Rat Coronary Arteries *via* Hydrogen Sulfide

Allicin-induced dilation in rat coronary arteries precontracted with KCl in a dose-dependent manner. The maximum vasodilation reached 85.11 ± 2.11% of the pre-contraction amplitude. After the application of PAG, the maximum relaxation induced by allicin was 49.37 ± 6.94%, which was significantly lower than that in the control group (**Figures 4A,B**). The inhibitory rate of PAG on the vasodilation effect of allicin was 42.4%. There was no significant difference in pEC_{50} between the two groups.

3.2.2 Allicin-Mediated Inhibition of Dose-dependent Potassium Chloride-Induced Contraction in Rat Coronary Arteries

KCl induced contractions in rat coronary arteries in a dose-dependent manner. No significant changes in E_{max} and pEC_{50} of

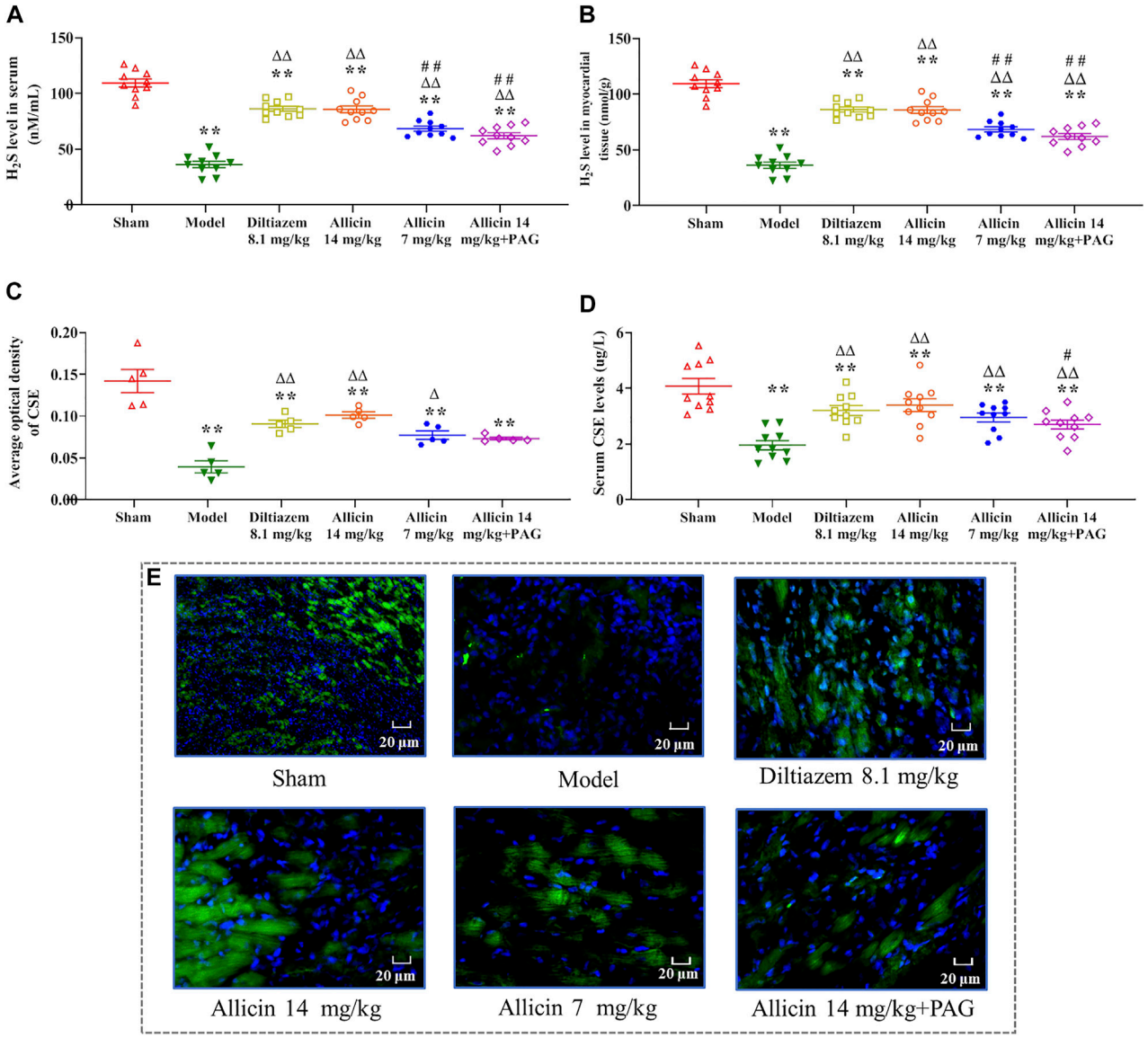

FIGURE 3 | Allicin increased H_2S and CSE levels. **(A)** Serum H_2S levels; **(B)** H_2S levels in myocardial tissue; **(C)** CSE levels in myocardial tissue; **(D)** Serum CSE levels. **(E)** Representative micrographs of heart sections from AMI rats stained to visualize the CSE enzyme (green) and nuclei (DAPI; blue), magnification ×400. Data are expressed as mean ± S.E.M (n = 5–12). $^{*}p < 0.05$, $^{**}p < 0.01$ vs. control; $^{\triangle}p < 0.05$, $^{\triangle\triangle}p < 0.01$ vs. the Model group; $^{\#}p < 0.05$, $^{\#\#}p < 0.01$ vs. the Allicin 14 mg/kg group. Abbreviations: CSE, cystathionine-γ-lyase; AMI, acute myocardial infarction; PAG, DL-propargylglycine.

KCl-induced concentration-contraction curves were observed after administration of allicin or allicin + PAG (**Figures 4C,D**).

3.2.3 Effects of Allicin on Receptor-Dependent Ca^{2+} Channel Agonist Dose-Response Curves in Rat Coronary Arteries

Following administration of allicin, the E_{max} values of the concentration-contraction curves induced by 5-HT, U46619, and ET-1 were 101.86 ± 2.16%, 102.19 ± 15.24%, and 120.77 ± 13.98%, respectively. These values were significantly lower than those of the control group (158.73 ± 12.63%, 146.56 ± 18.23%, and 173.51 ± 14.09%, respectively). Following administration of allicin + PAG, the E_{max} values of the concentration-contraction curves induced by 5-HT, U46619, and ET-1 were 133.91 ± 8.65%, 124.09 ± 6.64%, and 144.02 ± 5.22%. These values were significantly lower than those of the control group but were significantly higher than those of the allicin group (**Figure 5**).

3.2.4 The Weakening Effect of a K^+ Pathway Inhibitor on Allicin-Induced Vasodilation of Rat Coronary Arteries

The R_{max} of allicin in the TEA, 4-AP, and $BaCl_2$ groups was not significantly different compared with that of the control group

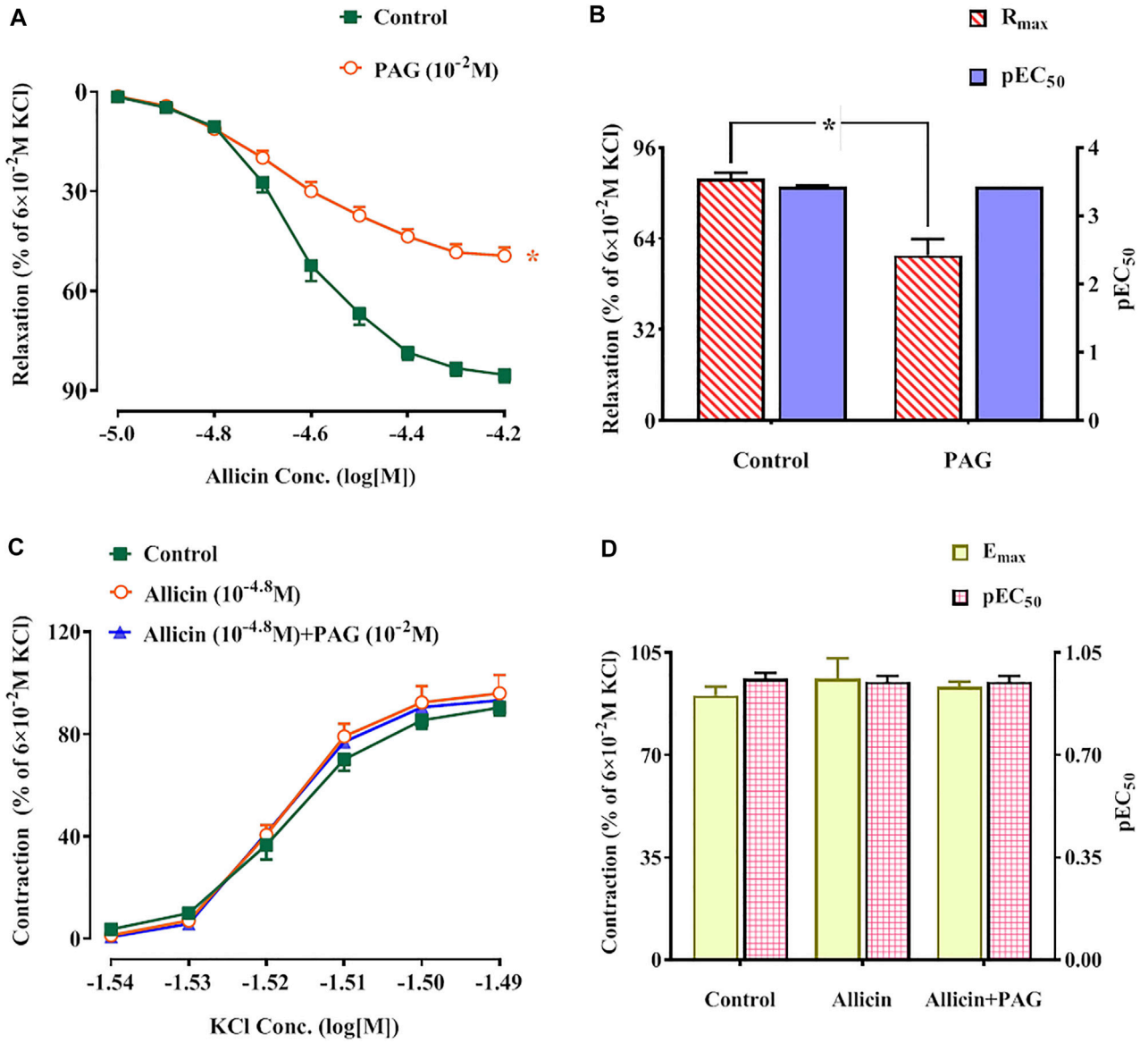

FIGURE 4 | (A,B) Allicin induced coronary artery dilation in rats, while PAG inhibited this effect. **(A)** Diastolic effect curves of allicin adding saline and PAG, respectively; **(B)** R_{max} and pEC_{50} of diastolic effect curve of allicin. **(C,D)** Effects of allicin on dose-response curves of KCl-induced contraction in rat coronary arteries and the intervention effects of PAG. **(C)** Diastolic effect curve of KCl; **(D)** R_{max} and pEC_{50} of diastolic effect curve of KCl. Data are presented as mean ± S.E.M (8 rings from 4–8 rats for each group). *$p < 0.05$ vs. control. Abbreviations: PAG, DL-propargylglycine; pEC_{50}, half-maximal effect; R_{max}, maximum relaxation; E_{max}, maximum contraction.

(82.90 ± 6.22%), whereas the R_{max} of allicin was significantly lower in the Glib group (46.98 ± 3.86%) than in the control group. No significant differences were observed in the R_{max} of allicin among the PAG, PAG + Glib, and Glib groups. Altogether, these data suggest that the response to allicin is mediated by receptor-dependent, rather than voltage-dependent, Ca^{2+} channels (**Figures 6A–D**).

3.2.5 The Inhibitory Effect of Allicin on Caffeine-Induced Coronary Artery Contraction in Ca^{2+}-free Solution

Caffeine (3×10^{-2} M) induced a transient and rapid contraction of rat coronary arteries in Ca^{2+}-free solution. The contraction amplitude was 40.70 ± 10.09% of the contraction induced by KCl (6×10^{-2} M). After administration of allicin, the contraction

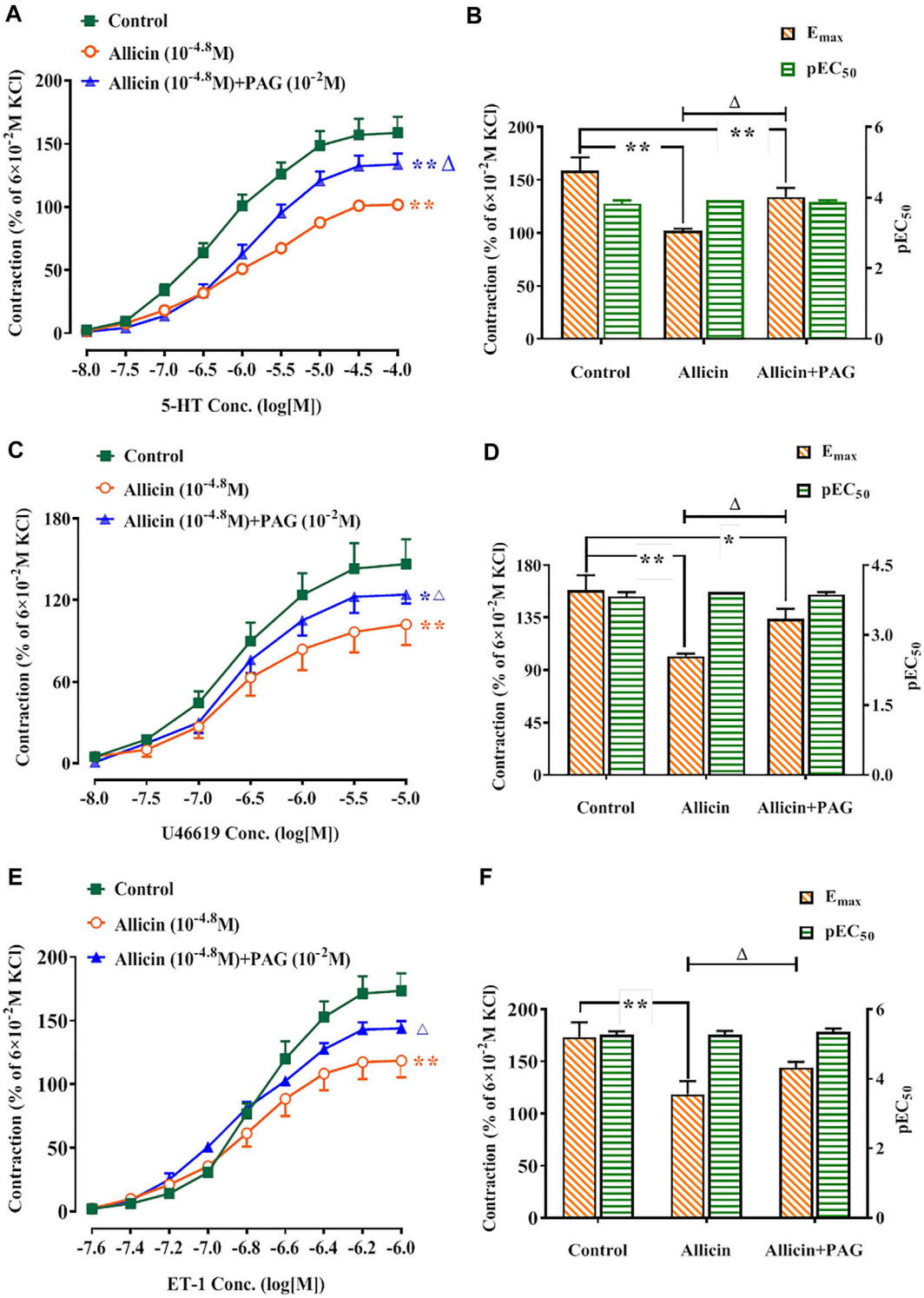

FIGURE 5 | Allicin inhibited 5-HT, U46619, and ET-1-induced contractions in rat coronary arteries and the intervention effects of PAG. **(A,C,E)** Diastolic effect curves of 5-HT, U46619, and ET-1; **(B,D,F)** R_{max} and pEC_{50} of diastolic effect curves of 5-HT, U46619, and ET-1. Data are presented as mean ± SEM (8 rings in each group from 4–8 rats). $^{*}p < 0.05$, $^{**}p < 0.01$ vs. control; $^{\triangle}p < 0.05$ vs. the Allicin group. Abbreviations: PAG, DL-propargylglycine; pEC_{50}, half-maximal effect; R_{max}, maximum relaxation; E_{max}, maximum contraction; 5-HT, 5-hydroxytryptamine; ET-1, endothelin 1.

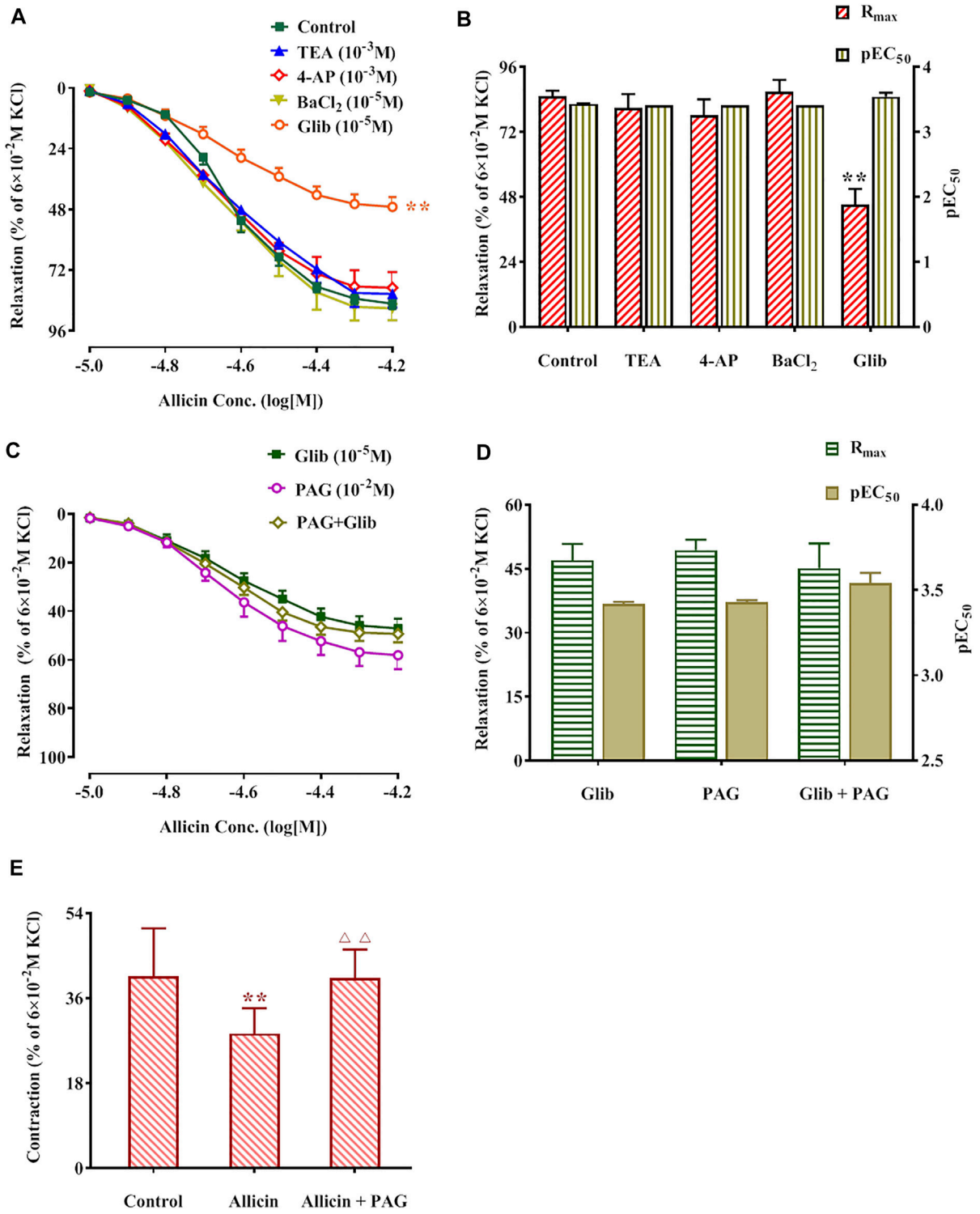

FIGURE 6 | Potassium pathway inhibitors reduced allicin-induced diastolic effects in rat coronary arteries via H_2S and allicin inhibited caffeine-induced coronary artery contraction. **(A,B)** The diastolic effect curves of allicin and R_{max} and pEC_{50} after adding saline and four potassium pathway inhibitors respectively; **(C,D)** The diastolic effect curves of allicin and R_{max} and pEC_{50} after adding PAG or/and Glib, respectively; **(E)** Effect of allicin on caffeine-induced contraction. Data are presented as mean ± S.E.M (8 rings in each group from 4–8 rats). $^{**}p < 0.01$ vs. control; $^{\triangle\triangle}p < 0.01$ vs. the Allicin group. Abbreviations: PAG, DL-propargylglycine; Glib, glibenclamide; 4-AP, 4-aminopyridine; TEA, tetraethylamine; pEC_{50}, half-maximal effect; R_{max}, maximum relaxation.

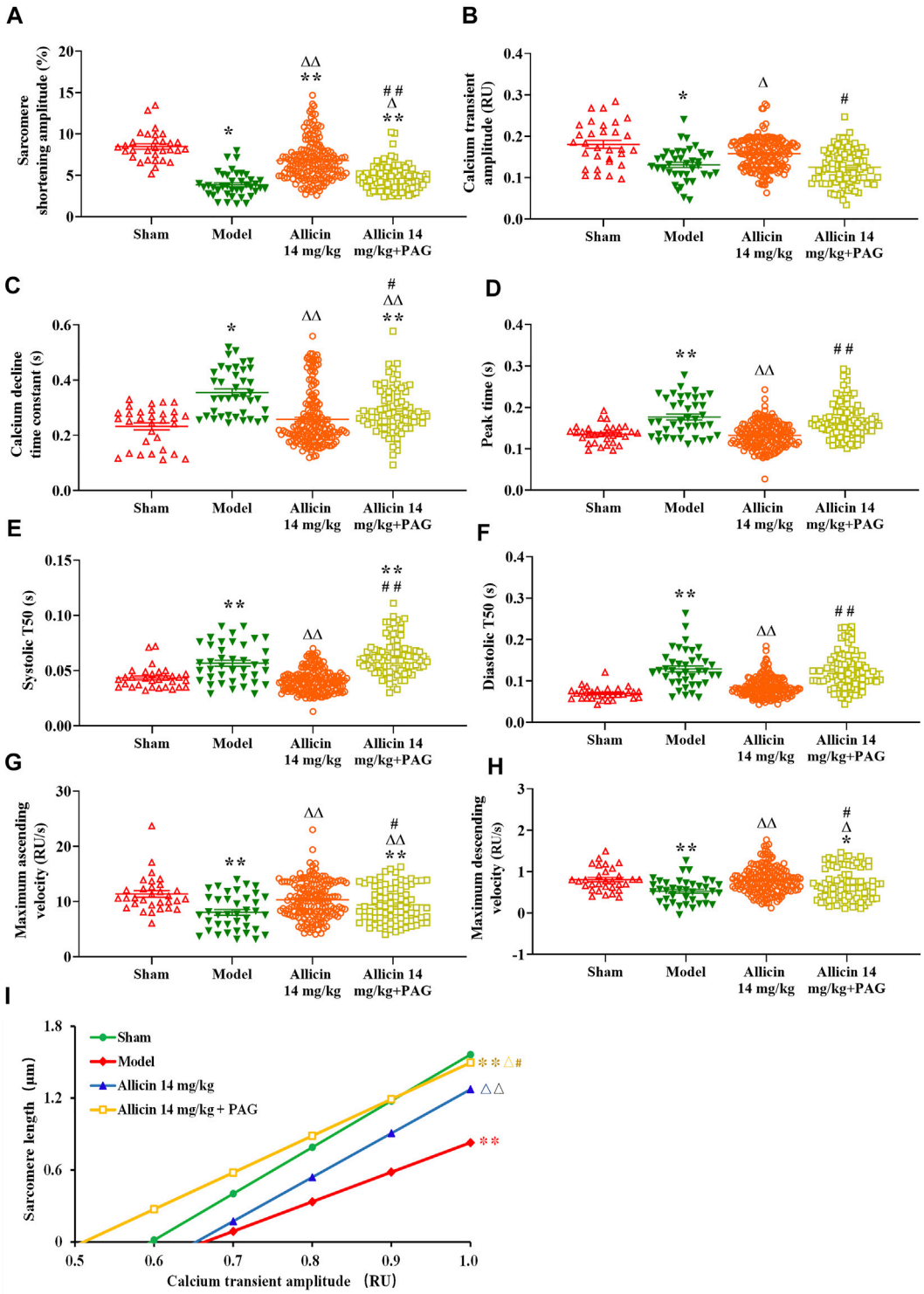

FIGURE 7 | Allicin enhanced cardiomyocyte sarcomere shortening and Ca^{2+} transients. **(A)** Contraction amplitude; **(B)** Calcium transient amplitude; **(C)** Ca^{2+} decline time constant; **(D)** Peak time; **(E)** Systolic T_{50}; **(F)** Diastolic T_{50}; **(G)** Maximum ascending and descending velocities; **(H)** Maximum decline time constant; **(I)** Myofilament sensitivity. Data are presented as mean ± S.E.M (n = 31–175 cardiomyocytes from 3–5 rats). $^{*}p < 0.05$, $^{**}p < 0.01$ vs. control; $^{\Delta}p < 0.05$, $^{\Delta\Delta}p < 0.01$ vs. the Model group; $^{\#}p < 0.05$, $^{\#\#}p < 0.01$ vs. the Allicin 14 mg/kg group. Abbreviations: PAG, DL-propargylglycine; T_{50}, half-time of decay.

amplitude induced by caffeine was 28.45 ± 5.42%, which was significantly lower than that in the control group. Caffeine-induced contraction amplitude was significantly higher in the allicin + PAG group (40.28 ± 6.05%) than in the allicin group (**Figure 6E**).

3.3 Allicin-Mediated Enhancement of Cardiomyocyte Sarcomere Shortening and Ca^{2+} Transients at the Infarct Border

3.3.1 Cardiomyocyte Sarcomere Shortening

Figure 7 shows that the contraction amplitude (3.85 ± 1.49%) was significantly lower, whereas peak time (0.17 ± 0.04 s), systolic T_{50} (0.056 ± 0.017 s), and diastolic T_{50} (0.128 ± 0.044 s) were significantly longer in the model group than in the sham group (8.47 ± 1.80%, 0.13 ± 0.02 s, 0.043 ± 0.009 s, and 0.069 ± 0.014 s, respectively). Contraction amplitude in the allicin 14 mg/kg (6.76 ± 2.43%) and allicin 14 mg/kg + PAG groups (4.65 ± 1.53%) was higher, whereas peak time, systolic T_{50}, and diastolic T_{50} in the allicin 14 mg/kg group (0.13 ± 0.02 s, 0.041 ± 0.010 s, 0.081 ± 0.033 s) was significantly lower than that in the model group. The addition of PAG significantly reduced the contraction amplitude in the allicin 14 mg/kg + PAG group (4.65 ± 1.53%) compared with the allicin 14 mg/kg group. Similarly, peak time, systolic T_{50}, and diastolic T_{50} were significantly longer in the allicin 14 mg/kg + PAG group (0.16 ± 0.04 s, 0.062 ± 0.016 s, and 0.122 ± 0.046 s, respectively) than in the allicin 14 mg/kg group, indicating that PAG significantly alleviated the effects of allicin.

3.3.2 Ca^{2+} Transients

AMI significantly reduced the amplitude, maximum ascending velocity, and maximum descending velocity of Ca^{2+} transients in the model group (0.13 ± 0.03 RU [ratio unit], 8.02 ± 3.20 RU/s, and 0.52 ± 0.28 RU/s, respectively) compared with the sham group (0.18 ± 0.05 RU, 11.36 ± 3.27 RU/s, and 0.80 ± 0.28 RU/s, respectively). The Ca^{2+} decline time constant in the model group (0.35 ± 0.08 s) was significantly longer than that in the sham group (0.23 ± 0.07 s) as well. Ca^{2+} transient amplitude in the allicin 14 mg/kg group (0.15 ± 0.03 RU) and maximum ascending and descending velocities of Ca^{2+} transients in the allicin 14 mg/kg (10.26 ± 3.42 RU/s and 0.79 ± 0.34 RU/s, respectively) and allicin 14 mg/kg + PAG groups (9.39 ± 3.26 RU/s and 0.68 ± 0.38 RU/s, respectively) were significantly higher than in the model group. The Ca^{2+} decline time constants in the allicin 14 mg/kg (0.25 ± 0.10 s) and allicin 14 mg/kg + PAG groups (0.28 ± 0.08 s) were significantly shorter than in the model group. Compared with the allicin 14 mg/kg group, the allicin 14 mg/kg + PAG group exhibited significantly lower Ca^{2+} transient amplitude and maximum ascending and descending velocities of Ca^{2+} transients, as well as significantly longer Ca^{2+} decline time constant (**Figure 7**).

3.3.3 Myofilament Sensitivity

Diastolic curves with good linear relationships were obtained from the nonlinear fitting curve between sarcomere length and Ca^{2+} transient amplitude. The slope of this curve was calculated to reflect myofilament sensitivity. Myofilament sensitivity of cardiomyocytes in the model group (2.46 ± 0.77) was significantly lower than in the sham group (3.86 ± 1.76). By contrast, myofilament sensitivity in the allicin 14 mg/kg and allicin 14 mg/kg + PAG groups was significantly higher than that in the model group. Myofilament sensitivity was significantly lower in the allicin 14 mg/kg + PAG group than in the allicin 14 mg/kg group (**Figure 7I**).

3.3.4 Sarco/Endoplasmic Reticulum Ca^{2+}-ATPase-Mediated Ca^{2+} Reabsorption and Na^+/Ca^{2+} Exchanger-Mediated Ca^{2+} Efflux

Tau_{NCX} and Tau_{SERCA} were significantly higher in the model group (6986.2 ± 5238.6 ms and 349.5 ± 63.5 ms, respectively) than in the sham group (2732.3 ± 1275.1 ms and 200.7 ± 93.6 ms, respectively). Compared with the model group, the Tau_{NCX} and Tau_{SERCA} of the allicin 14 mg/kg group (3202.9 ± 1473.1 ms and 246.4 ± 63.1 ms, respectively) and allicin 14 mg/kg + PAG group (3584.4 ± 768.0 ms and 246.4 ± 29.1 ms, respectively) were both significantly decreased. No significant differences were observed in Tau_{NCX} and Tau_{SERCA} between the allicin 14 mg/kg and allicin 14 mg/kg + PAG groups (**Figures 8A,B**).

3.3.5 Sarcoplasmic Reticulum Ca^{2+} Content and Ca^{2+} Leakage

The SR Ca^{2+} content of myocardial cells was threefold lower in the model group (0.53 ± 0.16 RU) than in the sham group (1.51 ± 0.37 RU). On the other hand, the allicin 14 mg/kg (1.43 ± 0.18 RU) and allicin 14 mg/kg + PAG (1.17 ± 0.13 RU) treatments induced significantly higher SR Ca^{2+} content when compared with the model group. SR Ca^{2+} content was significantly lower in the allicin 14 mg/kg + PAG group than in the allicin 14 mg/kg group.

Ca^{2+} leakage was significantly higher in the model group (0.097 ± 0.033 RU) than in the sham group (0.052 ± 0.040 RU), whereas allicin 14 mg/kg (0.056 ± 0.05 RU) and allicin 14 mg/kg + PAG (0.073 ± 0.044 RU) administration significantly decreased leakage compared with the model group. Ca^{2+} leakage was significantly higher in the allicin 14 mg/kg + PAG group than in the allicin 14 mg/kg group (**Figures 8C,D**).

4 DISCUSSION

AMI is a prevalent cardiovascular event (Lu et al., 2015). Despite early revascularization, timely medical therapy, and up-to-date mechanical circulatory support, AMI prognosis remains poor and patient mortality remains high. TCM, which is underscored by a rich 2000–3000-year history of medical theories concerning disease etiology and treatments, has been in the public eye due its therapeutic promise for AMI, among other conditions. Here, we investigated the therapeutic effects of allicin, a component of garlic, in a rat model of AMI. We demonstrated that allicin exerted anti-AMI effects, including improvements in cardiac function as well as reduction in infarct size and serum cTnI and LDH levels. In parallel, microscopic observations revealed that allicin significantly improved the detrimental morphological

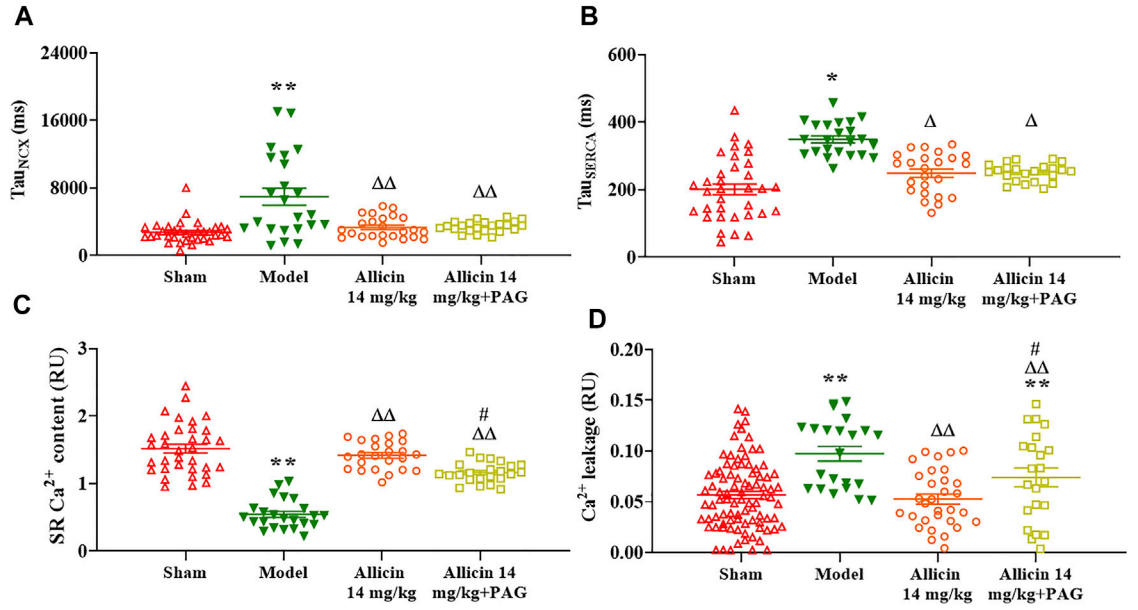

FIGURE 8 | Effect of allicin on myocardial Ca^{2+} transport. **(A,B)** Allicin enhanced SERCA reabsorption and NCX-induced calcium efflux in cardiomyocytes. **(C,D)** Allicin increased SR Ca^{2+} content and reduced Ca^{2+} leakage in cardiomyocytes. n = 22–89 cardiomyocytes from 3–5 rats. Data are presented as mean ± S.E.M. $^{*}p < 0.05$, $^{**}p < 0.01$ vs. control; $^{\triangle}p < 0.05$, $^{\triangle\triangle}p < 0.01$ vs. the Model group; $^{\#}p < 0.05$ vs. the Allicin 14 mg/kg group. Abbreviations: PAG, DL-propargylglycine; SERCA, sarco/endoplasmic reticulum Ca^{2+}-ATPase; NCX, Na^{+}/Ca^{2+} exchanger; SR, sarcoplasmic reticulum.

changes observed in myocardial tissue after AMI, supporting the protective effects of allicin against cardiac lesions and myocardial cell necrosis.

Garlic, as a food source and medicinal plant, is widely known for its cardiovascular properties (Zhou et al., 2021). Allicin is well-established as the main pharmacological component of garlic. Allicin is an enzymatic product of alliin and alliinase, and is produced when raw garlic cloves undergo cell rupture. Extensive evidence supports the cardioprotective effects of allicin. For instance, allicin protected rats against AMI and myocardial ischemia reperfusion injury by suppressing inflammation, fibrosis, apoptosis, and oxidative stress (Liu et al., 2019). We previously demonstrated that allicin exerted anti-AMI effects (Ma et al., 2017). This study builds upon our previous findings and provides insight into the mechanisms underlying the anti-AMI effects of allicin.

Patients who survive AMI frequently develop systolic heart failure due to the infarct-induced loss of a functional myocardium and the remodeling of the LV. This process involves cardiomyocyte necrosis and hypertrophy, LV wall thinning, infarct expansion, and collagen accumulation (Wollert and Drexler, 2010). Further, serum levels of the cytosolic enzymes cTnI and LDH are significantly increased when myocardial ischemia and hypoxia occur (Goyal et al., 2010; Cordwell et al., 2012). In the event of AMI, myocardial circulatory perfusion becomes insufficient, leading to ischemia and hypoxia of the myocardial tissue, structural and functional damage to cardiomyocytes, irreversible cellular necrosis, and serious damage to cardiac contractile function. Therefore, increasing the blood supply to coronary arteries and improving the function of cardiomyocytes are key to effectively prevent and treat adverse clinical events after AMI.

In AMI, coronary microvascular dysfunction results in the insufficient supply of blood and oxygen and may affect myocardial function at rest and during stress (Michelsen et al., 2018). Given the protective effects of allicin on AMI, elucidating the regulatory effects of this compound on the vasomotor function of coronary arteries in the context of AMI-induced damage would provide valuable mechanistic insight. In this study, we observed that allicin exerted concentration-dependent vasodilatory effects on rat coronary arteries. Given that Ca^{2+} concentration is a critical factor for vascular tone (Shen et al., 2009), we focused on Ca^{2+}-related vascular tension. Intracellular Ca^{2+} concentration is predominantly increased by Ca^{2+} influx and/or Ca^{2+} release from the SR (Guan et al., 2019). Ca^{2+} influx involves the opening of VDCCs and RDCCs. Ligands such as 5-HT, thromboxane A_2 (TXA_2), and ET-1, by binding to their corresponding G protein-coupled receptors, are the main activators of RDCCs, whereas VDCCs are predominantly activated by cations, including K^{+}. We demonstrated that allicin significantly inhibited the contractions induced by 5-HT, U46619, and ET-1 in rat coronary arteries, but it did not alter contractions induced by KCl, suggesting that RDCCs, rather than VDCCs, mediated the extracellular Ca^{2+} influx that contributed to vasodilation. Receptors mediating SR Ca^{2+} release include the inositol triphosphate and ryanodine receptors (RyRs), of which, the latter mediates more than 90% of SR Ca^{2+} release. In order to study the effects of allicin on RyR-mediated calcium release, we used caffeine in Ca^{2+}-free solution, which increased the intracellular Ca^{2+} concentration by

completely activating the RyRs in the SR (Garcia et al., 2019). Our findings indicated that allicin significantly inhibited caffeine-induced coronary artery contractions, suggesting that allicin-induced vasodilation of coronary arteries was associated with inhibition of the SR Ca^{2+} release mediated by RyRs.

The opening of K^+ channels, which leads to cell membrane hyperpolarization by promoting intracellular K^+ outflow, is a way to decrease intracellular Ca^{2+} concentration and induce vasodilation. To date, four types of K^+ channels with different activation mechanisms have been identified: these are the K_V, K_{Ca}, K_{ir}, and K_{ATP} channels (Lorigo et al., 2020). These channels inhibit the activation of VDCCs on the cell membrane, thus reducing extracellular Ca^{2+} influx. Further, they increase intracellular Ca^{2+} efflux by stimulating the NCX, thus reducing intracellular Ca^{2+} and causing vasodilation. To investigate the involvement of K^+ channels in allicin-induced vasodilation, we applied 4-AP, TEA, $BaCl_2$, and Glib separately on coronary arteries to observe their effects on allicin-induced vasodilation. Only Glib application significantly inhibited allicin-induced vasodilation, suggesting that the vasodilatory effects of allicin on coronary arteries were at least partly attributed to K_{ATP} channel opening but did not involve other K^+ channels.

Cardiomyocyte dysfunction is a direct consequence of AMI and leads to a decrease in cardiomyocyte vitality, which eventually results in heart failure and even death. Ca^{2+}-mediated excitation-contraction coupling is a requirement for correct cardiomyocyte contraction and relaxation (Palomeque et al., 2009; Lahiri et al., 2021). During cardiac systole, a small amount of extracellular Ca^{2+} enters the cytoplasm through L-type Ca^{2+} channels, which triggers the activation of the RyRs in the SR and leads to extensive Ca^{2+} release from the SR. Intracellular Ca^{2+} binds to troponin to cause cell contraction (Zhang et al., 2018). Intracellular Ca^{2+} can be rapidly recaptured by SERCA on the SR and transported out of cells through the NCX on the cell membrane, which causes cardiomyocytes to enter a diastolic state. Ca^{2+} transients reflect the rapid dynamic changes in cytoplasmic Ca^{2+} during cardiomyocyte contraction and relaxation, and the changes in velocity and amplitude represent changes in myocardial contractility. In addition, the sensitivity of cardiomyocyte myofilaments to Ca^{2+} affects the contractile function of cardiomyocytes. Under pathological conditions, there is a decrease in the amplitude and velocity of Ca^{2+} transients of cardiomyocytes, SR Ca^{2+} content, and myofilament sensitivity to Ca^{2+}. This leads to a decrease in cardiomyocyte contraction and relaxation function (D.M. Bers, 2002; Piacentino et al., 2003). In this study, we observed that allicin significantly increased the contractile amplitude of cardiomyocytes, maximum release and reabsorption rate of Ca^{2+} transients, and myofilament sensitivity of cardiomyocytes. Allicin also decreased the peak time, systolic T_{50}, diastolic T_{50}, and elimination constant of Ca^{2+} transient time. Collectively, these findings indicated that allicin significantly improved the contraction and relaxation function of myocardial cells.

In pathological states, intracellular Ca^{2+} is not reabsorbed by SERCA or expelled by the NCX in a timely manner at the end of cardiomyocyte contraction. Rather, intracellular Ca^{2+} accumulates in the cytoplasm, which hinders the separation of thin and thick myofilaments and leads to myocardial diastolic dysfunction. On the other hand, under physiological conditions, the elimination of Ca^{2+} transients is predominantly mediated by SERCA recapture, Ca^{2+} efflux by the NCX, and slow transport systems during end-diastole. In this regard, the contribution of slow transport systems is less than 1% (Matthew et al., 2004). In order to investigate the SR Ca^{2+} content and Ca^{2+} efflux induced by the NCX, we continuously perfused coronary arteries with caffeine in a Ca^{2+}-free environment, which completely opened the RyRs. This enabled all Ca^{2+} in the SR to be completely released and temporarily offset SERCA-induced Ca^{2+} reabsorption. Therefore, cytoplasmic Ca^{2+} concentration reflected the SR Ca^{2+} content, and the elimination of Ca^{2+} transients was considered to be predominantly accomplished by the NCX. We demonstrated that allicin significantly enhanced SERCA recapture and increased Ca^{2+} extrusion by the NCX, and increased the SR Ca^{2+} content. Furthermore, RyR dysfunction is known to cause Ca^{2+} leakage during diastole (Fischer et al., 2013), which leads to intracellular Ca^{2+} overload, SR Ca^{2+} content decrease, and eventually, abnormal cell contraction (Sheibani et al., 2017). Our data demonstrated that allicin significantly decreased Ca^{2+} leakage, suggesting its ability to regulate Ca^{2+} homeostasis.

H_2S functions as a gasotransmitter, similar to nitric oxide and carbon monoxide. H_2S exerts various cardiovascular effects, including vasodilation, blood pressure reduction, and myocardium protection. Endogenous H_2S, a potent vasodilator, is synthesized via the metabolic breakdown of L-cysteine by CSE, CBS, and 3-MST (Kanagy et al., 2017; Sheibani et al., 2017). Found predominantly in the cardiovascular system (Singh and Banerjee, 2011), CSE contributes to about 90% of total H_2S production in organs that express all three enzymes (Leigh et al., 2016). In addition, it has been reported that CSE also exists as a circulating enzyme that is secreted by endothelial cells into the circulatory system, where it circulates as a member of the plasma proteome (Bearden et al., 2010). Allicin, as a sulfur-containing compound, may exert its cardiovascular effects by increasing the production of H_2S. Furthermore, our previous research demonstrated that allicin reduced blood pressure by promoting H_2S production. Here, we expand upon our previous findings by demonstrating that the anti-AMI effects of allicin are at least partially underpinned by the production of H_2S mediated by CSE. In this regard, PAG, a CSE inhibitor, significantly attenuated, but did not completely abrogate, the positive effects that allicin exerts on AMI injury, coronary artery vasodilation, and calcium transport regulation in cardiomyocytes. In the present study, allicin increased the levels of H_2S and CSE with or without PAG, but PAG reversed this effect, indicating that PAG partially impedes the allicin-induced production of H_2S and CSE. Therefore, we speculate that allicin directly induces H_2S production both directly and indirectly by increasing the levels of CSE. Several studies have shown that the mechanisms underlying H_2S-induced vasorelaxation include the opening of K_{ATP} channels, closing of VDCC, and decreased concentration of intracellular Ca^{2+} (Holwerda et al., 2015; Hedegaard et al., 2016). It has been established that NaHS, an

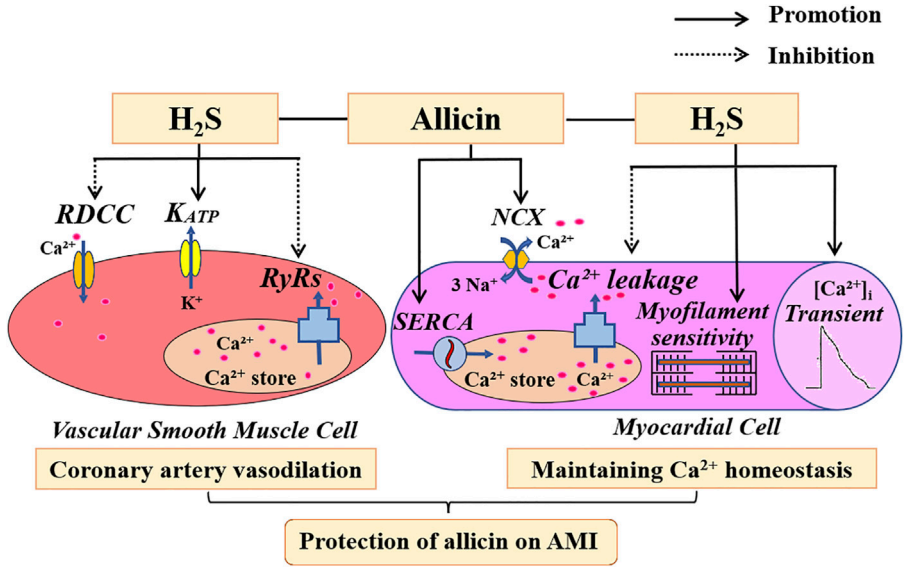

FIGURE 9 | The potential mechanism of action of allicin in an AMI rat model. Allicin administration resulted in concentration-dependent effects on coronary artery dilation, which were mediated by RDCC, K_{ATP}, and RyRs. Allicin administration improved Ca^{2+} homeostasis in the cardiomyocytes of rats with AMI by increasing cardiomyocyte contraction, Ca^{2+} transient amplitude, myofilament sensitivity, and SR Ca^{2+} content. Allicin also enhanced the Ca^{2+} uptake induced by SERCA and the Ca^{2+} removal induced by the NCX, and reduced Ca^{2+} leakage. H_2S is partially involved in the anti-AMI effects of allicin. Abbreviations: RDCC, receptor-dependent Ca^{2+} channels; K_{ATP}, ATP-sensitive potassium channels; RyRs, ryanodine receptors; SERCA, sarco/endoplasmic reticulum Ca^{2+}-ATPase; NCX, Na^+/Ca^{2+} exchanger; AMI, acute myocardial infarction.

H_2S-donor, improved diabetic cardiomyopathy by regulating the Ca^{2+}-handling system in the SR (Cheng et al., 2016). Consistent with the literature, our results showed that the effects of allicin on Ca^{2+} and K^+ currents are strictly superimposable to those exhibited by H_2S. These findings suggest that H_2S is involved in the anti-AMI effects of allicin, but other mechanisms are involved. Unexpectedly, our results showed that PAG weakened the effect of allicin on CSE production, causing a decrease in CSE levels. However, we are puzzled as to why PAG, an inhibitor of CSE activity, also reduces CSE level. After preliminary literature research, we found that quite a few studies reported that PAG could decrease CSE level (Li X. et al., 2017; Wang et al., 2019; Li Y. et al., 2020). The impact of PAG on CSE level, and the reason for such effect would require further in-depth studies.

An additional point worth noting is that most scholars believe that the CSE enzyme is mainly expressed in the cardiovascular system (Xu et al., 2014; Kolluru et al., 2015). Therefore, we selected a CSE enzyme inhibitor as a tool to explore the relationship between allicin-induced coronary vasodilation and H_2S. The results showed that the CSE inhibitor significantly weakened the vasodilatory effects of allicin on isolated rat coronary arteries, indicating that CSE is indeed involved in allicin-induced vasodilation by mediating H_2S production. However, a previous study on swine coronary arteries suggested that CBS was the most important enzyme for the production of H_2S under hypoxic conditions, and that the vasodilatory contribution from CSE and 3-MST becomes apparent only upon inhibition of CBS (Donovan et al., 2017). Another study pointed out that 3-MST, rather than CSE, was the main enzyme expressed in the coronary arteries of rats and mice (Kuo et al., 2016). Therefore, the role of the three H_2S-producing enzymes in coronary arteries is still debatable. In this study, we only evaluated the role of CSE, but not that of CBS or 3-MST; hence, this study cannot fully elucidate the role of each enzyme in the rat coronary artery. Our results showed that the CSE inhibitor inhibited allicin-induced vasodilation in coronary arteries by 42.4%, indicating that a considerable amount of CSE exists in rat coronary arteries, and that its role in inducing H_2S production cannot be neglected, as previously suggested in some studies (Chai et al., 2015; Luo et al., 2021). Regarding the controversy over the dominant role of each H_2S-producing enzyme in coronary arteries, four reasons could explain such discrepancies. First, the expression and activity of CSE, CBS, and 3-MST may vary across different species, and under different physiological or pathological conditions. Second, the levels of enzyme expression may not be proportional to the levels of activity, and indeed an inverse relationship may be present where lower expression results in higher activity. Third, enzyme activity may vary under different experimental conditions and methods, and lastly, the predominance of one H_2S-producing enzyme over the others may differ with or without drug intervention. Therefore, further in-depth studies are needed to better understand the dominant role of CSE, CBS, and 3-MST in coronary arteries.

5 CONCLUSION

Our study demonstrates that allicin may exert cardioprotective effects in a rat model of AMI injury by inducing coronary artery vasodilation and maintaining Ca^{2+} homeostasis via H_2S production. Allicin induced the vasodilation of coronary

arteries via favoring H_2S production by inhibiting the opening of RDCC, promoting the opening of K_{ATP}, and decreasing the Ca^{2+} release induced by the RyRs. Allicin regulated Ca^{2+} homeostasis by increasing cardiomyocyte contraction, Ca^{2+} transient amplitude, myofilament sensitivity, and SR Ca^{2+} content, and reducing SR Ca^{2+} leakage via H_2S production. Moreover, allicin enhanced the Ca^{2+} uptake induced by SERCA and Ca^{2+} removal induced by the NCX, in which H_2S is not involved. (**Figure 9**) This new understanding of the mechanisms underpinning the therapeutic effects of allicin will facilitate the development of effective therapeutic modalities for cardiac rehabilitation in humans.

DATA AVAILABILITY STATEMENT

The raw data supporting the conclusions of this article will be made available by the authors, without undue reservation.

ETHICS STATEMENT

The animal study was reviewed and approved by the Animal Care Committee, Xiyuan Hospital, China Academy of Chinese Medical Sciences (SYXK [JING] 2018-0018).

AUTHOR CONTRIBUTIONS

JZ, TC, and XS designed and conceived the study; TC, WL, and CY performed the experiments. QL was involved in experiments for the completion of the revised work. YL and JR participated in some experiments. JZ, TC, WL, and XS analyzed the data and wrote the paper. All authors read and approved the final manuscript.

FUNDING

This study was supported by grants from the National Nature Science Foundation of China (Grant No. 81973515), National Science and Technology Major Project of China (Grant No. 2017ZX09301061), and the Innovative Funding for PhD Students at China Academy of Chinese Medical Sciences.

ACKNOWLEDGMENTS

We are grateful to Dr. Shenglou Ni (Beijing University of Chinese Medicine) for his critical comments on the manuscript.

REFERENCES

Bearden, S. E., Beard, R. S., Jr, and Pfau, J. C. (2010). Extracellular Transsulfuration Generates Hydrogen Sulfide from Homocysteine and Protects Endothelium from Redox Stress. *Am. J. Physiol. Heart Circ. Physiol.* 299 (5), H1568–H1576. doi:10.1152/ajpheart.00555.2010

Benavides, G. A., Squadrito, G. L., Mills, R. W., Patel, H. D., Isbell, T. S., Patel, R. P., et al. (2007). Hydrogen Sulfide Mediates the Vasoactivity of Garlic. *Proc. Natl. Acad. Sci. U S A.* 104 (46), 17977–17982. doi:10.1073/pnas.0705710104

Bers, D. M. (2002). Cardiac Excitation-Contraction Coupling. *Nature* 415 (6868), 198–205. doi:10.1038/415198a

Chai, Q., Lu, T., Wang, X. L., and Lee, H. C. (2015). Hydrogen Sulfide Impairs Shear Stress-Induced Vasodilation in Mouse Coronary Arteries. *Pflugers. Arch.* 467 (2), 329–340. doi:10.1007/s00424-014-1526-y

Chen, C., Cheng, X. H., Ren, T., Wu, R. X., Zhou, C., Yuan, M., et al. (2019). Experimental Study on Effects of Jiawei Danshen Decoction on Endogenous H_2S Synthesis Pathway to Protect Myocardial Ischemia/reperfusion Injury. *J. Hunan. Univ. Tradit. Chin. Med.* 39 (10), 1183–1188. doi:10.3969/j.issn.1674-070X.2019.10.003

Cheng, Y. S., Dai, D. Z., Dai, Y., Zhu, D. D., and Liu, B. C. (2016). Exogenous Hydrogen Sulphide Ameliorates Diabetic Cardiomyopathy in Rats by Reversing Disordered Calcium-Handling System in Sarcoplasmic Reticulum. *J. Pharm. Pharmacol.* 68 (3), 379–388. doi:10.1111/jphp.12517

Cordwell, S. J., Edwards, A. V., Liddy, K. A., Moshkanbaryans, L., Solis, N., Parker, B. L., et al. (2012). Release of Tissue-specific Proteins into Coronary Perfusate as a Model for Biomarker Discovery in Myocardial Ischemia/reperfusion Injury. *J. Proteome. Res.* 11 (4), 2114–2126. doi:10.1021/pr2006928

Cui, T., Liu, W., Chen, S., Yu, C., Li, Y., and Zhang, J. Y. (2020). Antihypertensive Effects of Allicin on Spontaneously Hypertensive Rats via Vasorelaxation and Hydrogen Sulfide Mechanisms. *Biomed. Pharmacother.* 128, 110240. doi:10.1016/j.biopha.2020.110240

Donovan, J., Wong, P. S., Roberts, R. E., Garle, M. J., Alexander, S. P. H., Dunn, W. R., et al. (2017). A Critical Role for Cystathionine-β-Synthase in Hydrogen Sulfide-Mediated Hypoxic Relaxation of the Coronary Artery. *Vascul. Pharmacol.* 93-95, 20–32. doi:10.1016/j.vph.2017.05.004

Fischer, T. H., Maier, L. S., and Sossalla, S. (2013). The Ryanodine Receptor Leak: How a Tattered Receptor Plunges the Failing Heart into Crisis. *Heart Fail. Rev.* 18 (4), 475–483. doi:10.1007/s10741-012-9339-6

Garcia, D. C. G., Lopes, M. J., Mbiakop, U. C., Lemos, V. S., and Cortes, S. F. (2019). Activation of Cav1.2 and BKCa Is Involved in the Downregulation of Caffeine-Induced Contraction in Mice Mesenteric Arteries. *Life Sci.* 231, 116555. doi:10.1016/j.lfs.2019.116555

Goyal, S. N., Arora, S., Sharma, A. K., Joshi, S., Ray, R., Bhatia, J., et al. (2010). Preventive Effect of Crocin of *Crocus Sativus* on Hemodynamic, Biochemical, Histopathological and Ultrastuctural Alterations in Isoproterenol-Induced Cardiotoxicity in Rats. *Phytomedicine* 17 (3–4), 227–232. doi:10.1016/j.phymed.2009.08.009

Guan, Z., Baty, J. J., Zhang, S., Remedies, C. E., and Inscho, E. W. (2019). Rho Kinase Inhibitors Reduce Voltage-dependent Ca2+ Channel Signaling in Aortic and Renal Microvascular Smooth Muscle Cells. *Am. J. Physiol. Ren. Physiol.* 317 (5), F1132–F1141. doi:10.1152/ajprenal.00212.2018

Hedegaard, E. R., Gouliaev, A., Winther, A. K., Arcanjo, D. D., Aalling, M., Renaltan, N. S., et al. (2016). Involvement of Potassium Channels and Calcium-independent Mechanisms in Hydrogen Sulfide-Induced Relaxation of Rat Mesenteric Small Arteries. *J. Pharmacol. Exp. Ther.* 356 (1), 53–63. doi:10.1124/jpet.115.227017

Holwerda, K. M., Karumanchi, S. A., and Lely, A. T. (2015). Hydrogen Sulfide: Role in Vascular Physiology and Pathology. *Curr. Opin. Nephrol. Hypertens.* 24 (2), 170–176. doi:10.1097/MNH.0000000000000096

Kanagy, N. L., Szabo, C., and Papapetropoulos, A. (2017). Vascular Biology of Hydrogen Sulfide. *Am. J. Physiol. Cel Physiol.* 312 (5), C537–C549. doi:10.1152/ajpcell.00329.2016

Kolluru, G. K., Bir, S. C., Yuan, S., Shen, X., Pardue, S., Wang, R., et al. (2015). Cystathionine γ-lyase Regulates Arteriogenesis through NO-dependent Monocyte Recruitment. *Cardiovasc. Res.* 107 (4), 590–600. doi:10.1093/cvr/cvv198

Kuo, M. M., Kim, D. H., Jandu, S., Bergman, Y., Tan, S., Wang, H., et al. (2016). MPST but Not CSE Is the Primary Regulator of Hydrogen Sulfide Production and Function in the Coronary Artery. *Am. J. Physiol. Heart Circ. Physiol.* 310 (1), H71–H79. doi:10.1152/ajpheart.00574.2014

Lahiri, S. K., Aguilar-Sanchez, Y., and Wehrens, X. H. T. (2021). Mechanisms Underlying Pathological Ca2+ Handling in Diseases of the Heart. *Pflugers. Arch.* 473 (3), 331–347. doi:10.1007/s00424-020-02504-z

Lawson, L. D., and Hunsaker, S. M. (2018). Allicin Bioavailability and Bioequivalence from Garlic Supplements and Garlic Foods. *Nutrients* 10 (7), 812. doi:10.3390/nu10070812

Leigh, J., Saha, M. N., Mok, A., Champsi, O., Wang, R., Lobb, I., et al. (2016). Hydrogen Sulfide Induced Erythropoietin Synthesis Is Regulated by HIF Proteins. *J. Urol.* 196 (1), 251–260. doi:10.1016/j.juro.2016.01.113

Li, J., Cao, G. Y., Zhang, X. F., Meng, Z. Q., Gan, L., Li, J. X., et al. (2020). Chinese Medicine *She-Xiang-Xin-Tong-Ning*, Containing *Moschus, Corydalis* and *Ginseng*, Protects from Myocardial Ischemia Injury via Angiogenesis. *Am. J. Chin. Med.* 48 (1), 107–126. doi:10.1142/S0192415X20500068

Li, S., Chen, S., Yang, W., Liao, L., Li, S., Li, J., et al. (2017). Allicin Relaxes Isolated Mesenteric Arteries through Activation of PKA-KATP Channel in Rat. *J. Recept. Signal. Transduct. Res.* 37 (1), 17–24. doi:10.3109/10799893.2016.1155065

Li, X., Cheng, Q., Li, J., He, Y., Tian, P., and Xu, C. (2017). Significance of Hydrogen Sulfide in Sepsis-Induced Myocardial Injury in Rats. *Exp. Ther. Med.* 14 (3), 2153–2161. doi:10.3892/etm.2017.4742

Li Y, Y., Liu, M., Song, X., Zheng, X., Yi, J., Liu, D., et al. (2020). Exogenous Hydrogen Sulfide Ameliorates Diabetic Myocardial Fibrosis by Inhibiting Cell Aging through SIRT6/AMPK Autophagy. *Front. Pharmacol.* 11, 1150. doi:10.3389/fphar.2020.01150

Liu, H. X., Wang, S. R., Lei, Y., and Shang, J. J. (2011). Characteristics and Advantages of Traditional Chinese Medicine in the Treatment of Acute Myocardial Infarction. *J. Tradit. Chin. Med.* 31 (4), 269–272. doi:10.1016/s0254-6272(12)60002-8

Liu, S., He, Y., Shi, J., Liu, L., Ma, H., He, L., et al. (2019). Allicin Attenuates Myocardial Ischemia Reperfusion Injury in Rats by Inhibition of Inflammation and Oxidative Stress. *Transpl. Proc.* 51 (6), 2060–2065. doi:10.1016/j.transproceed.2019.04.039

Lorigo, M., Oliveira, N., and Cairrao, E. (2020). Clinical Importance of the Human Umbilical Artery Potassium Channels. *Cells* 9 (9), 1956. doi:10.3390/cells9091956

Lu, Z., Zhang, Y., Zhuang, P., Zhang, J., Zhou, H., Zhang, M., et al. (2015). Protective Effect of Suxiao Jiuxin Pill, a Traditional Chinese Medicine, against Acute Myocardial Ischemia in Dogs. *BMC. Complement. Altern. Med.* 15, 373. doi:10.1186/s12906-015-0908-9

Luo, Y., Liu, L. M., Xie, L., Zhao, H. L., Lu, Y. K., Wu, B. Q., et al. (2021). Activation of the CaR-CSE/H2S Pathway Confers Cardioprotection against Ischemia-Reperfusion Injury. *Exp. Cel. Res.* 398 (2), 112389. doi:10.1016/j.yexcr.2020.112389

Ma, L. N., Li, L. D., Li, S. C., Hao, X. M., Zhang, J. Y., He, P., et al. (2017). Allicin Improves Cardiac Function by Protecting against Apoptosis in Rat Model of Myocardial Infarction. *Chin. J. Integr. Med.* 23 (8), 589–597. doi:10.1007/s11655-016-2523-0

Martelli, A., Testai, L., Citi, V., Marino, A., Pugliesi, I., Barresi, E., et al. (2013). Arylthioamides as H2S Donors: L-Cysteine-Activated Releasing Properties and Vascular Effects *In Vitro* and *In Vivo*. *ACS. Med. Chem. Lett.* 4 (10), 904–908. doi:10.1021/ml400239a

Martelli, A., Piragine, E., Citi, V., Testai, L., Pagnotta, E., Ugolini, L., et al. (2020). Erucin Exhibits Vasorelaxing Effects and Antihypertensive Activity by H2 S-Releasing Properties. *Br. J. Pharmacol.* 177 (4), 824–835. doi:10.1111/bph.14645

Matthew, A., Shmygol, A., and Wray, S. (2004). Ca2+ Entry, Efflux and Release in Smooth Muscle. *Biol. Res.* 37 (4), 617–624. doi:10.4067/s0716-97602004000400017

McAloon, C. J., Boylan, L. M., Hamborg, T., Stallard, N., Osman, F., Lim, P. B., et al. (2016). The Changing Face of Cardiovascular Disease 2000-2012: an Analysis of the World Health Organisation Global Health Estimates Data. *Int. J. Cardiol.* 224, 256–264. doi:10.1016/j.ijcard.2016.09.026

Michelsen, M. M., Pena, A., Mygind, N. D., Bech, J., Gustafsson, I., Kastrup, J., et al. (2018). Coronary Microvascular Dysfunction and Myocardial Contractile reserve in Women with Angina and No Obstructive Coronary Artery Disease. *Echocardiography* 35 (2), 196–203. doi:10.1111/echo.13767

Mocayar Marón, F. J., Camargo, A. B., and Manucha, W. (2020). Allicin Pharmacology: Common Molecular Mechanisms against Neuroinflammation and Cardiovascular Diseases. *Life Sci.* 249, 117513. doi:10.1016/j.lfs.2020.117513

Palomeque, J., Rueda, O. V., Sapia, L., Valverde, C. A., Salas, M., Petroff, M. V., et al. (2009). Angiotensin II-Induced Oxidative Stress Resets the Ca2+ Dependence of Ca2+-Calmodulin Protein Kinase II and Promotes a Death Pathway Conserved across Different Species. *Circ. Res.* 105 (12), 1204–1212. doi:10.1161/CIRCRESAHA.109.204172

Piacentino, V., 3rd, Weber, C. R., Chen, X., Weisser-Thomas, J., Margulies, K. B., Bers, D. M., et al. (2003). Cellular Basis of Abnormal Calcium Transients of Failing Human Ventricular Myocytes. *Circ. Res.* 92 (6), 651–658. doi:10.1161/01.RES.0000062469.83985.9B

Puglisi, J. L., Goldspink, P. H., Gomes, A. V., Utter, M. S., Bers, D. M., and Solaro, R. J. (2014). Influence of a Constitutive Increase in Myofilament Ca2+-Sensitivity on Ca2+-Fluxes and Contraction of Mouse Heart Ventricular Myocytes. *Arch. Biochem. Biophys.* 552-553, 50–59. doi:10.1016/j.abb.2014.01.019

Santulli, G., Nakashima, R., Yuan, Q., and Marks, A. R. (2017). Intracellular Calcium Release Channels: an Update. *J. Physiol.* 595 (10), 3041–3051. doi:10.1113/JP272781

Sheibani, L., Lechuga, T. J., Zhang, H., Hameed, A., Wing, D. A., Kumar, S., et al. (2017). Augmented H2S Production via Cystathionine-Beta-Synthase Upregulation Plays a Role in Pregnancy-Associated Uterine Vasodilation. *Biol. Reprod.* 96 (3), 664–672. doi:10.1095/biolreprod.116.143834

Shen, B., Ye, C. L., Ye, K. H., Zhuang, L., and Jiang, J. H. (2009). Doxorubicin-induced Vasomotion and [Ca(2+)](i) Elevation in Vascular Smooth Muscle Cells from C57BL/6 Mice. *Acta Pharmacol. Sin.* 30 (11), 1488–1495. doi:10.1038/aps.2009.145

Singh, S., and Banerjee, R. (2011). PLP-dependent H(2)S Biogenesis. *Biochim. Biophys. Acta* 1814 (11), 1518–1527. doi:10.1016/j.bbapap.2011.02.004

Uren, N. G., Crake, T., Lefroy, D. C., de Silva, R., Davies, G. J., and Maseri, A. (1994). Reduced Coronary Vasodilator Function in Infarcted and normal Myocardium after Myocardial Infarction. *N. Engl. J. Med.* 331 (4), 222–227. doi:10.1056/NEJM199407283310402

Wang, Q., Wang, X. L., Liu, H. R., Rose, P., and Zhu, Y. Z. (2010). Protective Effects of Cysteine Analogues on Acute Myocardial Ischemia: Novel Modulators of Endogenous H(2)S Production. *Antioxid. Redox Signal.* 12 (10), 1155–1165. doi:10.1089/ars.2009.2947

Wang, R., Li, K., Wang, H., Jiao, H., Wang, X., Zhao, J., et al. (2019). Endogenous CSE/hydrogen Sulfide System Regulates the Effects of Glucocorticoids and Insulin on Muscle Protein Synthesis. *Oxid. Med. Cel. Longev.* 2019, 9752698. doi:10.1155/2019/9752698

Wang, Y. Z., Ngowi, E. E., Wang, D., Qi, H. W., Jing, M. R., Zhang, Y. X., et al. (2021). The Potential of Hydrogen Sulfide Donors in Treating Cardiovascular Diseases. *Int. J. Mol. Sci.* 22 (4), 2194. doi:10.3390/ijms22042194

Wollert, K. C., and Drexler, H. (2010). Cell Therapy for the Treatment of Coronary Heart Disease: a Critical Appraisal. *Nat. Rev. Cardiol.* 7 (4), 204–215. doi:10.1038/nrcardio.2010.1

Wu, Y., Zhang, Y., Zhang, J., Zhai, T., Hu, J., Luo, H., et al. (2020). Cathelicidin Aggravates Myocardial Ischemia/reperfusion Injury via Activating TLR4 Signaling and P2X7R/NLRP3 Inflammasome. *J. Mol. Cel. Cardiol.* 139, 75–86. doi:10.1016/j.yjmcc.2019.12.011

Xu, S., Liu, Z., and Liu, P. (2014). Targeting Hydrogen Sulfide as a Promising Therapeutic Strategy for Atherosclerosis. *Int. J. Cardiol.* 172 (2), 313–317. doi:10.1016/j.ijcard.2014.01.068

Xu, W., Li, X. P., Li, E. Z., Liu, Y. F., Zhao, J., Wei, L. N., et al. (2020). Protective Effects of Allicin on ISO-Induced Rat Model of Myocardial Infarction via JNK Signaling Pathway. *Pharmacology* 105 (9–10), 505–513. doi:10.1159/000503755

Zhang, Y., Jiao, L., Sun, L., Li, Y., Gao, Y., Xu, C., et al. (2018). LncRNA ZFAS1 as a SERCA2a Inhibitor to Cause Intracellular Ca2+ Overload and Contractile Dysfunction in a Mouse Model of Myocardial Infarction. *Circ. Res.* 122 (10), 1354–1368. doi:10.1161/CIRCRESAHA.117.312117

Zhang, J., Shi, X., Gao, J., Zhou, R., Guo, F., Zhang, Y., et al. (2021). Danhong Injection and Trimetazidine Protect Cardiomyocytes and Enhance Calcium Handling after Myocardial Infarction. *Evid. Based. Complement. Alternat. Med.* 2021, 2480465. doi:10.1155/2021/2480465

Zhou, D. D., Luo, M., Shang, A., Mao, Q. Q., Li, B. Y., Gan, R. Y., et al. (2021). Antioxidant Food Components for the Prevention and Treatment of Cardiovascular Diseases: Effects, Mechanisms, and Clinical Studies. *Oxid. Med. Cel. Longev.* 2021, 6627355. doi:10.1155/2021/6627355

Conflict of Interest: The authors declare that the research was conducted in the absence of any commercial or financial relationships that could be construed as a potential conflict of interest.

frontiers in Pharmacology

ORIGINAL RESEARCH
published: 24 January 2022
doi: 10.3389/fphar.2022.834296

Deletion of Smooth Muscle Lethal Giant Larvae 1 Promotes Neointimal Hyperplasia in Mice

Ya Zhang[1], Peidong Yuan[1,2], Xiaoping Ma[3], Qiming Deng[1], Jiangang Gao[4], Jianmin Yang[1], Tianran Zhang[5], Cheng Zhang[1]* and Wencheng Zhang[1,2]**

[1]The Key Laboratory of Cardiovascular Remodeling and Function Research, The State and Shandong Province Joint Key Laboratory of Translational Cardiovascular Medicine, Department of Cardiology, Chinese Ministry of Education, Chinese National Health Commission and Chinese Academy of Medical Sciences, Qilu Hospital, Cheeloo College of Medicine, Shandong University, Jinan, China, [2]Cardiovascular Disease Research Center of Shandong First Medical University, Central Hospital Affiliated to Shandong First Medical University, Jinan, China, [3]Department of Obstetrics and Gynecology, Liaocheng People's Hospital, Liaocheng, China, [4]School of Life Science and Key Laboratory of the Ministry of Education for Experimental Teratology, Shandong University, Jinan, China, [5]Department of Cardiology, The First Affiliated Hospital of Zhengzhou University, Zhengzhou, China

OPEN ACCESS

Edited by:
Qilong Wang,
Tianjin University of Traditional Chinese Medicine, China

Reviewed by:
Jinlong He,
Tianjin Medical University, China
Qiulun Lu,
Nanjing Medical University, China

***Correspondence:**
Tianran Zhang
714136498@qq.com
Cheng Zhang
zhangc@sdu.edu.cn
Wencheng Zhang
zhangwencheng@sdu.edu.cn

Specialty section:
This article was submitted to Cardiovascular and Smooth Muscle Pharmacology, a section of the journal Frontiers in Pharmacology

Received: 13 December 2021
Accepted: 06 January 2022
Published: 24 January 2022

Citation:
Zhang Y, Yuan P, Ma X, Deng Q, Gao J, Yang J, Zhang T, Zhang C and Zhang W (2022) Deletion of Smooth Muscle Lethal Giant Larvae 1 Promotes Neointimal Hyperplasia in Mice. Front. Pharmacol. 13:834296. doi: 10.3389/fphar.2022.834296

Vascular smooth muscle cell (VSMC) proliferation and migration contribute to neointimal hyperplasia after injury, which causes vascular remodeling related to arteriosclerosis, hypertension, and restenosis. Lethal giant larvae 1 (LGL1) is a highly conserved protein and plays an important role in cell polarity and tumor suppression. However, whether LGL1 affects neointimal hyperplasia is still unknown. In this study, we used smooth muscle-specific LGL1 knockout ($LGL1^{SMKO}$) mice generated by cross-breeding $LGL1^{flox/flox}$ mice with α-SMA-Cre mice. LGL1 expression was significantly decreased during both carotid artery ligation *in vivo* and PDGF-BB stimulation *in vitro*. LGL1 overexpression inhibited the proliferation and migration of VSMCs. Mechanistically, LGL1 could bind with signal transducer and activator of transcription 3 (STAT3) and promote its degradation *via* the proteasomal pathway. In the carotid artery ligation animal model, smooth muscle-specific deletion of LGL1 accelerated neointimal hyperplasia, which was attenuated by the STAT3 inhibitor SH-4-54. In conclusion, LGL1 may inhibit neointimal hyperplasia by repressing VSMC proliferation and migration *via* promoting STAT3 proteasomal degradation.

Keywords: LGL1, STAT3, neointimal hyperplasia, smooth muscle, proteasomal degradation

INTRODUCTION

Neointimal hyperplasia is a significant type of vascular remolding defined as the pathological accumulation of vascular smooth muscle cells (VSMCs) and extracellular matrix (ECM) in the intima. It is a process of excessive repair in the vascular wall caused by various activated cells and recycling substances responding to vessel injury (Zaman and Herath, 2008). Vascular injury inevitably occurs with various clinical procedures. Percutaneous coronary interventions such as balloon angioplasty and stents to treat ischemic coronary artery disease, vein grafts for coronary artery bypass graft surgery, and vascular access in hemodialysis can result in lumen re-narrowing and restenosis in a year after the operation (Schwartz et al., 1995; Roy-Chaudhury et al., 2001; Roy-Chaudhury et al., 2007; Harskamp et al., 2013; Byrne et al., 2017).

The behavior of VSMCs plays a vital role in neointimal hyperplasia. Gathering around the vessel lesion, activated inflammatory cells, and disturbed endothelial cells release a number of factors such as platelet-derived growth factor (PDGF) to stimulate the proliferation of VSMCs and subsequent

migration from the media layer of the vessel to the intima (Dzau et al., 1991; Majesky et al., 1991; Nabel et al., 1993; Grant et al., 1994; Dzau et al., 2002). Previous studies have revealed that neointimal hyperplasia is regulated by many proteins including signal transducer and activator of transcription 3 (STAT3) (Dutzmann et al., 2015). When VSMCs are activated by cytokines or growth factors, STAT3 is phosphorylated and translocates into the nucleus to regulate the expression of target genes involved in proliferation and migration (Park et al., 2000). Earlier researchers found that blocking STAT3 by adenovirus-expressing domain-negative STAT3 or siRNA could inhibit VSMC proliferation and migration, thus decreasing neointimal formation in models of carotid balloon injury or jugular vein-carotid artery bypass (Shibata et al., 2003; Wang et al., 2007; Sun et al., 2012). Similarly, the administration of STAT3 inhibitor downregulated its activity and suppressed VSMC proliferation and migration in neointimal hyperplasia (Lim et al., 2007; Daniel et al., 2012). Although the role of STAT3 in neointimal hyperplasia is clear, the regulation of STAT3 expression and activity needs further exploration.

Lethal giant larvae (LGL) proteins are a group of highly conserved proteins first discovered in Drosophila (Grifoni et al., 2004). LGL1 and LGL2 are two homologs in mammals (Russ et al., 2012). LGL1 maintains cell polarity and acts as a tumor suppressor (Bilder et al., 2000; Kuphal et al., 2006; Tian and Deng, 2008; Lu et al., 2009). In our recent study, LGL1 could inhibit vascular calcification *via* high mobility group box 1 (Zhang et al., 2020). Nonetheless, the role of LGL1 in neointimal hyperplasia after the vascular injury has not been elucidated.

Here, we used smooth muscle-specific LGL1 knockout ($LGL1^{SMKO}$) mice to explore the function of smooth-muscle LGL1 in neointimal hyperplasia. We found that LGL1 could inhibit neointimal hyperplasia after injury *via* STAT3.

MATERIALS AND METHODS

Reagents

Adenovirus-expressing LGL1 and its control green fluorescent protein (GFP) were purchased from Vigenebio (Maryland, United States). Recombinant human PDGF-BB was from Proteintech (Wuhan, China). 3-Methyladenine (3-MA), MG132 and SH-4-54 were from Selleck Chemicals (Shanghai, China). SH-4-54 could effectively inhibit the phosphorylation of STAT3. The IC50 of SH-4-54 to STAT3 is 300 nM (Kd). Chloroquine (CQ) was from MCE (Shanghai, China).

Mice

Smooth muscle-specific LGL1-knockout ($LGL1^{SMKO}$) mice were generated by cross-breeding $LGL1^{flox/flox}$ mice (Klezovitch et al., 2004) with transgenic Cre mice controlled by α-smooth muscle actin (α-SMA) promoter (Wu et al., 2007) as described (Zhang et al., 2020). Littermate $LGL1^{flox/flox}$/Cre- mice were used as controls (CTR). All mice were bred at a constant temperature of 25°C and under a 12-hr-day/night light cycle. All animal experiments were performed with the protocols approved by the Animal Care and Use Committee of Shandong University.

Animal Model for Neointimal Hyperplasia

We used common carotid artery (CCA) ligation to induce neointimal hyperplasia as reported previously (Wu et al., 2019). Briefly, 8-week-old mice were anesthetized with an intraperitoneal injection of sodium pentobarbital (40 mg/kg). A 10–15-mm median incision was made, and bilateral CCAs were carefully separated from veins and nerves. After exposing the left CCA, the ligation was performed below the bifurcation with 6–0 silk suture, above which are internal and external carotid arteries. The right CCA as a sham was processed as for the left CCA except for ligation. The neck incision was sutured, and animals were resuscitated in a warm and clean condition. After 3 weeks, mice were euthanized to collect tissues.

Primary Culture of VSMCs

Mice at 4–6 weeks old were euthanized with sodium pentobarbital (40 mg/kg). Aortas were isolated and placed in culture dishes containing phosphate buffered saline (PBS). After dissection of extravascular connective tissues and adventitia, VSMC-enriched tunica media was transferred into tubes with cell culture medium and then cut into about $1 \times 1\text{-mm}^3$ pieces. The tissue suspension was smeared evenly on the bottom of the culture bottle, which was inverted in a humidified incubator at 37°C and 5% CO_2 for 2 h until small blocks adhered firmly to the surface. Adequate cell culture medium containing 15% fetal bovine serum, 100 μg/ml streptomycin and 100 U/mL penicillin was supplied, and bottles were turned over in the incubator to observe crawling cells 5–7 days later. When cell confluency reached about 80–90%, cells were passaged and plated for further use.

Western Blot Analysis

The RIPA buffer (Solarbio. R0010) was used to extract proteins from cells and tissues. Proteins were fractionated by SDS-PAGE gel and transferred to PVDF membranes. After blocking with 5% skim dried milk/TBST for 1 h, membranes were incubated overnight at 4°C with primary antibodies, washed with TBST, incubated with corresponding secondary antibodies and observed by enhanced chemiluminescence (Pierce). The primary antibodies used were LGL1 monoclonal antibody (mAb) (CST, 12159s), GAPDH mAb (CST, 5174s), β-tubulin mAb (CST, 5568s), Cyclin D1 (CST, 55506s), proliferating cell nuclear antigen (PCNA) mAb (CST, 13110s), STAT3 mAb (CST, 9139s), and P-STAT3 (Y705) mAb (CST, 9145s). ImageJ software was used for analysis. All experiments were performed at least three times.

Co-Immunoprecipitation

VSMCs were lysed with lysis buffer (Beyotime, P0013) and incubated with IgG or anti-LGL1 antibody at 4°C overnight to form an antigen-antibody complex. Then protein A/G magnetic beads were added (MCE, HY-K0202). After washing and magnetic separation, the precipitation was dissolved with 1 × SDS loading buffer for western blot analysis.

Quantitative Real-Time Polymerase Chain Reaction

Total RNA was extracted from VSMCs and tissues by using an RNAfast200 kit (Fastagen, 220011), then a PrimeScript RT

reagent kit (Takara, RR0037A) was applied to reverse transcript total RNA to complementary DNA. PCR amplification was performed with the SYBR Premix Ex Taq (Takara, RR420A). The primers' sequences were as follows. LGL1: 5′-TACTGTGAT CAGCCCAAGACTG-3′ and 5′- GGAGGATCCCAAGATAGA GGAC-3′. GAPDH: 5′- GCACCGTCAAGGCTGAGAAC-3′ and 5′-TGGTGAAGACGCCAGTGGA-3′. Cyclin D1: 5′-AGG CGGATGAGAACAAGCAG-3′ and 5′- AGAAAGTGCGTT GTGCGGTA-3′. PCNA: 5′-TACAGCTTACTCTGCGCTCC-3′ and 5′-TTTTGGACATGCTGGTGAGGT-3′. STAT3: 5′-AGG ACATCAGTGGCAAGACC-3′ and 5′-CCTTGGGAATGT CGGGGTAG-3′.

Cell Proliferation Assay

Cell counting kit-8 (CCK-8) (Solarbio, CA1210) was used to assess cell proliferation. Briefly, VSMCs were seeded in 96-well plates at 5×10^3/well. After being induced with PDGF-BB for 48 h, the culture medium was replaced with 100 μL fresh medium, and 10 μL CCK-8 reagent was added to wells. Then plates were kept out of light and continuously incubated at 37°C and 5% CO_2 for 1 h in the incubator. The absorbance was detected at 450 nm by using a microplate reader (Molecular Devices, SpectraMax Plus 384) and optical density (OD) was recorded.

Wound Healing Assay

The scratch wound healing assay *in vitro* was used to evaluate cell migration. VSMCs were seeded in 12-well plates at 6×10^4/well. When cell confluency reached about 70–80%, a standard wound was made with a 200 μL micropipette tip for each well. VSMCs were then incubated for another 18 or 24 h. Images were captured under an inverted microscope (Nikon Instruments). Wound closure (%), defined as a cell coverage area in the wound divided by the total wound area, was calculated to represent migrative ability.

Hematoxylin and Eosin Staining

Carotid arteries were excised carefully from CTR and $LGL1^{SMKO}$ mice, fixed with 4% paraformaldehyde for 24 h and embedded in paraffin. Tissues were cut in serial 5-μm sections. After deparaffinization and rehydration, hematoxylin was used to stain the nucleus for 3 min. Differentiation was processed in 1% hydrochloric acid alcohol for 5 s. Then eosin was applied for cytoplasm and ECM staining for 2 min. The excessive stain was washed, then tissue was dehydrated in gradient alcohol and transparentized in xylene. The slides were sealed by neutral gum, and images were captured under a microscope (Nikon Instruments).

Immunohistochemistry

After deparaffinization and rehydration, slides were immersed in antigen repair buffer (Proteintech, PR30002) and underwent a microwave thermal repair method for 20 min. Endogenous peroxide was inactivated with 0.3% H_2O_2 at 37°C for 10 min and non-specific antibody binding was blocked with 5% bovine serum albumin. The slides were incubated with primary antibodies at 4°C overnight. After three cycles of washing with PBS, sections were incubated with secondary antibodies at 37°C for 30 min, then diaminobenzidine as a chromogen was dropped on sections for 2–5 min. The images were viewed under a microscope (Nikon Instruments).

Statistical Analysis

GraphPad Prism 9.0 (GraphPad Software, San Diego, CA) was used for all statistical analyses. All data are presented as mean ± SEM. The normality assumption of the data distribution was assessed by the Kolmogorov-Smirnov test. For the normal distribution, a two-tailed Student unpaired *t*-test was used to compare two groups. Differences between multiple groups with one variable were analyzed by one-way ANOVA followed by Bonferroni's post-hoc test. $p < 0.05$ was considered statistically significant.

RESULTS

LGL1 Expression was Decreased During Vascular Injury

To explore the relation between LGL1 level and vascular injury, we examined the expression of LGL1 in the mouse model of neointimal hyperplasia. The protein and mRNA levels of LGL1 were decreased in carotid arteries after ligation as compared with the sham group (**Figures 1A,B**). The reduced LGL1 expression was confirmed by immunohistochemistry (**Figure 1C**). Next, VSMCs were treated with PDGF-BB (20 ng/ml), a potent stimulator of VSMCs and a key mediator in vascular injury, for different times. LGL1 expression began to decrease after 12 h of stimulation (**Figure 1D**). Thus, the LGL1 level was related to vascular injury, which suggests that LGL1 may be involved in the development of neointimal hyperplasia.

LGL1 Overexpression Inhibited the Proliferation and Migration of VSMCs

To explore the role of LGL1 in vascular injury, VSMCs were infected with adenovirus-expressing GFP or LGL1, then treated with PDGF-BB. PDGF-BB could increase the protein expression of Cyclin D1 and PCNA, markers of cell proliferation, which was inhibited by LGL1 overexpression (**Figure 2A**). Similarly, PDGF-BB–upregulated Cyclin D1 and PCNA mRNA levels were also attenuated by LGL1 overexpression (**Figures 2B,C**). Cell viability assay revealed PDGF-BB promoted VSMC proliferation, which was suppressed by LGL1 overexpression (**Figure 2D**). Furthermore, on wound healing assay, LGL1 inhibited VSMC migration (**Figure 2E**). Hence, LGL1 overexpression inhibited the proliferation and migration of VSMCs.

LGL1 Deletion Aggravated the Proliferation and Migration of VSMCs

To comprehensively confirm the function of LGL1 in VSMCs, we cultured primary VSMCs from control and $LGL1^{SMKO}$ mice. PDGF-BB increased the protein expression of Cyclin D1 and PCNA, which was further upregulated by LGL1 deficiency (**Figure 3A**). The mRNA levels of Cyclin D1 and PCNA were further augmented by LGL1 deletion under PDGF-BB stimulation (**Figures 3B,C**). PDGF-BB–induced VSMC proliferation was enhanced by LGL1 deficiency (**Figure 3D**)

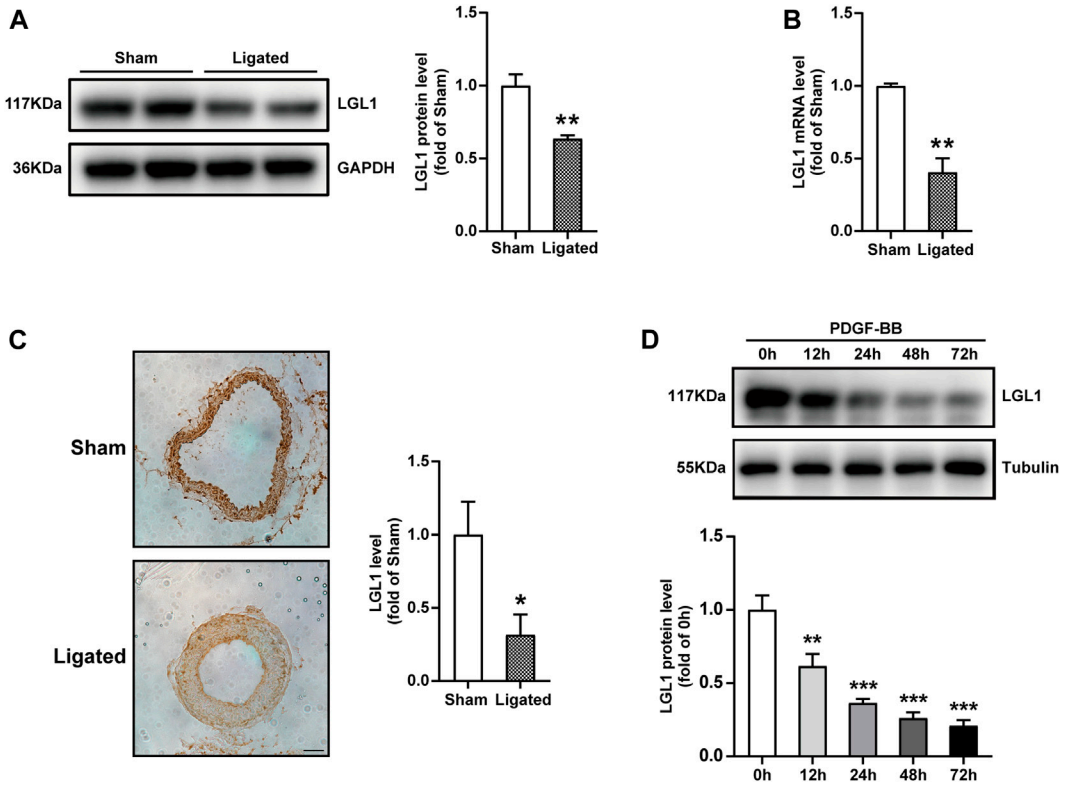

FIGURE 1 | LGL1 expression was decreased during vascular injury in mice. **(A,B)** Mice underwent left CCA ligation (Ligated) to induce neointimal hyperplasia; the right CCA was a control (Sham). Protein and mRNA levels of carotid artery LGL1 were tested by western blot analysis ($n = 4$) **(A)** and qRT-PCR ($n = 5$) **(B)**. $^{*}p < 0.05$ *vs.* Sham. **(C)** The expression of LGL1 from Sham and Ligated carotid arteries detected by immunohistochemistry ($n = 4$). Scale bar: 50 μm. $^{**}p < 0.01$ *vs.* Sham. **(D)** VSMCs were treated with PDGF-BB (20 ng/ml) for different times, then LGL1 expression was examined by western blot analysis ($n = 4$). $^{**}p < 0.01$, $^{***}p < 0.001$ *vs.* PDGF-BB 0 h.

and LGL1 deletion promoted cell migration on wound healing assay (**Figure 3E**). Thus, LGL1 deficiency aggravated the proliferation and migration of VSMCs.

LGL1 Could Bind With STAT3 and Promote its Degradation

To investigate the molecular mechanism of LGL1 in regulating the proliferation and migration of VSMCs, we analyzed various pathways and related molecules. LGL1 overexpression reduced both STAT3 and P-STAT3 (Y705) protein levels (**Figures 4A,B**) but not STAT3 mRNA level (**Figure 4B**). Thus, LGL1 may affect the STAT3 protein level by regulating its degradation. Immunoprecipitation assay revealed that LGL1 could bind with STAT3 (**Figure 4C**). There are three pathways to promote protein degradation: autophagy, lysosomal, and proteasome pathways. VSMCs were infected with adenovirus-expressing LGL1, then treated with the autophagy inhibitor 3-MA, lysosomal inhibitor CQ or proteasome inhibitor MG132 to explore the STAT3 degradation pathway. MG132 but not 3-MA or CQ could reverse the degradation of STAT3 induced by LGL1 overexpression (**Figures 4D–F**). Taken together, LGL1 could bind with STAT3 and promote its degradation *via* the proteasomal pathway.

LGL1 Inhibited the Proliferation and Migration of VSMCs *via* STAT3

To explore whether LGL1 regulates VSMC proliferation and migration *via* STAT3, we pretreated control and LGL1-deficient VSMCs with the STAT3 inhibitor SH-4-54 followed by PDGF-BB stimulation. LGL1 deficiency increased the protein and mRNA levels of Cyclin D1 and PCNA, which were attenuated by SH-4-54 (**Figures 5A–C**). Consistently, LGL1 deletion promoted cell proliferation under PDGF-BB stimulation, which was significantly suppressed by SH-4-54 treatment (**Figure 5D**). Furthermore, LGL1 deficiency-enhanced cell migration was also attenuated by the STAT3 inhibitor (**Figure 5E**). Therefore, *via* STAT3, LGL1 inhibited VSMC proliferation and migration, critical processes in neointimal hyperplasia.

Smooth Muscle-Specific Deletion of LGL1 Promoted Neointimal Hyperplasia *via* STAT3

To determine the role of LGL1 in neointimal hyperplasia *in vivo*, we subjected the control and $LGL1^{SMKO}$ mice to vascular injury by carotid ligation for 3 weeks. LGL1 deficiency significantly aggravated neointimal formation, as reflected by enlarged intima area and increased intima/media ratio (**Figure 6A**). Cyclin D1 and

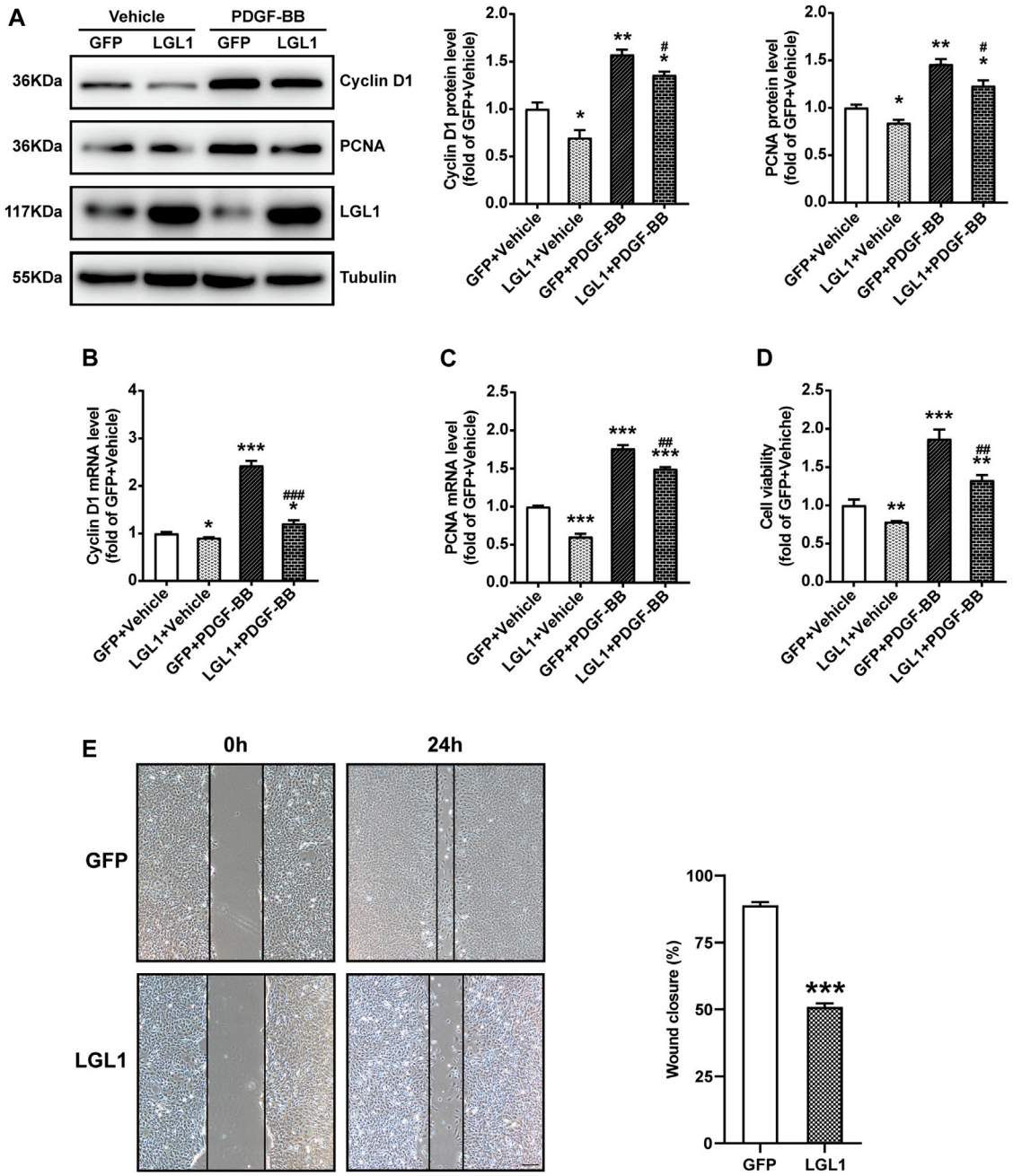

FIGURE 2 | LGL1 overexpression inhibited the proliferation and migration of VSMCs. **(A)** VSMCs were infected with adenovirus-expressing GFP or LGL1, then treated with PDGF-BB (20 ng/ml) for 48 h. The protein levels of Cyclin D1 and PCNA were detected by western blot ($n = 3$). $^{*}p < 0.05$, $^{**}p < 0.01$ *vs.* GFP + Vehicle. $^{\#}p < 0.05$ *vs.* GFP + PDGF-BB. **(B, C)** The mRNA levels of Cyclin D1 **(B)** and PCNA **(C)** were tested by qRT-PCR ($n = 4$). $^{*}p < 0.05$, $^{***}p < 0.001$ *vs.* GFP + Vehicle. $^{\#\#}p < 0.01$, $^{\#\#\#}p < 0.001$ *vs.* GFP + PDGF-BB. **(D)** Cell proliferation measured by CCK-8 assay ($n = 3$). $^{**}p < 0.01$, $^{***}p < 0.001$ *vs.* GFP + Vehicle. $^{\#\#}p < 0.01$ *vs.* GFP + PDGF-BB. **(E)** Cell migration evaluated by scratch wound healing assay ($n = 9$). Wound closure (%) represented migrative ability. Scale bar: 200 μm. $^{***}p < 0.001$ *vs.* GFP.

PCNA levels were increased in LGL1^{SMKO} mice, which agreed with the severe neointimal formation (**Figures 6B,C**). Carotid artery tissues harvested from mice post-surgery showed that ligation-induced upregulation of Cyclin D1 and PCNA was further enhanced by LGL1 deficiency (**Figure 6D**). Thus, smooth muscle-specific LGL1 knockout promoted neointimal formation.

STAT3 Inhibitor Attenuated Neointimal Hyperplasia in LGL1^{SMKO} Mice

To demonstrate whether LGL1 regulated neointimal hyperplasia *via* STAT3 *in vivo*, control and LGL1^{SMKO} mice were administrated with STAT3 inhibitor SH-4-54 and then induced to left CCA ligation for 3 weeks. Compared with

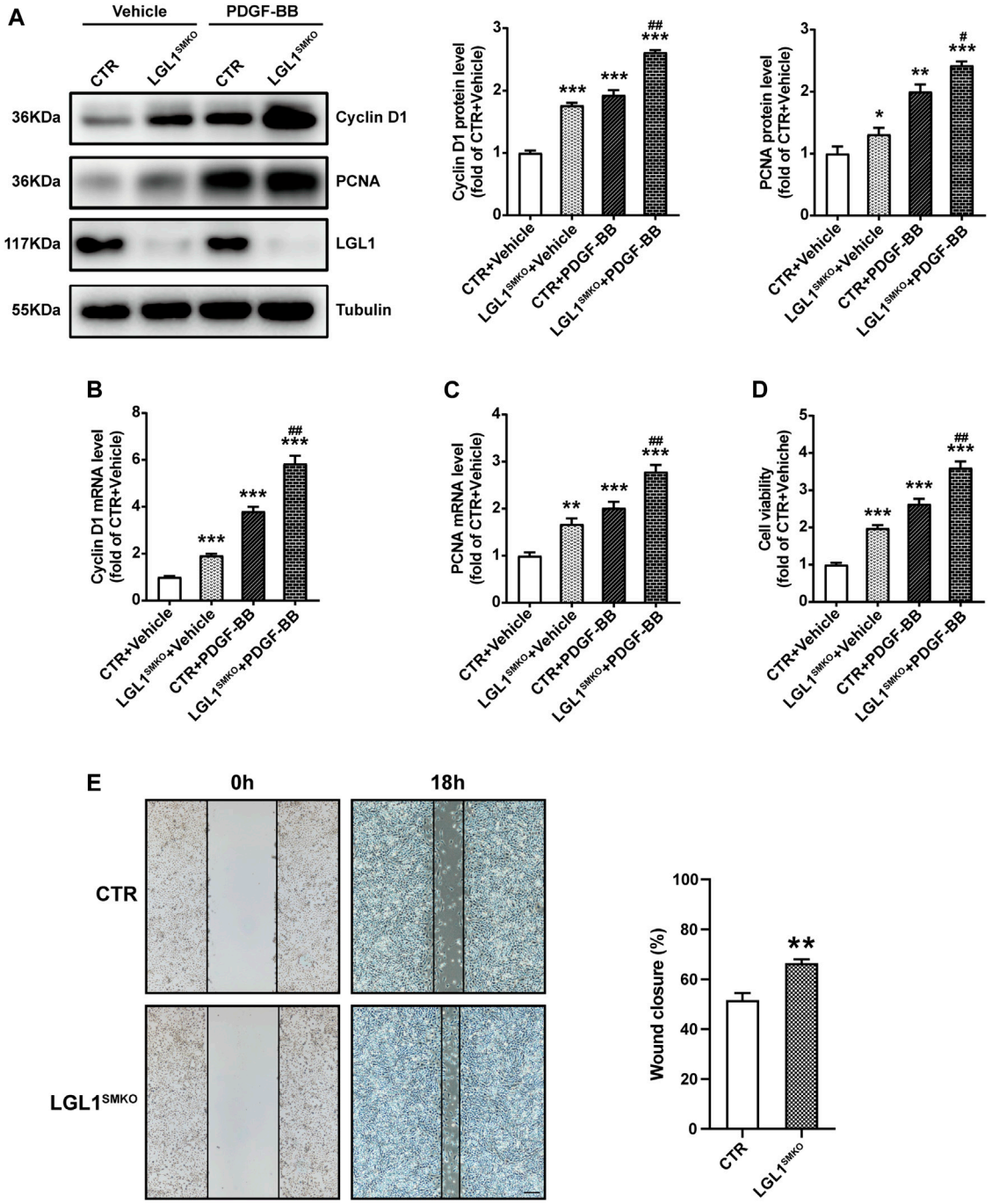

FIGURE 3 | LGL1 deficiency promoted the proliferation and migration of VSMCs. **(A)** Primary VSMCs were cultured from control (CTR) and LGL1^{SMKO} mice and treated with PDGF-BB for 48 h. The protein levels of Cyclin D1 and PCNA were detected by western blot analysis ($n = 3$). $^{*}p < 0.05$, $^{**}p < 0.01$, $^{***}p < 0.001$ *vs.* CTR + Vehicle. $^{\#}p < 0.05$, $^{\#\#}p < 0.01$ *vs.* CTR + PDGF-BB. **(B,C)** mRNA levels of Cyclin D1 **(B)** and PCNA **(C)** tested by qRT-PCR ($n = 4$). $^{**}p < 0.01$, $^{***}p < 0.001$ *vs.* CTR + Vehicle. $^{\#\#}p < 0.01$ *vs.* CTR + PDGF-BB. **(D)** Cell proliferation measured by CCK-8 assay ($n = 5$). $^{***}p < 0.001$ *vs.* CTR + Vehicle. $^{\#\#}p < 0.01$ *vs.* CTR + PDGF-BB. **(E)** Cell migration evaluated by scratch wound healing assay ($n = 4$). Wound closure (%) represented migrative ability. Scale bar: 200 μm. $^{**}p < 0.01$ *vs.* CTR.

control, LGL1^{SMKO} mice displayed aggravated neointimal hyperplasia, which was attenuated by SH-4-54 (**Figures 7A–C**). Taken together, LGL1 regulated the development of neointimal hyperplasia *via* STAT3 *in vivo*.

DISCUSSION

In this study, we found decreased LGL1 expression in both injured carotid arteries and PDGF-BB–induced VSMCs. To

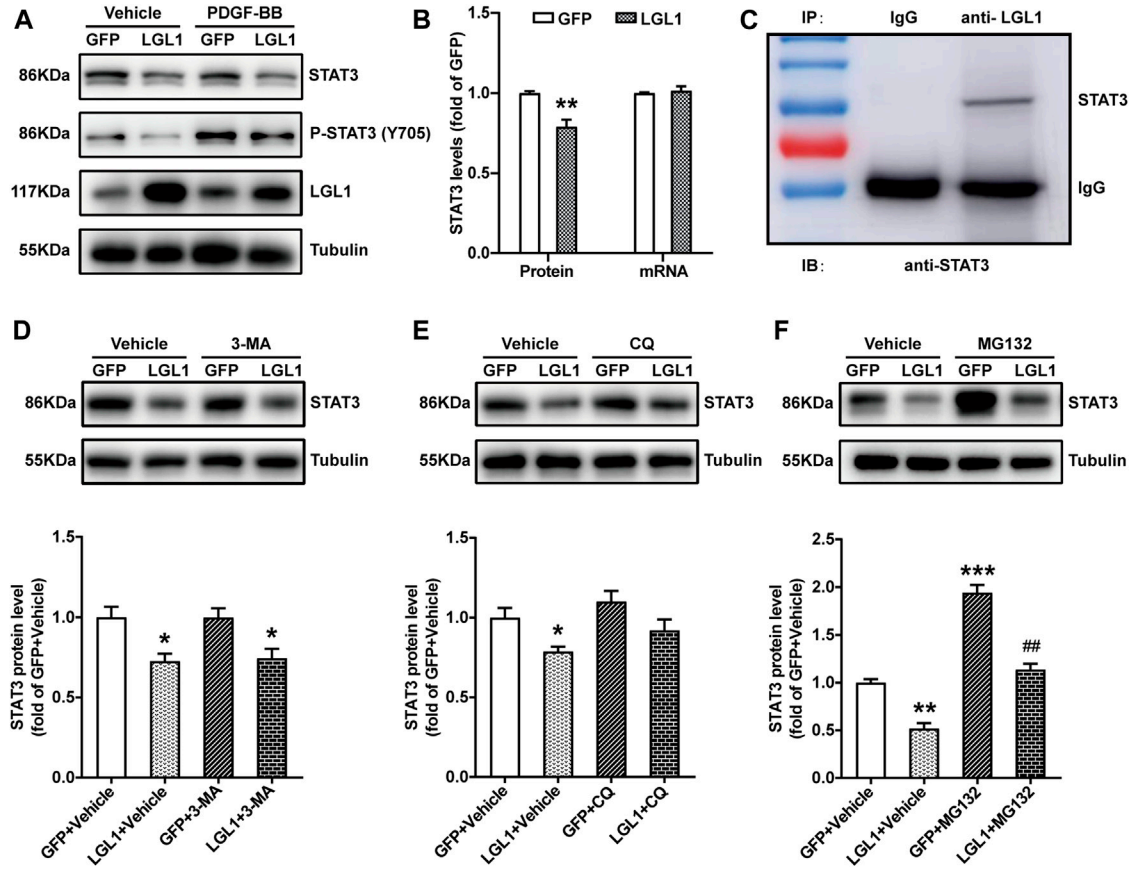

FIGURE 4 | LGL1 could bind with STAT3 and promote its degradation. **(A)** VSMCs were infected with adenovirus-expressing GFP or LGL1, then treated with PDGF-BB for 15 min. The protein levels of STAT3 and P-STAT3 (Y705) were measured by western blot analysis. **(B)** Statistical analysis of STAT3 protein and mRNA levels ($n = 4$). $^{**}p < 0.01$ *vs* GFP. **(C)** VSMC lysates were immunoprecipitated with IgG or anti-LGL1 antibody; STAT3 protein level was detected by western blot analysis. **(D–F)** VSMCs were infected with adenovirus-expressing GFP or LGL1, then treated with 10 mM of the autophagic inhibitor 3-MA for 24 h **(D)**, 10 μM of the lysosomal inhibitor CQ for 24 h **(E)** and 1 μM of the proteasome inhibitor MG132 for 6 h **(F)**; STAT3 protein level was detected by western blot analysis ($n = 3$). $^{*}p < 0.05$, $^{**}p < 0.01$, $^{***}p < 0.001$ *vs.* GFP + Vehicle. $^{\#\#}p < 0.01$ *vs.* LGL1 +Vehicle.

investigate the function of LGL1 in neointimal hyperplasia *in vivo*, we used smooth muscle-specific LGL1-knockout mice: LGL1 deficiency significantly aggravated neointimal formation. LGL1 overexpression inhibited PDGF-BB–stimulated proliferation and migration of VSMCs. Mechanistically, LGL1 could bind with STAT3 and promote its degradation *via* the proteasomal pathway (**Figure 7D**). Finally, STAT3 inhibitor treatment attenuated neointimal hyperplasia in $LGL1^{SMKO}$ mice. Our results reveal that LGL1 inhibited neointimal hyperplasia by promoting STAT3 degradation *via* the proteasomal pathway.

LGL1, located mainly in the cytoskeleton and plasma membrane (Strand et al., 1995; Kim et al., 2005), has a crucial role in cell polarity, cell division, and differentiation (Betschinger et al., 2003; Martin-Belmonte and Perez-Moreno, 2011; Dahan et al., 2012; Zhang et al., 2015). LGL1 alters its biological activity when phosphorylated by atypical protein kinase C (aPKC) (Graybill and Prehoda, 2014). Conjugated with Par/Cdc42/aPKC, LGL1 joins in the complex to regulate cell polarity and membrane development (Plant et al., 2003; Tocan et al., 2021). In addition, LGL1 in mammals acts as a tumor suppressor in many types of cancer progression (Tsuruga et al., 2007; Lu et al., 2009; Song et al., 2013; Liu et al., 2015). Moreover, LGL1 deficiency in the nervous system caused disrupted asymmetric cell division and lack of differentiation and hyperproliferation to apoptosis in progenitor cells, and mice developed tumors or severe brain dysplasia (Klezovitch et al., 2004; Daynac et al., 2018). Interestingly, the chimeric mice with a hematopoietic system deficient for LGL1 showed a stronger antiviral and antitumor effector $CD8^+$ T-cell response, which resulted in enhanced control of MC38-OVA tumors (Ramsbottom et al., 2016). Our recent study explored the role of LGL1 in vascular disease. LGL1 inhibited osteogenic differentiation by promoting degradation of high mobility group box protein 1 in vascular calcification (Zhang et al., 2020). In this study, we found that the protein and mRNA levels of LGL1 were decreased in carotid arteries after ligation, which indicates that vascular injury inhibited LGL1 expression at the transcriptional level. Moreover, LGL1 could inhibit neointimal hyperplasia after injury, which amplified the biological function of LGL1.

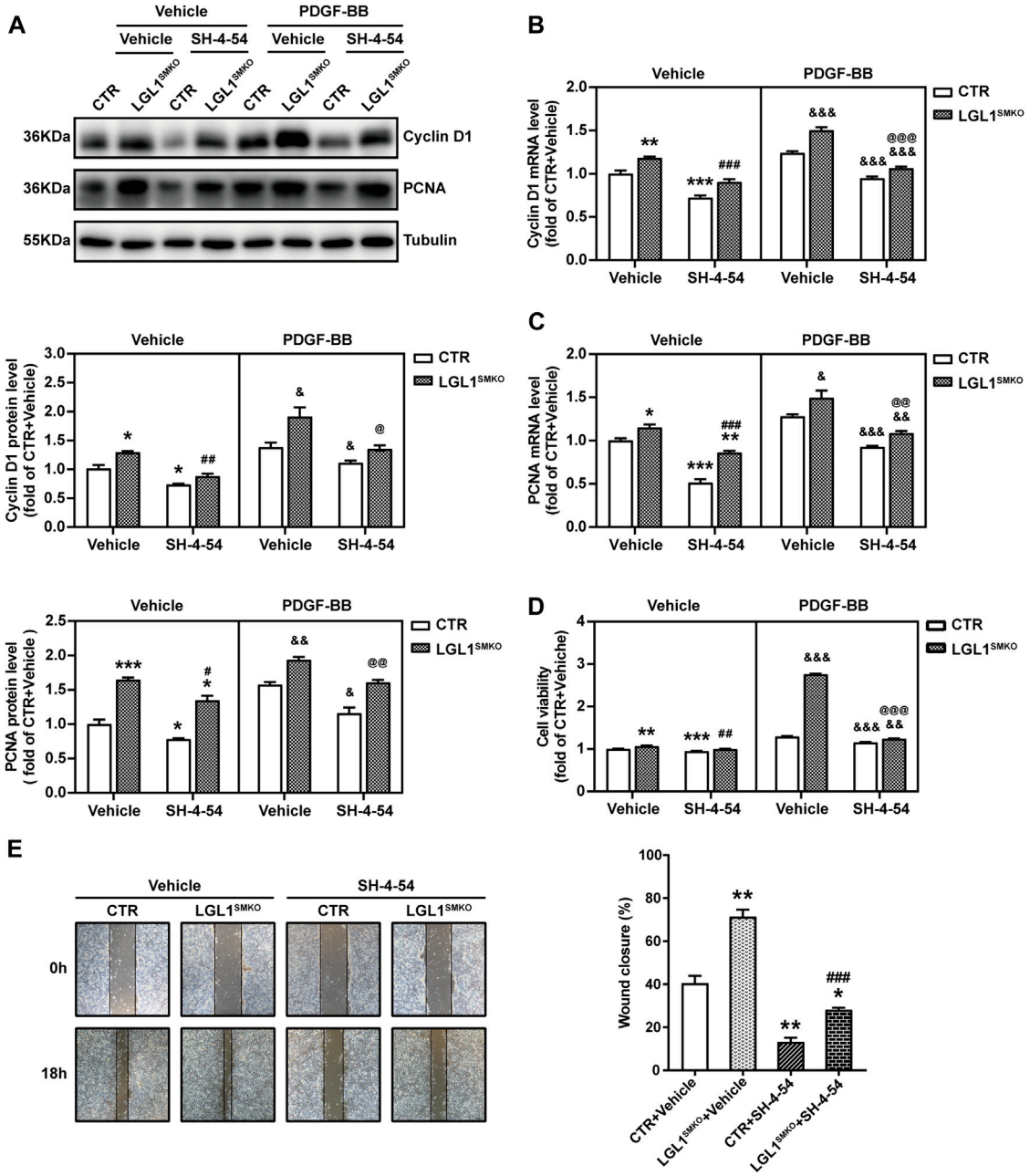

FIGURE 5 | LGL1 inhibited the proliferation and migration of VSMCs *via* STAT3. **(A)** Primary VSMCs were cultured from control (CTR) and LGL1^{SMKO} mice, pretreated with or without the STAT3 inhibitor SH-4-54 at 10 μM for 24 h, and stimulated with PDGF-BB for 48 h. Protein levels of Cyclin D1 and PCNA were detected by western blot analysis ($n = 3$). **(B,C)** mRNA levels of Cyclin D1 **(B)** and PCNA **(C)** tested by qRT-PCR ($n = 4$). **(D)** Cell proliferation measured by CCK-8 assay ($n = 8$). **(E)** Cell migration evaluated by the scratch wound healing assay ($n = 3$). Scale bar: 200 μm. $^{*}p < 0.05$, $^{**}p < 0.01$, $^{***}p < 0.001$ *vs.* CTR + Vehicle. $^{\#}p < 0.05$, $^{\#\#}p < 0.01$, $^{\#\#\#}p < 0.001$ *vs.* LGL1^{SMKO} + Vehicle. $^{\&}p < 0.05$, $^{\&\&}p < 0.01$, $^{\&\&\&}p < 0.001$ *vs.* CTR + PDGF-BB. $^{@}p < 0.05$, $^{@@}p < 0.01$, $^{@@@}p < 0.001$ *vs.* LGL1^{SMKO} + PDGF-BB.

STAT3 plays an important role in many pathological processes. When cells are stimulated by interleukin families, growth factors, angiotensin, erythropoietin, and colony-stimulating factors, tyrosine kinase-associated receptors in the cell membrane transduce the signal to tyrosine kinase (JAK), which phosphorylates STAT3 at Tyr705. Phosphorylated STAT3 dimers translocate into the nucleus to regulate the expression of target genes (Aggarwal et al., 2009; Brooks et al., 2014). STAT3 phosphorylation at Ser727 could increase the binding stability of DNA with STAT3 and augment its transcriptional activity (Yang et al., 2002). Acetylation at Lys685 was critical for STAT3 dimerization and transcriptional regulation (Yuan et al., 2005). SUMOylation at Lys451 caused the hyperphosphorylation of STAT3 and magnified its transcription activation (Zhou et al., 2016). Also, PIAS3, known as protein inhibitor of activated

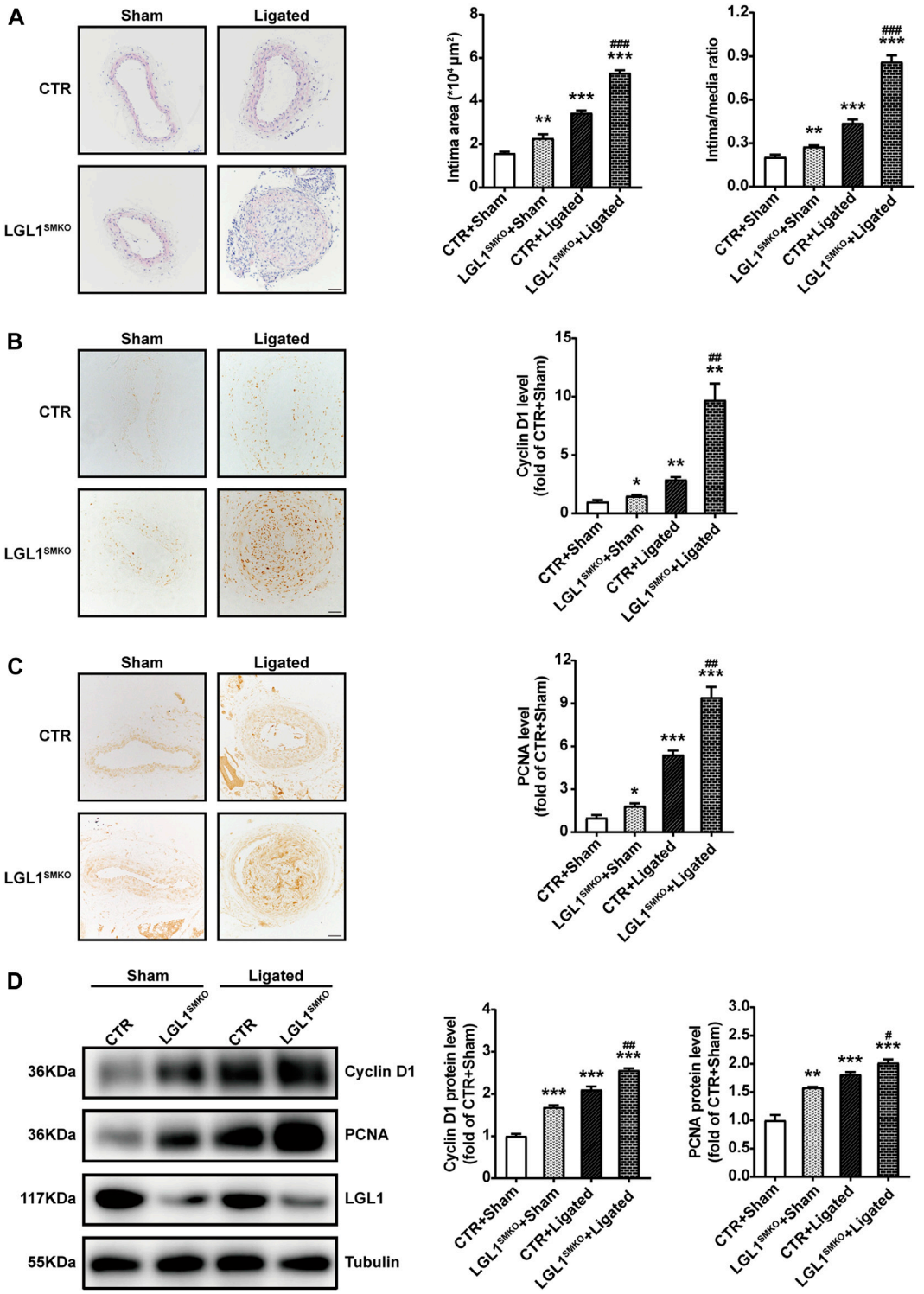

FIGURE 6 | Smooth muscle-specific deletion of LGL1 promoted neointimal hyperplasia *via* STAT3. **(A)** Control (CTR) and LGL1^{SMKO} mice underwent left CCA ligation (Ligated) to induce neointimal hyperplasia; right CCA was applied as control (Sham). Carotid arteries were stained with HE. The intimal area and intima/media ratio were calculated ($n = 6$). Scale bar: 50 μm. **(B,C)** Cyclin D1 **(B)** and PCNA **(C)** levels tested by immunohistochemistry ($n = 3$). Scale bar: 50 μm. **(D)** Protein levels of Cyclin D1 and PCNA detected by western blot analysis ($n = 4$). $^{*}p < 0.05$, $^{**}p < 0.01$, $^{***}p < 0.001$ *vs.* CTR + Sham. $^{\#}p < 0.05$, $^{\#\#}p < 0.01$, $^{\#\#\#}p < 0.001$ *vs.* CTR + Ligated.

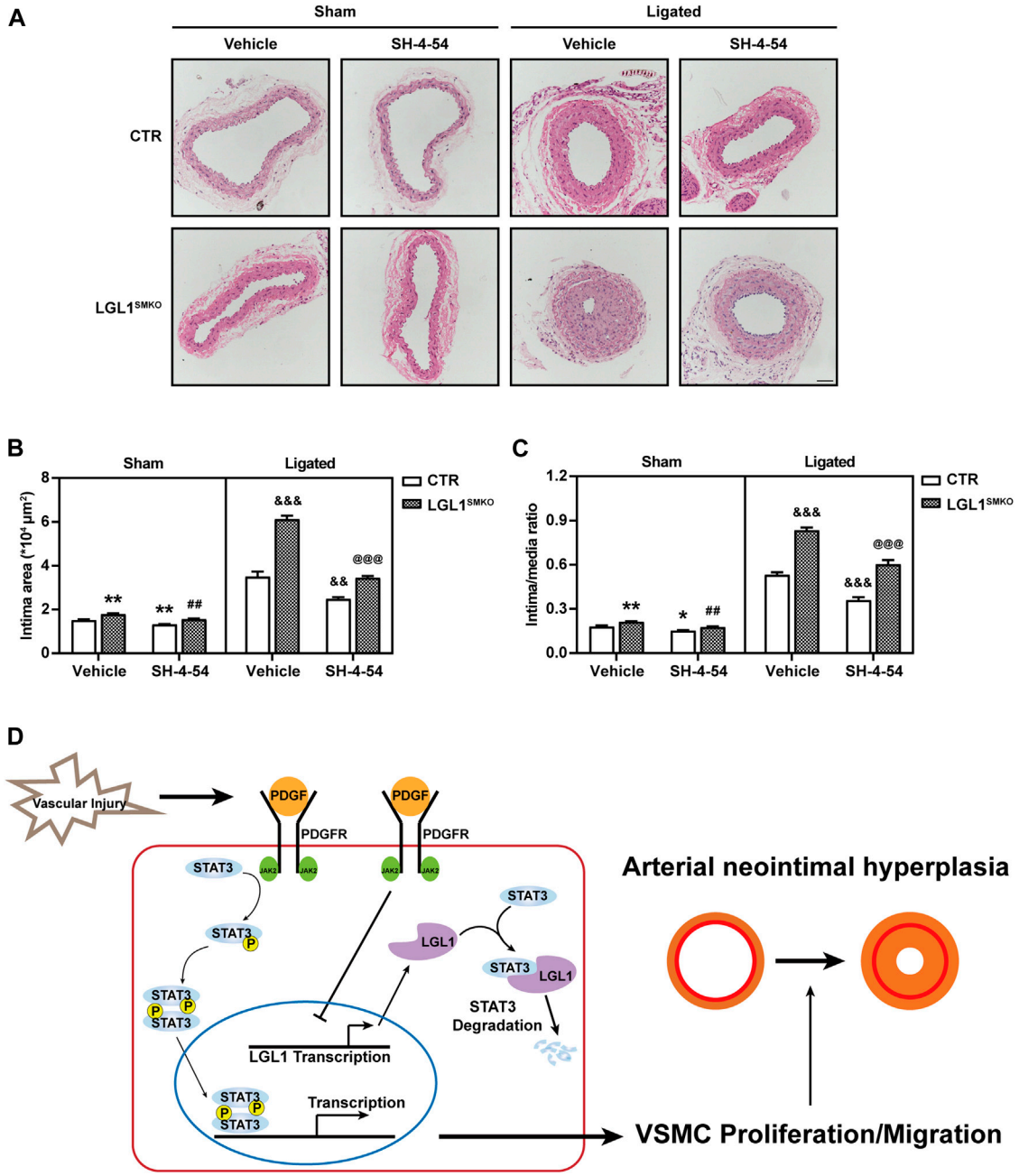

FIGURE 7 | STAT3 inhibitor attenuated neointimal hyperplasia in LGL1^{SMKO} mice. **(A)** CTR and LGL1^{SMKO} mice were administrated with STAT3 inhibitor SH-4-54 (10 mg/kg) daily and then underwent left CCA ligation for 21 days. Carotid arteries were stained with HE. **(B,C)** The intimal area **(B)** and intima/media ratio **(C)** were calculated ($n = 4$). Scale bar: 50 μm. $^{*}p < 0.05$, $^{**}p < 0.01$ *vs.* CTR + Vehicle + Sham. $^{\#\#}p < 0.01$ *vs.* LGL1^{SMKO} + Vehicle + Sham. $^{\&\&}p < 0.01$, $^{\&\&\&}p < 0.001$ *vs.* CTR + Vehicle + Ligated. $^{@@@}p < 0.001$ *vs.* LGL1^{SMKO} + Vehicle + Ligated. **(D)** Schematic diagram of neointimal hyperplasia inhibition by LGL1 *via* STAT3 degradation.

STAT3, could block the DNA-binding activity of STAT3 and inhibit STAT3-mediated gene expression (Chung et al., 1997). Moreover, the expression of STAT3 could be modulated by transcription factors such as PPARγ, Src and SMAD3, or microRNAs (miRNAs) such as miR-125a-5p and miR-519a (Xiao et al., 2017; Li et al., 2018; Xu et al., 2018; Liu et al., 2021; Zhang et al., 2021). In addition, some small molecules such as SD-36 could degrade STAT3 to disrupt its biological function (Bai et al., 2019; Zhou et al., 2019). In this study, we found that LGL1 could bind with STAT3 and promote its degradation *via* the proteasomal pathway. In our previous study, we demonstrated that LGL1 could inhibit vascular calcification by preventing osteogenic differentiation through degrading HMGB1 in the lysosomal pathway (Zhang et al., 2020). These results indicated that LGL1 might mediate the degradation of proteins in different

ways. The detailed mechanisms will be explored in future study. Moreover, the STAT3 inhibitor SH-4-54 attenuated the aggravated neointimal hyperplasia in LGL1^{SMKO} mice, which suggests that STAT3 may be a target for preventing and treating vascular diseases.

Neointimal hyperplasia is a complicated process referring to various cells and cellular cytokines. In response to injury, inflammatory cells along with platelets and fibrin recruit immediately around the impaired vascular surface and secrete cytokines such as PDGF-BB, which propel quiescent VSMCs in the tunica media to proliferate and migrate into the intima (Scott, 2006; Kim and Dean, 2011). The dysfunctional endothelium with released active mediators and degraded ECM induce VSMCs to transform from a "contractile" to a "synthetic" phenotype, which is more mobile and productive (Ip et al., 1990; Docherty et al., 1992; Scott, 2006; Park et al., 2020). During the process of neointimal hyperplasia, VSMCs are predominant. Inhibition of the proliferation and migration of VSMCs could be a promising strategy to treat neointima-related diseases such as atherosclerosis. In this study, we demonstrated that LGL1 could inhibit the proliferation and migration of VSMCs, which attenuated neointimal formation and increased our understanding of the mechanism of neointimal hyperplasia. Besides, in our previous study, we demonstrated that LGL1 could inhibit vascular calcification by preventing osteogenic differentiation through degrading HMGB1. These findings disclosed the vital role of LGL1 in vascular remodeling, which suggests that LGL1 may be the potential therapeutic target in the vascular remodeling-related diseases such as atherosclerosis.

In conclusion, we revealed that LGL1 could inhibit neointimal hyperplasia after vascular injury: it suppressed VSMC proliferation and migration by promoting STAT3 degradation *via* the proteasomal pathway. Our findings may shed light on the mechanism of neointimal formation and provide a novel strategy to treat vascular remodeling diseases.

DATA AVAILABILITY STATEMENT

The original contributions presented in the study are included in the article/Supplementary Material, further inquiries can be directed to the corresponding authors.

ETHICS STATEMENT

The animal study was reviewed and approved by the Animal Care and Use Committee of Shandong University.

AUTHOR CONTRIBUTIONS

YZ and PY designed and performed the research. XM, QD, JG, and JY analyzed data. YZ, TZ, CZ, and WZ conceived the project, reviewed the data, and wrote the manuscript.

FUNDING

This study was supported by grants from the Natural Science Foundation for Distinguished Young Scholars of Shandong Province (No. ZR2020JQ30), the National Natural Science Foundation of China (No. 81970198 and 81770473), and the Taishan Scholar Project of Shandong Province of China (No. tsqn20161066).

ACKNOWLEDGMENTS

The authors thank Prof. Valeri Vasioukhin from the Division of Human Biology, Fred Hutchinson Cancer Research Center, for providing the LGL1$^{flox/flox}$ mice.

REFERENCES

Aggarwal, B. B., Kunnumakkara, A. B., Harikumar, K. B., Gupta, S. R., Tharakan, S. T., Koca, C., et al. (2009). Signal Transducer and Activator of Transcription-3, Inflammation, and Cancer: How Intimate Is the Relationship? *Ann. N. Y Acad. Sci.* 1171, 59–76. doi:10.1111/j.1749-6632.2009.04911.x

Bai, L., Zhou, H., Xu, R., Zhao, Y., Chinnaswamy, K., McEachern, D., et al. (2019). A Potent and Selective Small-Molecule Degrader of STAT3 Achieves Complete Tumor Regression *In Vivo*. *Cancer Cell* 36 (5), 498–511.e17. doi:10.1016/j.ccell.2019.10.002

Betschinger, J., Mechtler, K., and Knoblich, J. A. (2003). The Par Complex Directs Asymmetric Cell Division by Phosphorylating the Cytoskeletal Protein Lgl. *Nature* 422 (6929), 326–330. doi:10.1038/nature01486

Bilder, D., Li, M., and Perrimon, N. (2000). Cooperative Regulation of Cell Polarity and Growth by Drosophila Tumor Suppressors. *Science* 289 (5476), 113–116. doi:10.1126/science.289.5476.113

Brooks, A. J., Dai, W., O'Mara, M. L., Abankwa, D., Chhabra, Y., Pelekanos, R. A., et al. (2014). Mechanism of Activation of Protein Kinase JAK2 by the Growth Hormone Receptor. *Science* 344 (6185), 1249783. doi:10.1126/science.1249783

Byrne, R. A., Stone, G. W., Ormiston, J., and Kastrati, A. (2017). Coronary Balloon Angioplasty, Stents, and Scaffolds. *Lancet* 390 (10096), 781–792. doi:10.1016/S0140-6736(17)31927-X

Chung, C. D., Liao, J., Liu, B., Rao, X., Jay, P., Berta, P., et al. (1997). Specific Inhibition of Stat3 Signal Transduction by PIAS3. *Science* 278 (5344), 1803–1805. doi:10.1126/science.278.5344.1803

Dahan, I., Yearim, A., Touboul, Y., and Ravid, S. (2012). The Tumor Suppressor Lgl1 Regulates NMII-A Cellular Distribution and Focal Adhesion Morphology to Optimize Cell Migration. *Mol. Biol. Cel* 23 (4), 591–601. doi:10.1091/mbc.E11-01-0015

Daniel, J. M., Dutzmann, J., Bielenberg, W., Widmer-Teske, R., Gündüz, D., Hamm, C. W., et al. (2012). Inhibition of STAT3 Signaling Prevents Vascular Smooth Muscle Cell Proliferation and Neointima Formation. *Basic Res. Cardiol.* 107 (3), 261. doi:10.1007/s00395-012-0261-9

Daynac, M., Chouchane, M., Collins, H. Y., Murphy, N. E., Andor, N., Niu, J., et al. (2018). Lgl1 Controls NG2 Endocytic Pathway to Regulate Oligodendrocyte Differentiation and Asymmetric Cell Division and Gliomagenesis. *Nat. Commun.* 9 (1), 2862. doi:10.1038/s41467-018-05099-3

Docherty, A. J., O'Connell, J., Crabbe, T., Angal, S., and Murphy, G. (1992). The Matrix Metalloproteinases and Their Natural Inhibitors: Prospects for Treating Degenerative Tissue Diseases. *Trends Biotechnol.* 10 (2), 200–207. doi:10.1016/0167-7799(92)90214-g

Dutzmann, J., Daniel, J. M., Bauersachs, J., Hilfiker-Kleiner, D., and Sedding, D. G. (2015). Emerging Translational Approaches to Target STAT3 Signalling and its Impact on Vascular Disease. *Cardiovasc. Res.* 106 (3), 365–374. doi:10.1093/cvr/cvv103

Dzau, V. J., Braun-Dullaeus, R. C., and Sedding, D. G. (2002). Vascular Proliferation and Atherosclerosis: New Perspectives and Therapeutic Strategies. *Nat. Med.* 8 (11), 1249–1256. doi:10.1038/nm1102-1249

Dzau, V. J., Gibbons, G. H., and Pratt, R. E. (1991). Molecular Mechanisms of Vascular Renin-Angiotensin System in Myointimal Hyperplasia. *Hypertension* 18 (4 Suppl. l), II100–5. doi:10.1161/01.hyp.18.4_suppl.ii100

Grant, M. B., Wargovich, T. J., Ellis, E. A., Caballero, S., Mansour, M., and Pepine, C. J. (1994). Localization of Insulin-like Growth Factor I and Inhibition of Coronary Smooth Muscle Cell Growth by Somatostatin Analogues in Human Coronary Smooth Muscle Cells. A Potential Treatment for Restenosis? *Circulation* 89 (4), 1511–1517. doi:10.1161/01.cir.89.4.1511

Graybill, C., and Prehoda, K. E. (2014). Ordered Multisite Phosphorylation of Lethal Giant Larvae by Atypical Protein Kinase C. *Biochemistry* 53 (30), 4931–4937. doi:10.1021/bi500748w

Grifoni, D., Garoia, F., Schimanski, C. C., Schmitz, G., Laurenti, E., Galle, P. R., et al. (2004). The Human Protein Hugl-1 Substitutes for Drosophila Lethal Giant Larvae Tumour Suppressor Function *In Vivo*. *Oncogene* 23 (53), 8688–8694. doi:10.1038/sj.onc.1208023

Harskamp, R. E., Lopes, R. D., Baisden, C. E., de Winter, R. J., and Alexander, J. H. (2013). Saphenous Vein Graft Failure after Coronary Artery Bypass Surgery: Pathophysiology, Management, and Future Directions. *Ann. Surg.* 257 (5), 824–833. doi:10.1097/SLA.0b013e318288c38d

Ip, J. H., Fuster, V., Badimon, L., Badimon, J., Taubman, M. B., and Chesebro, J. H. (1990). Syndromes of Accelerated Atherosclerosis: Role of Vascular Injury and Smooth Muscle Cell Proliferation. *J. Am. Coll. Cardiol.* 15 (7), 1667–1687. doi:10.1016/0735-1097(90)92845-s

Kim, M. S., and Dean, L. S. (2011). In-stent Restenosis. *Cardiovasc. Ther.* 29 (3), 190–198. doi:10.1111/j.1755-5922.2010.00155.x

Kim, Y. K., Kim, Y. S., and Baek, K. H. (2005). The WD-40 Repeat Motif of Lgl Tumor Suppressor Proteins Associated with Salt Tolerance and Temperature Sensitivity. *Biochem. Biophys. Res. Commun.* 331 (4), 922–928. doi:10.1016/j.bbrc.2005.04.017

Klezovitch, O., Fernandez, T. E., Tapscott, S. J., and Vasioukhin, V. (2004). Loss of Cell Polarity Causes Severe Brain Dysplasia in Lgl1 Knockout Mice. *Genes Dev.* 18 (5), 559–571. doi:10.1101/gad.1178004

Kuphal, S., Wallner, S., Schimanski, C. C., Bataille, F., Hofer, P., Strand, S., et al. (2006). Expression of Hugl-1 Is Strongly Reduced in Malignant Melanoma. *Oncogene* 25 (1), 103–110. doi:10.1038/sj.onc.1209008

Li, H., Chen, L., Li, J. J., Zhou, Q., Huang, A., Liu, W. W., et al. (2018). miR-519a Enhances Chemosensitivity and Promotes Autophagy in Glioblastoma by Targeting STAT3/Bcl2 Signaling Pathway. *J. Hematol. Oncol.* 11 (1), 70. doi:10.1186/s13045-018-0618-0

Lim, S. Y., Kim, Y. S., Ahn, Y., Jeong, M. H., Rok, L. S., Kim, J. H., et al. (2007). The Effects of Granulocyte-colony Stimulating Factor in Bare Stent and Sirolimus-Eluting Stent in Pigs Following Myocardial Infarction. *Int. J. Cardiol.* 118 (3), 304–311. doi:10.1016/j.ijcard.2006.07.018

Liu, X., Lu, D., Ma, P., Liu, H., Cao, Y., Sang, B., et al. (2015). Hugl-1 Inhibits Glioma Cell Growth in Intracranial Model. *J. Neurooncol.* 125 (1), 113–121. doi:10.1007/s11060-015-1901-3

Liu, Z., Meng, Y., Miao, Y., Yu, L., Wei, Q., Li, Y., et al. (2021). Propofol Ameliorates Renal Ischemia/reperfusion Injury by Enhancing Macrophage M2 Polarization through PPARγ/STAT3 Signaling. *Aging (Albany NY)* 13 (11), 15511–15522. doi:10.18632/aging.203107

Lu, X., Feng, X., Man, X., Yang, G., Tang, L., Du, D., et al. (2009). Aberrant Splicing of Hugl-1 Is Associated with Hepatocellular Carcinoma Progression. *Clin. Cancer Res.* 15 (10), 3287–3296. doi:10.1158/1078-0432.CCR-08-2078

Majesky, M. W., Lindner, V., Twardzik, D. R., Schwartz, S. M., and Reidy, M. A. (1991). Production of Transforming Growth Factor Beta 1 during Repair of Arterial Injury. *J. Clin. Invest.* 88 (3), 904–910. doi:10.1172/JCI115393

Martin-Belmonte, F., and Perez-Moreno, M. (2011). Epithelial Cell Polarity, Stem Cells and Cancer. *Nat. Rev. Cancer* 12 (1), 23–38. doi:10.1038/nrc3169

Nabel, E. G., Yang, Z., Liptay, S., San, H., Gordon, D., Haudenschild, C. C., et al. (1993). Recombinant Platelet-Derived Growth Factor B Gene Expression in Porcine Arteries Induce Intimal Hyperplasia *In Vivo*. *J. Clin. Invest.* 91 (4), 1822–1829. doi:10.1172/JCI116394

Park, K. S., Kang, S. N., Kim, D. H., Kim, H. B., Im, K. S., Park, W., et al. (2020). Late Endothelial Progenitor Cell-Capture Stents with CD146 Antibody and Nanostructure Reduce In-Stent Restenosis and Thrombosis. *Acta Biomater.* 111, 91–101. doi:10.1016/j.actbio.2020.05.011

Park, O. K., Schaefer, L. K., Wang, W., and Schaefer, T. S. (2000). Dimer Stability as a Determinant of Differential DNA Binding Activity of Stat3 Isoforms. *J. Biol. Chem.* 275 (41), 32244–32249. doi:10.1074/jbc.M005082200

Plant, P. J., Fawcett, J. P., Lin, D. C., Holdorf, A. D., Binns, K., Kulkarni, S., et al. (2003). A Polarity Complex of mPar-6 and Atypical PKC Binds, Phosphorylates and Regulates Mammalian Lgl. *Nat. Cel Biol* 5 (4), 301–308. doi:10.1038/ncb948

Ramsbottom, K. M., Sacirbegovic, F., Hawkins, E. D., Kallies, A., Belz, G. T., Van Ham, V., et al. (2016). Lethal Giant Larvae-1 Deficiency Enhances the CD8(+) Effector T-Cell Response to Antigen challenge *In Vivo*. *Immunol. Cel Biol* 94 (3), 306–311. doi:10.1038/icb.2015.82

Roy-Chaudhury, P., Arend, L., Zhang, J., Krishnamoorthy, M., Wang, Y., Banerjee, R., et al. (2007). Neointimal Hyperplasia in Early Arteriovenous Fistula Failure. *Am. J. Kidney Dis.* 50 (5), 782–790. doi:10.1053/j.ajkd.2007.07.019

Roy-Chaudhury, P., Kelly, B. S., Miller, M. A., Reaves, A., Armstrong, J., Nanayakkara, N., et al. (2001). Venous Neointimal Hyperplasia in Polytetrafluoroethylene Dialysis Grafts. *Kidney Int.* 59 (6), 2325–2334. doi:10.1046/j.1523-1755.2001.00750.x

Russ, A., Louderbough, J. M., Zarnescu, D., and Schroeder, J. A. (2012). Hugl1 and Hugl2 in Mammary Epithelial Cells: Polarity, Proliferation, and Differentiation. *PLoS One* 7 (10), e47734. doi:10.1371/journal.pone.0047734

Schwartz, S. M., deBlois, D., and O'Brien, E. R. (1995). The Intima. Soil for Atherosclerosis and Restenosis. *Circ. Res.* 77 (3), 445–465. doi:10.1161/01.res.77.3.445

Scott, N. A. (2006). Restenosis Following Implantation of Bare Metal Coronary Stents: Pathophysiology and Pathways Involved in the Vascular Response to Injury. *Adv. Drug Deliv. Rev.* 58 (3), 358–376. doi:10.1016/j.addr.2006.01.015

Shibata, R., Kai, H., Seki, Y., Kato, S., Wada, Y., Hanakawa, Y., et al. (2003). Inhibition of STAT3 Prevents Neointima Formation by Inhibiting Proliferation and Promoting Apoptosis of Neointimal Smooth Muscle Cells. *Hum. Gene Ther.* 14 (7), 601–610. doi:10.1089/104303403321618128

Song, J., Peng, X. L., Ji, M. Y., Ai, M. H., Zhang, J. X., and Dong, W. G. (2013). Hugl-1 Induces Apoptosis in Esophageal Carcinoma Cells Both *In Vitro* and *In Vivo*. *World J. Gastroenterol.* 19 (26), 4127–4136. doi:10.3748/wjg.v19.i26.4127

Strand, D., Unger, S., Corvi, R., Hartenstein, K., Schenkel, H., Kalmes, A., et al. (1995). A Human Homologue of the Drosophila Tumour Suppressor Gene L(2)gl Maps to 17p11.2-12 and Codes for a Cytoskeletal Protein that Associates with Nonmuscle Myosin II Heavy Chain. *Oncogene* 11 (2), 291–301.

Sun, J., Zheng, J., Ling, K. H., Zhao, K., Xie, Z., Li, B., et al. (2012). Preventing Intimal Thickening of Vein Grafts in Vein Artery Bypass Using STAT-3 siRNA. *J. Transl Med.* 10, 2. doi:10.1186/1479-5876-10-2

Tian, A. G., and Deng, W. M. (2008). Lgl and its Phosphorylation by aPKC Regulate Oocyte Polarity Formation in Drosophila. *Development* 135 (3), 463–471. doi:10.1242/dev.016253

Tocan, V., Hayase, J., Kamakura, S., Kohda, A., Ohga, S., Kohjima, M., et al. (2021). Hepatocyte Polarity Establishment and Apical Lumen Formation Are Organized by Par3, Cdc42, and aPKC in Conjunction with Lgl. *J. Biol. Chem.* 297, 101354. doi:10.1016/j.jbc.2021.101354

Tsuruga, T., Nakagawa, S., Watanabe, M., Takizawa, S., Matsumoto, Y., Nagasaka, K., et al. (2007). Loss of Hugl-1 Expression Associates with Lymph Node Metastasis in Endometrial Cancer. *Oncol. Res.* 16 (9), 431–435. doi:10.3727/000000007783980855

Wang, D., Liu, Z., Li, Q., Karpurapu, M., Kundumani-Sridharan, V., Cao, H., et al. (2007). An Essential Role for Gp130 in Neointima Formation Following Arterial Injury. *Circ. Res.* 100 (6), 807–816. doi:10.1161/01.RES.0000261350.61711.9e

Wu, W., Zhang, W., Choi, M., Zhao, J., Gao, P., Xue, M., et al. (2019). Vascular Smooth Muscle-MAPK14 Is Required for Neointimal Hyperplasia by Suppressing VSMC Differentiation and Inducing Proliferation and Inflammation. *Redox Biol.* 22, 101137. doi:10.1016/j.redox.2019.101137

Wu, Z., Yang, L., Cai, L., Zhang, M., Cheng, X., Yang, X., et al. (2007). Detection of Epithelial to Mesenchymal Transition in Airways of a Bleomycin Induced Pulmonary Fibrosis Model Derived from an Alpha-Smooth Muscle Actin-Cre Transgenic Mouse. *Respir. Res.* 8 (1), 1. doi:10.1186/1465-9921-8-1

Xiao, X., Fischbach, S., Zhang, T., Chen, C., Sheng, Q., Zimmerman, R., et al. (2017). SMAD3/Stat3 Signaling Mediates β-Cell Epithelial-Mesenchymal Transition in Chronic Pancreatitis-Related Diabetes. *Diabetes* 66 (10), 2646–2658. doi:10.2337/db17-0537

Xu, L., Li, Y., Yin, L., Qi, Y., Sun, H., Sun, P., et al. (2018). miR-125a-5p Ameliorates Hepatic Glycolipid Metabolism Disorder in Type 2 Diabetes Mellitus through Targeting of STAT3. *Theranostics* 8 (20), 5593–5609. doi:10.7150/thno.27425

Yang, E., Henriksen, M. A., Schaefer, O., Zakharova, N., and Darnell, J. E., Jr. (2002). Dissociation Time from DNA Determines Transcriptional Function in a STAT1 Linker Mutant. *J. Biol. Chem.* 277 (16), 13455–13462. doi:10.1074/jbc.M112038200

Yuan, Z. L., Guan, Y. J., Chatterjee, D., and Chin, Y. E. (2005). Stat3 Dimerization Regulated by Reversible Acetylation of a Single Lysine Residue. *Science* 307 (5707), 269–273. doi:10.1126/science.1105166

Zaman, A. G., and Herath, J. (2008). "Percutaneous Coronary Intervention in Saphenous Vein Graft Disease," in *Essential Interventional Cardiology*. Editors M. S. Norell, J. Perrins, B. Meier, and A. M. Lincoff. Second Edition (Philadelphia: W.B. Saunders), 309–318.

Zhang, H., Sweezey, N. B., and Kaplan, F. (2015). LGL1 Modulates Proliferation, Apoptosis, and Migration of Human Fetal Lung Fibroblasts. *Am. J. Physiol. Lung Cel Mol Physiol* 308 (4), L391–L402. doi:10.1152/ajplung.00119.2014

Zhang, T., Cao, G., Meng, X., Ouyang, C., Gao, J., Sun, Y., et al. (2020). Lethal Giant Larvae 1 Inhibits Smooth Muscle Calcification via High Mobility Group Box 1. *J. Mol. Cel Cardiol* 142, 39–52. doi:10.1016/j.yjmcc.2020.03.017

Zhang, X., Xu, H., Bi, X., Hou, G., Liu, A., Zhao, Y., et al. (2021). Src Acts as the Target of Matrine to Inhibit the Proliferation of Cancer Cells by Regulating Phosphorylation Signaling Pathways. *Cell Death Dis* 12 (10), 931. doi:10.1038/s41419-021-04221-6

Zhou, H., Bai, L., Xu, R., Zhao, Y., Chen, J., McEachern, D., et al. (2019). Structure-Based Discovery of SD-36 as a Potent, Selective, and Efficacious PROTAC Degrader of STAT3 Protein. *J. Med. Chem.* 62 (24), 11280–11300. doi:10.1021/acs.jmedchem.9b01530

Zhou, Z., Wang, M., Li, J., Xiao, M., Chin, Y. E., Cheng, J., et al. (2016). SUMOylation and SENP3 Regulate STAT3 Activation in Head and Neck Cancer. *Oncogene* 35 (45), 5826–5838. doi:10.1038/onc.2016.124

Conflict of Interest: The authors declare that the research was conducted in the absence of any commercial or financial relationships that could be construed as a potential conflict of interest.

Publisher's Note: All claims expressed in this article are solely those of the authors and do not necessarily represent those of their affiliated organizations, or those of the publisher, the editors and the reviewers. Any product that may be evaluated in this article, or claim that may be made by its manufacturer, is not guaranteed or endorsed by the publisher.

frontiers in Pharmacology

ORIGINAL RESEARCH
published: 27 January 2022
doi: 10.3389/fphar.2022.836710

Using Polyacrylamide Hydrogels to Model Physiological Aortic Stiffness Reveals that Microtubules Are Critical Regulators of Isolated Smooth Muscle Cell Morphology and Contractility

*Sultan Ahmed†, Robert. T. Johnson *†, Reesha Solanki, Teclino Afewerki, Finn Wostear and Derek. T. Warren*

School of Pharmacy, University of East Anglia, Norwich Research Park, Norwich, United Kingdom

OPEN ACCESS

Edited by:
Ping Song,
Georgia State University,
United States

Reviewed by:
Kunzhe Dong,
Augusta University, United States
Erzsébet Bartolák-Suki,
Boston University, United States

***Correspondence:**
Robert. T. Johnson
robert.johnson@uea.ac.uk

†These authors have contributed equally to this work and share first authorship

Specialty section:
This article was submitted to Cardiovascular and Smooth Muscle Pharmacology, a section of the journal Frontiers in Pharmacology

Received: *15 December 2021*
Accepted: *12 January 2022*
Published: *27 January 2022*

Citation:
Ahmed S, Johnson RT, Solanki R, Afewerki T, Wostear F and Warren DT (2022) Using Polyacrylamide Hydrogels to Model Physiological Aortic Stiffness Reveals that Microtubules Are Critical Regulators of Isolated Smooth Muscle Cell Morphology and Contractility. Front. Pharmacol. 13:836710. doi: 10.3389/fphar.2022.836710

Vascular smooth muscle cells (VSMCs) are the predominant cell type in the medial layer of the aortic wall and normally exist in a quiescent, contractile phenotype where actomyosin-derived contractile forces maintain vascular tone. However, VSMCs are not terminally differentiated and can dedifferentiate into a proliferative, synthetic phenotype. Actomyosin force generation is essential for the function of both phenotypes. Whilst much is already known about the mechanisms of VSMC actomyosin force generation, existing assays are either low throughput and time consuming, or qualitative and inconsistent. In this study, we use polyacrylamide hydrogels, tuned to mimic the physiological stiffness of the aortic wall, in a VSMC contractility assay. Isolated VSMC area decreases following stimulation with the contractile agonists angiotensin II or carbachol. Importantly, the angiotensin II induced reduction in cell area correlated with increased traction stress generation. Inhibition of actomyosin activity using blebbistatin or Y-27632 prevented angiotensin II mediated changes in VSMC morphology, suggesting that changes in VSMC morphology and actomyosin activity are core components of the contractile response. Furthermore, we show that microtubule stability is an essential regulator of isolated VSMC contractility. Treatment with either colchicine or paclitaxel uncoupled the morphological and/or traction stress responses of angiotensin II stimulated VSMCs. Our findings support the tensegrity model of cellular mechanics and we demonstrate that microtubules act to balance actomyosin-derived traction stress generation and regulate the morphological responses of VSMCs.

Keywords: actomyosin, contraction, matrix stiffness, microtubules, polyacrylamide hydrogel (PAH), traction force, vascular smooth muscle cell (VSMC)

INTRODUCTION

Vascular smooth muscle cells (VSMCs) are the predominant cell type in the medial layer of the arterial wall. VSMCs normally exist in a quiescent, contractile phenotype where actomyosin-derived contractile forces maintain vascular tone (Brozovich et al., 2016). However, VSMCs are not terminally differentiated and can down-regulate contractile markers and dedifferentiate into a proliferative, synthetic phenotype (Rzucidlo et al., 2007; Liu et al., 2015; Shi and Chen, 2016). Both

phenotypes retain the ability to generate actomyosin force that is essential for both VSMC contraction and migration (Ahmed and Warren, 2018; Afewerki et al., 2019). Contractile VSMCs possess a greater abundance of α-smooth muscle actin (αSMA) and smooth muscle-myosin heavy chain (SM-MyHC), that enhance their ability to generate actomyosin forces and contract (Rensen et al., 2007). However, both contractile and proliferative VSMCs generate actomyosin force via stimulating interactions between myosin II and filamentous actin. This process is regulated in both phenotypes by blood-borne factors, such as angiotensin II, that bind to receptors on the VSMC surface and mechanical factors including matrix stiffness and circumferential tension of the aortic wall (Qiu et al., 2010; Brozovich et al., 2016; Ahmed and Warren, 2018).

Young's modulus is a measure of material stiffness. Atomic force microscopy studies have determined that the Young's modulus of the medial layer of an elastic artery is between 5 and 37 kPa (Tracqui et al., 2011; Bae et al., 2016; Rezvani-Sharif et al., 2019). Microenvironment rigidity transmits 'outside-in' resistive forces to VSMCs and this process is dependent on focal adhesions that convey force between the extracellular matrix (ECM) and the cytoskeleton (Lacolley et al., 2017; Ahmed and Warren, 2018; Mohammed et al., 2019). VSMCs and other cell types respond to outside-in signals by exerting actomyosin based contractile forces on the matrix (inside-out forces) that scale with the outside-in resistive forces (Sun et al., 2008; Holle et al., 2018). Matrix rigidity rapidly activates Rho/ROCK signalling at ECM adhesions, initiating actin polymerisation and myosin light chain phosphorylation, thereby augmenting actomyosin activity (Ahmed and Warren, 2018). Actin cytoskeletal reorganisation and enhanced actomyosin activity increase VSMC integrated traction forces, the force VSMCs apply to the ECM (Li et al., 2020; Johnson et al., 2021). While much is known about VSMC actomyosin and contractile responses, we still lack an understanding of how VSMC structural and signalling components integrate to regulate these processes.

Extracellular mechanical forces, generated by the flow of blood and the mechanical properties of the ECM, programme the function of VSMCs (Johnson et al., 2021). In healthy arteries, VSMC contraction is initiated in response to blood pressure derived deformation of the arterial wall (Ye et al., 2014). However, these forces are not consistent and physiological cycle-by-cycle variations in blood pressure have been found to alter the contractile response of VSMCs (Bartolák-Suki et al., 2015; Bartolák-Suki and Suki, 2020). During ageing, the mechanical environment changes. Blood pressure increases, enhancing the compressional forces applied to the arterial wall; whilst the tensile strength and rigidity of the wall increases due to ECM remodelling (Tsamis et al., 2013). In response to these altered mechanical cues, VSMCs generate enhanced actomyosin derived contractile forces (Ye et al., 2014). This results in arterial stiffening, a hallmark of vascular ageing and cardiovascular disease onset (Glasser et al., 1997; Mitchell et al., 2010). How matrix stiffness induces enhanced VSMC actomyosin force production is unknown, but it is a response that is observed in many other cell types (Discher et al., 2005; Zhou et al., 2017; Pasqualini et al., 2018; Bastounis et al., 2019). It is therefore imperative that studies investigating VSMC physiological force generation take this mechanical property into account. Traditionally, many *in vitro* experiments have cultured isolated VSMCs on plastic or glass, materials whose stiffness is around a thousand times greater than that of the arterial wall (Minaisah et al., 2016). More recently, the role of matrix stiffness in regulating VSMCs has been investigated using polyacrylamide hydrogels, a substrate whose stiffness can be tuned to a desired kPa. These studies have identified that matrix stiffness is a regulator of VSMC phenotype, with enhanced stiffness altering the proliferative, migratory and adhesive properties of VSMCs (Wong et al., 2003; Xie et al., 2018; Nagayama and Nishimiya, 2020; Rickel et al., 2020). Furthermore, matrix rigidity promoted actin cytoskeleton remodelling and stress fiber formation, increasing VSMC stiffness and traction stress generation (Brown et al., 2010; Sazonova et al., 2015; Petit et al., 2019; Sanyour et al., 2019). Whilst these studies controlled ECM rigidity, many of them made use of high passage VSMCs and culture conditions that would promote the synthetic phenotype. Therefore, the findings have little relevance for understanding VSMC contractile function.

Actomyosin derived contractile forces place stress and intracellular tension upon the cell. In other cell types, these deformational forces are proposed to be balanced by the ECM and the microtubule network (Johnson et al., 2021). This relationship is described by the tensegrity model, whereby microtubules act as compression bearing struts, capable of resisting strain generated by the actin cytoskeleton (Stamenović, 2005; Brangwynne et al., 2006). The balance between compression and strain defines cell shape and stability (Stamenović, 2005). This model predicts that microtubule destabilisation will increase actomyosin derived force generation. In support of this, treatment with microtubule destabilisers, such as colchicine, result in enhanced force generation within coronary and aortic vessels (Sheridan et al., 1996; Platts et al., 1999, 2002; Paul et al., 2000; Zhang et al., 2000). However, our understanding of the role of microtubules in VSMC contractile agonist responses remains limited and some data contradicts the tensegrity model. For example, wire myography showed that microtubule stabilisation had no effect on the ability of isolated aortic rings to contract (Zhang et al., 2000). Dynamic instability, the ability of microtubules to constantly cycle through phases of growth and shrinkage, is an inherent characteristic that enables the microtubule network to rapidly reorganise in response to the changing mechanical requirements of the cell (Nogales, 2001). Whilst observations regarding the function of microtubule stability in VSMC contraction have been made, our understanding of the mechanisms behind these observations remains incomplete.

One of the largest obstacles for identifying different mechanisms of VSMC contraction remains the lack of *in vitro* tools. The current gold standard for assessing isolated cell actomyosin activity is traction force microscopy (TFM) (Muhamed et al., 2017). TFM is used to quantitatively measure the stress exerted by a cell on its substrate, which is then used as an indicator of cell contractility (Kraning-Rush et al.,

2012; Lekka et al., 2021). Additionally, atomic force microscopy (AFM) has been used to assess actomyosin cortical tension and the force transduced through individual focal adhesion complexes (Sanyour et al., 2019). However, these techniques have several limitations, mainly being time consuming and low throughput (Haase and Pelling, 2015; Colin-York and Fritzsche, 2018; Schierbaum et al., 2019). Collagen gel assays, that are easily performed with generic lab equipment and skills, provide an alternative to these techniques. Typical collagen assays involve the suspension of a cell population in a prefabricated collagen gel. Contraction is then assessed by observing dimensional changes of the gel (Ngo et al., 2006). Limitations of collagen gels primarily relate to the qualitative nature of the assay and inconsistencies in gel shape. Collagen gels also lack rigidity control and are softer than the physiological arterial wall. These limitations severely affect the reproducibility and reliability of such assays (Vernon and Gooden, 2002).

Previous studies have reported that isolated VSMCs display a reduction in cell area upon contractile agonist stimulation (Li et al., 1999; Wang et al., 2017; Halaidych et al., 2019). Suggesting that changes in VSMC morphology and actomyosin activity are important components of the VSMC contractile response. Given their limitations, existing *in vitro* VSMC contractility assays are not able to investigate these processes. In this study we develop and validate an approach for screening isolated VSMC contraction using cell area as a reporter. The assay uses polyacrylamide hydrogels that are easily fabricated and mimic the rigidity of the physiological elastic arterial wall (Minaisah et al., 2016; Porter et al., 2020). Moreover, we show that combined with TFM, this technique allows investigation into factors that regulate both VSMC morphology and traction stress generation. Finally, we identify microtubule stability as a key regulator of VSMC contractile responses.

MATERIALS AND METHODS

Polyacrylamide Hydrogel Preparation

Hydrogels were prepared as described previously (Minaisah et al., 2016). Briefly 30 mm coverslips were activated by treating with (3-Aminopropyl)triethoxysilane for 2 min, washed 3x in dH_2O and fixed in 0.5% glutaraldehyde for 40 min. Coverslips were subsequently washed 3x in dH_2O and left to air dry. The required volume of 12 kPa polyacrylamide hydrogel mix (7.5% acrylamide, 0.15% bis-acrylamide in water) was supplemented with 10% APS (1:100) and TEMED (1:1,000) before 50 µl of the solution was placed on a standard microscopy slide and covered by an activated coverslip. Once set, the fabricated 12 kPa hydrogel was removed, placed into a 6-well plate, washed 3x with dH_2O and crosslinked with sulfo-SANPAH (1:3,000) under UV illumination (365 nm). Finally, hydrogels were washed with PBS and functionalised with collagen I (0.1 mg/ml) for 10 min at room temperature. Hydrogel stiffness was previously confirmed using a JPK Nanowizard-3 atomic force microscope (Porter et al., 2020).

Vascular Smooth Muscle Cell Culture and Drug Treatments

Human adult aortic VSMCs (passage 3–10) were purchased from Cell Applications Inc. (354-05a). VSMCs were grown in growth media (Cell Applications Inc.), prior to being washed with Earle's Balanced Salt Solution (Thermo) and seeded in basal media (Cell Applications Inc.) onto 12 kPa hydrogels, 18 h prior to drug treatment. Standard VSMCs culture was performed as described previously (Ragnauth et al., 2010; Warren et al., 2015).

Quiescent VSMCs were stimulated with either angiotensin II (0.01–100 µM) (Merck) or carbachol (0.01–100 µM) (Merck) for 30 min. For all other drug treatments, quiescent VSMCs were pretreated with the stated dose for 30 min, prior to co-treatment with angiotensin II (10 µM) for an additional 30 min. Please see **Supplementary Table S1** for a list of compounds used in this study.

Immunofluorescence and VSMC Area/Volume Analysis

Following treatment, cells were fixed in 4% paraformaldehyde (actin cytoskeleton) or ice-cold methanol (microtubules), permeabilised with 0.5% NP40 and blocked in 3% BSA/PBS. Targets were visualized using antibodies raised against lamin A/C (SAB4200236, Sigma), or α-tubulin (3873S, CST) in combination with a relevant Alexa Fluor 488 secondary antibody (A1101 or A1103, Thermo). F-actin was stained using Rhodamine Phalloidin (R145, Thermo). All images were captured at 20x (cell area/volume) or 40x (microtubule organization) magnification using either a Zeiss LSM510-META or a Zeiss LSM980-Airyscan confocal microscope. Cell area was measured using FIJI, open-source software (Schindelin et al., 2012), whilst cell volume was calculated using Volocity 6.3.

Cold-Stable Microtubule Stability Assay

The number of cold-stable microtubules per cell was determined as previous (Atkinson et al., 2018). Briefly, after treatment, cells were placed on ice for 15 min before being washed once with PBS and twice with PEM buffer (80 µM PIPES pH 6.8, 1 mM EGTA, 1 mM $MgCl_2$, 0.5% Triton X-100 and 25% (w/v) glycerol) for 3 min. Cells were then fixed for 20 min in ice-cold MeOH and prepared for staining as detailed above. Cell nuclei were identified using DAPI. Images were captured at 40x magnification using an Axioplan Epifluorescent microscope.

Traction Force Microscopy

For Traction Force Microscopy (TFM), VSMCs were seeded onto 12 kPa hydrogels containing 0.5 µm red fluorescent (580/605) FluoSpheres (1:1,000) (Invitrogen). Imaging was performed using a Zeiss Axio Observer live cell imaging system that captured 20x magnification images every 2 min. TFM was performed either in real-time or as an end point assay whereby images were captured before and after cell lysis. Lysis was achieved by the addition of 0.5% Triton X-100. Drift was corrected using the ImageJ StackReg plugin and traction force was calculated using the ImageJ plugin described previously to measure FluoSphere displacement (Tseng

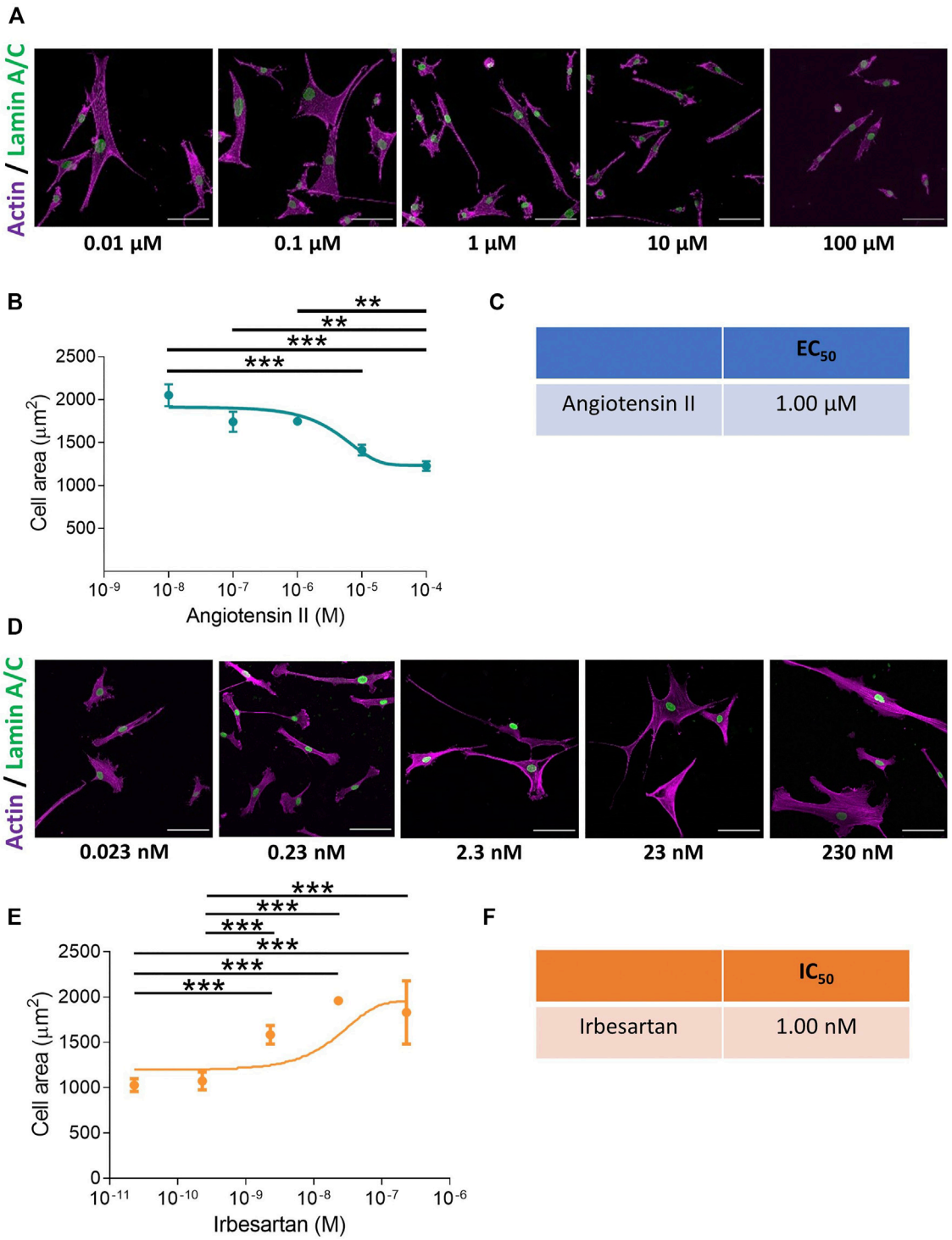

FIGURE 1 | VSMCs grown on pliable hydrogels display decreased area upon stimulation with the contractile agonist angiotensin II. **(A)** Representative images of isolated VSMCs cultured on 12 kPa polyacrylamide hydrogels treated with a range of angiotensin II concentrations for 30 min. Actin cytoskeleton (purple) and Lamin A/C labelled nuclei (green). Scale bar = 100 µm. **(B)** Isolated VSMC area, representative of 3 independent experiments with ≥150 cells analysed per condition. **(C)** EC_{50} of angiotensin II calculated from **(B)**. **(D)** Representative images of isolated VSMCs cultured on 12 kPa hydrogels and treated with angiotensin II (10 µM) for 30 min in the presence of a range of irbesartan concentrations. Actin cytoskeleton (purple) and Lamin A/C (green). Scale bar = 100 µm. **(E)** Isolated VSMC area, representative of 3 independent experiments with ≥50 cells analysed per condition. **(F)** IC_{50} of irbesartan calculated from **(E)**. (** = $p < 0.01$), (*** = $p < 0.001$).

et al., 2012). Briefly, bead displacement was measured using the first and last image of the movie sequence. The cell region was segmented by overlaying the traction map with the cell image, highlighting the cell traction region with an ROI and extracting the traction forces in each pixel by using the save XY coordinate function in FIJI (Porter et al., 2020).

Cell Viability Assay

Cell viability was determined using a RealTime-Glo™ MT Cell Viability Assay following manufacturers instruction. Briefly, 5,000 cells per well in a 96-well plate were exposed to a range of drug concentrations for 1 h, prior to luminescence being measured using a Wallac EnVision 2,103 Multilabel Reader (PerkinElmer).

Statistics

All statistical analyses were performed in GraphPad Prism 6.05. Dose response curves are presented as the mean data ± SEM (error bars) plotted on a logarithmic dose response scale. EC_{50} and IC_{50} data were generated by non-linear regression. Results are presented as mean ± SEM. Dot plot graphs are presented to show data distribution, with each point corresponding to an individual cell measurement. Bars indicate the mean value, ± SEM (error bars). Comparison of multiple groups was achieved using a one-way ANOVA analysis with Bonferroni post-hoc test. For comparison of two groups, unpaired student t-tests were performed. Analysis of the real time Angiotensin II contraction data was performed using non-linear regression. A one phase association analysis was performed on traction stress vs time data and a one phase decay analysis was performed on the VSMC area vs time data.

RESULTS

Contractile Agonist Stimulation Reduces VSMC Area on Pliable Hydrogels

We set out to develop a screen, performed at a physiologically relevant rigidity, to unravel mechanisms regulating VSMC actomyosin activity and contraction (**Supplementary Figure S1**). Quiescent VSMCs grown on pliable, 12 kPa hydrogels were treated with a concentration range of the contractile agonists, angiotensin II or carbachol. Contractile response was measured through changes in VSMC area, which previous studies have shown correlates with isolated VSMC contractile activity (Li et al., 1999; Wang et al., 2017; Halaidych et al., 2019). Analysis confirmed that contractile agonist stimulation resulted in a reduction in VSMC area (**Figures 1A,B** and **Supplementary Figures S2A,B**). Further analysis of VSMC area revealed the assay could be used to determine the EC_{50} values of both angiotensin II and carbachol (**Figure 1C** and **Supplementary Figures S2C**), confirming the assay could be used to measure and compare agonist potency. Subsequent experiments were performed with 10 μM angiotensin II, a dose that produced the maximal response (**Figures 1A,B**). To observe the effect of angiotensin II stimulation on isolated VSMC volume, we next performed confocal microscopy. Analysis revealed that angiotensin II stimulated VSMCs displayed a reduction in area, but no change in volume (**Supplementary Figure S3**).

To confirm that the change in area was specific for receptor activation, we utilised the angiotensin II antagonist irbesartan and the cholinergic antagonist, atropine. VSMCs grown on pliable hydrogels were stimulated with angiotensin II or carbachol in the presence of an increasing dose of irbesartan or atropine, respectively. As expected, irbesartan and atropine treatment prevented a reduction in VSMC area, confirming that these changes were driven by receptor activation (**Figures 1D–F** and **Supplementary Figure S4**).

Myosin II Mediated Traction Stress Drives Changes in Angiotensin II Stimulated VSMC Area

The above data demonstrated the validity of our approach in generating EC_{50} and IC_{50} data for agonists/antagonists of isolated VSMC contractile function. We next sought to confirm that changes in VSMC area were due to contraction and not due to membrane retraction. To do this, we performed traction force microscopy to measure the displacement of beads embedded within the hydrogels. Analysis revealed that angiotensin II treatment stimulated VSMCs to contract, with a significant reduction in cell area observed after 8 min (**Figures 2A,B**). Importantly, beads moved towards VSMCs and both maximal and integrated traction stress increased rapidly and plateaued after 8 min (**Figures 2A,C,D**). This data confirmed the correlation between reduced VSMC area and traction stress generation upon angiotensin II stimulation. To further confirm that actomyosin derived force was driving these changes in VSMC area, we next used the myosin II inhibitor blebbistatin and the ROCK inhibitor Y-27632. As expected, treatment with either blebbistatin or Y-27632 blocked the angiotensin II mediated reduction in area, however, actomyosin inhibited VSMCs possessed an increased volume, compared to their angiotensin II treated counterparts (**Figure 3**). This confirmed that actomyosin activation was driving VSMC contraction in our system.

Microtubule Destabilisation Alters the Morphological Response of Angiotensin II Stimulated VSMCs

Microtubule depolymerisation increases the constriction and myogenic tone of aortic and carotid tissues (Leite and Webb, 1998; Platts et al., 2002; Johnson et al., 2021). However, the precise impact of microtubule disruption on VSMC contraction remains unknown. To address this, we determined the impact of angiotensin II stimulated VSMC contraction upon microtubule organisation and stability. Angiotensin II stimulation promoted the microtubule network to reorganise, switching from a straight, elongated arrangement of parallel microtubules to a more interlinking meshwork of microtubules (**Supplementary Figure S5**). Although angiotensin II stimulation induced the reorganisation of the microtubule cytoskeleton, there was no change in the number of cold-stable microtubules between

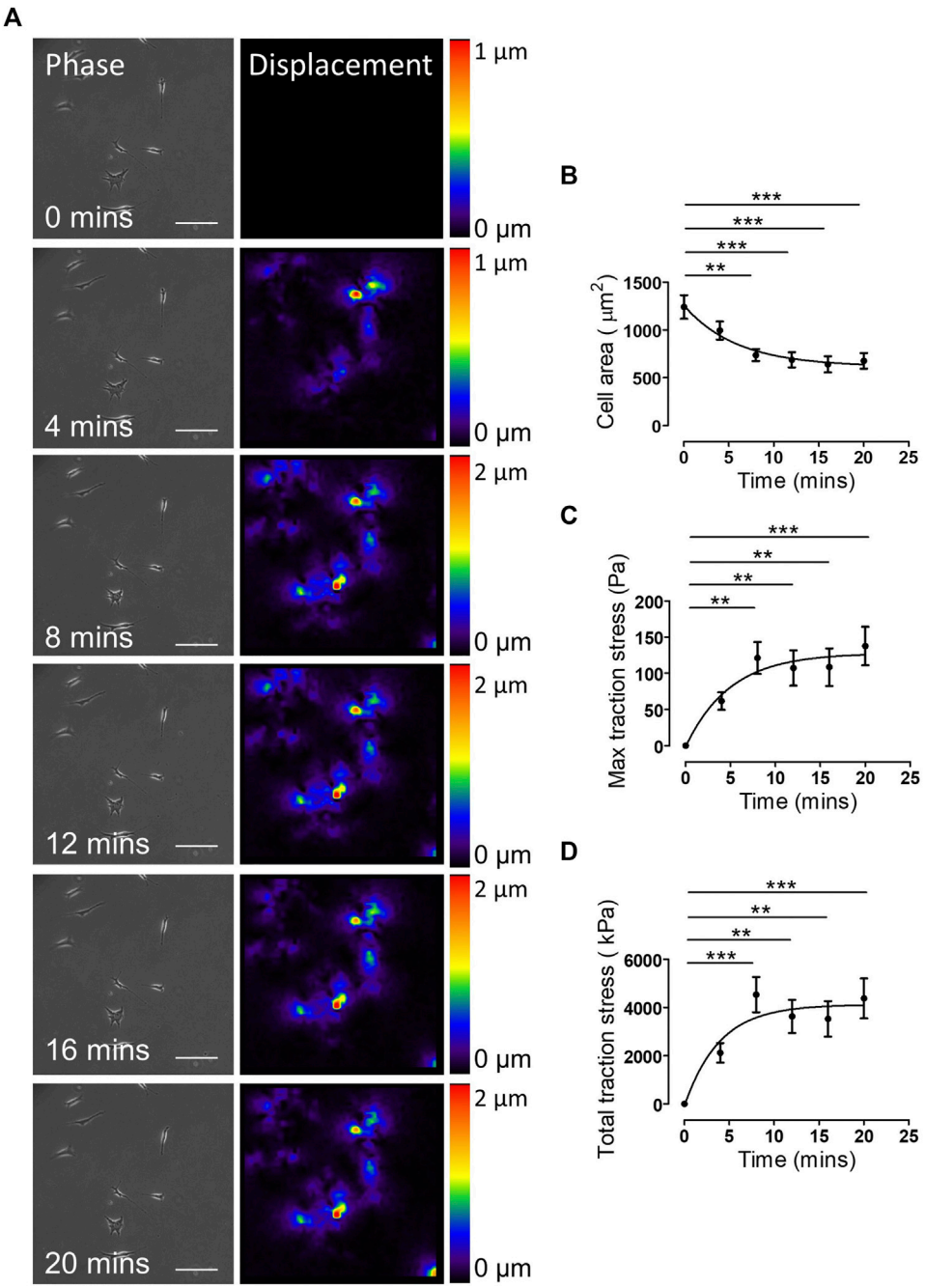

FIGURE 2 | Traction stress generation correlates with decreased VSMC area following angiotensin II stimulation. **(A)** Representative phase images and bead displacement heat maps of isolated VSMCs grown on 12 kPa polyacrylamide hydrogels and stimulated with angiotensin II over a 20 min time course. Scale bar = 100 µm. Displacement heat maps were generated by comparing the bead displacement for each time point to their initial positions at $t = 0$, as such there is no displacement at $t = 0$. **(B)** Isolated VSMC area, **(C)** maximum traction stress and **(D)** total traction stress generated at each time point compared to $t = 0$. Graphs represent the combined data from 3 independent experiments, with measurements taken from 35 VSMCs. (** = $p < 0.01$), (*** = $p < 0.001$).

quiescent and angiotensin II stimulated VSMCs (**Figures 4A,B**). Next, we used our assay to test the impact of microtubule disruption on VSMC contraction. Colchicine, a microtubule destabiliser, induced a concentration dependent increase in angiotensin II treated VSMC area, suggesting that microtubule depolymerisation was promoting VSMC relaxation (**Figures 4C–E**). In contrast, paclitaxel, a microtubule stabiliser, had no effect on the area of angiotensin II treated VSMCs (**Figures 4F,G**). Analysis confirmed that the concentrations of colchicine or paclitaxel used were sufficient to reduce or increase the number of cold-stable microtubules respectively (**Supplementary Figures S6A–D**). Furthermore, these concentrations produced no

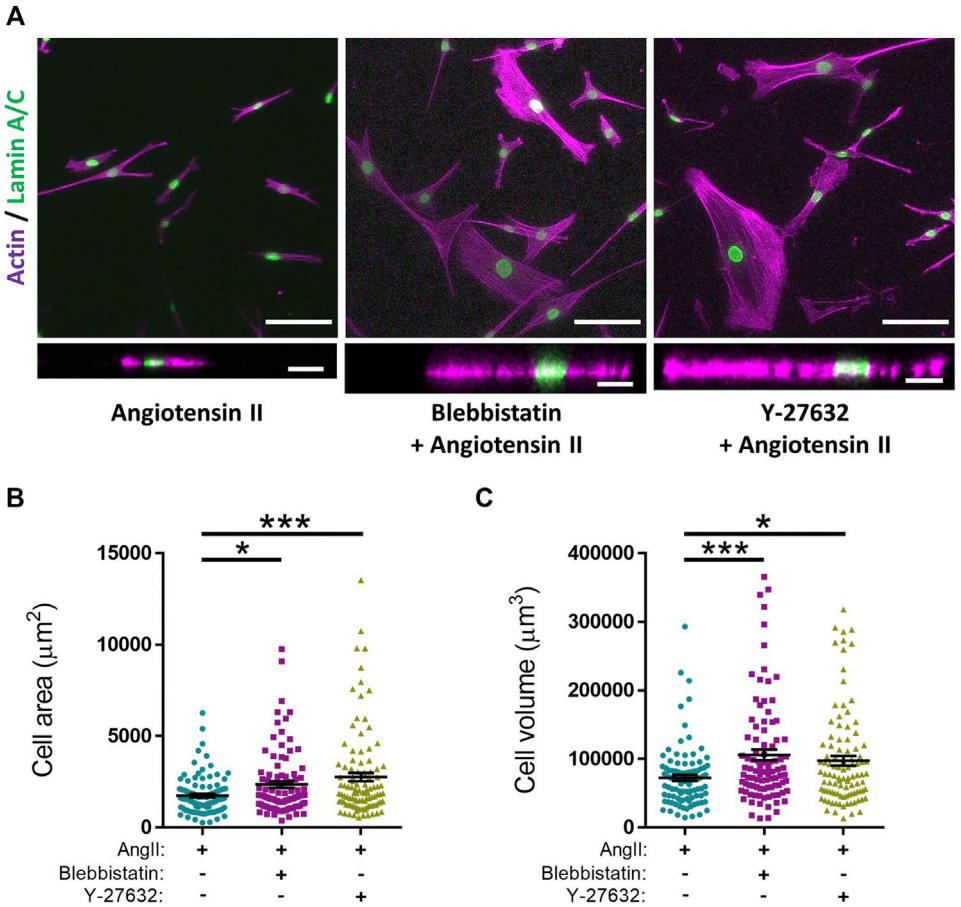

FIGURE 3 | Actomyosin inhibition prevents angiotensin II induced changes in VSMC area and increases VSMC volume on pliable hydrogels. **(A)** Representative images of isolated VSMCs cultured on 12 kPa polyacrylamide hydrogels pre-treated with either blebbistatin or Y-27632 for 30 min prior to cotreatment with angiotensin II (AngII) (10 μM) for an additional 30 min. Actin cytoskeleton (Rhodamine phalloidin, Purple) and Lamin A/C (green). Top—Representative XY images of VSMC area. Scale bar = 100 μm. Bottom—Representative XZ images of VSMC height. Scale bar = 30 μm. **(B)** Isolated VSMC area and **(C)** Isolated VSMC volume. Both **(B,C)** are representative of 3 independent experiments with ≥95 cell analysed per condition. (* = $p < 0.05$), (*** = $p < 0.001$).

significant reductions in cell viability (**Supplementary Figures S6E,F**). Surprisingly, confocal microscopy revealed that colchicine increased VSMC volume (**Figures 5A–C**), whereas the volume of paclitaxel treated VSMCs remained unchanged (**Figure 5D–F**).

Changes in Microtubule Stability Alters the Traction Stress Generation of Isolated VSMCs

The data above suggested that microtubule destabilisation was altering the angiotensin II induced area/volume response of isolated VSMCs. Previous studies using wire or pressure myography have reported that microtubule destabilisation increased VSMC force generation (Paul et al., 2000; Zhang et al., 2000; Platts et al., 2002). To confirm the impact of microtubule destabilisation on actomyosin activity, TFM was performed to measure traction stresses exerted by VSMCs. In agreement with previous studies, analysis revealed that pre-treatment with colchicine increased the maximal and total traction stress exerted by angiotensin II stimulated VSMCs (**Figures 6A–C**). Finally, we examined the effect of microtubule stabilisation on traction stress. Paclitaxel pre-treatment had no effect on maximal traction stress. However, total traction stress was reduced when compared to their untreated counterparts (**Figures 6D–F**). This confirmed that maintenance of microtubule dynamics was essential for VSMC actomyosin activity and force generation.

DISCUSSION

Whilst much is known about VSMC contractile responses in physiology, *in vitro* assays to examine this process remain limited. Tissue culture plastic and glass are approximately a thousand times stiffer than the aortic wall (Minaisah et al., 2016), meaning that changes in VSMC area are driven by membrane retraction rather than contraction. Existing technologies to examine the contractile response of isolated VSMCs are either low throughput, such as TFM, or are

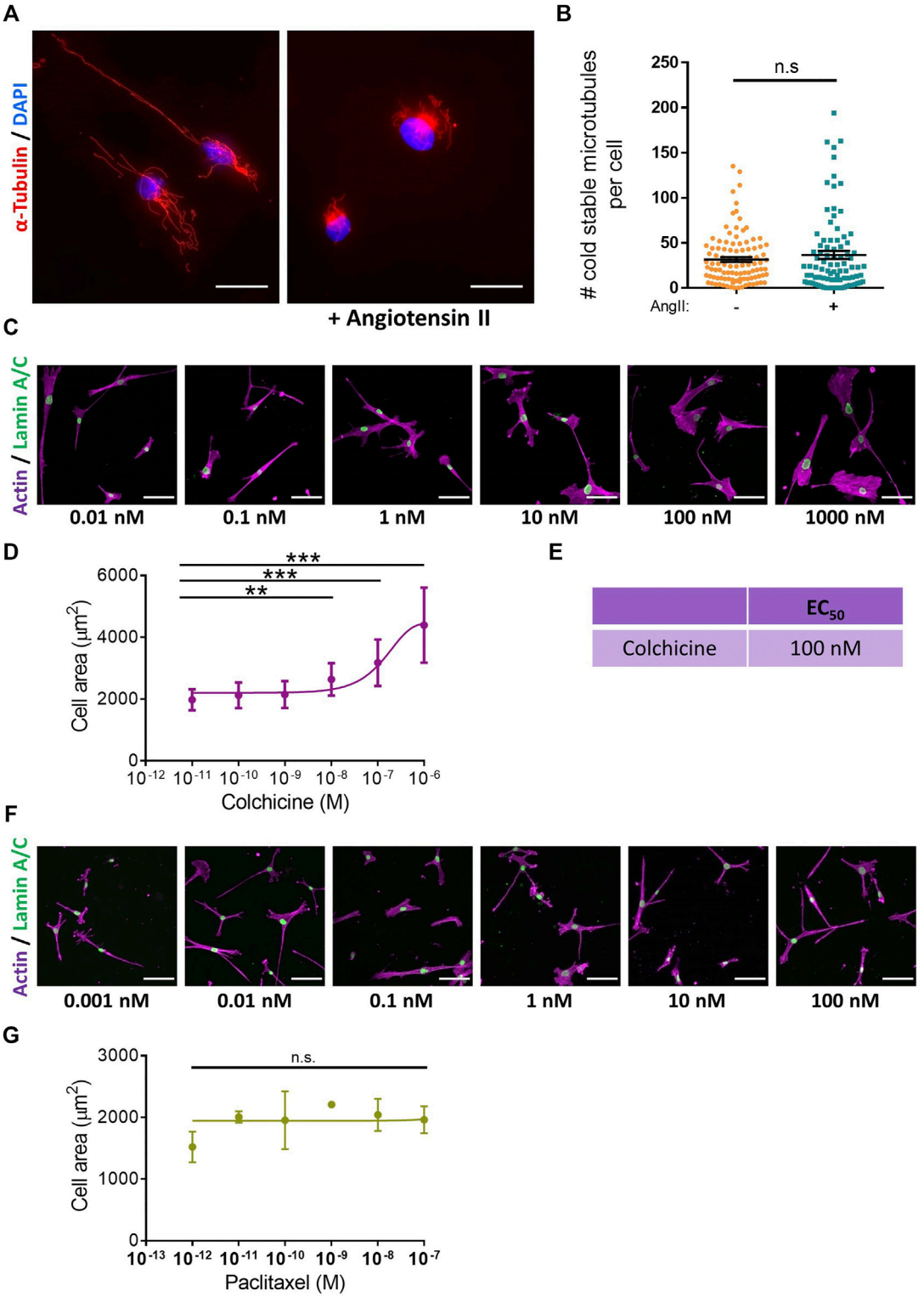

FIGURE 4 | Microtubule destabilisation prevents angiotensin II induced changes in VSMC area. **(A)** Representative images of isolated VSMCs cultured on 12 kPa polyacrylamide hydrogels, stained for cold-stable microtubules (α-tubulin, red) and cell nuclei (DAPI, blue). Scale bar = 50 μm. Angiotensin II (AngII) (10 μM) stimulation was performed for 30 min. **(B)** Number of cold-stable microtubules per cell, representative of 4 independent experiments, with ≥90 cells analysed per condition. **(C)** Representative images of isolated VSMCs cultured on 12 kPa hydrogels pre-treated with a range of colchicine concentrations for 30 min prior to cotreatment with angiotensin II (10 μM) for an additional 30 min. Actin cytoskeleton (purple) and Lamin A/C (green). Scale bar = 100 μm. **(D)** Isolated VSMC area, representative of 3

(*Continued*)

FIGURE 4 | independent experiments with ≥55 cells analysed per condition. **(E)** EC_{50} of colchicine calculated from **(D)**. **(F)** Representative images of isolated VSMCs cultured on 12 kPa hydrogels pre-treated with a range of paclitaxel concentrations for 30 min prior to cotreatment with angiotensin II (10 μM) for an additional 30 min. Actin cytoskeleton (purple) and Lamin A/C (green). Scale bar = 100 μm. **(G)** Isolated VSMC area, representative of 3 independent experiments with ≥65 cells analysed per condition. (n.s. = non-significant), (** = $p < 0.01$), (*** = $p < 0.001$).

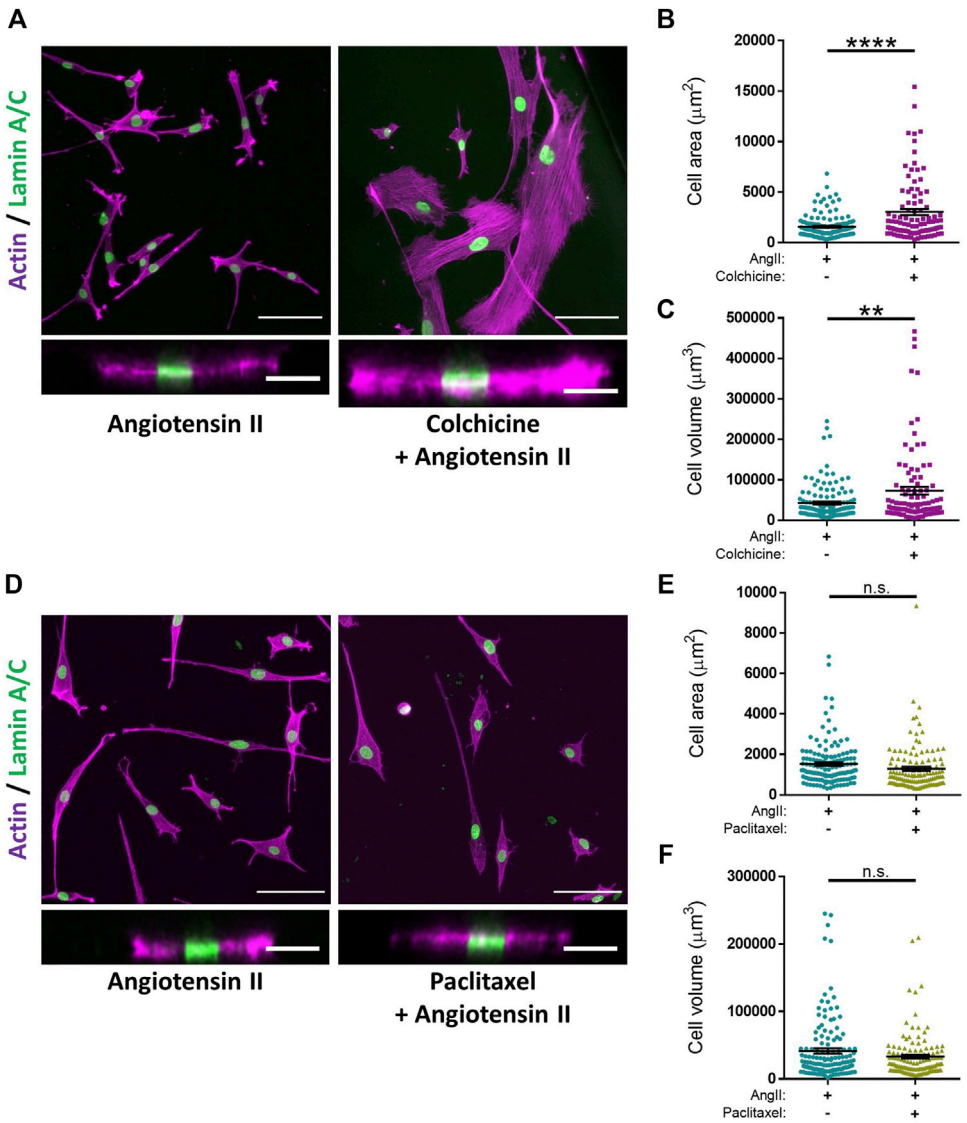

FIGURE 5 | Microtubule destabilisation alters angiotensin II stimulated VSMC volume on pliable hydrogels. **(A)** Representative images of isolated VSMCs cultured on 12 kPa polyacrylamide hydrogels pre-treated +/− colchicine (100 nM) for 30 min prior to cotreatment with angiotensin II (AngII) (10 μM) for an additional 30 min. Actin cytoskeleton (purple) and Lamin A/C (green). Top—Representative XY images of VSMC area. Scale bar = 100 μm. Bottom—Representative XZ images of VSMC height. Scale bar = 30 μm. **(B)** Isolated VSMC area and **(C)** Isolated VSMC volume. Both **B&C** are representative of 3 independent experiments with ≥100 cell analysed per condition. **(D)** Representative images of isolated VSMCs cultured on 12 kPa polyacrylamide hydrogels pre-treated +/− paclitaxel (1 nM) for 30 min prior to cotreatment with angiotensin II (AngII) (10 μM) for an additional 30 min. Actin cytoskeleton (purple) and Lamin A/C (green). Top—Representative XY images of VSMC area. Scale bar = 100 μm. Bottom—Representative XZ images of VSMC height. Scale bar = 30 μm. **(E)** Isolated VSMC area and **(F)** Isolated VSMC volume. Both **(E,F)** are representative of 3 independent experiments with ≥125 cell analysed per condition. (n.s. = non-significant), (** = $p < 0.01$), (**** = $p < 0.0001$).

inconsistent and lack rigidity control, such as the collagen gel assay (Vernon and Gooden, 2002; Colin-York and Fritzsche, 2018). We therefore set out to establish and validate a polyacrylamide hydrogel-based assay for screening the contractility of isolated VSMCs. Polyacrylamide hydrogels are widely used in cell biology and can be easily fabricated with generic research equipment and skills (Kandow et al., 2007; Caliari and Burdick, 2016; Minaisah et al., 2016; Mohammed et al., 2019). To enable VSMC attachment,

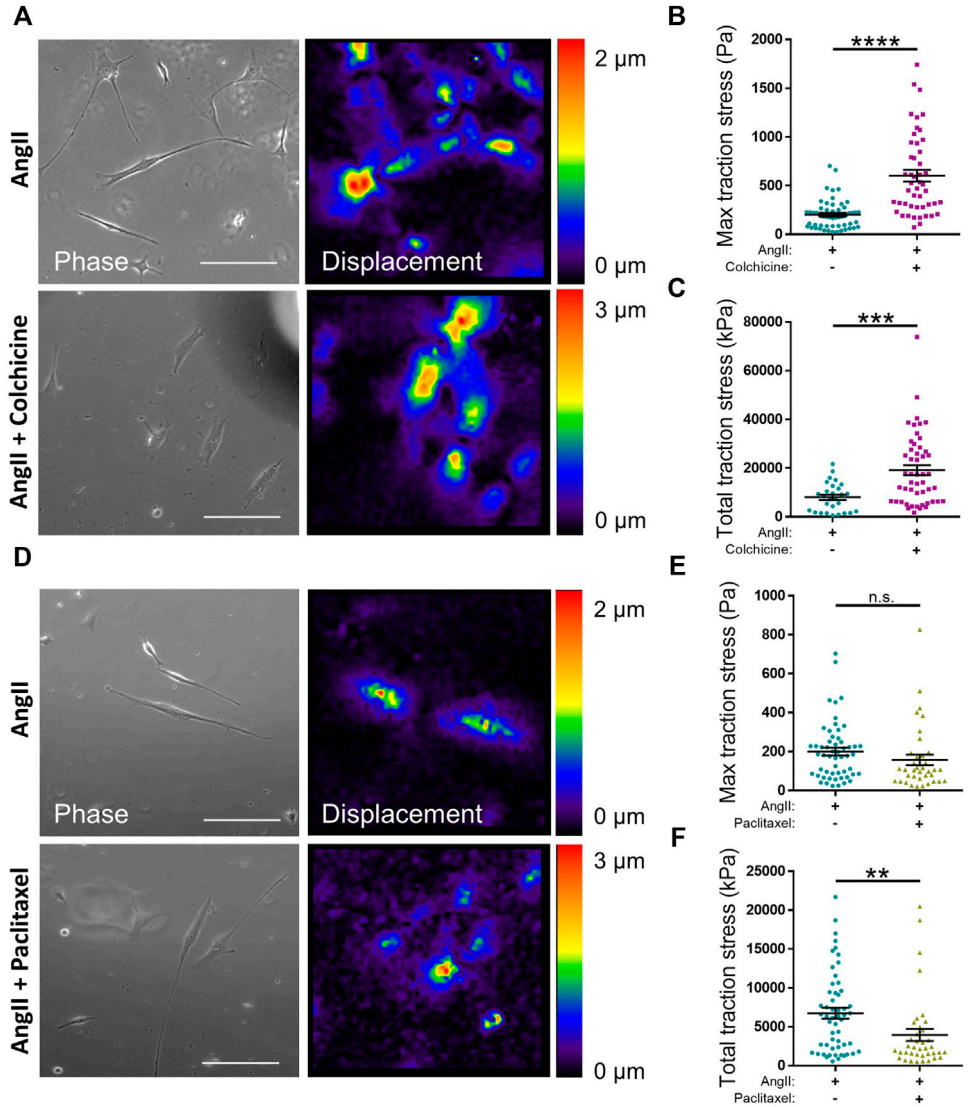

FIGURE 6 | Microtubule stability regulates angiotensin II induced VSMC traction stress generation. **(A)** Representative phase images and bead displacement heat maps of isolated VSMCs grown on 12 kPa polyacrylamide hydrogels. Cells were pre-treated +/− colchicine (100 nM) for 30 min prior to cotreatment with angiotensin II (AngII) (10 µM) for an additional 30 min. Scale bar = 100 µm. **(B)** Maximum traction stress and **(C)** Total traction stress generation. Both **(B,C)** are representative of 3 independent experiments with ≥48 cell analysed per condition. **(D)** Representative phase images and bead displacement heat maps of isolated VSMCs grown on 12 kPa polyacrylamide hydrogels. Cells were pre-treated +/− paclitaxel (1 nM) for 30 min prior to cotreatment with angiotensin II (AngII) (10 µM) for an additional 30 min. Scale bar = 100 µm. **(E)** Maximum traction stress generation and **(F)** Total traction stress generation. Both **(E,F)** are representative of 3 independent experiments with ≥38 cell analysed per condition. (n.s. = non-significant), (** = $p < 0.01$), (*** = $p < 0.001$), (**** = $p < 0.0001$).

polyacrylamide hydrogels mimicking physiological rigidity must be functionalised by ECM components such as collagen, fibronectin or lamin (Brown et al., 2010; Sazonova et al., 2015). Previous studies have utilised hydrogels of varying stiffness to identify matrix rigidity as a key regulator of VSMC morphology, migration, proliferation and phenotype. In response to matrix stiffness, VSMCs downregulate the expression of contractile markers SM-MyHC, calponin and smoothelin, whilst increasing the expression of proliferative genes Cyclin A and PCNA (proliferating cell nuclear antigen), in correlation with increased VSMC proliferation (Brown et al., 2010; Sazonova et al., 2015; Xie et al., 2018; Nagayama and Nishimiya, 2020). Additionally, VSMCs undergo durotaxis, preferentially migrating from soft to stiff matrix rigidity, although the effect of matrix stiffness on the rate of migration appears dependent on the ECM component (Wong et al., 2003; Rickel et al., 2020).

In our present study, we describe a novel assay in which agonist induced VSMC contraction is performed on a substrate of physiological stiffness. We demonstrate that changes in isolated VSMC area were driven by angiotensin II induced traction stress generation, that pulled the compliant hydrogels towards the VSMC, decreasing cell area (**Figures 1A**,**B**, **2**). Demonstrating that, isolated VSMC area can be used as a reporter of contractility on pliable hydrogels. VSMC volume remained unchanged by

contractile agonist stimulation (**Supplementary Figure S3**). Importantly, this assay was sensitive enough to generate EC_{50} and IC_{50} information of contractile agonists and antagonists, respectively (**Figures 1C,F**; **Supplementary Figures S2C, S4C**. Whilst TFM alone can measure the contractile response of VSMCs, it requires a large number of individual cells to be analysed in order to achieve consistent results (Petit et al., 2019). Through using cell area as a marker of VSMC contractility, a concentration range of potential agonists/antagonists can be rapidly trialed, identifying the efficacy and optimal dose of a compound. Changes in VSMC area can subsequently be correlated to altered traction force generation using TFM in a targeted approach. We also predict that our assay could easily be used in conjunction with siRNA mediated depletion or overexpression strategies. Immunofluorescent co-staining, using antibodies against the targeted protein, would ensure only depleted or overexpressing cells are analysed. Therefore, this assay possesses the flexibility to enable the precise interrogation of complex biological pathways that regulate VSMC contractile function.

We have used this polyacrylamide hydrogel-based assay to investigate the role of microtubule stability in isolated VSMC morphology and traction stress generation. We identify microtubule stability as a critical regulator of isolated VSMC contractility and show that proper microtubule stability is essential to couple VSMC morphology and traction stress generation (**Figures 4C–G**, **6**). Our findings fit the tensegrity model of cellular mechanics (Stamenović, 2005); microtubule destabilisation increased traction stress generation, whereas microtubule stabilisation had the opposite effect (**Figure 6**). Our findings are supported by previous studies that show microtubule destabilising agents promoted an increase in isometric force generation by wire myography (Sheridan et al., 1996; Platts et al., 1999, 2002; Paul et al., 2000; Zhang et al., 2000). Whilst overall microtubule stability is maintained (**Figures 4A,B**), angiotensin II induced contraction initiates remodelling of the microtubule network (**Supplementary Figure S5**). Further work is required to understand the importance of this reorganisation, however, a recent study has demonstrated that stretched-induced reorganisation of VSMC microtubules enhances the efficiency of mitochondrial ATP production, thereby increasing actomyosin force generation (Bartolák-Suki et al., 2015).

However, contradictory to our findings (**Figures 6D–F**), previous studies have shown that microtubule stabilisation does not alter VSMC force generation by wire myography (Zhang et al., 2000). In this study, we show that paclitaxel had no effect on VSMC morphology (**Figures 4F,G**) and this may potentially account for this discrepancy. Additionally, we identify the IC_{50} of colchicine to be within the nanomolar range (**Figures 4C–E**). Paclitaxel also demonstrated significant microtubule stabilisation when used in the nanomolar range (**Supplementary Figures S6C,D**). However, previous studies have used microtubule targeting agents in the tens of micromolar range (Platts et al., 1999; Paul et al., 2000; Zhang et al., 2000). Numerous studies have shown that these agents can be cytotoxic in micromolar and, in some cell lines, nanomolar ranges (Pasquier et al., 2006; Thomopoulou et al., 2016; Atkinson et al., 2018; Abbassi et al., 2019; Čermák et al., 2020). Meanwhile, in the present study we used these agents in nanomolar ranges, which had no effect on VSMC viability (**Supplementary Figures S6E,F**). Surprisingly, wire myography has shown that VSMC death does not trigger a reduction in isometric force generation (Clarke et al., 2006). Previously, a tamoxifen model that induced VSMC death resulted in the loss of approximately two thirds of VSMCs. However, the remaining VSMCs generated more contractile forces, resulting in the maintenance of the overall isometric force generation (Clarke et al., 2006). This observation may account for the divergence from the tensegrity model predictions, as seen in previous studies (Zhang et al., 2000). Clearly more research is needed to clarify the role of microtubules and cell death in regulating VSMC contractility and vascular tone.

As described above, our microtubule stabilisation/destabilisation traction stress data fits the tensegrity model of cellular mechanics (**Figure 6**). However, we also show that microtubule destabilisation/stabilisation uncoupled the morphological response from the amount of traction stress VSMCs generated following angiotensin II stimulation (**Figure 5**). In our assay, isolated VSMC volume was unchanged by contractile agonist stimulation and changes in area were driven by actomyosin induced contraction (**Supplementary Figures S2, S3**). Microtubule destabilisation promoted increased VSMC volume (**Figures 5A,C**), and we propose that this increased volume is enhancing spreading in these cells. We predicted that these cells were undergoing a hypertrophic response, however more work is needed to clarify how these cells respond over a longer time course. Surprisingly, inhibition of non-muscle myosin II or ROCK also resulted in enhanced VSMC volume (**Figures 3A,C**). This suggests that actin and microtubule networks may mechanically cooperate to regulate VSMC volume control. Much is known about the synergistic nature of microtubules and actomyosin activity. Indeed, non-muscle myosin II has been shown to suppress microtubule growth in order to stabilise cell morphology (Sato et al., 2020), whilst microtubule acetylation has been found to regulate actomyosin-derived force generation (Joo and Yamada, 2014; Seetharaman et al., 2021). Actomyosin and microtubule cross-talk also regulates morphology during differentiation and cell migration in a variety of cell types (Akhshi et al., 2014; Wu and Bezanilla, 2018; Seetharaman and Etienne-Manneville, 2020), suggesting that communication between these mechanical networks is fundamentally important in determining VSMC morphology.

DATA AVAILABILITY STATEMENT

The raw data supporting the conclusion of this article will be made available by the authors, without undue reservation.

AUTHOR CONTRIBUTIONS

SA, RJ, RS, TA, and FW were responsible for performing experiments and analysed data. DW analysed data. RJ and

DW were responsible for the design, writing and editing of this manuscript. SA and RJ contributed equally to this work and share first authorship.

FUNDING

This work was funded by a Biotechnology and Biological Sciences Research Council Research Grant BB/T007699/1 and two British Heart Foundation PhD Studentships (Nos. FS/17/32/32916 and FS/18/35/33681) awarded to DW.

ACKNOWLEDGMENTS

The authors would like to thank Dr. Stefan Bidula for his critical reading of this manuscript. This research was previously submitted as a preprint on the BioRxiv server (DOI: 10.1101/2021.12.14.472278).

SUPPLEMENTARY MATERIAL

The Supplementary Material for this article can be found online at: https://www.frontiersin.org/articles/10.3389/fphar.2022.836710/full#supplementary-material

REFERENCES

Abbassi, R. H., Recasens, A., Indurthi, D. C., Johns, T. G., Stringer, B. W., Day, B. W., et al. (2019). Lower Tubulin Expression in Glioblastoma Stem Cells Attenuates Efficacy of Microtubule-Targeting Agents. *ACS Pharmacol. Transl. Sci.* 2, 402–413. doi:10.1021/acsptsci.9b00045

Afewerki, T., Ahmed, S., and Warren, D. (2019). Emerging Regulators of Vascular Smooth Muscle Cell Migration. *J. Muscle Res. Cel Motil* 40, 185–196. doi:10.1007/s10974-019-09531-z

Ahmed, S., and Warren, D. T. (2018). Vascular Smooth Muscle Cell Contractile Function and Mechanotransduction. *Vp* 2, 36. doi:10.20517/2574-1209.2018.51

Akhshi, T. K., Wernike, D., and Piekny, A. (2014). Microtubules and Actin Crosstalk in Cell Migration and Division. *Cytoskeleton (Hoboken)* 71, 1–23. doi:10.1002/cm.21150

Atkinson, S. J., Gontarczyk, A. M., Alghamdi, A. A., Ellison, T. S., Johnson, R. T., Fowler, W. J., et al. (2018). The β3-integrin Endothelial Adhesome Regulates Microtubule-dependent Cell Migration. *EMBO Rep.* 19, 1. doi:10.15252/embr.201744578

Bae, Y. H., Liu, S. L., Byfield, F. J., Janmey, P. A., and Assoian, R. K. (2016). Measuring the Stiffness of *Ex Vivo* Mouse Aortas Using Atomic Force Microscopy. *J. Vis. Exp.* 54630, 1. doi:10.3791/54630

Bartolák-Suki, E., Imsirovic, J., Parameswaran, H., Wellman, T. J., Martinez, N., Allen, P. G., et al. (2015). Fluctuation-driven Mechanotransduction Regulates Mitochondrial-Network Structure and Function. *Nat. Mater.* 14, 1049–1057. doi:10.1038/nmat4358

Bartolák-Suki, E., and Suki, B. (2020). Tuning Mitochondrial Structure and Function to Criticality by Fluctuation-Driven Mechanotransduction. *Sci. Rep.* 10, 407. doi:10.1038/s41598-019-57301-1

Bastounis, E. E., Yeh, Y. T., and Theriot, J. A. (2019). Subendothelial Stiffness Alters Endothelial Cell Traction Force Generation while Exerting a Minimal Effect on the Transcriptome. *Sci. Rep.* 9, 18209. doi:10.1038/s41598-019-54336-2

Brangwynne, C. P., MacKintosh, F. C., Kumar, S., Geisse, N. A., Talbot, J., Mahadevan, L., et al. (2006). Microtubules Can bear Enhanced Compressive Loads in Living Cells Because of Lateral Reinforcement. *J. Cel Biol* 173, 733–741. doi:10.1083/jcb.200601060

Brown, X. Q., Bartolak-Suki, E., Williams, C., Walker, M. L., Weaver, V. M., and Wong, J. Y. (2010). Effect of Substrate Stiffness and PDGF on the Behavior of Vascular Smooth Muscle Cells: Implications for Atherosclerosis. *J. Cel Physiol* 225, 115–122. doi:10.1002/jcp.22202

Brozovich, F. V., Nicholson, C. J., Degen, C. V., Gao, Y. Z., Aggarwal, M., and Morgan, K. G. (2016). Mechanisms of Vascular Smooth Muscle Contraction and the Basis for Pharmacologic Treatment of Smooth Muscle Disorders. *Pharmacol. Rev.* 68, 476–532. doi:10.1124/pr.115.010652

Caliari, S. R., and Burdick, J. A. (2016). A Practical Guide to Hydrogels for Cell Culture. *Nat. Methods* 13, 405–414. doi:10.1038/nmeth.3839

Čermák, V., Dostál, V., Jelínek, M., Libusová, L., Kovář, J., Rösel, D., et al. (2020). Microtubule-targeting Agents and Their Impact on Cancer Treatment. *Eur. J. Cel Biol.* 99, 151075. doi:10.1016/j.ejcb.2020.151075

Clarke, M. C., Figg, N., Maguire, J. J., Davenport, A. P., Goddard, M., Littlewood, T. D., et al. (2006). Apoptosis of Vascular Smooth Muscle Cells Induces Features of Plaque Vulnerability in Atherosclerosis. *Nat. Med.* 12, 1075–1080. doi:10.1038/nm1459

Claudie, P., Alain, G., and Stéhane, A. (2019). Traction Force Measurements of Human Aortic Smooth Muscle Cells Reveal a Motor-Clutch Behavior. *Mol. Cell Biomech.* 16, 87–108. doi:10.32604/mcb.2019.06415

Colin-York, H., and Fritzsche, M. (2018). The Future of Traction Force Microscopy. *Curr. Opin. Biomed. Eng.* 5, 1–5. doi:10.1016/j.cobme.2017.10.002

Discher, D. E., Janmey, P., and Wang, Y. L. (2005). Tissue Cells Feel and Respond to the Stiffness of Their Substrate. *Science* 310, 1139–1143. doi:10.1126/science.1116995

Glasser, S. P., Arnett, D. K., McVeigh, G. E., Finkelstein, S. M., Bank, A. J., Morgan, D. J., et al. (1997). Vascular Compliance and Cardiovascular Disease: A Risk Factor or a Marker? *Am. J. Hypertens.* 10, 1175–1189. doi:10.1016/S0895-7061(97)00311-7

Haase, K., and Pelling, A. E. (2015). Investigating Cell Mechanics with Atomic Force Microscopy. *J. R. Soc. Interf.* 12, 20140970. doi:10.1098/rsif.2014.0970

Halaidych, O. V., Cochrane, A., van den Hil, F. E., Mummery, C. L., and Orlova, V. V. (2019). Quantitative Analysis of Intracellular Ca2+ Release and Contraction in hiPSC-Derived Vascular Smooth Muscle Cells. *Stem Cel Rep.* 12, 647–656. doi:10.1016/j.stemcr.2019.02.003

Holle, A. W., Young, J. L., Van Vliet, K. J., Kamm, R. D., Discher, D., Janmey, P., et al. (2018). Cell-Extracellular Matrix Mechanobiology: Forceful Tools and Emerging Needs for Basic and Translational Research. *Nano Lett.* 18, 1–8. doi:10.1021/acs.nanolett.7b04982

Johnson, R. T., Solanki, R., and Warren, D. T. (2021). Mechanical Programming of Arterial Smooth Muscle Cells in Health and Ageing. *Biophys. Rev.* 13, 757–768. doi:10.1007/s12551-021-00833-6

Joo, E. E., and Yamada, K. M. (2014). MYPT1 Regulates Contractility and Microtubule Acetylation to Modulate Integrin Adhesions and Matrix Assembly. *Nat. Commun.* 5, 3510. doi:10.1038/ncomms4510

Kandow, C. E., Georges, P. C., Janmey, P. A., and Beningo, K. A. (2007). "Polyacrylamide Hydrogels for Cell Mechanics: Steps toward Optimization and Alternative Uses," in *Methods in Cell Biology Cell Mechanics* (Academic Press), 29–46. doi:10.1016/S0091-679X(07)83002-0

Kraning-Rush, C. M., Carey, S. P., Califano, J. P., and Reinhart-King, C. A. (2012). "Quantifying Traction Stresses in Adherent Cells," in *Computational Methods in Cell Biology*. Editors A. R. Asthagiri and A. P. Arkin (Academic Press), 139–178. doi:10.1016/B978-0-12-388403-9.00006-0

Lacolley, P., Regnault, V., Segers, P., and Laurent, S. (2017). Vascular Smooth Muscle Cells and Arterial Stiffening: Relevance in Development, Aging, and Disease. *Physiol. Rev.* 97, 1555–1617. doi:10.1152/physrev.00003.2017

Leite, R., and Webb, R. C. (1998). Microtubule Disruption Potentiates Phenylephrine-Induced Vasoconstriction in Rat Mesenteric Arterial Bed. *Eur. J. Pharmacol.* 351, R1–R3. doi:10.1016/S0014-2999(98)00358-6

Lekka, M., Gnanachandran, K., Kubiak, A., Zieliński, T., and Zemła, J. (2021). Traction Force Microscopy - Measuring the Forces Exerted by Cells. *Micron* 150, 103138. doi:10.1016/j.micron.2021.103138

Li, S., Sims, S., Jiao, Y., Chow, L. H., and Pickering, J. G. (1999). Evidence from a Novel Human Cell Clone that Adult Vascular Smooth Muscle Cells Can Convert Reversibly between Noncontractile and Contractile Phenotypes. *Circ. Res.* 85, 338–348. doi:10.1161/01.res.85.4.338

Li, X., Ni, Q., He, X., Kong, J., Lim, S. M., Papoian, G. A., et al. (2020). Tensile Force-Induced Cytoskeletal Remodeling: Mechanics before Chemistry. *Plos Comput. Biol.* 16, e1007693. doi:10.1371/journal.pcbi.1007693

Liu, R., Leslie, K. L., and Martin, K. A. (2015). Epigenetic Regulation of Smooth Muscle Cell Plasticity. *Biochim. Biophys. Acta* 1849, 448–453. doi:10.1016/j.bbagrm.2014.06.004

Minaisah, R.-M., Cox, S., and Warren, D. T. (2016). "The Use of Polyacrylamide Hydrogels to Study the Effects of Matrix Stiffness on Nuclear Envelope Properties," in The Nuclear Envelope *Methods in Molecular Biology*. Editors S. Shackleton, P. Collas, and E. C. Schirmer (New York, NY: Springer New York), 233–239. doi:10.1007/978-1-4939-3530-7_15

Mitchell, G. F., Hwang, S. J., Vasan, R. S., Larson, M. G., Pencina, M. J., Hamburg, N. M., et al. (2010). Arterial Stiffness and Cardiovascular Events: the Framingham Heart Study. *Circulation* 121, 505–511. doi:10.1161/CIRCULATIONAHA.109.886655

Mohammed, D., Versaevel, M., Bruyère, C., Alaimo, L., Luciano, M., Vercruysse, E., et al. (2019). Innovative Tools for Mechanobiology: Unraveling Outside-In and Inside-Out Mechanotransduction. *Front. Bioeng. Biotechnol.* 7, 162. doi:10.3389/fbioe.2019.00162

Muhamed, I., Chowdhury, F., and Maruthamuthu, V. (2017). Biophysical Tools to Study Cellular Mechanotransduction. *Bioengineering (Basel)* 4, 12. doi:10.3390/bioengineering4010012

Nagayama, K., and Nishimiya, K. (2020). Moderate Substrate Stiffness Induces Vascular Smooth Muscle Cell Differentiation through Cellular Morphological and Tensional Changes. *Biomed. Mater. Eng.* 31, 157–167. doi:10.3233/BME-201087

Ngo, P., Ramalingam, P., Phillips, J. A., and Furuta, G. T. (2006). Collagen Gel Contraction Assay. *Methods Mol. Biol.* 341, 103–109. doi:10.1385/1-59745-113-4:103

Nogales, E. (2001). Structural Insight into Microtubule Function. *Annu. Rev. Biophys. Biomol. Struct.* 30, 397–420. doi:10.1146/annurev.biophys.30.1.397

Pasqualini, F. S., Agarwal, A., O'Connor, B. B., Liu, Q., Sheehy, S. P., and Parker, K. K. (2018). Traction Force Microscopy of Engineered Cardiac Tissues. *PLOS ONE* 13, e0194706. doi:10.1371/journal.pone.0194706

Pasquier, E., Honoré, S., and Braguer, D. (2006). Microtubule-targeting Agents in Angiogenesis: Where Do We Stand? *Drug Resist. Updat* 9, 74–86. doi:10.1016/j.drup.2006.04.003

Paul, R. J., Bowman, P. S., and Kolodney, M. S. (2000). Effects of Microtubule Disruption on Force, Velocity, Stiffness and [Ca(2+)](i) in Porcine Coronary Arteries. *Am. J. Physiol. Heart Circ. Physiol.* 279, H2493–H2501. doi:10.1152/ajpheart.2000.279.5.H2493

Platts, S. H., Falcone, J. C., Holton, W. T., Hill, M. A., and Meininger, G. A. (1999). Alteration of Microtubule Polymerization Modulates Arteriolar Vasomotor Tone. *Am. J. Physiol.* 277, H100–H106. doi:10.1152/ajpheart.1999.277.1.H100

Platts, S. H., Martinez-Lemus, L. A., and Meininger, G. A. (2002). Microtubule-Dependent Regulation of Vasomotor Tone Requires Rho-Kinase. *J. Vasc. Res.* 39, 173–182. doi:10.1159/000057765

Porter, L., Minaisah, R. M., Ahmed, S., Ali, S., Norton, R., Zhang, Q., et al. (2020). SUN1/2 Are Essential for RhoA/ROCK-Regulated Actomyosin Activity in Isolated Vascular Smooth Muscle Cells. *Cells* 9, 132. doi:10.3390/cells9010132

Qiu, H., Zhu, Y., Sun, Z., Trzeciakowski, J. P., Gansner, M., Depre, C., et al. (2010). Short Communication: Vascular Smooth Muscle Cell Stiffness as a Mechanism for Increased Aortic Stiffness with Aging. *Circ. Res.* 107, 615–619. doi:10.1161/CIRCRESAHA.110.221846

Ragnauth, C. D., Warren, D. T., Liu, Y., McNair, R., Tajsic, T., Figg, N., et al. (2010). Prelamin A Acts to Accelerate Smooth Muscle Cell Senescence and Is a Novel Biomarker of Human Vascular Aging. *Circulation* 121, 2200–2210. doi:10.1161/CIRCULATIONAHA.109.902056

Rensen, S. S., Doevendans, P. A., and van Eys, G. J. (2007). Regulation and Characteristics of Vascular Smooth Muscle Cell Phenotypic Diversity. *Neth. Heart J.* 15, 100–108. doi:10.1007/BF03085963

Rezvani-Sharif, A., Tafazzoli-Shadpour, M., and Avolio, A. (2019). Progressive Changes of Elastic Moduli of Arterial wall and Atherosclerotic Plaque Components during Plaque Development in Human Coronary Arteries. *Med. Biol. Eng. Comput.* 57, 731–740. doi:10.1007/s11517-018-1910-4

Rickel, A. P., Sanyour, H. J., Leyda, N. A., and Hong, Z. (2020). Extracellular Matrix Proteins and Substrate Stiffness Synergistically Regulate Vascular Smooth Muscle Cell Migration and Cortical Cytoskeleton Organization. *ACS Appl. Bio Mater.* 3, 2360–2369. doi:10.1021/acsabm.0c00100

Rzucidlo, E. M., Martin, K. A., and Powell, R. J. (2007). Regulation of Vascular Smooth Muscle Cell Differentiation. *J. Vasc. Surg.* 45 Suppl A, A25–A32. doi:10.1016/j.jvs.2007.03.001

Sanyour, H. J., Li, N., Rickel, A. P., Childs, J. D., Kinser, C. N., and Hong, Z. (2019). Membrane Cholesterol and Substrate Stiffness Co-ordinate to Induce the Remodelling of the Cytoskeleton and the Alteration in the Biomechanics of Vascular Smooth Muscle Cells. *Cardiovasc. Res.* 115, 1369–1380. doi:10.1093/cvr/cvy276

Sato, Y., Kamijo, K., Tsutsumi, M., Murakami, Y., and Takahashi, M. (2020). Nonmuscle Myosin IIA and IIB Differently Suppress Microtubule Growth to Stabilize Cell Morphology. *J. Biochem.* 167, 25–39. doi:10.1093/jb/mvz082

Sazonova, O. V., Isenberg, B. C., Herrmann, J., Lee, K. L., Purwada, A., Valentine, A. D., et al. (2015). Extracellular Matrix Presentation Modulates Vascular Smooth Muscle Cell Mechanotransduction. *Matrix Biol.* 41, 36–43. doi:10.1016/j.matbio.2014.11.001

Schierbaum, N., Rheinlaender, J., and Schäffer, T. E. (2019). Combined Atomic Force Microscopy (AFM) and Traction Force Microscopy (TFM) Reveals a Correlation between Viscoelastic Material Properties and Contractile Prestress of Living Cells. *Soft Matter* 15, 1721–1729. doi:10.1039/C8SM01585F

Schindelin, J., Arganda-Carreras, I., Frise, E., Kaynig, V., Longair, M., Pietzsch, T., et al. (2012). Fiji: an Open-Source Platform for Biological-Image Analysis. *Nat. Methods* 9, 676–682. doi:10.1038/nmeth.2019

Seetharaman, S., and Etienne-Manneville, S. (2020). Cytoskeletal Crosstalk in Cell Migration. *Trends Cel Biol* 30, 720–735. doi:10.1016/j.tcb.2020.06.004

Seetharaman, S., Vianay, B., Roca, V., Farrugia, A. J., De Pascalis, C., Boëda, B., et al. (2021). Microtubules Tune Mechanosensitive Cell Responses. *Nat. Mater.* 8, 1–12. doi:10.1038/s41563-021-01108-x

Sheridan, B. C., McIntyre, R. C., Meldrum, D. R., Cleveland, J. C., Agrafojo, J., Banerjee, A., et al. (1996). Microtubules Regulate Pulmonary Vascular Smooth Muscle Contraction. *J. Surg. Res.* 62, 284–287. doi:10.1006/jsre.1996.0209

Shi, N., and Chen, S. Y. (2016). Smooth Muscle Cell Differentiation: Model Systems, Regulatory Mechanisms, and Vascular Diseases. *J. Cel Physiol* 231, 777–787. doi:10.1002/jcp.25208

Stamenović, D. (2005). Microtubules May Harden or Soften Cells, Depending of the Extent of Cell Distension. *J. Biomech.* 38, 1728–1732. doi:10.1016/j.jbiomech.2004.07.016

Sun, Z., Martinez-Lemus, L. A., Hill, M. A., and Meininger, G. A. (2008). Extracellular Matrix-specific Focal Adhesions in Vascular Smooth Muscle Produce Mechanically Active Adhesion Sites. *Am. J. Physiol. Cel Physiol* 295, C268–C278. doi:10.1152/ajpcell.00516.2007

Thomopoulou, P., Sachs, J., Teusch, N., Mariappan, A., Gopalakrishnan, J., and Schmalz, H. G. (2016). New Colchicine-Derived Triazoles and Their Influence on Cytotoxicity and Microtubule Morphology. *ACS Med. Chem. Lett.* 7, 188–191. doi:10.1021/acsmedchemlett.5b00418

Tracqui, P., Broisat, A., Toczek, J., Mesnier, N., Ohayon, J., and Riou, L. (2011). Mapping Elasticity Moduli of Atherosclerotic Plaque *In Situ* via Atomic Force Microscopy. *J. Struct. Biol.* 174, 115–123. doi:10.1016/j.jsb.2011.01.010

Tsamis, A., Krawiec, J. T., and Vorp, D. A. (2013). Elastin and Collagen Fibre Microstructure of the Human Aorta in Ageing and Disease: a Review. *J. R. Soc. Interf.* 10, 20121004. doi:10.1098/rsif.2012.1004

Tseng, Q., Duchemin-Pelletier, E., Deshiere, A., Balland, M., Guillou, H., Filhol, O., et al. (2012). Spatial Organization of the Extracellular Matrix Regulates Cell-Cell junction Positioning. *Proc. Natl. Acad. Sci. U S A.* 109, 1506–1511. doi:10.1073/pnas.1106377109

Vernon, R. B., and Gooden, M. D. (2002). An Improved Method for the Collagen Gel Contraction Assay. In Vitro *Cel Dev Biol Anim* 38, 97–101. doi:10.1290/1071-2690(2002)038<0097:AIMFTC>2.0.CO;2

Wang, L., Qiu, P., Jiao, J., Hirai, H., Xiong, W., Zhang, J., et al. (2017). Yes-Associated Protein Inhibits Transcription of Myocardin and Attenuates Differentiation of Vascular Smooth Muscle Cell from Cardiovascular Progenitor Cell Lineage. *Stem Cells* 35, 351–361. doi:10.1002/stem.2484

Warren, D. T., Tajsic, T., Porter, L. J., Minaisah, R. M., Cobb, A., Jacob, A., et al. (2015). Nesprin-2-dependent ERK1/2 Compartmentalisation Regulates the DNA Damage Response in Vascular Smooth Muscle Cell Ageing. *Cell Death Differ* 22, 1540–1550. doi:10.1038/cdd.2015.12

Wong, J. Y., Velasco, A., Rajagopalan, P., and Pham, Q. (2003). Directed Movement of Vascular Smooth Muscle Cells on Gradient-Compliant Hydrogels. *Langmuir* 19, 1908–1913. doi:10.1021/la026403p

Wu, S. Z., and Bezanilla, M. (2018). Actin and Microtubule Cross Talk Mediates Persistent Polarized Growth. *J. Cel Biol* 217, 3531–3544. doi:10.1083/jcb.201802039

Xie, S. A., Zhang, T., Wang, J., Zhao, F., Zhang, Y. P., Yao, W. J., et al. (2018). Matrix Stiffness Determines the Phenotype of Vascular Smooth Muscle Cell *In Vitro* and *In Vivo*: Role of DNA Methyltransferase 1. *Biomaterials* 155, 203–216. doi:10.1016/j.biomaterials.2017.11.033

Ye, G. J., Nesmith, A. P., and Parker, K. K. (2014). The Role of Mechanotransduction on Vascular Smooth Muscle Myocytes' [corrected] Cytoskeleton and Contractile Function. *Anat. Rec. (Hoboken)* 297, 1758–1769. doi:10.1002/ar.22983

Zhang, D., Jin, N., Rhoades, R. A., Yancey, K. W., and Swartz, D. R. (2000). Influence of Microtubules on Vascular Smooth Muscle Contraction. *J. Muscle Res. Cel Motil* 21, 293–300. doi:10.1023/A:1005600118157

Zhou, D. W., Lee, T. T., Weng, S., Fu, J., and García, A. J. (2017). Effects of Substrate Stiffness and Actomyosin Contractility on Coupling between Force Transmission and Vinculin-Paxillin Recruitment at Single Focal Adhesions. *Mol. Biol. Cel* 28, 1901–1911. doi:10.1091/mbc.e17-02-0116

Conflict of Interest: The authors declare that the research was conducted in the absence of any commercial or financial relationships that could be construed as a potential conflict of interest.

Publisher's Note: All claims expressed in this article are solely those of the authors and do not necessarily represent those of their affiliated organizations, or those of the publisher, the editors and the reviewers. Any product that may be evaluated in this article, or claim that may be made by its manufacturer, is not guaranteed or endorsed by the publisher.

frontiers in Pharmacology

MINI REVIEW
published: 08 February 2022
doi: 10.3389/fphar.2022.828933

A Role of IL-17 in Rheumatoid Arthritis Patients Complicated With Atherosclerosis

Jiexin Wang, Linxi He, Weihong Li and Shangbin Lv*

Basic Medical College, Chengdu University of Traditional Chinese Medicine, Chengdu, China

Rheumatoid arthritis (RA) is mainly caused by joint inflammation. RA significantly increases the probability of cardiovascular disease. Although the progress of RA has been well controlled recently, the mortality of patients with RA complicated with cardiovascular disease is 1.5–3 times higher than that of patients with RA alone. The number of people with atherosclerosis in patients with RA is much higher than that in the general population, and atherosclerotic lesions develop more rapidly in patients with RA, which has become one of the primary factors resulting in the death of patients with RA. The rapid development of atherosclerosis in RA is induced by inflammation-related factors. Recent studies have reported that the expression of IL-17 is significantly upregulated in patients with RA and atherosclerosis. Simultaneously, there is evidence that IL-17 can regulate the proliferation, migration, and apoptosis of vascular endothelial cells and vascular smooth muscle cells through various ways and promote the secretion of several cytokines leading to the occurrence and development of atherosclerosis. Presently, there is no clear prevention or treatment plan for atherosclerosis in patients with RA. Therefore, this paper explores the mechanism of IL-17 in RA complicated with atherosclerosis and shows the reasons for the high incidence of atherosclerosis in patients with RA. It is hoped that the occurrence and development of atherosclerosis in patients with RA can be diagnosed or prevented in time in the early stage of lesions, and the prevention and treatment of cardiovascular complications in patients with RA can be enhanced to reduce mortality.

Keywords: rheumatoid arthritis, atherosclerosis, vascular smooth muscle cells, vascular endothelial cells, interleukin-17, inflammation

OPEN ACCESS

Edited by:
Qilong Wang,
Tianjin University of Traditional Chinese Medicine, China

Reviewed by:
Pawan Krishan,
Punjabi University, India
Junji Moriya,
The University of Tokyo Hospital, Japan

****Correspondence:***
Weihong Li
lwh@cdutcm.edu.cn

Specialty section:
This article was submitted to Cardiovascular and Smooth Muscle Pharmacology, a section of the journal Frontiers in Pharmacology

Received: *04 December 2021*
Accepted: *19 January 2022*
Published: *08 February 2022*

Citation:
Wang J, He L, Li W and Lv S (2022) A Role of IL-17 in Rheumatoid Arthritis Patients Complicated With Atherosclerosis. Front. Pharmacol. 13:828933. doi: 10.3389/fphar.2022.828933

INTRODUCTION

Rheumatoid arthritis (RA) is a progressive systemic inflammatory disease with unknown etiology, which affects about 0.2–1% of adults worldwide for a long time (Gabriel, 2001; Helmick et al., 2008; Myasoedova et al., 2010; Roth et al., 2017). RA is characterized by inflammatory changes in the joints, resulting in local swelling, pain, and stiffness, usually accompanied by the formation of autoantibodies, such as rheumatoid factor or antinitrate antibodies. Long-term inflammatory stimulation often causes damage and deformity of diseased joints and finally loss of labor ability (Scott et al., 2010; Lillegraven et al., 2012), which greatly impacts social and economic development. What is more severe is that RA, as an autoimmune inflammatory disease, causes local lesions in joint and leads to cardiovascular diseases, including atherosclerosis, cerebrovascular diseases, heart failure, and peripheral vascular diseases (Wolfe et al., 1994; del Rincón et al., 2001). Cardiovascular disease is one

of the major reasons for the increase in mortality of patients with RA. Some studies (Crowson et al., 2013; Winchester et al., 2016) have indicated that the mortality of patients with RA with cardiovascular disease is 1.5–3 times higher than that of patients with RA alone. Hence, the study on the mechanism of cardiovascular disease in RA is particularly essential to reduce the mortality of patients with RA. In previous studies, many factors causing cardiovascular disease in RA were found, such as hypertension (McEntegart et al., 2001; Erb et al., 2004), abnormal lipid metabolism (Situnayake and Kitas, 1997), obesity (Stavropoulos-Kalinoglou et al., 2007), smoking (Gerli et al., 2005), and inflammation, among which inflammatory changes are the core link of cardiovascular disease in RA and play an essential role in the occurrence, development, and outcome of the disease. Inflammation is a defense response of the body to stimulation; it is a highly complex process involving many cytokines that cause pathological changes in the lesion site and even the whole body, such as RA. Some studies have discovered several cytokines and chemokines in the synovial tissue of patients with RA. Under the action of these cytokines, dendritic cells (DCs) were activated (Khan et al., 2009); activated DCs expressed several interleukin (IL)-23 (Duvallet et al., 2011) and further stimulated T-cells to differentiate into helper T-cells 17 (TH17), and activated TH17 began expressing IL-17. IL-17 is a cytokine that acts on blood vessels and cardiomyocytes, aggravating inflammation, blood clotting, and thrombosis (Robert and Miossec, 2017). Therefore, blocking the expression of IL-17 or preventing its binding to the receptor may be key to treating cardiovascular diseases in patients with RA.

IL-17 refers to a single cytokine IL-17A or IL-17 family of cytokines composed of IL-17A, IL-17B, IL-17C, IL-17D, IL-17E (IL-25), and IL-17F. There is a large amount of IL-17 expression in the synovial tissue of RA (Chabaud et al., 1999), indicating that IL-17 plays a potential role in the pathogenesis of RA. This view has been verified by different experimental models of arthritis and supported by several human *in vitro* experiments (van den Berg and Miossec, 2009). Subsequently, due to the common pathogenesis of cardiovascular dysfunction and immune diseases (Abou-Raya and Abou-Raya, 2006; Prasad et al., 2015), IL-17 has the same effects on atherosclerosis and chronic inflammation (Ross, 1999; Hansson and Libby, 2006); thus, IL-17 may be involved in both processes. As an increasing number of chronic inflammatory diseases target IL-17 (Beringer et al., 2016), it is crucial to explore the positive or negative effects and related results of IL-17 in RA and cardiovascular diseases.

In view of the high mortality rate of patients with RA with cardiovascular disease, the occurrence and development of coronary heart disease caused by atherosclerosis is the major reason for its high mortality (Kitas et al., 1998; Van Doornum et al., 2002; Kitas and Erb, 2003). Therefore, it is imperative to reveal its pathogenesis to block the occurrence of lesions and decrease mortality. By reviewing previous studies on RA and atherosclerosis, this study shows the core mechanism of the high incidence of cardiovascular disease in patients with RA and provides a theoretical basis for blocking the occurrence and development of cardiovascular disease in patients with RA.

INFLAMMATION IS KEY TO ATHEROSCLEROSIS IN PATIENTS WITH RA

In previous studies, many factors were found to cause RA atherosclerosis, such as hypertension, abnormal lipid metabolism, obesity, smoking, and inflammation. Some studies have indicated that (Anyfanti et al., 2020) the increased incidence of hypertension in patients with RA is accompanied by vascular endothelial cell dysfunction, which is usually regarded as a precursor for hypertension. Vascular endothelial cell dysfunction eventually increases the prevalence of atherosclerosis. Regarding abnormal lipid metabolism, previous studies have indicated that elevated levels of low-density lipoprotein can cause cardiovascular disease, and high-density lipoprotein has a protective effect on atherosclerosis. Recent studies have shown that (García-Gómez et al., 2014) the effects of low-density lipoprotein and high-density lipoprotein vary from the actual data related to blood lipids in patients with RA. However, they also prove that abnormal lipid metabolism does increase the risk of atherosclerosis in patients with RA. There is a high amount of adipose tissue in patients with obesity. These adipose tissues act as energy storage organs and can be regarded as a complex dynamic endocrine organ that can secrete a large number of adipose factors (Kershaw and Flier, 2004). Some of these lipokines (such as chemotactic protein, lipoprotein troponin 2, vaspin, and omentin-1) exhibit strong immunomodulatory activity in the pathogenesis of RA (Xie and Chen, 2019). Simultaneously, RA correlates highly with the occurrence and development of atherosclerosis (Tsuji et al., 2001; Hemdahl et al., 2006; Folkesson et al., 2007; Yamawaki et al., 2010; Duan et al., 2011; Kadoglou et al., 2011; Yamawaki et al., 2011; Sivalingam et al., 2017; Wu et al., 2020), but its molecular and physiological mechanism is still unclear. Smoking is seen as a risk factor for RA development, and it is also a significant risk factor for cardiovascular disease in patients with RA (Salonen and Salonen, 1991; Diez-Roux et al., 1995; Silman et al., 1996; Wolfe, 2000; McEntegart et al., 2001; Padyukov et al., 2004; Goodson et al., 2005; Maradit-Kremers et al., 2005). Smoking can promote the manufacture of antinucleotide peptide autoantibodies in susceptible individuals with RA carrying HLA-DRB1 alleles, which cause the aggravation of inflammation and autoimmune diseases (Klareskog et al., 2006; Linn-Rasker et al., 2006), resulting in atherosclerosis (Kraan et al., 1998; Rantapää-Dahlqvist et al., 2003; Vossenaar and van Venrooij, 2004). From the above discussion, it is evident that traditional factors, whether hypertension, obesity, abnormal lipid metabolism, or smoking, will cause abnormal autoimmunity, causing the aggravation of vascular lesions in patients with RA.

Additionally, inflammation is considered the key mechanism of atherosclerosis. Previous studies have suggested that atherosclerosis is caused by the accumulation of lipids in the arterial wall, but new studies suggest that atherosclerosis is inextricably related to

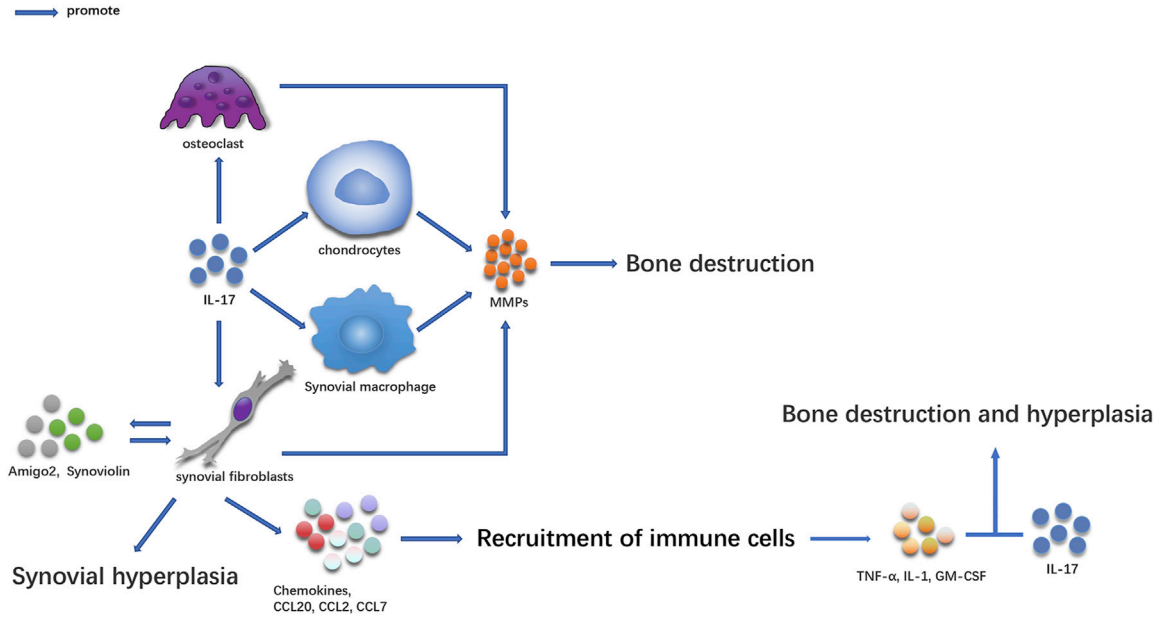

FIGURE 1 | The effect of IL-17 on bone in RA patients.

inflammation (Libby et al., 2009). Inflammation and autoantibodies may be involved in the occurrence and development of atherosclerotic diseases (Frostegård, 2013; Iseme et al., 2017). Alternatively, inflammation also plays an essential role in inducing plaque erosion and plaque stability, so the development of anti-inflammatory drugs to stabilize plaque is an option for preventing coronary artery disease (CAD) (Everett et al., 2013). The physiology and pathology of atherosclerosis are related to inflammatory lesions of RA synovium in many aspects. Macrophages, helper T-cells (TH1), tumor necrosis factor α (TNF- α), IL-6, and matrix metalloproteinases (MMPs) are all involved in the process (Pasceri and Yeh, 1999). Past studies have indicated that the immune system plays a double-edged role in atherosclerosis development. TH1CD4+ lymphocytes accelerate the formation of atherosclerosis, whereas regulatory T-cells can inhibit atherosclerosis by secreting cytokines, such as transforming growth factor (TGF)-α and IL-10. Changes in the types of cytokines cause an imbalance in T-cell subsets, thereby affecting the disease progression (Ait-Oufella et al., 2006). Additionally, infiltration, accumulation, and oxidation of low-density lipoprotein in the intima of blood vessels can cause inflammation of the arterial wall (Hansson, 2005), Oxidation of low-density lipoprotein results in the expression of adhesion molecules and inflammation-related factors in endothelial cells (Dai et al., 2004); leucocytes infiltrate into the intima through adhesion molecules and differentiate into macrophages under the action of cytokines, such as macrophage colony-stimulating factor and growth factors (Smith et al., 1995; Hansson, 2005). Macrophages, endothelial cells, apoptotic foam cells, and lipid fragments form plaques, leading to narrowing and closure of arteries (Hansson, 2005). Under the action of enzymes, such as inflammatory factors and MMPs, plaques may become unstable or even ruptured (Finn et al., 2010), and plaque rupture may cause thrombosis and blood flow blockage. Blockages of the heart and cerebral arteries cause heart attacks and strokes, respectively (Jones et al., 2003; Hansson, 2005).

In the early stage of RA disease, due to the reduction in the immune system's self-tolerance, various autoantibodies activate the immune system, resulting in immune cells infiltrating into the synovium of the joint. This process involves the participation of many cytokines, including TNF-α and IL. The levels of TNF-α, IL-17, IL-6, and IL-1 β in serum of patients with RA and cardiovascular disease were increased in varying degrees. These cytokines also participate in the activation of endothelial cells and vascular smooth muscle cells (VSMC), which is the key process in the formation of pannus in synovial tissue during RA lesions and also contributes to the pathogenesis of atherosclerotic heart disease.

BONE DESTRUCTION AND SYNOVIAL HYPERPLASIA IN RA ARE MEDIATED BY IL-17-GUIDED RA (FIGURE 1)

IL-17-secreting cells were first discovered in the synovium of patients with RA. Some studies have shown that there are many IL-17 and Th17 cells in serum and synovial supernatant of inflammatory joints in patients with RA (Kirkham et al., 2006; Shen et al., 2009; Gullick et al., 2010; Leipe et al., 2010; Raychaudhuri et al., 2012; Gullick et al., 2013). A large amount of IL-17 was also manufactured in peripheral blood mononuclear cells (PBMC) (Kim et al., 2005), and its concentration was higher than that in healthy people (Chabaud et al., 1999; Ziolkowska et al., 2000; Li et al., 2013). Several studies have proven that the content of IL-17 in synovial tissue and serum is directly related to the degree of RA joint injury (Kirkham et al., 2006; Schofield et al., 2016; Siloşi et al., 2016; Lee

and Bae, 2017; Costa et al., 2019). The increase in IL-17 levels in serum, synovial fluid, and PBMC is related to the expression of C-reactive protein, erythrocyte sedimentation rate, and rheumatoid factor (Roşu et al., 2012; El-Maghraby et al., 2019). IL-17 participates in the occurrence and development of the disease and plays an essential role in the pathogenesis of the disease (**Figure 1**) (Raza et al., 2005; Kokkonen et al., 2010).

IL-17 Causes Bone Destruction at the Lesion Site

In the pathogenesis of RA, IL-17 can cause an imbalance between osteoblasts and osteoclasts in several ways, which often occur in the pathological process of RA (Gravallese and Schett, 2018). The activity of osteoclasts in subchondral, trabecular, and cortical bone eroded areas increased in the joint where IL-17 was highly expressed (Lubberts et al., 2002; Lubberts et al., 2003; Lubberts et al., 2004). IL-17 causes bone destruction by increasing osteoclast formation induced by NF-KB ligand-receptor activator (RANKL) (Lubberts et al., 2004; Adamopoulos et al., 2010). IL-17 can also promote the release of MMPs in synoviocytes and chondrocytes, causing joint injury (Koenders et al., 2005; Agarwal et al., 2008). Collagen-induced arthritis (CIA) is a commonly used animal model for studying RA (Wu et al., 2018), High levels of IL-17 were found in CD4+T-cells and GDT cells in the joints of CIA mice (Pöllinger et al., 2011). Th17 cells transferred to subarticular cartilage osteoclasts to express IL-17, showing that IL-17 was involved in the bone destruction of CIA. Additionally, local injection of IL-17 into the knee joint aggravated arthritis and joint injury during CIA development (Lubberts et al., 2003). Local injection of adenovirus vector expressing mouse IL-17 into the joint can also accelerate the development of CIA and inflammation (Lubberts et al., 2002). Treatment using soluble IL-17 receptor fusion protein or anti-IL-17 antibody can enhance the severity of arthritis, cartilage injury, and bone loss (Lubberts et al., 2001; Bush et al., 2002; Lubberts et al., 2004; Pöllinger et al., 2011). IL-17 can also promote the production of collagen-specific T-cells and collagen-specific IgG2a and participate in CIA occurrence and development (Nakae et al., 2003). Anti-IL-17 can decrease the production and recruitment of inflammatory cells in CIA (Chao et al., 2011; Li et al., 2014).

IL-17 can Cause Synovium and Bone Hyperplasia in Diseased Joints

IL-17 can also cause synovial and bone hyperplasia while aggravating the inflammatory response of diseased joints. IL-17 promotes the proliferation and survival of synovial cells and induces synovial hyperplasia by inducing the expression of anti-apoptotic molecules, such as synovial protein and amigo2 (Toh et al., 2010; Lee et al., 2013; Benedetti et al., 2016). In the absence of osteoclasts, IL-17, and TNF promote bone proliferation by inducing osteogenic differentiation of mesenchymal stem cells (Osta et al., 2014). IL-17 induces the recruitment of T-cells and other immune cells by inducing the expression of neutrophil chemokine, CC chemokine ligand 20 (CCL20), CCL2, and CCL7 (Hattori et al., 2015). When several immune cells are recruited into the synovium, inflammation in this site is aggravated, and a specific pro-inflammatory cytokine environment is formed, which in turn promotes inflammatory synergism between IL-17 and other cytokines (such as TNF, GM-CSF, or IL-1) and aggravates bone destruction and proliferation in the diseased site. The combination of anti-IL-1 and anti-IL-17 antibodies can effectively inhibit bone and cartilage injury, downregulate the expression of IL-1b, IL-6, IL-17, interferon-gamma (IFN-γ), RANKL, and MMP-3 (Zhang et al., 2013; Li et al., 2014), and decrease the inflammatory changes of the lesion site. Therefore, IL-17 can participate in chronic lesions of RA in several ways.

IL-17 IS INVOLVED IN THE OCCURRENCE AND DEVELOPMENT OF ATHEROSCLEROSIS BY ACTING ON VASCULAR ENDOTHELIAL CELLS AND VSMC (FIGURE 2)

Early atherosclerotic CAD is associated with IL-17 (**Figure 2**). IL-17 is a cytokine that acts on blood vessels and cardiomyocytes and aggravates inflammation, coagulation, and thrombosis (Robert and Miossec, 2017). IL-17 can activate many downstream signaling pathways, including NF-KB, resulting in the expression of numerous pro-inflammatory cytokines (Iwakura et al., 2011). By binding to IL-17R on cells, IL-17 activates NF-KB under the action of conjugate protein ACT1 (Qian et al., 2007), causing the expression of different inflammatory factors, such as TNF-α, IL-6, IL-1β, monocyte chemoattractant protein-1, and intracellular adhesion molecule-1 (Feldmann et al., 2005; Liu et al., 2013; Soltanzadeh-Yamchi et al., 2018). These cytokines are involved in the formation and development of atherosclerotic plaque (Maracle et al., 2018; Song et al., 2018; Zhang et al., 2018). In the early stage, many animal models also observed direct evidence of the atherosclerotic effect of IL-17 (Erbel et al., 2009; van Es et al., 2009; Gao et al., 2010; Butcher et al., 2012; Zhang et al., 2012; Nordlohne and von Vietinghoff, 2019). Th17 cells play an essential role in the development of atherosclerotic plaque in mice, which may also affect atherosclerotic patients (Gao et al., 2010). By injecting IL-17 blocking antibody into apolipoprotein E deficient ($apoE^{-/-}$) mice, it was discovered that functional blocking of IL-17 could decrease atherosclerotic lesions and improve as well as decrease plaque vulnerability, cell infiltration, and tissue activation, proposing that IL-17 plays a vital role in atherosclerosis formation (Erbel et al., 2009).

IL-17 Regulates VSMC and Vascular Endothelial Cells, Leading to Atherosclerosis

The inflammatory reaction and proliferation of VSMC are the reasons for the progression of atherosclerosis (Chistiakov et al., 2015; Bennett et al., 2016). VSMC is mainly located in the middle layer of the vascular wall and plays a crucial role in atherosclerosis through proliferation, migration, apoptosis, and aging (Bennett

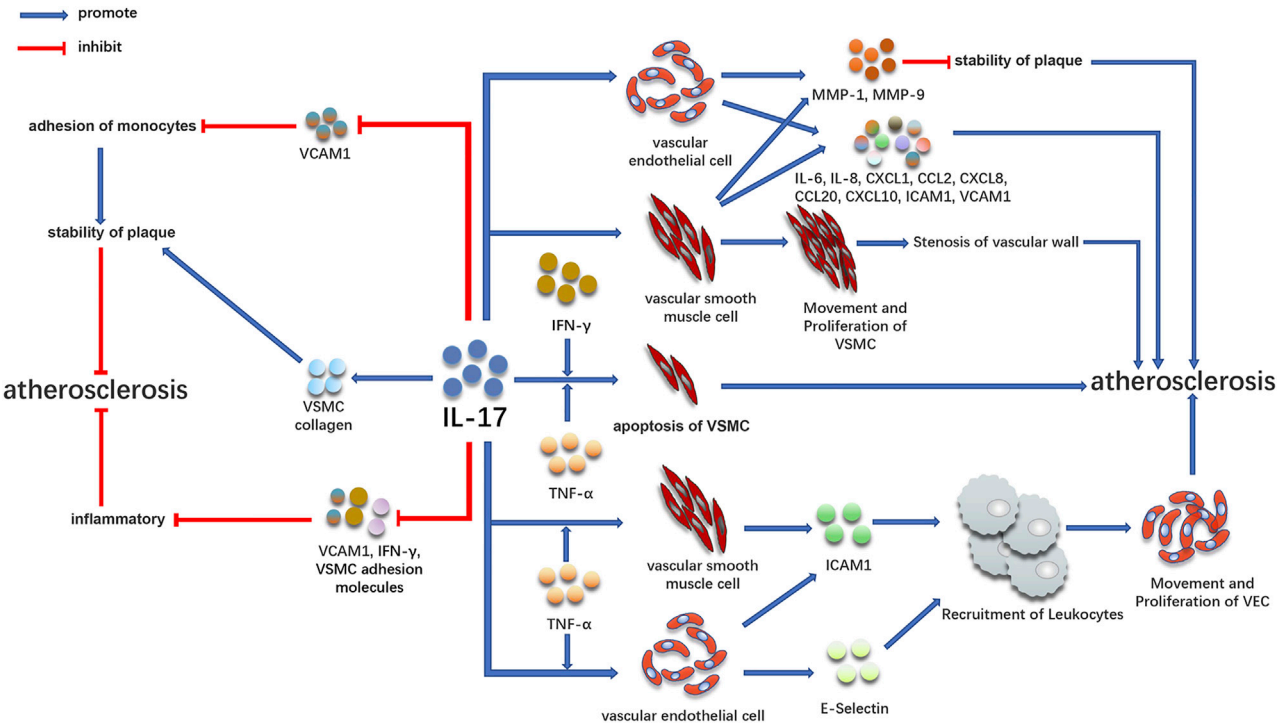

FIGURE 2 | Promoting and inhibiting effect of IL-17 in atherosclerosis. IL-17 is involved in the development of atherosclerosis by acting on vascular endothelial cells and VSMC. At the same time, IL-17 can play an anti-atherosclerotic effect by increasing plaque stability and inhibiting inflammation, which may be related to the staging of the disease.

et al., 2016). Under normal circumstances, VSMC in the arterial wall exhibits a contractile phenotype. When blood vessels are destroyed, VSMC exhibits proliferative and pro-inflammatory effects when it differentiates into a pro-inflammatory phenotype. Therefore, inflammation and excessive proliferation of VSMCs are the reasons for atherosclerosis progression (Chistiakov et al., 2015; Bennett et al., 2016). Persistent inflammatory stimulation plays a crucial role in atherosclerosis by promoting the proliferation and migration of VSMCs. IL-17 can cause the proliferation and migration of VSMCs dependent on NF-KB activator 1 (TRAF3IP2) and upregulate the expression of many mediators involved in angiogenesis and occlusive disease (Mummidi et al., 2019). IL-17 induces the production of pro-inflammatory cytokines (such as IL-6), chemokines (such as IL-8, CXCL-1, CCL-2, CXCL8, and CXCL10), and adhesion molecules (intercellular adhesion molecules 1ICAM1 and vascular cell adhesion molecules 1VCAM1) in vascular endothelial cells and VSMC (Fossiez et al., 1996; Eid et al., 2009; Erbel et al., 2009; Zhu et al., 2011; Erbel et al., 2014; Yuan et al., 2015), leading to atherosclerosis. Additionally, IL-17 can enhance the effect of TNF-α, further increase the expression of VCAM1 and ICAM1, and secrete IL-6, IL-8, and CCL20 by endothelial cells (Erbel et al., 2009; Hot et al., 2012). IL-17 may also aggravate atherosclerosis by increasing the expression of MMP1 and MMP9 and apoptosis of VSMCs and endothelial cells (Erbel et al., 2009; Zhu et al., 2011).

IL-17 Combined With Other Cytokines Mediates the Occurrence of Atherosclerosis

IL-17 can also play a role with other inflammatory factors in inducing atherosclerosis. In the clinical specimens of coronary atherosclerosis, IL-17 and IFN-γ exist simultaneously, and T-cells can secrete IL-17 and IFN-γ in coronary plaques. IL-17 and IFN-γ jointly induce the release of IL-6, CXCL1, CXCL2, CXCL5, CCL8, and CXCL10 from VSMC (Eid et al., 2009). These chemokines play an essential role in the stability and activation of various cell types (Rolin and Maghazachi, 2014); different chemokines are also involved in the occurrence of atherosclerosis in different ways (Weber and Noels, 2011; Lu, 2017). Additionally, IFN-γ is highly expressed in atherosclerotic lesions and inhibits the proliferation of VSMC. While reducing collagen production, it makes the fibrous cap thinner by many expressions of MMPs, resulting in plaque rupture more easily (Harvey and Ramji, 2005; Tedgui and Mallat, 2006). The synergistic effect of IFN-γ and TNF-α can promote the formation of atherosclerosis (Mehta et al., 2017); IL-17 combined with TNF-α or IFN-γ leads to atherosclerosis by accelerating the apoptosis of VSMC (Clarke et al., 2008; Erbel et al., 2009). *In vitro* studies have indicated that IL-17 combined with TNF-α has a strong effect on promoting coagulation and thrombosis of vascular endothelial cells (Hot et al., 2012). Additionally, the combination of IL-17 and TNF-α can

significantly increase E-selectin and intercellular adhesion molecules and promote the recruitment of leukocytes to form an inflammatory environment that causes the proliferation, migration, and invasion of endothelial cells (Robert and Miossec, 2017). These results suggest that IL-17 may promote the progression of atherosclerosis by inducing vascular inflammation, leukocyte recruitment, and plaque vulnerability.

IL-17 has an Anti-atherosclerotic Effect (Figure 2)

However, it is worth noting that IL-17 can also promote the production of VSMC collagen, promote plaque stabilization, and inhibit the pathogenesis of atherosclerosis (**Figure 2**) (Erbel et al., 2009; Taleb et al., 2009; Smith et al., 2010; Gisterå et al., 2013; Hansson et al., 2015; Robert and Miossec, 2017). Some studies have indicated that IL-17 can inhibit the role of vascular cell adhesion molecules, fibroblasts, and VSMC adhesion molecules as well as decrease the production of IFN-γ, indicating that it has anti-inflammatory effects (**Figure 2**) (Madhur et al., 2010; Danzaki et al., 2012). Animal experiments have indicated that IL-17 exhibits resistance to low-density lipoprotein receptor$^{-/-}$mouse atherosclerosis by improving the stability of plaques (Gisterå et al., 2013). The anti-atherosclerotic effect of IL-17 could be caused by inducing VSMC proliferation and downregulating the expression of VCAM1 in endothelial cells to inhibit the adhesion of monocytes to plaques to maintain the stability of plaques (**Figure 2**). Similarly, in a study of 981 patients with myocardial infarction, the high IL-17 expression in serum was significantly associated with low mortality and risk of recurrent myocardial infarction (Simon et al., 2013). VCAM1, as a biomarker of atherosclerosis, also exhibited a decreasing trend in these patients. The atherogenic and anti-atherosclerotic effects of IL-17 may be caused by the expression of IL-17 in various stages of the disease, in which the expression of IL-17 is highest in the early stage of atherosclerosis and reduced in the late stage of atherosclerosis.

SUMMARY AND PROSPECT

RA is an autoimmune disease significantly associated with the increased risk of atherosclerosis (Mellado et al., 2015). The leading cause of death of patients with RA is cardiovascular disease. Chronic inflammation seems to be the main potential pathogenic factor connecting RA and cardiovascular disease. However, the mechanism of the link between RA and cardiovascular disease is not fully understood. In this review, by summarizing the mechanism of IL-17 in the pathogenesis of RA and atherosclerosis, it was found that autoantibodies activate the immune system and cells manufacture many cytokines and chemokines to activate dendritic cells owing to the reduced self-tolerance of the immune system in patients with RA. IL-23 expressed by activated dendritic cells mediates the differentiation of T-cells into TH17, which results in the expression of IL-17. IL-17 plays a vital role in the expression of adhesion molecules, pro-inflammatory cytokines and chemokines, cartilage and bone hyperplasia, bone destruction, and the proliferation, migration, and apoptosis of vascular endothelial cells, as well as VSMC. Simultaneously, the levels of IL-17 and IL-17-expressing cells in the serum of patients with RA and atherosclerosis exhibited an increasing trend. What is essential is that autoimmune diseases and atherosclerosis have common pathogenesis, and IL-17 plays a major role in the pathogenesis of autoimmune diseases and atherosclerosis, which promotes the secretion of different cytokines and aggravates the disease process to some extent.

There is increasing evidence that the morbidity and mortality of CVS are increasing in patients with RA. When formulating treatment plans for autoimmune diseases, such as RA, attention should be paid not only to relieving patients' existing symptoms and reducing the injury of diseased joints but also to preventing cardiovascular diseases, especially the occurrence of RA, to decrease mortality to the greatest extent. IL-17 may be an essential index for the early diagnosis of RA complicated with atherosclerosis. In the early stage of RA, through the detection of IL-17, cardiovascular disease could be diagnosed in time and interventions could be initiated. IL-17 may become a potential target in treatment. Taking appropriate measures to decrease the expression of IL-17 or prevent it from binding to the receptor to reduce the symptoms of RA and decrease the possibility of atherosclerosis may be a feasible direction for treating RA complicated with cardiovascular disease. However, some studies have also suggested that IL-17 has an anti-atherosclerotic effect. So what is the reason that IL-17 has atherosclerotic and anti-atherosclerotic functions, and will this double-edged sword function change our view on the link between autoimmune and cardiovascular diseases? Will it provide us with new ideas for the prevention and treatment of these diseases? This will be our next research direction.

AUTHOR CONTRIBUTIONS

Conception and design of the study—JW and LH; Drafting the article—JW; Revising the article critically for important intellectual content—WL, LH, and SL; Final approval of the version to be submitted—JW, WL; Agreement to be accountable for all aspects of the work in ensuring that questions related to the accuracy or integrity of any part of the work are appropriately investigated and resolved—JW, WL, LH, and SL.

FUNDING

This work is supported by the National Key Research and Development Program of China (No. 2017YFC1703304), the National Natural Science Foundation of China (No. 81873204), Sichuan Science and Technology Program (No. 2021YFS0040).

ACKNOWLEDGMENTS

The authors would like to thank LH, WL and SL for their help and support in this study.

REFERENCES

Abou-Raya, A., and Abou-Raya, S. (2006). Inflammation: A Pivotal Link between Autoimmune Diseases and Atherosclerosis. *Autoimmun. Rev.* 5 (5), 331–337. doi:10.1016/j.autrev.2005.12.006

Adamopoulos, I. E., Chao, C. C., Geissler, R., Laface, D., Blumenschein, W., Iwakura, Y., et al. (2010). Interleukin-17A Upregulates Receptor Activator of NF-kappaB on Osteoclast Precursors. *Arthritis Res. Ther.* 12 (1), R29. doi:10.1186/ar2936

Agarwal, S., Misra, R., and Aggarwal, A. (2008). Interleukin 17 Levels Are Increased in Juvenile Idiopathic Arthritis Synovial Fluid and Induce Synovial Fibroblasts to Produce Proinflammatory Cytokines and Matrix Metalloproteinases. *J. Rheumatol.* 35 (3), 515–519. doi:10.1016/j.jbspin.2008.01.020

Ait-Oufella, H., Salomon, B. L., Potteaux, S., Robertson, A. K., Gourdy, P., Zoll, J., et al. (2006). Natural Regulatory T Cells Control the Development of Atherosclerosis in Mice. *Nat. Med.* 12 (2), 178–180. doi:10.1038/nm1343

Anyfanti, P., Gavriilaki, E., Douma, S., and Gkaliagkousi, E. (2020). Endothelial Dysfunction in Patients with Rheumatoid Arthritis: the Role of Hypertension. *Curr. Hypertens. Rep.* 22 (8), 56. doi:10.1007/s11906-020-01064-y

Benedetti, G., Bonaventura, P., Lavocat, F., and Miossec, P. (2016). IL-17A and TNF-α Increase the Expression of the Antiapoptotic Adhesion Molecule Amigo-2 in Arthritis Synoviocytes. *Front. Immunol.* 7, 254. doi:10.3389/fimmu.2016.00254

Bennett, M. R., Sinha, S., and Owens, G. K. (2016). Vascular Smooth Muscle Cells in Atherosclerosis. *Circ. Res.* 118 (4), 692–702. doi:10.1161/CIRCRESAHA.115.306361

Beringer, A., Noack, M., and Miossec, P. (2016). IL-17 in Chronic Inflammation: From Discovery to Targeting. *Trends Mol. Med.* 22 (3), 230–241. doi:10.1016/j.molmed.2016.01.001

Bush, K. A., Farmer, K. M., Walker, J. S., and Kirkham, B. W. (2002). Reduction of Joint Inflammation and Bone Erosion in Rat Adjuvant Arthritis by Treatment with Interleukin-17 Receptor IgG1 Fc Fusion Protein. *Arthritis Rheum.* 46 (3), 802–805. doi:10.1002/art.10173

Butcher, M. J., Gjurich, B. N., Phillips, T., and Galkina, E. V. (2012). The IL-17A/IL-17RA axis Plays a Proatherogenic Role via the Regulation of Aortic Myeloid Cell Recruitment. *Circ. Res.* 110 (5), 675–687. doi:10.1161/CIRCRESAHA.111.261784

Chabaud, M., Durand, J. M., Buchs, N., Fossiez, F., Page, G., Frappart, L., et al. (1999). Human Interleukin-17: A T Cell-Derived Proinflammatory Cytokine Produced by the Rheumatoid Synovium. *Arthritis Rheum.* 42 (5), 963–970. doi:10.1002/1529-0131(199905)42:5<963:AID-ANR15>3.0.CO;2-E

Chao, C. C., Chen, S. J., Adamopoulos, I. E., Davis, N., Hong, K., Vu, A., et al. (2011). Anti-IL-17A Therapy Protects against Bone Erosion in Experimental Models of Rheumatoid Arthritis. *Autoimmunity* 44 (3), 243–252. doi:10.3109/08916934.2010.517815

Chistiakov, D. A., Orekhov, A. N., and Bobryshev, Y. V. (2015). Vascular Smooth Muscle Cell in Atherosclerosis. *Acta Physiol. (Oxf)* 214 (1), 33–50. doi:10.1111/apha.12466

Clarke, M. C., Littlewood, T. D., Figg, N., Maguire, J. J., Davenport, A. P., Goddard, M., et al. (2008). Chronic Apoptosis of Vascular Smooth Muscle Cells Accelerates Atherosclerosis and Promotes Calcification and Medial Degeneration. *Circ. Res.* 102 (12), 1529–1538. doi:10.1161/CIRCRESAHA.108.175976

Costa, C. M., Santos, M. A. T. D., and Pernambuco, A. P. (2019). Elevated Levels of Inflammatory Markers in Women with Rheumatoid Arthritis. *J. Immunoassay Immunochem* 40 (5), 540–554. doi:10.1080/15321819.2019.1649695

Crowson, C. S., Liao, K. P., Davis, J. M., Solomon, D. H., Matteson, E. L., Knutson, K. L., et al. (2013). Rheumatoid Arthritis and Cardiovascular Disease. *Am. Heart J.* 166 (4), 622–e1. doi:10.1016/j.ahj.2013.07.010

Dai, G., Kaazempur-Mofrad, M. R., Natarajan, S., Zhang, Y., Vaughn, S., Blackman, B. R., et al. (2004). Distinct Endothelial Phenotypes Evoked by Arterial Waveforms Derived from Atherosclerosis-Susceptible and -resistant Regions of Human Vasculature. *Proc. Natl. Acad. Sci. U S A.* 101 (41), 14871–14876. doi:10.1073/pnas.0406073101

Danzaki, K., Matsui, Y., Ikesue, M., Ohta, D., Ito, K., Kanayama, M., et al. (2012). Interleukin-17A Deficiency Accelerates Unstable Atherosclerotic Plaque Formation in Apolipoprotein E-Deficient Mice. *Arterioscler Thromb. Vasc. Biol.* 32 (2), 273–280. doi:10.1161/ATVBAHA.111.229997

del Rincón, I. D., Williams, K., Stern, M. P., Freeman, G. L., and Escalante, A. (2001). High Incidence of Cardiovascular Events in a Rheumatoid Arthritis Cohort Not Explained by Traditional Cardiac Risk Factors. *Arthritis Rheum.* 44 (12), 2737–2745. doi:10.1002/1529-0131(200112)44:12<2737:AID-ART460>3.0.CO;2-%23

Diez-Roux, A. V., Nieto, F. J., Comstock, G. W., Howard, G., and Szklo, M. (1995). The Relationship of Active and Passive Smoking to Carotid Atherosclerosis 12-14 Years Later. *Prev. Med.* 24 (1), 48–55. doi:10.1006/pmed.1995.1007

Duan, X. Y., Xie, P. L., Ma, Y. L., and Tang, S. Y. (2011). Omentin Inhibits Osteoblastic Differentiation of Calcifying Vascular Smooth Muscle Cells through the PI3K/Akt Pathway. *Amino Acids* 41 (5), 1223–1231. doi:10.1007/s00726-010-0800-3

Duvallet, E., Semerano, L., Assier, E., Falgarone, G., and Boissier, M. C. (2011). Interleukin-23: a Key Cytokine in Inflammatory Diseases. *Ann. Med.* 43 (7), 503–511. doi:10.3109/07853890.2011.577093

Eid, R. E., Rao, D. A., Zhou, J., Lo, S. F., Ranjbaran, H., Gallo, A., et al. (2009). Interleukin-17 and Interferon-Gamma Are Produced Concomitantly by Human Coronary Artery-Infiltrating T Cells and Act Synergistically on Vascular Smooth Muscle Cells. *Circulation* 119 (10), 1424–1432. doi:10.1161/CIRCULATIONAHA.108.827618

El-Maghraby, H. M., Rabie, R. A., and Makram, W. K. (2019). Correlation between Relative Expression of IL 17 and PERP in Rheumatoid Arthritis Patients and Disease Activity. *Egypt. J. Immunol.* 26 (2), 19–29.

Erb, N., Pace, A. V., Douglas, K. M., Banks, M. J., and Kitas, G. D. (2004). Risk Assessment for Coronary Heart Disease in Rheumatoid Arthritis and Osteoarthritis. *Scand. J. Rheumatol.* 33 (5), 293–299. doi:10.1080/03009740410006899

Erbel, C., Akhavanpoor, M., Okuyucu, D., Wangler, S., Dietz, A., Zhao, L., et al. (2014). IL-17A Influences Essential Functions of the Monocyte/macrophage Lineage and Is Involved in Advanced Murine and Human Atherosclerosis. *J. Immunol.* 193 (9), 4344–4355. doi:10.4049/jimmunol.1400181

Erbel, C., Chen, L., Bea, F., Wangler, S., Celik, S., Lasitschka, F., et al. (2009). Inhibition of IL-17A Attenuates Atherosclerotic Lesion Development in apoE-Deficient Mice. *J. Immunol.* 183 (12), 8167–8175. doi:10.4049/jimmunol.0901126

Everett, B. M., Pradhan, A. D., Solomon, D. H., Paynter, N., Macfadyen, J., Zaharris, E., et al. (2013). Rationale and Design of the Cardiovascular Inflammation Reduction Trial: a Test of the Inflammatory Hypothesis of Atherothrombosis. *Am. Heart J.* 166 (2), 199–e15. doi:10.1016/j.ahj.2013.03.018

Feldmann, M., Brennan, F. M., Foxwell, B. M., Taylor, P. C., Williams, R. O., and Maini, R. N. (2005). Anti-TNF Therapy: where Have We Got to in 2005? *J. Autoimmun.* 25 (Suppl. l), 26–28. doi:10.1016/j.jaut.2005.09.006

Finn, A. V., Nakano, M., Narula, J., Kolodgie, F. D., and Virmani, R. (2010). Concept of Vulnerable/unstable Plaque. *Arterioscler Thromb. Vasc. Biol.* 30 (7), 1282–1292. doi:10.1161/ATVBAHA.108.179739

Folkesson, M., Kazi, M., Zhu, C., Silveira, A., Hemdahl, A. L., Hamsten, A., et al. (2007). Presence of NGAL/MMP-9 Complexes in Human Abdominal Aortic Aneurysms. *Thromb. Haemost.* 98 (2), 427–433. doi:10.1016/j.vph.2006.08.381

Fossiez, F., Djossou, O., Chomarat, P., Flores-Romo, L., Ait-Yahia, S., Maat, C., et al. (1996). T Cell Interleukin-17 Induces Stromal Cells to Produce Proinflammatory and Hematopoietic Cytokines. *J. Exp. Med.* 183 (6), 2593–2603. doi:10.1084/jem.183.6.2593

Frostegård, J. (2013). Immunity, Atherosclerosis and Cardiovascular Disease. *BMC Med.* 11, 117. doi:10.1186/1741-7015-11-117

Gabriel, S. E. (2001). The Epidemiology of Rheumatoid Arthritis. *Rheum. Dis. Clin. North. Am.* 27 (2), 269–281. doi:10.1016/s0889-857x(05)70201-5

Gao, Q., Jiang, Y., Ma, T., Zhu, F., Gao, F., Zhang, P., et al. (2010). A Critical Function of Th17 Proinflammatory Cells in the Development of Atherosclerotic Plaque in Mice. *J. Immunol.* 185 (10), 5820–5827. doi:10.4049/jimmunol.1000116

García-Gómez, C., Bianchi, M., de la Fuente, D., Badimon, L., Padró, T., Corbella, E., et al. (2014). Inflammation, Lipid Metabolism and Cardiovascular Risk in Rheumatoid Arthritis: A Qualitative Relationship? *World J. Orthop.* 5 (3), 304–311. doi:10.5312/wjo.v5.i3.304

Gerli, R., Sherer, Y., Vaudo, G., Schillaci, G., Gilburd, B., Giordano, A., et al. (2005). Early Atherosclerosis in Rheumatoid Arthritis: Effects of Smoking on Thickness

of the Carotid Artery Intima media. *Ann. N. Y Acad. Sci.* 1051, 281–290. doi:10.1196/annals.1361.069

Gisterå, A., Robertson, A. K., Andersson, J., Ketelhuth, D. F., Ovchinnikova, O., Nilsson, S. K., et al. (2013). Transforming Growth Factor-β Signaling in T Cells Promotes Stabilization of Atherosclerotic Plaques through an Interleukin-17-dependent Pathway. *Sci. Transl Med.* 5 (196), 196ra100196ra00. doi:10.1126/scitranslmed.3006133

Goodson, N. J., Symmons, D. P., Scott, D. G., Bunn, D., Lunt, M., and Silman, A. J. (2005). Baseline Levels of C-Reactive Protein and Prediction of Death from Cardiovascular Disease in Patients with Inflammatory Polyarthritis: a Ten-Year Followup Study of a Primary Care-Based Inception Cohort. *Arthritis Rheum.* 52 (8), 2293–2299. doi:10.1002/art.21204

Gravallese, E. M., and Schett, G. (2018). Effects of the IL-23-IL-17 Pathway on Bone in Spondyloarthritis. *Nat. Rev. Rheumatol.* 14 (11), 631–640. doi:10.1038/s41584-018-0091-8

Gullick, N. J., Abozaid, H. S., Jayaraj, D. M., Evans, H. G., Scott, D. L., Choy, E. H., et al. (2013). Enhanced and Persistent Levels of Interleukin (IL)-17$^+$ CD4$^+$ T Cells and Serum IL-17 in Patients with Early Inflammatory Arthritis. *Clin. Exp. Immunol.* 174 (2), 292–301. doi:10.1111/cei.12167

Gullick, N. J., Evans, H. G., Church, L. D., Jayaraj, D. M., Filer, A., Kirkham, B. W., et al. (2010). Linking Power Doppler Ultrasound to the Presence of Th17 Cells in the Rheumatoid Arthritis Joint. *PLoS One* 5 (9). doi:10.1371/journal.pone.0012516

Hansson, G. K. (2005). Inflammation, Atherosclerosis, and Coronary Artery Disease. *N. Engl. J. Med.* 352 (16), 1685–1695. doi:10.1056/NEJMra043430

Hansson, G. K., Libby, P., and Tabas, I. (2015). Inflammation and Plaque Vulnerability. *J. Intern. Med.* 278 (5), 483–493. doi:10.1111/joim.12406

Hansson, G. K., and Libby, P. (2006). The Immune Response in Atherosclerosis: a Double-Edged Sword. *Nat. Rev. Immunol.* 6 (7), 508–519. doi:10.1038/nri1882

Harvey, E. J., and Ramji, D. P. (2005). Interferon-gamma and Atherosclerosis: Pro- or Anti-atherogenic? *Cardiovasc. Res.* 67 (1), 11–20. doi:10.1016/j.cardiores.2005.04.019

Hattori, T., Ogura, N., Akutsu, M., Kawashima, M., Watanabe, S., Ito, K., et al. (2015). Gene Expression Profiling of IL-17A-Treated Synovial Fibroblasts from the Human Temporomandibular Joint. *Mediators Inflamm.* 2015, 436067. doi:10.1155/2015/436067

Helmick, C. G., Felson, D. T., Lawrence, R. C., Gabriel, S., Hirsch, R., Kwoh, C. K., et al. (2008). Estimates of the Prevalence of Arthritis and Other Rheumatic Conditions in the United States. Part I. *Arthritis Rheum.* 58 (1), 15–25. doi:10.1002/art.23177

Hemdahl, A. L., Gabrielsen, A., Zhu, C., Eriksson, P., Hedin, U., Kastrup, J., et al. (2006). Expression of Neutrophil Gelatinase-Associated Lipocalin in Atherosclerosis and Myocardial Infarction. *Arterioscler Thromb. Vasc. Biol.* 26 (1), 136–142. doi:10.1161/01.ATV.0000193567.88685.f4

Hot, A., Lenief, V., and Miossec, P. (2012). Combination of IL-17 and TNFα Induces a Pro-inflammatory, Pro-coagulant and Pro-thrombotic Phenotype in Human Endothelial Cells. *Ann. Rheum. Dis.* 71 (5), 768–776. doi:10.1136/annrheumdis-2011-200468

Iseme, R. A., McEvoy, M., Kelly, B., Agnew, L., Walker, F. R., Handley, T., et al. (2017). A Role for Autoantibodies in Atherogenesis. *Cardiovasc. Res.* 113 (10), 1102–1112. doi:10.1093/cvr/cvx112

Iwakura, Y., Ishigame, H., Saijo, S., and Nakae, S. (2011). Functional Specialization of Interleukin-17 Family Members. *Immunity* 34 (2), 149–162. doi:10.1016/j.immuni.2011.02.012

Jones, C. B., Sane, D. C., and Herrington, D. M. (2003). Matrix Metalloproteinases: a Review of Their Structure and Role in Acute Coronary Syndrome. *Cardiovasc. Res.* 59 (4), 812–823. doi:10.1016/s0008-6363(03)00516-9

Kadoglou, N. P., Gkontopoulos, A., Kapelouzou, A., Fotiadis, G., Theofilogiannakos, E. K., Kottas, G., et al. (2011). Serum Levels of Vaspin and Visfatin in Patients with Coronary Artery Disease-Kozani Study. *Clin. Chim. Acta* 412 (1-2), 48–52. doi:10.1016/j.cca.2010.09.012

Kershaw, E. E., and Flier, J. S. (2004). Adipose Tissue as an Endocrine Organ. *J. Clin. Endocrinol. Metab.* 89 (6), 2548–2556. doi:10.1210/jc.2004-0395

Khan, S., Greenberg, J. D., and Bhardwaj, N. (2009). Dendritic Cells as Targets for Therapy in Rheumatoid Arthritis. *Nat. Rev. Rheumatol.* 5 (10), 566–571. doi:10.1038/nrrheum.2009.185

Kim, K. W., Cho, M. L., Park, M. K., Yoon, C. H., Park, S. H., Lee, S. H., et al. (2005). Increased Interleukin-17 Production via a Phosphoinositide 3-kinase/Akt and Nuclear Factor kappaB-dependent Pathway in Patients with Rheumatoid Arthritis. *Arthritis Res. Ther.* 7 (1), R139–R148. doi:10.1186/ar1470

Kirkham, B. W., Lassere, M. N., Edmonds, J. P., Juhasz, K. M., Bird, P. A., Lee, C. S., et al. (2006). Synovial Membrane Cytokine Expression Is Predictive of Joint Damage Progression in Rheumatoid Arthritis: a Two-Year Prospective Study (The DAMAGE Study Cohort). *Arthritis Rheum.* 54 (4), 1122–1131. doi:10.1002/art.21749

Kitas, G., Banks, M., and Bacon, P. (1998). Accelerated Atherosclerosis as a Cause of Cardiovascular Death in RA. *Pathogenesis* 1 (2), 73–83.

Kitas, G. D., and Erb, N. (2003). Tackling Ischaemic Heart Disease in Rheumatoid Arthritis. *Rheumatology (Oxford)* 42 (5), 607–613. doi:10.1093/rheumatology/keg175

Klareskog, L., Stolt, P., Lundberg, K., Källberg, H., Bengtsson, C., Grunewald, J., et al. (2006). A New Model for an Etiology of Rheumatoid Arthritis: Smoking May Trigger HLA-DR (Shared Epitope)-Restricted Immune Reactions to Autoantigens Modified by Citrullination. *Arthritis Rheum.* 54 (1), 38–46. doi:10.1002/art.21575

Koenders, M. I., Kolls, J. K., Oppers-Walgreen, B., van den Bersselaar, L., Joosten, L. A., Schurr, J. R., et al. (2005). Interleukin-17 Receptor Deficiency Results in Impaired Synovial Expression of Interleukin-1 and Matrix Metalloproteinases 3, 9, and 13 and Prevents Cartilage Destruction during Chronic Reactivated Streptococcal Cell wall-induced Arthritis. *Arthritis Rheum.* 52 (10), 3239–3247. doi:10.1002/art.21342

Kokkonen, H., Söderström, I., Rocklöv, J., Hallmans, G., Lejon, K., and Rantapää Dahlqvist, S. (2010). Up-regulation of Cytokines and Chemokines Predates the Onset of Rheumatoid Arthritis. *Arthritis Rheum.* 62 (2), 383–391. doi:10.1002/art.27186

Kraan, M. C., Versendaal, H., Jonker, M., Bresnihan, B., Post, W. J., t Hart, B. A., et al. (1998). Asymptomatic Synovitis Precedes Clinically Manifest Arthritis. *Arthritis Rheum.* 41 (8), 1481–1488. doi:10.1002/1529-0131(199808)41:8<1481:AID-ART19>3.0.CO;2-O

Lee, S. Y., Kwok, S. K., Son, H. J., Ryu, J. G., Kim, E. K., Oh, H. J., et al. (2013). IL-17-mediated Bcl-2 Expression Regulates Survival of Fibroblast-like Synoviocytes in Rheumatoid Arthritis through STAT3 Activation. *Arthritis Res. Ther.* 15 (1), R31. doi:10.1186/ar4179

Lee, Y. H., and Bae, S. C. (2017). Associations between Circulating IL-17 Levels and Rheumatoid Arthritis and between IL-17 Gene Polymorphisms and Disease Susceptibility: a Meta-Analysis. *Postgrad. Med. J.* 93 (1102), 465–471. doi:10.1136/postgradmedj-2016-134637

Leipe, J., Grunke, M., Dechant, C., Reindl, C., Kerzendorf, U., Schulze-Koops, H., et al. (2010). Role of Th17 Cells in Human Autoimmune Arthritis. *Arthritis Rheum.* 62 (10), 2876–2885. doi:10.1002/art.27622

Li, N., Wang, J. C., Liang, T. H., Zhu, M. H., Wang, J. Y., Fu, X. L., et al. (2013). Pathologic Finding of Increased Expression of Interleukin-17 in the Synovial Tissue of Rheumatoid Arthritis Patients. *Int. J. Clin. Exp. Pathol.* 6 (7), 1375–1379. doi:10.1159/000354821

Li, Q., Ren, G., Xu, L., Wang, Q., Qi, J., Wang, W., et al. (2014). Therapeutic Efficacy of Three Bispecific Antibodies on Collagen-Induced Arthritis Mouse Model. *Int. Immunopharmacol* 21 (1), 119–127. doi:10.1016/j.intimp.2014.04.018

Libby, P., Ridker, P. M., and Hansson, G. K. (2009). Inflammation in Atherosclerosis: from Pathophysiology to Practice. *J. Am. Coll. Cardiol.* 54 (23), 2129–2138. doi:10.1016/j.jacc.2009.09.009

Lillegraven, S., van der Heijde, D., Uhlig, T., Kvien, T. K., and Haavardsholm, E. A. (2012). What Is the Clinical Relevance of Erosions and Joint Space Narrowing in RA? *Nat. Rev. Rheumatol.* 8 (2), 117–120. doi:10.1038/nrrheum.2011.202

Linn-Rasker, S. P., van der Helm-van Mil, A. H., van Gaalen, F. A., Kloppenburg, M., de Vries, R. R., le Cessie, S., et al. (2006). Smoking Is a Risk Factor for Anti-CCP Antibodies Only in Rheumatoid Arthritis Patients Who Carry HLA-DRB1 Shared Epitope Alleles. *Ann. Rheum. Dis.* 65 (3), 366–371. doi:10.1136/ard.2005.041079

Liu, C. L., Shen, D. L., Zhu, K., Tang, J. N., Hai, Q. M., and Zhang, J. Y. (2013). Levels of Interleukin-33 and Interleukin-6 in Patients with Acute Coronary Syndrome or Stable Angina. *Clin. Invest. Med.* 36 (4), E234–E241. doi:10.25011/cim.v36i4.19957

Lu, X. (2017). The Impact of IL-17 in Atherosclerosis. *Curr. Med. Chem.* 24 (21), 2345–2358. doi:10.2174/0929867324666170419150614

Lubberts, E., Joosten, L. A., Oppers, B., van den Bersselaar, L., Coenen-de Roo, C. J., Kolls, J. K., et al. (2001). IL-1-independent Role of IL-17 in Synovial

Inflammation and Joint Destruction during Collagen-Induced Arthritis. *J. Immunol.* 167 (2), 1004–1013. doi:10.4049/jimmunol.167.2.1004

Lubberts, E., Joosten, L. A., van de Loo, F. A., Schwarzenberger, P., Kolls, J., and van den Berg, W. B. (2002). Overexpression of IL-17 in the Knee Joint of Collagen Type II Immunized Mice Promotes Collagen Arthritis and Aggravates Joint Destruction. *Inflamm. Res.* 51 (2), 102–104. doi:10.1007/BF02684010

Lubberts, E., Koenders, M. I., Oppers-Walgreen, B., van den Bersselaar, L., Coenen-de Roo, C. J., Joosten, L. A., et al. (2004). Treatment with a Neutralizing Anti-murine Interleukin-17 Antibody after the Onset of Collagen-Induced Arthritis Reduces Joint Inflammation, Cartilage Destruction, and Bone Erosion. *Arthritis Rheum.* 50 (2), 650–659. doi:10.1002/art.20001

Lubberts, E., van den Bersselaar, L., Oppers-Walgreen, B., Schwarzenberger, P., Coenen-de Roo, C. J., Kolls, J. K., et al. (2003). IL-17 Promotes Bone Erosion in Murine Collagen-Induced Arthritis through Loss of the Receptor Activator of NF-Kappa B Ligand/osteoprotegerin Balance. *J. Immunol.* 170 (5), 2655–2662. doi:10.4049/jimmunol.170.5.2655

Madhur, M. S., Lob, H. E., McCann, L. A., Iwakura, Y., Blinder, Y., Guzik, T. J., et al. (2010). Interleukin 17 Promotes Angiotensin II-Induced Hypertension and Vascular Dysfunction. *Hypertension* 55 (2), 500–507. doi:10.1161/HYPERTENSIONAHA.109.145094

Maracle, C. X., Agca, R., Helder, B., Meeuwsen, J. A. L., Niessen, H. W. M., Biessen, E. A. L., et al. (2018). Noncanonical NF-Kb Signaling in Microvessels of Atherosclerotic Lesions Is Associated with Inflammation, Atheromatous Plaque Morphology and Myocardial Infarction. *Atherosclerosis* 270, 33–41. doi:10.1016/j.atherosclerosis.2018.01.032

Maradit-Kremers, H., Nicola, P. J., Crowson, C. S., Ballman, K. V., and Gabriel, S. E. (2005). Cardiovascular Death in Rheumatoid Arthritis: a Population-Based Study. *Arthritis Rheum.* 52 (3), 722–732. doi:10.1002/art.20878

McEntegart, A., Capell, H. A., Creran, D., Rumley, A., Woodward, M., and Lowe, G. D. (2001). Cardiovascular Risk Factors, Including Thrombotic Variables, in a Population with Rheumatoid Arthritis. *Rheumatology (Oxford)* 40 (6), 640–644. doi:10.1093/rheumatology/40.6.640

Mehta, N. N., Teague, H. L., Swindell, W. R., Baumer, Y., Ward, N. L., Xing, X., et al. (2017). IFN-γ and TNF-α Synergism May Provide a Link between Psoriasis and Inflammatory Atherogenesis. *Sci. Rep.* 7 (1), 13831. doi:10.1038/s41598-017-14365-1

Mellado, M., Martínez-Muñoz, L., Cascio, G., Lucas, P., Pablos, J. L., and Rodríguez-Frade, J. M. (2015). T Cell Migration in Rheumatoid Arthritis. *Front. Immunol.* 6, 384. doi:10.3389/fimmu.2015.00384

Mummidi, S., Das, N. A., Carpenter, A. J., Yoshida, T., Yariswamy, M., Mostany, R., et al. (2019). RECK Suppresses Interleukin-17/traf3ip2-Mediated MMP-13 Activation and Human Aortic Smooth Muscle Cell Migration and Proliferation. *J. Cell Physiol* 234 (12), 22242–22259. doi:10.1002/jcp.28792

Myasoedova, E., Crowson, C. S., Kremers, H. M., Therneau, T. M., and Gabriel, S. E. (2010). Is the Incidence of Rheumatoid Arthritis Rising?: Results from Olmsted County, Minnesota, 1955-2007. *Arthritis Rheum.* 62 (6), 1576–1582. doi:10.1002/art.27425

Nakae, S., Nambu, A., Sudo, K., and Iwakura, Y. (2003). Suppression of Immune Induction of Collagen-Induced Arthritis in IL-17-deficient Mice. *J. Immunol.* 171 (11), 6173–6177. doi:10.4049/jimmunol.171.11.6173

Nordlohne, J., and von Vietinghoff, S. (2019). Interleukin 17A in Atherosclerosis - Regulation and Pathophysiologic Effector Function. *Cytokine* 122, 154089. doi:10.1016/j.cyto.2017.06.016

Osta, B., Lavocat, F., Eljaafari, A., and Miossec, P. (2014). Effects of Interleukin-17A on Osteogenic Differentiation of Isolated Human Mesenchymal Stem Cells. *Front. Immunol.* 5, 425. doi:10.3389/fimmu.2014.00425

Padyukov, L., Silva, C., Stolt, P., Alfredsson, L., and Klareskog, L. (2004). A Gene-Environment Interaction between Smoking and Shared Epitope Genes in HLA-DR Provides a High Risk of Seropositive Rheumatoid Arthritis. *Arthritis Rheum.* 50 (10), 3085–3092. doi:10.1002/art.20553

Pasceri, V., and Yeh, E. T. (1999). A Tale of Two Diseases: Atherosclerosis and Rheumatoid Arthritis. *Circulation* 100 (21), 2124–2126. doi:10.1161/01.cir.100.21.2124

Pöllinger, B., Junt, T., Metzler, B., Walker, U. A., Tyndall, A., Allard, C., et al. (2011). Th17 Cells, Not IL-17+ γδ T Cells, Drive Arthritic Bone Destruction in Mice and Humans. *J. Immunol.* 186 (4), 2602–2612. doi:10.4049/jimmunol.1003370

Prasad, M., Hermann, J., Gabriel, S. E., Weyand, C. M., Mulvagh, S., Mankad, R., et al. (2015). Cardiorheumatology: Cardiac Involvement in Systemic Rheumatic Disease. *Nat. Rev. Cardiol.* 12 (3), 168–176. doi:10.1038/nrcardio.2014.206

Qian, Y., Liu, C., Hartupee, J., Altuntas, C. Z., Gulen, M. F., Jane-Wit, D., et al. (2007). The Adaptor Act1 Is Required for Interleukin 17-dependent Signaling Associated with Autoimmune and Inflammatory Disease. *Nat. Immunol.* 8 (3), 247–256. doi:10.1038/ni1439

Rantapää-Dahlqvist, S., de Jong, B. A., Berglin, E., Hallmans, G., Wadell, G., Stenlund, H., et al. (2003). Antibodies against Cyclic Citrullinated Peptide and IgA Rheumatoid Factor Predict the Development of Rheumatoid Arthritis. *Arthritis Rheum.* 48 (10), 2741–2749. doi:10.1002/art.11223

Raychaudhuri, S. P., Raychaudhuri, S. K., and Genovese, M. C. (2012). IL-17 Receptor and its Functional Significance in Psoriatic Arthritis. *Mol. Cell Biochem* 359 (1-2), 419–429. doi:10.1007/s11010-011-1036-6

Raza, K., Falciani, F., Curnow, S. J., Ross, E. J., Lee, C. Y., Akbar, A. N., et al. (2005). Early Rheumatoid Arthritis Is Characterized by a Distinct and Transient Synovial Fluid Cytokine Profile of T Cell and Stromal Cell Origin. *Arthritis Res. Ther.* 7 (4), R784–R795. doi:10.1186/ar1733

Robert, M., and Miossec, P. (2017). Effects of Interleukin 17 on the Cardiovascular System. *Autoimmun. Rev.* 16 (9), 984–991. doi:10.1016/j.autrev.2017.07.009

Rolin, J., and Maghazachi, A. A. (2014). Implications of Chemokines, Chemokine Receptors, and Inflammatory Lipids in Atherosclerosis. *J. Leukoc. Biol.* 95 (4), 575–585. doi:10.1189/jlb.1113571

Ross, R. (1999). Atherosclerosis--an Inflammatory Disease. *N. Engl. J. Med.* 340 (2), 115–126. doi:10.1056/NEJM199901143400207

Roşu, A., Mărgăritescu, C., Stepan, A., Mușetescu, A., and Ene, M. (2012). IL-17 Patterns in Synovium, Serum and Synovial Fluid from Treatment-Naïve, Early Rheumatoid Arthritis Patients. *Rom. J. Morphol. Embryol.* 53 (1), 73–80.

Roth, G. A., Johnson, C., Abajobir, A., Abd-Allah, F., Abera, S. F., Abyu, G., et al. (2017). Global, Regional, and National Burden of Cardiovascular Diseases for 10 Causes, 1990 to 2015. *J. Am. Coll. Cardiol.* 70 (1), 1–25. doi:10.1016/j.jacc.2017.04.052

Salonen, R., and Salonen, J. T. (1991). Determinants of Carotid Intima-media Thickness: a Population-Based Ultrasonography Study in Eastern Finnish Men. *J. Intern. Med.* 229 (3), 225–231. doi:10.1111/j.1365-2796.1991.tb00336.x

Schofield, C., Fischer, S. K., Townsend, M. J., Mosesova, S., Peng, K., Setiadi, A. F., et al. (2016). Characterization of IL-17AA and IL-17FF in Rheumatoid Arthritis and Multiple Sclerosis. *Bioanalysis* 8 (22), 2317–2327. doi:10.4155/bio-2016-0207

Scott, D. L., Wolfe, F., and Huizinga, T. W. (2010). Rheumatoid Arthritis. *Lancet* 376 (9746), 1094–1108. doi:10.1016/S0140-6736(10)60826-4

Shen, H., Goodall, J. C., and Hill Gaston, J. S. (2009). Frequency and Phenotype of Peripheral Blood Th17 Cells in Ankylosing Spondylitis and Rheumatoid Arthritis. *Arthritis Rheum.* 60 (6), 1647–1656. doi:10.1002/art.24568

Silman, A. J., Newman, J., and MacGregor, A. J. (1996). Cigarette Smoking Increases the Risk of Rheumatoid Arthritis. Results from a Nationwide Study of Disease-Discordant Twins. *Arthritis Rheum.* 39 (5), 732–735. doi:10.1002/art.1780390504

Siloşi, I., Boldeanu, M. V., Cojocaru, M., Biciuşcă, V., Pădureanu, V., Bogdan, M., et al. (2016). The Relationship of Cytokines IL-13 and IL-17 with Autoantibodies Profile in Early Rheumatoid Arthritis. *J. Immunol. Res.* 2016, 3109135. doi:10.1155/2016/3109135

Simon, T., Taleb, S., Danchin, N., Laurans, L., Rousseau, B., Cattan, S., et al. (2013). Circulating Levels of Interleukin-17 and Cardiovascular Outcomes in Patients with Acute Myocardial Infarction. *Eur. Heart J.* 34 (8), 570–577. doi:10.1093/eurheartj/ehs263

Situnayake, R. D., and Kitas, G. (1997). Dyslipidemia and Rheumatoid Arthritis. *Ann. Rheum. Dis.* 56 (6), 341–342. doi:10.1136/ard.56.6.341

Sivalingam, Z., Larsen, S. B., Grove, E. L., Hvas, A. M., Kristensen, S. D., and Magnusson, N. E. (2017). Neutrophil Gelatinase-Associated Lipocalin as a Risk Marker in Cardiovascular Disease. *Clin. Chem. Lab. Med.* 56 (1), 5–18. doi:10.1515/cclm-2017-0120

Smith, E., Prasad, K. M., Butcher, M., Dobrian, A., Kolls, J. K., Ley, K., et al. (2010). Blockade of interleukin-17A Results in Reduced Atherosclerosis in Apolipoprotein E-Deficient Mice. *Circulation* 121 (15), 1746–1755. doi:10.1161/CIRCULATIONAHA.109.924886

Smith, J. D., Trogan, E., Ginsberg, M., Grigaux, C., Tian, J., and Miyata, M. (1995). Decreased Atherosclerosis in Mice Deficient in Both Macrophage colony-

stimulating Factor (Op) and Apolipoprotein E. *Proc. Natl. Acad. Sci. U S A.* 92 (18), 8264–8268. doi:10.1073/pnas.92.18.8264

Soltanzadeh-Yamchi, M., Shahbazi, M., Aslani, S., and Mohammadnia-Afrouzi, M. (2018). MicroRNA Signature of Regulatory T Cells in Health and Autoimmunity. *Biomed. Pharmacother.* 100, 316–323. doi:10.1016/j.biopha.2018.02.030

Song, D., Fang, G., Mao, S. Z., Ye, X., Liu, G., Miller, E. J., et al. (2018). Reply to: "Comments and Question on "Selective Inhibition of endothelial NF-Kb Signaling Attenuates Chronic Intermittent Hypoxia-Induced Atherosclerosis in Mice"". *Atherosclerosis* 272, 248–275. doi:10.1016/j.atherosclerosis.2018.01.02710.1016/j.atherosclerosis.2018.03.034

Stavropoulos-Kalinoglou, A., Metsios, G. S., Koutedakis, Y., Nevill, A. M., Douglas, K. M., Jamurtas, A., et al. (2007). Redefining Overweight and Obesity in Rheumatoid Arthritis Patients. *Ann. Rheum. Dis.* 66 (10), 1316–1321. doi:10.1136/ard.2006.060319

Taleb, S., Romain, M., Ramkhelawon, B., Uyttenhove, C., Pasterkamp, G., Herbin, O., et al. (2009). Loss of SOCS3 Expression in T Cells Reveals a Regulatory Role for Interleukin-17 in Atherosclerosis. *J. Exp. Med.* 206 (10), 2067–2077. doi:10.1084/jem.20090545

Tedgui, A., and Mallat, Z. (2006). Cytokines in Atherosclerosis: Pathogenic and Regulatory Pathways. *Physiol. Rev.* 86 (2), 515–581. doi:10.1152/physrev.00024.2005

Toh, M. L., Gonzales, G., Koenders, M. I., Tournadre, A., Boyle, D., Lubberts, E., et al. (2010). Role of Interleukin 17 in Arthritis Chronicity through Survival of Synoviocytes via Regulation of Synoviolin Expression. *PLoS One* 5 (10), e13416. doi:10.1371/journal.pone.0013416

Tsuji, S., Uehori, J., Matsumoto, M., Suzuki, Y., Matsuhisa, A., Toyoshima, K., et al. (2001). Human Intelectin Is a Novel Soluble Lectin that Recognizes Galactofuranose in Carbohydrate Chains of Bacterial Cell wall. *J. Biol. Chem.* 276 (26), 23456–23463. doi:10.1074/jbc.M103162200

van den Berg, W. B., and Miossec, P. (2009). IL-17 as a Future Therapeutic Target for Rheumatoid Arthritis. *Nat. Rev. Rheumatol.* 5 (10), 549–553. doi:10.1038/nrrheum.2009.179

Van Doornum, S., McColl, G., and Wicks, I. P. (2002). Accelerated Atherosclerosis: an Extraarticular Feature of Rheumatoid Arthritis? *Arthritis Rheum.* 46 (4), 862–873. doi:10.1002/art.10089

van Es, T., van Puijvelde, G. H., Ramos, O. H., Segers, F. M., Joosten, L. A., van den Berg, W. B., et al. (2009). Attenuated Atherosclerosis upon IL-17R Signaling Disruption in LDLr Deficient Mice. *Biochem. Biophys. Res. Commun.* 388 (2), 261–265. doi:10.1016/j.bbrc.2009.07.152

Vossenaar, E. R., and van Venrooij, W. J. (2004). Citrullinated Proteins: sparks that May Ignite the Fire in Rheumatoid Arthritis. *Arthritis Res. Ther.* 6 (3), 107–111. doi:10.1186/ar1184

Weber, C., and Noels, H. (2011). Atherosclerosis: Current Pathogenesis and Therapeutic Options. *Nat. Med.* 17 (11), 1410–1422. doi:10.1038/nm.2538

Winchester, R., Giles, J. T., Nativ, S., Downer, K., Zhang, H. Z., Bag-Ozbek, A., et al. (2016). Association of Elevations of Specific T Cell and Monocyte Subpopulations in Rheumatoid Arthritis with Subclinical Coronary Artery Atherosclerosis. *Arthritis Rheumatol.* 68 (1), 92–102. doi:10.1002/art.39419

Wolfe, F., Mitchell, D. M., Sibley, J. T., Fries, J. F., Bloch, D. A., Williams, C. A., et al. (1994). The Mortality of Rheumatoid Arthritis. *Arthritis Rheum.* 37 (4), 481–494. doi:10.1002/art.1780370408

Wolfe, F. (2000). The Effect of Smoking on Clinical, Laboratory, and Radiographic Status in Rheumatoid Arthritis. *J. Rheumatol.* 27 (3), 630–637. doi:10.1097/00002281-200003000-00010

Wu, Q., Chen, Y., Chen, S., Wu, X., and Nong, W. (2020). Correlation between Adiponectin, Chemerin, Vascular Endothelial Growth Factor and Epicardial Fat Volume in Patients with Coronary Artery Disease. *Exp. Ther. Med.* 19 (2), 1095–1102. doi:10.3892/etm.2019.8299

Wu, S., Meng, Z., and Zhang, Y. (2018). Correlation between Rheumatoid Arthritis and Immunological Changes in a Rheumatoid Arthritis Rat Model. *J. Biol. Regul. Homeost Agents* 32 (6), 1461–1466.

Xie, C., and Chen, Q. (2019). Adipokines: New Therapeutic Target for Osteoarthritis? *Curr. Rheumatol. Rep.* 21 (12), 71. doi:10.1007/s11926-019-0868-z

Yamawaki, H., Kuramoto, J., Kameshima, S., Usui, T., Okada, M., and Hara, Y. (2011). Omentin, a Novel Adipocytokine Inhibits TNF-Induced Vascular Inflammation in Human Endothelial Cells. *Biochem. Biophys. Res. Commun.* 408 (2), 339–343. doi:10.1016/j.bbrc.2011.04.039

Yamawaki, H., Tsubaki, N., Mukohda, M., Okada, M., and Hara, Y. (2010). Omentin, a Novel Adipokine, Induces Vasodilation in Rat Isolated Blood Vessels. *Biochem. Biophys. Res. Commun.* 393 (4), 668–672. doi:10.1016/j.bbrc.2010.02.053

Yuan, S., Zhang, S., Zhuang, Y., Zhang, H., Bai, J., and Hou, Q. (2015). Interleukin-17 Stimulates STAT3-Mediated Endothelial Cell Activation for Neutrophil Recruitment. *Cell Physiol Biochem* 36 (6), 2340–2356. doi:10.1159/000430197

Zhang, K., Zhang, F., Yang, J. M., Kong, J., Meng, X., Zhang, M., et al. (2018). Silencing of Non-POU-domain-containing Octamer-Binding Protein Stabilizes Atherosclerotic Plaque in Apolipoprotein E-Knockout Mice via NF-Kb Signaling Pathway. *Int. J. Cardiol.* 263, 96–103. doi:10.1016/j.ijcard.2018.04.018

Zhang, S., Yuan, J., Yu, M., Fan, H., Guo, Z. Q., Yang, R., et al. (2012). IL-17A Facilitates Platelet Function through the ERK2 Signaling Pathway in Patients with Acute Coronary Syndrome. *PLoS One* 7 (7), e40641. doi:10.1371/journal.pone.0040641

Zhang, Y., Ren, G., Guo, M., Ye, X., Zhao, J., Xu, L., et al. (2013). Synergistic Effects of Interleukin-1β and interleukin-17A Antibodies on Collagen-Induced Arthritis Mouse Model. *Int. Immunopharmacol* 15 (2), 199–205. doi:10.1016/j.intimp.2012.12.010

Zhu, F., Wang, Q., Guo, C., Wang, X., Cao, X., Shi, Y., et al. (2011). IL-17 Induces Apoptosis of Vascular Endothelial Cells: a Potential Mechanism for Human Acute Coronary Syndrome. *Clin. Immunol.* 141 (2), 152–160. doi:10.1016/j.clim.2011.07.003

Ziolkowska, M., Koc, A., Luszczykiewicz, G., Ksiezopolska-Pietrzak, K., Klimczak, E., Chwalinska-Sadowska, H., et al. (2000). High Levels of IL-17 in Rheumatoid Arthritis Patients: IL-15 Triggers *In Vitro* IL-17 Production via Cyclosporin A-Sensitive Mechanism. *J. Immunol.* 164 (5), 2832–2838. doi:10.4049/jimmunol.164.5.2832

Conflict of Interest: The authors declare that the research was conducted in the absence of any commercial or financial relationships that could be construed as a potential conflict of interest.

frontiers in Pharmacology

ORIGINAL RESEARCH
published: 07 February 2022
doi: 10.3389/fphar.2022.798053

Daprodustat Accelerates High Phosphate-Induced Calcification Through the Activation of HIF-1 Signaling

Andrea Tóth[1,2], *Dávid Máté Csiki*[1,2], *Béla Nagy Jr.*[3], *Enikő Balogh*[1], *Gréta Lente*[1,2], *Haneen Ababneh*[1,2], *Árpád Szöőr*[4] *and Viktória Jeney*[1*†]

[1]MTA-DE Lendület Vascular Pathophysiology Research Group, Research Centre for Molecular Medicine, Faculty of Medicine, University of Debrecen, Debrecen, Hungary, [2]Doctoral School of Molecular Cell and Immune Biology, Faculty of Medicine, University of Debrecen, Debrecen, Hungary, [3]Department of Laboratory Medicine, Faculty of Medicine, University of Debrecen, Debrecen, Hungary, [4]Department of Biophysics and Cell Biology, Faculty of Medicine, University of Debrecen, Debrecen, Hungary

OPEN ACCESS

Edited by:
Vicky E. MacRae, University of Edinburgh, United Kingdom

Reviewed by:
Deliang Zhang, Eunice Kennedy Shriver National Institute of Child Health and Human Development (NICHD), United States
Andrew Bahn, University of Otago, New Zealand

***Correspondence:**
Viktória Jeney
jeney.viktoria@med.unideb.hu

†ORCID:
Viktória Jeney
orcid.org/0000-0003-4942-7091

Specialty section:
This article was submitted to Cardiovascular and Smooth Muscle Pharmacology, a section of the journal Frontiers in Pharmacology

Received: *19 October 2021*
Accepted: *13 January 2022*
Published: *07 February 2022*

Citation:
Tóth A, Csiki DM, Nagy B, Balogh E, Lente G, Ababneh H, Szöőr Á and Jeney V (2022) Daprodustat Accelerates High Phosphate-Induced Calcification Through the Activation of HIF-1 Signaling. Front. Pharmacol. 13:798053. doi: 10.3389/fphar.2022.798053

Aims: Chronic kidney disease (CKD) is frequently associated with other chronic diseases including anemia. Daprodustat (DPD) is a prolyl hydroxylase inhibitor, a member of a family of those new generation drugs that increase erythropoiesis *via* activation of the hypoxia-inducible factor 1 (HIF-1) pathway. Previous studies showed that HIF-1 activation is ultimately linked to acceleration of vascular calcification. We aimed to investigate the effect of DPD on high phosphate-induced calcification.

Methods and Results: We investigated the effect of DPD on calcification in primary human aortic vascular smooth muscle cells (VSMCs), in mouse aorta rings, and an adenine and high phosphate-induced CKD murine model. DPD stabilized HIF-1α and HIF-2α and activated the HIF-1 pathway in VSMCs. Treatment with DPD increased phosphate-induced calcification in cultured VSMCs and murine aorta rings. Oral administration of DPD to adenine and high phosphate-induced CKD mice corrected anemia but increased aortic calcification as assessed by osteosense staining. The inhibition of the transcriptional activity of HIF-1 by chetomin or silencing of HIF-1α attenuated the effect of DPD on VSMC calcification.

Conclusion: Clinical studies with a long follow-up period are needed to evaluate the possible risk of sustained activation of HIF-1 by DPD in accelerating medial calcification in CKD patients with hyperphosphatemia.

Keywords: chronic kidney disease (CKD), vascular calcification, anemia, hypoxia-inducible factor-1, prolyl hydroxylase inhibitor (PHI), daprodustat, vascular smooth muscle cell

Abbreviations: AR, alizarin red; CKD, chronic kidney disease; Ctrl, control; DMEM, Dublecco's modified eagle medium; DMSO, dimethyl sulphoxide; DPBS, Dulbecco's phosphate-buffered saline; DPD, daprodustat; ECM, extracellular matrix; EPO, erythropoietin; ER, endoplasmic reticulum; ESAs, erythropoiesis-stimulating agents; FBS, fetal bovine serum; FDA, U.S. Food and Drug Administration; GM, growth medium; H&E, hematoxylin eosin; HIF-1, hypoxia inducible factor 1; MCV, mean cell volume; OCN, osteocalcin; OD, optical density; OM, osteogenic medium; PHD, prolyl hydroxylase domain-containing; PHI, prolyl hydroxylase inhibitor; Pi, inorganic phosphate; RBC, red blood cell; VEGF-A, vascular endothelial growth factor A; VSMCs, vascular smooth muscle cells.

INTRODUCTION

Chronic kidney disease (CKD) is an irreversible and progressive disease associated with alteration of the renal structure and decline of kidney functions (Webster et al., 2017). CKD is a public health problem worldwide affecting about 10% of the general population in high- and middle-income countries (Webster et al., 2017). CKD is frequently associated with other chronic diseases, including anemia (Babitt and Lin, 2012), metabolic bone diseases (Martin and González, 2007), and cardiovascular diseases (Sarnak et al., 2003; Di Angelantonio et al., 2007). CKD patients have five to ten times higher risk of premature death than the general population, which is largely attributed to death from cardiovascular diseases (Sarnak et al., 2003; Di Angelantonio et al., 2007; Webster et al., 2017).

CKD-associated anemia is a considerable burden because it significantly worsens the quality of life of CKD patients, increases hospitalization, causes cognitive impairment, propagates the progression of CKD, and increases the risk of cardiovascular events and mortality. The etiology of CKD-associated anemia is complex with the contribution of reduced production of erythropoietin (EPO), a kidney-derived factor responsible for stimulating erythropoiesis, shortened red blood cell lifespan, and iron deficiency (Babitt and Lin, 2012; Hanna et al., 2021). Accordingly, anemia in patients with advanced CKD was targeted with EPO or erythropoiesis-stimulating agents (ESAs) (Eschbach et al., 1987), along with oral or intravenous iron supplementation (Gafter-Gvili et al., 2019; Batchelor et al., 2020). Red blood cell transfusion remained a treatment option only for blood loss or severe hyporesponsiveness for ESAs (Locatelli et al., 2013).

The treatment of CKD-associated anemia was revolutionized by the introduction of EPO and ESAs, but safety concerns of ESA use have lately been emerged (Robles, 2016). Trials showed that ESA treatment increases the risks for cardiovascular events and probably increases risk for death, serious cardiovascular events, and the development of end-stage renal disease (Palmer et al., 2010; Koulouridis et al., 2013; McCullough et al., 2013). Consequently, following the U.S. Food and Drug Administration (FDA) warning, the use of ESAs has markedly decreased, even in patients with very low hemoglobin levels (<10 mg/dl), and currently, the administration of ESAs is recommended only to avoid red blood cell transfusion.

An alternative therapeutic strategy has emerged to treat CKD-associated anemia that relies on the modulation of the hypoxia-inducible factor (HIF) pathway (Locatelli et al., 2017). The activation of the HIF pathway leads to transcriptional activation of numerous genes, including EPO, and a subsequent increase in erythropoiesis (Semenza and Wang, 1992). Therefore, small-molecule stabilizers of the HIF pathway have been developed (Maxwell and Eckardt, 2016). These molecules inhibit the activity of HIF prolyl hydroxylase domain–containing (PHD) enzymes, which are responsible for hydroxylation of the oxygen-sensitive alpha subunits of HIF at conserved proline residues under normoxic conditions (Semenza, 2001). Proline-hydroxylated α subunits are recognized and ubiquitinated by the von Hippel–Lindau E3 ubiquitin ligase, followed by rapid proteasomal degradation (Jaakkola et al., 2001; Metzen and Ratcliffe, 2004). PHD inhibitors (PHIs) mimic the effect of hypoxia and result in stabilization of the HIF α subunits, nuclear translocation, assembly of the HIF transcription complex, and eventually HIF activation with increased production of EPO.

Morbidity and mortality of CKD patients are largely associated with vascular calcification, an actively regulated process in which vascular smooth muscle cells (VSMCs) undergo an osteochondrogenic transdifferentiation process (Jono et al., 2000; Schoppet et al., 2008; Giachelli, 2009; Paloian and Giachelli, 2014). Various inhibitors and inducers of vascular calcification have been identified, and recent studies highlighted the potential role of hypoxia and the HIF-1 pathway activation in vascular calcification (Mokas et al., 2016; Balogh et al., 2019). Because 1) PHIs target the HIF pathway and 2) hypoxia-mediated activation of HIF-1 induces the calcification of VSMCs, here, we investigated the effect of the PHI daprodustat (GSK1278863, DPD) on calcification in both *in vitro* and *in vivo* conditions.

MATERIALS AND METHODS

Materials

All the reagents were purchased from Sigma-Aldrich Co. (St. Louis, MO, United States) unless otherwise specified.

Cell Culture and Treatments

Human aortic VSMCs (354-05; Cell Applications Inc., San Diego, CA, United States) were maintained in a growth medium (GM) that was prepared by supplementing Dulbecco's modified Eagle medium (DMEM, D6171, Sigma) with 10% FBS (10270-106, Gibco, Grand Island, NY, United States), antibiotic–antimycotic solution (A5955, Sigma), sodium pyruvate (S8636, Sigma), and L-glutamine (G7513, Sigma). Cells were maintained at 37°C in a humidified atmosphere containing 5% CO_2. Cells were grown till they reach confluence and used from passages 5 to 8. To induce calcification, we cultured VSMCs in an osteogenic medium (OM) that was obtained by supplementing GM with different concentrations of inorganic phosphate (Pi) (NaH_2PO_4-Na_2HPO_4, 1–2.5 mmol/L, pH 7.4). DPD (HY-17608, MedChemExpress, NJ, United States) was dissolved in dimethyl sulfoxide (DMSO, D2438, Sigma) to make a stock solution (25 mmol/L) and used in concentrations between 1 and 100 μmol/L. A hypoxic condition was obtained by placing the cells into a modular incubator chamber (Billups-Rothenburg Inc. Del Mar, CA, United States), which was connected to a gas bottle containing a mixture of 1% O_2, 5% CO_2, and 94% of N_2 (Messer Group GmbH, Bad Soden, Germany). A continuous slow flow (0.1 L/min) was applied throughout the experiment. In some experiments, we used chetomin (stock solution: 12.5 μmol/L in DMSO; working concentration: 12.5 nmol/L; C8106, Sigma) to inhibit the HIF-1 signaling pathway. Uric acid stock solution (80 mmol/L) was prepared in 1 mmol/L NaOH.

Alizarin Red (AR) Staining and Quantification

After washing with DPBS, the cells were fixed in 4% paraformaldehyde (16005, Sigma) and rinsed with deionized

water thoroughly. Cells were stained with Alizarin Red S (A5533, Sigma) solution (2%, pH 4.2) for 20 min at room temperature. Excessive dye was removed by several washes in deionized water. To quantify AR staining in 96-well plates, we added 100 µL of hexadecylpyridinium chloride (C9002, Sigma) solution (100 mmol/L) to the wells and measured optical density (OD) at 560 nm using hexadecylpyridinium chloride solution as blank.

Quantification of Ca Deposition

Cells grown on 96-well plates were washed twice with DPBS and decalcified with HCl (30721, Sigma, 0.6 mol/L) for 30 min at room temperature. The Ca content of the HCl supernatants was determined by using a QuantiChrome Calcium Assay Kit (DICA-500, Gentaur, Kampenhout, Belgium). Following decalcification, cells were washed twice with DPBS and solubilized with a solution of NaOH (S8045, Sigma, 0.1 mol/L) and sodium dodecyl sulfate (11667289001, Sigma, 0.1%), and protein content of samples were measured using the BCA protein assay kit (23225, Pierce Biotechnology, Rockford, IL, United States). The Ca content of the cells was normalized to protein content and expressed as mg/mg protein. The observer who performed all the Ca measurements was blinded to the group assignment.

Quantification of OCN and VEGF-A

For OCN detection, the ECM of the cells grown on 6-well plates was dissolved in 100 µL of EDTA (E6758, Sigma, 0.5 mol/L, pH 6.9). OCN content of the EDTA-solubilized ECM samples was quantified by an enzyme-linked immunosorbent assay (ELISA) (DY1419-05, DuoSet ELISA, R&D, Minneapolis, MN, United States), according to manufacturer's protocol. VEGF-A levels were quantified from the cellular supernatant using a VEGF-A ELISA kit (DY293B-05, DuoSet ELISA, R&D, Minneapolis, MN, United States). The observer who performed all the ELISA measurements was blinded to the group assignment.

Ex Vivo Aorta Organ Culture Model and Quantification of Aortic Calcium

C57BL/6 mice (8- to 12-week-old male, n = 18) were exterminated by CO_2 inhalation and perfused with 5 ml of sterile DPBS. The entire aorta was harvested and cleaned under aseptic conditions and cut into pieces. Aorta rings were randomly divided into three groups and maintained in control, high Pi (2 mmol/L Pi), and high Pi (2 mmol/L Pi) plus DPD (25 µmol/L) conditions, respectively. The culturing medium was DMEM (D6171, Sigma) supplemented with 10% FBS (10,270-106, Gibco, Grand Island, NY, United States), antibiotic–antimycotic solution (A5955, Sigma), sodium pyruvate (S8636, Sigma), l-glutamine (G7513, Sigma), and 2.5 µg/ml amphotericin B (171,375, Millipore). The medium was changed every 2 days. After the 3rd, 5th, and 7th day, the aorta pieces were washed in DPBS, opened longitudinally and decalcified in 25 µL of 0.6 mmol/L HCl overnight. The Ca content was determined by using the QuantiChrom Ca-assay kit, as described earlier. The observer who performed aorta Ca measurements was blinded to the group assignment.

CKD Induction and DPD Treatment in Mice

Animal care and experimental procedures were performed in accordance with the institutional and national guidelines and was approved by the Institutional Ethics Committee of University of Debrecen (registration number 3/2018/DEMÁB). Animal studies were reported in compliance with the ARRIVE guidelines. Male C57BL/6 mice (8- to 12-week-old, n = 25) were randomly divided into 5 groups, control (Ctrl), CKD, CKD + DPD (5 mg/kg/day), CKD + DPD (10 mg/kg/day), and CKD + DPD (15 mg/kg/day). CKD was induced by a two-phase diet as described previously (Tani et al., 2017). In the first 6 weeks, the mice received a diet containing 0.2% adenine and 0.7% phosphate, followed by a diet containing 0.2% adenine and 1.8% phosphate (S8106-S075 and S8893-S006, respectively; Ssniff, Soest, Germany) for 3 weeks. Mice were housed in cages with standard beddings and unlimited access to food and water. DPD (HY-17608, MedChemExpress, NJ, United States) was suspended in 1% methylcellulose and was daily administered orally at a dose of 5/10/15 mg/kg between weeks 7 and 9. At the end of the experiment mice were euthanized by CO_2 inhalation, blood was collected by cardiac puncture and aortas were harvested for calcium analysis and histology. In a separate experiment, C57BL/6 mice (8- to 12-week-old male, n = 15) were randomly divided into three groups: Ctrl, CKD, and CKD + DPD (15 mg/kg/day). The experiment was performed as the previous one, and aorta calcification was assessed by near-infrared imaging (detailed separately).

Laboratory Analysis of Renal Function and Anemia in CKD Mice

Serum phosphorous, urea creatinine, and uric acid levels were determined in mice by kinetic assays on a Cobas® c502 instrument (Roche Diagnostics, Mannheim, Germany). K_3-EDTA anticoagulated whole blood murine samples were analyzed by a Siemens Advia 2120i hematology analyzer (Tarrytown, NY, United States) with the 800 Mouse C57BL program of Multispecies software. Hemoglobin concentration was measured by using a cyanide-free colorimetric method. Hematocrit values were determined as a calculated parameter derived from the red blood cell count (RBC in T/L) and mean cell volume (MCV in fL). The number of RBCs was multiplied by the MCV of the sample RBCs and was divided by 1,000. The observer who performed these measurements was blinded to the group assignment.

Near-Infrared Imaging and Quantification of Aortic Calcification

OsteoSense dye (OsteoSense 680 EX and NEV10020EX; PerkinElmer, MA, United States) and near-infrared imaging were used to evaluate aorta calcification in mice as previously described (Malhotra et al., 2019). Mice (Ctrl, CKD, and CKD + DPD; n = 5/group) were anesthetized with isoflurane and injected with 2 nmol OsteoSense dye dissolved in 100 µL DPBS retro-orbitally. After 24 hours, mice were killed by CO_2 inhalation; the mice were perfused with 5 ml of ice-cold PBS, and aortas were isolated, cleaned, and analyzed *ex vivo* by an IVIS Spectrum *In*

Vivo Imaging System (PerkinElmer, MA, United States). The observer who performed this measurement was blinded to the group assignment.

Histology

Aortic rings were fixed in 10% neutral-buffered formalin (HT501640; Sigma), embedded in paraffin blocks, and cut into 4-μm-thick cross sections. After deparaffinization and rehydration, we performed von Kossa staining and hematoxylin eosin (H&E) counterstaining on the sections, according to manufacturer's protocol (von Kossa Kit, ab150687; Abcam, Cambridge, United Kingdom). The observer who performed histology was blinded to the group assignment.

Western Blot Analysis

VSMCs were lysed in the Laemmli lysis buffer (38,733, Sigma). Proteins were resolved by SDS-PAGE (7.5 and 10%) and transferred to nitrocellulose membranes (1060003; Amersham, GE Healthcare, Chicago, IL, United States). Western blotting was performed by using anti-HIF1α antibody (GTX127309, GeneTex, Irvine, CA, United States) at 0.5 μg/ml concentration, anti-HIF2α antibody (#7096, Cell Signaling Technology, Danvers, MA, United States) at 2.5 μg/ml concentration, and anti-Glut-1 antibody (GTX1309, GeneTex) at 0.5 μg/ml concentration. After binding of the primary antibodies, membranes were incubated with horseradish peroxidase–linked rabbit (NA-934) and mouse IgG (NA-931) (Amersham, GE Healthcare) at 0.5 μg/ml concentration. Antigen–antibody complexes were visualized using the enhanced chemiluminescence system Clarity Western ECL (170-5060, BioRad, Hercules, CA, United States). Chemiluminescent signals were detected conventionally on an X-ray film or digitally by using a C-Digit Blot Scanner (LI-COR Biosciences, Lincoln, NE, United States). After detection, the membranes were stripped and reprobed for β-actin using an anti-β-actin antibody (sc-47778, Santa Cruz Biotechnology Inc., Dallas, TX, United States) at 0.2 μg/ml concentration. Western blots were repeated three times with independent sample sets and blots were quantified by using the inbuilt software on the C-Digit Blot Scanner.

RNA Silencing

To knock-down HIF-1α gene expression, we used *Silencer*® select siRNA construct targeting HIF-1α (assay IDs #AM16708, Thermo Fisher Scientific). As a control, we used negative control #1 construct (#4390843, Thermo Fisher Scientific). The Lipofectamine® RNAiMAX reagent (13778075, Invitrogen, Carlsbad, CA, United States) was used to transfect VSMCs, according to manufacturer's protocol.

Statistical Analysis

Group size was equal in all experiments, and no data points were excluded from the analysis. Data are presented as mean ±SD with individual data points. Statistical analyses were performed with GraphPad Prism software (version 8.01, San Diego, CA, United States). Comparisons between more than two groups were carried out by one-way ANOVA, followed by Tukey's multiple comparisons test. To compare each treatment group with a single control group, we performed one-way ANOVA, followed by Dunnett's *post hoc* test. Time course experiments were analyzed by two-way ANOVA, followed by Tukey's multiple comparisons test. The value of $p < 0.05$ was considered significant.

RESULTS

Hypoxia Accelerates Pi-Induced ECM Calcification in VSMCs

A previous study by Mokas et al. showed that hypoxia amplifies the pro-calcification effect of elevated inorganic phosphate (Pi) (Mokas et al., 2016). To confirm this finding, first, we set up an *in vitro* model of vascular calcification with cultured human VSMCs maintained in a calcification medium that was supplemented with different concentrations of Pi (0–2.5 mmol/L) under normoxic (21% O_2) and hypoxic (1% O_2) conditions. Calcification was evaluated by AR staining after 6 days of treatment (**Figure 1A**). We found increased intensity of AR staining at all tested Pi concentrations under hypoxia in comparison to normoxic condition (**Figure 1A**). Interestingly, hypoxia increased AR staining intensity over normoxia control after 6 days of treatment even in normal phosphate condition. Measurement of Ca levels confirmed the result of AR staining, having more Ca in the extracellular matrix (ECM) of VSMCs under hypoxic condition than normoxic groups (**Figure 1B**). In a time course experiment, we investigated the kinetics of calcification in the presence of a calcification medium containing 2.5 mmol/L excess Pi under normoxic and hypoxic conditions (**Figure 1C**). Results show that calcification is significantly higher on both days 4 and 6 under hypoxia than under normoxia (**Figure 1C**). These results confirm the previously established pro-calcifying effect of hypoxia under normal and high Pi conditions (Mokas et al., 2016; Balogh et al., 2019).

DPD Activates the HIF-1 Pathway and Increases Pi-Induced Calcification in VSMCs *In Vitro* and Aorta *Ex Vivo*

DPD is a prolyl hydroxylase inhibitor; therefore, next, we investigated its effect on HIF-1 activation in VSMCs. We found that DPD (1–100 μmol/L) increased the expression of both HIF-1α and HIF-2α in a dose-dependent manner (**Figures 2A–C**). This was accompanied by increased expression of glucose transporter 1 (Glut-1) and vascular endothelial growth factor A (VEGF-A), which are characteristic target genes of the HIF-1 pathway (**Figures 2A,D,E**).

Then we addressed the effect of DPD on Pi-induced calcification of VSMCs. We treated VSMCs in the osteogenic medium supplemented with various concentrations of Pi (1.5–2.5 mmol/L) in the presence or absence of DPD (10 μmol/L). Calcification was assessed by AR staining after 6 days of exposure. The osteogenic medium supplemented

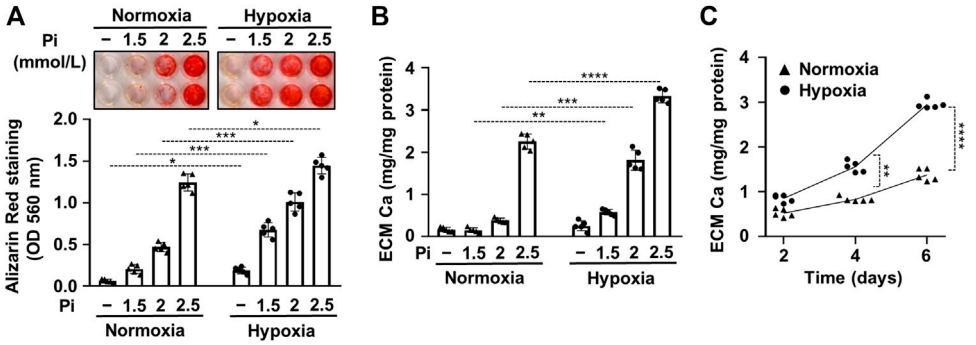

FIGURE 1 | Hypoxia increases Pi-mediated extracellular matrix calcification of VSMCs. Confluent VSMCs were exposed to a calcification medium containing Pi (1.5–2.5 mmol/L) under normoxic (21% O_2) and hypoxic conditions (1% O_2). **(A)** Ca deposition in the ECM (day 6) evaluated by AR staining. Representative image and quantification are depicted. **(B)** Ca content of the HCl-solubilized ECM. **(C)** Time course of Ca accumulation under normoxic and hypoxic conditions in the presence of 2.5 mmol/L Pi. **(A–C)** Data are expressed as mean ± SD, $n = 5$. **(A,B)** Ordinary one-way ANOVA followed by Tukey's multiple comparisons test were used to obtain p values. **(C)** Multiple t tests to compare normoxia and hypoxia samples at each time points were performed to obtain p values. *$p < 0.05$, **$p < 0.01$, ***$p < 0.005$, ****$p < 0.001$.

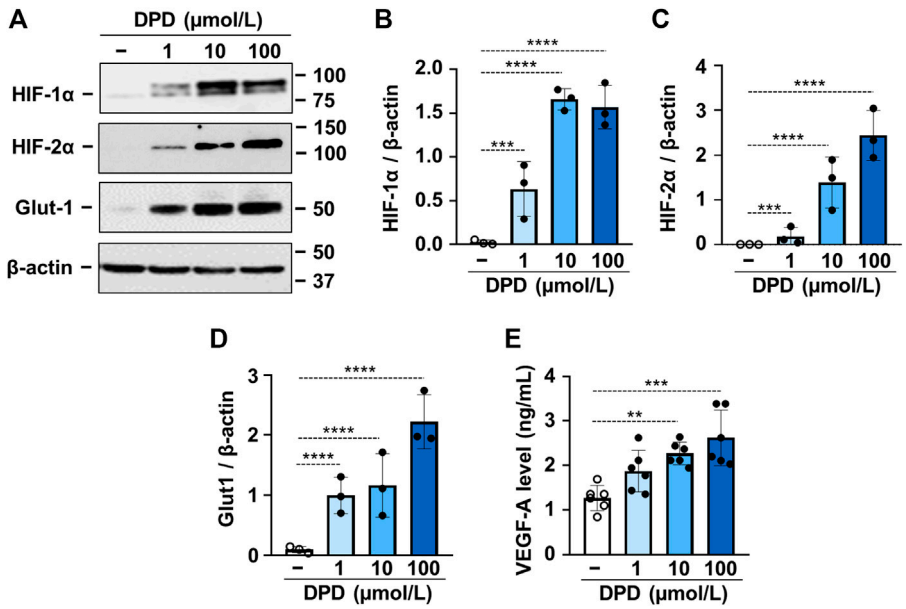

FIGURE 2 | DPD triggers hypoxia response in VSMCs. VSMCs were cultured in the absence or presence of DPD (1–100 μmol/L). **(A–D)** Protein expression of HIF-1α, HIF-2α, and Glut-1 in whole cell lysates was evaluated after 24 h. Membranes were reprobed for β-actin. **(A)** Representative Western blots and densitometry analyses on the relative expression of **(B)** HIF-1α, **(C)** HIF-2α, and **(D)** Glut-1 normalized to β-actin are depicted ($n = 3$). **(E)** VEGF-A levels (24 h) were determined from cellular supernatant by ELISA ($n = 6$). Data are expressed as mean ± SD. **(A–D)** Ordinary one-way ANOVA followed by Dunnett's multiple comparisons test and **(E)** ordinary one-way ANOVA followed by Tukey's multiple comparisons test were used to obtain p values. **$p < 0.01$, ***$p < 0.005$, ****$p < 0.001$.

with 2.0 mmol/L Pi triggered calcification only in the presence of DPD. Higher Pi (2.5 mmol/L) induced calcification in both the absence and presence of DPD, but the extent of calcification was higher in the DPD-treated cells (**Figure 3A**). Next, we performed a time course experiment and measured the Ca content of the extracellular matrix after 2nd, 4th, and 6 th days of exposure to high Pi (2 mmol/L) in the absence or presence of DPD (**Figure 3B**). DPD significantly increased Ca content of the ECM on days 4 and 6 (**Figure 3B**). Next, we investigated the effect of DPD on the expression of osteocalcin (OCN), a major non-collagenous protein of the bone matrix, and an established marker of osteochondrogenic transdifferentiation of VSMCs. We found that DPD (10 μmol/L) largely enhanced Pi-induced increase in OCN production in VSMCs ($p < 0.0001$, **Figure 3C**). For further confirmation, we set up an *ex vivo* tissue culture model and investigated the effect of DPD on

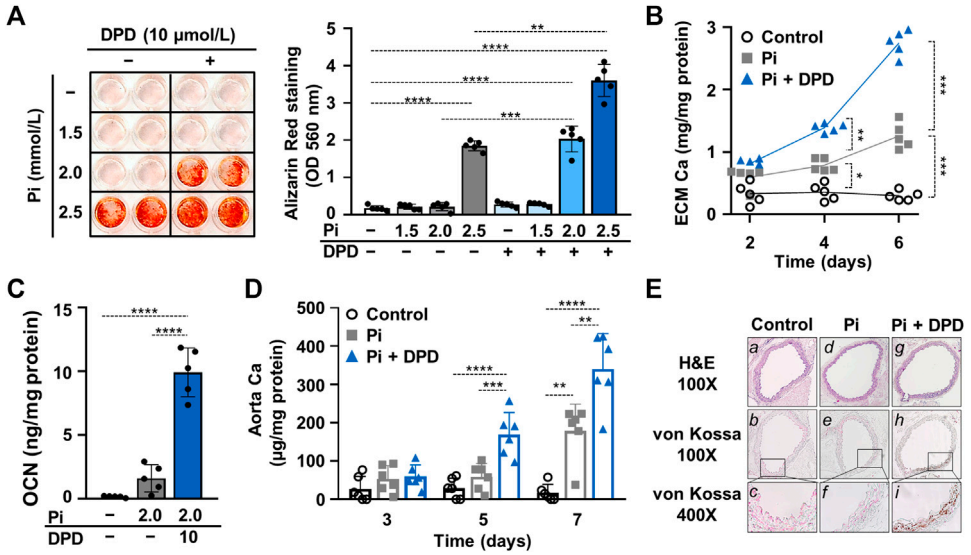

FIGURE 3 | DPD increases Pi-mediated ECM calcification and osteochondrogenic transdifferentiation of VSMCs and accelerates aorta ring calcification. **(A–C)** VSMCs were cultured in an osteogenic medium (excess Pi: 1.5–2.5 mmol/L) in the presence or absence of DPD (10 µmol/L). **(A)** Representative AR staining (day 6) and quantification. **(B)** Time course of Ca accumulation induced by Pi (2 mmol/L) and Pi + DPD (10 µmol/L) (day 2, 4, and 6). **(C)** OCN level (day 6) in EDTA-solubilized ECM samples. **(D)** Aortic rings obtained from C57BL/6 mice were cultured in control, high Pi (2 mmol/L), and high Pi + DPD (25 µmol/L) conditions. Ca content of aorta rings normalized to protein level (day 3, day 5, and day 7). **(E)** Histological analysis of *ex vivo* cultured aortic rings from C57BL/6 mice. Representative H&E and von Kossa-stained aortic sections of untreated, Pi-, and Pi + DPD-treated aorta rings (day 7). Magnification: ×100 and ×400. Data are expressed as mean ± SD, $n = 5$. **(A,C)** Ordinary one-way ANOVA followed by Tukey's multiple comparisons test and **(B,D)** two-way ANOVA followed by Tukey's multiple comparisons test were used to obtain p values. $^{*}p < 0.05$, $^{**}p < 0.01$, $^{***}p < 0.005$, $^{****}p < 0.001$.

aorta calcification. We cultured cleaned aorta pieces of C57BL/6 mice under control, high Pi (2 mmol/L), and high Pi + DPD (25 µmol/L) conditions and measured Ca levels of aorta rings on day 3, day 5, and day 7. High Pi increased Ca content of the aorta on day 7, whereas when high Pi and DPD were applied together, aorta calcification started already on day 5 (**Figure 3D**). The calcium content was higher in the aorta rings treated with Pi + DPD than in Pi-treated aorta rings on day 7 (345.9 ± 102.7 vs. 178.3 ± 70.7 µg/mg protein, **Figure 3D**). After 7 days of treatment, we performed von Kossa staining on the specimens of the descending thoracic aorta to visualize calcification. von Kossa staining revealed calcification in the media layer of the aorta that was treated with Pi + DPD but not in control or Pi-treated aorta specimens (**Figure 3E**). These results suggest that DPD is a pro-calcification agent that increases Pi-induced calcification of VSMCs and mouse aorta in a synergistic way.

DPD Administration Successfully Corrects Anemia but Increases Aorta Calcification in a Mice Model of CKD

Then we studied the effect of DPD on anemia and vascular calcification in the murine model of CKD. Mice were fed with a diet containing adenine (0.2%) and elevated phosphate (0.7%) for 6 weeks, and then the phosphate content of the diet was further increased up to 1.8%; mice received this diet for an additional 3 weeks. To determine the efficient dose of DPD that corrects anemia in this particular CKD model, we administered DPD in three different doses: 5, 10, and 15 mg/body weight kg/day orally in the last 3 weeks of the experiment (**Figure 4A**). The development of CKD with the adenine plus high phosphate diet was associated with significant decrease in body weight (**Figure 4B**) and increased serum phosphorous, urea, and creatinine levels (**Figures 4C–E**), regardless of DPD treatment. Parallel to the development of CKD, mice became anemic, and their condition was characterized by reduced Hb concentration, decreased red blood cell count, and low hematocrit levels (**Figures 4F–H**). Low doses of DPD (5 and 10 mg/kg/day) did not improved anemia, but the highest dose (15 mg/kg/day) efficiently corrected anemia in CKD mice, resulting in normalized Hb concentration, RBC count, and hematocrit levels similar to the controls with normal renal function (**Figures 4F–H**).

Next, we also addressed the effect of DPD on aorta calcification *in vivo*. Macroscopic fluorescence reflectance imaging technics was used to investigate the osteogenic activity in whole mouse aortas. Osteosense, a near-infrared fluorescent imaging agent was administered intravenously 24 h before imaging. Fluorescent intensity of the aorta was higher in CKD mice than in control mice with normal renal function ($6.41 \times 10^8 \pm 3.22 \times 10^8$ vs. $1.38 \times 10^9 \pm 3.58 \times 10^8$ p/s, $p < 0.05$, **Figure 5A**). Moreover, the osteogenic activity was higher in the aortas derived from DPD-treated CKD mice than in vehicle-treated CKD mice ($2.82 \times 10^9 \pm 1.06 \times 10^9$ vs. $1.38 \times 10^9 \pm 3.58 \times$

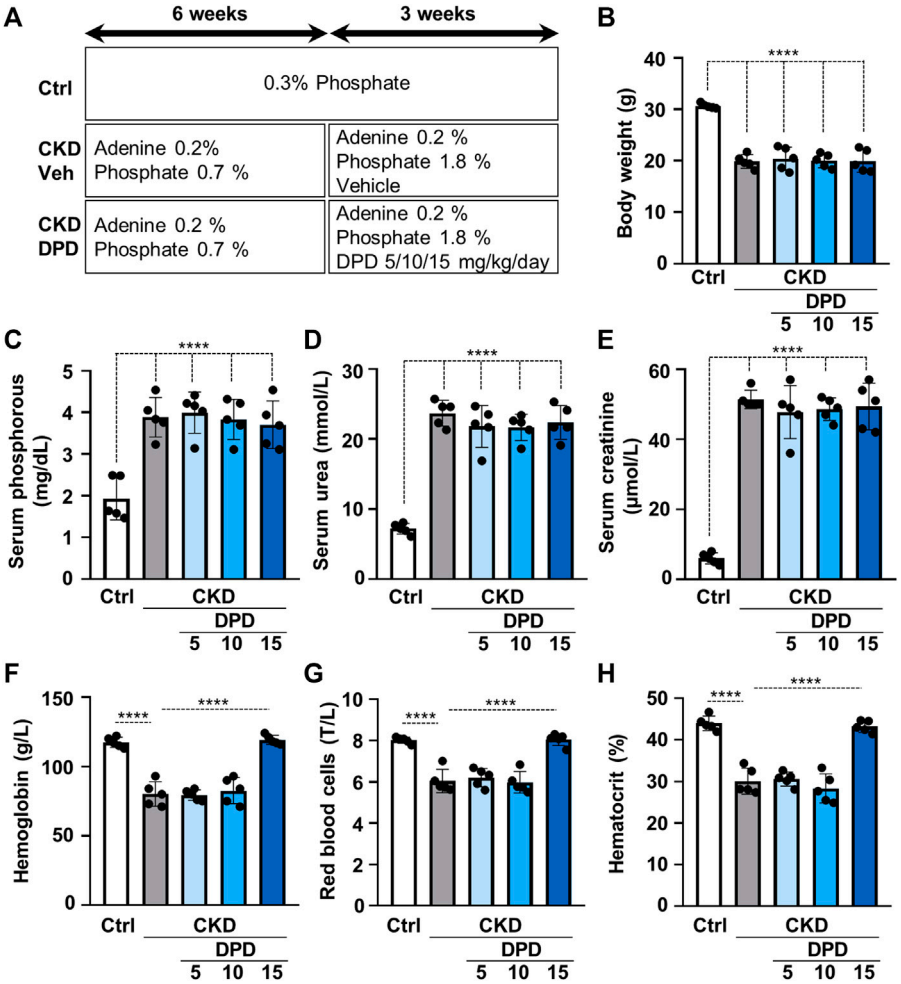

FIGURE 4 | Dose-dependent effect of DPD treatment on renal function and anemia in C57BL/6 mice fed an adenine plus high Pi diet. **(A)** Scheme of the experimental protocol. **(B)** Body weight, **(C)** serum phosphorous, **(D)** serum urea, **(E)** serum creatinine, **(F)** whole blood hemoglobin concentration with **(G)** red blood cell count (T/L), and **(H)** hematocrit values were determined. Data are expressed as mean ± SD, $n = 5$. Ordinary one-way ANOVA followed by Tukey's multiple comparisons test were used to calculate p values. ****$p < 0.001$.

10^8 p/s, $p < 0.05$, **Figure 5A**). Parallel with this, the Ca level of the aorta was higher in DPD-treated mice than in vehicle-treated CKD mice (4.76 ± 1.89 vs. 10.19 ± 4.97 µg/mg tissue, $p < 0.05$, **Figure 5B**). von Kossa staining also revealed starting calcification in the media layer of the aorta obtained from DPD-treated CKD mice, whereas calcification was undetectable in vehicle-treated CKD mice and in control mice with normal renal function (**Figure 5C**).

HIF-1 Activation Is Critically Involved in DPD-Facilitated Calcification in VSMCs

After establishing that DPD triggers HIF-1 activation in VSMCs, we raised the question whether this mechanism plays a role in the DPD-induced calcification process. To address this, we first used chetomin, a chemical inhibitor of HIF-1 transcriptional activity and investigated the calcification of VSMCs in response to Pi + DPD. As revealed by AR staining, chetomin partially attenuated Pi + DPD-induced calcification of VSMCs (**Figure 6A**). The inhibitory effect of chetomin on Pi + DPD-induced calcification was confirmed by Ca and OCN measurements from the ECM (**Figures 6B,C**). Furthermore, siRNA-manipulated knockdown of HIF-1α, the regulatory subunit of the HIF-1 complex, attenuated VSMCs calcification as detected by AR staining, as well as Ca and OCN measurements from the ECM (**Figures 6D–G**).

Uric Acid Retention Is Not Involved in the Pro-Calcification Effect of DPD

DPD is an organic anion which might interfere with transport of other organic anions, specifically uric acid. Uric acid is an important uremic toxin, and recent evidence showed that soluble uric acid promotes atherosclerosis (Kimura et al.,

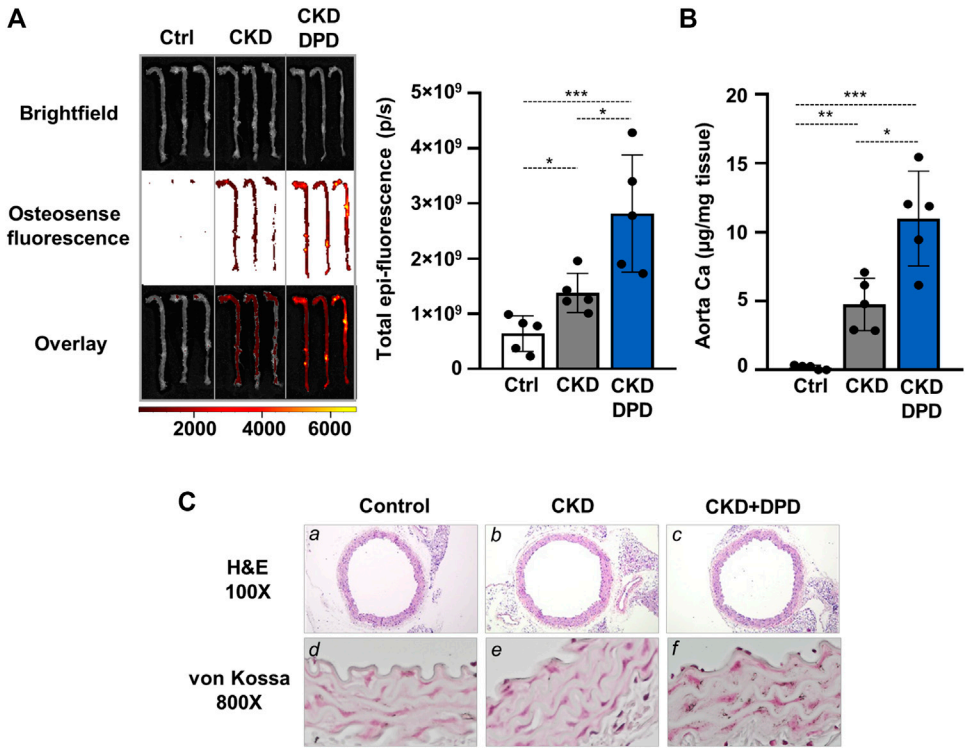

FIGURE 5 | DPD increases aorta calcification in CKD mice with hyperphosphatemia. Mice were treated as detailed in **Figure 4A**. **(A)** Bright-field and macroscopic fluorescence reflectance imaging of calcification and quantification in control, CKD, and CKD + DPD mice (n = 5/group). **(B)** Ca content of aortas derived from control, CKD, and CKD + DPD mice normalized to protein level (n = 5/group). **(C)** Histological analysis of aorta obtained from control, CKD, and CKD + DPD mice. Representative H&E and von Kossa-stained aortic sections. Magnification: ×100, ×800. Data are expressed as mean ± SD, n = 5. Ordinary one-way ANOVA followed by Tukey's multiple comparisons test was used to calculate p values. *p < 0.05, **p < 0.01, ***p < 0.005.

2020). To see whether the pro-calcification effect of DPD relies on uric acid retention, we first determined uric acid levels in mice serum. The induction of CKD and DPD treatment was performed, as shown in **Figure 4A**. The uric acid level in CKD mice was almost twice as high as the control, whereas its level did not differ between CKD and CKD + DPD (15 mg/kg/day) mice (**Figure 7A**). Then using an *in vitro* approach, we investigated whether uric acid increases Pi-induced VSMCs calcification. We induced VSMC calcification with Pi (2 mmol/L) in the presence or absence of uric acid (400 and 600 µmol/L). As revealed by AR staining, uric acid did not modify Pi-induced calcification of VSMCs (**Figure 7B**). This result was confirmed by Ca measurements from the ECM (**Figure 7C**).

DISCUSSION

CKD-associated medial calcification is an actively regulated process that involves complex interactions of multiple calcification inducers, inhibitors, and circulating and local factors (Jono et al., 2000; Schoppet et al., 2008; Giachelli, 2009; Paloian and Giachelli, 2014). Transdifferentiation of VSMCs into osteoblast/chondrocyte-like cells is the major cellular mechanism of vascular calcification (Jono et al., 2000; Schoppet et al., 2008; Giachelli, 2009; Paloian and Giachelli, 2014). High Pi is a potent inducer of osteochondrogenic phenotype switch of VSMCs, and it is one of the most relevant inducer of vascular calcification in CKD (Jono et al., 2000; Schoppet et al., 2008; Giachelli, 2009; Paloian and Giachelli, 2014). Studies have shown that hypoxia and HIF-1 signaling are closely associated with kidney disease, and recent evidence proved their implication in vascular calcification (Nangaku and Eckardt, 2007; Gunaratnam and Bonventre, 2009; Mokas et al., 2016; Balogh et al., 2019).

CKD is often accompanied by anemia that requires treatment. DPD is a new generation drug to treat anemia in CKD patients. A recent phase 3 study compared the efficacy and safety of DPD with an ESA (darbepoetin alfa) over 1 year of treatment (Akizawa et al., 2020). That study revealed that oral DPD was generally well tolerated and is non-inferior to ESA in the maintenance of hemoglobin concentration in Japanese dialyzed CKD patients (Akizawa et al., 2020).

DPD is a PHI which acts through the activation of the HIF pathways. Our study provides evidence of a role for DPD in the progression of vascular calcification during CKD. We described

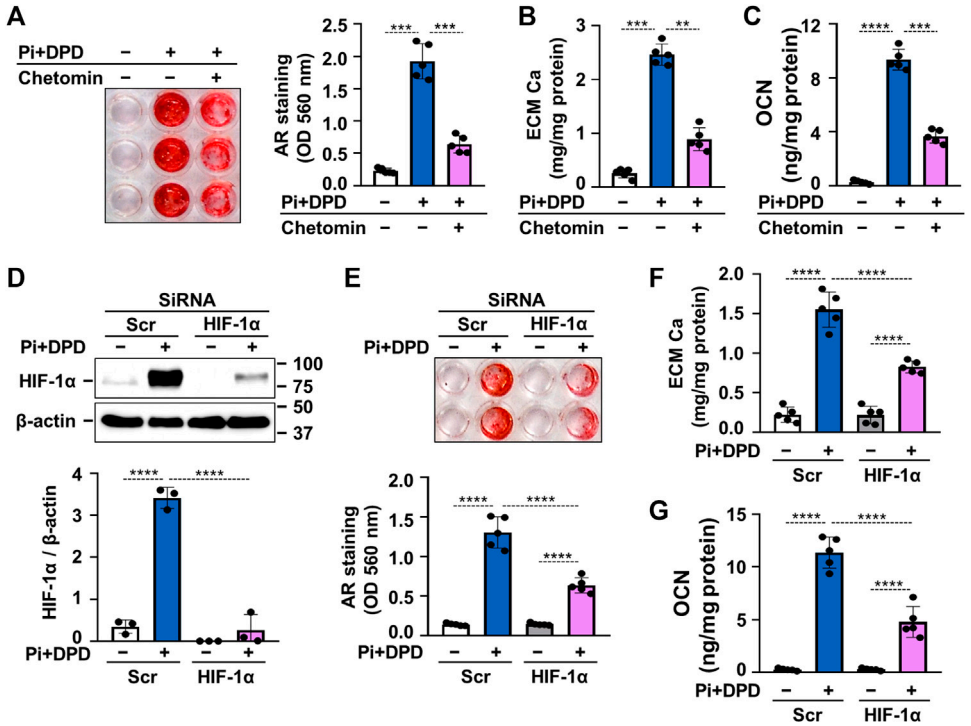

FIGURE 6 | DPD increases calcification of VSMCs through HIF-1 activation. **(A–C)** VSMCs were exposed to Pi (2 mmol/L) and DPD (10 μmol/L) in the presence or absence of HIF-1 inhibitor, chetomin (12.5 nmol/L). **(A)** Representative AR staining (day 4) and quantification. **(B)** Ca content of HCl-solubilized ECM (day 4). **(C)** OCN level in EDTA-solubilized ECM samples (day 6). **(D–G)** VSMCs were exposed to Pi (2 mmol/L) and DPD (10 μmol/L) in the presence of HIF-1α or scrambled siRNA. **(D)** Protein expression of HIF-1α in whole cell lysates (24 h). Membranes were reprobed for β-actin. Representative Western blots and relative expression of HIF-1α normalized to β-actin. **(E)** Representative AR staining (day 4) and quantification. **(F)** Ca content of HCl-solubilized ECM (day 4). **(G)** OCN level in EDTA-solubilized ECM samples (day 6). Data are expressed as mean ± SD, $n = 5$ except **(D)**, where $n = 3$. Ordinary one-way ANOVA followed by Tukey's multiple comparisons tests were used to calculate p values. $^{**}p < 0.01$, $^{***}p < 0.005$, $^{****}p < 0.001$.

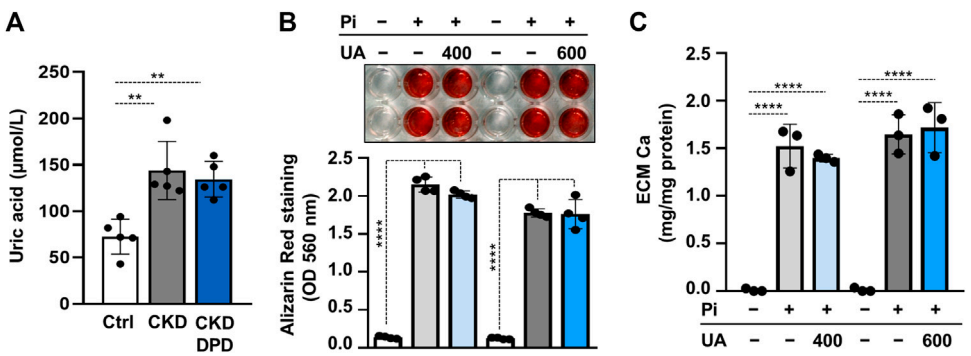

FIGURE 7 | Uric acid retention is not involved in the pro-calcification effect of DPD. **(A)** Serum uric acid levels in control (Ctrl), CKD, and CKD + DPD (15 mg/kg/day) mice ($n = 5$). **(B,C)** VSMCs were exposed to Pi (2 mmol/L) in the presence of uric acid (UA, 400 or 600 μmol/L) or vehicle. **(B)** Representative AR staining (day 4) and quantification ($n = 4$). **(C)** Ca content of HCl-solubilized ECM (day 4, $n = 3$). Data are expressed as mean ± SD. Ordinary one-way ANOVA followed by Tukey's multiple comparison tests were used to calculate p values. $^{**}p < 0.01$, $^{****}p < 0.001$.

synergistic effects between DPD and high Pi during osteochondrogenic differentiation of VSMCs. We report that oral administration of DPD accelerates high Pi-induced calcification in a mouse model of CKD. We also established HIF-1α as major functional contributor of DPD-driven calcification.

Hydroxylation at specific prolyl residues initiates ubiquitination and proteolytic destruction of the regulatory α subunits of HIFs by the ubiquitin/proteasome pathway (Jaakkola et al., 2001). DPD is an inhibitor of prolyl hydroxylases, and here, we show that DPD treatment increases both HIF-1α and HIF-2α expressions in VSMCs (**Figure 2**). Upon stabilization, HIF α subunits are translocated into the nucleus, heterodimerizes with HIF β subunits, recruits coactivator molecules, that is, p300 and CREB-binding protein, and the complex activates transcription of certain genes controlling cell metabolism and angiogenesis that foster cell survival in a low oxygen environment. Our results revealed that DPD upregulates Glut-1, an important target gene of HIF, proving that DPD potently activated the HIF pathway in human VSMCs (**Figure 2**).

Growing evidence suggests that diseases with hypoxemia and/or hypoxia, such as asthma, chronic obstructive pulmonary disease, and obstructive sleep apnea are associated with increased vascular calcification (Green et al., 2006; Williams et al., 2014; Tachikawa et al., 2015). Moreover, Mokas et al. showed that hypoxia synergizes with high Pi to enhance osteochondrogenic transdifferentiation of VSMCs (Mokas et al., 2016). Furthermore, we reported recently that hypoxia itself is a pro-calcifying factor and is able to induce osteochondrogenic transdifferentiation and ECM calcification of VSMCs (Balogh et al., 2019). These observations warranted us to test the pro-calcifying potential of DPD.

We chose a cellular model of vascular calcification in which we induced calcification of VSMCs with high Pi because DPD is a drug intended to be used in progressive CKD patients who develop positive phosphate balance. Here, we reported that similar to hypoxia, DPD intensifies high Pi-induced osteochondrogenic transdifferentiation, ECM calcification of VSMCs *in vitro*, and aorta calcification *ex vivo* (**Figure 3**). Similar results were obtained in previous studies with another PHI, roxadustat (FG-4592), that also enhanced VSMCs calcification under high phosphate conditions (Mokas et al., 2016; Nagy et al., 2020).

Several phase 3 and phase 2 studies demonstrated that DPD is effective in improving hemoglobin levels of CKD patients (Ishii et al., 2021). These clinical trials have not reported serious adverse events or obvious off-target effects of DPD (Li et al., 2018; Ishii et al., 2021). In 2020, DPD was approved for the treatment of patients with CKD-associated anemia in Japan (Dhillon, 2020).

After seeing the pro-calcifying action of DPD in elevated phosphate condition *in vitro*, we aimed to test the effect of DPD on anemia and calcification *in vivo*. In order to do this, we applied an adenine-induced CKD mice model, in which high-phosphate condition was approached by a diet rich in phosphorous. We tested three doses of DPD (5, 10, and 15 mg/kg/day) and found that DPD at the dose of 15 mg/kg/day corrected anemia of CKD mice completely, whereas the lower doses did not improve the hematological parameters (**Figure 4**). This dose is higher than the dose reported earlier by Ariazi et al. who tested the effect of DPD (3, 10, and 30 mg/kg/day) on the Hb level and reticulocyte number in normal female B6D2F1 mice during the preclinical characterization of DPD (Ariazi et al., 2017). They found that a daily administration of 3 mg/kg DPD increased the reticulocyte number and hemoglobin concentration significantly. There could be several reasons for this discrepancy, such as the mice model (CKD vs. healthy), the initial anemia status (moderate to severe anemia vs. non-anemia), the gender (male vs. female), or the genetic background (C57BL/6 vs. B6D2F1). Here, we reported that besides its beneficial effect in correcting anemia, DPD at the dose of 15 mg/kg/day accelerated aorta calcification in CKD mice with high plasma phosphate levels (**Figure 5**). We showed that DPD stabilized both HIF-1α and HIF-2α in VSMCs. Chetomin that blocks the interaction of HIF α subunits with transcriptional co-activators, thereby attenuating hypoxia-inducible transcription, inhibited calcification triggered by DPD + Pi (**Figure 6**). Both the ubiquitously expressed HIF-1α and the more cell-specific HIF-2α are important regulators of the hypoxia response (Loboda et al., 2010). Although both HIF-1α and HIF-2α subunits heterodimerize with the HIF-1β subunit in the nucleus, and the HIF1 and HIF2 bind to the same hypoxia responsive elements of target genes, their effect on the expression of some genes may be specific (Loboda et al., 2010). There is a consensus that the PHIs increase EPO expression mainly through HIF-2. On the other hand, previous reports provided evidence that sustained HIF-1α stabilization induces VSMC calcification in both normal and high phosphate conditions (Mokas et al., 2016; Balogh et al., 2019). Therefore, focusing on HIF-1α, here, we showed that the pro-calcifying effect of DPD is dependent on HIF-1α stabilization (**Figure 6**).

Uremic toxins accumulate in CKD patient's plasma and contribute to the pathology of the disease. One example is uric acid, an end-product of purine metabolism that normally excreted through the urine (Kumagai et al., 2017). Excess uric acid can precipitate causing gout, whereas soluble uric acid promotes atherosclerosis and further exacerbates CKD (Kumagai et al., 2017; Kimura et al., 2020). There are conflicting results about the association between uric acid levels and vascular calcification (Neogi et al., 2011; Malik et al., 2016; Yan et al., 2019). Here, we tested the hypothesis that DPD interferes with urinary excretion of uric acid, and uric acid increases VSMCs calcification. Our results showed that uric acid levels were similar in DPD-treated and non-treated CKD mice, and uric acid does not influence Pi-induced VSMCs calcification (**Figure 7**).

To our knowledge, this is the first study that addressed the potential pro-calcifying effect of DPD. We found that DPD treatment accelerates phosphate-induced vascular calcification *in vitro* in primary VSMCs, *ex vivo* in mouse aorta rings, and *in vivo* in a murine CKD model with a high plasma phosphorous level. We assumed that administration of DPD in CKD patients with hyperphosphatemia could increase the risk of vascular calcification. Further investigation with an extended follow-up

period is warranted to evaluate the possible risks of sustained HIF elevation by DPD in accelerating calcification in CKD patients with hyperphosphatemia.

DATA AVAILABILITY STATEMENT

The raw data supporting the conclusion of this article will be made available by the authors, without undue reservation.

ETHICS STATEMENT

The animal study was reviewed and approved by the Institutional Ethics Committee of University of Debrecen.

AUTHOR CONTRIBUTIONS

VJ and AT designed the research; AT, DC, BN, EB, GL, HA, ÃS, and VJ performed the experiments; VJ, AT, DC, BN, EB, GL, and ÃS analyzed and interpreted the data; and VJ and AT wrote the manuscript. The manuscript was reviewed and edited by all authors.

FUNDING

This work was funded by the Hungarian National Research, Development and In-novation Office (NKFIH) (K131535 to VJ and FK135327 to BN), and the Hungarian Academy of Sciences (MTA-DE Lendület Vascular Pathophysiology Research Group, grant number 96050 to VJ).

REFERENCES

Akizawa, T., Nangaku, M., Yonekawa, T., Okuda, N., Kawamatsu, S., Onoue, T., et al. (2020). Efficacy and Safety of Daprodustat Compared with Darbepoetin Alfa in Japanese Hemodialysis Patients with Anemia: A Randomized, Double-Blind, Phase 3 Trial. *Clin. J. Am. Soc. Nephrol.* 15, 1155–1165. doi:10.2215/CJN.16011219

Ariazi, J. L., Duffy, K. J., Adams, D. F., Fitch, D. M., Luo, L., Pappalardi, M., et al. (2017). Discovery and Preclinical Characterization of GSK1278863 (Daprodustat), a Small Molecule Hypoxia Inducible Factor-Prolyl Hydroxylase Inhibitor for Anemia. *J. Pharmacol. Exp. Ther.* 363, 336–347. doi:10.1124/JPET.117.242503

Babitt, J. L., and Lin, H. Y. (2012). Mechanisms of Anemia in CKD. *J. Am. Soc. Nephrol.* 23, 1631–1634. doi:10.1681/ASN.2011111078

Balogh, E., Tóth, A., Méhes, G., Trencsényi, G., Paragh, G., and Jeney, V. (2019). Hypoxia Triggers Osteochondrogenic Differentiation of Vascular Smooth Muscle Cells in an HIF-1 (Hypoxia-Inducible Factor 1)-Dependent and Reactive Oxygen Species-dependent Manner. *Arterioscler Thromb. Vasc. Biol.* 39, 1088–1099. doi:10.1161/ATVBAHA.119.312509

Batchelor, E. K., Kapitsinou, P., Pergola, P. E., Kovesdy, C. P., and Jalal, D. I. (2020). Iron Deficiency in Chronic Kidney Disease: Updates on Pathophysiology, Diagnosis, and Treatment. *J. Am. Soc. Nephrol.* 31, 456–468. doi:10.1681/ASN.2019020213

Dhillon, S. (2020). Daprodustat: First Approval. *Drugs* 80, 1491–1497. doi:10.1007/s40265-020-01384-y

Di Angelantonio, E., Danesh, J., Eiriksdottir, G., and Gudnason, V. (2007). Renal Function and Risk of Coronary Heart Disease in General Populations: New Prospective Study and Systematic Review. *Plos Med.* 4, e270. doi:10.1371/journal.pmed.0040270

Eschbach, J. W., Egrie, J. C., Downing, M. R., Browne, J. K., and Adamson, J. W. (1987). Correction of the Anemia of End-Stage Renal Disease with Recombinant Human Erythropoietin. Results of a Combined Phase I and II Clinical Trial. *N. Engl. J. Med.* 316, 73–78. doi:10.1056/NEJM198701083160203

Gafter-Gvili, A., Schechter, A., and Rozen-Zvi, B. (2019). Iron Deficiency Anemia in Chronic Kidney Disease. *Acta Haematol.* 142, 44–50. doi:10.1159/000496492

Giachelli, C. M. (2009). The Emerging Role of Phosphate in Vascular Calcification. *Kidney Int.* 75, 890–897. doi:10.1038/ki.2008.644

Green, F. H., Butt, J. C., James, A. L., and Carroll, N. G. (2006). Abnormalities of the Bronchial Arteries in Asthma. *Chest* 130, 1025–1033. doi:10.1378/chest.130.4.1025

Gunaratnam, L., and Bonventre, J. V. (2009). HIF in Kidney Disease and Development. *J. Am. Soc. Nephrol.* 20, 1877–1887. doi:10.1681/ASN.2008070804

Hanna, R. M., Streja, E., and Kalantar-Zadeh, K. (2021). Burden of Anemia in Chronic Kidney Disease: Beyond Erythropoietin. *Adv. Ther.* 38, 52–75. doi:10.1007/s12325-020-01524-6

Ishii, T., Tanaka, T., and Nangaku, M. (2021). Profile of Daprodustat in the Treatment of Renal Anemia Due to Chronic Kidney Disease. *Tcrm* Vol. 17, 155–163. doi:10.2147/TCRM.S293879

Jaakkola, P., Mole, D. R., Tian, Y. M., Wilson, M. I., Gielbert, J., Gaskell, S. J., et al. (2001). Targeting of HIF-alpha to the von Hippel-Lindau ubiquitylation complex by O2-regulated prolyl hydroxylation. *Science* 292, 468–472. doi:10.1126/science.1059796

Jono, S., McKee, M. D., Murry, C. E., Shioi, A., Nishizawa, Y., Mori, K., et al. (2000). Phosphate Regulation of Vascular Smooth Muscle Cell Calcification. *Circ. Res.* 87. doi:10.1161/01.res.87.7.e10

Kimura, Y., Yanagida, T., Onda, A., Tsukui, D., Hosoyamada, M., and Kono, H. (2020). Soluble Uric Acid Promotes Atherosclerosis via AMPK (AMP-Activated Protein Kinase)-Mediated Inflammation. *Arterioscler. Thromb. Vasc. Biol.* 40, 570–582. doi:10.1161/ATVBAHA.119.313224

Koulouridis, I., Alfayez, M., Trikalinos, T. A., Balk, E. M., and Jaber, B. L. (2013). Dose of Erythropoiesis-Stimulating Agents and Adverse Outcomes in CKD: A Metaregression Analysis. *Am. J. Kidney Dis.* 61, 44–56. doi:10.1053/j.ajkd.2012.07.014

Kumagai, T., Ota, T., Tamura, Y., Chang, W. X., Shibata, S., and Uchida, S. (2017). Time to Target Uric Acid to Retard CKD Progression. *Clin. Exp. Nephrol.* 21, 182–192. doi:10.1007/S10157-016-1288-2

Li, W., Zhao, Y., and Fu, P. (2018). Hypoxia Induced Factor in Chronic Kidney Disease: Friend or Foe. *Front. Med. (Lausanne)* 4, 259. doi:10.3389/fmed.2017.00259

Loboda, A., Jozkowicz, A., and Dulak, J. (2010). HIF-1 and HIF-2 Transcription Factors-Ssimilar but Not Identical. *Mol. Cell* 29, 435–442. doi:10.1007/S10059-010-0067-2

Locatelli, F., Bárány, P., Covic, A., De Francisco, A., Del Vecchio, L., Goldsmith, D., et al. (2013). Kidney Disease: Improving Global Outcomes Guidelines on Anaemia Management in Chronic Kidney Disease: A European Renal Best Practice Position Statement. *Nephrol. Dial. Transpl.* 28, 1346–1359. doi:10.1093/ndt/gft033

Locatelli, F., Fishbane, S., Block, G. A., and MacDougall, I. C. (2017). Targeting Hypoxia-Inducible Factors for the Treatment of Anemia in Chronic Kidney Disease Patients. *Am. J. Nephrol.* 45, 187–199. doi:10.1159/000455166

Malhotra, R., Mauer, A. C., Lino Cardenas, C. L., Guo, X., Yao, J., Zhang, X., et al. (2019). HDAC9 Is Implicated in Atherosclerotic Aortic Calcification and Affects Vascular Smooth Muscle Cell Phenotype. *Nat. Genet.* 51, 1580–1587. doi:10.1038/s41588-019-0514-8

Malik, R., Aneni, E. C., Shahrayar, S., Freitas, W. M., Ali, S. S., Veledar, E., et al. (2016). Elevated Serum Uric Acid Is Associated with Vascular Inflammation but Not Coronary Artery Calcification in the Healthy Octogenarians: the Brazilian Study on Healthy Aging. *Aging Clin. Exp. Res.* 28, 359–362. doi:10.1007/S40520-015-0395-3

Martin, K. J., and González, E. A. (2007). Metabolic Bone Disease in Chronic Kidney Disease. *J. Am. Soc. Nephrol.* 18, 875–885. doi:10.1681/ASN.2006070771

Maxwell, P. H., and Eckardt, K. U. (2016). HIF Prolyl Hydroxylase Inhibitors for the Treatment of Renal Anaemia and beyond. *Nat. Rev. Nephrol.* 12, 157–168. doi:10.1038/nrneph.2015.193

McCullough, P. A., Barnhart, H. X., Inrig, J. K., Reddan, D., Sapp, S., Patel, U. D., et al. (2013). Cardiovascular Toxicity of Epoetin-Alfa in Patients with Chronic Kidney Disease. *Am. J. Nephrol.* 37, 549–558. doi:10.1159/000351175

Metzen, E., and Ratcliffe, P. J. (2004). HIF Hydroxylation and Cellular Oxygen Sensing. *Biol. Chem.* 385, 223–230. doi:10.1515/BC.2004.016

Mokas, S., Larivière, R., Lamalice, L., Gobeil, S., Cornfield, D. N., Agharazii, M., et al. (2016). Hypoxia-inducible Factor-1 Plays a Role in Phosphate-Induced Vascular Smooth Muscle Cell Calcification. *Kidney Int.* 90, 598–609. doi:10.1016/j.kint.2016.05.020

Nagy, A., Pethő, D., Gáll, T., Zavaczki, E., Nyitrai, M., Posta, J., et al. (2020). Zinc Inhibits HIF-Prolyl Hydroxylase Inhibitor-Aggravated VSMC Calcification Induced by High Phosphate. *Front. Physiol.* 10, 1584. doi:10.3389/FPHYS.2019.01584

Nangaku, M., and Eckardt, K. U. (2007). Hypoxia and the HIF System in Kidney Disease. *J. Mol. Med. (Berl)* 85, 1325–1330. doi:10.1007/s00109-007-0278-y

Neogi, T., Terkeltaub, R., Ellison, R. C., Hunt, S., and Zhang, Y. (2011). Serum Urate Is Not Associated with Coronary Artery Calcification: the NHLBI Family Heart Study. *J. Rheumatol.* 38, 111–117. doi:10.3899/JRHEUM.100639

Palmer, S. C., Navaneethan, S. D., Craig, J. C., Johnson, D. W., Tonelli, M., Garg, A. X., et al. (2010). Meta-analysis: Erythropoiesis-Stimulating Agents in Patients with Chronic Kidney Disease. *Ann. Intern. Med.* 153, 23–33. doi:10.7326/0003-4819-153-1-201007060-00252

Paloian, N. J., and Giachelli, C. M. (2014). A Current Understanding of Vascular Calcification in CKD. *Am. J. Physiol. Ren. Physiol* 307, F891–F900. doi:10.1152/ajprenal.00163.2014

Robles, N. R. (2016). The Safety of Erythropoiesis-Stimulating Agents for the Treatment of Anemia Resulting from Chronic Kidney Disease. *Clin. Drug Investig.* 36, 421–431. doi:10.1007/s40261-016-0378-y

Sarnak, M. J., Levey, A. S., Schoolwerth, A. C., Coresh, J., Culleton, B., Hamm, L. L., et al. (2003). Kidney Disease as a Risk Factor for Development of Cardiovascular Disease: A Statement from the American Heart Association Councils on Kidney in Cardiovascular Disease, High Blood Pressure Research, Clinical Cardiology, and Epidemiology and Prevention. *Circulation* 108, 2154–2169. doi:10.1161/01.CIR.0000095676.90936.80

Schoppet, M., Shroff, R. C., Hofbauer, L. C., and Shanahan, C. M. (2008). Exploring the Biology of Vascular Calcification in Chronic Kidney Disease: What's Circulating. *Kidney Int.* 73, 384–390. doi:10.1038/sj.ki.5002696

Semenza, G. L. (2001). HIF-1, O(2), and the 3 PHDs: How Animal Cells Signal Hypoxia to the Nucleus. *Cell* 107, 1–3. doi:10.1016/S0092-8674(01)00518-9

Semenza, G. L., and Wang, G. L. (1992). A Nuclear Factor Induced by Hypoxia via De Novo Protein Synthesis Binds to the Human Erythropoietin Gene Enhancer at a Site Required for Transcriptional Activation. *Mol. Cel. Biol.* 12, 5447–5454. doi:10.1128/mcb.12.12.5447

Tachikawa, R., Koyasu, S., Matsumoto, T., Hamada, S., Azuma, M., Murase, K., et al. (2015). Obstructive Sleep Apnea and Abdominal Aortic Calcification: Is There An association Independent of Comorbid Risk Factors. *Atherosclerosis* 241, 6–11. doi:10.1016/j.atherosclerosis.2015.04.801

Tani, T., Orimo, H., Shimizu, A., and Tsuruoka, S. (2017). Development of a Novel Chronic Kidney Disease Mouse Model to Evaluate the Progression of Hyperphosphatemia and Associated mineral Bone Disease. *Sci. Rep.* 7, 2233. doi:10.1038/s41598-017-02351-6

Webster, A. C., Nagler, E. V., Morton, R. L., and Masson, P. (2017). Chronic Kidney Disease. *Lancet* 389, 1238–1252. doi:10.1016/S0140-6736(16)32064-5

Williams, M. C., Murchison, J. T., Edwards, L. D., Agustí, A., Bakke, P., Calverley, P. M., et al. (2014). Coronary Artery Calcification Is Increased in Patients with COPD and Associated with Increased Morbidity and Mortality. *Thorax* 69, 718–723. doi:10.1136/thoraxjnl-2012-203151

Yan, B., Liu, D., Zhu, J., and Pang, X. (2019). The Effects of Hyperuricemia on the Differentiation and Proliferation of Osteoblasts and Vascular Smooth Muscle Cells Are Implicated in the Elevated Risk of Osteopenia and Vascular Calcification in Gout: An *In Vivo* and *In Vitro* Analysis. *J. Cel. Biochem.* 120, 19660–19672. doi:10.1002/JCB.29272

Conflict of Interest: The authors declare that the research was conducted in the absence of any commercial or financial relationships that could be construed as a potential conflict of interest.

Publisher's Note: All claims expressed in this article are solely those of the authors and do not necessarily represent those of their affiliated organizations, or those of the publisher, the editors, and the reviewers. Any product that may be evaluated in this article, or claim that may be made by its manufacturer, is not guaranteed or endorsed by the publisher.

frontiers in Pharmacology

ORIGINAL RESEARCH
published: 11 March 2022
doi: 10.3389/fphar.2022.841435

A Novel Modulator of the Renin–Angiotensin System, Benzoylaconitine, Attenuates Hypertension by Targeting ACE/ACE2 in Enhancing Vasodilation and Alleviating Vascular Inflammation

Qi-Qiang Zhang[1†], *Feng-Hua Chen*[1†], *Fei Wang*[2], *Xue-Mei Di*[1], *Wei Li*[2] *and Hai Zhang*[1*]

[1]*Shanghai First Maternity and Infant Hospital, School of Medicine, Tongji University, Shanghai, China,* [2]*School of Pharmacy, Shandong University of Traditional Chinese Medicine, Jinan, China*

OPEN ACCESS

Edited by:
Vicky E MacRae, University of Edinburgh, United Kingdom

Reviewed by:
Satomi Kagota, Mukogawa Women's University, Japan
Xiaofei Chen, Second Military Medical University, China

***Correspondence:**
Hai Zhang
zhxdks2005@126.com

[†]*These authors have contributed equally to this work*

Specialty section:
This article was submitted to Cardiovascular and Smooth Muscle Pharmacology, a section of the journal Frontiers in Pharmacology

Received: *22 December 2021*
Accepted: *09 February 2022*
Published: *11 March 2022*

Citation:
Zhang Q-Q, Chen F-H, Wang F, Di X-M, Li W and Zhang H (2022) A Novel Modulator of the Renin–Angiotensin System, Benzoylaconitine, Attenuates Hypertension by Targeting ACE/ACE2 in Enhancing Vasodilation and Alleviating Vascular Inflammation. Front. Pharmacol. 13:841435. doi: 10.3389/fphar.2022.841435

The monoester alkaloids in *Aconitum carmichaelii*, including benzoylaconitine (BAC), benzoylmesaconine, and benzoylhypaconitine, were found to have anti-hypertensive effects in spontaneously hypertension rats (SHRs), of which BAC is the strongest. However, its antihypertensive target and underlying molecular mechanisms remain unclear. In this study, first, we screened the antihypertensive targets of BAC by using the CVDPlatform (www.cbligand.org/CVD) and found that ACE/ACE2 are the most possible targets. Then, we verified the effect of BAC on ACE/ACE2 by virtual docking, SPR, enzyme activity assay, and HUVECs cell experiment. We found that BAC could bind with ACE/ACE2, inhibit ACE activity and protein expression, and activate ACE2 enzyme activity. Using vascular function test *in vitro,* we found that BAC could target ACE/ACE2 to enhance endothelium-dependent vasorelaxation. In BAC-treated SHRs, the levels of ACE and AngII in serum were reduced while Ang (1–7) was increased significantly, and the expression of ACE was reduced, which suggested that BAC can inhibit ACE and activate ACE2 to inhibit AngI to AngII and promote AngII to Ang (1–7) to inhibit vasoconstriction and finally attenuate hypertension. Furthermore, the signaling pathways with regard to vasorelaxation and vascular inflammation were investigated. The results showed that BAC could significantly activate Akt/eNOS, increase NO production, and promote endothelial-related vasodilation; BAC could also reduce inflammatory factors TNF-α and IL6, inhibition of COX-2 expression, and IKB-α phosphorylation to reduce vascular inflammation in SHRs. In brief, BAC targets ACE/ACE2 to enhance endothelium-dependent vasorelaxation

Abbreviations: ACEIs, angiotensin-converting enzyme inhibitors; Ang, angiotensin; ARBs, Ang II receptor blockers; BAC, benzoylaconitine; BMC, benzoylmesaconine; BHC, benzoylhypaconitine; CCK-8, Cell Counting Kit-8; DAPI, 4′,6-diamidino-2-phenylindole dihydrochloride; DBP, diastolic blood pressure; EC50, 50% effective concentration; ECM, endothelial cell medium; HUVECs, human umbilical vein endothelial cells; IC50, 50% inhibiting concentration; LD50, median lethal dose; MAP, mean arterial pressure; MDAs, monoester-diterpenoid alkaloids; RAS, renin–angiotensin system; SHRs, spontaneously hypertension rats; SD rats, Sprague-Dawley rats; DMSO, dimethyl sulfoxide; SPR, surface plasmon resonance; rhACE, recombinant human ACE; PBS, phosphate buffered saline; SBP, systolic blood pressure; UHPLC-MS/MS, ultra-high-performance liquid chromatography-tandem mass spectrometry.

and reduce vascular inflammation to attenuate hypertension as a potential modulator of the renin–angiotensin system.

Keywords: benzoylaconitine, antihypertensive effect, ACE, ACE2, renin–angiotensin system

INTRODUCTION

Hypertension is a high-risk chronic disease and is the leading cause of death globally, accounting for 10.4 million deaths per year worldwide (GBD 2017 Risk Factor Collaborators, 2018). It manifests primarily as high blood pressure and other cardiovascular complications, such as cardiovascular, neural, and renal diseases (Chockalingam, 2008). Drug therapy is the main treatment for hypertension. Besides regular medicines, angiotensin-converting enzyme inhibitors (ACEI), Ang II receptor blockers (ARB), calcium blockers, diuretics, and so on (Chockalingam, 2008), many traditional Chinese herbs have been used to clinically treat hypertension, especially *Aconitum carmichaelii*, which is officially recorded in Chinese pharmacopoeia and has been used to treat cardiovascular disease for many years.

A. carmichaelii is also known as "Fu Zi" sourced from the lateral root of *A. carmichaelii Debx*. It is beneficial for combating cardiovascular diseases, such as hypertension and heart failure (Xu et al., 2021). Alkaloids are considered the most predominant active ingredients in *A.* carmichaelii, which can be divided into three groups, including diester-diterpenoid alkaloids, monoester-diterpenoid alkaloids (MDAs), and alcohol-amine alkaloids. Some earlier studies demonstrated that diester-diterpenoid alkaloids, especially aconitine, are powerful agents for treating hypertension and contribute to their strong cardiovascular effects (Wang et al., 2020b). Unfortunately, they are not considered for clinical use owing to their toxic effects (Lin et al., 2004). In our previous study, systematic analysis of alkaloids using ultra-high-performance liquid chromatography-tandem mass spectrometry (UHPLC-MS/MS) revealed that diester-diterpenoid alkaloids could be transformed to MDAs by boiling or metabolism *in vivo*, and MDAs mainly contain benzoylaconitine (BAC), benzoylmesaconine (BMC), and benzoylhypaconitine (BHC) (Zhang et al., 2014; Zhang H. et al., 2015). Pharmacokinetic analysis in our previous study indicated that these MDAs had a low T_{max} value and high $t_{1/2}$ (Zhang W. et al., 2015; Zhang et al., 2016b), which indicated that they can be absorbed rapidly and metabolized or excreted slowly. In addition, BAC was also found to be safer as its oral median lethal dose (*LD50*) is 1,500 mg kg^{-1} in mice (Wada et al., 2005). According to this evidence, we conferred that MDAs are potential therapeutic drugs for anti-hypertension.

However, the anti-hypertensive effect and targets of three MDAs are still unclear. In our previous study, we constructed the CVD intelligent analysis platform (www.cbligand.org/CVD) for the target screening and verification of anti-hypertensive compounds of traditional Chinese medicinal herbs (Zhang et al., 2016a). This platform involved main targets of the coagulation system, RAS system, adrenaline system, HMGCoA system, etc. We have successfully used the CVDPlatform to screen the active components and possible targets of a traditional Chinese herbal formula (Wang et al., 2020a).

Based on our preliminary study on the antihypertensive effect of three MDAs, we have carried out our research from the following aspects in this study: (1) evaluate the anti-hypertensive action of MDAs in spontaneously hypertension rats (SHRs) by i.v. injection and oral administration, and verify that BAC is the best one; (2) screen and identify the targets of BAC for anti-hypertension in the CVDPlatform; (3) verify the binding and effect between the BAC and its targets *via* virtual dock, SPR assay, and enzyme activity test; (4) verify the role of BAC on its targets in HUVECs; (5) verify the effect of BAC for anti-hypertension in SHRs; and (6) clarify the molecular mechanism by investigating the signaling pathways with regard to vasorelaxation and vascular inflammation. We hope that this study could provide support for drug discovery and clinical therapy of BAC for anti-hypertension.

MATERIALS AND METHODS

Animal Model and Ethics Statement

This study was performed in accordance with the Chinese legislation and regulations of Laboratory Animals of the Chinese Animal Welfare Committee. The protocols for this study were approved by the ethics committee of the Tongji University School of Medicine (Shanghai, China, No. TJBG00121313) and authorized by the Shanghai First Maternity and Infant Hospital, Tongji University School of Medicine (Shanghai, 201204, China).

Fifteen-week-old male SHRs (280.0 ± 10 g) and 10-week-old male Sprague–Dawley (SD) rats (310.0 ± 10 g) were obtained from Charles River Co., Ltd. (Beijing, China). The animals were housed at the Tongji University Animal Center for a week for acclimatization, where they were exposed to a 12-h light/12-h dark cycle under conditions of controlled temperature of 25 ± 2°C and relative humidity of 45% ± 5%. All rats were provided access to standard rat chow and water *ad libitum*. This protocol was approved by the University of Tongji Animal Welfare Committee in accordance with the guidelines issued by the China Council on Animal Care and adhered to the *Guide for the Care and Use of Laboratory Animals* published by the United States National Institutes of Health.

Surgical Procedure

The SHRs were surgically implanted with a catheter *via* the left femoral artery, vein, and stomach after anesthetizing with 2% pentobarbital sodium (40 mg kg^{-1} i.p.,). A pressure sensor was inserted into the terminal of the arterial catheter and connected to a PowerLab system (ADInstruments, New South Wales, Australia) for real-time blood pressure monitoring.

TABLE 1 | Information on BAC, BHC, and BMC.

Full name	Abbreviation	Formula	MW (g/mol)
Benzoylaconitine	BAC	$C_{32}H_{45}NO_{10}$	604
Benzoylmesaconine	BMC	$C_{31}H_{43}NO_{10}$	590
Benzoylhypaconitine	BHC	$C_{31}H_{43}NO_9$	574

Dosage Information

All three MDAs (BAC, BMC, and BHC) were purchased from Nature-Standard Co., Ltd. (Shanghai, China) and their purities were all over 98%. Information on the three MDAs is shown in **Table 1**. The anti-hypertensive effects of MDAs were studied in both acute and chronic experiments. The 16-week-old SHRs were used in animal experiments, and each group had six rats. In the acute experiment, drug administration was *via* i.v. injection. For i.v. injection, the animals were randomly assigned into four groups: vehicle (0.1% DMSO–0.9% salt solution, $n = 6$), low-dose group (0.6 mg kg^{-1} body weight, $n = 6$), medium-dose group (2 mg kg^{-1} body weight, $n = 6$), and high-dose group (6 mg kg^{-1} body weight, $n = 6$). The drug was administered using a venous catheter. In chronic experiments, the animals were randomly assigned into five groups: vehicle (5% Tween 80–0.9% salt solution, $n = 6$), captopril group (5 mg kg^{-1} body weight, $n = 6$), low-dose group (3 mg kg^{-1} body weight, $n = 6$), medium-dose group (10 mg kg^{-1} body weight, $n = 6$), and high-dose group (30 mg kg^{-1} body weight, $n = 6$). Oral administration with drug or 5% Tween 80–0.9% salt solution was carried out once a day, and continued for 14 days. The drugs were dissolved in 0.1% DMSO–0.9% salt solution for intravenous injection and in 5% Tween 80–0.9% salt solution for oral administration. Blood pressure was recorded in real time.

Blood Pressure Recording

Real-time blood pressure level was monitored after drug treatment in the acute and chronic experiments. All animals were surgically implanted with a catheter in the left femoral artery. After connection to the monitor, all animals were placed at room temperature of 25°C for 0.5–1 h and the average blood pressure value was calculated based on a real-time blood pressure curve (10 s of every 30 s).

Target Screening, Virtual Docking, and Surface Plasmon Resonance Assay

To screen the potential targets of the MDAs in hypertension, a CVDPlatform (www.cbligand.org/CVD) was used as previously reported (Zhang et al., 2016a). The results of database screening were verified by virtual docking with Discovery Studio 3.5 (BIOVIA, San Diego, CA, United States) and then validated in the SPR assay. In the SPR assay, a solution of protein standards was prepared, and the concentration of recombinant human ACE (rhACE) protein and rhACE2 (Proteintech, Rosemont, IL, United States) solution was set to 500 μg ml^{-1}. After combining with the chips, a series of concentrations of compounds, which were double-diluted at each step with 5% DMSO–1.05 × phosphate buffered saline (PBS) solution, were tested for their binding affinity to the proteins. Finally, the level of binding between the proteins and each molecule was determined based on the K_d value.

Enzyme Kinetics Study

ACE and ACE2 activities were measured using the ACE activity assay kit and SensoLyte390 ACE2 activity assay kit (Anaspec, Fremont, CA, United States), respectively, according to the manufacturer's instructions with some modifications. Briefly, rhACE solution dissolved in deionized water was used for analysis. ACE activity was measured in a reaction system with 50 μl of the sample and 50 μl of the ACE substrate solution with or without BAC (10^{-4} to 10^{-2} μM). ACE2 activity was assayed in the same manner as ACE activity. All assays were performed every 10 s for 30 min at 37°C using a Varioskan LUX fluorescence microplate reader (Thermo Fisher Scientific, Waltham, MA, United States). The autofluorescence value in each assay was subtracted from the measured values to generate the final results. The relative fluorescence unit of each sample was normalized to the corresponding total protein concentration, which was measured using a Pierce BCA protein assay kit (Thermo Fisher Scientific).

Cell Culture and Treatment

Human umbilical vein endothelial cells (HUVECs) were isolated from umbilical cords as previously described (Jaffe et al., 1973). They were purchased from ATCC (cat# CRL-1444, Manassas, VA, United States) and cultured in endothelial cell medium (ECM, ScienCell, Carlsbad, CA, United States) supplemented with 5% FBS, 1% endothelial cell growth supplement, and 1% antibiotics (Sigma, St. Louis, MO, United States). Cells harvested between the third and tenth passages were used in the experiments. Cells were cultured until they were ~80% confluent. After pre-starving in a quiescing ECM supplemented with 1% FBS and 1% antibiotics for 24 h, the cells were treated using different concentrations of BAC (Control, DMSO, 25, 50, and 100 μM, dissolved in 0.1% DMSO–DMEM) with or without MG132, an inhibitor of proteasome, at 20 nM or 40 nM for 24 h. Then, cell samples were collected for Western blot analysis or immunofluorescence staining.

Drug Cytotoxicity

The potential of cells to maintain or recover viability after treatment with each agent was determined. Cell viability can be distinguished from the all-or-nothing states of life and death using a quantifiable index between 0 and 1 (or 0 and 100%). Cell viability was measured by a Cell Counting Kit-8 (CCK-8) Assay Kit (EnoGene, Nanjing, China). The cells (1×10^4) were seeded in a 96-well plate. After reaching 90% density and starving for 24 h, the cells were treated with different concentrations of BAC (0, 12.5, 25, 50, 100, 200, and 400 μM) or with 0.1% DMSO for 48 h. CCK-8 reagent (10 μl) was added to fresh medium (100 μl) in each well. After 1 h of incubation, the absorbance was measured at

450 nm using a microplate reader (Thermo Fisher Scientific). The measurement of cell viability at each concentration was repeated three times.

Immunofluorescence Staining

After treatment with different concentrations of BAC (Control, DMSO, 25, 50, and 100 μM, dissolved in 0.1% DMSO–DMEM) for 24 h, the cells were washed with PBS three times, fixed in 4% paraformaldehyde for 20 min, permeabilized with 0.3% Triton X-100 for 20 min, and then blocked with 5% BSA for 30 min at room temperature of 25°C. Next, the cells were treated with primary antibodies against ACE (1:100, ABclonal) and ACE2 (1:100, ABclonal) at 4°C overnight, followed by treatment with fluorescein isothiocyanate-labeled secondary antibody (1:400, Beyotime, Wuhan, China) for 1 h at room temperature (25°C). 4′,6-Diamidino-2-phenylindole dihydrochloride (DAPI, Beyotime) was used for nuclear staining. The samples were analyzed using a confocal laser scanning microscope (Zeiss LSM 510 META, Oberkochen, Germany).

Histological and Immunofluorescence Staining Analysis

After euthanizing the rats with sodium pentobarbital (100 mg kg^{-1}, i.p.) administration in combination with isoflurane inhalation, the aortas were harvested directly according to a previously described method. The aortas were fixed in 4% paraformaldehyde for 24 h and embedded in paraffin. The cross-sections (5 μm) were stained with hematoxylin and eosin or subjected to immunostaining. Immunofluorescence staining for ACE and ACE2 was performed according to the manufacturer's instructions (Servicebio, Wuhan, China).

Western Blot Analysis

The cell samples and tissue sample were collected and placed in ice rapidly. All samples were washed with PBS and lysed in a buffer containing protease inhibitors (Roche, Basel, Switzerland). Total proteins were extracted after incubation in lysis buffer for 15 min on ice. The supernatants were collected after centrifugation (12,000 × *g*, 4°C, 10 min). Mitochondrial proteins were isolated using a mitochondrial isolation kit (YEASEN, Shanghai, China). Protein concentration in cell lysates was measured using a Bio-Rad DC Protein Assay Kit (Pierce, Rockford, United States). The proteins (20 μg) were separated by electrophoresis at 100 V for 80 min in a 10% polyacrylamide gel and electrotransferred (Bio-Rad) to polyvinylidene fluoride membranes at 110 V for 70 min. To prevent non-specific binding, the membranes were blocked by treating with 5% milk for 60 min at 20°C. The proteins were treated with primary antibodies against ACE (1: 1,000; cat#A2805, ABclonal, Shanghai, China), ACE2 (1: 1,000; cat#A4612, ABclonal), eNOS (1:1,000; cat#A20985, ABclonal), p-eNOS^{Ser1177} (1:1,000; cat#AP0515, ABclonal), COX-2 (1:1,000; cat#A3560, ABclonal), IKB-α (1:1,000; cat#A11397, ABclonal), p-IKB-α (1:1,000; cat#AP0707, ABclonal), and GAPDH (1:10,000; cat#AC027, ABclonal) at 4°C overnight, and were then treated with HRP-secondary antibodies (1:15,000; ABclonal) at 25°C for 1 h. After washing three times with TBS-Tween (for 5 min), the membrane was observed.

Plasma Biomarker Analysis

Blood samples were collected from the left femoral artery of rats at the end point, followed by centrifugation at 1,000 × *g* for 15 min at 4°C. Only serum was collected and stored at −80°C until analysis. The concentrations of circulating ACE, ACE2, Ang I, Ang II, Ang (1–7), TNF-α, and IL-6 in serum were measured using the ELISA kits [ACE, cat#xy-R2401c, X-Y Biotechnology, Shanghai, China; ACE2, cat#xy-ACE2-Ra, X-Y Biotechnology; Ang I, cat#xy-E12541, X-Y Biotechnology; Ang II, cat#xy-R1430c, X-Y Biotechnology; Ang (1–7), cat#xy-Ang1-7-Ra, X-Y Biotechnology; TNF-α, cat#GM1149, Servicebio, Shanghai, China; IL-6, cat#GM1154, Servicebio] according to the manufacturer's instructions. The absorbance was measured using a microplate reader (Thermo Fisher Scientific) at 450 nm and calculated according to the standard curve. Each experimental group had three duplicate wells, and the experiment was repeated three times.

Vascular Function

Endothelium-dependent vasorelaxation using aorta was evaluated as previously described (Liao et al., 2019). Briefly, after euthanizing the SD rat with sodium pentobarbital (100 mg kg^{-1}, i.p.) administration in combination with isoflurane inhalation, thoracic aorta (diameter: 150–250 μm, length: 2 mm) was mounted on two tungsten wires and attached to a tension sensor system (ADInstruments). After balancing for 2 h in Krebs' solution at 37°C, arteries were exposed to 10 μM of phenylephrine (PE, Sigma-Aldrich, St. Louis, MO, United States) twice, followed by a single dose of acetylcholine (Ach, 3 μm, Sigma-Aldrich, St. Louis, MO, United States) to evaluate the integrity of the vessel. Afterward, the vessel was pre-constricted to maximum using AngI (Sigma-Aldrich) at 10^{-2} μM and then treated with a series concentration of BAC or A779 (Sigma-Aldrich) or captopril at 10^{-6} to 10^{-1} μM. Lastly, a cumulative concentration response curve to BAC with A779 (at 10^{-2} μM) was performed to assess the endothelium-dependent vasorelaxation.

Measurement of Total NO

Total NO levels in serum obtained from SHRs treated with vehicle, BAC, or captopril for 14 days were quantified by using total nitric oxide assay kit (Beyotime, Shanghai, China) as described previously. The absorbance was measured using a microplate reader (Thermo Fisher Scientific) at 540 nm and calculated according to the standard curve. Each experimental group had three duplicate wells, and the experiment was repeated three times.

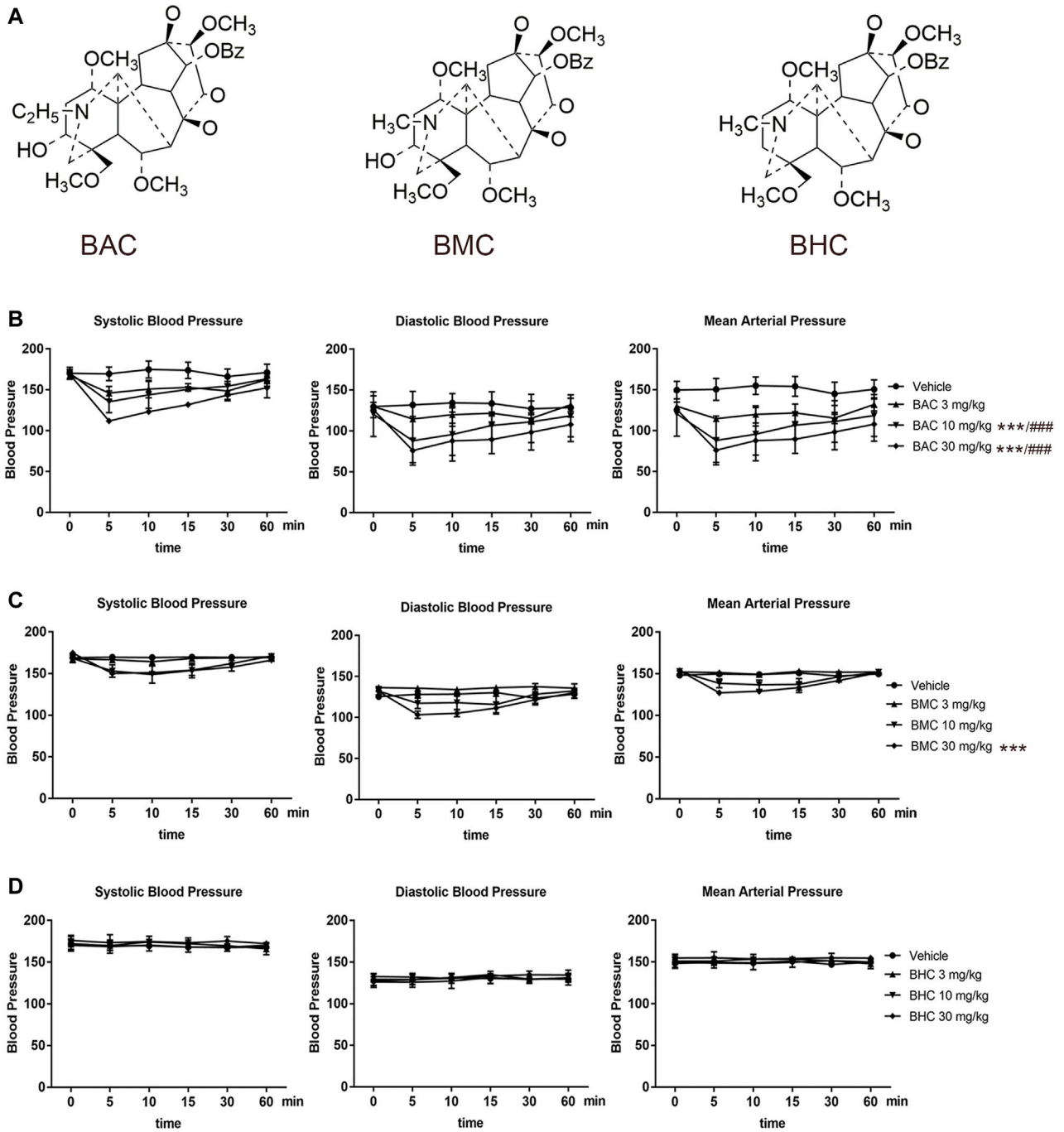

FIGURE 1 | Anti-hypertensive effect of three monoester alkaloids (MDAs). **(A)** Structure of MDAs. Left to right were benzoylaconitine (BAC), benzoylmesaconine (BMC), and benzoylhypaconitine (BHC). **(B–D)** Blood pressure measurement and heart rate recording after intravenous administration of drugs in spontaneous hypertension rats (SHRs). SHRs were divided into four groups randomly. The experimental groups were the vehicle group ($n = 6$), the low-dose group (0.6 mg kg^{-1}, $n = 6$), the medium-dose group (2 mg kg^{-1}, $n = 6$), and the high-dose group (6 mg kg^{-1}, $n = 6$). **(B)** To BAC, **(C)** to BMC, and **(D)** to BHC. The experimental results were expressed by mean ± SEM, $^{*}p < 0.005$, as compared with the vehicle control, $^{\#\#\#}p < 0.005$, as compared with the BMC or BHC in the same dosage.

Data and Statistical Analysis

Data are expressed as mean ± SEM. Differences between two groups were compared using a two-tailed Student's *t*-test. Differences among multiple groups were analyzed using two-way ANOVA followed by Bonferroni's post-hoc test. Differences with $p < 0.05$ were considered statistically significant.

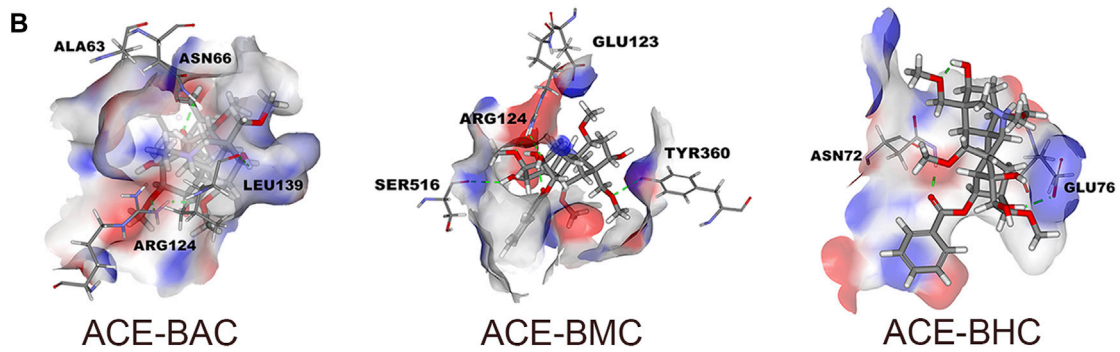

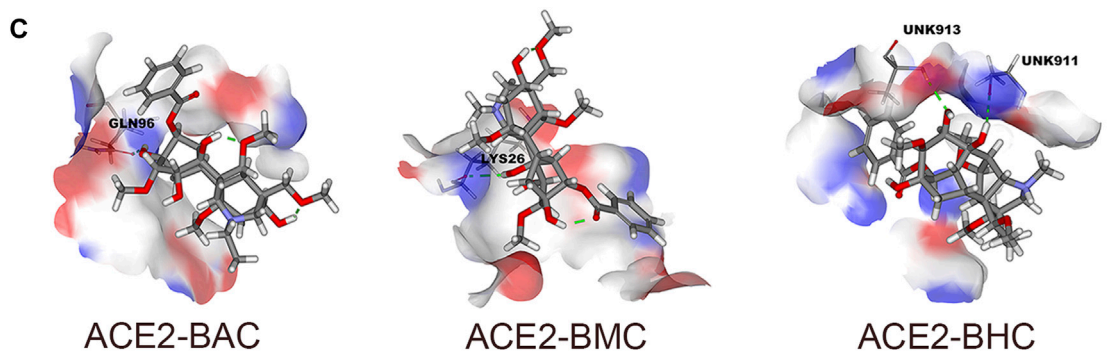

D

Protein	Protein Sequence	Compound	Libdock_Score	CDOCK_Score
ACE	642-1230	BAC	147	74.4
		BMC	118	67.6
		BHC	98.3	32.3
ACE2	1-615	BAC	106	39.4
		BMC	105	34.1
		BHC	87.5	23.9

FIGURE 2 | MDAs bound with ACE and ACE2 in Virtual Docking. Target screening and virtual docking of MDAs. **(A)** Drug molecular potential target screening based on the CVD-Platform online analysis platform. **(B,C)** Molecular docking of MDAs at ACE and ACE2 active sites. Drug molecules interact with amino acid residues of ACE and ACE2 mainly through hydrogen bonds. Blue: donor; Red: acceptor. **(D)** Docking results of MDAs with ACE and ACE2. The docking modes including Libdock (high throughput) and CDOCK (precision docking).

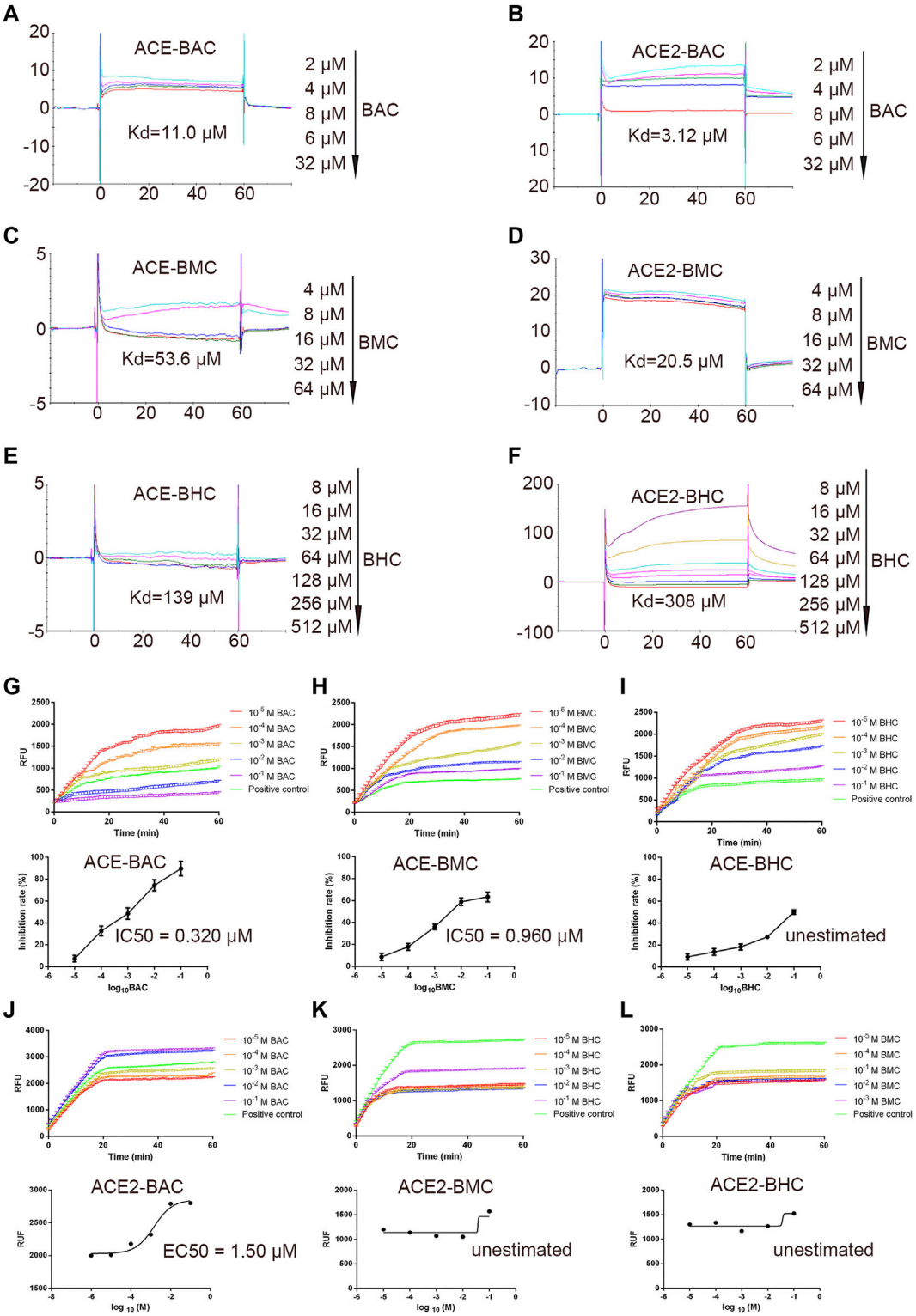

FIGURE 3 | *In vitro* binding and bioactivity verification of MDAs with proteins ACE and ACE2 under cell-free conditions. **(A–F)** Binding verification between protein and molecules were measured by SPR. A series of concentration step of drug diluted with 5% DMSO–1.05*PBS was reacted with the protein in chip, the electrical signal value was recorded, and the dissociation constant K_d value was determined. **(A)** ACE with BAC, **(B)** ACE with BMC, **(C)** ACE with BHC, **(D)** ACE2 with BAC, **(E)** ACE2 with BMC, and **(F)** ACE2 with BHC. **(G–L)** Bioactivity verification of MDAs by enzyme kinetics experiment. Dose-dependent hrACE2 activity in the presence of MDAs. Then, MDAs of series of concentrations were added into the system respectively. Results were analyzed by GraphPad Prism 7.0 software. Each group was repeated three times. **(A)** ACE and BAC, **(B)** ACE and BMC, **(C)** ACE and BHC, **(D)** ACE2 and BAC, **(E)** ACE2 and BMC, and **(F)** ACE2 and BHC. The value was expressed by mean ± SEM.

RESULTS

MDAs Attenuated High Arterial Pressure in SHRs

The structures of the three MDAs are shown in **Figure 1A**. We determined whether they elicited anti-hypertensive effects *via* experiments on rats with acute and chronic hypertension by assessing systolic blood pressure (SBP), diastolic blood pressure (DBP), mean arterial pressure (MAP), and heart rate (HR). In the acute experiment, we observed that BAC and BMC exerted observable anti-hypertensive effects but BHC did not. Even at the lowest dose (0.6 mg kg^{-1}), BAC administered *via* i.v. injection for 1–5 min could lower SBP, DBP, and MAP by more than 20 mmHg, with the anti-hypertensive effect lasting for at least 30 min. At a medium dose (2 mg kg^{-1}) and high dose (6 mg kg^{-1}), BAC had a better effect (**Figure 1B**). The effect of BMC was weaker than that of BAC as blood pressure was reduced by approximately 20 mmHg only at a dosage of 6 mg kg^{-1} (**Figure 1C**). BHC at a dosage lower than 6 mg kg^{-1} exerted no anti-hypertensive effects (**Figure 1D**). Heart rate had no significant change after drug administration. Thus, BAC is the best candidate drug for lowering blood pressure among these MDAs. The results showed that at medium and high dosage, BAC and BMC exerted anti-hypertensive effects in a dose-dependent manner.

MDAs Bound With ACE and ACE2 in Virtual Docking and SPR Assay

After screening in the CVDPlatform, ACE and ACE2 were found to be potential targets of the three MDAs (**Figure 2A**). To verify the binding relationship of MDAs with ACE and ACE2, virtual docking (a method in virtuality) was used. In virtual docking, the Libdock results of BAC, BMC, and BHC were 147, 118, and 98.3 with ACE and 106, 105, and 87.5 with ACE2. The CDOCK results of BAC, BMC, and BHC were 74.4, 67.6, and 32.3 with ACE and 39.4, 34.1, and 23.9 with ACE2, respectively. Comparing the dock score of each molecule and protein, BAC and BMC were found to have a better binding relationship with ACE owing to hydrogen bonding (**Figure 2B**), whereas their binding relationship with ACE2 was ambiguous (**Figures 2C,D**). BHC appeared to have the weakest binding relationship among these compounds. In summary, among these three MDAs, BAC showed the best binding with both ACE and ACE2, followed by BMC and BHC.

MDAs Bind With ACE/ACE2 and Affected Their Activity Under Cell-Free Conditions *In Vitro*

The SPR assay was used to identify the binding between the drugs and proteins (Nguyen et al., 2015). The results showed that MDAs interacted with the rhACE protein with a K_d of 11.0, 53.6, and 139 μM (**Figures 3A,C,E**). They interacted with the rhACE2 protein with a K_d of 3.12, 20.5, and 308 μM (**Figures 3B,D,F**). These are consistent with the results of virtual docking. In order to further verify the effect of MDAs on the biological activities of ACE and ACE2 proteins, enzyme kinetics experiments were carried out. According to the experimental results, we observed that BAC and BMC clearly inhibited ACE activity, and their IC_{50} values were 0.320 and 0.960 μM, respectively (**Figures 3G,H**). However, BHC had little effect on ACE activity, and its IC_{50} value could not be determined (**Figure 3I**). Moreover, MDAs were found to have an excitatory effect on ACE2 activity. Among them, BAC had the most significant effect, and its EC_{50} value was 1.50 μM (**Figure 3J**), while BMC and BHC played weaker pharmacodynamics effects, and their EC_{50} values could not be determined (**Figures 3K–L**-L). Taken together, the results showed that BAC had the strongest effect on ACE and ACE2 under cell-free conditions.

Benzoylaconitine Inhibited the Protein Expression of ACE Directly in HUVECs

Binding of BAC with ACE prompted us to examine whether BAC affects the expression of ACE and ACE2 in HUVECs, which are model cells for studying hypertension. Cell viability experiment was used to evaluate the toxicity of BAC on HUVECs, and the results showed that BAC at a dose lower than 100 μM had no significant effect (**Figure 4A**). The protein expression of ACE and ACE2 in RAS was measured by Western blotting and immunofluorescence staining, and we found that BAC can inhibit the expression of ACE, but does not affect the protein expression of ACE2 (**Figures 4B–D**). Adding proteasome inhibitor, MG132, we further found that BAC could promote ACE protein degradation to inhibit the expression level of ACE directly.

Benzoylaconitine Attenuated Hypertension in SHRs

In view of the above results, BAC showed the most significant anti-hypertensive effect. Thus, a long-term animal experiment was conducted using BAC. Captopril (5 mg kg^{-1}) was used as a positive control for this experiment. The process of this experiment is shown in **Figure 5A**. The SBP, DBP, and MAP of SHRs were 172 ± 6 mmHg, 130 ± 5 mmHg, and 151 ± 5 mmHg, respectively. After 14 days of oral administration, the SBP, DBP, and MAP reduced in the medium-dose group (10 mg kg^{-1}) and the high-dose group (30 mg kg^{-1}). The SBP, DBP, and MAP of the medium-dose group were 154 ± 6 mmHg, 119 ± 8 mmHg, and 136 ± 7 mmHg, respectively, and those of the high-dose group were 139 ± 6 mmHg, 101 ± 7 mmHg, and 121 ± 6 mmHg, respectively. However, the blood pressure of the low-dose group did not significantly differ from the vehicle group (**Figures 5B–D**). Heart rate changed in the high-dose group and captopril group, and they had similar heart rate changes, which means that BAC could also reduce the heart rate after long-term drug treatment (**Figure 5E**). The vascular smooth muscle was thicker in the absence of BAC treatment. This suggests that BAC could reverse smooth muscle remodeling to play an anti-hypertensive effect (**Figure 5F**).

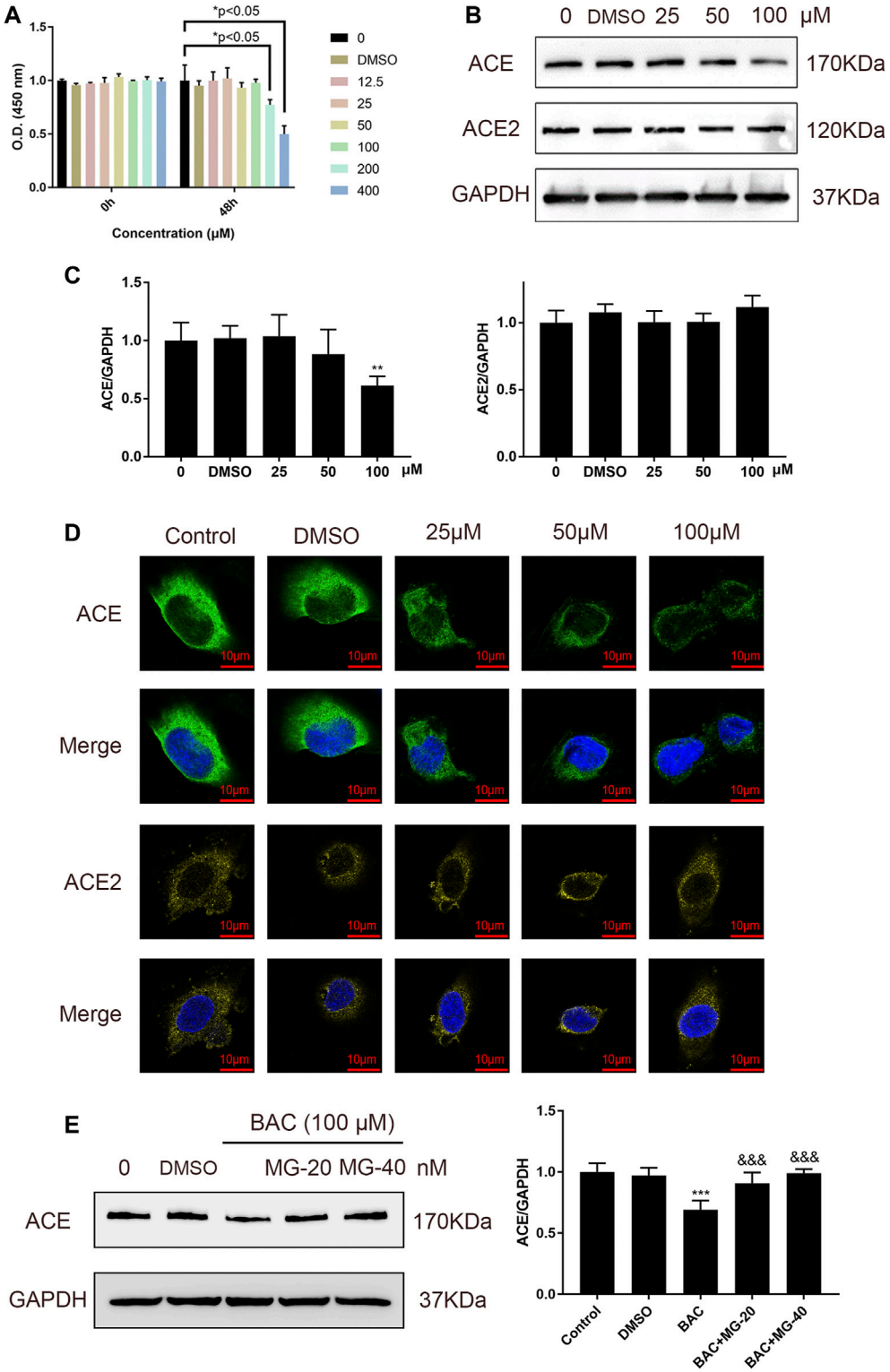

FIGURE 4 | BAC inhibited ACE directly in HUVECs. **(A)** Starved HUVECs were preconditioned with a series of BAC (0, 12.5, 25, 50, 100, 200, and 400 μM) or with 0.1% DMSO for 48 h and then measured by CCK-8 assay ($n = 3$) at 450 nm. *$p < 0.05$ compared with 0 group. **(B,C)** After being starved, HUVECs were treated with serial concentrations of BAC (0, DMSO, 25, 50, and 100 μM) for 24 h to extract protein, and the protein quantity of ACE and ACE2 was detected by Western blot. The gray value of protein was determined by ImageJ. **(D)** Representative image of fluorescence immunoassay for protein expression and fluorescence localization of ACE and ACE2. Starved HUVECs were treated with serial concentrations of BAC (0, DMSO, 25, 50, and 100 μM) for 24 h and measured by fluorescence immunoassay. **(E)** After being starved, HUVECs were treated with BAC (100 μM) and with or without MG132 at 20 nM or 40 nM for 24 h. The protein quantity of ACE was detected by Western blot. The gray value of protein was determined by ImageJ. The value was expressed by mean ± SEM. **$p < 0.05$, ***$p < 0.05$, as compared with the 0 group.

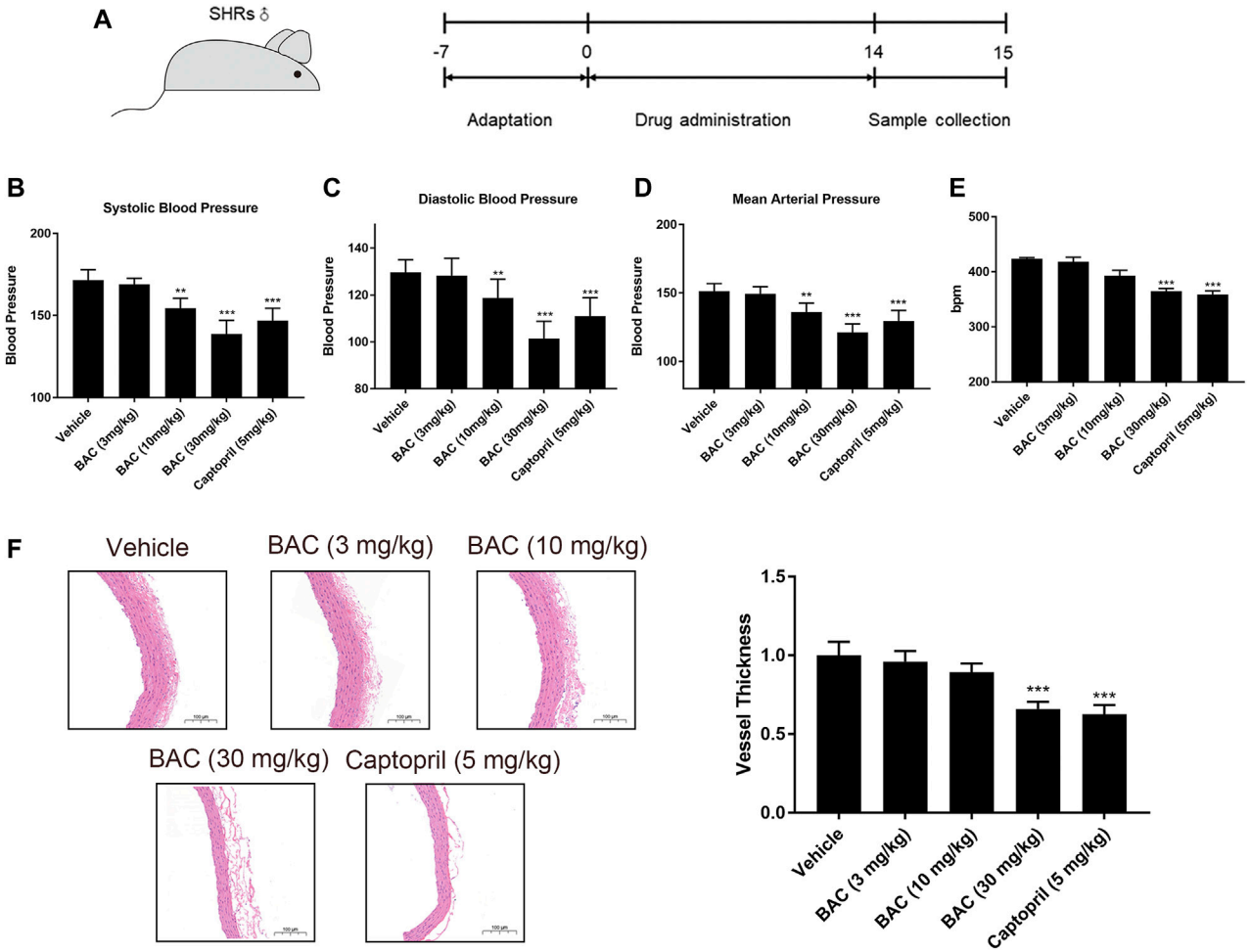

FIGURE 5 | BAC attenuated hypertension in SHRs after a 14-day oral administration. The experimental groups were the vehicle group ($n = 6$), the low-dose group (3 mg kg^{-1}, $n = 6$), the medium-dose group (10 mg kg^{-1}, $n = 6$), the high-dose group (30 mg kg^{-1}, $n = 6$), and the captopril group (5 mg kg^{-1}, $n = 6$). All rats were given a 14-day oral administration. **(A)** The process of animal administration and sample collection in our research. **(B–D)** BAC reduced the blood pressure of SHRs measured after 14 days of oral administration. **(B)** Systolic blood pressure (SBP), **(C)** diastolic blood pressure (DBP), and **(D)** mean arterial pressure (MAP). **(E)** Heart rate recording. **(F)** Representative hematoxylin and eosin stain image of SHRs with or without BAC oral administration. Data represented as mean ± SEM from six animals per treatment group. $^{**}p < 0.05$, $^{***}p < 0.005$, as compared with the vehicle control.

Benzoylaconitine Attenuated Hypertension Through Regulating RAS in SHRs

Vascular function was performed in isolated vascular rings as in a previous study (Liao et al., 2019). The results demonstrated that BAC could attenuate Ang I-induced vascular constriction, and it could be abolished by Mas inhibitor, A779 (**Figure 6A**). The serological experiments related to the RAS were carried out in this study. The results showed that the levels of ACE and Ang II decreased, the levels of Ang (1–7) significantly increased after BAC treatment, but that of Ang I and ACE2 did not change in the blood of SHRs (**Figure 6B**). The effect of BAC on RAS protein expressions was also determined in SHRs after 14 days of BAC oral administration by Western blotting and tissue immunofluorescence. We found that BAC significantly downregulated ACE expression, while it had no effect on ACE2 expression in the aorta (**Figures 6C–E**). These results suggested that BAC could not only inhibit the activity and protein expression of ACE but also activate the ACE2 activity in a dose-dependent manner.

Benzoylaconitine Activated Endothelium-dependent Vasorelaxation and Reduced Vascular Inflammation

Concentration of total NO in serum was measured in SHRs, and the results suggested that BAC could increase NO level in a dose-dependent manner in SHRs (**Figure 7A**). In the vessel of SHRs, we assessed the protein expression and phosphorylation of eNOS in SHRs by Western blotting. As anticipated, the p-Akt and p-eNOS^{Ser1177} were activated, which indicated NO release in SHR tissue (**Figures 7B,C**). We further found that BAC reduced the level of TNF-α and IL-6 in serum and downregulated expression of COX-2 and phosphorylation of IKB-α (**Figures 7D–F**), which were

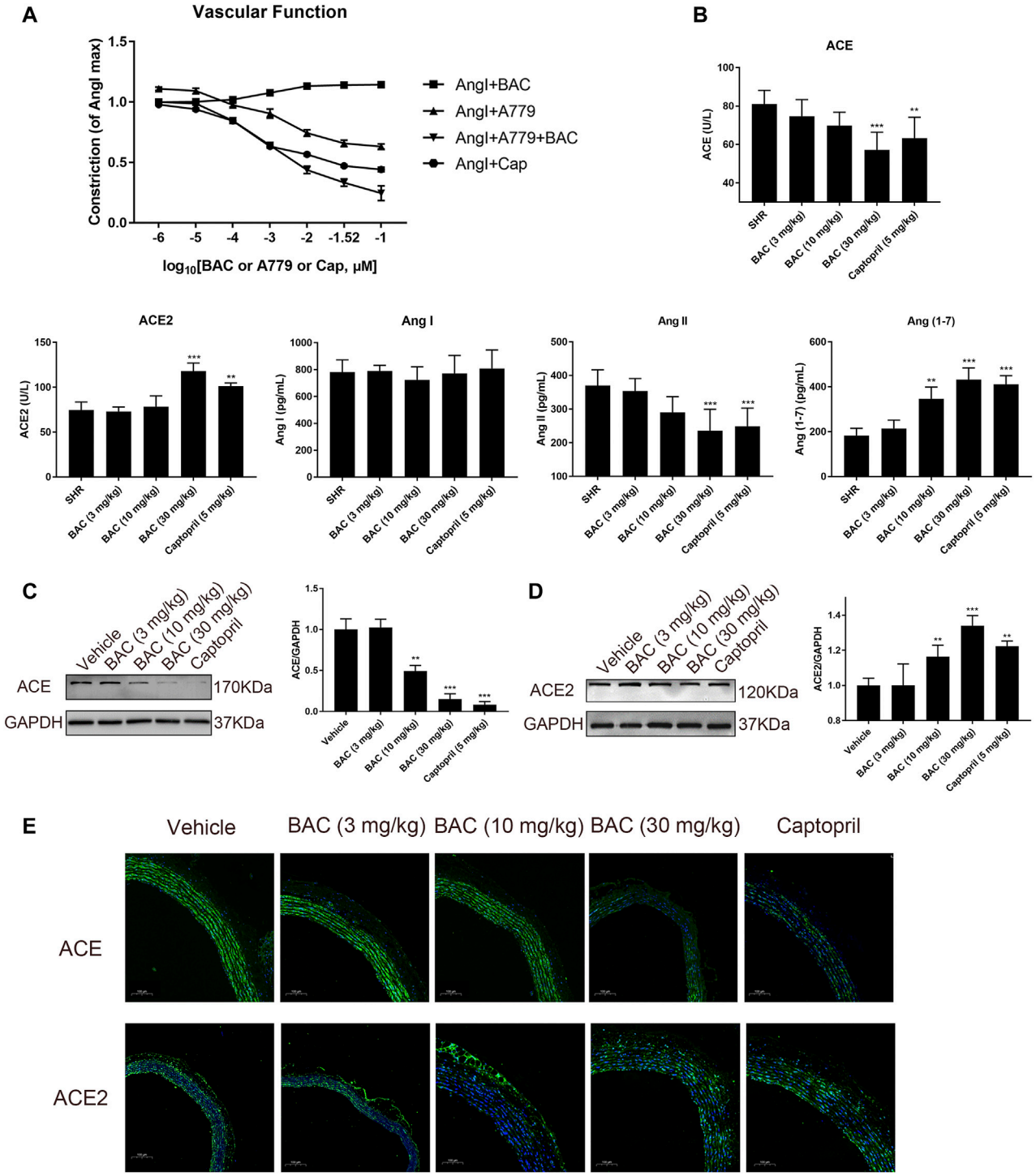

FIGURE 6 | BAC attenuated vascular constriction and regulated the RAS in SHRs. **(A)** *Ex vivo* cumulative response curve was performed with isolated aorta. Tissue was isolated from SD rat and balanced for 2 h in Krebs' solution at 37°C and then it was stimulated with Ang I at 10^{-2} μM and a series concentration of BAC or A779 or captopril at 10^{-6} to 10^{-1} μM. Abbreviations: Ang I + BAC: Ang I at 10^{-2} μM and a series concentration of BAC; Ang I + A779: Ang I at 10^{-2} μM and a series concentration of A779; Ang I + A779 + BAC: Ang I at 10^{-2} μM, A779 at 10^{-1} μM and a series concentration of BAC; Ang I + Cap: Ang I at 10^{-2} μM and a series concentration of captopril. **(B–E)** The experimental groups were the vehicle group ($n = 6$), the low-dose group (3 mg kg^{-1}, $n = 6$), the medium-dose group (10 mg kg^{-1}, $n = 6$), the high-dose group (30 mg kg^{-1}, $n = 6$), and the captopril group (5 mg kg^{-1}, $n = 6$). All rats were given a 14-day oral administration. **(B)** Plasma from the rats were collected at the end point to evaluate the levels of circulating, including ACE, ACE2, Ang I, Ang II, and Ang (1–7) concentration. **(C,D)** Total proteins were extracted from aorta of SHRs. Expressions of **(C)** ACE and **(D)** ACE2 were normalized to GAPDH. The gray value of protein blotting was measured by ImageJ. **(E)** Representative image of fluorescence immunoassay for protein expression and fluorescence localization of ACE and ACE2. The value was expressed by mean ± SEM. $^{**}p < 0.05$, $^{***}p < 0.05$, as compared with the vehicle group.

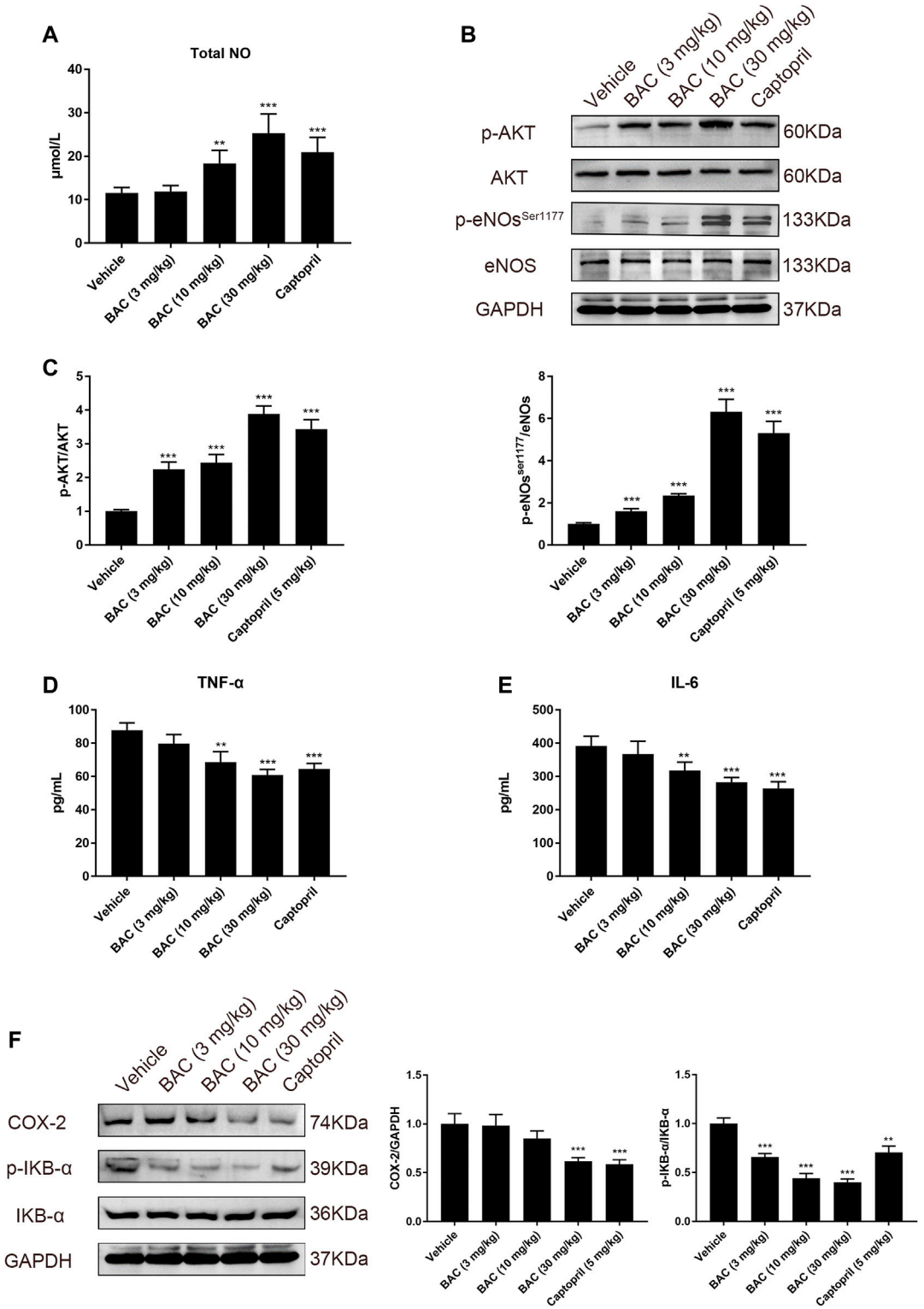

FIGURE 7 | BAC activated the NO system and reduced vascular inflammation in SHRs. The experimental groups were the vehicle group ($n = 6$), the low-dose group (3 mg kg^{-1}, $n = 6$), the medium-dose group (10 mg kg^{-1}, $n = 6$), the high-dose group (30 mg kg^{-1}, $n = 6$), and the captopril group (5 mg kg^{-1}, $n = 6$). All rats were given a 14-day oral administration. Serum and tissues were collected at the end point. Total proteins were extracted from aorta of SHRs. **(A)** Total NO in serum was measured by total nitric oxide assay kit at 540 nm. **(B,C)** Protein quantities of p-Akt, Akt, eNOs, and p-$NO^{ser1177}$ were detected by Western blot, and gray values were quantified by ImageJ. **(D,E)** The TNF-α and IL-6 in serum were measured by a microplate reader at 450 nm. **(F)** Protein quantities of COX-2, p-IKB-α, and IKB-α were detected by Western blot, and gray values were quantified by ImageJ. The value was expressed by mean ± SEM. ***$p < 0.05$, as compared with the vehicle group.

markers of vascular inflammation. These results suggested that BAC targeted the ACE/ACE2 to modulate the vasorelaxation and vascular inflammation.

DISCUSSION

Natural products such as herbal medicine are abundant sources of compounds for drug discovery for anti-hypertension. The MDAs, a series of natural products derived from "Fu Zi", have potential protective effects against hypertension (Zhang et al., 2016a; Zhang et al., 2016b). However, the systematic evaluation of the blood-pressure-lowering effects of MDAs, the study of their targets, and pharmacological mechanism are still incomplete.

In this study, we used a real-time blood pressure monitoring system in MDA-treated SHRs to evaluate their effect. We found that BAC is the most effective in lowering blood pressure among the MDAs. The CVDPlatform is a very effective intelligent target screening platform that we previously built (Zhang et al., 2016a). In this study, we screen the potential targets of BAC in the CVDPlatform and found that ACE/ACE2 are the potential targets for anti-hypertension. We further validated their binding and activities by using virtual dock, SPR, and enzyme activity assays under cell-free conditions and found that BAC could bind with ACE/ACE2, inhibit ACE activity, and activate ACE2 activity in a dose-dependent manner. In BAC-treated HUVECs, we investigated the protein expression of ACE/ACE2 and found the BAC directly inhibited the protein expression of ACE by promoting its degradation and had no effect on the protein expression of ACE2. In the BAC-treated isolated vessel, we found that BAC could inhibit Ang I-induced vasoconstriction and promote ACE2-related vasorelaxation. In long-term BAC-treated SHRs, BAC significantly lowered blood and heart rate, and reduced vessel thickness. Furthermore, BAC reduced the level of ACE and Ang II, increased the level of Ang (1–7), and had no effect on the level of ACE2 in blood circulation. In SHR vessel tissue, BAC inhibited the protein expression of ACE and had little effect on ACE2. ACE and ACE2 are the main regulatory enzymes in RAS and the key targets for anti-hypertension (Stroth and Unger, 1999; Oudit et al., 2003). ACE is the key enzyme in the generation of Ang II from Ang I, and AngII is a well-known vasoconstrictor that contributes to increased vascular tone and blood pressure (Lonn et al., 1994). Hyperactivity of ACE increases the level of Ang II, which leads to arterial vasoconstriction and glomerular effects, such as promotion of inflammation, hypertrophy, and fibrosis in arteries (Griendling et al., 1993). These effects also contribute to elevating blood pressure and heart rate in the process of hypertension (Lavoie and Sigmund, 2003; Crowley et al., 2006). ACE2 has contradictory actions to ACE. ACE2 metabolizes Ang II into smaller non-hypertensive metabolites, such as Ang (1–7), which is an active substance for lowering blood pressure and reducing heart rate (Ferrario et al., 1997). Multiple studies have indicated that ACE2 is involved in counterbalancing the detrimental effects of Ang II and exerting protective effects, such as anti-fibrosis, antioxidant, and anti-inflammatory effects, within and beyond the cardiovascular system (Donoghue et al., 2000; Crackower et al., 2002; Oudit et al., 2003; Burrell et al., 2004; Ocaranza et al., 2006; Reudelhuber, 2006). Taken together, BAC could directly inhibit the activity and protein expression of ACE and increased the activity of ACE2 to attenuate hypertension.

To clarify the underlying pharmacological mechanism of BAC on anti-hypertension by targeting ACE/ACE2, we further studied the endothelium-dependent vasorelaxation and vascular inflammation in BAC-treated SHRs. Endothelium-dependent vasorelaxation (Knox et al., 2019) and vascular inflammation are the most important events in hypertension. The Akt/eNOS signaling pathway is closely related to endothelium-dependent vasorelaxation, and the inflammatory factors are directly related to vascular inflammation. The eNOS phosphorylation induced by Akt is a key event in the production of NO, which is a direct mediator for endothelium-dependent vasorelaxation (Palmer et al., 1988; Bhandari et al., 2006), while the release of TNF-α and IL-6, the activation of COX-2 expression, and IKB-α phosphorylation are a series of marker events of vascular inflammation. As previously reported, inhibition of ACE and activation of ACE2 can promote vasodilation associated with Akt/eNOS signaling pathway and reduce vascular inflammation (Bader et al., 2018; Shi et al., 2019). In our study, we found that BAC increased total serum NO, and activated Akt/eNOS pathway in BAC-treated SHRs, while the level of TNF-α and IL-6, expression of COX-2, and phosphorylation of IKB-α decreased. These findings suggested that BAC could promote endothelium-dependent vasorelaxation and ameliorate vascular inflammation to attenuate hypertension by inhibiting ACE and activating ACE2.

CONCLUSION

BAC targets ACE/ACE2 to enhance endothelium-dependent vasorelaxation and reduce vascular inflammation to attenuate hypertension as a potential modulator of the renin–angiotensin system.

DATA AVAILABILITY STATEMENT

The original contributions presented in the study are included in the article/**Supplementary Materials**, further inquiries can be directed to the corresponding author.

ETHICS STATEMENT

The animal study was reviewed and approved by the Ethics Committee of the Tongji University School of Medicine (Shanghai, China, No. TJBG00121313).

AUTHOR CONTRIBUTIONS

HZ identified the problem and proposed the study. Q-QZ, F-HC, FW, X-MD, and HZ designed the protocol and carried out the

experiments. Q-QZ, F-HC, FW, and X-MD performed *in vivo* and *in vitro* experiments. Q-QZ and HZ wrote the manuscript. All authors read and approved the manuscript for publication.

FUNDING

This work was financially supported by the National Natural Science Foundation of China (NSFC, 81973504) and the Natural Science Foundation of Shanghai Science and Technology Commission (18ZR1430200).

SUPPLEMENTARY MATERIAL

The Supplementary Material for this article can be found online at: https://www.frontiersin.org/articles/10.3389/fphar.2022.841435/full#supplementary-material

REFERENCES

Bader, M., Alenina, N., Young, D., Santos, R. A. S., and Touyz, R. M. (2018). The Meaning of Mas. *Hypertension* 72 (5), 1072–1075. doi:10.1161/hypertensionaha.118.10918

Bhandari, V., Choo-Wing, R., Chapoval, S. P., Lee, C. G., Tang, C., Kim, Y. K., et al. (2006). Essential Role of Nitric Oxide in VEGF-Induced, Asthma-like Angiogenic, Inflammatory, Mucus, and Physiologic Responses in the Lung. *Proc. Natl. Acad. Sci. U S A.* 103 (29), 11021–11026. doi:10.1073/pnas.0601057103

Burrell, L. M., Johnston, C. I., Tikellis, C., and Cooper, M. E. (2004). ACE2, a New Regulator of the Renin-Angiotensin System. *Trends Endocrinol. Metab.* 15 (4), 166–169. doi:10.1016/j.tem.2004.03.001

Chockalingam, A. (2008). World Hypertension Day and Global Awareness. *Can. J. Cardiol.* 24 (6), 441–444. doi:10.1016/s0828-282x(08)70617-2

Crackower, M. A., Sarao, R., Oudit, G. Y., Yagil, C., Kozieradzki, I., Scanga, S. E., et al. (2002). Angiotensin-converting Enzyme 2 Is an Essential Regulator of Heart Function. *Nature* 417 (6891), 822–828. doi:10.1038/nature00786

Crowley, S. D., Gurley, S. B., Herrera, M. J., Ruiz, P., Griffiths, R., Kumar, A. P., et al. (2006). Angiotensin II Causes Hypertension and Cardiac Hypertrophy through its Receptors in the Kidney. *Proc. Natl. Acad. Sci. U S A.* 103 (47), 17985–17990. doi:10.1073/pnas.0605545103

Donoghue, M., Hsieh, F., Baronas, E., Godbout, K., Gosselin, M., Stagliano, N., et al. (2000). A Novel Angiotensin-Converting Enzyme-Related Carboxypeptidase (ACE2) Converts Angiotensin I to Angiotensin 1-9. *Circ. Res.* 87 (5), E1–E9. doi:10.1161/01.res.87.5.e1

Ferrario, C. M., Chappell, M. C., Tallant, E. A., Brosnihan, K. B., and Diz, D. I. (1997). Counterregulatory Actions of Angiotensin-(1-7). *Hypertension* 30 (3 Pt 2), 535–541. doi:10.1161/01.hyp.30.3.535

GBD 2017 Risk Factor Collaborators (2018). Global, Regional, and National Comparative Risk Assessment of 84 Behavioural, Environmental and Occupational, and Metabolic Risks or Clusters of Risks for 195 Countries and Territories, 1990-2017: a Systematic Analysis for the Global Burden of Disease Study 2017. *Lancet* 392 (10159), 1923–1994. doi:10.1016/s0140-6736(18)32225-6

Griendling, K. K., Murphy, T. J., and Alexander, R. W. (1993). Molecular Biology of the Renin-Angiotensin System. *Circulation* 87 (6), 1816–1828. doi:10.1161/01.cir.87.6.1816

Jaffe, E. A., Nachman, R. L., Becker, C. G., and Minick, C. R. (1973). Culture of Human Endothelial Cells Derived from Umbilical Veins. Identification by Morphologic and Immunologic Criteria. *J. Clin. Invest.* 52 (11), 2745–2756. doi:10.1172/jci107470

Knox, M., Vinet, R., Fuentes, L., Morales, B., and Martínez, J. L. (2019). A Review of Endothelium-dependent and -Independent Vasodilation Induced by Phytochemicals in Isolated Rat Aorta. *Animals (Basel)* 9 (9). 623, doi:10.3390/ani9090623

Lavoie, J. L., and Sigmund, C. D. (2003). Minireview: Overview of the Renin-Angiotensin System-Aan Endocrine and Paracrine System. *Endocrinology* 144 (6), 2179–2183. doi:10.1210/en.2003-0150

Liao, W., Fan, H., Davidge, S. T., and Wu, J. (2019). Egg White-Derived Antihypertensive Peptide IRW (Ile-Arg-Trp) Reduces Blood Pressure in Spontaneously Hypertensive Rats via the ACE2/Ang (1-7)/Mas Receptor Axis. *Mol. Nutr. Food Res.* 63 (9), e1900063. doi:10.1002/mnfr.201900063

Lin, C. C., Chan, T. Y., and Deng, J. F. (2004). Clinical Features and Management of Herb-Induced Aconitine Poisoning. *Ann. Emerg. Med.* 43 (5), 574–579. doi:10.1016/j.annemergmed.2003.10.046

Lonn, E. M., Yusuf, S., Jha, P., Montague, T. J., Teo, K. K., Benedict, C. R., et al. (1994). Emerging Role of Angiotensin-Converting Enzyme Inhibitors in Cardiac and Vascular protection. *Circulation* 90 (4), 2056–2069. doi:10.1161/01.cir.90.4.2056

Nguyen, H. H., Park, J., Kang, S., and Kim, M. (2015). Surface Plasmon Resonance: a Versatile Technique for Biosensor Applications. *Sensors (Basel)* 15 (5), 10481–10510. doi:10.3390/s150510481

Ocaranza, M. P., Godoy, I., Jalil, J. E., Varas, M., Collantes, P., Pinto, M., et al. (2006). Enalapril Attenuates Downregulation of Angiotensin-Converting Enzyme 2 in the Late Phase of Ventricular Dysfunction in Myocardial Infarcted Rat. *Hypertension* 48 (4), 572–578. doi:10.1161/01.Hyp.0000237862.94083.45

Oudit, G. Y., Crackower, M. A., Backx, P. H., and Penninger, J. M. (2003). The Role of ACE2 in Cardiovascular Physiology. *Trends Cardiovasc. Med.* 13 (3), 93–101. doi:10.1016/s1050-1738(02)00233-5

Palmer, R. M., Ashton, D. S., and Moncada, S. (1988). Vascular Endothelial Cells Synthesize Nitric Oxide from L-Arginine. *Nature* 333 (6174), 664–666. doi:10.1038/333664a0

Reudelhuber, T. L. (2006). A Place in Our Hearts for the Lowly Angiotensin 1-7 Peptide? *Hypertension* 47 (5), 811–815. doi:10.1161/01.Hyp.0000209020.69734.73

Shi, X., Guan, Y., Jiang, S., Li, T., Sun, B., and Cheng, H. (2019). Renin-angiotensin System Inhibitor Attenuates Oxidative Stress Induced Human Coronary Artery Endothelial Cell Dysfunction via the PI3K/AKT/mTOR Pathway. *Arch. Med. Sci.* 15 (1), 152–164. doi:10.5114/aoms.2018.74026

Stroth, U., and Unger, T. (1999). The Renin-Angiotensin System and its Receptors. *J. Cardiovasc. Pharmacol.* 33 Suppl 1 (Suppl. 1), S21–S23. doi:10.1097/00005344-199900001-00005

Wada, K., Nihira, M., Hayakawa, H., Tomita, Y., Hayashida, M., and Ohno, Y. (2005). Effects of Long-Term Administrations of Aconitine on Electrocardiogram and Tissue Concentrations of Aconitine and its Metabolites in Mice. *Forensic Sci. Int.* 148 (1), 21–29. doi:10.1016/j.forsciint.2004.04.016

Wang, H. Q., Liu, M., Wang, L., Lan, F., Zhang, Y. H., Xia, J. E., et al. (2020a). Identification of a Novel BACE1 Inhibitor, Timosaponin A-III, for Treatment of Alzheimer's Disease by a Cell Extraction and Chemogenomics Target Knowledgebase-Guided Method. *Phytomedicine* 75, 153244. doi:10.1016/j.phymed.2020.153244

Wang, X. Y., Zhou, Q. M., Guo, L., Dai, O., Meng, C. W., Miao, L. L., et al. (2021b). Cardioprotective Effects and Concentration-Response Relationship of Aminoalcohol-Diterpenoid Alkaloids from Aconitum Carmichaelii. *Fitoterapia* 149, 104822. doi:10.1016/j.fitote.2020.104822

Xu, X., Xie, X., Zhang, H., Wang, P., Li, G., Chen, J., et al. (2021). Water-soluble Alkaloids Extracted from Aconiti Radix Lateralis Praeparata Protect against Chronic Heart Failure in Rats via a Calcium Signaling Pathway. *Biomed. Pharmacother.* 135, 111184. doi:10.1016/j.biopha.2020.111184

Zhang, H., Liu, M., Zhang, W., Chen, J., Zhu, Z., Cao, H., et al. (2015a). Comparative Pharmacokinetics of Three Monoester-Diterpenoid Alkaloids after Oral Administration of Acontium Carmichaeli Extract and its Compatibility with Other Herbal Medicines in Sini Decoction to Rats. *Biomed. Chromatogr.* 29 (7), 1076–1083. doi:10.1002/bmc.3394

Zhang, H., Ma, S., Feng, Z., Wang, D., Li, C., Cao, Y., et al. (2016a). Cardiovascular Disease Chemogenomics Knowledgebase-Guided Target Identification and Drug Synergy Mechanism Study of an Herbal Formula. *Sci. Rep.* 6, 33963. doi:10.1038/srep33963

Zhang, H., Sun, S., Zhang, W., Xie, X., Zhu, Z., Chai, Y., et al. (2016b). Biological Activities and Pharmacokinetics of Aconitine, Benzoylaconine, and Aconine after Oral Administration in Rats. *Drug Test. Anal.* 8 (8), 839–846. doi:10.1002/dta.1858

Zhang, H., Wu, Q., Li, W., Sun, S., Zhang, W., Zhu, Z., et al. (2014). Absorption and Metabolism of Three Monoester-Diterpenoid Alkaloids in Aconitum Carmichaeli after Oral Administration to Rats by HPLC-MS. *J. Ethnopharmacol* 154 (3), 645–652. doi:10.1016/j.jep.2014.04.039

Zhang, W., Zhang, H., Sun, S., Sun, F. F., Chen, J., Zhao, L., et al. (2015b). Comparative Pharmacokinetics of Hypaconitine after Oral Administration of Pure Hypaconitine, Aconitum Carmichaelii Extract and Sini Decoction to Rats. *Molecules* 20 (1), 1560–1570. doi:10.3390/molecules20011560

Conflict of Interest: The authors declare that the research was conducted in the absence of any commercial or financial relationships that could be construed as a potential conflict of interest.

Publisher's Note: All claims expressed in this article are solely those of the authors and do not necessarily represent those of their affiliated organizations, or those of the publisher, the editors, and the reviewers. Any product that may be evaluated in this article, or claim that may be made by its manufacturer, is not guaranteed or endorsed by the publisher.

frontiers | Frontiers in Pharmacology

REVIEW
published: 10 May 2022
doi: 10.3389/fphar.2022.857331

Effect of Extracellular Vesicles From Multiple Cells on Vascular Smooth Muscle Cells in Atherosclerosis

*Tong Li[1†], Baofu Wang[1†], Hao Ding[2†], Shiqi Chen[1], Weiting Cheng[1], Yang Li[1], Xiaoxiao Wu[1], Lei Wang[1], Yangyang Jiang[1], Ziwen Lu[1], Yu Teng[1], Sha Su[1], Xiaowan Han[3] and Mingjing Zhao[1]**

[1]Key Laboratory of Chinese Internal Medicine of Ministry of Education, Dongzhimen Hospital, Beijing University of Chinese Medicine, Beijing, China, [2]Department of Oncology, Shanxi Traditional Chinese Medical Hospital, Taiyuan, China, [3]Department of Cardiac Rehabilitation, Dongzhimen Hospital, Beijing University of Chinese Medicine, Beijing, China

OPEN ACCESS

Edited by:
Qilong Wang,
Tianjin University of Traditional Chinese Medicine, China

Reviewed by:
Qiaobing Huang,
Southern Medical University, China
Yanwei Xing,
China Academy of Chinese Medical Sciences, China
Sarah Jane George,
University of Bristol, United Kingdom

***Correspondence:**
Mingjing Zhao
mjgx2004@163.com

[†]These authors have contributed equally to this work and share first authorship

Specialty section:
This article was submitted to Cardiovascular and Smooth Muscle Pharmacology, a section of the journal Frontiers in Pharmacology

Received: 18 January 2022
Accepted: 05 April 2022
Published: 10 May 2022

Citation:
Li T, Wang B, Ding H, Chen S, Cheng W, Li Y, Wu X, Wang L, Jiang Y, Lu Z, Teng Y, Su S, Han X and Zhao M (2022) Effect of Extracellular Vesicles From Multiple Cells on Vascular Smooth Muscle Cells in Atherosclerosis. Front. Pharmacol. 13:857331. doi: 10.3389/fphar.2022.857331

Atherosclerosis (AS)-related diseases are still the main cause of death in clinical patients. The phenotype switching, proliferation, migration, and secretion of vascular smooth muscle cells (VSMCs) have a pivotal role in atherosclerosis. Although numerous research studies have elucidated the role of VSMCs in AS, their potential functional regulations continue to be explored. The formation of AS involves various cells, such as endothelial cells, smooth muscle cells, and macrophages. Therefore, intercellular communication of blood vessels cannot be ignored due to closely connected endothelia, media, and adventitia. Extracellular vesicles (EVs), as the vectors of cell-to-cell communication, can deliver proteins and nucleic acids of parent cells to the recipient cells. EVs have emerged as being central in intercellular communication and play a vital role in the pathophysiologic mechanisms of AS. This review summarizes the effects of extracellular vesicles (EVs) derived from multiple cells (endothelial cells, macrophages, mesenchymal stem cells, etc.) on VSMCs in AS. The key findings of this review are as follows: 1) endothelial cell–derived EVs (EEVs) have anti- or pro-atherogenic effects on VSMCs; 2) macrophage-derived EVs (MEVs) aggravate the proliferation and migration of VSMCs; 3) mesenchymal stem cells can inhibit VSMCs; and 4) the proliferation and migration of VSMCs can be inhibited by the treatment of EVs with atherosclerosis-protective factors and promoted by noxious stimulants. These results suggested that EVs have the same functional properties as treated parent cells, which might provide vital guidance for treating AS.

Keywords: atherosclerosis, endothelial cells, extracellular vesicles, macrophages, vascular smooth muscle cells

Abbreviations: 5-HTT, 5-hydroxytryptamine transporter; α-SMA, smooth muscle acting; ABCA1, ATP-binding cassette transporter A1; ACTA2, actin alpha 2; AS, atherosclerosis; ECM, extracellular matrix; ECs, endothelial cells; EEVs, endothelial cell–derived EVs; EMPs, endothelial microparticles; EPCs, endothelial progenitor cells; EVs, extracellular vesicles; ICAM-1, intercellular cell adhesion molecule-1; IL-1β, interleukin-1β; KLF2, Krüppel-like factor 2; LncRNA, long noncoding RNA; LRP6, lipoprotein receptor–related protein 6; MAPK, mitogen-activated protein kinase; MCP-1, monocyte chemoattractant protein-1; MEVs, macrophage-derived EV; MoEVs, monocyte-derived EVs; MMPs matrix metalloproteinases.

INTRODUCTION

Atherosclerosis (AS) is a chronic inflammation of the vascular system caused by the interaction of endothelial dysfunction, lipid metabolism disorder, and infiltration of inflammatory cells (Li et al., 2018). Vascular smooth muscle cells (VSMCs) are major cells in the media layer of arteries, critical for maintaining the integrity of the arterial wall. Under physiological conditions, VSMCs exhibit low proliferation and synthesis. The cellular function and phenotype can be regulated by cytokines and hemorheology (Wan et al., 2019; Ledard et al., 2020). The proliferation and migration of VSMCs and secretion of extracellular matrix (ECM) are critical steps in the occurrence and development of AS. In early AS, VSMCs transform from a contractile to synthetic phenotype and phagocytose lipids and then transform into foam cells, thus participating in the formation of lipid pools. VSMCs then proliferate and secrete ECM, resulting in the thickening of the pathological intima while preventing the rupture of fiber caps and stabilizing plaques in advanced AS (Basatemur et al., 2019). In addition, a series of cells, such as adventitial fibroblasts, endothelial cells (ECs), and macrophages act on VSMCs, affecting their proliferation, migration, and apoptosis, thus regulating the formation and development of AS.

Extracellular vesicles (EVs) have a significant mediating role in regulating vascular function and are closely related to the occurrence and development of cardiovascular diseases (Hulsmans and Holvoet, 2013). EVs contain proteins, RNAs, and lipids and represent an astonishing tool for transferring biochemical properties from cell to cell (Charla et al., 2020). EVs carry molecular signatures of both health and disease and are thus considered indicators of diagnosis and prognosis, and sometimes as a vector of AS-targeted therapy. Over the years, the application of EVs in the diagnosis, prognosis, and treatment of AS has been investigated. This review summarizes the effects of EVs from multiple cells (endothelial cells, macrophages, mesenchymal stem cells, etc.) on VSMCs in AS.

ROLE OF VASCULAR SMOOTH MUSCLE CELLS IN ATHEROSCLEROSIS

Vascular Smooth Muscle Cells' Phenotypic Switching

Normally, VSMCs are in a contractile phenotype. When stimulated, VSMCs dedifferentiate to a synthetic state characterized by decreased myofilament density and contractile protein expression. During this phase, the expression of the contractile protein, alpha smooth muscle actin (α-SMA), and smooth muscle 22α decreases, while the expression of synthetic markers osteopontin and retinol-binding protein increases (Lacolley et al., 2017; Lu et al., 2018). Synthetic VSMCs show increased proliferation and migration ability, which are accompanied by secretion of ECM, matrix metalloproteinases (MMPs), pro-inflammatory cytokines, and exosomes. Exosomes trigger the differentiation of adjacent VSMCs into osteochondral VSMCs, which are characterized by runt-related transcription factor 2 and osteopontin expression, calcium deposition release, and calcification vesicles (Kapustin and Shanahan, 2016; Durham et al., 2018).

VSMC-derived intermediate cells, termed "SEM" cells, are pluripotent and can differentiate into macrophage-like and fibrochondrocyte-like cells (Pan et al., 2020). Macrophage colony–stimulating factors can induce the transformation of SEM cells into $CD68^+$ macrophages, while at the same time, very few $CD68^+$ cells were found induced by non-SEM cells (Manzanero, 2012). A previous study also showed that the level of various fibroblast markers, such as collagen type I, fibronectin, fibroblast-specific protein 1, and vimentin, is remarkably increased in SEM cells treated with connective tissue growth factor (Lee et al., 2010). Moreover, VSMCs' transition to SEM cells is reversible. The marker of VSMCs' actin alpha 2 (ACTA2) is infrequent in SEM and non-SEM cells (mainly VSMC-derived fibrochondrocyte), yet a higher percentage of ACTA2+ cells was found in SEM cells than in non-SEM cells after induction of the transforming growth factor β1 (TGF-β1, VSMCs' differentiation promoter) for 3 days (Pan et al., 2020).

Vascular Smooth Muscle Cells' Proliferation and Migration

Accumulation of VSMCs is a marker of atherosclerosis and vascular injury. In the past, it was believed that AS was the involvement of media VSMCs after endothelial injury and that the continuous proliferation of VSMCs was accumulated by lesion injury or inflammation. Now, the proliferation of VSMCs or cells derived from advanced atherosclerotic plaques is found to be low. Recent lineage-tracing studies have suggested that VSMCs' proliferation begin in the media, after which the cells migrate to the intima, where they continue to divide in the oligoclonal mode (Chappell et al., 2016). The cells proliferate to form fibrous caps and then invade the plaque core (Misra et al., 2018); VSMCs in injury-induced neointimal lesions and atherosclerotic plaques are oligoclonal derived from a few dilated cells. Lineage tracing also indicates that a single VSMC contributes to the formation of α-SMA–positive fibrous cap and Mac3-expressing macrophage-like plaque core cells. The co-staining of phenotypic markers further identifies the double-positive $\alpha\text{-SMA}^+$ $Mac3^+$ cell population, specific to the VSMC-derived plaque cells. On the contrary, VSMC-derived cells producing neointima after a vascular injury usually retain the expression of VSMC markers, and the upregulation of Mac3 in these cells is not obvious. It has also been demonstrated that the extensive proliferation of a low proportion of highly plastic VSMCs leads to the accumulation of VSMCs after injury and in atherosclerotic plaques. Thus, therapeutic targeting of these hyper-proliferative VSMCs may effectively reduce vascular diseases without affecting the vascular integrity.

External factors participate in regulating cells proliferation. Noncoding RNA can interact with proteins, DNA, and RNA to participate in VSMCs' proliferation. The expression of miR143/145 decreases in atherosclerotic vascular cells and can block

VSMC de-differentiation and proliferation by inhibiting KLF4 and Elk1 through binding with their mRNA 3′UTR region (Cordes et al., 2009). Mahmoud et al. (2019) suggested that long noncoding RNA (LncRNA) SMILR promotes VSMCs' proliferation by directly regulating mitosis, and its expression is increased in stable and unstable atherosclerotic plaques. Moreover, LncRNA MALAT1 stimulates proliferation and migration of VSMCs and promotes aortic stiffness (Song et al., 2018; Yu et al., 2018).

VSMCs generally migrate to the intima and proliferate to form fibrous caps (Allahverdian et al., 2018). Migration of VSMCs in the media may be preceded by both mitotic and non-mitotic VSMCs, which promote the formation of lesions (Webster et al., 1974; Clowes and Schwartz, 1985). However, the lineage-tracing study showed that VSMCs' migration was independent of proliferation and was not a major factor in the pathogenesis of the disease. Similarly, neointimal plaques derived from VSMCs were observed to connect with media plaques expressing the same color, suggesting that VSMCs proliferate in the media and thus predate migration (Chappell et al., 2016).

miRNA also has an important role in the migration of VSMCs. Studies have shown that miRNA-26a, miRNA-181b, miRNA-135b-5p, and miRNA-499a-3p promote the migration of VSMCs, while miRNA-599 and miRNA-132 have a negative effect (Gao et al., 2016). For example, miRNA-181b can promote proliferation and migration of VSMCs by activating phosphatidylinositol kinase-3(PI3K)/mitogen-activated protein kinase (MAPK) (Li et al., 2015), while miRNA-599 inhibits VSMCs migration by targeting TGF-β2 mRNA, thereby decreasing the expression of proliferating nuclear antigen (Xie et al., 2015).

Vascular Smooth Muscle Cells' Secretion

VSMCs secrete various biologically active molecules, namely, matrix proteins and pro-inflammatory mediators, some of which are encapsulated in vesicles that are released from the cell surface and transmit signals between cells. ECM produced by VSMCs is the main structural component of the vascular wall. The interaction between the two is a dynamic bidirectional process, and the content of the ECM depends on the balance of production and degradation (Barallobre-Barreiro et al., 2020).

During early plaque formation, MMPs affect VSMCs' migration by degrading the connective tissue structure around VSMCs (Johnson, 2017). A variety of matrix-degrading enzymes are secreted by synthetic VSMCs that can lead to the death of the neighboring cells (Johnson, 2017; Allahverdian et al., 2018). Pro-inflammatory cytokines interleukin-1β (IL-1β), IL-6, and monocyte chemoattractant protein-1 (MCP-1) promote atherosclerosis by stimulating monocyte recruitment and cell death (Orr et al., 2010). Synthetic VSMCs express a series of adhesion molecules and toll-like receptors that promote monocyte recruitment and regulate intracellular inflammatory signals.

In addition, VSMCs secrete EVs, which contain phosphatidylserine PS, annexin A6, and a low concentration of calcification inhibitors that may lead to vascular calcification (Kapustin et al., 2015). Proudfoot et al. (2000) suggested that matrix vesicles containing apoptotic VSMC remnants can serve as nucleation sites for plaques calcification. In addition, Schurgers et al. (2018) found that osteochondrocyte-like VSMCs secreted calcified vesicles which can promote calcification. Senescent cells released more EVs than non-senescent cells, promoting cell proliferation, inflammatory response, wound healing, and DNA damage (Borghesan et al., 2019; Basisty et al., 2020).

ROLE OF EXTRACELLULAR VESICLES–REGULATED VASCULAR SMOOTH MUSCLE CELLS IN ATHEROSCLEROSIS

Characterization of Extracellular Vesicles

EVs are membrane-bound phospholipid vesicles secreted by cells. EVs carry proteins, nucleic acids, and other substances transmitted between cells and have a critical role in regulating cell homeostasis and pathological development (Colombo et al., 2014; Lo Cicero et al., 2015). According to biogenesis, origin, and size, EVs can be classified into exosomes (40–200 nm), microvesicles (MVs) and microparticles (200–2000 nm in size), and apoptotic bodies (500–2000 nm) (Shao et al., 2018; van Niel et al., 2018). The production of exosomes can be divided into three steps: firstly, the endosome is formed by the inward budding of the cellular plasma membrane. Further inward budding of the endosome then leads to the formation of a multivesicular body (Piper and Katzmann, 2007). Finally, the multivesicular body fuses with the plasma membrane, releasing the vesicles (Théry, 2011). MVs are produced by outward budding and division of the plasma membrane (Raposo and Stoorvogel, 2013).

The lipid distribution of the membrane bilayer is asymmetrical. The outer layer is enriched with phosphatidylcholine and sphingomyelin, while the inner layer is predominantly composed of phosphatidylserine and phosphatidylethanolamine (Zwaal and Schroit, 1997). The influx of cytoplasmic $Ca2^{+}$ can disrupt this asymmetry by activating enzymes that facilitate the mixing of transport lipids. This activation leads to a redistribution of phospholipid bilayers across the membrane, promoting membrane blistering. $Ca2^{+}$-dependent proteolysis simultaneously degrades membrane-associated cytoskeleton, accelerating the budding process (Hugel et al., 2005). High-speed centrifugation (<100000*g*) and flow cytometry are used to extract and detect specific MVs of different cell origins. Exosomes are commonly isolated by ultracentrifugation or by using commercial kits. The morphology of exosomes is then examined by transmission electron microscopy, while the size is evaluated by nanoparticle tracking analysis. EV-associated proteins, such as tetraspanin proteins (namely, CD9, CD63, and CD81), are detected by western blotting.

Exosomes and MVs contain nucleic acids, namely, miRNAs, mRNA (Valadi et al., 2007; Skog et al., 2008), DNA (Balaj et al., 2011; Thakur et al., 2014), and other noncoding RNAs. The use of EVs' RNA as diagnostic biomarkers has become a hot research

TABLE 1 | EVs-mediated crosstalk between multiple cells and VSMCs in AS.

	Vesicular origin	Type	Stimulants	Cargo mediators	Target pathway	Functions	References
Anti-atherogenic↓	ECs	MVs	KLF2	miR-143/145	KLF2/miR-143/145	Prevented VSMCs' de-differentiation, limited the progression of atherosclerosis	Hergenreider et al. (2012)
		MVs	5-HTT inhibitors	miR-195	miR-195/5-HTT/Erk22/24	Inhibited VSMCs' proliferation and migration	Gu et al. (2017)
		MVs	miR-126 mimic and inhibitor	miR-126-3p	miR-126-3p/LRP6	Inhibited proliferation and migration of VSMCs and neointima formation	Jansen et al. (2017)
		Exosomes	miR-33a-5p antagomir	miR-33a-5p	miR-33a-5p/ABCA1/ApoA-I	Increased ABCA1 expression, enhanced ApoA-I–mediated cholesterol efflux, inhibited the development of AS	Stamatikos et al. (2020)
		Exosomes	-	-	-	Reduced VSMCs' proliferation and migration and lipid accumulation	Xiang et al. (2021)
	MSCs	Exosomes	miR-221 agomir	miRNA-221	miRNA-221/NAT1/IGF2/IGF2R	Suppressed atherosclerotic plaque formation	Guo et al. (2020)
	Adipose MSCs	Exosomes	-	-	MAPK/Akt	Inhibited proliferation and migration of VSMCs	Liu et al. (2016a)
Pro-atherogenic ↑	EPCs	Exosomes	-	-	-	Promoted VSMCs' proliferation and migration	Kong et al. (2018)
	ECs	Exosomes	CD137	-	TET2/CD137/PDGF-BB	Promoted phenotypic switching of VSMCs and neointimal formation	Li et al. (2020)
		Exosomes	ox-LDL	LINC01005	LINC01005/KLF4/miR-128-3p	Promoted VSMCs' phenotype switch, proliferation, and migration	Zhang et al. (2020)
	Macrophages	EVs	Western diet	-	-	Promoted VSMCs' proliferation	Wang et al. (2018a)
		Exosomes	ox-LDL	-	Erk/Akt	Promoted adhesion and migration of VSMCs	Niu et al. (2016)
		Exosomes	Nicotine	miR-21-3p	miR-21-3p/PTEN	Promoted proliferation and migration of VSMCs	Zhu et al. (2019)
		Exosomes	ox-LDL	miR-106-3p	miR-106-3p/CASP9	Promoted proliferation and migration of VSMCs	Liu et al. (2020)
		Exosomes	ox-LDL	miRNA-503-5p	miRNA-503-5p/Smad7/Smurf1/Smurf2/TGF-β	Promoted proliferation and migration of VSMCs	Wang et al. (2021a)
		Exosomes	ox-LDL	LIPCAR	LIPCAR/CDK2/PCNA	Promoted proliferation and migration of VSMCs	Hu et al. (2021)

5-HTT, 5-hydroxytryptamine transporter; VSMCs, vascular smooth muscle cells; ECs, endothelial cells; EPCs, endothelial progenitor cells; KLF2, Krüppel-like factor 2; LRP6, lipoprotein receptor–related protein 6; MSCs, mesenchymal stem cells; MVs, microvesicles; ox-LDL, oxidized low-density lipoprotein.

topic in recent years. EVs have already been used as biomarkers for autoimmune and circulatory diseases and cancer (Happel et al., 2020; Xu et al., 2020).

Extracellular Vesicles–Mediated Crosstalk Between Multiples Cells and Vascular Smooth Muscle Cells in Atherosclerosis

Intercellular communication is a vital part of regulating vascular function. EVs mediate the communication between cells during the development of atherosclerosis and play a role in delivering proteins, nucleic acids, or other active substances to the receptor cells. Through a comprehensive literature search, 16 studies were extracted to summarize the effect of extracellular vesicles derived from multiple cells on smooth muscle cells. EVs derived from endothelial cells, macrophages, and mesenchymal stem cells exert various effects on VSMCs' proliferation and migration. Krüppel-like factor 2 (KLF2), 5-hydroxytryptamine transporter (5-HTT) inhibitor, miR-33a-5p antagomir, and miR-221 agomir are the protective factors of atherosclerosis. After being treated with the above-mentioned factors, EVs could inhibit the proliferation and migration of VSMCs. However, EVs produced by pro-atherogenic factors, such as oxidized low-density lipoprotein (ox-LDL) and nicotine, promoted the proliferation and migration of VSMCs. More in-depth studies have found that miR-33a-5p, miR-126, and miR-221 carried by the vesicles had a protective effect on VSMCs, while others, such as miR-128-3p, miR-21, miR-106, miR-503-5p, and LIPCAR showed detrimental effects. More study details are given in **Table 1** and **Figure 1**.

Effect of Endothelial Cell–Derived Extracellular Vesicles on Vascular Smooth Muscle Cells in Atherosclerosis

EEVs can regulate endothelial barrier function, control VSMCs' phenotype, modulate monocytes activation, and affect atherosclerotic lesion formation in AS (Njock et al., 2015; Zheng et al., 2017; Wang et al., 2021). The blood vessels are

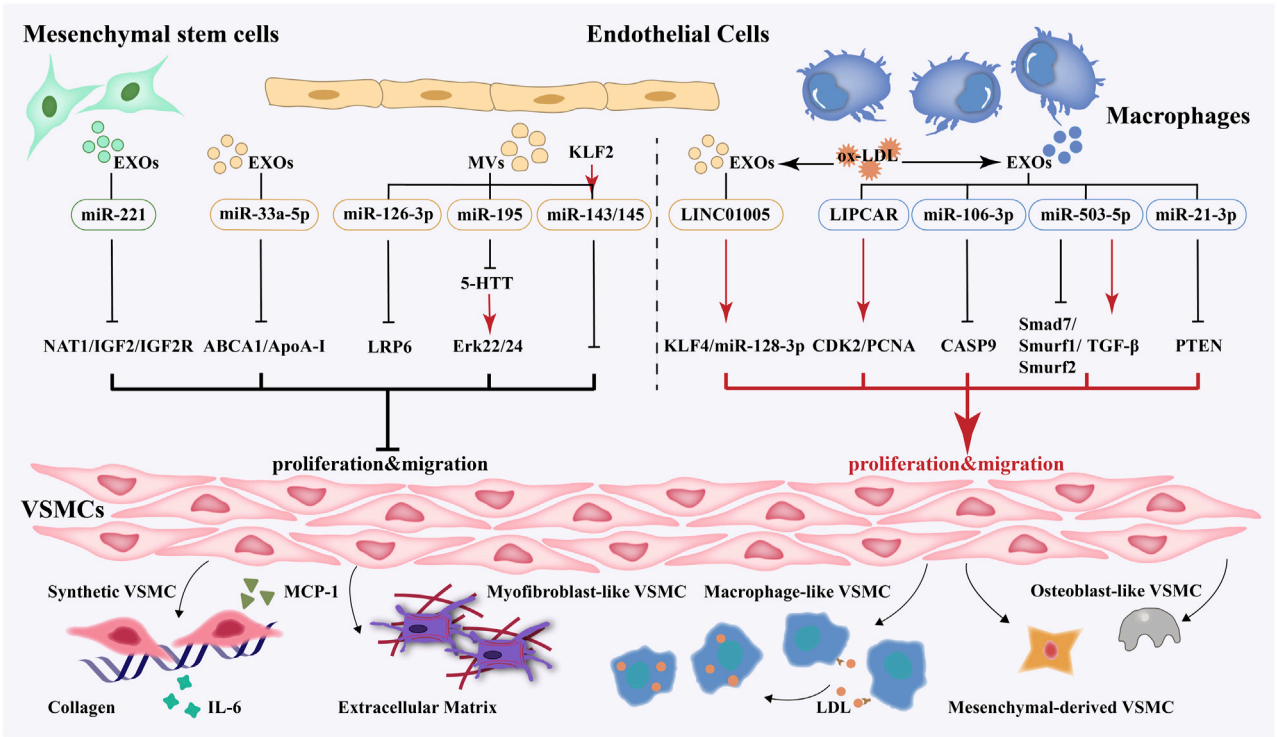

FIGURE 1 | EVs-mediated crosstalk between multiple cells and VSMCs and phenotype switching, proliferation, migration and secretion of VSMCs.

mainly composed of ECs and VSMCs; the interaction between the two is essential for the repair and remodeling of blood vessel growth (Li et al., 2018). Activation, proliferation, and migration of VSMCs can promote the formation of atherosclerotic plaques. VSMCs' phenotype is regulated by several environmental factors, such as growth factors, cytokines, and injury stimulation (Owens et al., 2004; Davis-Dusenbery et al., 2011). As a novel intercellular communication vector, EVs have received extensive attention. Evidence has shown that EEVs may have both anti- or pro-atherogenic effects on VSMCs.

The protective effects are mainly associated with miRNA contained in EVs. Boon and Horrevoets (2009) indicated that KLF2 has an important role in anti-atherosclerosis by regulating endothelial biological activity, mediating atherosclerosis induced by shear stress and protecting the endothelial phenotype. KLF2 binds to miR-143/145 and induces an increment of the cluster which regulates the phenotype of VSMCs. EVs released by KLF2-stimulated HUVECs were enriched in miR-143/145, and the expression of miR-143/145–targeted genes declined in coculture VSMCs. When miR-143/145–deficient ECs are cocultured with VSMCs, the miRNA targets were suppressed in VSMCs. KLF2 conversion led to a 30-fold enrichment of miR-143/145 in EVs, while the exosomes-depleted supernatant did not show an upregulation of the miR-143/145 levels. In addition, EVs produced by the endothelial cells expressing KLF2 also reduced the formation of atherosclerotic aortic lesions in $ApoE^{-/-}$ mice. The results suggested that KLF2 mediates miR-143/145 transferred from endothelial cells to VSMCs in EVs to maintain the differentiation status of VSMCs and atheroprotective effects (Hergenreider et al., 2012).

5-hydroxytryptamine is an important bioactive substance in the body, which promotes the formation of macrophage-derived foam cells. It can also promote the proliferation and migration of VSMCs through LDL and ox-LDL (Koba et al., 1999), as well as 5-hydroxytryptamine transporter (5-HTT) (Wang et al., 2015). The level of 5-HTT increased in the injured carotid artery and the overexpression of 5-HTT–induced VSMCs' proliferation. ECs' conditional medium (EC-CM) hampered the proliferation and expression of 5-HTT in SMCs. After ECs' transfection with miR-195 inhibitors, EC-CM was added to culture VSMCs and the expression of 5-HTT did not decline in them. These results showed that EEVs transforming miR-195 to VSMCs restrained the expression of 5-HTT, thereby inhibiting the proliferation of VSMCs by enhancing Erk42/44 phosphorylation level (Gu et al., 2017).

Lipid accumulation of intimal macrophages and VSMCs are also an essential driving factor for AS (Tabas et al., 2015). ATP-binding cassette transporter A1 (ABCA1) can transport intracellular cholesterol to ApoA-I, forming a high-density lipoprotein precursor, such that excess cholesterol can be transported to the liver for reuse after metabolism or excretion, thus reducing the formation of foam cells and inhibiting the occurrence and development of AS (Qian et al., 2017). Cholesterol accumulation in VSMCs induces cell differentiation into foam cell phenotype. In addition, cholesterol deposition in VSMCs downregulates the expression

of VSMC markers ACTA2 and calmodulin and increases the expression of inflammation-related genes. Endothelial cells release exosomes containing miR-33a-5p, a microRNA that restrained cholesterol efflux by silencing ABCA1. Stamatikos et al. (2020) transfected ECs with anti-miR-33a-5p, which was then incubated with macrophages or VSMCs. Exosome-mediated transfer of anti-miR-33a-5p increased ABCA1 expression and enhanced ApoA-I–mediated cholesterol efflux, inhibiting the development of AS. However, the effects were not observed when exosomes were removed from the medium. Furthermore, EEVs absorbed by VSMCs suppressed the proliferation, migration, and lipid deposition of VSMCs, while LPS-induced EEVs promoted the proliferation of VSMCs. Also, GW4689, an inhibitor of EVs, prevented the effect of EEVs on the proliferation and migration of VSMCs (Xiang et al., 2021).

Injections with endothelial microparticles (EMPs) reduced neointima formation in mice after vascular injury. Low-density lipoprotein receptor–related protein 6 (LRP6), a target of miR-126, is involved in regulating the proliferation of VSMCs and neointima formation. Upregulation of miR-126 in EMPs can reduce LRP expression, thereby inhibiting the proliferation and migration of VSMCs and neointima formation. The results indicated that EMPs delivered miR-126-3p to VSMCs and inhibited the expression of LRP6, thus reducing VSMCs' proliferation and disrupting neointima formation and vascular remodeling (Jansen et al., 2017).

Recent studies have shown that endothelial progenitor cells (EPCs) do not directly differentiate into mature ECs but utilize paracrine mechanisms through which they potentially participate in enhancing re-endothelialization (Hagensen et al., 2010, 2012). EPC-derived exosomes were injected into rats to investigate whether they could regulate re-endothelialization. It was found that the re-endothelialization area of the exosomes group was bigger than that of the control group, and both the intimal-to-medial area ratio and VSMCs proliferation in the exosomes group were markedly decreased when compared with those in the control group. At the same time, Kong et al. (2018) found that the exosomes promoted VSMCs' proliferation and migration *in vitro*.

EEVs promote atherosclerosis. TET2 is expressed in endothelial cells and can protect cells against inflammation. It is also regarded as a regulator of the transition to the VSMCs' phenotype, and its reduction leads to VSMCs' de-differentiation. The activation of CD137 signaling in ECs has a key role in inducing the immune and inflammatory response of AS. Injection with EC-derived exosomes significantly declined the intima/media ratio and neointima area, whereas CD137L (CD137 ligand) reversed the effect. Exosomes derived from ECs decreased the migration of PDGF-BB–induced VSMCs; however, the endothelial CD137 pathway was activated during this process, and the TET2 content of the endothelial-derived exosomes was repressed, promoting the phenotype switch and migration of VSMCs. Overexpression of TET2 in exosomes weakened the CD137 signaling–stimulated pro-phenotypic switch of VSMCs *in vitro* and *in vivo*, thus eventually attenuating plaque formation and AS development (Li et al., 2020).

LncRNA, a type of noncoding RNA, regulates gene expression at the transcriptional, posttranscriptional, and epigenetic levels (Kwok and Tay, 2017). It can be transferred from EVs of parent to recipient cells. Exosomal LINC01005 from ECs treated with ox-LDL promoted VSMCs' phenotype switch, proliferation, and migration by enhancing KLF4 expression *via* competitively binding to miR-128-3p. Of note, the effects were negated by upregulation of miR-128-3p *via* miR-128-3p mimic and silencing of KLF4 (Zhang et al., 2020).

Effect of Macrophage-Derived Extracellular Vesicles on Vascular Smooth Muscle Cells in Atherosclerosis

MEVs can induce macrophages polarization, modulate proliferation and migration of VSMCs, and regulate inflammatory response and lipid deposition in AS (Nguyen et al., 2018; Zhang et al., 2019; Bouchareychas et al., 2020). Macrophages and VSMCs have a critical role in plaque necrosis and rupture. Macrophages can secrete pro-inflammatory factors to maintain local inflammation in plaque. At the same time, they interact with T cells and VSMCs to enhance inflammation and promote lipoprotein retention (Moore et al., 2013). The transformation of VSMCs into the macrophage phenotype may be driven by lipid accumulation due to the cholesterol load in the culture (Rong et al., 2003), and also reversed by stimulating cholesterol efflux through ApoA-I and high-density lipoprotein (Allahverdian et al., 2014). Previous studies have suggested that MEVs promote smooth muscle cell proliferation and migration, thereby contributing to the development of atherosclerosis.

Four out of six studies made use of involved ox-LDL to treat macrophages (Niu et al., 2016; Liu et al., 2020; Hu et al., 2021; Wang et al., 2021a). Ox-LDL promotes the migration and proliferation of VSMCs by activating MAPK and other signaling pathways, upregulating the expression of adhesion molecules, inflammatory factors, and chemokines (Liu et al., 2014). Yet, high concentrations of ox-LDL can induce apoptosis of VSMCs, resulting in decreased plaque stability and easy rupture (Obermayer et al., 2018). In addition, ox-LDL stimulates vascular endothelial cells to express chemokines that induce monocytes to adhere to the vascular endothelium and move to the subintimal layer. The monocytes then differentiate into macrophages, which engulf ox-LDL receptors to form foam cells (Chistiakov et al., 2019).

Niu et al. (2016) found a higher level of leukocyte-derived EVs in patients with atherosclerosis than in healthy subjects. These EVs accelerated the migration and adhesion of VSMCs. Moreover, *in vitro* experiments suggested that foam cells produced more EVs than normal macrophages. In addition, proteomic results suggested that foam cell–derived EVs might promote adhesion and migration of VSMCs by regulating the actin skeleton and local adhesion pathways. Further validation revealed that foam cell–derived EVs may activate ERK and Akt pathway proteins.

In ox-LDL–treated macrophages, miR-106a-3p was significantly enriched in the exosomes, which were absorbed by VSMCs, causing a reduction in its target gene CASP9. miR-106a-3p overexpression and exosomes knockdown promoted and repressed proliferation and migration of VSMCs, respectively. This research revealed that exosomal miR-106a–mediated macrophage–VSMC crosstalk promoted VSMC proliferation and suppressed apoptosis *via* inhibition of CASP9 expression, thus further promoting the development of atherosclerosis (Liu et al., 2020).

Wang et al. (2021) found that EVs released by ox-LDL–treated macrophages containing miRNA-503-5p increased the proliferation and migration of VSMCs, while downregulation miR-503-5p attenuated these effects. Also, proliferation and migration of VSMCs were accelerated by downregulating the expressions of Smad7, Smurf1, and Smurf2 and elevating TGF-β, then exacerbating AS.

LncRNA LIPCAR participates in the development of AS, while excessive expression of LIPCAR significantly promotes phenotype switching, proliferation, and migration of VSMCs (Wang et al., 2019). The level of LIPCAR increased in exosomes from human myeloid leukemia mononuclear cells (THP-1) which was treated with ox-LDL. Furthermore, Hu et al. (2021) suggested that exosomes accelerated the proliferation and migration of VSMCs by upregulating CDK2 and PCNA, while this effect could be reversed by LIPCAR.

EVs stimulated by smoke and hyperlipidemia, risk factors of AS, display pro-atherogenic effects. Cigarette smoke is one of the risk factors of atherosclerosis (Messner and Bernhard, 2014). Wang et al. (2019) suggested that nicotine, a major component of cigarettes, not only directly activated the migration and proliferation of plaque cells but also enhanced the pro-inflammatory communication between macrophages and VSMCs, thereby promoting the occurrence of AS. Nicotine stimulated macrophages to produce exosomes, enriched with miR-21-3p, which were reported to join in vascular injury and repair (Liu et al., 2016). In a previous study, VSMCs were transfected with miR-21-3p mimics and miR-21-3p inhibitors and then incubated with EVs. After miR-21-3p mimic transfection, the migration and proliferation of VSMCs were obviously increased. The target gene of miR-21, phosphate and tensin homolog (PTEN), was selectively knocked down and the increment of the migration and proliferation of VSMCs emerged. The expression of PTEN was inhibited and VSMCs' proliferation and migration were enhanced by EVs-treated VSMCs, which exacerbated atherosclerosis progression (Zhu et al., 2019).

EVs derived from macrophage foam cells, which were isolated from mice fed on Western diet, promoted VSMCs proliferation. However, the exact mechanism is unclear (Wang et al., 2018).

Effect of Mesenchymal Stem Cell–Derived Extracellular Vesicles on Vascular Smooth Muscle Cells in Atherosclerosis

Mesenchymal stem cells (MSCs) are considered pluripotent stem cells with great therapeutic potential. MSCs replace damaged tissue by differentiating into various cell lineages, regulate immune response, and secrete EVs by paracrine function. Mesenchymal stem cells–extracellular vesicles (MSCs-EVs) harbor anti-atherogenic effects, such as inhibiting intimal hyperplasia, suppressing inflammation, and promoting M2 macrophage polarization (Chen et al., 2016; Li et al., 2019). Two studies of MSCs-EVs have shown a protective effect on VSMCs. Adipose mesenchymal stem cells–derived EVs inhibited the proliferation and migration of VSMCs. The expression of IL-6 and MCP-1 and the phosphorylation of MAPK and Akt declined after treatment with EVs.

The involvement of pro-inflammatory cytokines might promote the proliferation and migration of VSMCs (Liu et al., 2016). miR-221 is downregulated in patients with AS and in AS plaques (Tsai et al., 2013), and the lack of miR-221 enhances plaque instability and rupture (Bazan et al., 2015). Simultaneously, elevated miR-221 may stabilize vulnerable atherosclerotic plaques by inhibiting inflammation (Ye et al., 2018). Transmission of miR-221 from EVs derived from MSCs can inhibit lipid deposition and atherosclerotic plaque formation. EVs with high miR-221 expression increased miR-221 in the aorta and reduced NAT1 and atherosclerotic plaque formation in $ApoE^{-/-}$ mice. MSCs-EVs, including miR-221, were absorbed by ox-LDL–treated VSMCs and decreased the target gene NAT1, thereby suppressing the activation of the IGF2/IGF2R signaling pathway to inhibit atherosclerotic plaque formation (Guo et al., 2020).

EFFECT OF MULTIPLE EXTRACELLULAR VESICLES ON NONVASCULAR SMOOTH MUSCLE CELLS IN ATHEROSCLEROSIS

According to the existing literature, EVs have been proven to possess anti- or pro-atherogenic effects. EVs could regulate vascular inflammation, cholesterol metabolism, angiogenesis, plaque stability, and thrombosis through intercellular communication.

Monocytes and macrophages are important cell types those participate in atherosclerotic inflammation progression. The monocyte-derived EVs (MoEVs) isolated from human atherosclerotic plaques increase intercellular cell adhesion molecule-1 (ICAM-1), vascular cell adhesion molecule, and E-selectin, leading to increased leukocyte adhesion and transmigration (Rautou et al., 2011). In addition, MoEVs induce endothelial cells and leukocytes to release pro-inflammatory cytokines, in particular IL-6 and IL-8, which in turn promote the adhesion of cells (Boulanger et al., 2017). Hoyer et al. (2012) found mounting monocyte and T-cell infiltrated into the vessel wall, and enhanced plaque formation in $ApoE^{-/-}$ mice treated with MoEVs. *In vitro* study showed MoEVs increased the generation of pro-inflammation factors of chemokine receptor 2, intracellular reactive oxygen species, IL-6, and ICAM-1. EVs are capable of enhancing immunomodulatory responses and diminishing pro-inflammatory responses. EEVs transfer miR-10a to the monocyte by targeting the inflammatory pathway of NF-κB/MAP3K7/IRAK4 to repress inflammatory signaling

(Njock et al., 2015). In addition, EEVs reduce the M1 macrophage phenotype with a transition to the M2 anti-inflammatory macrophage phenotype and can be absorbed by the neighboring ECs and transferred to recipient cells through functional miR-222, promoting anti-inflammatory effects by decreasing ICAM-1 expression (Deng et al., 2019).

The dynamic balance between cholesterol uptake, synthesis, and efflux regulates cholesterol homeostasis in macrophages. This process is closely regulated by EVs-mediated cellular interaction. Cholesterol efflux can reduce intracellular cholesterol accumulation, preventing the formation of foam cells and the occurrence of AS. Moreover, cholesterol efflux is correlated with miR-3129-5p of adipocyte-derived EVs. The more the adipocyte-derived EVs are released, the lower the cholesterol efflux from macrophages and ABCA1 is expressed (Barberio et al., 2019). $CD4^+$-activated T lymphocytes infiltrate atherosclerotic plaques, induce T lymphocyte-releasing exosomes, and promote cholesterol accumulation and the expression of tumor necrosis factor-α (TNF-α) in THP-1, thereby facilitating AS (Zakharova et al., 2007). However, platelet-derived EVs (PEVs) exert anti-cholesterol aggregation effects and inhibit atherosclerotic thrombosis by suppressing ox-LDL binding and cholesterol accumulating in macrophages, affecting the class B scavenger receptor CD36 and inhibiting platelet thrombosis (Srikanthan et al., 2014).

The accumulation of EVs in atherosclerotic plaque indicates an endogenous signal of plaque neovascularization and vulnerability (Leroyer et al., 2008). EVs regulate angiogenesis and plaque stability, a major event in the switching from stable to unstable lesions. $CD40^+$ EVs in atherosclerotic plaque stimulate endothelial proliferation and angiogenesis and may be involved in intra-plaque neovascularization. The CD40L-expressing EVs isolated from human atherosclerotic lesions stimulate endothelial cell proliferation and promote angiogenesis by involving vascular endothelial growth factor and PI3K/Akt following connection with endothelial CD40 (Leroyer et al., 2008). In addition, the transfer of microRNAs from EVs to recipient ECs can regulate angiogenesis. For example, under IL-3 stimulation, EVs secreted by ECs are transported to ECs' recipients through miR-126-3p and pSTAT5 to induce angiogenesis (Lombardo et al., 2016). The promotion of angiogenesis in advanced plaques leads to instability and rupture of the plaque, thus accelerating the development of AS. Insulin-resistant adipocyte-derived exosomes can enter into HUVECs and atherosclerotic plaques, promote tube formation, increase vasa vasorum angiogenesis, the plaque burden, the vulnerability index, and the expression of angiogenesis-related factors (Wang et al., 2018).

Activated platelets releasing PEVs is an integral part of the thrombotic process. The procoagulant activity of platelet EVs in blood circulation is much higher than that of activated platelets (Sinauridze et al., 2007). PSGL-1 on PEVs activates platelets by binding to P-selectin in the endothelial injured area, which is conducive to thrombosis and atherosclerosis, and promotes the expansion of lesions (Suades et al., 2012). High levels of PEVs have been found in patients with coronary disease. Several studies have confirmed that increased PEV levels can enhance platelet and fibrin adhesion under high shear stress, injuring the atherosclerotic vessel wall (Suades et al., 2012; Mause, 2013). Tissue factor (TF) initiating coagulation is exposed to triggered thrombus formation (Biró et al., 2003). TF^+ monocyte EVs, the second largest group of thrombogenic EVs, follow platelet EVs (Aharon et al., 2008). They are abundant in human atherosclerotic plaques and may be aggregated in the vascular injury site by combining with activated platelets (Del Conde et al., 2005; Furie and Furie, 2008).

ROLE OF EXTRACELLULAR VESICLES AS A DRUG VECTOR

The use of endogenous exosomes as drug vectors has good biocompatibility and non-immunogenicity. It can improve the effective utilization rate and reduce the drug clearance rate. A recent study evaluated the anti-atherosclerotic effect of platelet-derived EV loaded with NLRP3 inhibitor MCC950. In ApoE-deficient mice, intravenous administration of PEVs mitigated inflammatory processes and atherosclerotic plaque formation, and inhibited macrophage and T-cell proliferation (Ma et al., 2021). Exosomes have also been used as drug vectors in the study of Chinese traditional medicine monomers. For example, exosomes loaded with curcumin increased the concentration and stability of curcumin *in vivo* and improved its therapeutic effect without obvious adverse reactions (Sun et al., 2010). However, the research on drug vectors of exosomes is still in its early phase, thus extensive research is still needed to optimize the targeting of exosomes as drug delivery vectors in the future.

CONCLUSION

This review summarized the effect of multiple cells–derived EVs on VSMCs in atherosclerosis. Endothelial cell–derived EVs have dual effects on VSMCs, while macrophage-derived EVs can promote the proliferation and migration of VSMCs and impair AS. Moreover, studies on EVs derived from mesenchymal stem cells showed that these particular EVs have inhibiting effects on VSMCs. We also found that EVs containing miR-33a-5p, miR-126, and miR-221 were able to inhibit the proliferation and migration of VSMCs, displaying protective effects on AS, whereas miR-128-3p, miR-21, miR-106, miR-503-5p, and LIPCAR further aggravated the disease. Additionally, studies suggested that EVs derived from source cells treated with beneficial factors have an important role in anti-atherosclerosis, and the harmful stimulants promote the development of AS. Therefore, EVs used as drug vectors may be a novel approach in treating AS. This review also provides new insight into the complexity of VSMCs biology and the potential of cells as a target for therapeutic strategies in AS. Under physiological conditions, EVs mediate intercellular communication and are involved in maintaining homeostasis; under a pathological state, however, EVs are released by the parent cell and participate in the occurrence and development of the disease. The pro-atherogenic and anti-atherogenic EVs' balance in different stages of atherosclerosis is still not very clear. Further studies are needed to verify whether the effect of

EVs *in vivo* is consistent with that *in vitro*. Also, the methods for extraction and purification of EVs have not yet been unified. At this stage, EVs are still recommended only as auxiliary diagnostic indicators for a certain disease. Their limited clinical transformation and small numbers make them currently unavailable for the treatment of disease. Therefore, an in-depth study of EVs' function and improvement in the rate of EVs' acquisition is of great value for their clinical application.

AUTHOR CONTRIBUTIONS

TL, BW, and HD have contributed equally to this work and share first authorship. Theme and design of the review: TL and BW; article retrieval: SC and WC; data extraction: YL, XW, and YJ; verification of data: ZL, YT, and SS; table and picture drawing: HD; writing of the manuscript: TL, BW, and HD; critical revision of the manuscript for intellectual content: LW, XH, and MZ; obtaining funding: MZ.

FUNDING

This study was supported by the National Natural Science Foundation of China (Grant No. 81774127) and Enterprise Sponsored Research (Grant No. 2019110002000200).

REFERENCES

Aharon, A., Tamari, T., and Brenner, B. (2008). Monocyte-derived Microparticles and Exosomes Induce Procoagulant and Apoptotic Effects on Endothelial Cells. *Thromb. Haemost.* 100, 878–885. doi:10.1160/th07-11-0691

Allahverdian, S., Chaabane, C., Boukais, K., Francis, G. A., and Bochaton-Piallat, M. L. (2018). Smooth Muscle Cell Fate and Plasticity in Atherosclerosis. *Cardiovasc. Res.* 114, 540–550. doi:10.1093/cvr/cvy022

Allahverdian, S., Chehroudi, A. C., McManus, B. M., Abraham, T., and Francis, G. A. (2014). Contribution of Intimal Smooth Muscle Cells to Cholesterol Accumulation and Macrophage-like Cells in Human Atherosclerosis. *Circulation* 129, 1551–1559. doi:10.1161/CIRCULATIONAHA.113.005015

Balaj, L., Lessard, R., Dai, L., Cho, Y. J., Pomeroy, S. L., Breakefield, X. O., et al. (2011). Tumour Microvesicles Contain Retrotransposon Elements and Amplified Oncogene Sequences. *Nat. Commun.* 2, 180. doi:10.1038/ncomms1180

Barallobre-Barreiro, J., Loeys, B., Mayr, M., Rienks, M., Verstraeten, A., and Kovacic, J. C. (2020). Extracellular Matrix in Vascular Disease, Part 2/4: JACC Focus Seminar. *J. Am. Coll. Cardiol.* 75, 2189–2203. doi:10.1016/j.jacc.2020.03.018

Barberio, M. D., Kasselman, L. J., Playford, M. P., Epstein, S. B., Renna, H. A., Goldberg, M., et al. (2019). Cholesterol Efflux Alterations in Adolescent Obesity: Role of Adipose-Derived Extracellular Vesical microRNAs. *J. Transl Med.* 17, 232. doi:10.1186/s12967-019-1980-6

Basatemur, G. L., Jørgensen, H. F., Clarke, M. C. H., Bennett, M. R., and Mallat, Z. (2019). Vascular Smooth Muscle Cells in Atherosclerosis. *Nat. Rev. Cardiol.* 16, 727–744. doi:10.1038/s41569-019-0227-9

Basisty, N., Kale, A., Jeon, O. H., Kuehnemann, C., Payne, T., Rao, C., et al. (2020). A Proteomic Atlas of Senescence-Associated Secretomes for Aging Biomarker Development. *Plos Biol.* 18, e3000599. doi:10.1371/journal.pbio.3000599

Bazan, H. A., Hatfield, S. A., O'Malley, C. B., Brooks, A. J., Lightell, D., Jr, and Woods, T. C. (2015). Acute Loss of miR-221 and miR-222 in the Atherosclerotic Plaque Shoulder Accompanies Plaque Rupture. *Stroke* 46, 3285–3287. doi:10.1161/STROKEAHA.115.010567

Biró, E., Sturk-Maquelin, K. N., Vogel, G. M., Meuleman, D. G., Smit, M. J., Hack, C. E., et al. (2003). Human Cell-Derived Microparticles Promote Thrombus Formation *In Vivo* in a Tissue Factor-dependent Manner. *J. Thromb. Haemost.* 1, 2561–2568. doi:10.1046/j.1538-7836.2003.00456.x

Boon, R. A., and Horrevoets, A. J. (2009). Key Transcriptional Regulators of the Vasoprotective Effects of Shear Stress. *Hamostaseologie* 29 (39-40), 39–43. doi:10.1055/s-0037-1616937

Borghesan, M., Fafián-Labora, J., Eleftheriadou, O., Carpintero-Fernández, P., Paez-Ribes, M., Vizcay-Barrena, G., et al. (2019). Small Extracellular Vesicles Are Key Regulators of Non-cell Autonomous Intercellular Communication in Senescence via the Interferon Protein IFITM3. *Cell Rep* 27, 3956–e6. e6. doi:10.1016/j.celrep.2019.05.095

Bouchareychas, L., Duong, P., Covarrubias, S., Alsop, E., Phu, T. A., Chung, A., et al. (2020). Macrophage Exosomes Resolve Atherosclerosis by Regulating Hematopoiesis and Inflammation via MicroRNA Cargo. *Cel Rep* 32, 107881. doi:10.1016/j.celrep.2020.107881

Boulanger, C. M., Loyer, X., Rautou, P. E., and Amabile, N. (2017). Extracellular Vesicles in Coronary Artery Disease. *Nat. Rev. Cardiol.* 14, 259–272. doi:10.1038/nrcardio.2017.7

Chappell, J., Harman, J. L., Narasimhan, V. M., Yu, H., Foote, K., Simons, B. D., et al. (2016). Extensive Proliferation of a Subset of Differentiated, yet Plastic, Medial Vascular Smooth Muscle Cells Contributes to Neointimal Formation in Mouse Injury and Atherosclerosis Models. *Circ. Res.* 119, 1313–1323. doi:10.1161/CIRCRESAHA.116.309799

Charla, E., Mercer, J., Maffia, P., and Nicklin, S. A. (2020). Extracellular Vesicle Signalling in Atherosclerosis. *Cell. Signal.* 75, 109751. doi:10.1016/j.cellsig.2020.109751

Chen, W., Huang, Y., Han, J., Yu, L., Li, Y., Lu, Z., et al. (2016). Immunomodulatory Effects of Mesenchymal Stromal Cells-Derived Exosome. *Immunol. Res.* 64, 831–840. doi:10.1007/s12026-016-8798-6

Chistiakov, D. A., Kashirskikh, D. A., Khotina, V. A., Grechko, A. V., and Orekhov, A. N. (2019). Immune-Inflammatory Responses in Atherosclerosis: The Role of Myeloid Cells. *J. Clin. Med.* 8, 1798. doi:10.3390/jcm8111798

Clowes, A. W., and Schwartz, S. M. (1985). Significance of Quiescent Smooth Muscle Migration in the Injured Rat Carotid Artery. *Circ. Res.* 56, 139–145. doi:10.1161/01.res.56.1.139

Colombo, M., Raposo, G., and Théry, C. (2014). Biogenesis, Secretion, and Intercellular Interactions of Exosomes and Other Extracellular Vesicles. *Annu. Rev. Cel Dev. Biol.* 30, 255–289. doi:10.1146/annurev-cellbio-101512-122326

Cordes, K. R., Sheehy, N. T., White, M. P., Berry, E. C., Morton, S. U., Muth, A. N., et al. (2009). miR-145 and miR-143 Regulate Smooth Muscle Cell Fate and Plasticity. *Nature* 460, 705–710. doi:10.1038/nature08195

Davis-Dusenbery, B. N., Wu, C., and Hata, A. (2011). Micromanaging Vascular Smooth Muscle Cell Differentiation and Phenotypic Modulation. *Arterioscler. Thromb. Vasc. Biol.* 31, 2370–2377. doi:10.1161/ATVBAHA.111.226670

Del Conde, I., Shrimpton, C. N., Thiagarajan, P., and López, J. A. (2005). Tissue-factor-bearing Microvesicles Arise from Lipid Rafts and Fuse with Activated Platelets to Initiate Coagulation. *Blood* 106, 1604–1611. doi:10.1182/blood-2004-03-1095

Deng, W., Tang, T., Hou, Y., Zeng, Q., Wang, Y., Fan, W., et al. (2019). Extracellular Vesicles in Atherosclerosis. *Clin. Chim. Acta* 495, 109–117. doi:10.1016/j.cca.2019.04.051

Durham, A. L., Speer, M. Y., Scatena, M., Giachelli, C. M., and Shanahan, C. M. (2018). Role of Smooth Muscle Cells in Vascular Calcification: Implications in Atherosclerosis and Arterial Stiffness. *Cardiovasc. Res.* 114, 590–600. doi:10.1093/cvr/cvy010

Furie, B., and Furie, B. C. (2008). Mechanisms of Thrombus Formation. *N. Engl. J. Med.* 359, 938–949. doi:10.1056/NEJMra0801082

Gao, Y., Peng, J., Ren, Z., He, N. Y., Li, Q., Zhao, X. S., et al. (2016). Functional Regulatory Roles of microRNAs in Atherosclerosis. *Clin. Chim. Acta* 460, 164–171. doi:10.1016/j.cca.2016.06.044

Gu, J., Zhang, H., Ji, B., Jiang, H., Zhao, T., Jiang, R., et al. (2017). Vesicle miR-195 Derived from Endothelial Cells Inhibits Expression of Serotonin Transporter in Vessel Smooth Muscle Cells. *Sci. Rep.* 7, 43546. doi:10.1038/srep43546

Guo, Z., Zhao, Z., Yang, C., and Song, C. (2020). Transfer of microRNA-221 from Mesenchymal Stem Cell-Derived Extracellular Vesicles Inhibits Atherosclerotic Plaque Formation. *Transl Res.* 226, 83–95. doi:10.1016/j.trsl.2020.07.003

Hagensen, M. K., Raarup, M. K., Mortensen, M. B., Thim, T., Nyengaard, J. R., Falk, E., et al. (2012). Circulating Endothelial Progenitor Cells Do Not Contribute to Regeneration of Endothelium after Murine Arterial Injury. *Cardiovasc. Res.* 93, 223–231. doi:10.1093/cvr/cvr278

Hagensen, M. K., Shim, J., Thim, T., Falk, E., and Bentzon, J. F. (2010). Circulating Endothelial Progenitor Cells Do Not Contribute to Plaque Endothelium in Murine Atherosclerosis. *Circulation* 121, 898–905. doi:10.1161/CIRCULATIONAHA.109.885459

Happel, C., Ganguly, A., and Tagle, D. A. (2020). Extracellular RNAs as Potential Biomarkers for Cancer. *J. Cancer Metastasis Treat.* 6, 32. doi:10.20517/2394-4722.2020.71

Hergenreider, E., Heydt, S., Tréguer, K., Boettger, T., Horrevoets, A. J., Zeiher, A. M., et al. (2012). Atheroprotective Communication between Endothelial Cells and Smooth Muscle Cells through miRNAs. *Nat. Cel Biol.* 14, 249–256. doi:10.1038/ncb2441

Hoyer, F. F., Giesen, M. K., Nunes França, C., Lütjohann, D., Nickenig, G., and Werner, N. (2012). Monocytic Microparticles Promote Atherogenesis by Modulating Inflammatory Cells in Mice. *J. Cel. Mol. Med.* 16, 2777–2788. doi:10.1111/j.1582-4934.2012.01595.x

Hu, N., Zeng, X., Tang, F., and Xiong, S. (2021). Exosomal Long Non-coding RNA LIPCAR Derived from oxLDL-Treated THP-1 Cells Regulates the Proliferation of Human Umbilical Vein Endothelial Cells and Human Vascular Smooth Muscle Cells. *Biochem. Biophys. Res. Commun.* 575, 65–72. doi:10.1016/j.bbrc.2021.08.053

Hugel, B., Martínez, M. C., Kunzelmann, C., and Freyssinet, J. M. (2005). Membrane Microparticles: Two Sides of the coin. *Physiology (Bethesda)* 20, 22–27. doi:10.1152/physiol.00029.2004

Hulsmans, M., and Holvoet, P. (2013). MicroRNA-containing Microvesicles Regulating Inflammation in Association with Atherosclerotic Disease. *Cardiovasc. Res.* 100, 7–18. doi:10.1093/cvr/cvt161

Jansen, F., Stumpf, T., Proebsting, S., Franklin, B. S., Wenzel, D., Pfeifer, P., et al. (2017). Intercellular Transfer of miR-126-3p by Endothelial Microparticles Reduces Vascular Smooth Muscle Cell Proliferation and Limits Neointima Formation by Inhibiting LRP6. *J. Mol. Cel. Cardiol.* 104, 43–52. doi:10.1016/j.yjmcc.2016.12.005

Johnson, J. L. (2017). Metalloproteinases in Atherosclerosis. *Eur. J. Pharmacol.* 816, 93–106. doi:10.1016/j.ejphar.2017.09.007

Kapustin, A. N., Chatrou, M. L., Drozdov, I., Zheng, Y., Davidson, S. M., Soong, D., et al. (2015). Vascular Smooth Muscle Cell Calcification Is Mediated by Regulated Exosome Secretion. *Circ. Res.* 116, 1312–1323. doi:10.1161/CIRCRESAHA.116.305012

Kapustin, A. N., and Shanahan, C. M. (2016). Emerging Roles for Vascular Smooth Muscle Cell Exosomes in Calcification and Coagulation. *J. Physiol.* 594, 2905–2914. doi:10.1113/JP271340

Koba, S., Pakala, R., Watanabe, T., Katagiri, T., and Benedict, C. R. (1999). Vascular Smooth Muscle Proliferation: Synergistic Interaction between Serotonin and Low Density Lipoproteins. *J. Am. Coll. Cardiol.* 34, 1644–1651. doi:10.1016/s0735-1097(99)00349-6

Kong, J., Wang, F., Zhang, J., Cui, Y., Pan, L., Zhang, W., et al. (2018). Exosomes of Endothelial Progenitor Cells Inhibit Neointima Formation after Carotid Artery Injury. *J. Surg. Res.* 232, 398–407. doi:10.1016/j.jss.2018.06.066

Kwok, Z. H., and Tay, Y. (2017). Long Noncoding RNAs: Lincs between Human Health and Disease. *Biochem. Soc. Trans.* 45, 805–812. doi:10.1042/BST20160376

Lacolley, P., Regnault, V., Segers, P., and Laurent, S. (2017). Vascular Smooth Muscle Cells and Arterial Stiffening: Relevance in Development, Aging, and Disease. *Physiol. Rev.* 97, 1555–1617. doi:10.1152/physrev.00003.2017

Ledard, N., Liboz, A., Blondeau, B., Babiak, M., Moulin, C., Vallin, B., et al. (2020). Slug, a Cancer-Related Transcription Factor, Is Involved in Vascular Smooth Muscle Cell Transdifferentiation Induced by Platelet-Derived Growth Factor-BB during Atherosclerosis. *J. Am. Heart Assoc.* 9, e014276. doi:10.1161/JAHA.119.014276

Lee, C. H., Shah, B., Moioli, E. K., and Mao, J. J. (2010). CTGF Directs Fibroblast Differentiation from Human Mesenchymal Stem/stromal Cells and Defines Connective Tissue Healing in a Rodent Injury Model. *J. Clin. Invest.* 120, 3340–3349. doi:10.1172/JCI43230

Leroyer, A. S., Rautou, P. E., Silvestre, J. S., Castier, Y., Lesèche, G., Devue, C., et al. (2008). CD40 Ligand+ Microparticles from Human Atherosclerotic Plaques Stimulate Endothelial Proliferation and Angiogenesis a Potential Mechanism for Intraplaque Neovascularization. *J. Am. Coll. Cardiol.* 52, 1302–1311. doi:10.1016/j.jacc.2008.07.032

Li, B., Zang, G., Zhong, W., Chen, R., Zhang, Y., Yang, P., et al. (2020). Activation of CD137 Signaling Promotes Neointimal Formation by Attenuating TET2 and Transferrring from Endothelial Cell-Derived Exosomes to Vascular Smooth Muscle Cells. *Biomed. Pharmacotherpharmacother* 121, 109593. doi:10.1016/j.biopha.2019.109593

Li, J., Xue, H., Li, T., Chu, X., Xin, D., Xiong, Y., et al. (2019). Exosomes Derived from Mesenchymal Stem Cells Attenuate the Progression of Atherosclerosis in ApoE-/- Mice via miR-Let7 Mediated Infiltration and Polarization of M2 Macrophage. *Biochem. Biophys. Res. Commun.* 510, 565–572. doi:10.1016/j.bbrc.2019.02.005

Li, M., Qian, M., Kyler, K., and Xu, J. (2018a). Endothelial-Vascular Smooth Muscle Cells Interactions in Atherosclerosis. *Front. Cardiovasc. Med.* 5, 151. doi:10.3389/fcvm.2018.00151

Li, T. J., Chen, Y. L., Gua, C. J., Xue, S. J., Ma, S. M., and Li, X. D. (2015). MicroRNA 181b Promotes Vascular Smooth Muscle Cells Proliferation through Activation of PI3K and MAPK Pathways. *Int. J. Clin. Exp. Pathol.* 8, 10375–10384.

Li, T., Zhao, M. J., Han, X. W., Zhao, Y. Z., Yang, T., Wang, L., et al. (2018b). The Role of Adventitial Fibroblast in Atherosclerosis and Restenosis post-PCI. *Chin. J. Integr. Med. Cardio-Cerebrovascular Dis.* 16 (01), 49–53. doi:10.5772/intechopen.98546

Liu, J., Ren, Y., Kang, L., and Zhang, L. (2014). Oxidized Low-Density Lipoprotein Increases the Proliferation and Migration of Human Coronary Artery Smooth Muscle Cells through the Upregulation of Osteopontin. *Int. J. Mol. Med.* 33, 1341–1347. doi:10.3892/ijmm.2014.1681

Liu, R., Shen, H., Ma, J., Sun, L., and Wei, M. (2016a). Extracellular Vesicles Derived from Adipose Mesenchymal Stem Cells Regulate the Phenotype of Smooth Muscle Cells to Limit Intimal Hyperplasia. *Cardiovasc. Drugs Ther.* 30, 111–118. doi:10.1007/s10557-015-6630-5

Liu, Y., Luo, F., Wang, B., Li, H., Xu, Y., Liu, X., et al. (2016b). STAT3-regulated Exosomal miR-21 Promotes Angiogenesis and Is Involved in Neoplastic Processes of Transformed Human Bronchial Epithelial Cells. *Cancer Lett.* 370, 125–135. doi:10.1016/j.canlet.2015.10.011

Liu, Y., Zhang, W. L., Gu, J. J., Sun, Y. Q., Cui, H. Z., Bu, J. Q., et al. (2020). Exosome-mediated miR-106a-3p Derived from Ox-LDL Exposed Macrophages Accelerated Cell Proliferation and Repressed Cell Apoptosis of Human Vascular Smooth Muscle Cells. *Eur. Rev. Med. Pharmacol. Sci.* 24, 7039–7050. doi:10.26355/eurrev_202006_21697

Lo Cicero, A., Stahl, P. D., and Raposo, G. (2015). Extracellular Vesicles Shuffling Intercellular Messages: for Good or for Bad. *Curr. Opin. Cel Biol.* 35, 69–77. doi:10.1016/j.ceb.2015.04.013

Lombardo, G., Dentelli, P., Togliatto, G., Rosso, A., Gili, M., Gallo, S., et al. (2016). Activated Stat5 Trafficking via Endothelial Cell-Derived Extracellular Vesicles Controls IL-3 Pro-angiogenic Paracrine Action. *Sci. Rep.* 6, 25689. doi:10.1038/srep25689

Lu, Q. B., Wan, M. Y., Wang, P. Y., Zhang, C. X., Xu, D. Y., Liao, X., et al. (2018). Chicoric Acid Prevents PDGF-BB-Induced VSMC Dedifferentiation, Proliferation and Migration by Suppressing ROS/NFκB/mTOR/P70S6K Signaling cascade. *Redox Biol.* 14, 656–668. doi:10.1016/j.redox.2017.11.012

Ma, Q., Fan, Q., Han, X., Dong, Z., Xu, J., Bai, J., et al. (2021). Platelet-derived Extracellular Vesicles to Target Plaque Inflammation for Effective Anti-atherosclerotic Therapy. *J. Control. Release* 329, 445–453. doi:10.1016/j.jconrel.2020.11.064

Mahmoud, A. D., Ballantyne, M. D., Miscianinov, V., Pinel, K., Hung, J., Scanlon, J. P., et al. (2019). The Human-specific and Smooth Muscle Cell-Enriched LncRNA SMILR Promotes Proliferation by Regulating Mitotic CENPF mRNA and Drives Cell-Cycle Progression Which Can Be Targeted to Limit Vascular Remodeling. *Circ. Res.* 125, 535–551. doi:10.1161/CIRCRESAHA.119.314876

Manzanero, S. (2012). Generation of Mouse Bone Marrow-Derived Macrophages. *Methods Mol. Biol.* 844, 177–181. doi:10.1007/978-1-61779-527-5_12

Mause, S. F. (2013). Platelet Microparticles: Reinforcing the Hegemony of Platelets in Atherothrombosis. *Thromb. Haemost.* 109, 5–6. doi:10.1160/TH12-11-0817

Messner, B., and Bernhard, D. (2014). Smoking and Cardiovascular Disease: Mechanisms of Endothelial Dysfunction and Early Atherogenesis. *Arterioscler. Thromb. Vasc. Biol.* 34, 509–515. doi:10.1161/ATVBAHA.113.300156

Misra, A., Feng, Z., Chandran, R. R., Kabir, I., Rotllan, N., Aryal, B., et al. (2018). Integrin Beta3 Regulates Clonality and Fate of Smooth Muscle-Derived Atherosclerotic Plaque Cells. *Nat. Commun.* 9, 2073. doi:10.1038/s41467-018-04447-7

Moore, K. J., Sheedy, F. J., and Fisher, E. A. (2013). Macrophages in Atherosclerosis: a Dynamic Balance. *Nat. Rev. Immunol.* 13, 709–721. doi:10.1038/nri3520

Nguyen, M. A., Karunakaran, D., Geoffrion, M., Cheng, H. S., Tandoc, K., Perisic Matic, L., et al. (2018). Extracellular Vesicles Secreted by Atherogenic Macrophages Transfer MicroRNA to Inhibit Cell Migration. *Arterioscler. Thromb. Vasc. Biol.* 38, 49–63. doi:10.1161/ATVBAHA.117.309795

Niu, C., Wang, X., Zhao, M., Cai, T., Liu, P., Li, J., et al. (2016). Macrophage Foam Cell-Derived Extracellular Vesicles Promote Vascular Smooth Muscle Cell Migration and Adhesion. *J. Am. Heart Assoc.* 5, e004099. doi:10.1161/JAHA.116.004099

Njock, M. S., Cheng, H. S., Dang, L. T., Nazari-Jahantigh, M., Lau, A. C., Boudreau, E., et al. (2015). Endothelial Cells Suppress Monocyte Activation through Secretion of Extracellular Vesicles Containing Antiinflammatory microRNAs. *Blood* 125, 3202–3212. doi:10.1182/blood-2014-11-611046

Obermayer, G., Afonyushkin, T., and Binder, C. J. (2018). Oxidized Low-Density Lipoprotein in Inflammation-Driven Thrombosis. *J. Thromb. Haemost.* 16, 418–428. doi:10.1111/jth.13925

Orr, A. W., Hastings, N. E., Blackman, B. R., and Wamhoff, B. R. (2010). Complex Regulation and Function of the Inflammatory Smooth Muscle Cell Phenotype in Atherosclerosis. *J. Vasc. Res.* 47, 168–180. doi:10.1159/000250095

Owens, G. K., Kumar, M. S., and Wamhoff, B. R. (2004). Molecular Regulation of Vascular Smooth Muscle Cell Differentiation in Development and Disease. *Physiol. Rev.* 84, 767–801. doi:10.1152/physrev.00041.2003

Pan, H., Xue, C., Auerbach, B. J., Fan, J., Bashore, A. C., Cui, J., et al. (2020). Single-Cell Genomics Reveals a Novel Cell State during Smooth Muscle Cell Phenotypic Switching and Potential Therapeutic Targets for Atherosclerosis in Mouse and Human. *Circulation* 142, 2060–2075. doi:10.1161/CIRCULATIONAHA.120.048378

Piper, R. C., and Katzmann, D. J. (2007). Biogenesis and Function of Multivesicular Bodies. *Annu. Rev. Cel Dev. Biol.* 23, 519–547. doi:10.1146/annurev.cellbio.23.090506.123319

Proudfoot, D., Skepper, J. N., Hegyi, L., Bennett, M. R., Shanahan, C. M., and Weissberg, P. L. (2000). Apoptosis Regulates Human Vascular Calcification *In Vitro*: Evidence for Initiation of Vascular Calcification by Apoptotic Bodies. *Circ. Res.* 87, 1055–1062. doi:10.1161/01.res.87.11.1055

Qian, H., Zhao, X., Cao, P., Lei, J., Yan, N., and Gong, X. (2017). Structure of the Human Lipid Exporter ABCA1. *Cell* 169, 1228–e10. e10. doi:10.1016/j.cell.2017.05.020

Raposo, G., and Stoorvogel, W. (2013). Extracellular Vesicles: Exosomes, Microvesicles, and Friends. *J. Cel Biol.* 200, 373–383. doi:10.1083/jcb.201211138

Rautou, P. E., Leroyer, A. S., Ramkhelawon, B., Devue, C., Duflaut, D., Vion, A. C., et al. (2011). Microparticles from Human Atherosclerotic Plaques Promote Endothelial ICAM-1-dependent Monocyte Adhesion and Transendothelial Migration. *Circ. Res.* 108, 335–343. doi:10.1161/CIRCRESAHA.110.237420

Rong, J. X., Shapiro, M., Trogan, E., and Fisher, E. A. (2003). Transdifferentiation of Mouse Aortic Smooth Muscle Cells to a Macrophage-like State after Cholesterol Loading. *Proc. Natl. Acad. Sci. U S A.* 100, 13531–13536. doi:10.1073/pnas.1735526100

Schurgers, L. J., Akbulut, A. C., Kaczor, D. M., Halder, M., Koenen, R. R., and Kramann, R. (2018). Initiation and Propagation of Vascular Calcification Is Regulated by a Concert of Platelet- and Smooth Muscle Cell-Derived Extracellular Vesicles. *Front. Cardiovasc. Med.* 5, 36. doi:10.3389/fcvm.2018.00036

Shao, H., Im, H., Castro, C. M., Breakefield, X., Weissleder, R., and Lee, H. (2018). New Technologies for Analysis of Extracellular Vesicles. *Chem. Rev.* 118, 1917–1950. doi:10.1021/acs.chemrev.7b00534

Sinauridze, E. I., Kireev, D. A., Popenko, N. Y., Pichugin, A. V., Panteleev, M. A., Krymskaya, O. V., et al. (2007). Platelet Microparticle Membranes Have 50- to 100-fold Higher Specific Procoagulant Activity Than Activated Platelets. *Thromb. Haemost.* 97, 425–434.

Skog, J., Würdinger, T., van Rijn, S., Meijer, D. H., Gainche, L., Sena-Esteves, M., et al. (2008). Glioblastoma Microvesicles Transport RNA and Proteins that Promote Tumour Growth and Provide Diagnostic Biomarkers. *Nat. Cel Biol.* 10, 1470–1476. doi:10.1038/ncb1800

Song, T. F., Huang, L. W., Yuan, Y., Wang, H. Q., He, H. P., Ma, W. J., et al. (2018). LncRNA MALAT1 Regulates Smooth Muscle Cell Phenotype Switch via Activation of Autophagy. *Oncotarget* 9, 4411–4426. doi:10.18632/oncotarget.23230

Srikanthan, S., Li, W., Silverstein, R. L., and McIntyre, T. M. (2014). Exosome Poly-Ubiquitin Inhibits Platelet Activation, Downregulates CD36 and Inhibits Pro-atherothombotic Cellular Functions. *J. Thromb. Haemost.* 12, 1906–1917. doi:10.1111/jth.12712

Stamatikos, A., Knight, E., Vojtech, L., Bi, L., Wacker, B. K., Tang, C., et al. (2020). Exosome-Mediated Transfer of Anti-miR-33a-5p from Transduced Endothelial Cells Enhances Macrophage and Vascular Smooth Muscle Cell Cholesterol Efflux. *Hum. Gene Ther.* 31, 219–232. doi:10.1089/hum.2019.245

Suades, R., Padró, T., Vilahur, G., and Badimon, L. (2012). Circulating and Platelet-Derived Microparticles in Human Blood Enhance Thrombosis on Atherosclerotic Plaques. *Thromb. Haemost.* 108, 1208–1219. doi:10.1160/TH12-07-0486

Sun, D., Zhuang, X., Xiang, X., Liu, Y., Zhang, S., Liu, C., et al. (2010). A Novel Nanoparticle Drug Delivery System: the Anti-inflammatory Activity of Curcumin Is Enhanced when Encapsulated in Exosomes. *Mol. Ther.* 18, 1606–1614. doi:10.1038/mt.2010.105

Tabas, I., García-Cardeña, G., and Owens, G. K. (2015). Recent Insights into the Cellular Biology of Atherosclerosis. *J. Cel Biol.* 209, 13–22. doi:10.1083/jcb.201412052

Thakur, B. K., Zhang, H., Becker, A., Matei, I., Huang, Y., Costa-Silva, B., et al. (2014). Double-stranded DNA in Exosomes: a Novel Biomarker in Cancer Detection. *Cell Res* 24, 766–769. doi:10.1038/cr.2014.44

Théry, C. (2011). Exosomes: Secreted Vesicles and Intercellular Communications. *F1000 Biol. Rep.* 3, 15. doi:10.3410/B3-15

Tsai, P. C., Liao, Y. C., Wang, Y. S., Lin, H. F., Lin, R. T., and Juo, S. H. (2013). Serum microRNA-21 and microRNA-221 as Potential Biomarkers for Cerebrovascular Disease. *J. Vasc. Res.* 50, 346–354. doi:10.1159/000351767

Valadi, H., Ekström, K., Bossios, A., Sjöstrand, M., Lee, J. J., and Lötvall, J. O. (2007). Exosome-mediated Transfer of mRNAs and microRNAs Is a Novel Mechanism of Genetic Exchange between Cells. *Nat. Cel Biol.* 9, 654–659. doi:10.1038/ncb1596

van Niel, G., D'Angelo, G., and Raposo, G. (2018). Shedding Light on the Cell Biology of Extracellular Vesicles. *Nat. Rev. Mol. Cel Biol.* 19, 213–228. doi:10.1038/nrm.2017.125

Wan, W., Ding, Y., Xie, Z., Li, Q., Yan, F., Budbazar, E., et al. (2019). PDGFR-β Modulates Vascular Smooth Muscle Cell Phenotype via IRF-9/sirt-1/nf-Kb Pathway in Subarachnoid Hemorrhage Rats. *J. Cereb. Blood Flow Metab.* 39, 1369–1380. doi:10.1177/0271678X18760954

Wang, C., Li, Z., Liu, Y., and Yuan, L. (2021a). Exosomes in Atherosclerosis: Performers, Bystanders, Biomarkers, and Therapeutic Targets. *Theranostics* 11, 3996–4010. doi:10.7150/thno.56035

Wang, F., Chen, F. F., Shang, Y. Y., Li, Y., Wang, Z. H., Han, L., et al. (2018a). Insulin Resistance Adipocyte-Derived Exosomes Aggravate Atherosclerosis by Increasing Vasa Vasorum Angiogenesis in Diabetic ApoE-/- Mice. *Int. J. Cardiol.* 265, 181–187. doi:10.1016/j.ijcard.2018.04.028

Wang, J., Yannie, P., and Ghosh, S. (2018b). Western Diet Feeding Increases Secretion of Extracellular Vesicles from Macrophage Foam Cells that Promotes Smooth Muscle Cell Proliferation. *Circulation* 138, 15827. doi:10.1161/circ.138.suppl_1.15827?cookieSet=1

Wang, Q. J., Wang, D., and Tang, C. C. (2015). The 5-hydroxytryptamine Transporter Is Functional in Human Coronary Artery Smooth Muscle Cells Proliferation and Is Regulated by Interleukin-1 Beta. *Int. J. Clin. Exp. Med.* 8, 6947–6956.

Wang, X., Li, D., Chen, H., Wei, X., and Xu, X. (2019a). Expression of Long Noncoding RNA LIPCAR Promotes Cell Proliferation, Cell Migration, and

Change in Phenotype of Vascular Smooth Muscle Cells. *Med. Sci. Monit.* 25, 7645–7651. doi:10.12659/MSM.915681

Wang, Y., Xu, Z., Wang, X., Zheng, J., Peng, L., Zhou, Y., et al. (2021b). Extracellular-vesicle Containing miRNA-503-5p Released by Macrophages Contributes to Atherosclerosis. *Aging (Albany NY)* 13, 12239–12257. doi:10.18632/aging.103855

Wang, Z., Liu, B., Zhu, J., Wang, D., and Wang, Y. (2019b). Nicotine-mediated Autophagy of Vascular Smooth Muscle Cell Accelerates Atherosclerosis via nAChRs/ROS/NF-κB Signaling Pathway. *Atherosclerosis* 284, 1–10. doi:10.1016/j.atherosclerosis.2019.02.008

Webster, W. S., Bishop, S. P., and Geer, J. C. (1974). Experimental Aortic Intimal Thickening. I. Morphology and Source of Intimal Cells. *Am. J. Pathol.* 76, 245–264.

Xiang, D., Li, Y., Cao, Y., Huang, Y., Zhou, L., Lin, X., et al. (2021). Different Effects of Endothelial Extracellular Vesicles and LPS-Induced Endothelial Extracellular Vesicles on Vascular Smooth Muscle Cells: Role of Curcumin and its Derivatives. *Front. Cardiovasc. Med.* 8, 649352. doi:10.3389/fcvm.2021.649352

Xie, B., Zhang, C., Kang, K., and Jiang, S. (2015). miR-599 Inhibits Vascular Smooth Muscle Cells Proliferation and Migration by Targeting TGFB2. *PLoS ONE* 10, e0141512. doi:10.1371/journal.pone.0141512

Xu, K., Liu, Q., Wu, K., Liu, L., Zhao, M., Yang, H., et al. (2020). Extracellular Vesicles as Potential Biomarkers and Therapeutic Approaches in Autoimmune Diseases. *J. Transl Med.* 18, 432. doi:10.1186/s12967-020-02609-0

Ye, J., Wang, C., Wang, D., and Yuan, H. (2018). LncRBA GSA5, Up-Regulated by Ox-LDL, Aggravates Inflammatory Response and MMP Expression in THP-1 Macrophages by Acting like a Sponge for miR-221. *Exp. Cel Res.* 369, 348–355. doi:10.1016/j.yexcr.2018.05.039

Yu, C. K., Xu, T., Assoian, R. K., and Rader, D. J. (2018). Mining the Stiffness-Sensitive Transcriptome in Human Vascular Smooth Muscle Cells Identifies Long Noncoding RNA Stiffness Regulators. *Arterioscler. Thromb. Vasc. Biol.* 38, 164–173. doi:10.1161/ATVBAHA.117.310237

Zakharova, L., Svetlova, M., and Fomina, A. F. (2007). T Cell Exosomes Induce Cholesterol Accumulation in Human Monocytes via Phosphatidylserine Receptor. *J. Cel. Physiol.* 212, 174–181. doi:10.1002/jcp.21013

Zhang, Y. G., Song, Y., Guo, X. L., Miao, R. Y., Fu, Y. Q., Miao, C. F., et al. (2019). Exosomes Derived from oxLDL-Stimulated Macrophages Induce Neutrophil Extracellular Traps to Drive Atherosclerosis. *Cell Cycle* 18, 2674–2684. doi:10.1080/15384101.2019.1654797

Zhang, Z., Yi, D., Zhou, J., Zheng, Y., Gao, Z., Hu, X., et al. (2020). Exosomal LINC01005 Derived from Oxidized Low-Density Lipoprotein-Treated Endothelial Cells Regulates Vascular Smooth Muscle Cell Phenotypic Switch. *Biofactors* 46, 743–753. doi:10.1002/biof.1665

Zheng, B., Yin, W. N., Suzuki, T., Zhang, X. H., Zhang, Y., Song, L. L., et al. (2017). Exosome-Mediated miR-155 Transfer from Smooth Muscle Cells to Endothelial Cells Induces Endothelial Injury and Promotes Atherosclerosis. *Mol. Ther.* 25, 1279–1294. doi:10.1016/j.ymthe.2017.03.031

Zhu, J., Liu, B., Wang, Z., Wang, D., Ni, H., Zhang, L., et al. (2019). Exosomes from Nicotine-Stimulated Macrophages Accelerate Atherosclerosis through miR-21-3p/PTEN-Mediated VSMC Migration and Proliferation. *Theranostics* 9, 6901–6919. doi:10.7150/thno.37357

Zwaal, R. F., and Schroit, A. J. (1997). Pathophysiologic Implications of Membrane Phospholipid Asymmetry in Blood Cells. *Blood* 89, 1121–1132. doi:10.1182/blood.v89.4.1121

Conflict of Interest: The authors declare that the research was conducted in the absence of any commercial or financial relationships that could be construed as a potential conflict of interest.

Publisher's Note: All claims expressed in this article are solely those of the authors and do not necessarily represent those of their affiliated organizations, or those of the publisher, the editors, and the reviewers. Any product that may be evaluated in this article, or claim that may be made by its manufacturer, is not guaranteed or endorsed by the publisher.

frontiers | Frontiers in Pharmacology

ORIGINAL RESEARCH
published: 24 May 2022
doi: 10.3389/fphar.2022.816059

Serum Homocysteine Level Predictive Capability for Severity of Restenosis Post Percutaneous Coronary Intervention

Jiqiang Guo[1,2,3†], Ying Gao[1,2,3†], Mohammad Ahmed[4], Pengfei Dong[4], Yuping Gao[2,3], Zhihua Gong[2,3], Jinwen Liu[2,3], Yajie Mao[2,3], Zhijie Yue[2,3], Qingli Zheng[1], Jiansheng Li[2,3], Jianrong Rong[2,3], Yongnian Zhou[2,3], Meiwen An[1], Linxia Gu[4]* and Jin Zhang[2]**

[1]College of Biomedical Engineering, Taiyuan University of Technology, Taiyuan, China, [2]Shanxi Bethune Hospital, Shanxi Academy of Medical Sciences, Tongji Shanxi Hospital, Third Hospital of Shanxi Medical University, Taiyuan, China, [3]Tongji Hospital, Tongji Medical College, Huazhong University of Science and Technology, Wuhan, China, [4]Department of Biomedical and Chemical Engineering and Sciences, Florida Institute of Technology, Melbourne, FL, United States

OPEN ACCESS

Edited by:
Qilong Wang,
Tianjin University of Traditional Chinese Medicine, China

Reviewed by:
Yuanli Chen,
Hefei University of Technology, China
Dipti Deshpande,
Kirkland and Ellis, United States

***Correspondence:**
Meiwen An
meiwen_an@163.com
Linxia Gu
Linxia.gu@gmail.com
Jin Zhang
zhangjin_99@126.com

[†]These authors have contributed equally to this work

Specialty section:
This article was submitted to Cardiovascular and Smooth Muscle Pharmacology, a section of the journal Frontiers in Pharmacology

Received: 16 November 2021
Accepted: 21 February 2022
Published: 24 May 2022

Citation:
Guo J, Gao Y, Ahmed M, Dong P, Gao Y, Gong Z, Liu J, Mao Y, Yue Z, Zheng Q, Li J, Rong J, Zhou Y, An M, Gu L and Zhang J (2022) Serum Homocysteine Level Predictive Capability for Severity of Restenosis Post Percutaneous Coronary Intervention. Front. Pharmacol. 13:816059. doi: 10.3389/fphar.2022.816059

Background: In stent restenosis (ISR) is one of the major complications after stent implantation. Thus, there is a growing interest in identifying a biomarker for the onset of ISR. High levels of serum homocysteine (Hcy) have been associated with the progression of cardiovascular disease. Therefore, the study was carried out to quantify the correlation between serum Hcy and ISR severity. Compared with coronary angiography (CAG), Hcy levels provided a significantly better clinical detection of ISR severity after PCI.

Methods: A total of 155 patients were recruited from Shanxi Bethune hospital, from 6 months to 2 years post PCI. Serum Hcy levels and postoperative angiography results were used to differentiate the patients into two experimental groups: ISR (>50% diametrical stenosis), and non-ISR. The non-ISR included two subgroups: intimal hyperplasia (10–50% diametrical stenosis), and recovery (<10% diametrical stenosis). In addition, a group of 80 healthy individuals was used as a negative control. The correlation between homocysteine level and ISR severity t was analyzed for all groups. In addition, the correlation between serum Hcy level and the severity of ISR in the experimental group was analyzed by the Pearson correlation test.

Results: The serum Hcy level in the experimental group and control group was determined to be (20.21 ± 11.42) μmol/L and (15.11 ± 10.25) μmol/L respectively. The level of serum Hcy in the experimental group was significantly higher than in the control group (t-value of 2.385; p-value of 0.019). The serum Hcy level in the restenosis and the intimal hyperplasia group was (25.72 ± 13.71) μmol/L and (17.35 ± 7.70) μmol/L respectively. The serum Hcy level in the restenosis group was significantly higher than in the intimal hyperplasia group (t-value of 2.215; p-value of 0.033). The level of serum Hcy in the group without a plaque in the stent was (16.30 ± 6.08) μmol/L, whereas in the control group was (15.11 ± 10.25) μmol/L. The no plaque group had a slightly higher serum Hcy level than the control group (t-value of 0.634; p-value of 0.528). All included patients were divided into four quartiles based on the serum Hcy concentration: quartile 1

(8.90–13.20 μmol/L), quartile 2 (13.30–16.45 μmol/L), quartile 3 (16.60–24.25 μmol/L) and quartile 4 (24.30-65.30 μ mol/L). The incidence of ISR was 5, 6.25, 7.5 and 15%, in the 1,2,3 and four quartiles respectively. The serum Hcy level in the experimental group was (20.21 ± 11.42) μmol/L, the severity of in-stent restenosis was (0.25 ± 0.31), (*R*-value was 0.234; *p*-value was 0.037), indicating a correlation between serum Hcy and the severity of restenosis ($p < 0.05$). Taking coronary angiography as the gold standard, a ROC curve analysis was performed on the serum Hcy levels for the experimental group. The area under the curve (AUC) was 0.718 (95% *CI* 0.585-0.854, $p < 0.001$), indicating that the serum Hcy concentration could predict ISR. On the ROC curve, the best critical value of serum Hcy concentration for predicting ISR was 20.05 μmol/L, with a sensitivity of 45% and specificity of 88.1%.

Conclusion: A positive correlation was observed between homocysteine and the severity of restenosis after PCI, The level of Hcy could serve as a predictive biomarker for the severity of ISR.

Keywords: homocysteine, in stent restenosis, severity, percutaneous coronary intervention, ROC curve

1 INTRODUCTION

The continuous improvement in people's living standard, the change of lifestyle and eating habits have aggregated the incidence rate of coronary heart disease, especially towards the younger ages. Therefore the occurrence and development of coronary heart disease significantly reduces patient's quality of life. Percutaneous coronary intervention (PCI), also known as stenting, is the popular treatment procedure to open clogged arteries with the advantages of short operation time and minimal invasiveness (Bennett 2003). However, stent restenosis (ISR) is one of the major complications following PCI (Giulio and David 2013). The ISR is a complex pathophysiological process, including vascular inflammation, vascular remodeling caused by endothelial injury, and excessive proliferation and migration of vascular smooth muscle cells. Large-scale clinical trials have shown that the incidence of ISR of bare metal stents is approximately 20–30%. However, drug-eluting stents could reduce the risk of restenosis to 5–10% (Paudel et al., 2005).

A variety of cytokines and inflammatory factors such as nuclear factors-κB (NF-κB), tumor necrosis factor-α (TNF-α), platelet derived growth factor (PDGF) have been associated with the incidence of coronary ISR (Guildford et al., 2011). The high homocysteine (Hcy) level, i.e., hyperhomocysteinemia, has attracted increasing attention in treating coronary heart disease. High Hcy level was positively correlated with the severity of coronary heart disease, atrial fibrillation, stroke, arteriosclerosis, and other cardiovascular disorders (CADS) (Chen et al., 2018; Dhar et al., 2018; Kubota et al., 2019). Hcy is a sulfur-containing amino acid, which can be easily detected in the blood. It is mainly metabolized by methionine (MET) through two main pathways: re-methylation to methionine or reverses sulfurization to cysteine (Kim et al., 2018). Moreover gene mutations encoding enzymes in the Hcy metabolic pathway, an increased homocysteine level can be attributed to vitamin deficiency, excessive methionine intake, or the use of some drugs and other factors (Kumar et al., 2017). However, there is a lack of information regarding the correlation between. Hcy and restenosis. Bakoyiannis et al. (2015) considered Hcy as the risk factor for the efficacy of percutaneous transluminal coronary angioplasty (PTCA). A lower Hcy level could improve the prognosis after PTCA. .De Luca et al., 2005 demonstrated a positive relationship between the Hcy level and the carotid restenosis within 2 years post endarterectomy. Whereas Wong et al., 2004 observed no direct relationship between the level of Hcy and ISI, a higher Hcy level increased the risk of mortality after PCI. However, all these observations were qualitative. Hcy level is important in predicting the disease risk, controlling disease complications and affecting disease outcomes. Hcy level monitoring might be conducive to early detection and diagnosis of diseases, and early prevention of serious complications. However, no quantitative analysis was observed between the Hcy level and the ISR severity. Thus, the study examines the correlation between Hcy and ISR severity, to identify the prediction capacity of Hcy.

2 METHODS

2.1 Patients

In a retrospective study, 155 patients were recruited from Shanxi Bethune hospital as the experimental group 6 months to 2 years following PCI, while 80 healthy individuals were recruited as the negative control group. The clinical data collected in this study was obtained from the inpatient medical record system (patient admission course record), test data system, PCI registration system, and image diagnosis report workstation of the cardiovascular department of Shanxi Bethune hospital. The data included gender, age, serum Hcy levels, and postoperative angiographic results. The clinical data of the experimental group was used to subdivide the group further based on the severity of restenosis after stent implantation. There were 48 cases in the stent restenosis group, 30 cases in the intimal hyperplasia group and 77 cases in the plaque free group. The average age of all patients in the experimental group was (59.89 ± 3.15) years, with 78 male and 77

female patients. The negative control group consisted of 43 males and 37 females ranging from 18 to 60 years of age: the average age of (40.12 ± 4.13 years). The experimental and control groups were comparable for age or sex ratio ($p > 0.05$). All patients had good compliance with the drug treatment after PCI. The patients who successfully received PCI underwent routine coronary angiography in the Shanxi Bethune hospital for recurrent chest distress, chest pain, palpitation, shortness of breath, acid reflux, heartburn, and other symptoms. All procedures were carried out per Shanxi Bethune hospital's clinical medical ethics standards. The research protocol was approved by the clinical medical ethics committee, and informed consent was obtained from the subjects.

Inclusion Criteria: 1) a complete medical history,2) complaints of stable or unstable angina pectoris leading to further coronary angiography within 6 months to 2 years post stent implantation, and 3) the patient receiving conventional antiplatelet drugs (aspirin 100 mg/Day and clopidogrel 75 mg/Day) and statins for at least 1 year after PCI. The international common visual diameter method was used to calculate the degree of coronary artery stenosis independently, and then the average value was obtained for analysis, (see Eq. 1). Exclusion Criteria:1) taking anti-infective drugs, anti-inflammatory drugs, or glucocorticoids affecting immune function, 2) liver insufficiency, renal insufficiency, impaired right ventricular function, and acute heart failure, 3) recent history of surgery and ulcers, and 4) myocarditis, cardiomyopathy, acute and chronic infection, cardiogenic shock, severe lung disease, severe arrhythmia, blood system disease, peripheral vascular embolism disease, immune system disease, malignant tumor, or severe anemia.

Eq. 1: Degree of stenosis = (Normal vessel diameter near the heart at the stenosis - Vessel diameter at the stenosis)/Vessel diameter near the heart at the stenosis×100%.

2.2 Measures

The patient's gender, age, BMI, coronary heart disease risk factors (hypertension, hyperlipidemia, diabetes, smoking, etc.), relevant laboratory examination indices, coronary angiography characteristics (vascular lesion location), and stent placement conditions (stent diameter, number, length) were collected for the experimental group. Other information includes postoperative medication such as clopidogrel for at least 1 year after stent implantation, aspirin enteric coated tablets, statins β- Receptor blockers and angiotensin converting enzyme inhibitors were also obtained.

A total of 155 patients in the experimental group were hospitalized for coronary angiography 6 months to 2 years post PCI. The following day, the elbow venous blood was taken on an empty stomach and sent to the laboratory for hematological examination. Total 5.0 ml of venous blood was collected in a tube containing coagulant separation glue, and the serum Hcy level was detected by the Beckman Kurt AU5800 automatic biochemical analyzer. The cyclic enzyme method was used to determine Hcy levels for the experimental and control group.

All patients underwent coronary angiography in Shanxi Bethune hospital's cardiovascular interventional catheter room of ISR grouping criteria: related to a plaque in the stent, the patients were further divided into plaque in the stent group and no plaque in the stent group. According to the severity, the plaque in the stent group was divided into the in-stent restenosis and in-stent intimal hyperplasia group. In stent restenosis group: plaques in the stent, and the lumen were lost in the whole process of the stent and/or 5 mm segments at both ends of the stent, resulting in the degree of lumen stenosis ≥50%, and the degree of restenosis can be quantified; In-stent intimal hyperplasia group: plaques in the stent, and the lumen were lost in the whole process of the stent and/or in the 5 mm segment at both ends of the stent, resulting in the stenosis of the lumen ranging from 0 to 50%; No plaque in stent group: no plaque in the whole length of the stent and/or 5 mm segments at both ends of the stent.

2.3 Statistical Methods

Excel software was used to establish a database and SPSS 19.0 software was used for statistical analysis. Quantitative data (or measurement data) was described by mean ± standard deviation ($\bar{x} \pm s$) or median. *t*-test, or analysis of variance, was used for inter-group comparisons. The Pearson method was used for the correlation analysis. Multivariate stepwise logistic regression analysis was used to determine the predictors of ISR. A p less than 0.05 was considered statistically significant. The ROC curve was drawn and the area under the curve (AUC) was calculated to determine the accuracy of predicting the Hcy risk. The Youden index method determined the best cutoff point; the maximum sensitivity and specificity determine the critical point. The AUC was compared using medcalc statistical software.

3 RESULTS

3.1 Clinical Characteristics of Patients

According to the severity of restenosis, or lack thereof, the experimental group was divided into the ISR group (n = 48) or the non-ISR group (n = 107; subdivided into intimal hyperplasia group n = 30 and normal coronary lumen group n = 77). No significant difference in gender, average age, smoking, or hypertension was observed between the two groups. Compared with the non-ISR group, the ISR patients had a significantly higher proportion of diabetes mellitus, longer stent implantations, higher serum hs-CRP, HMGB1 concentrations, longer stent lengths, and smaller lumen diameters (**Table 1**), No correlation was observed between ISR occurrence and age, gender, smoking history, diabetic history, location of the lesion, or hypertension drugs. However, a relationship between ISR and hypertensive history, number of stent implantations, stent length, stent diameter, the diameter of the reference vessel, serum inflammatory factor CRP and HMGB1 levels were observed.

3.2 The Higher Serum Hcy, Levels Revise and Remove Comma

The clinical data were collected for 155 patients after PCI was collected in the experimental group, while the physical

TABLE 1 | Comparison of serum Hcy levels between non ISR group and ISR group.

Group		Non-ISR group (n = 107)	ISR group (n = 48)	*p* Value
Age (y)		55.23 ± 1.09	57.83 ± 2.16	0.18
Male gender (n, %)		50 (46.4)	28 (58.3)	0.57
Smoking (n, %)		63 (58.9)	30 (62.5)	0.49
Diabetes (n, %)		24.6 ± 3.2	25.5 ± 3.8	0.57
Hypertension (n, %)		86 (80.7)	42 (86.7)	0.046
Target vessels (n, %)	Left anterior descending	50 (46.5)	26 (54.2)	0.61
	Left circumflex	25 (23.2)	14 (29.2)	0.44
	Right coronary artery	31 (28.6)	16 (33.3)	0.42
Stent number (n)		2.10 ± 0.076	1.96 ± 0.068	0.041
Stent length (mm)		19.34 ± 0.5	21.88 ± 0.48	0.026
Stent diameter (mm)		3.13 ± 0.46	2.91 ± 0.54	<0.01
References vessel diameter (mm)		3.05 ± 0.48	2.89 ± 0.43	<0.01
hs-CRP (mg/l)		2.21 ± 1.05	2.77 ± 1.40	0.046
HMGB1 (μg/l)		15.45 ± 7.72	23.95 ± 11.05	0.013
β-blocker (n, %)		21 (37.5)	10 (41.7)	0.62
ACEI/ARB (n, %)		27 (48.2)	13 (54.2)	0.70
CCB (n, %)		29 (51.8)	14 (58.3)	0.35

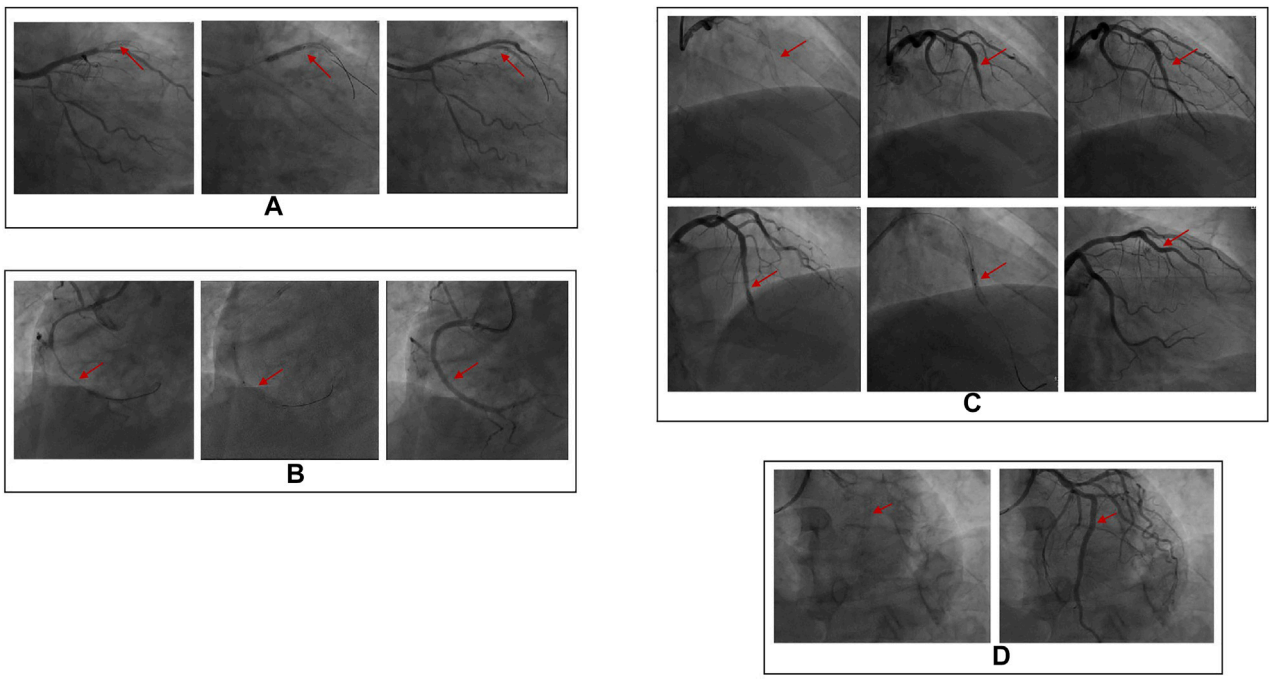

FIGURE 1 | DSA images of plaque formation in stent and the severity of plaque on vascular blockage. **(A)** In stent restenosis (complete occlusion), stent shadow can be seen in the proximal part of lad, complete occlusion in the middle part of LAD (100% stenosis), TIMI grade 0; **(B)** In stent restenosis (partial occlusion), stent shadow can be seen in the proximal part of RCA, and 70% stenosis in the proximal part of RCA; **(C)** There are plaques (intimal hyperplasia) in the stent, stent shadow can be seen in the middle of lad, and intimal hyperplasia in the stent. **(D)** There is no plaque (unobstructed blood flow) in the stent. The stent shadow can be seen in the proximal and middle part of RCA, and the blood flow in the stent is unobstructed.

examination data were obtained for 80 healthy individuals was collected in the control group. DSA images of plaque formed in the stent and the degree of vascular blockage caused by plaque in the experimental group are shown in **Figure 1**. The serum Hcy level in the experimental group was significantly higher than the control group (**Table 2**) (*t*-value was 2.385, the *p*-value was 0.019). Besides, a correlation was observed between coronary atherosclerosis and Hcy levels. The higher serum Hcy, levels were associated with the increased vulnerability for coronary atherosclerosis. In the experimental group, the serum Hcy level of ISR patients (48 cases) was comparable with the intimal hyperplasia patients (30 cases) (**Table 3**). The ISR

TABLE 2 | Comparison of serum Hcy levels between experimental group and control group.

Variables	Hcy (μmol/L)	Number of Cases(n)	*t* value	*p* value
Experience group	20.21 ± 11.42	155	2.385	0.019
Control group	15.11 ± 10.25	80		

TABLE 3 | Comparison of serum Hcy levels between restenosis group and intimal hyperplasia group.

Variables	Experience group		Control group		*t* value	*p* value
	Hcy (μmol/L)	Number of Cases(n)	Hcy (μmol/L)	Number of Cases(n)		
Restenosis group	25.72 ± 13.71	48	15.11 ± 10.25	80	3.527	0.001
Intimal hyperplasia group	17.35 ± 7.70	30			0.789	0.434
No plaque in stent group	16.30 ± 6.08	77			0.634	0.528
t value	6.784					
p value	0.000					

TABLE 4 | Comparison of serum Hcy levels between plaque group and plaque free group in stent.

Variables	Plaque group in stent		No plaque in stent group		*t* value	*p* value
	Hcy (μmol/L)	Number of Cases(n)	Hcy (μmol/L)	Number of Cases(n)		
Restenosis group	25.72 ± 13.71	48	16.30 ± 6.08	77	3.783	0.000
Intimal hyperplasia group	17.35 ± 7.70	30			0.539	0.592
t value	2.215					
p value	0.033					

TABLE 5 | Comparison of serum Hcy levels between plaque free group and control group.

Variables	Plaque group in stent		Control group		*t* value	*p* value
	Hcy (μmol/L)	Number of Cases(n)	Hcy (μmol/L)	Number of Cases(n)		
Plaque group in stent	22.37 ± 12.28	78	15.11 ± 10.25	80	2.872	0.005
No plaque in stent group	16.30 ± 6.08	77			0.634	0.528
t value	2.801					
p value	0.006					

group revealed a serum Hcy level of 25.72 ± 13.71 μmol/L whereas the intimal hyperplasia group had a Hcy level of 17.35 ± 7.70 μmol/L. The difference between the two groups was statistically significant with the *t*-value was 2.215 and the *p*-value was 0.033. Among both the ISR and intimal hyperplasia groups, 77 patients had a serum Hcy level of 22.37 ± 12.28 μmol/L. Patients without a plaque in the stent after PCI revealed an Hcy level of 16.30 ± 6.08 μmol/L. A significant difference was observed between the plaque versus no plaque groups (*t*-value was 2.801 and the *p*-value was 0.006). The plaque free group had a lower Hcy level (**Table 4**), the higher the serum Hcy level, the greater the probability and severity of ISR. Patients with a plaque in the stent after PCI had an Hcy level of 22.37 ± 12.28 μmol/L whereas patients in the plaque free group had the level of 16.30 ± 6.08 μmol/L. The healthy subjects in the control group had a level of 15.11 ± 10.25 μmol/L, which was further lower than the no plaque group. The difference between the no plaque group and

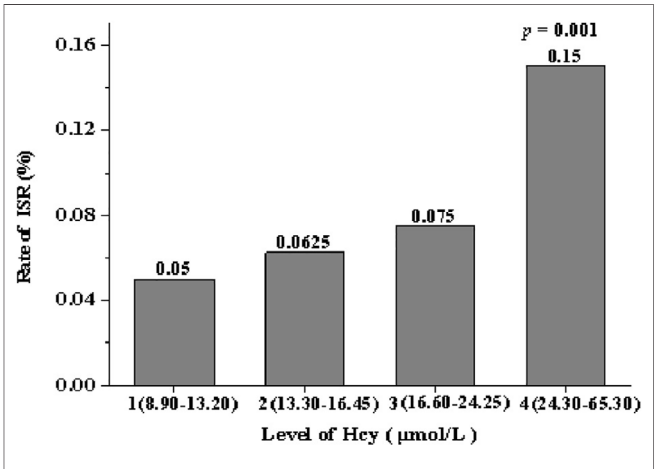

FIGURE 2 | Rate of ISR stratified by quartile of level of Hcy.

TABLE 6 | Pearson correlation between serum Hcy value and in stent restenosis severity.

Variables	Detection result	Number of Cases(n)	*r* value	*p* value
Hcy (μmol/L)	20.21 ± 11.42	155	0.266	0.003
In stent restenosis severi (%)	0.25 ± 0.31	155		

TABLE 7 | Logistic regression analysis of restenosis severity.

Variables	R	95% CI	*p* value
Serum Hcy	0.266	22.19-61.45	0.003

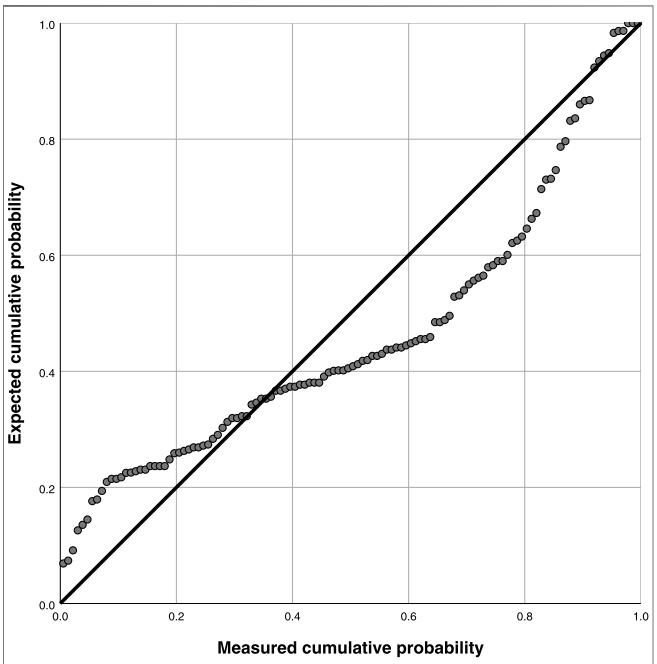

FIGURE 3 | Logistic regression analysis of serum Hcy level and the severity of in stent restenosis.

control group was statistically significant (*t*-value was 2.872 and the *p*-value was 0.005). No statistically significant difference was observed in serum Hcy levels of the plaque free group (*t*-value was 0.634 and the *p*-value was 0.528), (**Table 5**).

The experimental group was further divided into four quartiles (n = 20 each quartile) depending on the concentration of serum Hcy: quartile 1 (8.90–13.20 μmol/L), quartile 2 (13.30–16.45 μmol/L), quartile 3 (16.60–24.25 μmol/L) and quartile 4 (24.30–65.30 μmol/L). From quartile one to quartile 4, the incidence of ISR was 5, 6.25, 7.5 and 15%, respectively. The incidence of ISR in patients in quartile four was significantly higher than in other groups (p = 0.001), and the incidence of ISR increased gradually between these quartiles (**Figure 2**).

Of the 155 patients in the experimental group, the severity of ISR in the intimal hyperplasia group was calculated as 0.25, whereas the non-plaque group was 0.00. The correlation between serum Hcy levels and ISR severity was analyzed by the Pearson correlation test (**Table 6**). The level of serum Hcy in the experimental group was calculated as 20.21 ± 11.42 μmol/L, and the severity of ISR was 0.25 ± 0.31 (r = 0.234, p = 0.037).

Table 7 and **Figure 3** demonstrate the goodness of fit coefficient (0.266), with multiple linearities. There was significant linearity since a regression coefficient p was less than 0.05 indicating a linear relationship (p = 0.003). (Linear regression equation: $y = 16.717 + 10.876x$, 95% *CI*: 22.19–61.45).

3.3 Correlation Analysis Between the Severity of in Stent Restenosis and Diseased Vessels

A total of 82 patients (52.90%) had vascular lesions in the left anterior descending branch in the experimental group., In the ISR group, the most significant incidence of ISR was related to the left anterior descending coronary artery (LAD) in 26 cases (54.17%), followed by 16 cases (33.33%) in the right coronary artery (RCA), 4 cases (8.33%) in the left circumflex artery (LCX), and 2 cases (4.17%) in the left main coronary artery, (LM) (**Table 8**).

3.4 ROC Curve Analysis Value of Serum Hcy Level in Predicting the Severity of in Stent Restenosis

Taking coronary angiography as the gold standard, the ROC curve was used to explore the relationship between the serum Hcy level and ISR in the experimental group (**Figure 4**). Taking Youden index = sensitivity + specificity - 1, the area under the curve was AUC 0.718 (95% CI 0.585-0.854, $p < 0.001$), indicating that serum Hcy concentration could predict ISR. The best critical value of serum Hcy concentration on the ROC curve for predicting ISR was 20.05 μmol/L with a sensitivity of 45%, and specificity of 88.1%. Compared with other study populations, a serum Hcy value of 20.05 μmol/L significantly increased the risk of restenosis.

4 DISCUSSION

The incidence of coronary is increasing amongst younger age groups, as a consequence of dietary changes and increased stress (Assimes 2016). PCI is the popular method to treat coronary heart disease. Though PCI significantly improves the quality-of-life index of patients. ISR is a major adverse event post PCI. The incidence of ISR with bare-metal stents is 20–30%, whereas the emergence of drug-eluting stents reduces ISR incidence to a certain extent, (about 5–10%). Still, drug-eluting stents inhibit intimal hyperplasia and growth of endodermal cells (ECS) while promoting the formation and development of ISR to a certain

TABLE 8 | Pearson correlation between diseased vessels and the severity of in stent restenosis.

Diseased vessel	RCA	LAD	LM	LCX	Total
Restenosis	16 (33.33%)	26 (54.17%)	2 (4.17%)	4 (8.33%)	48 (30.97%)
Intimal hyperplasia	3 (8.57%)	24 (68.57%)	2 (5.72%)	6 (17.14%)	35 (22.58%)
No plaque in stent group	16 (22.22%)	32 (44.44%)	2 (2.78%)	22 (30.56%)	72 (46.45%)
Total	35 (22.58%)	82 (52.90%)	6 (3.87%)	32 (20.65%)	155 (100%)
X^2 value		15.814			
p value		0.015			

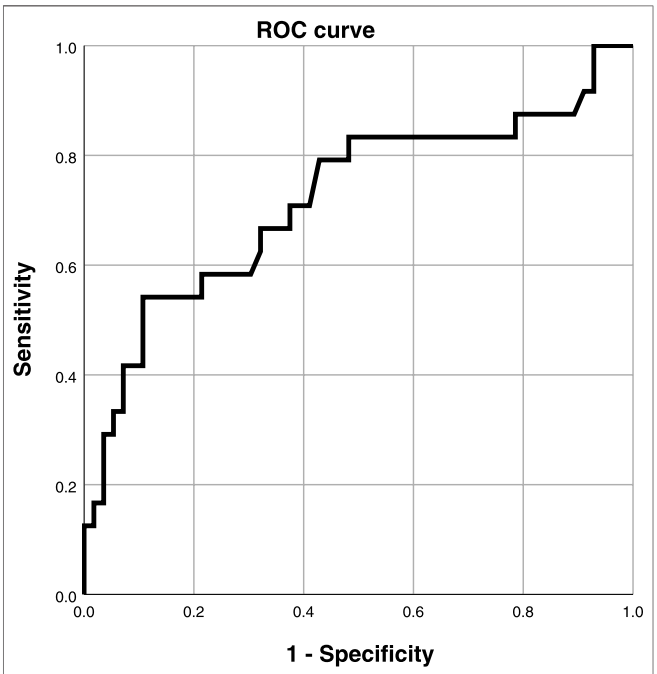

FIGURE 4 | ROC curve of serum Hcy level.

extent (Tian et al., 2013). The efficacy of biodegradable stents depends on their degradability, however, discontinuity or thrombosis might occur in the degradation process doubling the risk of thrombosis in the stent (Byrne et al., 2015). Current strategies focus on mitigating the ISR, including improving myocardial perfusion, reducing cardiomyocyte necrosis, etc.

During PCI, the balloon expands the stent to enlarge the lumen and push the lesion outwards (Philip 2015). To ensure the complete expansion of the stent and maximum elimination of residual plaque in the blood vessel clinicians often choose to over-expand the stent. Due to the abnormal stress induced by the stent, the ECS in the lesion area experience damage in varying degrees. The ECS injurypromotes the inflammatory cells such as neutrophils and macrophages to start the repair mechanism. This cascade causes an inflammatory response causing the release of inflammatory factors at the damaged part of the vascular endothelium. Under the combined action of many chemokines and inflammatory factors, vascular smooth muscle cells (SMC) proliferate and migrate to the damaged vascular intima, and the abnormal proliferation of vascular smooth muscle cells (Hu et al., 2015) contributes to the formation and development of ISR. In addition, the change in the elastic contraction of blood vessels promotes the occurrence of ISR (Kokkinidis et al., 2019).

Hcy is a sulfur-containing amino acid formed after the demethylation of methionine. Though it is an intermediate product of the methionine cycle, it is an unnecessary amino acid for the human body (Otsuka et al., 2012). Foods with high protein content, such as meat and milk, contain a large amount of methionine which can be transformed into Hcy. Other components in the body, such as vitamins B6, B9, B12, folic acid, betaine, etc catalyzes the conversion of Hcy to glutathione (GSH) and S - adenosylmethionine (SAM). As a result, the serum Hcy positively correlates with methionine concentration in the daily diet.In contrast, a negative correlation of Hcy was observed with the concentration of vitamins B6, B9, B12, folic acid, and betaine in the human body (Ganguly and Alam 2015).

The levels of serum Hcy in the ideal human body are low. The Hcy can be converted into GSH and SAM beneficial to the human body. However, genetic defects, nutrient deficiency, smoking, heavy drinking, and improper diet (excessive intake of foods containing too much lysine or too little intake of vitamins B6, B9, B12, folic acid and betaine) can alter this balance. This imbalance causes an imbalance of nutritional state, resulting in the accumulation of Hcy content and an overall increase in Hcy level in the blood. Studies have shown that elevated serum Hcy can increase the body's oxidative stress pressure, causeing endothelial cell damage, nitric oxide depletion, reduced endothelial relaxation function, formation of oxidized low-density lipoprotein, and promotion of pre-atherosclerotic state and pre-thrombotic state (Spence 2006; Eichinger 2010; Graeme et al., 2012).

The increase of Hcy levels affects the gene expression of vascular endothelial cells, leading to a toxic effect on the endothelial cells and apoptosis. Therefore, arterial vascular smooth muscle cells overgrow and proliferate, resulting in vascular endothelial wall thickening, arterial elasticity damage and the formation of joint sclerosis plaque in stents. These conditions contribute to be the potential pathogenesis of ISR. However, human serum Hcy level is affected by genetic factors, nutritional and dietary factors, life factors, drug factors, and other factors (Nygrd et al., 1995; Nagele et al., 2011; Naik et al., 2011; Nilsson et al., 2014; Hildebrandt et al., 2015; Jung et al., 2015), These factors include lack of cystine sulfide-β-Synthetase (CBS), methylenetetrahydrofolate reductase (MTHFR), Methionine synthase (MS), methionine adenosyltransferase (MAT) folic acid, vitamin B6, vitamin B12 and othergenetic factors. Besides smoking, drinking, lack of physical exercise and other living

habits, antiepileptic drugs, metformin, methotrexate, thiazide diuretics, niacin, rosiglitazone and drugs for hypothyroidism, renal failure, malignant tumor and other diseases, can also increase the blood Hcy level.

De et al. (De Luca et al., 2005) showed that patients with moderate or severe high Hcy levels might have a higher risk of restenosis and subacute thrombosis. Hcy promotes the proliferation of intravascular SMC, inducing SMC to enter the division stage and rapidly proliferate and differentiate in a short period (Zeng et al., 2010); Hcy can also affect the normal metabolism of blood lipids in the human body. Hcy can cause the oxidative modification of low density lipoprotein (LDL), form oxidized low-density lipoprotein (ox LDL), and reduce the concentration of high-density lipoprotein (HDL). In addition, Hcy can reduce NO production and cause damage to vascular function by combining with NO secreted by endothelial cells and ox LDL, leading to limited vascular endothelial relaxation function (Dionisio et al., 2010). High Hcy content can also cause an imbalance of the coagulation and fibrinolysis system. In addition, Hcy activates metalloproteinases, activates inflammatory cells, promotes the production of a variety of inflammatory factors such as monocyte chemoattractant protein, tumor necrosis factor and interleukin family, and promotes neutrophil migration to accelerate the damage to vascular endothelium (Kugler et al., 2015).

Studies have observed that high homocysteine levels increase the risk of restenosis after coronary angioplasty. Elevated homocysteine levels are also known to increase the risk of all-cause mortality, mace and heart death after PCI, suggesting that serum Hcy is a potential risk factor for ISR (Hong et al., 2005). The dose-response meta-analysis supported a linear relationship between homocysteine levels and all-cause mortality in the general population. Specifically, an increase in hcy levels of 5 μmol/l was correlated with the risk of all-cause mortality increase by 1.336 times (Zhang et al., 2019). The alterations of Hcy levels in patients who underwent carotid endarterectomy (CEA) with venous patch closure technique were collected pre- and post-operation in a prospective design. Hcy levels were significantly correlated with both the presence of complicated atheromatous plaque and the degree of internal carotid artery restenosis after CEA (Bakoyiannis et al., 2015; Vidale et al., 2017). However, the relationship between Hcy levels and long-term outcomes post PCI remained inconsistent and contradictory (Stangl et al., 2000; Zairis et al., 2002; Ortolani et al., 2004). Some studies have shown that extending the intake of oral folic acid decreased the plasma Hcy level. Therefore, long-term oral folic acid tablets can reduce the plasma Hcy level and reduce the incidence of coronary stent restenosis. Therefore, folic acid can be used as the secondary prevention of in stent restenosis. Moreover, with its low price and high-cost performance, folic acid can be recommended in the clinic (Schnyder et al., 2001; Schnyder et al., 2002; Hong et al., 2005; Bleie et al., 2008).

There are three main methods of detecting for serum Hcy, circulating enzyme method, isotope method, immunoassay and chromatography. However, the use of these methods is limited in clinical practice due to the involved in operational complexity. In this study, the circulating enzyme method determines the serum Hcy level. The circulating enzyme method uses enzyme-substrate specificity to amplify the target substance. It has the advantages of mild reaction, good specificity, high sensitivity, environmental protection, and no pollution, and it has been widely popularized in clinics (Ortolani et al., 2004).

We have demonstrated that the level of serum Hcy in the experimental and control group was 20.21 ± 11.42 μmol/L and 15.11 ± 10.25 μmol/L, respectively. The serum Hcy in the experimental group was significantly higher than in the control group. Serum Hcy in the groups with plaque in the stent was 22.37 ± 12.28 μmol/L whereas in the plaque free group was 16.30 ± 6.08 μmol/L. The serum Hcy in the plaque group was higher than in the no plaque group. The serum Hcy level was 25.72 ± 13.71 μmol/L in the ISR group and 17.35 ± 7.70 μmol/L in the intimal hyperplasia group. The serum Hcy in the ISR group was higher than in the intimal hyperplasia group. The level of serum Hcy in the group without a plaque in the stent was 16.30 ± 6.08 μmol/L whereas the control group had a level of 15.11 ± 10.25 μmol/L.A small difference was observed in serum Hcy levels between the plaque free group and the control group, indicating a correlation between serum Hcy levels and ISR. Pearson correlation test showed a correlation between serum Hcy value and ISR severity. Using CAG as the gold standard, the ROC curve analysis of serum Hcy level in the experimental group showed that the serum Hcy levels had a certain predictive value for ISR severity.

Overall, a positive correlation was found between serum Hcy level and ISR severity, suggesting that serum Hcy is a risk factor for ISR and a significant predictor of cardiovascular disease. Furthermore, it has a certain predictive value for the formation, development and severity of ISR after PCI. Therefore, early intervention to reduce preoperative and postoperative serum Hcy levels might be helpful to prevent ISR.

5 CONCLUSION

A positive correlation was observed between the serum Hcy level and ISR severity. In addition, the ROC curve analysis demonstrated that the serum Hcy level could serve as a predictive biomarker for ISR severity after PCI. However, other hematological indexes might alter the correlation between serum Hcy and ISR severity, which was not considered in this present study. Future multi-center research with a large cohort is required to validate the current findings in clinical practices.

DATA AVAILABILITY STATEMENT

The original contributions presented in the study are included in the article/Supplementary Material, further inquiries can be directed to the corresponding authors.

AUTHOR CONTRIBUTIONS

All authors listed have made a substantial, direct, and intellectual contribution to the work and approved it for publication.

FUNDING

This work is supported by the National Natural ScienceFoundation of China (No. 31870934), Shanxi Provincial Health Commission Project "The research on intelligent and accurate detection of medical devices in Shanxi Province (provincial key training laboratory)(No. 2020SYS14)", The principal Investigator of Shanxi Bethune hospital (Shanxi Academy of Medical Sciences) (No: 2021RC001) and Shanxi Provincial Health Commission project Mechanical and biologicalmechanism of stent stress regulating HMGB1 in stentrestenosis (No: 2021146).

REFERENCES

Assimes, T. L. (2016). Genetics. Implications for Prevention and Management of Coronary Artery Disease-ScienceDirectGenetics: Implications for Prevention and Management of Coronary Artery Disease. *J. Am. Coll. Cardiol.* 68 (25), 2797–2818. doi:10.1016/j.jacc.2016.10.039

Bakoyiannis, C., Karaolanis, G., Moris, D., Palla, V., Skrapari, I., Bastounis, E., et al. (2015). Homocysteine as a Risk Factor of Restenosis after Carotid Endarterectomy. *Int. Angiol* 34 (2), 166–71.

Bennett, M. R. (2003). In-stent Stenosis: Pathology and Implications for the Development of Drug Eluting Stents. *Heart* 89, 218–224. doi:10.1136/heart.89.2.218

Bleie, O., Strand, E., and Loland, K. H. (2008). Homocysteine Lowering B-Vitamin Therapy and In-Stent Restenosis. A WENBIT Sub Study. *Circulation* 118 (12), E472

Byrne, R. A., Joner, M., and Kastrati, A. (2015). Stent Thrombosis and Restenosis: what Have We Learned and where Are We Going? the Andreas Grüntzig Lecture ESC 2014. *Eur. Heart J.* 36 (47), 3320–3331. doi:10.1093/eurheartj/ehv511

Chen, L., Wang, B., Wang, J., Ban, Q., Wu, H., Song, Y., et al. (2018). Association between Serum Total Homocysteine and Arterial Stiffness in Adults: a Community-Based Study. *J. Clin. Hypertens. (Greenwich)* 20 (4), 686–693. doi:10.1111/jch.13246

De Luca, G., Suryapranata, H., Gregorio, G., Lange, H., and Chiariello, M. (2005). Homocysteine and its Effects on In-Stent Restenosis. *Circulation* 112 (19), e307–11. doi:10.1161/CIRCULATIONAHA.105.573923

Dhar, I., Svingen, G. F. T., Pedersen, E. R., DeRatt, B., Ulvik, A., Strand, E., et al. (2018). Plasma Cystathionine and Risk of Acute Myocardial Infarction Among Patients with Coronary Heart Disease: Results from Two Independent Cohorts. *Int. J. Cardiol.* 266, 24–30. doi:10.1016/j.ijcard.2018.04.083

Dionisio, N., Jardín, I., Salido, G. M., and Rosado, J. A. (2010). Homocysteine, Intracellular Signaling and Thrombotic Disorders. *Curr. Med. Chem.* 17 (27), 3109–3119. doi:10.2174/092986710791959783

Eichinger, S. (2010). Are B Vitamins a Risk Factor for Venous Thromboembolism? Yes. *J. Thromb. Haemost.* 4 (2), 307–308. doi:10.1111/j.1538-7836.2006.01711.x

Ganguly, P., and Alam, S. F. (2015). Role of Homocysteine in the Development of Cardiovascular Disease. *Nutr. J.* 14, 6–15. doi:10.1186/1475-2891-14-6

Graeme, J. H., John, W. E., and Qilong, Y. (2012). Antiplatelet Therapy and the Effects of B Vitamins in Patients with Previous Stroke or Transient Ischaemic Attack: a post-hoc Sobanalysis of VITATOPS. A Randomized, Placebo-Controlled Trial. *Lancet Neurol.* 11 (6), 512. doi:10.1016/S1474-4422(12)70091-1

Guildford, A. L., Stewart, H. J., Morris, C., and Santin, M. (2011). Substrate-induced Phenotypic Switches of Human Smooth Muscle Cells: an *In Vitro* Study of In-Stent Restenosis Activation Pathways. *J. R. Soc. Interf.* 8 (58), 641–649. doi:10.1098/rsif.2010.0532

Hildebrandt, W., Sauer, R., Bonaterra, G., Dugi, K. A., Edler, L., and Kinscherf, R. (2015). Oral N-Acetylcysteine Reduces Plasma Homocysteine Concentrations Regardless of Lipid or Smoking Status. *Am. J. Clin. Nutr.* 102 (5), 1014–1024. doi:10.3945/ajcn.114.101964

Hong, Y. J., Jeong, M. H., Lim, S. Y., Lee, S. R., Kim, K. H., Sohn, I. S., et al. (2005). Elevated Preprocedural High-Sensitivity C-Reactive Protein Levels Are Associated with Neointimal Hyperplasia and Restenosis Development after Successful Coronary Artery Stenting. *Circ. J.* 69 (12), 1477–1483. doi:10.1253/circj.69.1477

Hu, X., Wang, Z., Wu, H., Jiang, W., and Hu, R. (2015). Ras ssDNA Aptamer Inhibits Vascular Smooth Muscle Cell Proliferation and Migration through MAPK and PI3K Pathways. *Int. J. Mol. Med.* 35 (5), 1355–1361. doi:10.3892/ijmm.2015.2139

Jung, S., Je, Y., Giovannucci, E. L., Rosner, B., Ogino, S., and Cho, E. (2015). Derivation and Validation of Homocysteine Score in u.S. Men and Women. *J. Nutr.* 145 (1), 96–104. doi:10.3945/jn.114.192716

Kim, J., Kim, H., Roh, H., and Kwon, Y. (2018). Causes of Hyperhomocysteinemia and its Pathological Significance. *Arch. Pharm. Res.* 41 (4), 372–383. doi:10.1007/s12272-018-1016-4

Kokkinidis, D. G., Waldo, S. W., and Armstrong, E. J. (2017). Treatment of Coronary Artery In-Stent Restenosis. *Expert Rev. Cardiovasc. Ther.* 15 (3), 191–202. doi:10.1080/14779072.2017.1284588

Kubota, Y., Alonso, A., and Heckbert, S. R. (2019). *Homocysteine and Incident Atrial Fibrillation: The Atherosclerosis Risk in Communities Study and the Multi-Ethnic Study of Atherosclerosis. Heart Lung Circ.* 28 (4), 615–622. doi:10.1016/j.hlc.2018.03.007

Kugler, E., Cohen, E., Goldberg, E., Nardi, Y., Levi, A., Krause, I., et al. (2015). C Reactive Protein and Long-Term Risk for Chronic Kidney Disease: A Historical Prospective Study. *J. Nephrol.* 28 (3), 321–327. doi:10.1007/s40620-014-0116-6

Kumar, A., Palfrey, H. A., Pathak, R., Kadowitz, P. J., Gettys, T. W., and Murthy, S. N. (2017). The Metabolism and Significance of Homocysteine in Nutrition and Health. *Nutr. Metab. (Lond)* 14, 78. doi:10.1186/s12986-017-0233-z

Nagele, P., Meissner, K., Francis, A., Födinger, M., and Saccone, N. L. (2011). Genetic and Environmental Determinants of Plasma Total Homocysteine Levels: Impact of Population-wide Folate Fortification. *Pharmacogenet Genomics* 21 (7), 426–431. doi:10.1097/FPC.0b013e32834741ff

Naik, S., Joglekar, C., Bhat, D., Lubree, H., Rege, S., Raut, K., et al. (2011). Marked Gender Difference in Plasma Total Homocysteine Concentrations in Indian Adults with Low Vitamin B_{12}. *Int. J. Vitam Nutr. Res.* 81 (5), 306–316. doi:10.1024/0300-9831/a000078

Nilsson, T. K., Böttiger, A. K., Henríquez, P., and Serra Majem, L. (2014). MTHFR Polymorphisms and Serum Cobalamin Affect Plasma Homocysteine Concentrations Differentially in Females and Males. *Mol. Med. Rep.* 10 (5), 2706–2712. doi:10.3892/mmr.2014.2521

Giulio, G. S., and David, R. H. (2013). Drug-eluting Coronary-Artery Stents. *New Engl. J. Med.* 368 (3), 254–65. doi:10.1056/NEJMra1210816

Nygrd, O., Vollset, S., and Refsum, H. (1995). Total Plasma Homocysteine and Cardiovascular Risk Profile. The Hordaland Homocysteine Study[J]. *JAMA* 274 (19), 1526. doi:10.1001/jama.1995.03530190040032

Ortolani, P., Marzocchi, A., Marrozzini, C., Palmerini, T., Aquilina, M., Corlianò, L., et al. (2004). Clinical Relevance of Homocysteine Levels in Patients Receiving Coronary Stenting for Unstable Angina. *Ital. Heart J.* 5 (3), 189

Otsuka, F., Finn, A. V., Yazdani, S. K., Nakano, M., Kolodgie, F. D., and Virmani, R. (2012). The Importance of the Endothelium in Atherothrombosis and Coronary Stenting. *Nat. Rev. Cardiol.* 9 (8), 439–453. doi:10.1038/nrcardio.2012.64

Paudel, B., Xuan, G. J., and Chun, Z. F. (2005). Analysis of Clinical Factors Affecting the Restenosis Following Percutaneous Coronary Intervention. *Nepal Med. Coll. J.* 7 (2), 101.

Philip, F. (2015). Duration of Triple Therapy in Patients Requiring Oral Anticoagulation after Drug-Eluting Stent Implantation. *J. Am. Coll. Cardiol.* 66 (9), 1088–1089. doi:10.1016/j.jacc.2015.05.077

Schnyder, G., Roffi, M., Flammer, Y., Pin, R., and Hess, O. M. (2002). Association of Plasma Homocysteine with Restenosis after Percutaneous Coronary Angioplasty. *Eur. Heart J.* 23 (9), 726–733. doi:10.1053/euhj.2001.2962

Schnyder, G., Roffi, M., Pin, R., Flammer, Y., Lange, H., Eberli, F. R., et al. (2001). Decreased Rate of Coronary Restenosis after Lowering of Plasma Homocysteine Levels. *N. Engl. J. Med.* 345 (22), 1593–1600. doi:10.1056/NEJMoa011364

Spence, J. D. (2006). Nutrition and Stroke Prevention. *Stroke. Stroke A. J. Cereb. Circ.* 37, 2430–2435. doi:10.1161/01.str.0000199621.28234.e2

Stangl, K., Cascorbi, I., Stangl, V., Laule, M., Dschietzig, T., Richter, C., et al. (2000). Hyperhomocysteinaemia and Adverse Events Complicating Coronary Catheter Interventions. *Int. J. Cardiol.* 76 (2–3), 211–217. doi:10.1016/s0167-5273(00)00380-6

Tian, R., Shu-Zheng, L. V., and Liu, H. (2013). Clinical Follow up Observation of Drug Eluting Stent and Bare Metal Stent for Coronary Heart Disease. *Chin. J. Difficult Complicated Cases* 12 (002), 90. doi:10.3969/j.issn.1671-6450.2013.02.003

Vidale, S., Bellocchi, S., and Caronno, R. (2017). The Association between Homocysteine and Carotid Restenosis after Endarterectomy: A Meta-Analysis. *Jul Eu.n .l Neuro.y* 24 (5), 366

Wong, C. K., Hammett, C. J., The, R., French, J. K., Gao, W., Webber, B. J., et al. (2004). Lack of Association between Baseline Plasma Homocysteine Concentrations and Restenosis Rates after a First Elective Percutaneous Coronary Intervention without Stenting. *Heart* 90 (11), 1299–1302. doi:10.1136/hrt.2003.020701

Zairis, M. N., Ambrose, J. A., Manousakis, S. J., Stefanidis, A. S., Papadaki, O. A., Bilianou, H. I., et al. (2002). The Impact of Plasma Levels of C-Reactive Protein, Lipoprotein (A) and Homocysteine on the Long-Term Prognosis after Successful Coronary Stenting: The Global Evaluation of New Events and Restenosis after Stent Implantation Study. *J. Am. Coll. Cardiol.* 40 (8), 1375–1382. doi:10.1016/s0735-1097(02)02267-2

Zeng, X. K., Guan, Y. F., Remick, D. G., and Wang, X. (2010). Signal Pathways Underlying Homocysteine-Induced Production of MCP-1 and IL-8 in Cultured Human Whole Blood. *Acta Pharmacol. Sin* 26 (1), 85–91. doi:10.1111/j.1745-7254.2005.00005.x

Zhang, Z., Xiao, S., Yang, C., Ye, R., Hu, X., and Chen, X. (2019). Association of Elevated Plasma Homocysteine Level with Restenosis and Clinical Outcomes after Percutaneous Coronary Interventions: a Systemic Review and Meta-Analysis. *Cardiovasc. Drugs Ther.* 33 (4), 353–361. doi:10.1007/s10557-019-06866-0

Conflict of Interest: The authors declare that the research was conducted in the absence of any commercial or financial relationships that could be construed as a potential conflict of interest.

Publisher's Note: All claims expressed in this article are solely those of the authors and do not necessarily represent those of their affiliated organizations, or those of the publisher, the editors, and the reviewers. Any product that may be evaluated in this article, or claim that may be made by its manufacturer, is not guaranteed or endorsed by the publisher.

frontiers | Frontiers in Pharmacology

ORIGINAL RESEARCH
published: 12 July 2022
doi: 10.3389/fphar.2022.861319

Theaflavin-3,3′-Digallate from Black Tea Inhibits Neointima Formation Through Suppression of the PDGFRβ Pathway in Vascular Smooth Muscle Cells

Yichen Wu[1,2†], *Min Chen*[1,3,4†], *Zilong Chen*[1,2], *Jiangcheng Shu*[1,2], *Luoying Zhang*[5], *Jiong Hu*[6], *Hongjun Yu*[7], *Kai Huang*[1,3,2,4*] *and Minglu Liang*[1,3,4*]

[1]*Clinic Center of Human Gene Research, Union Hospital, Tongji Medical College, Huazhong University of Science and Technology, Wuhan, China,* [2]*Department of Cardiology, Union Hospital, Tongji Medical College, Huazhong University of Science and Technology, Wuhan, China,* [3]*Hubei Key Laboratory of Metabolic Abnormalities and Vascular Aging, Huazhong University of Science and Technology, Wuhan, China,* [4]*Hubei Clinical Research Center of Metabolic and Cardiovascular Disease, Wuhan, China,* [5]*Key Laboratory of Molecular Biophysics of the Ministry of Education, College of Life Science and Technology, Huazhong University of Science and Technology, Wuhan, China,* [6]*Department of Histology and Embryology School of Basic Medicine, Tongji Medical College Huazhong University of Science and Technology, Wuhan, China,* [7]*Department of Biochemistry and Molecular Biology, School of Basic Medicine and Tongji Medical College, Huazhong University of Science and Technology, Wuhan, China*

OPEN ACCESS

Edited by:
Qilong Wang,
Tianjin University of Traditional Chinese Medicine, China

Reviewed by:
Xiaoyan Dai,
Guangzhou Medical University, China
Quanwei He,
Huazhong University of Science and Technology, China

***Correspondence:**
Kai Huang
Huangkai1@hust.edu.cn
Minglu Liang
liangml@hust.edu.cn

†These authors have contributed equally to this work and share the first authorship

Specialty section:
This article was submitted to Cardiovascular and Smooth Muscle Pharmacology, a section of the journal Frontiers in Pharmacology

Received: *24 January 2022*
Accepted: *02 June 2022*
Published: *12 July 2022*

Citation:
Wu Y, Chen M, Chen Z, Shu J, Zhang L, Hu J, Yu H, Huang K and Liang M (2022) Theaflavin-3,3′-Digallate from Black Tea Inhibits Neointima Formation Through Suppression of the PDGFRβ Pathway in Vascular Smooth Muscle Cells. Front. Pharmacol. 13:861319. doi: 10.3389/fphar.2022.861319

The abnormal neointima formation caused by the phenotypic switching of vascular smooth cells (VSMCs) into a synthetic state plays a key role in the pathogenesis of various vascular diseases, including atherosclerosis and postangioplasty restenosis. Theaflavin-3,3′-digallate (TF3) in black tea has been reported to exert antiinflammatory and anticancer effects, but its role in neointima formation remains unclear. Here, we delineated a remarkable effect of TF3 in suppressing neointima formation of VSMCs *in vivo* as well as the ability of primary rat aortic smooth cells (RASMCs) to proliferate and migrate *in vitro*. Further study confirmed that the effects of TF3 on PDGF-BB–induced RASMCs were due to reduced phosphorylation of PDGFRβ, which led to the repression of downstream pathways. We concluded that TF3 may act as a repressor in the progression of neointima formation and serve as a potential therapeutic candidate for excessive phenotypic switching of VSMCs.

Keywords: vascular smooth muscle cells, neointima formation, phenotypic switching, TF3, PDGFRβ signaling pathway

INTRODUCTION

Arteriosclerotic cardiovascular diseases (ASCVD), such as atherosclerosis, coronary heart disease, and postangioplasty restenosis (RS), are the main causes of mortality worldwide (Mortensen and Nordestgaard, 2018). Vascular remodeling resulting in an aberrant phenotype of medial smooth muscle cells is pervasively accepted as the primary pathological basis of ASCVD (Beach et al., 2013). In contrast to other mature cells, such as endothelial cells and fibroblasts, medial smooth muscle cells, which enable blood vessels to maintain structural and functional homeostasis under normal conditions, exhibit extensive plasticity to switch from a quiescent contractile phenotype to an

active synthetic phenotype (Chistiakov et al., 2015). This aberrant transition in VSMC phenotype dramatically accelerates the pathogenesis of ASCVD (Chappell et al., 2016; Augstein et al., 2018), especially when induced by various pathogenic stimuli and stress signals, including vascular injury and mechanical force (Owens et al., 2004; Davis-Dusenbery et al., 2011; Heusch et al., 2014). For example, during the progression of postangioplasty restenosis (RS), injury-induced synthetic VSMCs express elevated proliferative factors and decreased contractile markers (Rensen et al., 2007; Frismantiene et al., 2018), migrate from the primary media to the intima, and secrete a large amount of extracellular matrix, leading to pathological thickening and vascular restenosis, which severely damage vessel functions.

The PDGFs are a number of cytokines belonging to the cystine knot protein superfamily. They exist as homo or heterodimers combined by four different monomers, namely, PDGF-A, PDGF-B, PDGF-C, and PDGF-D, and function as classical regulators of cell growth and cell division (Boor et al., 2014). PDGF-BB has been verified for its contribution to the formation of neointima after vascular injury (Raines, 2004; Tallquist and Kazlauskas, 2004; Shawky and Segar, 2017), and has become one of the most commonly used factors to induce fibroblast and VSMC proliferation and migration. Here, we used it to induce the synthetic phenotype of VSMCs *in vitro*.

Black tea, a fermented tea, provides multiple health benefits, such as refreshing effects and antiaging activity (Yang and Landau, 2000). The fermentation process of black tea results in the formation of theaflavins, comprising a mixture of theaflavin (TF1), theaflavin-3-gallate (TF2a), theaflavin-3′-gallate (TF2b), and theaflavin-3,3′-digallate (TF3), which is regarded as the most beneficial component of black tea (Liang et al., 1999). Previous studies have shown that theaflavins, especially TF3, can block nitric oxide synthase by downregulating NF-κB activation in macrophages (Lin et al., 1999). TF3 was recently reported to inhibit osteoclast formation and prevent ovariectomy-induced bone loss via suppression of the ERK pathway (Hu et al., 2017). Moreover, studies concerning the beneficial antioxidant, antiangiogenic, and antitumor effects of TF3 have also been published (Lin et al., 2000; Leung et al., 2001; Lee et al., 2004; Cai et al., 2007; Gao et al., 2016). However, whether TF3 can regulate the phenotypic switching of VSMCs remains unknown. Here, we elucidated the effect of TF3 on the regulation of injury and PDGF-BB–induced VSMC phenotypic switching and the underlying mechanisms.

MATERIALS AND METHODS

Animals

C57BL/6 mice (8-weeks old) and male Sprague Dawley rats (170 g) were used in our experiments. The animals were housed on a 12:12-h light–dark cycle in a temperature-controlled and humidity-controlled room with free access to standard chow and tap water. All animal studies were approved by the Institutional Animal Care and Use Committee of Huazhong University of Science and Technology.

Animal Experiments

The anesthetized C57BL/6 mice ($n \geq 6$ for each group) were supine with their necks fully exposed and hair removed. First, the common carotid artery, the external carotid artery, and the internal carotid artery were carefully separated, and then the blood flow in a unilateral carotid artery was completely blocked using a ligature near the distal bifurcation. The same separation was performed for the carotid vessels on the other side as a sham operation. The mice were randomly injected intraperitoneally with normal saline (vehicle) or TF3 (10 mg/kg) the day before the operation and once every other day after ligation. Then, 14 and 28 days later, tissue sections were taken from the proximal end of the suture junction for histological tests.

Histomorphometry

Tissue sections were fixed in 4% paraformaldehyde (PFA) and embedded in paraffin by Bios Biological Company. Serial 5-mm-thick transverse sections were stained in batches with hematoxylin and eosin and Masson to better differentiate intimal hyperplasia. Digital photographs were taken using an inverted microscope (OLYMPUS IX73). ImageJ software was used for morphometric analyses.

Immunofluorescence

Slides of different sections were dewaxed in xylene, boiled for 10 min in citrate buffer for antigen retrieval, and exposed to blocking solution (5% goat serum in phosphate-buffered saline [PBS]) for 1 h at room temperature. PCNA (CST, #2586, 1: 100 dilutions), MMP9 (Abcam, ab38898, 1:100 dilutions), α-SMA (Proteintech, 67735-1-lg, 1:100 dilutions), p-AKT (CST, #9231, 1: 100 dilutions), and p-ERK1/2 (Abclonal, AP0974, 1: 100 dilutions) were diluted in blocking solution and applied to the slides overnight at 4°C in a humidified chamber. The next day, slides were incubated with appropriate Alexa Fluor 488-, Alexa Fluor 555-conjugated secondary antibodies diluted 1:500 in blocking solution for 1 h at room temperature. DAPI (Servicebio, G1012) was then mounted on slides for 15 min. All immunofluorescence micrographs were taken using a confocal microscope (Nikon).

The cells were fixed in 4% PFA for 15 min at room temperature after reaching confluence, immunostained with α-SMA (Proteintech, 67735-1-lg, 1:100 dilutions) and SM22 (proteintech 10493-1-AP, 1:100 dilutions) antibodies overnight at 4°C, and then incubated with the indicated secondary antibodies for 1 h at 37°C. Nuclei were stained with DAPI for 20 min at 37°C. Photos were taken under a fluorescence microscope (Olympus).

Cell Culture

For primary RASMC culture, the aorta of normal male rats was digested using collagenase II (Worthington) at a concentration of 2 mg/ml for 10 min, and then the adventitia was carefully stripped using microscopic tweezers. Endothelial cells were gently wiped off with a cotton swab. After overnight culture at 37°C in a 5%

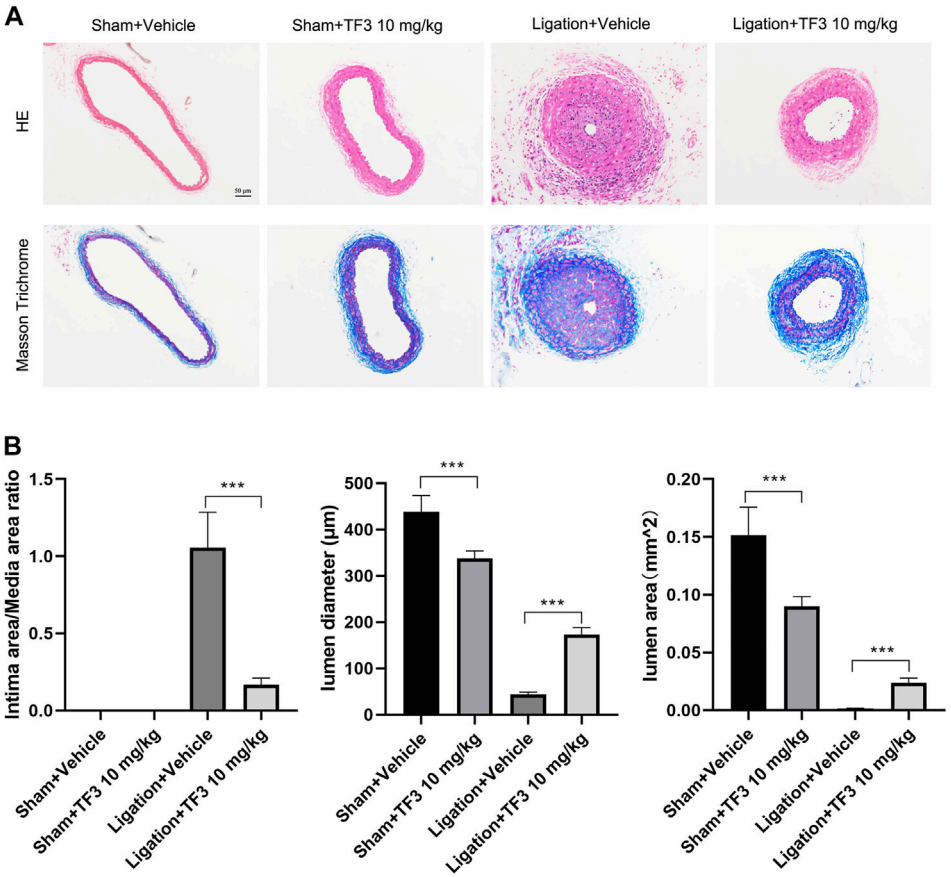

FIGURE 1 | Effect of theaflavin-3,3′-digallate (TF3) on carotid artery ligation–induced neointimal hyperplasia. **(A)** TF3 (10 mg/kg) or vehicle was intraperitoneally injected after carotid artery ligation. Mice were sacrificed 14 days after the surgery. Hematoxylin and eosin-stained and Masson trichrome-stained sections of all groups are shown. Scale bar, 50 μm. **(B)** Quantification of the ratio of intima to media (I/M ratio), lumen diameter, and lumen area. The data are presented as the mean ± SEM (n = 7). ***$p < 0.001$.

CO_2 incubator in Dulbecco's Modified Eagle Medium (DMEM) containing 10% FBS (Gibco), the remaining aorta was cut into pieces using microscissors and digested using collagenase II at 3 mg/ml for 30 min. Then, elastase (1 mg/ml, Worthington) was added for another 60 min. RASMCs were centrifuged, resuspended, and cultured in DMEM containing 10% FBS at 37°C in a 5% CO_2 incubator. Primary mouse smooth muscle cells (mSMCs) were isolated in the same way. Then, 0.2 mg/ml collagenase II was used to remove the adventitia. After overnight culture, 1.0 mg/ml collagenase II and 0.1 mg/ml elastase were used for further digestion. All SMCs used for experiments were between the third and fifth passages.

CCK-8 Assay

To estimate cell proliferation, RASMCs were seeded onto 96-well plates (5,000/well) and cultured in DMEM containing 10% FBS to near confluence. RASMCs were then cultured with FBS-free DMEM for 24 h and treated with PBS as a control or 20 ng/ml PDGF-BB (GenScript, Z03179) with or without adding different concentrations of TF3 (1, 10, and 20 μM) 1 h before exposure. The cells were incubated using CCK-8 for 2 h, and the absorbance at 450 nm was detected using a microplate reader (Multiskan FC, Thermo Fisher Scientific, Rockford, IL, United States).

Western Blotting

RASMCs cultured in 6-well plates were starved in FBS-free DMEM for 24 h after nearly reaching confluence. The cells were pretreated with vehicle or different concentrations of TF3 1 h before stimulation. Total protein was extracted from the cells after 48 h, and the protein concentration was determined with a Pierce™ BCA protein assay kit (Thermo Scientific™, 23227), according to the manufacturer's instructions. Then, western blot was conducted with primary antibodies against MYH11(Proteintech, 18569-1-AP, 1:1000 dilutions), α-SMA (Proteintech, 67735-1-lg, 1:1000 dilutions), SM22 (Proteintech, 10493-1-AP, 1:1000 dilutions), PCNA (CST, #2586, 1:1000 dilutions), cyclin E (CST, #20808, 1:1000 dilutions), CDK1 (Proteintech, 19532-1-AP, 1:1000 dilutions), CDK2 (Proteintech, 10122-1-AP, 1:1000 dilutions), CDK4 (Proteintech, 11026-1-AP, 1:1000 dilutions), MMP2 (Proteintech, 10373-2-AP, 1:1000 dilutions), MMP9 (Abcam,

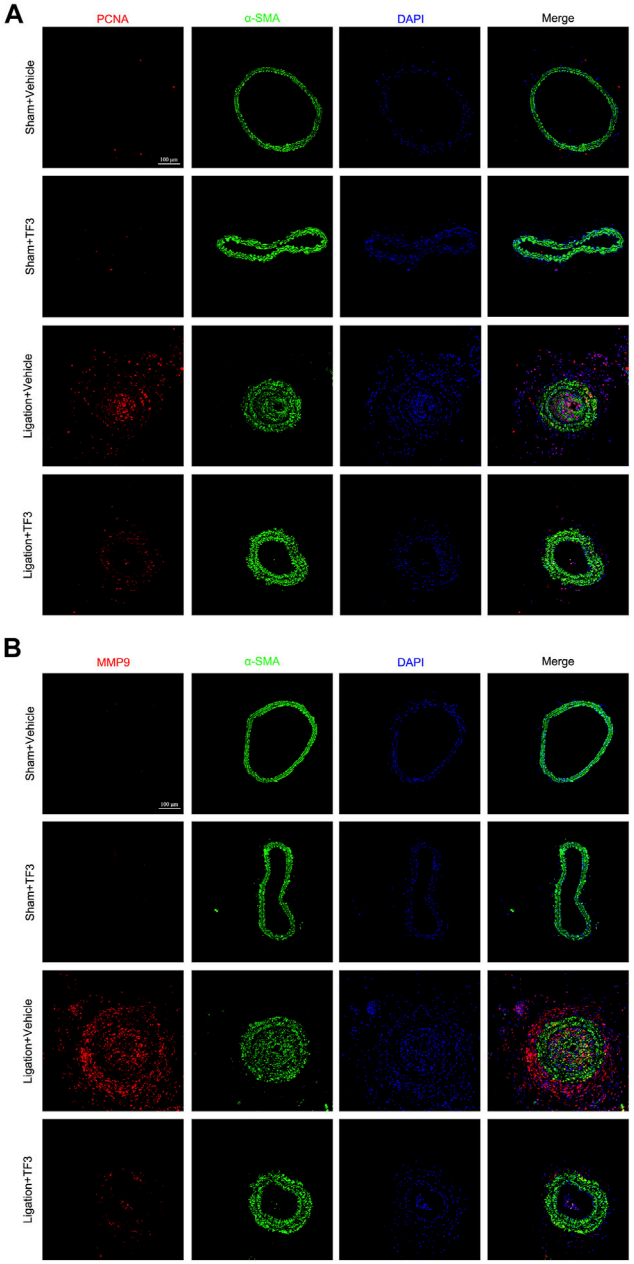

FIGURE 2 | Effect of theaflavin-3,3′-digallate (TF3) on carotid artery ligation–induced neointimal hyperplasia. TF3 (10 mg/kg) or vehicle was intraperitoneally injected after carotid artery ligation. **(A)** Immunofluorescence staining of PCNA (red), α-SMA (green), and DAPI (blue) are shown. **(B)** Immunofluorescence staining of MMP9 (red), α-SMA (green), and DAPI (blue) are shown. Scale bar, 100 μm.

ab38898, 1:1000 dilutions), α-tubulin (Proteintech, 11224-1-AP, 1:1000 dilutions), GAPDH (Proteintech, 60004-1-lg, 1:1000 dilutions), p-ERK1/2 (CST, #5726, 1:1000 dilutions), p-JNK (CST, #4668, 1:1000 dilutions), p-p38 (CST, #9216, 1:1000 dilutions), ERK1/2 (ABclonal, A4782, 1:1000 dilutions), JNK (CST, #9252, 1:1000 dilutions), p38 (Proteintech, 14064-1-AP, 1:1000 dilutions), p-mTOR (CST, #5536, 1:1000 dilutions), mTOR (Bimake, A5866, 1:1000 dilutions), p-Akt (CST, #9271, 1:1000 dilutions), Akt (CST, #4691, 1:1000 dilutions), p-PDGF receptor beta (CST, #3161, 1:1000 dilutions), PDGF receptor beta (Bimake, A5541, 1:1000 dilutions), p-PLCγ1 (CST, #2821, 1:1000 dilutions), PLCγ1 (CST, #5690, 1:1000 dilutions), p-Src (CST, #6943, 1:1000 dilutions), and Src (CST, #2109, 1:1000 dilutions) at 4°C overnight. The blots were then incubated with secondary antibodies and visualized using ECL. ImageJ software was used for gray value analyses.

EdU Assay

RASMCs were seeded onto 96-well plates (5,000/well) and cultured in DMEM containing 10% FBS until almost confluent. After starvation for 24 h, the cells were pretreated with vehicle or different concentrations of TF3 1 h before stimulation. Then, 48 h later, an EdU assay was performed following the standard protocol of the Cell-Light™ EdU Apollo®567 *in vitro* imaging kit (RiboBio, C10310-1). Photographs were taken using an inverted microscope (OLYMPUS IX73). ImageJ software was used for cell counting analyses.

Wound Healing Migration Assay

RASMCs were seeded onto 6-well plates and grown to confluence. A straight line was scratched into the cells with a 200-μl pipette tip. The cells were pretreated with vehicle or different concentrations of TF3 1 h before stimulation. Then, they were allowed to migrate, and photographs from the same viewpoint were taken when the wound was made and 48 h later using an inverted microscope (OLYMPUS IX73). ImageJ software was used for wound area measurements.

Transwell Assay

Flamed forceps were used to place the upper transwell chamber into a regular 24-well plate. Then, 100 μl of serum-free medium was added, and the chamber was placed back into the incubator for >1 h. Starved RASMCs were pretreated with vehicle or different concentrations of TF3 1 h before stimulation. The cells were incubated for 24 h, trypsinized, and resuspended in serum-free media so that 2×10^5 cells were cultured in 100 μl of medium. Then, 500 μl of fully supplemented medium (containing 10% FBS) was added to the lower chamber. Flamed forceps were used to transfer the upper chambers above the lower chamber. Care was taken to avoid trapping air bubbles below the surface of the membrane. The cell suspension was immediately added to each of the upper chambers followed by incubation for another 24 h. Then, the medium was aspirated from the upper chamber, and the inserts were transferred into another well containing PBS for washing. The inside of the upper chamber was scraped with a cotton swab to remove the cells from the inside of the well. Cells on the underside of the insert were stained by placing the insert into crystal violet solution for 15 min, and photos were taken using an inverted microscope (OLYMPUS IX73). ImageJ software was used for cell counting analyses.

Statistical Analysis

The data are expressed as the mean ± SEM values. The Shapiro–Wilk tests and two-tailed unpaired students' tests were used to determine significance of differences between two groups. Statistical significance was indicated by p values < 0.05.

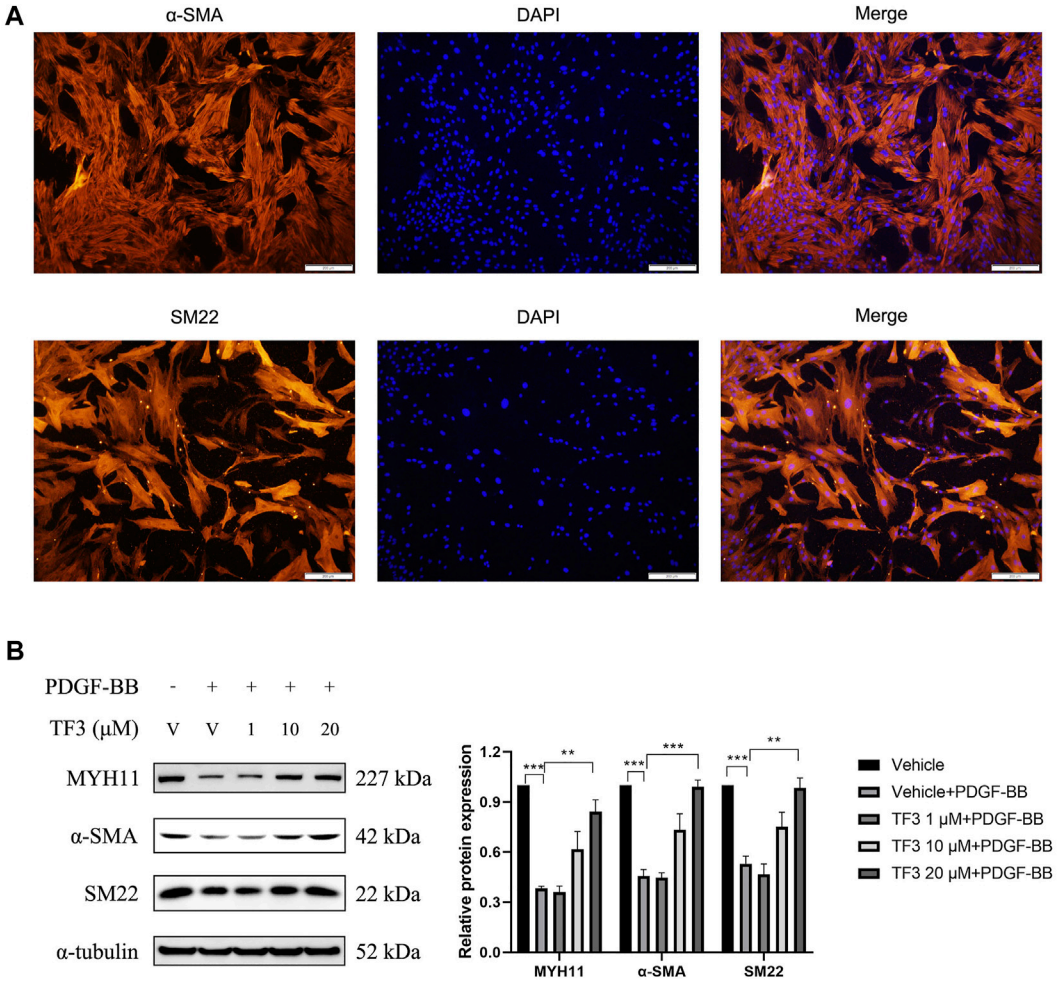

FIGURE 3 | Effects of theaflavin-3,3′-digallate (TF3) on PDGF-BB–induced phenotypic switching in RASMCs. **(A)** RASMCs were stained with α-SMA (red) and DAPI (blue). Scale bar, 200 μm **(B)** The serum-starved RASMCs were pretreated with 1, 10, or 20-μM TF3 for 1 h, and then, the cells were stimulated with 20 ng/ml PDGF-BB for 48 h. The levels of contractile proteins MYH11, α-SMA, and SM22 were detected using western blot. Each experiment was performed in triplicate. $^{**}p < 0.01$, $^{***}p < 0.001$.

RESULTS

TF3 Attenuates Carotid Artery Ligation–Induced Neointimal Hyperplasia

To assess the effect of TF3 on neointimal hyperplasia after vascular injury, we used the carotid artery ligation (CAL) model, which gave rise to the progression of vascular restenosis. TF3 (10 mg/kg) or vehicle was intraperitoneally injected one day before CAL and repeated every other day. Compared with the vehicle-treated sham surgery group, the vehicle-treated ligation surgery group showed well-developed neointimal hyperplasia after 14 days. The sections stained with HE and Masson trichrome solutions were used to highlight the media (**Figure 1A**). Compared with the vehicle-treated ligation surgery group, the TF3-treated ligation surgery group showed a prominently reduced ratio of intima to media (I/M ratio) with apparently larger lumen diameter and lumen area (**Figure 1B**). There was also a significant difference between the two sham surgery groups of vehicle- and TF3-treated mice in lumen sizes due to their different levels of compensatory dilatation. Immunofluorescence staining showed that the TF3-treated ligation surgery group had sharply declined PCNA and MMP9 expression compared to vehicle-treated surgery group (**Figure 2**). HE and Masson staining were also performed 28 days after surgery (**Supplementary Figure S1**) as well as immunofluorescence assay (**Supplementary Figure S2**). These results indicate that TF3 significantly attenuates neointimal hyperplasia induced by CAL.

TF3 Attenuates PDGF-BB–Induced Phenotypic Switching in RASMCs

Phenotypic switching of VSMCs is a main character of vascular restenosis after PCI. First, immunofluorescence staining of α-

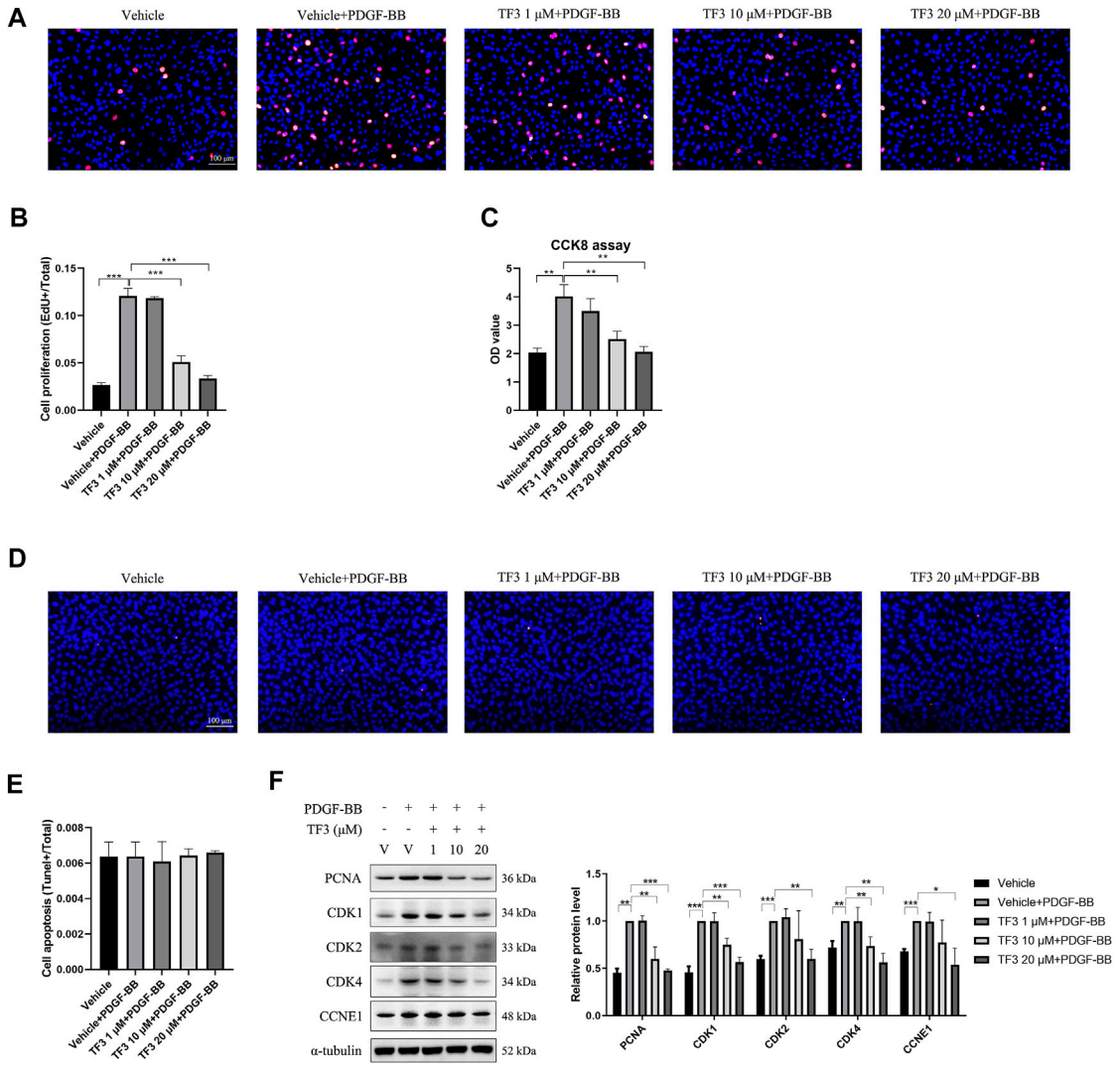

FIGURE 4 | Effects of theaflavin-3,3′-digallate (TF3) on PDGF-BB–induced proliferation in rat aortic smooth cells (RASMCs). Serum-starved RASMCs were pretreated with 1-, 10-, or 20-μM TF3 for 1 h and then stimulated with 20 ng/ml PDGF-BB for 48 h. **(A)** An EdU assay was performed to evaluate the proliferation of RASMCs. **(B)** Statistical data of the EdU assay are shown. **(C)** The effect of TF3 on PDGF-BB–induced proliferation of RASMCs was also measured using CCK-8 assay. **(D)** The effect of TF3 on PDGF-BB–induced apoptosis of RASMCs was measured using terminal deoxynucleotidyl transferase dUTP nick-end labeling (TUNEL) assay. **(E)** Statistical data from the TUNEL assay are shown. **(F)** The levels of the cell proliferation-associated proteins PCNA, CDK1, CDK2, CDK4, and CCNE1 were detected by western blotting. The western blot data are shown. Each experiment was performed in triplicate. Scale bar, 100 μm, $^{*}p < 0.05$, $^{**}p < 0.01$, $^{***}p < 0.001$.

SMA and SM22 was used to identify the phenotype of the RASMCs, as shown in **Figure 3A**, and then, to evaluate the cytotoxicity of TF3 for RASMCs, MTT assay was conducted to test the cell viability. As shown in **Supplementary Figure S3**, TF3 was nontoxic for RASMCs at concentrations of at least 80 μM. Therefore, we selected the safety concentrations of 1, 10, and 20 μM for further experiments. Western blot was conducted to investigate whether TF3 is able to reverse PDGF-BB–induced phenotypic switching in RASMCs. The results showed that the protein expressions of MYH11, α-SMA, and SM22, which were recognized to be the contractile markers of VSMCs, were reduced after PDGF-BB (20 ng/ml) stimulation, and pretreatment of 1, 10, and 20 μM TF3 could reverse this phenomenon in a concentration-dependent manner (**Figure 3B**).

TF3 Inhibits PDGF-BB–Induced RASMC Proliferation

One of the features of neointimal hyperplasia is the abnormal proliferation and migration of VSMCs toward the intima layer. Therefore, we tested the antiproliferative effect of TF3 on PDGF-BB-stimulated RASMCs. EdU assay showed that the proliferation rate of RASMCs was increased after stimulation with PDGF-BB (20 ng/ml) for 48 h compared with the nontreated control, and pretreatment

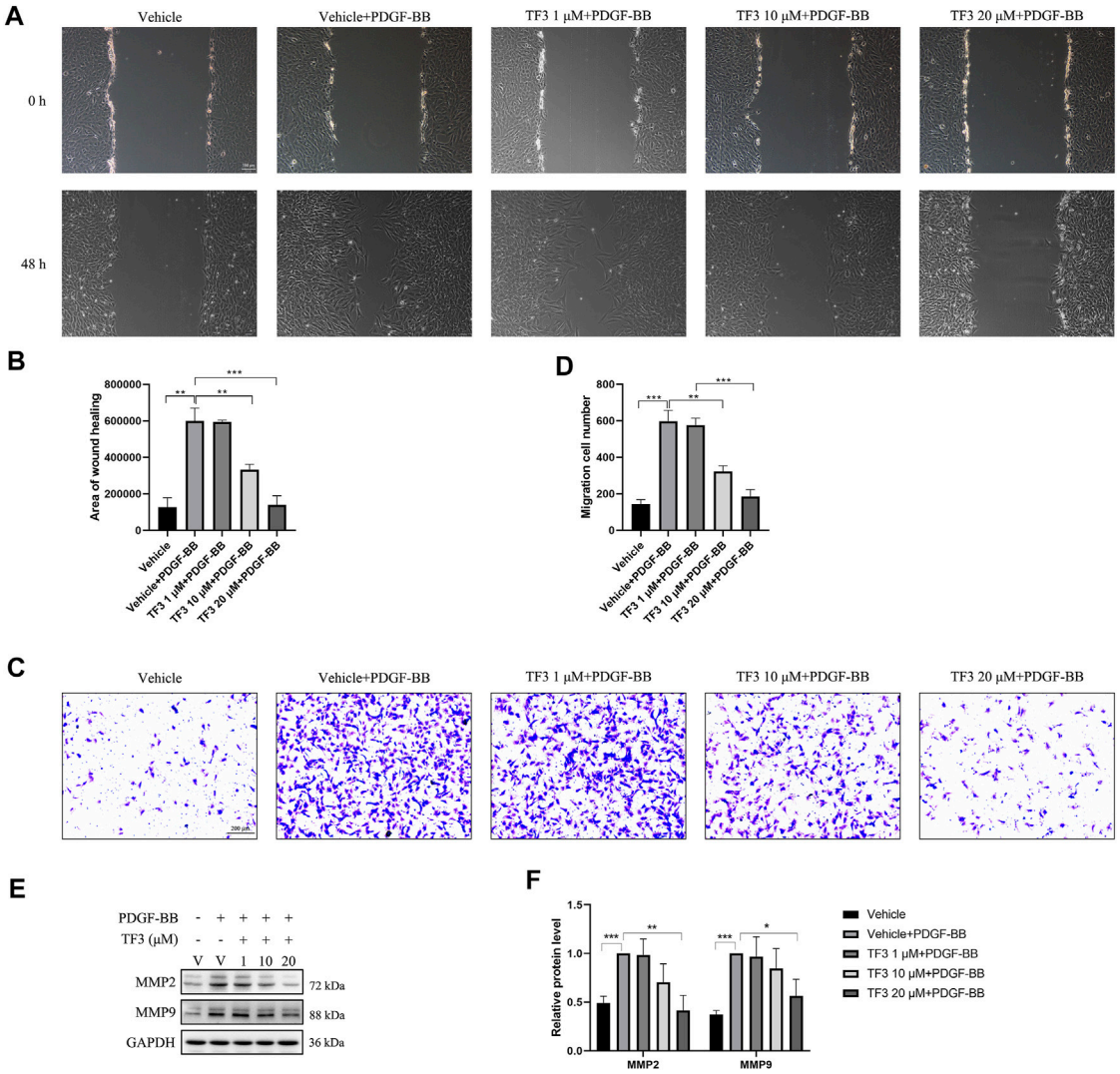

FIGURE 5 | Effects of theaflavin-3,3′-digallate (TF3) on PDGF-BB–induced migration in rat aortic smooth cells (RASMCs). Serum-starved RASMCs were pretreated with 1-, 10-, or 20-μM TF3 for 1 h and then stimulated with 20 ng/ml PDGF-BB for 48 h. **(A)** The wound healing migration assay was performed as indicated. Scale bar, 100 μm **(B)** The statistical data of the wound healing assay are shown. **(C)** The transwell assay was performed as indicated. Scale bar, 200 μm **(D)** The statistical data of the transwell assay are shown. **(E)** The levels of the cell migration-associated proteins MMP2 and MMP9 were detected by western blot. **(F)** The statistical data of the western blot analysis are shown. Each experiment was performed in triplicate. *$p < 0.05$, **$p < 0.01$, ***$p < 0.001$.

with TF3 suppressed this phenomenon in a concentration-dependent manner (**Figures 4A,B**). A CCK-8 assay was performed to further confirm this antiproliferative effect, in which the cells pretreated with TF3 showed much less proliferative capacity than the PDGF-BB stimulation group (**Figure 4C**). The terminal deoxynucleotidyl transferase dUTP nick-end labeling (TUNEL) assay showed that PDGF-BB and TF3 had no effect on cell apoptosis (**Figures 4D,E**). The results of western blot provided more evidence that the expressions of PCNA, CDK1, CDK2, CDK4, and CCNE1 were increased after stimulation with PDGF-BB, and pretreatment with TF3 suppressed them in a concentration-dependent manner (**Figure 4F**).

TF3 Inhibits PDGF-BB–Induced RASMC Migration

To evaluate the effect of TF3 on PDGF-BB–induced RASMC migration, we performed a wound healing migration assay. As shown in **Figures 5A,B**, the cells migrated to near confluence after 48 h of PDGF-BB stimulation, and pretreatment with TF3 inhibited PDGF-BB–induced migration in a concentration-dependent manner compared with the PDGF-BB stimulation group. As expected, the transwell assay and western blot analysis showed consistent results to further prove that TF3 prevents RASMC migration under PDGF-BB induction (**Figures 5C–F**).

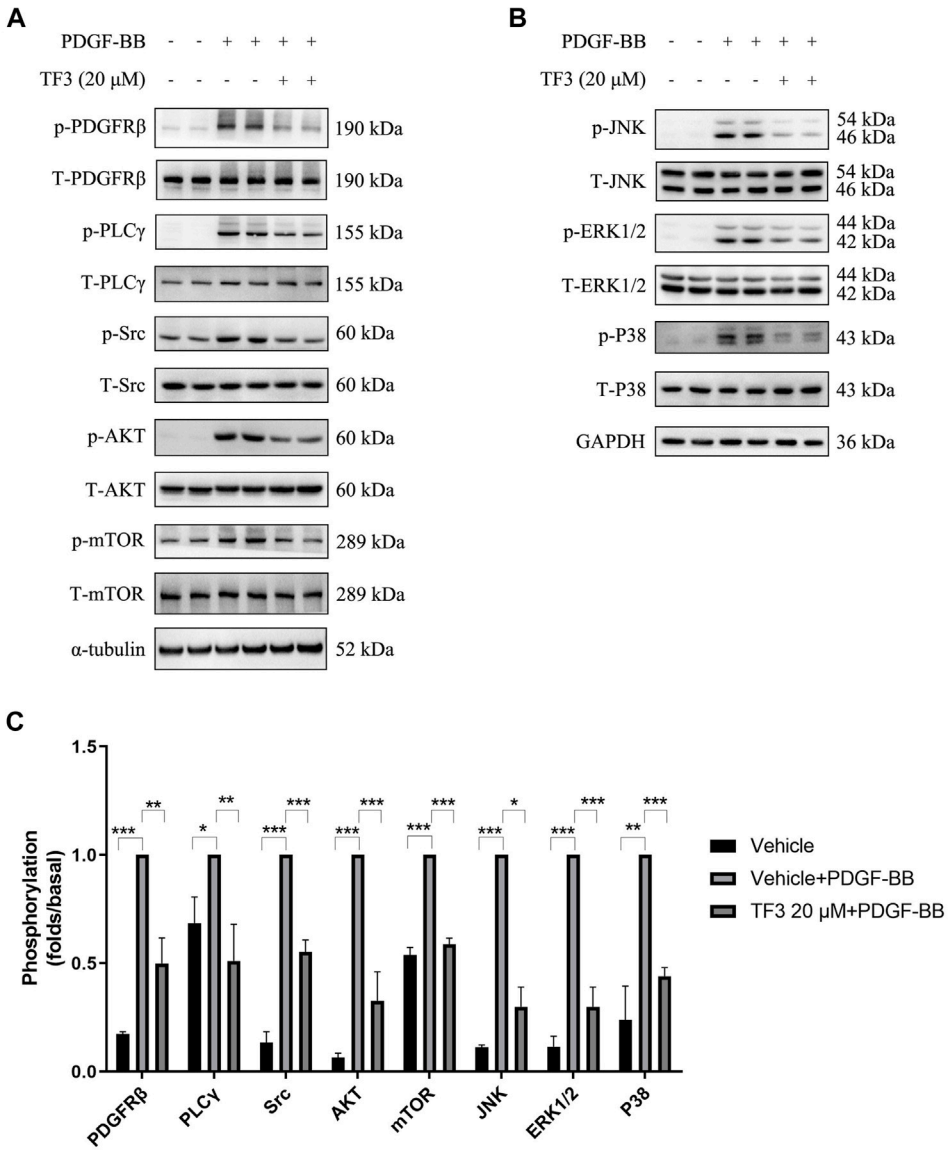

FIGURE 6 | Theaflavin-3,3′-digallate (TF3) suppresses the activation of PDGFRβ and its downstream pathways in PDGF-BB–induced rat aortic smooth cells (RASMCs). The cells were serum-starved for 24 h and then stimulated with PDGF-BB (20 ng/ml) with or without pretreatment with 20 μM TF3. Cell extract was harvested after 10 min of stimulation. **(A,B)** Western blotting was performed using antibodies against the classical PDGFRβ and MAPK signaling pathways. **(C)** The statistical data of the western blot are shown. Each experiment was performed in triplicate. $^{*}p < 0.05$, $^{**}p < 0.01$, $^{***}p < 0.001$.

TF3 Suppresses the Activation of PDGFRβ and Its Downstream Pathways in PDGF-BB–Induced RASMCs

PDGF-BB can bind to both PDGFRα and PDGFRβ on the surface of the cell membrane. Since the expression of β-receptors is approximately 10-fold higher than that of α-receptors (Bornfeldt et al., 1995), we tested whether TF3 targets PDGFRβ and its downstream pathways. Upon stimulation of the receptor, a series of tyrosine residues in the receptor subunits were phosphorylated. Next, ligands, such as phospholipase C-gamma 1 (PLC-γ1) and the Src family, bound with the receptor through specific phosphotyrosine residues (Claesson-Welsh, 1994) and were subsequently phosphorylated. In addition, it has been previously shown that PDGF-BB promotes RASMC proliferation and migration through activation of the PI3K/Akt/mTOR and classic MAPK pathways, the inhibition of which can postpone the above progression (Song et al., 2016; Fairaq et al., 2017; Zhang et al., 2018).

Our experiments confirmed the time-dependent manner of PDGF-BB-triggered activation in the abovementioned pathways (data not shown), and we chose 10 min as the time point to evaluate the extent of phosphorylation. Western blotting was conducted using antibodies against the classical PDGFRβ and

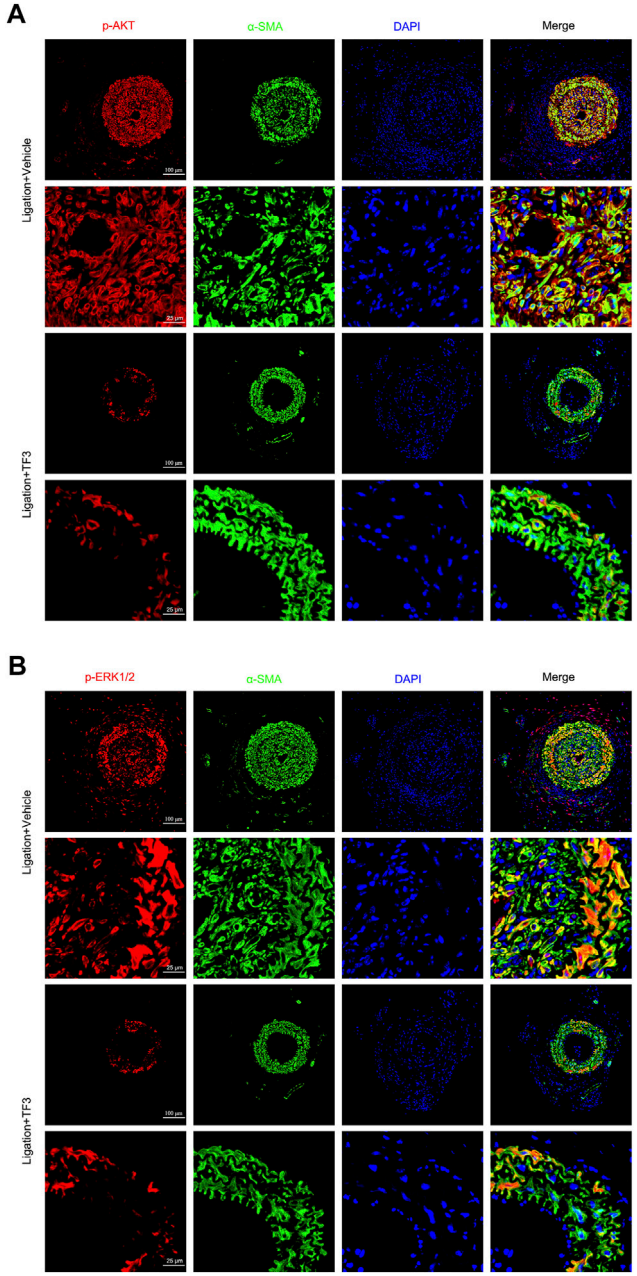

FIGURE 7 | Theaflavin-3,3′-digallate (TF3) suppresses the activation of AKT and ERK1/2 during carotid artery ligation–induced neointimal hyperplasia. TF3 (10 mg/kg) or vehicle was intraperitoneally injected after carotid artery ligation. **(A)** Immunofluorescence staining of p-AKT (red), α-SMA (green), and DAPI (blue) (above) and their enlarged view (below) are shown. **(B)** Immunofluorescence staining of p-ERK (red), α-SMA (green), and DAPI (blue) (above) and their enlarged view (below) are shown. Scale bars, 100 and 25 μm.

MAPK signaling pathway components after 10 min of PDGF-BB stimulation. Under the premise that the total amount of these proteins remained the same, the expressions of p-PDGFRβ (Tyr751), p-PLCγ (Tyr783), p-Src (Tyr416), p-AKT (Ser473), p-mTOR (Ser2448), p-JNK (Thr183/Tyr185), p-ERK1/2 (Tyr204), and p-P38 (Thr180/Tyr182) were found to be increased after PDGF-BB stimulation, and pretreatment with 20 μM TF3 obviously diminished the phosphorylation of these proteins after PDGF-BB stimulation (**Figure 6**).

In order to further explore whether TF3 has the same effect *in vivo*, we conducted immunofluorescence assay at 14 days after CAL, and a strong reduction of p-AKT and p-ERK1/2 was detected under TF3 injection (**Figure 7** and **Supplementary Figure S4**). In addition, using AKT activator SC79 (Wen et al., 2020) (Selleck, S7863) and ERK1/2 activator TPA (Xiao et al., 2019) (Shanghai yuanye Bio-Technology, B50767), we conducted CCK-8 and wound healing assay *in vitro*. Results revealed that pretreatment with SC79 (5 ug/ml) or TPA (150 nM) reversed the inhibition effects on cell proliferation and migration by TF3 under PDGF-BB stimulation to some extent (**Figure 8**). These results indicated that TF3 suppresses the activation of PDGFRβ and its downstream pathways during PDGF-BB stimulation to perform its pronounced effect on maintaining the contractile phenotype of RASMCs both *in vivo* and *in vitro*.

DISCUSSION

In the present study, we delineated that TF3 ameliorates neointimal hyperplasia *in vivo* to a large extent. Intraperitoneal injection of TF3 significantly reduced the I/M ratio after CAL as well as maintained the vessel structure. The expression levels of PCNA and MMP9 were decreased in the vascular media and intima after TF3 intervention.

Unlike cardiac or skeletal muscle cells, VSMCs are highly versatile in response to the environment change in vessel walls. Contractile VSMCs regulate the structure of blood vessels under normal conditions. In case of vascular injury, they undergo phenotypic changes from the quiescent contractile phenotype to the proliferative and migratory synthetic phenotype. PDGF-BB was found to have a key role in the modulation of this conversion (Xu et al., 2009) as it was sharply elevated in the initiation stage during neointimal hyperplasia and promoted the accumulation of VSMCs after balloon injury. Therefore, we conducted *in vitro* experiments on RASMCs using PDGF-BB as stimulation. Our results demonstrated that the expression of the contractile factors (MYH11, α-SMA, and SM22) of RASMCs were reduced after PDGF-BB stimulation, and pretreatment of TF3 can reverse this phenotypic switching to a large extent. While converting to the synthetic phenotype, RASMCs are excessively capable of proliferating and migrating as well as secreting various extracellular matrix proteins and cytokines (An et al., 2017). To observe the proliferative activity, we performed CCK8 and EdU assays. According to the results, the enhanced proliferative ability after PDGF-BB stimuli can be suppressed by TF3 to a large extent. Consistent with this finding, western blotting revealed a great decrease in the levels of some proliferation-associated proteins (PCNA, CDK1, CDK2, CDK4, and CCNE1), and TUNEL staining

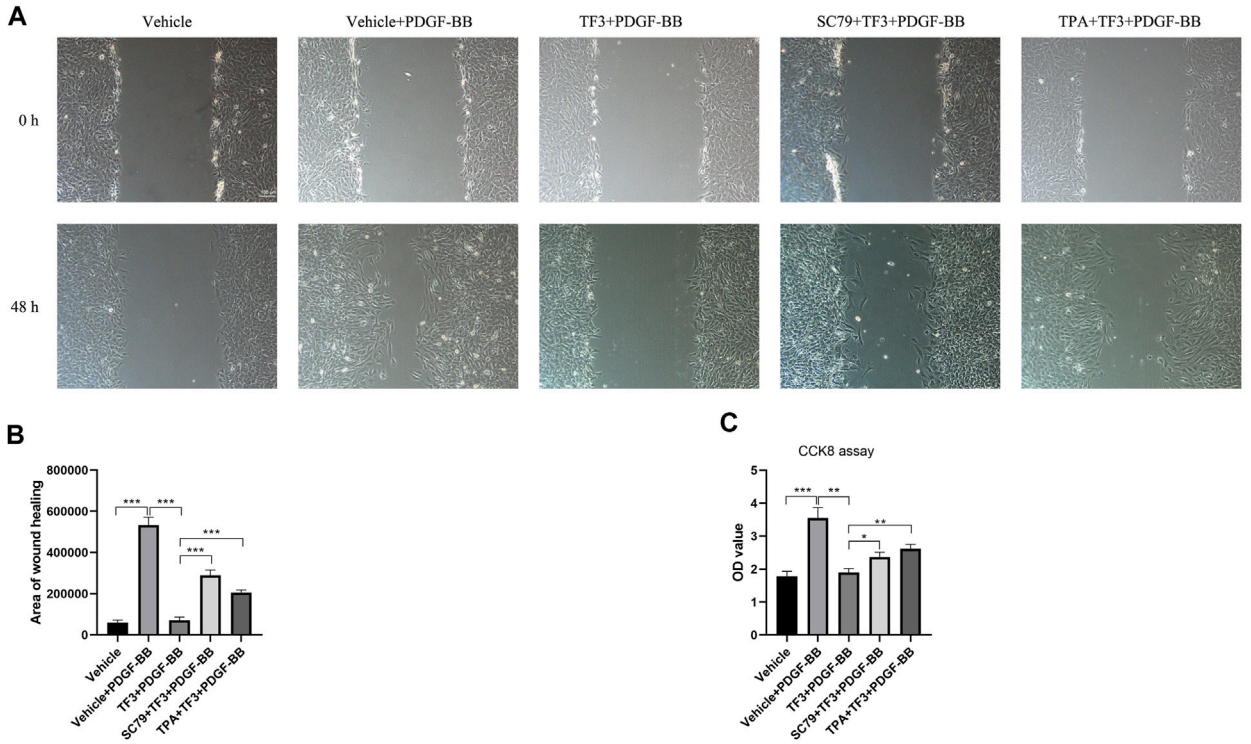

FIGURE 8 | Activation of AKT and ERK1/2 abrogate the effects of theaflavin-3,3′-digallate (TF3) on rat aortic smooth cells (RASMCs) under PDGF-BB stimulation. Serum-starved RASMCs were pretreated with 20-μM TF3, 5 ug/ml SC79, and 150 nM TPA for 1 h and then stimulated with 20 ng/ml PDGF-BB for 48 h. **(A)** The wound healing migration assay was performed as indicated. Scale bar, 100 μm **(B)** The statistical data of the wound healing assay is shown. **(C)** The CCK-8 assay was performed as indicated. Each experiment was performed in triplicate. $^{*}p < 0.05$, $^{**}p < 0.01$, $^{***}p < 0.001$.

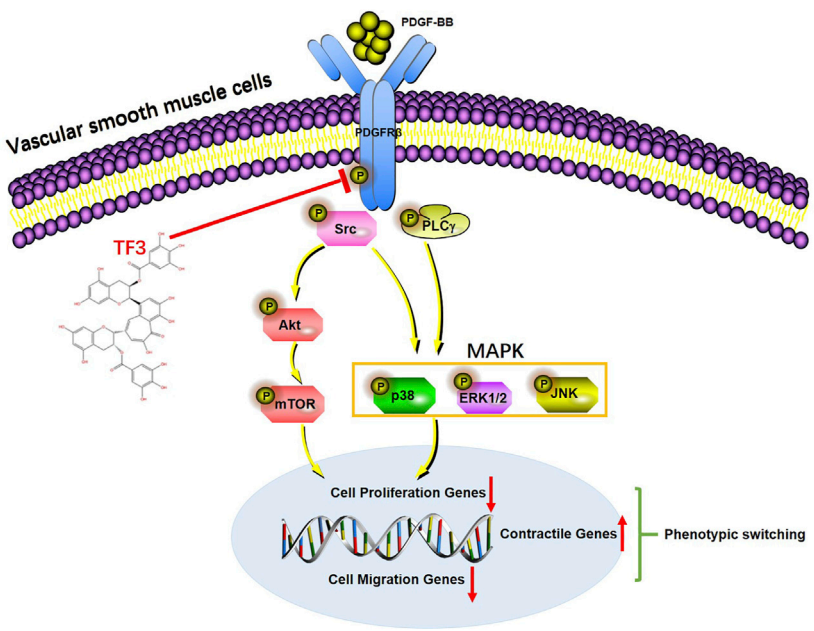

FIGURE 9 | A working model of the effect of theaflavin-3,3′-digallate (TF3) in PDGF-BB–induced phenotypic switching. Under vessel injury, vascular smooth cells (VSMCs) undergo phenotypic switching that leads to neointimal hyperplasia. TF3 inhibits the activation of PDGFRβ and its downstream pathways to suppress PDGF-BB–induced VSMC phenotypic switching and thus reduces neointimal hyperplasia.

showed that there was apparently no increase in cell apoptosis. Moreover, wound healing and transwell assays further demonstrated the ability of TF3 to inhibit VSMC migration. Cells pretreated with TF3 exhibited attenuated migratory ability compared to the control group, and western blot analysis later confirmed the decreased level of some migration-associated proteins (MMP2 and MMP9). Therefore, we verified that TF3 is an active inhibitor of the contractile-to-synthetic phenotype switch.

Consistent with previous studies, PDGF-BB triggers the phenotypic switching of RASMCs by binding and activating PDGFRβ; and molecules, such as PLCγ1 and the Src family, are subsequently bound to the receptor and phosphorylated. In addition, the PI3K/Akt/mTOR and MAPK pathways are also involved in PDGF-BB–induced phenotypic switching (Shao et al., 2020; Osman et al., 2021). Western blot analysis confirmed the explicit inhibitory effect of TF3 on the phosphorylation of p-PDGFRβ, p-PLCγ, p-Src, p-AKT, p-mTOR, p-JNK, p-ERK1/2, and p-P38 after 10 min of stimulation. It should be noted that phosphorylation levels of p-PDGFRβ, p-AKT, and p-ERK1/2 were also downregulated by TF3 in primary mSMCs (**Supplementary Figure S5**). In line with *in vitro* results, activation of p-AKT and p-ERK1/2 pathways were also suppressed by TF3 *in vivo*. SC79 and TPA, activators of AKT and ERK1/2, respectively, abrogated the effects of TF3 on inhibiting RASMC phenotypic switching. Taken together, these results proved that TF3 suppresses the activation of PDGFRβ and its downstream pathways under PDGF-BB stimulation.

In summary, we demonstrated that TF3 acts as a key repressor of PDGF-BB–induced VSMC phenotypic switching by inhibiting the activation of PDGFRβ and its downstream pathways (**Figure 9**). These findings suggest that intervention with TF3 may prevent some proliferative vascular diseases, such as neointimal hyperplasia, after percutaneous coronary intervention and serve as a potential therapeutic candidate for controlling the abnormal phenotypic switching of VSMCs.

DATA AVAILABILITY STATEMENT

The original contributions presented in the study are included in the article/**Supplementary Material**, and further inquiries can be directed to the corresponding authors.

ETHICS STATEMENT

The animal study was reviewed and approved by The Institutional Animal Care and Use Committee (IACUC) of Huazhong University of Science and Technology. Written informed consent was obtained from the owners for the participation of their animals in this study.

AUTHOR CONTRIBUTIONS

ML and KH conceived and designed the experiments. YW and MC performed the experiments and prepared the manuscript. JS, ZC, LZ, JH, and HY analyzed the data for the work. ML and KH prepared and revised the manuscript. All authors gave final approval.

FUNDING

This study was funded by the National Natural Science Foundation of China (No: 91949201 and No: 81830014) and the Natural Science Foundation of Hubei Province (2020CFB429).

SUPPLEMENTARY MATERIAL

The Supplementary Material for this article can be found online at: https://www.frontiersin.org/articles/10.3389/fphar.2022.861319/full#supplementary-material

REFERENCES

An, Z., Liu, Y., Song, Z. G., Tang, H., Yuan, Y., and Xu, Z. Y. (2017). Mechanisms of Aortic Dissection Smooth Muscle Cell Phenotype Switch. *J. Thorac. Cardiovasc Surg.* 154 (5), 1511–e6. doi:10.1016/j.jtcvs.2017.05.066

Augstein, A., Mierke, J., Poitz, D. M., and Strasser, R. H. (2018). Sox9 Is Increased in Arterial Plaque and Stenosis, Associated with Synthetic Phenotype of Vascular Smooth Muscle Cells and Causes Alterations in Extracellular Matrix and Calcification. *Biochim. Biophys. Acta Mol. Basis Dis.* 1864 (8), 2526–2537. doi:10.1016/j.bbadis.2018.05.009

Beach, J. M., Mihaljevic, T., Svensson, L. G., Rajeswaran, J., Marwick, T., Griffin, B., et al. (2013). Coronary Artery Disease and Outcomes of Aortic Valve Replacement for Severe Aortic Stenosis. *J. Am. Coll. Cardiol.* 61 (8), 837–848. doi:10.1016/j.jacc.2012.10.049

Boor, P., Ostendorf, T., and Floege, J. (2014). PDGF and the Progression of Renal Disease. *Nephrol. Dial. Transpl.* 29 (Suppl. 1), i45–i54. doi:10.1093/ndt/gft273

Bornfeldt, K. E., Raines, E. W., Graves, L. M., Skinner, M. P., Krebs, E. G., and Ross, R. (1995). Platelet-derived Growth Factor. Distinct Signal Transduction Pathways Associated with Migration versus Proliferation. *Ann. N. Y. Acad. Sci.* 766, 416–430. doi:10.1111/j.1749-6632.1995.tb26691.x

Cai, F., Li, C., Wu, J., Min, Q., Ouyang, C., Zheng, M., et al. (2007). Modulation of the Oxidative Stress and Nuclear Factor kappaB Activation by Theaflavin 3,3'-gallate in the Rats Exposed to Cerebral Ischemia-Reperfusion. *Folia Biol. (Praha)* 53 (5), 164–172.

Chappell, J., Harman, J. L., Narasimhan, V. M., Yu, H., Foote, K., Simons, B. D., et al. (2016). Extensive Proliferation of a Subset of Differentiated, yet Plastic, Medial Vascular Smooth Muscle Cells Contributes to Neointimal Formation in Mouse Injury and Atherosclerosis Models. *Circ. Res.* 119 (12), 1313–1323. doi:10.1161/CIRCRESAHA.116.309799

Chistiakov, D. A., Orekhov, A. N., and Bobryshev, Y. V. (2015). Vascular Smooth Muscle Cell in Atherosclerosis. *Acta Physiol. (Oxf)* 214 (1), 33–50. doi:10.1111/apha.12466

Claesson-Welsh, L. (1994). Signal Transduction by the PDGF Receptors. *Prog. Growth Factor Res.* 5 (1), 37–54. doi:10.1016/0955-2235(94)90016-7

Davis-Dusenbery, B. N., Wu, C., and Hata, A. (2011). Micromanaging Vascular Smooth Muscle Cell Differentiation and Phenotypic Modulation. *Arterioscler. Thromb. Vasc. Biol.* 31 (11), 2370–2377. doi:10.1161/atvbaha.111.226670

Fairaq, A., Shawky, N. M., Osman, I., Pichavaram, P., and Segar, L. (2017). AdipoRon, an Adiponectin Receptor Agonist, Attenuates PDGF-Induced VSMC Proliferation through Inhibition of mTOR Signaling Independent of AMPK: Implications toward Suppression of Neointimal Hyperplasia. *Pharmacol. Res.* 119, 289–302. doi:10.1016/j.phrs.2017.02.016

Frismantiene, A., Philippova, M., Erne, P., and Resink, T. J. (2018). Smooth Muscle Cell-Driven Vascular Diseases and Molecular Mechanisms of VSMC Plasticity. *Cell Signal* 52, 48–64. doi:10.1016/j.cellsig.2018.08.019

Gao, Y., Rankin, G. O., Tu, Y., and Chen, Y. C. (2016). Theaflavin-3, 3'-digallate Decreases Human Ovarian Carcinoma OVCAR-3 Cell-Induced Angiogenesis via Akt and Notch-1 Pathways, Not via MAPK Pathways. *Int. J. Oncol.* 48 (1), 281–292. doi:10.3892/ijo.2015.3257

Heusch, G., Libby, P., Gersh, B., Yellon, D., Böhm, M., Lopaschuk, G., et al. (2014). Cardiovascular Remodelling in Coronary Artery Disease and Heart Failure. *Lancet* 383 (9932), 1933–1943. doi:10.1016/s0140-6736(14)60107-0

Hu, X., Ping, Z., Gan, M., Tao, Y., Wang, L., Shi, J., et al. (2017). Theaflavin-3,3'-digallate Represses Osteoclastogenesis and Prevents Wear Debris-Induced Osteolysis via Suppression of ERK Pathway. *Acta Biomater.* 48, 479–488. doi:10.1016/j.actbio.2016.11.022

Lee, H. H., Ho, C. T., and Lin, J. K. (2004). Theaflavin-3,3'-digallate and Penta-O-Galloyl-Beta-D-Glucose Inhibit Rat Liver Microsomal 5alpha-Reductase Activity and the Expression of Androgen Receptor in LNCaP Prostate Cancer Cells. *Carcinogenesis* 25 (7), 1109–1118. doi:10.1093/carcin/bgh106

Leung, L. K., Su, Y., Chen, R., Zhang, Z., Huang, Y., and Chen, Z. Y. (2001). Theaflavins in Black Tea and Catechins in Green Tea Are Equally Effective Antioxidants. *J. Nutr.* 131 (9), 2248–2251. doi:10.1093/jn/131.9.2248

Liang, Y. C., Chen, Y. C., Lin, Y. L., Lin-Shiau, S. Y., Ho, C. T., and Lin, J. K. (1999). Suppression of Extracellular Signals and Cell Proliferation by the Black Tea Polyphenol, Theaflavin-3,3'-Digallate. *Carcinogenesis* 20 (4), 733–736. doi:10.1093/carcin/20.4.733

Lin, J. K., Chen, P. C., Ho, C. T., and Lin-Shiau, S. Y. (2000). Inhibition of Xanthine Oxidase and Suppression of Intracellular Reactive Oxygen Species in HL-60 Cells by Theaflavin-3,3'-Digallate, (-)-Epigallocatechin-3-Gallate, and Propyl Gallate. *J. Agric. Food Chem.* 48 (7), 2736–2743. doi:10.1021/jf000066d

Lin, Y. L., Tsai, S. H., Lin-Shiau, S. Y., Ho, C. T., and Lin, J. K. (1999). Theaflavin-3,3'-digallate from Black Tea Blocks the Nitric Oxide Synthase by Down-Regulating the Activation of NF-kappaB in Macrophages. *Eur. J. Pharmacol.* 367 (2-3), 379–388. doi:10.1016/s0014-2999(98)00953-4

Mortensen, M. B., and Nordestgaard, B. G. (2018). Comparison of Five Major Guidelines for Statin Use in Primary Prevention in a Contemporary General Population. *Ann. Intern Med.* 168 (2), 85–92. doi:10.7326/M17-0681

Osman, I., Dong, K., Kang, X., Yu, L., Xu, F., Ahmed, A. S. I., et al. (2021). YAP1/TEAD1 Upregulate Platelet-Derived Growth Factor Receptor Beta to Promote Vascular Smooth Muscle Cell Proliferation and Neointima Formation. *J. Mol. Cell Cardiol.* 156, 20–32. doi:10.1016/j.yjmcc.2021.03.005

Owens, G. K., Kumar, M. S., and Wamhoff, B. R. (2004). Molecular Regulation of Vascular Smooth Muscle Cell Differentiation in Development and Disease. *Physiol. Rev.* 84 (3), 767–801. doi:10.1152/physrev.00041.2003

Raines, E. W. (2004). PDGF and Cardiovascular Disease. *Cytokine Growth Factor Rev.* 15 (4), 237–254. doi:10.1016/j.cytogfr.2004.03.004

Rensen, S. S. M., Doevendans, P. A. F. M., and van Eys, G. J. J. M. (2007). Regulation and Characteristics of Vascular Smooth Muscle Cell Phenotypic Diversity. *Neth. Heart J.* 15, 100–108. doi:10.1007/BF03085963

Shao, W., Li, X., Peng, J., Fan, S., Liang, M., and Huang, K. (2020). Apatinib Attenuates Phenotypic Switching of Arterial Smooth Muscle Cells in Vascular Remodelling by Targeting the PDGF Receptor-β. *J. Cell Mol. Med.* 24 (17), 10128–10139. doi:10.1111/jcmm.15623

Shawky, N. M., and Segar, L. (2017). Sulforaphane Inhibits Platelet-Derived Growth Factor-Induced Vascular Smooth Muscle Cell Proliferation by Targeting mTOR/p70S6kinase Signaling Independent of Nrf2 Activation. *Pharmacol. Res.* 119, 251–264. doi:10.1016/j.phrs.2017.02.010

Song, Y., Wu, Y., Su, X., Zhu, Y., Liu, L., Pan, Y., et al. (2016). Activation of AMPK Inhibits PDGF-Induced Pulmonary Arterial Smooth Muscle Cells Proliferation and its Potential Mechanisms. *Pharmacol. Res.* 107, 117–124. doi:10.1016/j.phrs.2016.03.010

Tallquist, M., and Kazlauskas, A. (2004). PDGF Signaling in Cells and Mice. *Cytokine Growth Factor Rev.* 15 (4), 205–213. doi:10.1016/j.cytogfr.2004.03.003

Wen, L., Wang, K., Zhang, F., Tan, Y., Shang, X., Zhu, Y., et al. (2020). AKT Activation by SC79 to Transiently Re-open Pathological Blood Brain Barrier for Improved Functionalized Nanoparticles Therapy of Glioblastoma. *Biomaterials* 237, 119793. doi:10.1016/j.biomaterials.2020.119793

Xiao, Y., Liang, M. R., Liu, C. C., Wang, Y. N., Zeng, Y., Zhou, J., et al. (2019). Overexpression of P16 Reversed the MDR1-Mediated DDP Resistance in the Cervical Adenocarcinoma by Activating the ERK1/2 Signaling Pathway. *Cell Div.* 14, 6. doi:10.1186/s13008-019-0048-6

Xu, X., Lu, H., Lin, H., Li, X., Ni, M., Sun, H., et al. (2009). Aortic Adventitial Angiogenesis and Lymphangiogenesis Promote Intimal Inflammation and Hyperplasia. *Cardiovasc Pathol.* 18 (5), 269–278. doi:10.1016/j.carpath.2008.07.004

Yang, C. S., and Landau, J. M. (2000). Effects of Tea Consumption on Nutrition and Health. *J. Nutr.* 130 (10), 2409–2412. doi:10.1093/jn/130.10.2409

Zhang, L., Xu, Z., Wu, Y., Liao, J., Zeng, F., and Shi, L. (2018). Akt/eNOS and MAPK Signaling Pathways Mediated the Phenotypic Switching of Thoracic Aorta Vascular Smooth Muscle Cells in Aging/hypertensive Rats. *Physiol. Res.* 67 (4), 543–553. doi:10.33549/physiolres.933779

Conflict of Interest: The authors declare that the research was conducted in the absence of any commercial or financial relationships that could be construed as a potential conflict of interest.

Publisher's Note: All claims expressed in this article are solely those of the authors and do not necessarily represent those of their affiliated organizations, or those of the publisher, the editors, and the reviewers. Any product that may be evaluated in this article, or claim that may be made by its manufacturer, is not guaranteed or endorsed by the publisher.

Advantages of publishing in Frontiers

OPEN ACCESS
Articles are free to read for greatest visibility and readership

FAST PUBLICATION
Around 90 days from submission to decision

HIGH QUALITY PEER-REVIEW
Rigorous, collaborative, and constructive peer-review

TRANSPARENT PEER-REVIEW
Editors and reviewers acknowledged by name on published articles

Frontiers
Avenue du Tribunal-Fédéral 34
1005 Lausanne | Switzerland

Visit us: www.frontiersin.org
Contact us: frontiersin.org/about/contact

REPRODUCIBILITY OF RESEARCH
Support open data and methods to enhance research reproducibility

DIGITAL PUBLISHING
Articles designed for optimal readership across devices

FOLLOW US
@frontiersin

IMPACT METRICS
Advanced article metrics track visibility across digital media

EXTENSIVE PROMOTION
Marketing and promotion of impactful research

LOOP RESEARCH NETWORK
Our network increases your article's readership